# Interpretation of Resistivity Data

Interpretation of

Resistivity Data

By ROBERT G. VAN NOSTRAND *and* KENNETH L. COOK

GEOLOGICAL SURVEY PROFESSIONAL PAPER 499

A presentation of mathematical potential
theory and practical field application for
the direct-current methods of electrical
resistivity prospecting

CONTENTS

ILLUSTRATIONS

[All plates are in pocket]

TABLES

SYMBOLS

The following symbols are the principal ones used in the text. The symbols which are used in a restricted sense with no chance of ambiguity are excluded from the list. Also excluded are certain vector and scalar differential operations, which are defined in the section on useful coordinate systems. Where a given symbol has more than one meaning, the meanings are such that there is little chance for ambiguity. Distances are in meters, potentials in volts, and currents in amperes.

a	Separation between adjacent electrodes in Wenner configuration.
A, B	Current electrodes in Schlumberger configuration and well logging.
A, B, C, D	Arbitrary constants in solutions to differential equations.
b	Width of dike.
b	Length of current stake.
b	Geometric parameter in spheroidal or bipolar coordinates.
C, C_1, C_2	Current electrodes. Subscript 1 used to define easternmost or northernmost electrode.
C', C''	Image positions of a current electrode.
e	Constant equal to 2.718.
E	Electric field in Schlumberger configuration.
$f(x)$	A function of x.
$F(a, b; c; x)$	$1+\dfrac{(a)(b)}{c}\,x+\dfrac{a(a+1)(b)(b+1)}{2!c(c+1)}\,x^2+\ \dots$ and is called the hypergeometric series.
h_1, h_2, h_3	Geometric parameters in generalized coordinates.
i	$\sqrt{-1}$.
i	Summation index.
I	Total current.
$I_\nu(u)$	Modified Bessel function, defined by equation 73 or 75A.
J	Current density.
J_x, J_y, J_z	Components of current density.
$J_x]_{x=0}$	x component of current density evaluated at $x=0$.
$J_n(u)$	Bessel function, defined by equation 69.
k	Reflection factor.
k_{ij}	$(\rho_j-\rho_i)/(\rho_j+\rho_i)$.
$K_\nu(u)$	Modified Bessel function, defined by equation 71, 72, or 75.
$\ln x$	Natural logarithm of x.
l	Half distance between C_1 and C_2.
L	Distance between C_1 and C_2, $L=2l$.
m	Abbreviation for meters.
m	Summation index.
$m!$	$(1)(2)(3)\ \dots\ (m-1)(m)=m$ factorial.
M, N	Potential electrodes in Schlumberger configuration or well logging.
n	Summation index.
p	Variable of integration.
P, P_1, P_2	Potential electrodes or point at which potential is measured.
PDR	Potential-drop ratio.
$P_n(u)$	Legendre polynomial, defined by equations 56 and 57.
$P_n^m(u)$	Associated Legendre polynomial of the first kind, defined by equation 55. $P_n^m(u)=P_n(u)$ when $m=0$.
$P_{p-\frac{1}{2}}^m(u)$	Associated Legendre function of the first kind (where p and u are continuously variable), defined by equations 55, 62, 86, and 87.
$P_n'^m(u)$	$\dfrac{\partial P_n^m(u)}{\partial u}$.
$Q_n(u)$	Legendre function of the second kind as defined by equation 84.
$Q_n^m(u)$	Associated Legendre function of the second kind defined by equations 55 and 83 if the corresponding Q's replace the P's in these equations (see also equation 84). $Q_n^m(u)=Q_n(u)$ when $m=0$.
r	Radial distance in spherical or cylindrical coordinates.
R, R_1, R_{12}, etc.	Interelectrode distances.
U	Potential.

x

$u_1,\ u_2,\ u_3$	Variables in generalized coordinates.
U_{1B}	Potential in medium 1 due to current electrode in medium 2 (given by subscript "B").
V	Potential difference.
V_{10}	Potential difference between P_1 and P_0.
V	A vector.
x	Linear distance on earth's surface.
$x,\ y,\ z$	Rectangular coordinates.
z	Depth, increasingly positive downward.
z	Axial distance in cylindrical coordinates.
α	Dip of fault plane or bed.
α	Angle between profile and strike of vertical fault or bed.
$\Gamma(x)$	$\int_0^\infty u^{x-1}e^{-u}du=(x-1)!$, the latter only if x is a positive integer.
δ_{mn}	Constant equal to 1 if $m=n$ or zero if $m\neq n$.
$\delta(p-p')$	Impulse or delta function defined by equation 60.
ζ	Variable in oblate spheroidal coordinates.
η	Variable in prolate spheroidal coordinates.
θ	Latitude angle in spherical coordinates.
μ	Variable in oblate spheroidal coordinates.
ξ	Variable in prolate spheroidal coordinates.
π	Constant equal to 3.1416.
ρ	Resistivity.
ρ_a	Apparent resistivity.
$\rho_1,\ \rho_2$	Apparent resistivity in Lee configuration: ρ_1 is for north or east partitioning plane.
$\rho_1,\ \rho_2,\ \rho',\ \rho''$	True resistivities of formations.
σ	Variable in bipolar coordinates.
σ	Conductivity.
τ	Variable in bipolar coordinates.
ϕ	Azimuthal angle in all coordinate systems used.
$\psi_n^m(u)$	$P_n^m(u)/Q_n^m(u)$.
$\psi_n'^m(u)$	$P_n'^m(u)/Q_n'^m(u)$ where the primes on $P_n^m(u)$ and $Q_n^m(u)$ have the usual meaning of differentiation with respect to the argument.
$\Psi_n^m(u)$	$P_n'^m(u)-\psi_n^m(u)Q_n'^m(u)$.
$\psi_m(tr)$	$K_m(tr)/I_m(tr)$.
$\psi_m'(tr)$	$\dfrac{\partial K_m(tr)}{\partial r}\Big/\dfrac{\partial I_m(tr)}{\partial r}$.

INTERPRETATION OF RESISTIVITY DATA

By Robert G. Van Nostrand and Kenneth L. Cook

ABSTRACT

Electrical prospecting has grown from Fox's investigations of natural earth currents in 1830, through Schlumberger's successful use of applied direct currents, to a diversified art employing both alternating currents and electromagnetic fields, as well as direct currents. Early resistivity data were interpreted by empirical methods, which are still used widely. Other interpretative methods include direct interpretation by transforming the resistivity data into geologic information using mathematical transformation formulas; this method is as as yet restricted to horizontal bedding. This treatise is largely restricted to comparative interpretation—that is, the comparison of field data with theoretical curves over assumed ore bodies and geologic structures.

A logical and mathematical interpretation of resistivity data, even at present only partly successful, was initiated in 1928 by Hummel. The mathematical approach to electrical-resistivity prospecting draws upon all the principles of potential fields and especially of electric-current flow. The assumption that the current electrodes are point electrodes is valid at points whose distances from the electrode are a few times the dimensions of the electrode. The electric current field around this point electrode can be calculated from the fact that the field obeys Laplace's equation everywhere except at the electrode itself. If the earth is not uniform, but is divided into distinct zones of various resistivities, the solutions to Laplace's equation are subject to suitable boundary conditions. In some special cases, the terms in the solution are identifiable with electric fields that would be due to images of the original source; and these solutions can therefore be obtained directly by use of the less sophisticated image theory instead of the higher mathematics necessary for harmonic analysis. These special cases include horizontal bedding, buried perfectly conducting spheres, and a single geologic boundary dipping at certain specific angles.

The mathematical solutions are used to compute the potential distribution about the current electrode in a given problem. Using the reciprocity principle and the principle of superposition, the potential distribution and then the apparent resistivity are computed for various electrode configurations.

The many theoretical apparent-resistivity curves presented in this treatise, which include horizontal and vertical profiles for various electrode configurations, may be used for comparison with observed field curves for specific resistivity contrasts in such problems as vertical or dipping faults, vertical dikes, filled sinks, horizontal bedding, and buried spheres. The curves presented may be used for comparison with other resistivity contrasts, by inference, or the equations may serve as the basis for computation of other curves for further values of the various parameters. The analysis for outcropping volcanic necks or cones, filled channels, buried dome structures, and buried vertical faults is also treated briefly.

The apparent-resistivity curves may serve as the basis for general conclusions not limited to any specific problem, and facilitate the choice of field techniques in the exploration of ore bodies and geologic structures with resistivity methods. It is shown, for example, that a roughly spherical body buried deeper than its radius would be difficult to find by resistivity methods; that a profile crossing an outcropping vertical dike displays at least two peaks and not one as might be supposed; that an equal-resistivity map is sensitive to the direction in which the profiles are laid out; and that the value of the apparent resistivity can and does rise above the highest value of the true resistivity of the medium or fall below the lowest value of the true resistivity. It is demonstrated that many paradoxes exist in the apparent-resistivity curves and that theoretical curves are necessary for a correct interpretation of the resistivity field data over ore bodies and geologic structures.

A comprehensive bibliography on the resistivity method of prospecting is included.

INTRODUCTION

This treatise is the result of field and theoretical work carried on intermittently since 1951, when we first started a concerted attack on many of the problems incident to the interpretation of resistivity data. In previous field work, during resistivity surveys, we had encountered specific problems over vertical discontinuities such as dikes, faults, and brecciated zones. Interpretation was hampered because the analysis for such simple features was not available for the Lee configuration, which was used principally by the U.S. Geological Survey. In 1951, during a resistivity survey in the the Tri-State zinc and lead mining district, it was realized further that no theoretical analysis had been developed for features such as ellipsoidal and hemispherical sinks, which gave characteristic and well-defined anomalies in this district.

As a consequence, we began what eventually evolved into a systematic study of the interpretation of resistivity data, the results of which are presented here. The early work was confined to apparent-resistivity anomalies for various configurations over simple plane boundaries, such as vertical insulating and conducting planes, and vertical faults. This elementary work evolved into the study of more complex forms including vertical dikes, dipping faults, and various curved surfaces such as hemispherical sinks. To this was added the wealth of material already available concerning horizontal beds.

The typical method of attack on a given problem took the following form: The necessary formulas were

1

derived to describe the potential due to a point source of current in the presence of the given geologic feature; these equations were then used to calculate theoretical apparent-resistivity data from which were constructed albums of curves for typical values of the parameters; and, finally, these curves were compared with field anomalies over similar geologic features. In those cases for which we have been able to complete our treatment, this is also the sequence in which our material is given.

Our objectives in writing such a treatise were—

1. To develop in English under a single cover the subject of direct-current electrical prospecting, such that the discussion will serve both as a text for students and as a reference for more advanced workers. The only other book-length treatments of electrical prospecting are in foreign languages, namely that by Krayev (1951), in Russian, and that by Fritsch (1949b), in German.

2. To present the theory necessary to solve problems in electrical prospecting.

3. To present a wealth of theoretical resistivity curves based on this treatment, including a sufficiently large number of examples for which the conclusions drawn may be of general, as well as of practical utility.

4. To show how the theoretical results and curves can be used to interpret field data.

5. To compare present field techniques in the light of these curves and data and to devise additional techniques where they are necessary or helpful.

6. To assemble a comprehensive bibliography on the subject of surface-resistivity methods of electrical prospecting.

Because of limitations of time and space, the study has been only partly successful in meeting the objectives. For example, particularly in studying buried structures, we have done little more than present the basic mathematical solutions. Although our solutions are based solely on the exact and classical methods of differential equations, we suggest that someone carry the attack further by using numerical approximation methods, and thereby extend the possibilities from a limited number of regularly shaped bodies to an unlimited number of structures, including those irregular in shape.

Our treatment of horizontal bedding is limited essentially to the principles involved. Rather than include resistivity profiles for two- , three- , and four-layer cases, which have already been published elsewhere, we merely indicate where these published curves may be found.

Our coverage of vertical features such as dikes and faults, and of filled hemispherical sinks is reasonably exhaustive. We not only have accumulated material from a wide variety of sources but also have added much that is our own. The utility of this material goes beyond the geologic features shown specifically, inasmuch as inferences may be drawn that make some of the conclusions applicable to other features. More complicated structures are generally difficult for quantitative analysis and often lead to solutions that vary but little from these vertical features.

It must be emphasized that this volume deals with direct-current methods of prospecting. The results are applicable to alternating-current prospecting only in the limit of zero frequency, or in practice, very low frequencies. Even for perfectly homogeneous ground, the depth of penetration for alternating current is not proportional to the electrode spread but reaches an asymptotic value as the distance between the electrodes is increased. The same is true of commutated and interrupted currents which in general have several components of different penetration.

ACKNOWLEDGMENTS

DEVELOPMENT OF ELECTRICAL PROSPECTING
EARLY HISTORY

Electrical prospecting is the art of measuring electrical properties of rocks in the study of the structure and composition of those layers of the earth which are sufficiently shallow to be exploited by man. Like many other arts, electrical prospecting was conceived long ago, and the elaborate instruments and carefully devised methods of today result from ideas that evolved in the minds of men more than 2 centuries ago.

The earliest work in electrical prospecting appears to have been done by Gray and Wheeler in 1720 and by Watson in 1746 (Jakosky, 1950, p. 8). Gray and Wheeler made electrical studies of rocks and listed their electric conductivities. Watson discovered independently that the ground is an electrical conductor. He also found that an electric current passed through the ground between two electrodes two miles apart fluctuates in an erratic manner different from that where wire is used to complete the circuit.

The next recorded work in electrical prospecting was done by Robert W. Fox. In fact, we prefer to think that Fox made the first real contributions to the art. Fox was a prominent scientist of his day and lived most of his life (1789-1877) near Falmouth. England, where he did research on such matters as high-pressure steam, geothermics, electricity, and terrestrial magnetism (Kelly, 1938a). As revealed in his own publications, he was well versed in geologic matters. Among other geophysical accomplishments, he designed the first dip circle for the determination of magnetic dip and magnetic intensity aboard ship (Kelly, 1938a), and he was one of the first to recognize the existence of the geothermal gradient in the earth (Fox, 1830).

Fox conducted his original experiments in 1830 in the copper mines of Cornwall, where he made the momentous discovery that there are natural electric currents associated with sulfide ore deposits. Underground in several mines, he succeeded in measuring an electric current flowing between two points on the same vein as well as between two points on different veins. His electrodes consisted of copper plates that were wedged against the vein to make contact. The minerals in the veins included galena, copper, and iron pyrites. His insensitive galvanometer consisted of a 3¼-inch compass needle enclosed by 25 turns of wire. He sometimes used as much as 1,800 feet of connecting wire in these experiments. At first, he coated the wire with sealing wax for insulation, but later he dispensed with such precautions as being unnecessary.

Fox reported that the measured current varied in proportion to the abundance of copper ore in the veins; and, where there was little or no ore, there was little action. This fact led him to conclude, "Hence it seems likely that electro-magnetism may become useful to the practical miner in determining with some degree of probability at least, the relative quantity of ore in veins, and the direction in which it most abounds." He also observed the striking resemblance between the current phenomena associated with veins and those of galvanic batteries which were known at that time.

In 1834 Fox conducted further experiments "in order to prove that the electrical action is derived from the vein, and that it is not in any degree excited by the mere contact of the metal with the ore, as some have surmised." (Fox, 1835a.) He reported that the character and direction of the current was the same whether contact was made to the ground through two copper plates or through a pair of zinc plates; also, the same was true even when the plates were discarded and the ends of the wire alone made contact with the ore.

In his 1834 experiments, Fox constructed the prototype of the present-day bucking potentiometer. According to Fox (1835a), "The galvanic apparatus consisted of a plate of copper, and another of zinc, plunged into strong brine, to which some sulphuric acid was added, and each plate exposed about 180 square inches to the action of the liquid." In searching for an effect, he sometimes connected the cell so as to oppose the natural current and sometimes so as to augment the earth current. At one position of the search electrodes he obtained no measurable current through his galvanometer. He concluded that the veins supplied electric energy and suggested that "this method may become useful to the practical miner, in helping him appreciate the value of his discoveries, and enabling him to ascertain whether the ores in distant parts of a vein are connected or insulated, or whether what appear to be parallel veins are really so, or ramifications of the same vein."

Through 1843, Fox (1843a,b) performed further experiments to show conclusively that current actually was flowing through the earth. In one set of experiments he demonstrated that even with one terminal of zinc and the other of copper, "the current continued to deflect the needle from 50 to 60 degrees, notwithstanding that any action between the copper . . . and the zinc . . ., if it had existed, would have been in an opposite direction, and have tended more or less to counteract the influence of the actual current." In his last experiments, Fox used precautions that he had not previously used. He kept his wires apart and insulated them from the walls of the mine by means of poles, because he had by that time come to believe that "electric currents will traverse a very considerable thickness of rock or strata."

As word of his work spread, other workers commenced similar studies. In 1833, in Germany, von Strombeck (1833) attempted unsuccessfully to confirm Fox's results by careful experiments on a large vein in which quartz, sphalerite, galena, chalcopyrite, and tetrahedrite occurred. From his lack of success von Strombeck concluded that Fox's result were not applicable to veins generally. Henwood (1841) and Reich (1839) were more successful in verifying the results of Fox and, apparently, were able to come closer to the true meaning of the phenomena than was Fox. In 1837,

Henwood, who had been Fox's coworker in his 1830 experiments, made analogous experiments with electrodes at times as far apart as 3,600 feet. His results corroborated those of Fox but he insisted that currents are obtained only when the electrodes are in contact with the vein and not when they are in contact with the barren country rock. Henwood concluded that the currents are purely local and are probably of thermoelectric origin. In 1841, Henwood found that

the nature and position of the small metallic plates employed materially affect, not only the intensity, but in some cases also the directions of the currents; and also that there is a considerable difference in the results when the same plates of metal are placed on different ingredients in the veins, even though these may be in immediate contact with each other.

In 1839, Reich repeated all of Fox's experiments, confirming the latter's results. However, Reich was convinced that the currents are electrochemical phenomena and not, as Henwood believed, thermoelectric. In 1844 Reich published the results of studies of the currents probably existing in the rocks surrounding the vein, rather than along or within the vein.

Fox also saw fit to study the electrical properties of individual minerals. In his 1830 paper he listed 21 minerals as conductors, poor conductors, or nonconductors. Fox considered pyrite as one of the best commonly occurring mineral conductors and sphalerite as a nonconductor. He recognized that shale "seemed to possess the property of conducting common electricity in a slight degree, but only in the direction of cleavage, perhaps owing to the moisture it retained." He also noted the paradox that silver, zinc, and copper in the metallic state are excellent conductors, but combined as sulfides they are considerably less conducting; he classified the sulfides of silver and zinc as nonconductors and copper sulfide as one of the best mineral conductors.

Later, Fox (1835b, 1838) endeavored to classify minerals with reference to their electrical activity. He showed that ores possess the electrochemical properties of metals, particularly with respect to the galvanic action resulting when two ores, such as copper pyrites and "vitreous copper ore," are placed in mine water. He established to his own satisfaction that copper ores are more active than those of lead, and he believed that his field observations were consistent with this fact.

In 1871, W. Skey also performed experiments on single minerals. He enlarged the known list of conducting minerals and determined the direction of the current when conducting minerals in contact with solutions are connected by a wire (Wells, 1914). He reemphasized Fox's viewpoint that conducting minerals can be the electrodes of galvanic cells; and, in addition,

he called attention to the accelerating action of one mineral on another in chemical changes.

These experiments were very significant and made a considerable contribution to the art of electrical prospecting. However, the limited concept of electrical phenomena in general, which prevailed at that time, restricted the conclusions of the workers. Although self-potentials as we know them certainly existed, it is probable that they were obscured by the large potential differences that exist when two electrodes are placed in chemically different solutions. Moreover, Fox's criterion for the "activity" of the earth materials was the magnitude of the current which flowed in the measuring circuit. When the electrodes were placed in barren earth of comparatively high resistivity, the contact resistance was high and little or no current flowed, which fact explains why these early authors reported no activity.

Fox was also apparently the first to postulate the existence of telluric currents and their effect on the geomagnetic field, although his reasoning was naive. Fox (1830) wrote:

. . . assuming that metalliferous veins exist more or less in primitive rocks generally, . . . , it may I think be presumed, that the electrical currents, which so affect the needle of the galvanometer, may likewise influence the direction of the magnetic needle on the surface of the earth; at least no explanation of this phenomenon appears to be so plausible, or so near-connected with ascertained facts. Even the cause of the variations of the needle, mysterious as it has hitherto appeared to be, may probably be referred to the relative energies of the opposing electrical currents, which are perhaps subject to occasional modifications; and the appearance of earthquakes and volcanic action, from time to time, seem to countenance the probability of such changes.

Fox (1832) modified and supplemented his theory as a result of his experiments on the thermoelectricity of such rocks as slate, greenstone, and serpentine. He found that these rocks differed in their electrical properties; when heated, some specimens became electrically positive, others electrically negative, on the hot end. From these experiments he drew the following conclusions concerning telluric currents and related phenomena:

On the hypothesis of the existence of a very elevated temperature in the interior of the globe, it would necessarily follow from the preceding experiments that electrical currents would be produced from this cause, taking frequently different, and even opposite directions, and exerting an important influence on all the phenomena of terrestrial magnetism, both such as are general, and also such as appear to be local anomalies.

The later researches of Fox satisfied him that the directions of these currents are probably much influenced by the geological structure of the globe; which would in most cases tend to give them more or less obliquity to the parallels of latitude. He ascribed diurnal changes in the direction and intensity of

terrestrial magnetism to the successive action of the sun on the different portions of the globe.

Other studies concerning the origin of natural earth currents were made by A. C. Becquerel. Even prior to 1865 he made rather extensive studies of the electric currents obtained between masses of water and the surrounding rocks under different conditions (Matteucci, 1865). From 1865 to 1867, during a study of the effects produced in capillary action, Becquerel also noted the deposition of copper in capillary spaces and suggested that the phenomenon was of an electrochemical nature (Wells, 1914).

The name that stands out in the early descriptions of telluric currents is Charles Matteucci. As early as 1847, the Greenwich Observatory had noted the correlation between strong "spontaneous electric currents," as observed in telegraph wires, and the intensity of the aurora borealis (Matteucci, 1865). Matteucci observed the two coincident phenomena in the same year and subsequently became interested in telluric currents. He was familiar with the work on electric currents that had been done by Fox (Matteucci, 1867).

In 1865, Matteucci (1865) strung up guttapercha covered copper wire (well insulated for that time) on military telegraph poles on the St. Maurice plain in France. One wire was in the plane of the magnetic meridian and a second was normal to this direction. Each wire was 6 kilometers long. Contact with the ground at each end of the wire was made by means of a nonpolarizing electrode which consisted of a strip of amalgamated zinc immersed in a porous porcelain pot containing a saturated solution of zinc sulfate. The porous pot was brought in contact with water in a porous porcelain vase which was in turn embedded in the soil. Matteucci used a galvanometer in series with the line to measure currents directly. He observed the diurnal variations and other fluctuations in the flow of telluric currents. These experiments were followed by others in which he used lines as much as 36 kilometers long (Matteucci, 1867).

Until Matteucci's time, little or no attempt had been made to describe the phenomena quantitatively, and no systematic experiments had been performed with a preorganized plan. Generally, conclusions had been made from the deflection of a galvanometer needle without sufficient consideration of the probable variation of the resistance of the different circuits. During the period between 1844 and 1882, research on the electrical activity of ores bodies was apparently abandoned. The results of Fox and Reich had led Bernhard von Cotta to recommend earnestly that these experiments should be further pursued, as they seemed likely to lead to results of practical discovery of ore bodies. If this recommendation was ever carried out, there is no record of the work until 1882, when Carl Barus (1882) published his classic paper "On the electrical activity of ore bodies." The following account of his contribution is taken from that paper.

Carl Barus was a physicist invited to join the U.S. Geological Survey for the express purpose of continuing the investigation of the electrical activity of ore bodies. The invitation had been extended at the suggestion of George F. Becker, U.S. Geological Survey, who had long felt an interest in this subject. Barus made his electrical measurements during 1880 and 1881 on the Comstock lode and in the Eureka mining district, both in Nevada. Becker realized that neither of these two districts was the best choice, but they were the only ones accessible through extensive workings.

Actually, Barus did have difficulty in making the measurements of the small potentials found in the two districts in which he worked. The mine workings along the Comstock lode at that time were without exception in very barren or nearly exhausted parts of the vein. Therefore, there were probably more minerals possessing anomalous electrical properties in the country rock than there was ore in the ore stopes. In such a situation, the term "ore body" was hardly an applicable term. Also the mines were hot and permitted only intermittent work. Barus found no evidence of currents due to the lode itself on the Comstock. For various reasons, he abandoned the work on the Comstock without ever trying there the better techniques which he developed as his studies progressed.

The geologic conditions were more suitable for such tests at Eureka; but, in the light of our present knowledge, they were still far from satisfactory. The ore is principally lead carbonate, lead sulfate, and iron oxides. It contains silver and gold in variable quantities and occurs in huge, apparently isolated masses in limestone. The large unmined ore bodies were at a mean distance of about 400 feet from the surface and in some places extended upward within 100 feet of the surface. Because of extensive workings, the electrical surveys could be made over, through, and under the ore bodies.

After studying the then available literature, Barus concluded that his problem was not difficult, as it consisted simply in measuring the earth's potential at many points near the ore body and in tracing the equipotential surfaces. He assumed at the outstart the validity of Reich's hypothesis that any lode currents present are due to electrochemical action. He reasoned that currents are generated, analogous to local currents in a battery, at the contacts between the variety of ore minerals which are commonly present in a single ore body. He reasoned further that such

currents would be constant both in magnitude and direction because the process had been going on for a very long time. Therefore, the equipotentials would have fixed and definable positions relative to the ore body. He also realized that, if an ore body generates electric currents, a self-potential anomaly may be found even though the electrodes do not actually touch the ore body. Barus anticipated that the potential gradient would be a maximum near the ore body and would die out farther from the ore body.

Barus' first electrodes were gads, which are pointed iron or steel bars used for loosening ore. Unlike Fox, Barus took great pains to avoid leaks in the copper wire connecting the electrodes with the galvanometer. In the hot and damp atmosphere of the Comstock, he found that wire covered with a double thickness of cotton and waxed proved inadequate, as did guttapercha wire. After testing a number of devices, he suspended the wire from silk or waxed cotton threads; care was taken to prevent the wire from touching either rock or timbers. He followed this plan of "swinging" the line throughout his measurements.

In his experiments on the Comstock, the use of dry electrodes caused circuit resistances of 1,000 to 8,000 ohms, and with these electrodes he measured voltages from 10 to 90 millivolts. With wet electrodes the resistance was one-third to one-sixth as much and the voltages remained about the same. When the electrodes were interchanged, both the resistances and potentials changed by large amounts. From these facts plus the evidence that the direction of the electromotive force followed no observable law, Barus concluded that electrode potentials were of the same order of magnitude as the potential differences due to the electrical activity of the lode.

In his early work in the Eureka district, Barus sought first of all to eliminate the troublesome electrode effects. He recognized that the use of metallic electrodes was undesirable, and was thus led to the invention of an ingenious nonpolarizing electrode which he referred to as a "bag."

His nonpolarizing electrode consisted of an amalgamated metal strip immersed in zinc sulfate solution. The solution was contained in a nearly cylindrical bag 1 to 1½ inches in diameter and 6 to 10 inches in length. The sides were made with a piece of beef gut plugged at both ends with cork. Barus attached the beef gut snugly to the cork with twine. A hole in the top cork permitted insertion of the zinc terminal into the solution in the bag. A wooden stick, to which the zinc was affixed for support, also passed centrally through the top cork and a short way into the bottom cork to make the device more fieldworthy.

For field use this nonpolarizing electrode was fitted into a hole of just the right size which had been drilled into the rock at an angle of about 30° from the vertical. Before inserting the bag the hole was filled with water that had previously been placed in contact with zinc for sufficient time to precipitate all dissolved matter which might act upon the electrode.

Barus attained an accuracy of measuring ground potentials that is close to what is accomplished in modern self-potential surveys. The potential between two of his similar nonpolarizing electrodes placed in the same liquid was seldom found to be greater than five millivolts and was usually much less. For his work in the Eureka district Barus measured potentials with great accuracy, using a Grunow galvanometer. The readings of this instrument are magnified by an optical lever device.

His field technique for measuring potentials was similar to that used today. He kept one nonpolarizing electrode fixed in position and moved a second one about, measuring the potential difference between them. He took the added precaution of using a total of four electrodes in order to check his results. The station intervals between successive readings of the movable electrode averaged from 50 to 80 feet. He plotted self-potentials against position along the traverse, as is commonly done today.

Barus published data on two profiles, both taken in the Richmond mine, Eureka district. The first profile, which started on the 400-foot level and passed to the 500-foot level, was 1,332 feet long. It passed through the ore body and far into the barren country rock on either side of the ore body. His self-potential anomalies did not exceed 36 millivolts along this traverse. He noted that a negative self-potential anomaly of about 20 millivolts occurred in the area of the ore body; but as this anomaly was no larger than his noise level, he concluded that no prediction as to the occurrence of ore or electroactive material would be justified. He attributed at least part of the noise level to the passage of his movable electrode over "a great number of varieties of rock, and therefore also, probably through a great variety of absorbed liquids, holding more or less saline matter in solution."

Barus had more success in the profile along the 600-foot level in the Richmond mine. The traverse was 1,630 feet in length and passed beneath the ore body without actually entering it. All stations were in essentially the same kind of rock. A negative self-potential anomaly of about 80 millivolts over a horizontal distance of about 800 feet coincided with the region of ore. Barus found that the potential anomaly along this traverse remained unchanged, even after an interval of 4 months. He thus reasoned that the

anomaly indicated the seat of the potential and was associated with the ore body.

Because of the small anomalies he had observed, Barus was forced to conclude that his experiments "cannot be said to have settled the question as to whether lode currents will or will not be of practical assistance to the prospector." He felt that, especially in the light of the work done by Fox and Reich, it was probable–but not certain–that the currents were associated with the ore. Barus had met with indifferent success principally because of the unfortunate choice of sites for his experiments, but his contributions were a milestone in the art of electrical prospecting.

Barus also made measurements of the capacity of the rocks in place to carry an electric current. He found that fissured, impermeable, or especially dry rocks tend to have a maximum resistance; whereas porous or moist rocks have a minimum resistance. From these facts he seems to have been the first person to conclude "that the conductivity of the rock is largely, if not wholly, due to the presence of moisture in its pores, and is therefore electrolytic."

As a result of his work on self-potentials, Barus made several recommendations, some of which later became the basis for the experiments of R. C. Wells. Although Barus himself used only self-potential profiles, he thought that a single line survey was far from adequate and that "The endeavor should be made to map the equipotentials as surfaces traversing the whole mine, carefully considering their position and contour relative to any ore already in sight, and their change of form on leaving it." In this same trend of thought, he also advocated that surveys be made on the surface of the earth over a large area in the region of the mine. He felt that the field work would be enhanced by a continuation of Fox's study of the electrical properties of ore and the associated minerals of the heavy metals. He also believed that a study should be made of the effects of electric-potential changes with depth which Matteucci had emphasized.

From 1890 to 1910, advances in the field of electrochemistry were applied to the geological problems of alteration and replacement processes in ore deposits, and although the research was directed principally toward the solution of these problems, it eventually proved to be a boon to the art of electrical prospecting because of basic principals that evolved in this research.

In 1891 Braun proved that certain phenomena attending the formation of sulfides and the deposition of copper in capillary spaces are of electrochemical nature, as Becquerel had suggested (Wells, 1914). Experiments similar to those suggested by Barus were made in 1897 by Bernfield, who particularly studied the electric behavior of galena, and in 1912 by Gotts-

chalk and Buehler, who showed that the oxidation and solution of certain natural sulfides are accelerated by the presence of pyrite and marcasite. Gottschalk and Buehler ascribed this catalytic action partly to electric action. They listed many conducting minerals and tabulated the electromotive forces shown by several minerals with respect to copper, water serving as an electrolyte. They also pointed out that the electrolytic action of the sulfides "would be analogous in every respect to the action of metals" (Wells, 1914).

R. C. Wells (1914), of the U.S. Geological Survey, made systematic and comprehensive investigations on the electric activity of ore bodies in order to apply a knowledge of this subject to the problems of ore deposition. In this approach Wells was following the recommendations of Barus, whom he quoted.

Wells commenced his studies by thoroughly familiarizing himself with the works of the persons mentioned above. He extended the work of Gottschalk and Buehler by showing quantitatively the effect of varying concentrations of the ions in solution on the contact potential between a mineral and the solution. He showed that different minerals employed as electrodes exhibit different potentials in a given solution and also that the potentials shown by most minerals, certainly the initial values, depend to a marked degree on the nature of the solution in contact with the minerals. With common minerals such as pyrite, galena, and magnetite on the one hand and various naturally occurring solutions such as acidified ferric sulfate and sulfuric acid on the other, he learned that the contact potentials are of the order of 500 to 1,100 millivolts.

Wells next showed by laboratory experiments that, when using a resistance of 3,000 ohms in series with the circuit to simulate the resistance of geologic strata, the external current produced by electrodes of pyrite immersed in normal solutions of sodium sulfide and acidified ferric sulfide, respectively, amounted to about three-tenths of a milliampere with an effective electromotive force of about 1 volt. The solutions were in separate beakers connected by a wick-type bridge saturated with normal sodium sulfate solution. Using the results of these and similar experiments in which polarization effects were studied, he reasoned that ". . . sufficient evidence has been presented above to show that appreciable currents may be developed by various combinations of solutions and minerals."

In spite of the relatively large potentials and currents created by these electrochemical processes and measured by him in the laboratory, Wells was still greatly influenced in his thinking by the relatively small anomalies that Barus had found in the field. Yet he believed that Barus' results "do not exclude the possi-

bility that local electric action may be a potent agency in hastening chemical adjustments or that very small currents acting for long periods would be capable of accomplishing great results."

Wells' principal contribution to electrical prospecting lies in the fact that he was the first to recognize the major cause of self-potential anomalies near ore bodies and to specify the direction in which the current flows near an ore body. Because of the importance of this classic observation, we quote Wells (p. 64) directly:

> If a considerable mass of ore is in contact near the surface with an oxidizing solution—for example, acidified ferric sulphate—and at depth with a less oxidized solution—as ferrous sulphate (there being also any circuitous liquid connection)—electric action should result in the oxidation of the lower solution and reduction of the upper solution until equilibrium is attained. The current would pass downward in the solid conductor and upward in the electrolytic conductor—a vein solution, for example—in which the current would consist in the migration of cations upward and of anions downward.

Wells emphasized that the currents, and their effects, might manifest themselves in an extended zone round-about an ore body, and he called this phenomena "chemical action at a distance."

Early attempts to use the resistivity and allied electrical methods, other than self-potential, were qualitative only. Neither potential differences for fixed electrode spacings, nor even equipotential lines, as suggested by Barus, were observed. Several qualitative approaches to these electrical methods were tried just before and at the turn of the century and finally culminated at about the start of the First World War in more quantitative approaches to the subject. These experiments were at first carried on independently by what evolved into the American, French, Swedish, and other schools of electrical prospecting.

Even as major advances were being made, a prevalent attitude was expressed in 1914 by George Otis Smith, Director of the U.S. Geological Survey, who stated (Wells, 1914, preface):

> It should be emphasized that the results thus far obtained afford no adequate basis for any method of electric prospecting nor any promise of the development of such a method by connecting the presence of ore deposits with readily or definitely measurable electric activity.

FRENCH SCHOOL

Conrad Schlumberger (1878–1936) was perhaps the most colorful personality in the field of electrical prospecting. He and his colleagues initiated what some called the "Schlumberger school" (Migaux, 1941a) but which we designate the "French school." As a combination geologist, physicist, and miner, Conrad Schlumberger was in a unique position to develop techniques of geophysical prospecting not only when they were needed by the mining industry but also at a

time when general technical knowledge had only recently become available to furnish an adequate background for his studies. The use of electric fields was doubly attractive to him—first, because of the ease with which an artificial electrical field can be applied to the earth, and, second, because the electrical resistivity of earth materials varies more widely than any other property.

Schlumberger's first approach to electrical prospecting was to map equipotential lines about a point source of current. Schlumberger at first tried both an alternating-current inductor and a 1,000-cycle vibrator as sources of current; whence in principle he was able to map equipotential lines using a phone as a null indicator. Because of direct induction into his measuring lines, however, he changed to a direct-current source with a potentiometer and nonpolarizing potential electrodes to measure potential differences quantitatively. He was then able to make both equipotential-line maps about a single electrode and potential profiles between two current electrodes.

If the ground is homogeneous, or if the only resistivity variation lies in that found going from one horizontal bed to another below it, the equipotential lines would be concentric circles with the current electrode at their common center. If there are lateral variations in the earth resistivity, however, these variations would express themselves in distortions of the circles.

Schlumberger, in the summer of 1912, assembled the necessary equipment and field-tested it successfully at his ancestral home of Val Richer, in Normandy (Schlumberger, 1920b). From 1912 until 1914, he carried out a long series of experiments at Calvados, in Normandy, where hematite and siderite are important iron ore minerals in Silurian formations. The Silurian here consists of sandstone overlain by about 300 feet of shale, which contains the iron ore, and a series of unmineralized shale and sandstone. The beds are generally upturned and are covered unconformably by horizontal beds of Jurassic limestone as much as 270 feet thick. Schlumberger showed by these experiments that his new method was a valuable tool in roughly delineating the ore-bearing formations and he even went so far as to show qualitatively the direction of dip of the beds. In his memoirs (1920b), he gives several field examples that have often been reprinted by other authors.

Almost from the beginning of his work, Schlumberger was aware of natural-potential differences which exist in the earth (Schlumberger, 1920b, p. 34–35), undoubtedly because they interfered with his potential measurements. He attributed them to two causes, namely, those due to chemical action and those due to telluric currents which are associated with the terrestrial

electric and magnetic fields described above. His approach to correcting for these spontaneous potentials was the direct one; he measured their values and then subtracted them from his measured potentials when current was flowing. He also suggested that one might take potential measurements with the current flowing first in one direction and then in the opposite; the natural ground potential is eliminated from this pair of readings by taking a simple average.

Conrad Schlumberger also recognized early the geophysical importance of the spontaneous potentials due to the oxidation of sulfide ores. By means of this effect he made one of the earliest geophysical discoveries of a sulfide ore body. Early in 1914 (Migaux, 1941a, p. 16) at Bor in Serbia, he found a rich deposit of chalcopyrite in an area where exploration had already been abandoned.

The equipotential-line method is less sensitive to variations in lateral resistivity than one would desire and rather insensitive to horizontal discontinuities in resistivity. Therefore, it seemed reasonable that Conrad Schlumberger, even as he was writing his memoir in 1920, was turning to the concept of earth resistivity, which had been promulgated by Wenner in 1915. (See discussion of the American school.) He used the configuration of electrodes proposed by Wenner and in connection with his measurements he independently proposed the use of a double commutating device to overcome the difficulties imposed by natural earth potentials. His proposal was described in a French patent issued to him on September 15, 1925. The technique has come to be known in this country as the Gish-Rooney technique after the men who also described it independently in 1925.

The Schlumberger group eventually standardized upon an electrode configuration in which the potential electrodes are close enough together that the electric field midway between the current electrodes is the quantity which is effectively measured. We choose to call this arrangement the Schlumberger configuration.

In 1920 Conrad Schlumberger first successfully measured earth resistivity in the iron-bearing basin of May-Saint-Andié. During 1923 he successfully delineated, by the resistivity method, the Arisesti dome in Rumania (Rothé and Rothé, 1952, p. 410; Migaux, 1941a, p. 16). This delineation work constituted the first practical application of any geophysical method to the field of petroleum exploration. In 1926 and 1927 he discovered, with the resistivity method, several salt domes in the upper Rhine Valley in Alsace (Carrette and Kelly, 1928). During this phase of development, Schlumberger was joined in his efforts by his brother Marcel, as well as by many others, including his son-in-law, H. G. Doll, and E. G. Leonardon, S. S. Stefanesco,

Raymond Maillet, V. A. Kostitzin, and E. Poldini. He left teaching in 1923 and, in 1926, inaugurated La Societé de Prospection Electrique, which eventually led to such world-wide organizations as the Compagnie Générale de Géophysique and the Schlumberger Well Surveying Corporation. The Compagnie Générale de Géophysique has continued to this day carrying on successful surface electrical-prospecting projects in almost every part of the world. Projects include civil engineering, mining geophysics, and petroleum exploration. Reports on most of these projects still are kept in the confidential files of the mining and oil companies for whom the work was done. Many of the later contributions of the French school were theoretical in nature and are thus recounted in later sections.

In 1927 the Schlumberger group conceived the idea of electric logging (Migaux, 1941a, p. 17) which initially used, with only slight modification, the principles that apply in surface prospecting. The in-hole technique was tried initially in 1928 in an oil field in Alsace. Successes followed in 1929 in fields in Venezuela, the United States, and Russia; and the use of electric logging was thoroughly entrenched.

In about 1934, the Schlumberger group initiated work on the telluric current method of prospecting (Schlumberger, 1939, p. 272-3). This method evolved from the principle that, in using such configurations as the Wenner, the deeper the investigation the larger must be the electrode separation; in the limit, the current electrodes must be placed infinitely far apart to create a uniform electric current field. The sheets of telluric currents which flow in the earth, however, already furnish a field which has approximately the characteristics desired. Since the method uses a natural field, only potential measuring devices need be used. A fundamental difference between this and conventional methods stems from the extreme difficulty in measuring accurately the true potential differences between two points on the ground. In order to circumvent these difficulties due to spurious electrode effects, one measures the very low frequency variations in the potential differences. The data at a given station are useless alone and must always be compared to a record made at the same time at a base station. The telluric method has been developed to a fine degree and now furnishes a valuable tool in widespread reconnaissance surveys (Migaux, 1951). It is used particularly in Europe and North Africa, where there are many crews now (1955) at work.

Louis Cagniard is the latest member of the French school to make a significant contribution to electrical prospecting. In order to establish a technique which would have the advantages of the telluric method but which would eliminate the disadvantage of requiring

a base station, he has devised his magneto-telluric method (Cagniard, 1953). Instead of measuring only the variations in the telluric field, he also proposed to measure the corresponding variations in the horizontal component of the geomagnetic field. Then, using well-established principles of electrodynamics, he claims to be able to predict the nature of the substrata without referring his data to data taken at a base station. At present (1955), he is preparing his apparatus. Lacking knowledge of a thorough field test of his method, we are not in a position to judge the field-worthiness of the magneto-telluric method. Some applicable observatory data do, however, point to the strong possibility of this method's having equal success with the other ideas of the French school.

AMERICAN SCHOOL

We have traced the development of fundamental experimental studies in the United States through the work of R. C. Wells. We will now consider the more practical aspects of electrical prospecting as they developed during the early part of the 20th century in the United States and Canada. This phase actually started somewhat before the 20th century when, in America in 1883, Fred Brown devised and patented a resistance method of prospecting that was shortly afterward improved by McClatchey (Barton, 1927).

About 1902, Leo Daft and Alfred Williams, in their English and American patents, suggested the use of potential-difference observations for resistivity work (Heiland, 1932b). They devised a method in which a low-frequency alternating current was sent into the ground by means of electrodes, and the resulting current distribution was studied by means of a sensitive telephone receiver connected to two search electrodes placed on the ground (Barton, 1927). They were troubled by serious difficulties due to induction between the transmitter and receiver (Migaux, 1941a); and, owing to the inherent weakness in this type of measurement, the reliability of the observations depended largely on the personal impression and skill of the observer. They noted, however, that ore bodies changed the intensity of the electric field.

The father of modern quantitative resistivity methods in the United States was Frank Wenner, a physicist at the U.S. Bureau of Standards. In his work for the Bureau, Wenner (1912) was a specialist in the design of standards of resistance and in the accurate measurement of resistances. His analysis of the theory of the four-terminal resistance-measuring device and its applications resulted in two important contributions to electrical prospecting. The first contribution, which was made in 1912 and which has received inadequate emphasis in the geophysical literature, consisted of

giving a clear statement of the theorem of reciprocity as applied to his four-electrode measurement. We will discuss this principle, together with its applications and limitations, in a later section (p. 38). Wenner's second major contribution, for which he is known primarily, was his invention in 1915 of what is designated today as the Wenner configuration of electrodes (Wenner, 1915). As a natural outgrowth of his measurements of the resistivity of metals, he placed four electrodes on the ground, spaced at equal intervals along a straight line. Current was made to flow through the ground between the two outer electrodes while the potential difference was measured between the two inner electrodes. Wenner recognized the difficulties that arise from polarization effects when direct current is used with metal electrodes, and for this reason he used alternating current (not commuted, which was introduced later). Wenner applied from 50 to 150 volts across his current electrodes, which were 3 or 4 centimeters in diameter and initially placed 30 to 50 centimeters apart at a depth of 125 centimeters. The current was read by means of an ammeter. Across this current line was connected a 10:1 or 20:1 stepdown transformer with the low voltage side of the transformer connected to the ends of a slide-wire potentiometer. A vibration galvanometer, a phase shifter, and a voltmeter were employed in the low-voltage circuit to measure the potential difference between the two inner electrodes. Wenner did not state what frequency he used, but it was apparently less than 300 cycles per second. The apparent resistivity, which he called "effective resistivity," was calculated from the measured ohmic resistance and the geometry of the electrode configuration.

Wenner called attention to the fact that the measured apparent resistivity

. . . depends mainly upon the resistivity near and between the inner or potential electrodes, and very little upon the resistivity at distances from them equal to or more than the distance between the outer or current electrodes, providing the four electrodes are approximately uniformly spaced.

Although Wenner himself in 1915 used his method only for determining resistivities in an area a few meters or less in radius, he pointed out that it is possible to measure resistivities to a much greater depth by placing the electrodes a much greater distance apart and that such measurements could be made with the electrodes "practically on the surface." He stated that, by estimating the effect of the surface layer from results obtained with the electrodes close together, one could gain some idea as to the resistivity at different depths. He also suggested that "such a measurement might be of assistance in locating deposits of ore of high conductivity."

Some of Wenner's contemporaries at the Bureau of Standards also contributed to the knowledge of electrical prospecting by discovering certain fundamental principles involved in the flow of current through the earth. One such person was Burton McCollum, an electrical engineer. Although McCollum's immediate objective was to study electrolysis as it concerned current leakage along railway tracks, and corrosion of pipes and other metallic structures, his studies led to the measurement of the resistance of soils and of polarization.

McCollum and Logan (1913) recognized two general types of electrolytic corrosion—that due to "self-corrosion" currents between the pipe and the earth and that due to the fact that the pipe forms part of the circuit for stray currents flowing in the earth. They studied quantitatively how the rate of corrosion depends on current density, moisture in the soil, temperature, depth of burial of the metal, the presence of oxygen and chemicals in the ground water, and the kind of iron involved. They also initiated polarization studies in soils and measured the polarization effects of metals. For example, they noted that as soon as 6 volts is applied between two short lengths of pipe buried about 12 feet apart "the current drops off rapidly with time, especially during the first few minutes, due to the setting up of counter emf's and the formation of film resistances." Their extensive polarization studies continued through most of their work but was limited to electrode effects which are relatively unimportant in ordinary resistivity prospecting. They demonstrated that the polarization voltage or back emf is a function of the electrolyte, the character of the electrode, the current density at the electrode, and the time the current has been flowing (McCollum and Logan, 1915).

McCollum and Logan (1913) initially made measurements of the resistivity of the soil in place by means of the voltmeter-ammeter method. In order to overcome polarization and other electrochemical effects, they used alternating currents. The technique was to expose a block of earth by making two excavations close together and several feet deep. A "guard ring" arrangement of electrodes was used so that current was caused to flow through the block of earth essentially in parallel lines. The resistance of the block of earth was then measured by noting the potential drop across the block and the current flowing through it. Later, McCollum and Logan (1915) used the technique devised by Wenner to measure the soil resistivity.

In the laboratory, McCollum and Logan (1915) determined the resistivity of soil samples by compressing the sample into the shape of a cylinder and by applying the voltmeter-ammeter measurements to the flow of alternating current through the sample. Using this method, they tested samples of soil from many widely separated places in the United States; in each sample, they took great care to preserve the original moisture content of the soil. In connection with these tests they showed quantitatively the effect of moisture content and the effect of temperature on the resistivity Since they found that the resistivity increases tremendously when the soil temperature is below the freezing point of water, they cautioned that resistivity measurements of the soil should not be made when the atmospheric temperature is too low.

McCollum and Ahlborn (1916) developed and used nonpolarizing electrodes to measure potential differences on the earth's surface in connection with their studies of leakage currents along electric-railway tracks. This electrode was similar in principle to the one which Matteucci (1865) had devised some 50 years earlier. The nonpolarizing electrode of McCollum and Ahlborn consisted of a copper electrode immersed in a saturated copper sulfate solution contained in a porous cement cup An excess of copper sulfate crystals was provided to insure that the solution would always be saturated. The cup was 5 centimeters in outer diameter and 21 centimeters high; it was covered at the top by a hardwood lid held on by friction tape. Another type of nonpolarizing electrode consisted of an iron tube containing a solution of ferric chloride, the lower end of the tube being closed with a porous plug. The outside of the tube was insulated so that electrical contact with the earth was made only through the porous plug, usually a moist sponge. They remarked that the resistance between their electrode and moist soil rarely exceeded 250 ohms which was unimportant with the use of a high-sensitivity voltmeter. In the field, the nonpolarizing electrodes were placed in holes that had been partly filled with water.

In 1916 McCollum and Ahlborn reported that they could locate concealed metal conductors such as buried pipes and rails. Their system apparently worked best when used to locate buried cross bonds in the tracks and buried metallic connections between pipes. A high-frequency buzzer was connected in series with a battery between the two pipe systems at a convenient point. The resulting electromagnetic induction signal caused by this intermittent current in the pipe system was detected by an exploring coil and a telephone receiver that was carried along the surface of the earth.

McCollum (1921) designed a device for measuring the soil resistivity and current density in the earth surrounding pipes or other objects of interest. His electrode arrangement was an inverted Wenner system, with the inner pair of electrodes for current electrodes and the outer pair as potential electrodes; the fixed electrode spacing of the probe was about 3 inches.

The potential electrodes were of the nonpolarizing type so that self-potentials could be measured. A hand-driven commutator provided alternating current between the two inner electrodes, and a simultaneously commutated voltage was read between the two potential electrodes. The unique feature of McCollum's device was its capacity for indicating in a single operation both the voltage due to the impressed current and the natural ground potential. The current density then is the natural potential gradient divided by the earth resistivity, both of which can be computed from the measured quantities. Measurements could be made on the wall of a pit, in a hole, or at the surface of the earth. Later, McCollum and Logan (1927a, b) produced a more refined model of the instrument. This instrument actually embodied the principles of the modern electrical well-logging instruments.

Concurrently with the early electrical studies at the Bureau of Standards, H. R. Conklin (1917), after 3 years of laboratory and field tests, reported using a high-frequency electromagnetic method in an attempt to find conducting sulfides (galena and pyrite) in the Tri-State zinc and lead district. His work constituted the first serious experiments with the electromagnetic method (Lundberg, 1929). His primary transmitting coil, in the shape of a circle 200 feet in diameter, was laid on the ground; and the electromagnetic field produced within the loop was measured by two small identical exploring coils that were balanced against each other in series opposition and were connected through a detector to a galvanometer. With one coil held stationary, the other was moved along a curve in such a way that the galvanometer reading remained zero. Over homogeneous subsoil each traced curve or contour, called by Conklin an "isogonic line," was a circle. Inhomogeneities in the earth produced deviations from this normal shape. He believed that his device with a primary coil 200 feet in diameter would give a recognizable response for a conductor lying within 130 feet of the surface. He did not say how large the conductor should be. His field experiments in the Tri-State district lasted over a year but resulted mostly in the discovery of pyrite as the conducting body causing the disturbance. The principles of his method were sound, but, just as is true of Barus, it is unfortunate that he tried the new technique in a district now believed unsuited to electromagnetic techniques. In 1922, Sundberg introduced Conklin's method into Sweden (Rust, 1938).

S. F. Kelly brought to North America the self-potential method as it had been developed and perfected by the Schlumberger school. Using non-polarizing electrodes and a potentiometer that was sensitive to one millivolt, he measured the self-potential along straight-line profiles and also mapped equipotential lines about a fixed current electrode.

At Ducktown, Tenn., where the ore bodies consist principally of pyrrhotite, pyrite, and chalcopyrite and are within 100 feet of the surface, Kelly (1922) found that the equipotential curve outlined the strike and shape of the ore body rather well, but the negative center was not pronounced. At Wilkes-Barre, Pa., where anthracite coal veins 3 to 12 feet thick are exposed, self-potential anomalies were detected over the coal veins. Schlumberger had previously discovered this same phenomenon. Near Sudbury, Ontario, where nickel-bearing pyrrhotite occurs beneath an overburden of nearly 200 feet, Kelly found self-potential anomalies over the ore or mineralized zones. In the Porcupine camp, Ontario, he found a self-potential anomaly along a profile over veins containing auriferous pyrite. At Cobalt, Ontario, where the mineralization consists of native silver in veins of smaltite, small but recognizable self-potential anomalies were obtained when 5- to 10-foot station intervals were taken. Other experiments included work on copper-bearing sulfide deposits at Flin Flon Lake and Lake Athapapuskow, Manitoba.

The first discovery of a new deposit in North America through the use of the self-potential method was made by Kelly (1924). The anomaly was found in the Lake Athapapuskow region of Manitoba. It was more than 400 millivolts in maximum amplitude and extended several hundred feet along one of his profiles. Unfortunately, the deposit was not commercially valuable, but trenching did reveal "a narrow set of interlacing pyrite and chalcopyrite stringers."

In the Keweenaw Peninsula, where native copper occurs as veins in basalt and quartz porphyry conglomerate, no distinctive self-potentials attributable to the copper were obtained. As a result, Kelly (1922) experimented with Schlumberger's original method of mapping equipotential lines about a fixed current electrode. The area chosen was one in which an 18-foot-thick vein of copper with a dip of about 51° lay between basaltic walls and was covered by overburden less than 5 feet thick. Current was introduced into the ground through a fixed current electrode that consisted of "about ten copper bars, ½ in. square and 1½ ft. long, driven into the ground in a circle of about 10 ft. radius," all connected together with bare copper wire. The second electrode was placed 1,500 feet from the fixed electrode in a direction perpendicular to the strike of the vein; Kelly considered this electrode to be, in effect, at infinity. When the fixed current electrode was placed over the probable apex of the vein, the equipotential lines were elongated in the direction of the strike, because the vein was of lower resistivity than the surrounding country rock. When the fixed

current electrode was placed on either side of the vein, the equipotential lines were flattened near the vein on the side of the current electrode and were bulged out on the far side. From the degree of flattening and bulging, Kelly could predict whether the current electrode was on the foot-wall or hanging-wall side of the vein. Kelly concluded that the equipotential-line method could be used to explore for tilted strata that are hidden by a shallow overburden and to detect faults that contain water of greater conductivity than the country rock.

Some of the greatest contributions to electrical prospecting, especially those in early field measurements, were made during the 1920's by Gish and Rooney, who were studying telluric currents for the Department of Terrestrial Magnetism at the Carnegie Institution of Washington.

Gish (1923) gave the general requirements for measuring telluric currents. To define them completely, it was necessary to measure both the natural potentials from which the surface-potential gradients may be determined and also the resistivity of the earth in the same region. In connection with the natural potential V in his equations, he stated (p. 91) that

It is entirely probable that V is not in all cases an analytical function of the space coordinates. For example, polarization, or electrochemical effects, may exist across planes where two different geological formations meet, thus giving rise to discontinuities. Consequently, unless the structure in the region where earth currents are to be studied is very homogeneous it would seem advisable to make a survey of the earth potentials and thus determine the magnitude of such discontinuities as occur.

To study the earth currents, Gish had installed at Carnegie Institution's observatory at Watheroo, Australia, lines and equipment for the continuous recording of natural potentials. Lines were laid, both east and west and north and south. The work of Mauchly (1918) had indicated that carefully buried electrodes of lead were more suitable for long-range telluric-current studies than were nonpolarizing electrodes. For this reason, Gish used buried lead electrodes.

During late 1923, Gish (1924b) made preliminary resistivity measurements of the earth by modifying the McCollum "earth-current meter" and using the Wenner configuration. In all, four vertical resistivity profiles were taken, in which the electrode separation was varied regularly from 3 to 60 feet. Gish recognized that both lateral and depth variations manifested themselves in these vertical profiles. During the fall of 1924 Rooney and Gish (1925a, b) measured the resistivity of still larger volumes of earth and correlated changes in resistivity with changes in the strata. The areas surveyed were all in the vicinity of Washington, D.C. During 1924 and 1925 they occupied several hundred stations in taking both vertical and horizontal profiles (Gish and Rooney, 1925). Their test measurements of earth resistivity were made in four areas: (1) in a small tract in the northwestern part of the District of Columbia, where they studied the effects of a ravine 30 feet deep that was artificially filled with loose material of higher resistivity than the country rock; (2) in a fairly level site near College Park, Md., where they determined a thickness of 100 to 300 feet for the unconsolidated Pleistocene deposits overlying granite, and where they found a high resistivity zone over a surface-gravel deposit; (3) at Bradley Hills, Md., where a resistivity minimum at an electrode separation of 70 feet in their resistivity vertical profile was interpreted as the depth to the granite-gneiss bedrock; and (4) at the surface of the water in the Tidal Basin in Washington, where they mounted the Wenner configuration on a float and obtained a resistivity value for the water that compared quite favorably with corresponding laboratory measurements. Later work included resistivity studies near the Carnegie Institution's Watheroo Observatory where a surface layer of dry sand of high resistivity gave them considerable trouble in getting sufficient current into the ground, and led them to conclude that "practically all the resistance of the measuring circuits can be considered as concentrated at or near the contact surfaces of the electrodes and the ground" (Rooney and Gish, 1927). A similar condition at their potential electrodes reduced the sensitivity of the potential galvanometer.

During the summer of 1927, Rooney and several members of faculty of the Michigan College of Mines and Technology jointly conducted a series of earth-resistivity measurements (Rooney, 1927; Hotchkiss, Rooney, and Fisher, 1928). Their purpose was to use the copper country of northern Michigan, where the geological structure is well known, to determine the value of resistivity measurements to help indicate geological structure at depth. Their results were not consistent. Failure to obtain expected changes in slope on the apparent resistivity curves corresponding to several known geological discontinuities were attributed to local conditions, such as topographic relief.

Two major contributions evolved from the work of Gish and Rooney. The first involved instrumentation and the second an empirical method of interpretation. Gish (1924b) started with the McCollum "earth current meter" and modified its design, as time went on, into what is now known as the "Gish-Rooney double commutator." The original purpose of the double commutator was to apply current to the ground alternately in opposite directions to overcome polarization and self-potential effects and at the same time to measure the commutated potential between the potential electrodes

as though it were a constant potential in one direction. The final form of the double commutator was designed by Gish (1926). The separate commutators for the current and potential circuits were so adjusted that the current circuit was always closed before and opened after the potential circuit. In this way, the potential circuit is ideally never connected while there are transients in the current circuit. The current circuit of the equipment at Watheroo was designed in this manner, so that it worked satisfactorily when passing two amperes at 1,000 volts. Gish was able to improve the operation of the equipment by placing a 20-microfarad condenser "in one of the lines which connects with an intermediate electrode." The commutator was turned by hand about 30 times per second; hence, the current instruments, because of the inertia of their parts, registered on the instruments as a steady current.

In all their work Gish and Rooney (1925) were striving for some sort of empirical rule upon which they could depend. As a result of their early work, they reasoned (p. 162) that

The value of the resistivity thus found must, however, in general be considered an average in which the resistivity of the earth near the line of terminals is the more heavily weighted, while the weighting diminishes with distance from this line until at a depth, or lateral distance, equal to the distance between adjacent terminals the weights have become so small that all the earth beyond this range contributes comparatively little to the total result. Thus, the body of earth involved in a single determination has linear dimensions of the same order as the interval between terminals. By increasing this interval, greater depths of earth may be included so that from a series of such measurements a fairly satisfactory knowledge of the variation of resistivity with depth can be obtained provided the series are repeated at positions suitably distributed over the region.

As will be illustrated in a later section, this rule that the "depth of penetration" equals the electrode separation has been the subject of severe criticism from most of the theoretical workers in resistivity interpretation; in spite of the opposition, the rule is still used literally in the field.

In his work in Michigan, Rooney (1927) tried to apply a related empirical rule that a major discontinuity in slope of the apparent resistivity curve occurs at an electrode separation approximately equal to the depth of the horizontal geological feature causing the discontinuity in slope. He was unsuccessful in that particular area, but the enunciation of this rule precipitated a continuous argument between proponents of the "curve matching" method of interpretation and proponents of the empirical method. Both groups have reported some outstanding success and both have had failures. The theoretical aspects of this question will be included in a later section.

Gish and Rooney (1925) also suggested the possibility of a quantitative approach to the problem of resistivity interpretation. For example, when speaking of the two-layer case, they reasoned that

if the resistivity changes abruptly at a certain depth, if the boundary between the two types of earth is approximately plane, and if each part is homogeneous, then from a series of measurements with different electrode separations, a set of observational equations may be set up in which the two unknown resistivities are given weights which are a determinable function of the electrode separation. The solution of the normal equations will then yield the absolute resistivities of the two parts.

In 1927, Scott Turner, then director of the U.S. Bureau of Mines, recognized the possible value of a study of modern prospecting methods and initiated a program of investigation that has had a profound influence on the art of electrical prospecting. Turner began the investigation by employing A. S. Eve and D. A. Keys, both professors of physics at McGill Univeristy, and C. A. Heiland, professor of geophysics at the Colorado School of Mines. F. W. Lee also began his work with the Bureau of Mines the same year. Eve and Keys (1927) published a brief but excellent summary of geophysical methods being used at that time. Emphasis was placed on the possible use of the basic principles of these methods for finding ore deposits. Eve and Keys (1928) published the results of electrical tests that they had made during 1927 at various test sites selected by C. A. Heiland near Caribou, in Boulder County, Colo. The tests were made over small deposits of titaniferous magnetite in porphyritic monzonite. The excellent electrical conductivity of the deposits rendered them particularly adaptable to electrical-prospecting methods, and their strong magnetic properties enabled Heiland and Malkovsky to make an accurate magnetic survey with which the electrical data could be compared with confidence.

In this work, Eve and Keys tested various methods. They used the Lundberg method of mapping equipotential lines between parallel line electrodes excited by direct current. They observed a spreading of the equipotential lines over the known conductor. They also determined the equipotentials in a field between parallel wires excited by a 1300-cycle-per-second alternating current. For this audible frequency, a telephone receiver with a probe of bare copper wire, instead of porous pots, was used for charting the equipotentials. They also tried various electromagnetic methods, including radio frequency techniques, and self-potential methods. For the self-potential method, they found that the use of a potentiometer was superior to a direct-reading microammeter.

In these tests Eve and Keys (1929) devised a "leapfrog" method. Three parallel copper wires X, Y, and Z, each 100 feet long, were well pegged to the earth 100

feet apart and every peg was well watered. A known voltage was impressed across the outer wires X and Z and, while the direct current was flowing, the potential differences between the central wire Y and the outside wires was taken with a portable voltmeter. Asymmetry in the potential-drop readings would indicate which of the two sections between the wires was the better conducting ground. Then the three pegs of X were pulled up and the wire was leap-frogged over Y and Z to a new position A, located 100 feet from wire Z. Measurements were then repeated with the current flowing between Y and A. This procedure was repeated several times. By finding the ratios of the voltage drops, the relative conductivity of each 100-foot-wide zone could be obtained and this was designated a "figure of merit" for that area. This method, which Eve and Keys designated the "triple leapfrog" method, was used to outline successfully the general area of the magnetite body in the test area in Colorado. In dry areas this method worked well; but in marshy areas or in areas of abrupt change from dry to wet conditions, the stake resistances varied so much that the method failed. Thus, in northern Quebec where the method was also tried, the great variations in stake resistances and the difficulty of making good contact on rock as compared with swamp rendered the indications valueless. For this reason, Eve and Keys (1929, p. 80) predicted that the Gish-Rooney method "is likely to have wider applicability than the leapfrog method." It should be noted, however, that the principle which Eve and Keys tried to evoke is the same one which the Lee configuration, to be described later, employs successfully. They also used a "single leapfrog" method, which involves only stake electrodes instead of line electrodes, but they found the same objections to both systems.

Eve, Keys, and Lee (1929) devoted the summer of 1928 to obtaining information on the depth attainable by electrical-prospecting methods. The tests were made at Barton Hill and Fisher Hill, N.Y., over magnetite bodies so that the electrical measurements could be checked by magnetic methods; the two experimental areas had also been tested by diamond-drilling.

For this work Lee (1928) suggested and used the "Megger" to measure earth resistivity with the Wenner configuration. A Megger is a type of ohmmeter which has long been used as a standard electrical engineering tool for testing "grounds" and insulation resistances. It is based on the principle of simultaneous commutation, but differs from the Gish-Rooney arrangement in that a direct-reading ohmmeter, of the cross-coil type giving the ratio of voltage to current, is substituted for the ammeter and potentiometer; moreover, the current in the Megger is generated by a hand-driven magneto-

generator. The repetition rate of this instrument is about 50 times per second. The original Megger had only four terminals corresponding to the four electrodes of the Wenner configuration, but later models could accommodate three potential electrodes in addition to the two current electrodes, thus making it possible to use the Megger with the Lee configuration.

During this work in 1928 a careful comparison of vertical-profile measurements with the Wenner configuration were made by Lee using the Megger, by Rooney using the Gish-Rooney equipment, and by Eve and Keys using the direct-current method in which the current is reversed manually and the final potential difference used is the average of the direct and reverse readings. The electrode positions in all these methods were effectively the same. At Fisher Hill all three methods gave the same qualitative results; however, the Megger gave systematically lower apparent-resistivity readings than the Gish-Rooney equipment, which in turn gave consistently lower readings than the direct-current method. Lee (1928) claimed that the Megger registered low because it requires that some of the current flows through its measuring coils, which are in parallel with the earth circuit; this source of error could be minimized by keeping the stake resistances as low as possible. It is also possible that some of the lower readings for both the Megger and Gish-Rooney apparatus could have been due to transient phenomena which were not entirely compensated.

At Barton Hill, where a dipping sheet of conducting magnetite was known from drilling to lie at a depth of about 700 feet, a less exact comparison was made between measurements taken with the Megger and the Gish-Rooney equipment. Identical electrodes were not used at Barton Hill, and only one profile was exactly duplicated in location by the two methods. Reasonable agreement was reported between the true well-data depths and the depths indicated by abrupt changes in apparent-resistivity curves at 500 to 700 feet; somewhat better accord with the drill data was obtained with the Gish-Rooney equipment. Lee (1928) concluded that the Megger, as it was then built for general electrical engineering, was not entirely suited for geophysical exploration, and he listed the various improvements that he deemed desirable if the instrument was to be used for exploration.

Weaver (1928) proposed an electrode configuration in which the two potential electrodes are placed symmetrically along a line perpendicular to the line joining the current electrodes and midway between these electrodes. In the spring of 1925 Weaver had made model studies with this method over an almost perfectly conducting mass, 4 by 3 feet in horizontal dimension, 8 inches thick, and buried 4 feet. Each of the four

electrodes was located at the corner of a square of which the diagonal was 8 feet, and the whole configuration of four electrodes was moved from point to point along the line joining the power electrodes over the conducting body. The potential differences which he measured were indicative of the asymmetry in the current field as the configuration was moved over the conducting body.

At Fisher Hill, Eve, Keys, and Lee (1929) gave Weaver's method a thorough trial with the Megger. Using the same square configuration of electrodes, with a diagonal of the square equal to 200 feet, they took readings at stations spaced 100 feet apart on several traverses. Their anomalies were difficult to interpret and they concluded that "with a full knowledge of the ore distribution it is possible to discern its influence, but as a method of determining the unknown this scheme seems to involve unnecessary perplexity as compared with more direct methods." Lee, Scharon, and Sandberg (1946) successfully used a combination of the Weaver and Lee configurations to map dipping contacts in the Newton Flats area of California. The new system consisted simply in adding two potential electrodes to the regular Lee configuration; the new electrodes were placed on a line through the midpoint of the configuration and perpendicular to the original line of electrodes.

Crosby and Leonardon (1928) applied electrical methods successfully to map bedrock topography at a proposed dam site on the upper Connecticut River in what was apparently the first engineering application of these methods in the United States. The bedrock consisted of a high-resistivity Precambrian schist overlain by about 150 feet or less of glacial drift; the resistivity contrast was about 10:1. The Schlumberger method of taking a vertical profile about a single electrode was used. Of the results of the measurements at eight holes where tests were made prior to the full-scale survey, five gave accurate depths within 5 percent and the others were within 20 percent.

Pullen (1929) made laboratory resistivity measurements, by both alternating- and direct-current techniques, on many cores mostly of metamorphic rocks from the Mineville district of New York and on hand specimens of serpentine and chromite. He found that (1) resistivity measurements varied with time because of electrical polarization, (2) the rate of polarization differs in various rocks, (3) resistivity varies as a function of applied voltage and frequency, (4) water content greatly alters the resistivity of materials, and (5) the resistivity of an ore containing conducting minerals may be high if the ore minerals are disseminated.

Lee, Joyce, and Boyer (1929) pointed out the advantage of measuring resistivity by the Gish-Rooney method over mapping equipotentials at the surface of the ground when an artificial current is impressed through the ground, and they suggested various other configurations for measuring earth resistivity. As designated by us, these new configurations were the asymmetrical Wenner configuration in which the second current electrode in an otherwise conventional Wenner configuration is placed effectively at infinity, the Lee configuration in which a third potential electrode is placed midway between the two potential electrodes of the Wenner configuration, and azimuth measurements in which the asymmetrical Wenner configuration is rotated about the single current electrode. Actually azimuth measurements should be added as an additional technique in the class with vertical and horizontal profiling.

They made a comparison in the field between vertical resistivity profiles with the Wenner configuration, the Lee configuration, and the asymmetrical Wenner configuration. Electrode separations were taken up to 600 feet. Various methods of plotting were used to ascertain which method best correlated with the 200-foot depth to a highly resistive traprock known from drilling data to lie in the test area. Apparently lateral variations in resistivity prevented a definite conclusion to be made by the authors, although each configuration gave indication of approximate correct depth of the traprock by a break in the apparent-resistivity curve.

Their field tests confirmed Pullen's laboratory work which showed that the resistivity measured is affected by the magnitude of the current flowing. In taking a vertical resistivity profile up to an electrode separation of 700 feet, they changed the current flowing through the ground by 50 percent for each set of electrode positions; the apparent resistivity decreased in some cases and increased in others, with no general rule governing the change.

Lee (1930) gave results obtained with the Lee partitioning method and the asymmetrical Wenner configuration over two ore deposits near Sudbury, Ontario. Both properties had been thoroughly tested by diamond-drilling and mine exploration, thus making good test areas. In one of the deposits the low-resistivity ore which comprised pyrrhotite, pentlandite, and chalcopyrite in various proportions, was covered by about 100 feet of glacial till. Measurements with the asymmetrical Wenner configuration gave accurate indication of depth to the water table and indicated an area of low resistivity at a station 100 feet south of the ore body, but it did not differentiate between conditions in directions roundabout the station as clearly as did measurements with the Lee configuration about the same station. Results over a second ore body were apparently inconclusive with both configurations.

J. H. Swartz (1931) performed a group of experiments on the resistivity of artificial beds. For this purpose, he dug in the ground a large hole 15 feet long, 12 feet wide, and 3 feet deep. He filled the hole with alternating layers of clay and sand, making a total of seven layers. Lateral changes in topography and lithologic character were also modelled. Vertical resistivity profiles were taken with both the Lee and Wenner configurations. Direct-current methods, using small nonpolarizing electrodes, were employed; and Lee's instruments and field equipment were used. The Lee configuration seemed to give better correlation with the known geologic conditions within the model than did the Wenner configuration. For the Lee configuration, the depth at which a given true resistivity change occurred in the model corresponded in the eyes of the author with striking accuracy to the value of the electrode separation at which breaks occurred in the vertical resistivity profiles. Swartz said that if topographic effects are present, the depth reached must always be measured beneath the current stake on the side of the Lee partitioning plane under consideration, and not beneath the station at the center of the configuration. Swartz explained this as due to the fact that the equipotential shell on which the measurement is made surrounds the current stake and not the station. Swartz also used a single-electrode probe method by using direct-current techniques and measuring the potential drop with porous potential electrodes. When using the asymmetrical Wenner configuration with a fixed current electrode, the results were less clearcut than with the Lee configuration and were difficult to interpret. When using a constant spacing between the potential electrodes and moving them along the surface away from the single fixed current electrode, in a technique which he attributed to Schlumberger, Swartz found rapid variations in the apparent-resistivity curve but no apparent resemblance between this curve and that for the asymmetrical Wenner configuration. Moreover, he could find no rational means of interpreting the curve.

Lee and Swartz (1930) conducted experiments over oil-bearing beds in Allen County, Ky., where the oil formations occur at very shallow depth in porous lenses of limestone. Both the direct-current technique and the Gish-Rooney commutator technique were used. The work was continued and extended by Swartz (1932) in nearby areas where the strata are essentially horizontal, simplifying interpretation. Using the Lee configuration, Swartz interpreted the resistivity highs on the vertical resistivity profiles as indicative of oil- or gas-bearing formations directly; indications were obtained to a depth of 800 feet that correlated well with drilling results.

Swartz established the facts that the vertical resistivity profiles at certain places in his area were jagged rather than smooth and that these jagged breaks always occurred within the same range of electrode separation, indicating that they were apparently characteristic of stratigraphic horizons. Swartz recognized the necessity of disentangling depth effects from those produced by the horizontal movment of the current stakes during vertical-profile measurements; and he discussed methods of procedure for recognizing such lateral effects, if present.

He confirmed to his own satisfaction his earlier model results that the depth of the geologic discontinuity for horizontal beds is given by the value of the electrode separation at which a break occurs in the vertical resistivity profile. He clearly recognized that theoretically the observed vertical profiles should show no sharp changes and that boundaries should not be detected by breaks in his curves. However, he had observed the breaks, about which he commented: "How much significance they possess and how far interpretations of this nature can be useful are at this time still open to questions" (Swartz, 1932).

In the years following the early 1930's most of the work done by the American school, as well as the other schools considered herein, consisted of making improvements of instrumentation, refining already established field techniques, and theoretical interpretation.

OTHER WORKERS

In addition to the investigators in France and in North America, the Scandinavians also have made significant contributions to electrical prospecting through their basic interest in mining problems. From the beginning their interest in electrical prospecting has tended more toward the electromagnetic and the equipotential-line resistivity method.

In 1904 Trustedt in Finland suggested using an electromagnetic method for prospecting (Lundberg, 1929).

In 1906, in Sweden, the Daft-Williams method was tried in thorough experiments by Petersson and Wallin that served as a starting point for a long series of Swedish experiments on electrical prospecting (Barton, 1927). As described by Petersson (1907), who as early as 1907 had formed the "Electrical Ore Finding Company, London," the method was of the very low frequency type. He impressed directly into the ground through two electrodes an alternating current of 10 to 40 milliamperes using a voltage of 5,000 to 60,000 volts. A mercury circuit breaker acted as a buzzer that interrupted the current 300 times per minute. The intensity of the sound in a telephone receiver, which obtained its signal from

two electrodes driven into the ground, gave an indication of the ground conductivity (Heiland, 1932b). Although the method was qualitative, it was used successfully in Sweden in 1906 in tests on an ore body over which a vertical magnetic anomaly had also been found (Petersson, 1907).

In 1907, an official systematic test of the Daft-Williams method was made in Sweden by the Swedish Institute of Iron and Steel (Lundberg, 1929). The chief object of these early experiments was to test the feasibility of using the method to locate nonmagnetic specularite ore. The results of the tests indicated clearly the possibilities of the method, but the tests were not followed up. Further experiments with the Daft-Williams method were made in Sweden by the Geological Survey of Sweden—in 1912 by Tegengren and Bodman and in 1913 by Bergstrom (Lundberg, 1929). Bergstrom modified the method to include the mapping of equipotential lines, using the null or minimum signal in his phone as an indicator. The similarity is apparent between this method and the technique introduced by Conrad Schlumberger for mapping equipotential lines about a point electrode through which direct current was flowing. Detailed studies and tests were made with this new method. The apparatus filled all the requirements of field efficiency, but the field survey maps were difficult to interpret.

In 1907 a Norwegian named Muenster made the first discovery of a previously unknown ore deposit of commercial value with electrical-prospecting methods. The discovery was made in Nautanen, Lapland (northern Sweden), through the use of the self-potential method as it had been described by Barus (Lundberg, 1929). His self-potential measurements were taken along each of several profiles, as profiling techniques had already been systematized in Swedish magnetic surveys for iron ore.

During the decade following 1907 other attempts were made in Sweden to discover an electrical method that would be both reliable and convenient for the investigation of ore deposits. A brief account of some of these extensive operations are given in the Year Book of the Geological Survey of Sweden for 1913. Bergstrom (1914), in a report on trials that had been made with electrical prospecting, drew up the first plan for a practical method of prospecting that was later developed and improved in Sweden as well as in other countries. During World War I, the urgent need for sulfide ores stimulated renewed development of electrical methods in Sweden. However, no practical apparatus or method was perfected until the mining engineers, Hans Lundberg and Harry Nathorst, in-

vented their equipment in 1918 (Barton, 1927; Gavelin, 1923).

The Lundberg and Nathorst system, usually designated as the "old Lundberg method," comprised an arrangement of two parallel line electrodes which were about 1,000 meters long and which were laid on the ground about 1,000 meters apart. Contact with the ground was accomplished by metal pegs driven into the ground at regular intervals and attached to the bare cable of which the line electrode was made. By means of these line electrodes Lundberg sought a simple homogeneous field such that the equipotential lines would be straight and parallel to the electrodes in a homogeneous earth. He reasoned that a good conductor at depth in the lesser conducting country rock would cause the equipotential lines at the surface to be thrust apart, since the conductor would serve to concentrate the flow of current. Contrariwise, a poorer conductor than the country rock would act as an obstacle to the current, thus causing a constriction of the equipotential lines at the surface of the earth. In his thinking, Lundberg emphasized the enormous differences on the conductivity of different rock types and of different minerals. He also emphasized that the conductivity of rocks and soils depends on their moisture content.

Lundberg and Nathorst passed an alternating current of audio frequency (50 to 10,000 cycles per second) through the earth between the line electrodes (Lundberg, 1928a). The equipotential lines—or more correctly, curves of equal root-mean-square potential—were traced between the current electrodes by means of two metal "searching rods." Points of equipotential were located by finding a null point with telephone earphones when the rods were forced into the ground to make contact. Also, direct potential observations were made with a resistance bridge. The techniques as used by Lundberg and his associates in his early work were good for the detection of conducting sulfide ore bodies within about 300 feet of the surface.

Lundberg's early discoveries with his equipotential-line method constitute geophysical triumphs that stand as a milestone in the art of electrical prospecting. In the autumn of 1918 he discovered the Kristineberg ore field in northern Sweden and delineated the separate ore bodies of that field during the following summer. Here the ore, comprising pyrite and chalcopyrite, was at a shallow depth beneath the glacial overburden. The ore bodies were hidden, and workers using surface geology had been misled because boulders containing pyrite ore were found in the till along a northerly trend; the electrical survey showed that the ore bodies actually trend eastward.

In 1919 another sulfide ore body was discovered at Remdalen by an electrical survey in the Vasterbotten Mountains (Lundberg, 1929). During 1919 to 1922 a series of intermittent electrical surveys over a drift-covered area about 30 miles east of the first discovery at Kristineberg culminated in the discovery of the Bjurfors ore field in the summer of 1922. Here the ore was hidden as it had been in the previous field, and the only surface indication was a boulder containing ore nearly 2 miles from the original deposit. The Geological Survey of Sweden cooperated in the geological aspects of the search which was complicated by the variation of the direction of glacial striae and the glacial transport of the ore boulders that had probably been diverted by a nearby prominent hill. By December 1922, Lundberg had investigated or tested about 60 deposits of ore with his equipotential-line method (Sundberg and others, 1923).

The main development of electromagnetic methods in Sweden occurred in 1921 when Karl Sundberg, a mining engineer, began to experiment with a number of these methods (Lundberg, 1926b). During that year, the first new ore body to be discovered with electromagnetic methods was found in northern Sweden by Sundberg's method (Lundberg, 1929). He used both electromagnetic galvanic methods, in which current is introduced into the earth directly through electrodes, and induction methods, in which current is caused to flow in the ore body inductively by currents varying in loops of wire insulated from the ground. Lundberg and his company used these methods in the field with considerable success. By 1928, Lundberg (1928b) and his associates had discovered between 40 and 50 commercial ore bodies in Sweden. He had also made discoveries in North America. In Newfoundland, for example, he found by the equipotential-line method the well-known Lucky Strike ore body near Buchans after following a zone of weak mineralization for about a mile.

The Germans also made lasting contributions to the art of electrical prospecting, especially through their fundamental research in electromagnetic and electrochemical processes. During 1910 and 1911 in Germany, Lowy and Leimback used a high-frequency electromagnetic method for a large number of experiments. However, low penetration caused failure to obtain useful results (Migaux, 1941a; Lundberg, 1929). In 1913 K. Schilowsky patented a method to study the electromagnetic effect of subsurface disturbances (Rust, 1938).

Richard Ambronn was one of the most active German students in the field. He made several suggestions for improving the equipotential-line method. Most of his own work, as well as that of his German contemporaries, dealt with the electromagnetic method, which will not be considered further. Other workers in this category were Mueller, Fritsch, and Belluigi. The last-named is an Italian. One of Ambronn's greatest contributions was his text on the elements of geophysics, originally published in 1926 in German and later translated into English by Margaret C. Cobb. This book contains a comprehensive bibliography of papers on electrical methods to the year 1926.

During February 1928 to February 1930, the Imperial Geophysical Experimental Survey was organized in London and was conducted in Australia. Its purpose was not to find minerals but to test the applicability of the various geophysical methods under various field conditions. The report of that series of experiments (Broughton Edge and Laby, 1931) remains even today a classic in the geophysical literature. The wide range of geophysical methods tested included self-potential, resistivity, potential mapping, and electromagnetic, all of which were often tried in the same mineral region. The work was usually done in areas of known mineral occurrences and with relatively good geologic control. Thus, the report contains a good comparison of the various methods, together with the uses and limitations of each. This report also contains some theoretical development which parallels work by other authors reported in the next section of this treatise, but which apparently was done quite independently.

In 1924 Petrowsky (1925c), made detailed investigations at Ridder's mine near Altai, in central Asia, where he measured not only natural earth currents but also artificial direct currents, using Sherwin Kelly's method with some of his own modifications. To introduce current into the ground, Petrowsky used what he termed the "dot system" of arranging electrodes. This system consisted of a great number of small electrodes placed along the boundary of the field to be investigated and connected together with wires so as to keep them in a state of equal potential. This system was apparently similar to ones proposed by Lundberg and Schlumberger. In 1926 Petrowsky, Skaryatin, and Kleiman (1927) made systematic electrical surveys in the Beloretsk mining district in an abandoned mine where pyrite occurs at a depth of about 16 meters. Both direct- and alternating-current resistivity techniques were used. The current was introduced into the ground through two simulated line electrodes, each of which consisted of 21 stake electrodes. For the equipotential-line survey, they used 1,000-cycle alternating current, mapping the equipotential lines with probes and an earphone. In order to measure potential gradients with direct current, they used nonpolarizing electrodes and a galvanometer. Their results of the

equipotential-line survey show a bulge of the equipotential lines over the known conducting ore body.

There have undoubtedly been many other investigations of electrical prospecting in the U.S.S.R. However, the comparative difficulty in searching the Russian literature, not only because of the language barrier but also because of the inaccessibility of many Russian references, makes it doubtful whether the work of the Russians has had much influence on the development of the techniques which we will report in the main part of this treatise. For these reasons, we are not able to report further on the Russian work, except for some theoretical studies that will be discussed later.

Many more names should be added to the list already given above for workers in electrical prospecting in all parts of the world. The most notable of these are given in the following section.

DEVELOPMENT OF THEORY

The theory used in the art of electrical prospecting is based entirely upon electrical-potential theory. The equations of Laplace and Poisson and the potential theory, as developed by Maxwell and extended by others, constitute the foundation upon which rests today the interpretation of resistivity data. Most of the problems arising in electrical exploration are not new in that they involve recent theories, but they are new in that they involve the application of classical theories to specific situations that previously were not of interest.

As early as 1887 Franz Neumann derived the equation for the potential at any point in or on the earth near two current electrodes, placed on the earth's surface, between which a current I is flowing. Where ρ is the resistivity of the homogeneous earth and the distances from the two electrodes are r_1 and r_2, the potential is

$$U = \frac{I\rho}{2\pi}\left(\frac{1}{r_1} - \frac{1}{r_2}\right).$$

Newmann, at the same time, also developed the corresponding formula applicable when the two electrodes are on the surface of a homogeneous sphere. Equations comparable to that given above were used in 1912 by Schlumberger (1920b) to describe his normal equipotential lines about one or two point electrodes and in 1915 by Wenner to derive the expression for the apparent resistivity as determined with his electrode configuration.

In spite of the very early application of this theory, the real development of quantitative resistivity interpretation did not begin until nearly 1930. Warren Weaver (1930) gave a pictorial résumé of the prospecting problems which had already been solved for both point electrodes and long-line electrodes. The geologic features that he included are:

1. One or more parallel vertical planes across which the resistivity suddenly changes. This situation would include a vertical fault which he included, a vertical dike or brecciated zone which he implied but did not show, and three vertical planes of discontinuity separating four media of different resistivities, an example of which he also showed.
2. One or more parallel horizontal planes across which the resistivity suddenly changes. This situation includes the two- and four-layer cases, examples of which he showed, and other multilayer cases which he implied.
3. A buried sphere imbedded in a homogeneous earth.
4. A sphere buried beneath a horizontal layer differing in resistivity from the material in which the sphere is imbedded.

Weaver did not give the solutions for these problems, but stated only that the solutions were available and showed selected examples of the resistivity curves.

Although knowledge in the field has broadened since that time, there have been very few new basic principles added to the concepts summarized by Weaver. In the same paper Weaver also pointed out other important geologic features which were still wanting of solutions. These included a buried ellipsoid imbedded in a homogeneous earth, a vertical dike covered by overburden, a fault of infinite displacement covered by overburden, a fault with finite displacement and a dipping fault or dike. Of these solutions, the fault with finite displacement and the dipping dike even yet have not been solved exactly.

The most widespread interest in electrical-prospecting theory has been in its application to the problem of horizontal bedding. This emphasis clearly arose in the hope that resistivity prospecting would eventually help to locate structural oil traps, a hope that has not been fulfilled. The mathematical analysis involved in the layered-earth problem was indicated by Maxwell (1891). However, the main development of this subject occurred from 1929 onward, and was accomplished by a group of men who for the most part worked independently of each other. Hummel (1929 c, d) used the image theory to derive formulas for the two- and three-layer problems. For the two-layer case Hummel gave a table which facilitates computation of the formulas, and he gave several sample curves for the Wenner configuration. Hummel confirmed the fact, already pointed out by Weaver (1928), that for a two-layer case a bed of better conductivity at depth can be detected more readily than a bed of lesser conductivity, other factors being equal. When the second layer is perfectly insulating, Hummel showed

that the curve of apparent resistivity plotted against electrode separation is asymptotic to a straight line which passes through the origin and has a slope of 1.386. The limiting value of the slope is effectively reached when the electrode separation a is 1.5 times the thickness of the upper bed. Similarly, Hummel showed that for this limiting case the apparent resistivity is 1.5 times the resistivity of the upper bed when the electrode separation equals the thickness of the bed. For all practical purposes these limiting cases are reached if the resistivity of the lower bed is more than 10 times that of the upper bed. Hummel also showed some curves for the three-layer case and demonstrated how a graphic approximation can be used in the interpretation of the three-layer case.

Stefanesco, Schlumberger, and Schlumberger (1930) also solved the problem of the distribution of potential inside an earth composed of horizontal layers, each of which was homogeneous and isotropic. Following the suggestion of Ollendorf (1928), they started with the appropriate differential equation and obtained their solution in the form of integrals involving zero-order Bessel functions of the first kind. They extended their solution of the two-layer case to the three- and four-layer cases, and they showed how it could be carried to any number of layers. They demonstrated the equivalence of their solutions and those given by Hummel, but they preferred their own because they thought that the series representations of Hummel were too cumbersome.

Lancaster-Jones (1930), in a completely independent effort, duplicated the analysis of Hummel and came to many of Hummel's conclusions. In addition, he emphasized the fact that the influence of buried layers manifests itself for very small electrode separations. As a result of his theoretical work, Lancaster-Jones concluded that Gish and Rooney's (1925) empirical rule for the Wenner configuration that "the electrode spacing equals the depth of penetration" should be taken only as an approximate guide. He also cautioned against using breaks in the resistivity curves for estimating depth of a horizontal layer, as many workers advocate. However, he added an empirical rule that, when the bottom bed of a two-layer problem has the higher resistivity, an inflection point occurs in the Wenner resistivity curve when the electrode separation equals 1½ times the thickness of the upper bed. More than 20 years later, Palmer and Hough (1953) investigated systematically the question of inflection points for the two-layer case. They set up an expression for the apparent resistivity for a symmetrical electrode arrangement with the potential electrodes separated by an arbitrary fraction of the distance between the current electrodes. They differentiated this expression twice

with respect to the distance between the current electrodes. Using approximations, they determined the values of this distance at which there were inflection points in the resistivity curves for specific ratios of the potential electrode separation to the current electrode separation. For the Wenner configuration, this ratio is one-third. Palmer and Hough concluded that the Gish-Rooney rule can be theoretically justified only for high negative values of the reflection factor and that the Lancaster-Jones rule is applicable only for positive reflection factors of about one-half. For all preliminary approximations, in which the inflection point is used in the field, they recommend the rule that the thickness of the top layer is equal to one-quarter the distance between the current electrodes at the inflection point.

Tagg (1930) also criticized the depth rule used by American workers and emphasized that no theoretical proof had shown that a break or abrupt change occurs in apparent-resistivity curves for horizontal beds. At the same time he outlined the method for depth determination which now bears his name. Unlike previous empirical methods, Tagg's graphical solution of the problem is theoretically exact.

Ehrenburg and Watson (1931) generalized the use of images to apply to a mutilayer problem, provided the thicknesses of succeeding beds are a series of rational numbers. They gave both numerical calculations and sample curves for two- and three-layer cases. These authors emphasized once more "that in not one case does a maximum, minimum, or point of inflection correspond in electrode spacing to the depth of an abrupt change in resistivity." Roman (1931), in the most comprehensive treatment up to his time, used image theory to calculate the potential due to a current electrode at the surface of a two-layer earth. For the quantity $k = (\rho'' - \rho')/(\rho'' + \rho')$ he designated the term "reflection factor," which has since been used almost universally to specify resistivity contrast. Here, ρ' is the resistivity of the upper bed and ρ'' is the resistivity of the lower bed. Roman concluded his discussion by giving a table from which the theoretical apparent resistivity could be calculated for any given electrode separation with the Wenner configuration over a given two-layer earth. His table included all reflection factors from -1 to $+1$ in increments of one-tenth. He later (Roman, 1934) gave apparent-resistivity curves, based on these tables, and thus became the principal advocate of "curve matching." One of his most important contributions was in plotting these curves on logarithmic paper. This technique removes the scale factor from the problem and eliminates the necessity of plotting a separate family of master curves for each new geologic problem. Roman's

(1933) treatment of the two-layer problem was the first satisfactory image analysis for this problem.

L. V. King (1933), Morris Muskat (1933), and L. B. Slichter (1933) went much further than solving the basic multilayer problem analytically; each, in his own way, gave a formal solution to the problem based on harmonic analysis and then went on to investigate some of the ramifications of the solution. King departed from the usual viewpoint by solving his potential problems in terms of an "electric current function" and by replacing the usual apparent resistivity with a "surface gradient characteristic." These quantities can be easily related to the quantities more commonly used in electrical prospecting. The fact that these terms are rarely used in geophysics does not detract from the contribution which King made in his mathematical analysis. Muskat, working quite independently, covered much the same ground mathematically as did King but extended King's work in many respects. However, he worked directly with the potential functions and the apparent resistivity.

Both King and Muskat used more sophisticated mathematics than had been used by previous authors. They expanded their solutions in terms of certain hyperbolic functions instead of the usual powers of the reflecting factor. They also obtained a variety of solutions which contained expansions in terms of many types of Bessel functions other than the ordinary Bessel function of zero order. From his basic solutions for the two-layer problem, Muskat derived separate expansions suitable for numerical computations for radial distances from the current electrode both large and small in comparison to the thickness of the top layer. He also included other special expansions. He concluded that his results compare very favorably with the laborious calculations required when the series of images are summed directly. These computation shortcuts for the two-layer problem did not serve the progress of electrical prospecting directly because the necessary computing had already been done by Roman and others. However, the authors did show how to apply their methods to multilayer problems and thus served to enlighten persons who were to do later work on the more complicated cases.

Slichter considered another line of thought in resistivity interpretation. He regarded the problem of homogeneous horizontal multiple layers as an unusual boundary-value problem in that the function to be determined is one which expresses the unknown variation of the resistivity with depth, whereas the potential function itself is considered to be known on the boundary, which in this problem is the surface of the earth. Slichter sought to replace the trial-and-error method of curve matching by a more direct method of interpretation. The basis of his idea was to use transformation theory to solve for the resistivity function directly from the potentials observed on the earth's surface—a possibility which King (1933) also pointed out. In working out his theory of direct interpretation, Slichter also developed some new forms for the solutions to what he called the "inverse problem"—that is to say, solutions for the potential as a function of an assumed resistivity distribution with depth. Actually, Slichter did little more than to propose the direct interpretation method, to show that it was possible, and to prove that a unique solution existed if the resistivity is a continuous function only of depth.

Stevenson (1934) continued the work on the direct interpretation method. At first, he assumed that resistivity was a continuous function of position, not only of depth; which assumption he showed did not lead to a unique solution. Where resistivity is a function of depth only, Stevenson gave an approximate solution which is to be compared to Slichter's exact solution. However, Stevenson claimed that his approximate solution, based on successive approximations, might still give a rough answer where Slichter's method would break down completely—namely, where the resistivity is a stepwise function of depth, which is the situation of most interest in geophysics. Actually Stevenson admitted that neither his method nor Slichter's is particularly good from the practical viewpoint. He demonstrated his statements with computations on a three-layer curve that Muskat had published. A serious disadvantage of both methods from the practical point of view, even when they work, is the large amount of computation required for each individual case. Stevenson (1935) later obtained solutions of the direct problem in the form of Fourier series, but the following year he admitted error and stated that Fourier series are not valid for this unless the resistivity as a function of depth can be expressed as a Fourier series. If the resistivity is a stepwise function, it cannot be expressed as a Fourier series.

King (1934) indicated that, although no unique solution for the variation of resistivity with depth for the multilayer problem—that is, that in which the resistivity function is not continuous with depth—can be obtained from the knowledge of the potential about a point source of current, it is possible to obtain a solution when the potential is known near an infinite line electrode.

Evjen (1938) investigated the possibility of calculating the strength of images and their depths from a knowledge of potential measurements made at the surface only. He stated that the exact solution can be obtained by a double infinite integral involving Bessel

functions of complex argument, but he discounted the value of this method on the grounds that field measurements were not accurate enough to warrant an exact solution. Instead he turned to an iteration method to solve the problem. He finally concluded that, although the problem of direct analysis theoretically has a unique solution, the solution can rarely be realized in practice.

Pekeris (1940), starting with Slichter's exact method, showed how it could be used to determine the variation of resistivity with depth for a horizontally stratified earth. To test his method, Pekeris treated potential data from three unknown (to him) situations: two three-layer problems and one for a conductivity function continuously varying with depth. The computed results for small values of depth were in good agreement with the actual conditions of the problem. His method, however, requires a large amount of computational time. Keck and Colby (1942) solved the problem of determining earth conductivity from surface measurements, when it is a continuous function of depth only, by a perturbation method.

Additions and refinements of the above-mentioned studies of horizontal-layer problems have appeared in the literature from time to time. Most of these have been concerned with theoretical curves for multilayer problems or empirical methods of interpreting resistivity data. Poldini (1932) showed how three-layer problems can be interpreted by curve matching with two-layer curves, provided the bottom bed is assumed to be sufficiently deep. Pirson (1934) revealed a successive approximation method for the interpretation of resistivity curves when Tagg's charts for the two-layer problem are applied to the three-layer problem. Tagg (1935) stated that sometimes it is almost impossible to use Poldini's method to obtain satisfactory results and that Pirson's method may become very laborious. Tagg offered a method of his own to overcome the objections by applying his two-layer method to a three-layer problem.

Watson (1934) gave eight apparent-resistivity curves for the four-layer problem, chiefly to show the chances for error when an empirical rule is used for depth determination. He also showed the results of 14 model experiments to serve as a check for his mathematical analysis. Watson and Johnson (1938) gave additional families of curves for both three- and four-layer problems.

Rosenzweig (1938) gave a method, similar to Tagg's, of computing the thickness of the top layer and reflection factors for the two-layer problem. The following year he proposed a solution of the two-layer problem based on "lens-sources." He also extended this method to the multiple-layer case. He claimed that his method is more systematic than the method necessarily

used for computations based on the image theory. Longacre (1941) suggested a modification of Tagg's method for the three-layer case. He showed examples of how it worked and stated that situations where it would not work were easily recognized. Moore (1944) proposed an empirical cumulative-curve method, which he emphasized was without theoretical basis but which became the object of severe criticism by Muskat (1944).

Recently, several large albums of tables and curves for multiple-layer cases have been published. Roman (1960) extended his tables for two-layers; the Compagnie Générale de Géophysique (1955) published three-layer data for the Schlumberger configuration; and Mooney and Wetzel (1956) published an album consisting of one sheet with 20 two-layer curves, 35 sheets with about 350 three-layer curves, and over 200 sheets with more than 2,000 four-layer curves for the Wenner configuration.

In all these, the authors assumed that the material within any given horizontal layer is homogeneous and isotropic. This assumption is questionable, especially for shales.

Slichter (1933) solved Laplace's equation for anisotropic media but immediately specialized his solution so that it applied only to isotropic layers, whose resistivities vary with depth only.

Maillet and Doll (1932) considered completely the propagation of current in anisotropic media in terms of tensor analysis. They discussed and gave examples of the conditions under which the potentials in a current-flow problem remain invariant at homologous points under transformation of the space metric and of the conductivity tensor. They used a coefficient of anisotropy which is defined as the square root of the ratio of the "longitudinal resistivity" to the "transverse resistivity."

Schlumberger and others (1933b) recognized the problem of anisotropy and made a praiseworthy contribution to the study of anisotropic media. They commenced their study by examining the current flowing parallel to and perpendicular to the contact between two thin, homogeneous, isotropic beds. They then extended the analysis to include many thin, parallel beds. They defined a coefficient of anisotropy as the reciprocal of the one used by Maillet and Doll. They also distinguished between a microscopic anisotropy, which depends on preferred orientation of the grains in the rock, and a macroscopic anisotropy, arising from a thin-layering which is visible to the naked eye. They extended their theory to include multiple-layer problems and showed that solutions which are unique under the assumption of homogeneous and isotropic beds are no longer unique when the beds are anisotropic. They demonstrated this ambiguity of

the resistivity method by giving three different geological situations that would give the same vertical resistivity profiles. They showed how their concept of anisotropy could be used to detect qualitatively such features as dipping beds, synclines, and anticlines. Maillet and Doll had also presented this possibility.

Pirson (1935) solved the problem of anisotropy theoretically by reducing the original space into one in which the scales are changed to compensate for the anisotropy so that Laplace's equation in its usual form is valid. He then used Hummel's solutions for the ordinary horizontal-layer problem and transformed them into solutions valid for the anisotropic layers. In these new solutions the strengths of the images are not changed, but their positions are changed.

Maillet (1947) discussed in detail the fundamental equations in the direct-current method of electrical prospecting for the case of horizontal strata only. He established the relationship between the earth resistivity as a function of depth and the apparent resistivity as a function of electrode separation. He also defined a new diagram which he called the "Dar Zarrouk curve." In this classic paper Maillet effectively integrated much of the fundamental mathematical material that had been developed by the Schlumberger school during the previous generation and, in addition, introduced new fundamental ideas. He reviewed and extended his previous work on anisotropy and recognized the "principle of equivalence" originally promulgated by Pirson.

Theoretical treatments of types of geological problems other than horizontal beds have scarcely reached the volume of this subject alone, although work on the other subjects had as early a start (Weaver, 1930). Tagg (1930) gave, apparently for the first time, the formulas and apparent-resistivity curves for horizontal and vertical resistivity profiles across a vertical fault. The curves are for the Wenner configuration. Each of his families contains curves for all values of the reflection factor from $+1$ to -1 in increments of one-tenth between adjacent curves. For the first time Tagg showed that a horizontal profile contains four discontinuities in slope when it crosses a fault. In this paper Tagg gave a family of vertical resistivity profiles made with the electrode configuration oriented both perpendicular to and parallel to the fault. He showed that the effect of the fault in the parallel orientation is practically negligible if the distance from the traverse to the fault is 4 times the electrode separation a.

L. G. Howell (Hubbert, 1932: Discussion) gave formulas and curves for horizontal profiles with the Wenner configuration across both a perfectly conducting and perfectly insulating vertical thin sheet. His solutions, which were based on the method of images,

offered a possible solution to the problem of a filled fault zone, on both sides of which there was identical country rock.

Although some applicable papers on a related problem in electrical well-logging (for example, Buckner, 1954) were published during the ensuing interval, few studies of vertical boundaries were published until Lögn (1954) discussed the general problem. He used the method introduced by Stefanesco and others (1930, 1932) to solve for the potential functions which he used to get apparent-resistivity expressions. His electrode configuration resembles the Schlumberger configuration except that it uses only one current electrode. Lögn extended the previous mathematics on the subject by developing expressions for the apparent resistivity over very thin vertical sheets.

Because of long-standing interest in mining problems in Scandinavia, it is not surprising that early studies of the electrical effect of dikes and similar bodies were made in that region. From these studies evolved the potential-drop-ratio method, a technique still widely used. Lundberg and Zuschlag (1931) introduced the potential-drop-ratio method and showed typical potential-drop-ratio curves over a vertical fault and a vertical dike. They also showed the corresponding curves for the two-layer problem and claimed an advantage in the resolution of the potential-drop-ratio method over ordinary resistivity methods.

Hedström (1932), using the method of images, derived formulas and gave curves associated with a vertical dike in an otherwise uniform country rock. He considered only one current electrode in the vicinity of the dike and plotted the ratio of the potential when the dike is present to the normal potential for a homogeneous earth. He plotted families of curves for resistivity contrasts of 3:1 and of 10:1. Each family contained curves for distances from the electrode to the dike equal to the width of the dike and 2½, 5, 10, and 20 times the width of the dike. He included curves for corresponding cases when the resistivity of the dike was less than the resistivity of the country rock. He demonstrated that for a dike of a given width the potential at a given point on the far side of the dike from the current electrode is the same whether the resistivity contrast is 3:1 or 1:3. He also made similar studies of the situation in which the country rock on either side of the dike has different resistivities.

Hedström next studied the gradient over the same features. As a result of his studies, he concluded that it would be more advantageous to base interpretation on the potential gradient rather than on the potential. Only for a vertical fault did he conclude that anomalies in both quantities would be of the same magnitude. Actually, his findings point to the advantage of the

resistivity methods over the earlier potential-mapping methods.

The dipping-bed problem has been the subject of a long study which began in the mid-1930's. Aldredge (1937) attempted a general solution to the problem using the method of images, which is applicable in special cases only. Aldredge's theoretical work, without modification, became the basis for four other papers (Sanjeevareddi, 1936[1]; Jameson, 1941; Carreño, 1948; and Trudu, 1952), all of which obviously contain the same shortcomings in theory as did Aldredge's original paper. The final expression of the image school appeared in a paper by Unz (1953) in which he pointed out the restrictions, as well as the possibilities, of the image theory. He showed how image theory can be used to make adequate approximations in certain problems. The correctness of these approximations was discussed and illustrated by Van Nostrand and Cook (1955).

Correct general solutions of the dipping-bed problem had their beginning in the corresponding dielectric wedge problems in electrostatic theory. The most notable electrostatic solutions were published by MacDonald (1895), Rice (1940), and Grinberg (1940). The first geophysical application was published by Skal'skaya (1948). She used Fourier-Bessel transformations to solve an integral equation. She applied her general solutions, which are applicable to cases with both arbitrary dip and arbitrary resistivity contrasts, to many special cases to show when image theory is valid. She also manipulated her solutions into convenient forms for computation for certain special angles. Chastenet de Géry and Kunetz (1956) worked out much more refined computational forms of Skal'skaya's solution. Moreover, they reported that the Compagnie Générale de Géophysique had computed sets of curves for the Schlumberger configuration for angles that are submultiples of π down to $\pi/12$. They presented some of these curves.

Two other general solutions of the dipping-bed problem have been given by Maeda (1955) and Huber (1955). Maeda is the only geophysical writer to solve directly the differential equation; he carried his solution to the form of the summations originally published by Rice. Huber pointed out that the infinite-series solution of MacDonald and Rice, and thus of Maeda, is inconvenient for numerical computations, especially because it contains Legendre functions of the second kind which have a singularity when the argument is unity. Huber, therefore, transformed Rice's solution into the general solution which had been derived earlier

by Skal'skaya, and Maeda. The methods used by Skal'skaya, Maeda, and Huber are distinct and independent.

Work on buried bodies of finite extent has been restricted largely to buried spheres. Maxwell (1891) developed the theory for the disturbance due to a conducting sphere placed in a uniform electric current and in an otherwise homogeneous medium. Petrowsky (1928a) studied the potential distribution at the surface of the earth due to a buried electrically polarized sphere. His analysis is particularly useful in the interpretation of self-potential anomalies over sulfide ore deposits, and has been used recently as a basis for more specific interpretive techniques.

The most general solution of the buried-sphere problem with arbitrary resistivity contrast is the one given by Webb (1931a). He developed a formula for the potential at the surface of the earth due to a buried sphere of finite resistivity contrast with the surrounding medium when a point current electrode is located at the surface. The boundary condition requiring that no current flows across the earth's surface is satisfied by placing an image sphere above the earth's surface. The resulting complication of interaction between the original sphere and its image is handled by means of a special transformation in spherical harmonics. He showed to what degree of approximation the various parts of his solution are valid. Webb (1931b) extended his theory for buried spheres to obtain similar solutions for both buried prolate spheroids and buried oblate spheroids.

Apparently incognizant of Webb's work, Lipskaya (1949a, b, and 1953) made a comprehensive study of the buried-sphere problem. In her first paper she solved the problem of the buried perfectly conducting sphere through the use of bipolar coordinates. She obtained her solution by superposing two solutions given by Neumann (1887) for the corresponding electrostatic problem, one for the disturbance due to two spheres kept at zero potential in the presence of a point charge and the other for the potential distribution about two spheres maintained at some constant potential. She gave no curves in this paper.

In her second paper Lipskaya solved the problem by the iterated application of the method of images. The degree of approximation afforded by each of the first three terms in the resulting series is given and compared with the exact solution as obtained in her first paper. She illustrated these approximations with curves. She also plotted curves showing the intensity of the electric field on the earth's surface for different positions of the electrode and for different depths of the sphere. She ended her discussion with some resistivity profiles made with a two-electrode configuration. In 1953 she con-

[1] Sanjeevareddi, B. S., 1936, A theoretical and experimental investigation of the earth-resistivity method as applied to dipping strata: Colorado School Mines, Dept. Geophysics Series Pub., no. 69, 25 p. (unpublished Master's thesis).

tinued her studies by discussing the problem of a buried sphere with finite resistivity contrast. Following Lipskaya's earlier work, Van Nostrand (1953) showed that a sphere with its center buried to a depth equal to its diameter cannot be expected to be found in a resistivity survey with the Wenner configuration.

Cook and Van Nostrand (1954) discussed electrical surveying over filled sinks. They gave the applicable solutions of Laplace's equation in both prolate and oblate spheroidal coordinates, as well as in spherical coordinates. They showed a wide variety of resistivity curves to be expected with the Lee and Wenner configurations over and near filled sinks. Seigel (1952) also used these same mathematical solutions, independently derived, to evolve techniques for studying an underground ore body which has been penetrated by a bore hole. Clark and Salt (1951) had previously used an image solution for deriving a method of locating a buried ore body passed by a drill hole. The solutions of Seigel and Clark and Salt are only approximate because of the disturbing effect of the earth's surface.

Frank and von Mises (1935), collaborating with Noether and Ollendorf, gave the exact solution for the potential at the earth's surface due to a point current electrode over a buried cylinder with its axis horizontal (Huber, 1949). The problem was solved exactly by means of Hankel's function, but the solution is so complicated that numerical values can be obtained only by an unusually troublesome amount of computation. Tikhonov (1942) also studied this problem. Huber (1949) recognized the difficulty of computations based on von Mises' solution and suggested that studies should be restricted to the region midway between the two point electrodes where the current field is approximately uniform when the earth is homogeneous. He tried to analyze the error due to the assumption of a homogeneous field. Then he gave potential curves over a buried cylinder in a homogeneous field. Later Huber (1953) gave curves for the values of the potential on the surface of a perfectly insulating cylinder of infinite length due to a point-current electrode which is also on the surface of the cylinder.

Mukhina (1950a, b) has given apparently the only solutions for potentials due to a point source near a buried dike or fault. The problem is not easily solved and his solutions are only approximate. However, the solution of this problem, even in an approximate way, marks an important step forward in the interpretation of resistivity data. This problem was one of the unsolved problems listed by Weaver (1930).

The above theoretical work was concerned mostly with the Wenner and related configurations. The same basic potential theory applies to electrical studies using an infinite line electrode for the current source.

The mathematics in the latter is somewhat different because this type of field leads to a logarithmic potential. Many more problems can be solved in this "two-dimensional" case because of the applicability of conformal mapping.

It was shown early that the potential anomaly over a perfectly conducting spherical ore body is greater with a line electrode than with a point electrode (Sundberg and others, 1923). However, with the advent of resistivity prospecting, which is superior in resolving power to potential mapping, the use of line electrodes assumed a minor role. One of the earliest and most comprehensive theoretical studies on line electrodes was made by Peters and Bardeen (1930), who derived the expressions for the potential due to two parallel infinitely long line electrodes lying on the surface of a homogeneous, isotropic earth. They investigated the current density and the depth of current penetration for this current electrode configuration, and used the image theory to derive formulas for the potential for this configuration over a two-layer earth. After deriving the formulas they charted, both in profile and plan view, the potentials at the earth's surface between and outside the two line-current electrodes for several resistivity contrasts and for several thicknesses of the top layer. They did the same for certain three-layer problems. They also applied the image theory— but only for angles for which it is applicable—to the dipping-bed problem when the line electrodes are parallel to the strike. In this problem they worked only with a lower bed that was perfectly insulating or perfectly conducting. Peters and Bardeen also derived the equation for the potential over a buried conducting sphere near two line electrodes. In this problem, they used the method of inversion. They found that a sphere, whose radius equals one-fourth the distance between the line-current electrodes, produced negligible perturbation on the normal potential distribution when its top is buried to a depth equal to its radius.

Muskat (1935) gave an extensive treatment of the potential distribution about a line-current electrode on the surface of a horizontally stratified earth. He gave a complete analysis of the problem for both two and three layers. Following Slichter's analysis for a point electrode, he also outlined briefly the solution for the direct interpretation problem for the line electrode. Muskat's studies of the line electrode are especially instructive because he followed the same thorough approach he had used in his analysis of the point electrode, and he makes many appropriate comparisons of the two problems.

Although the line electrodes are of questionable practical value, the same "two-dimensional" mathe-

matics is useful in obtaining approximations to certain three-dimensional problems which are difficult to solve exactly. Kiyono (1950a, b, c) used this technique extensively to study resistivity curves with the Wenner configuration in which line-current electrodes and point-potential electrodes are used. He made model experiments which proved that his two-dimensional approximations are sufficiently accurate. Using this method, Kiyono computed and plotted horizontal resistivity profiles over a variety of features which included a buried fault modelled by a buried semi-infinite horizontal plate; a dike modelled by a buried semi-infinite vertical plate; an anticline modelled by a vertical wedge-shaped projection protruding from a horizontal plane; and a syncline similarly modelled. In each of these cases the buried body was perfectly conducting. Kiyono (1952a, b) also applied this method to several topographic features which might affect an electrical survey, as Hurd (1944) had done previously by model experiments.

In many respects an insight into the fundamental concepts was slower in being realized than were solutions to some of the geologic problems. Lee and others (1929) analyzed the potential field about two electrodes on the earth's surface, as Schlumberger (1920b) had done about a single electrode, when the earth is homogeneous and isotropic. They concluded that, even though the equipotential shells are fourth-order surfaces, these shells may be approximated by a family of accentric spheres whose centers fall on the surface of the earth. Weaver (1928) had already given the potential distribution about a current electrode in homogeneous ground and had presented a curve showing the fraction of the total current, from a dipole (two current electrodes, one a source and the other a sink) which penetrates below a given depth for homogeneous ground. Stefanesco (1929) gave a carefully prepared chart of the current flow lines and the equipotential lines for a horizontal dipole on the surface of the earth and he gave the equations for these families of curves. He also derived the expressions for the electric field due to this dipole. He went on to derive expressions for the magnetic field due to the current flowing, which was the main purpose of his paper.

Once again, the most extensive treatment of the subject is due to Muskat (1932) who studied the electrical problem because of its analogy with the flow of fluids in porous media. He analyzed the problem in terms of an electrode placed at the center of a cylindrical disk of very large radius and of uniform resistivity. He first studied the point electrode at the surface of the disk. Later, he used an image method, introduced by Samsioe (1931) in aless complete treatment of the same problem, to study the potential distribution about a partially penetrating, vertical-line electrode. Although he used image theory, he indicated that he could have used the more sophisticated approach with Bessel and Hankel functions. His solution is valid only for constant flux density along the penetrating electrode. Muskat's discussion is strictly valid only for a two-layer case in which the bottom layer is perfectly insulating, but his analysis is fundamental and can be used as a guide in analyzing certain features of any two-layer problem.

FUNDAMENTALS OF PROSPECTING WITH DIRECT CURRENT

In all direct-current methods of prospecting, current is impressed artificially into the ground and the effects of this current on or within the ground are obtained by measurements of potential, differences of potential, ratio of potential differences, or some parameter that is related directly to these variables. The fundamental theory involved in each of the different methods is the same and is predicated upon the validity of Laplace's equation for obtaining the electrical potential and the pattern of current flow about one or more current electrodes placed on or within the ground. The principal differences among the various methods of direct-current prospecting lie in the number and spacing of the current and potential electrodes employed, the variable electric quantity determined, and the manner of plotting the resulting data.

FUNDAMENTAL CONSIDERATIONS
POINT SOURCE OF CURRENT

The usual practice in the theoretical treatment of electrical prospecting is to assume that each separate geologic unit—for example, each of the beds in a layered sequence—is electrically homogeneous and isotropic. Although the assumption is not strictly valid, it does lead to useful conclusions.

Consider a point source of current placed on the surface of the earth, as is illustrated in figure 1. I amperes of current flow through the source C into the earth whose true resistivity is ρ ohm-meters. The distance, without regard to sign, from the potential electrode P to the current electrode C is R meters. It is now required to determine the potential at P due to the current flowing into the ground through the current electrode. As is usual, we refer the potential at the point P to the potential at infinity which we consider to be zero.

Since the medium is isotropic, the current flow outward from C must be the same in all directions into the earth; no current flows upward because the air has infinite resistivity. Hence, the current lines are uniformly spaced radial lines and the equipotential sur-
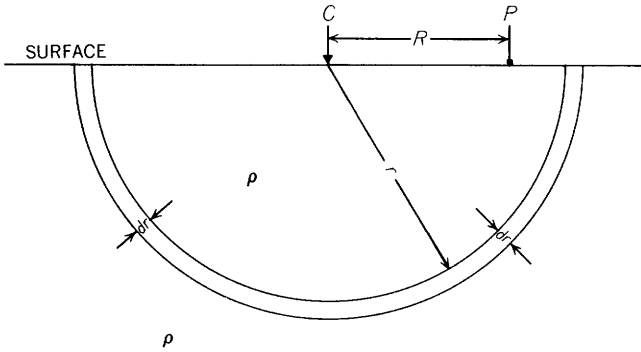
FIGURE 1.—Diagram showing a point source of current placed on the surface of the earth and the various symbols used in the problem.

faces are concentric hemispheres with their centers at C. Consider two of these equipotential surfaces, the first of radius r and the second of infinitesimally greater radius $r+dr$. All the current I must flow outward through the shell bounded by these equipotential lines. Because this shell is very thin, we may assume the flow of current through the shell to be linear and apply Ohm's law in its usual simple form for linear conductors. Thus, the potential drop dU from the inner surface to the outer surface of the shell is

$$dU = I\left(\frac{\rho dr}{2\pi r^2}\right),\tag{1}$$

where dr is the length and $2\pi r^2$ is the mean cross-sectional area of our linear conductor. In order to get the potential at P with respect to that at infinity, we integrate equation 1 from R to infinity:

$$U = \int_R^\infty dU = \frac{I\rho}{2\pi}\int_R^\infty \frac{dr}{r^2} = \frac{I\rho}{2\pi R}.\tag{2}$$

In the practical units that are being used, the potential U is in volts. Equation 2 is the basic equation of this whole study.

The assumption of a point electrode in electrical prospecting is at best only approximate. Therefore, it is useful to realize to what extent this approximation is valid. The following section represents an analysis of this problem.

CURRENT FROM A DRIVEN STAKE

The usual form of current electrode is a steel stake which is driven into the ground to a depth of 18 to 24 inches. Usually the stake is cylindrical in shape except for a point at the end. Muskat (1932) developed a theory which would be applicable to a truly cylindrical stake, but we feel that his theory is overly complicated for presentation here. The usual approximation for the stake is a point electrode. An approximation, much more satisfactory than the point electrode, would be a vertical-line electrode of the proper length. We

will, therefore, develop an expression for the potential due to a vertical-line electrode in a homogeneous earth and compare this expression with the corresponding one for a point electrode in order to determine under what circumstances the corresponding approximation is justified. In addition, we will use this opportunity to illustrate an important concept in the solution of potential problems—namely, the use of symmetry to facilitate mathematical treatment.

Consider an infinite medium of resistivity ρ in which we establish a rectangular coordinate system with the positive z-axis directed downward. We then place an electrode in the form of a line extending along the z-axis from $z=+b$ to $z=-b$ (fig. 2), through which a
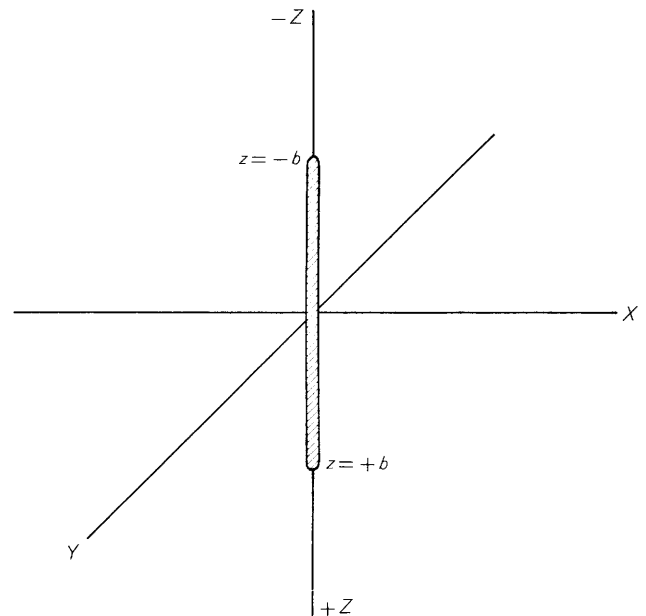
FIGURE 2.—Vertical line electrode of length $2b$ extending along the z-axis.

current $2I$ passes into the medium. We further assume that the same fraction of current emanates from each element of the line electrode—that is, that there is a constant flux density along the electrode. We will discuss and justify this assumption later.

Considering each element of length of the electrode to be a point source of current of strength Idz/b, we are now able to use equation 2, modified by changing $2\pi R$ in the denominator to $4\pi R$ which is necessary when one is considering an infinite instead of a semi-infinite medium. The total potential at some point P is then the sum of the potentials at P due to each of the infinitesimal elements of the line source of current. We note that R is a variable given by $R = \sqrt{x^2 + y^2 + (z_0 - z)^2}$. The variables without subscripts refer to the coordinates of the point P, and z_0

refers to the coordinate of a given element of the source. Then,

$$U = \frac{I\rho}{4b\pi} \int_{-b}^{b} \frac{dz_0}{\sqrt{x^2 + y^2 + (z_0 - z)^2}}$$

or, after integrating,

$$U = \frac{I\rho}{4b\pi} \ln \frac{\sqrt{x^2 + y^2 + (b-z)^2} + (b-z)}{\sqrt{x^2 + y^2 + (b+z)^2} - (b+z)}. \quad (3)$$

From symmetry considerations it can easily be seen that no current flows across the xy-plane; all the current flowing out of the lower half of the line source remains in the lower half-space. Therefore, we do not disturb the current field in the lower half-space if we discard the upper half of the line source and consider the upper half-space to be air with infinite resistivity. In this case, a current I flows from the electrode into the ground.

It can be shown that the equipotential surfaces described by equation 3 are confocal prolate ellipsoids of revolution. The z-axis is the axis of revolution and the points $z=+b$ and $z=-b$ are the foci of the ellipsoids. Let us consider the ellipsoid on whose surface the potential is 1,000 volts. If we choose a stake whose surface coincides with the given ellipsoid and we maintain the potential of that stake at 1,000 volts, I amperes will flow into the ground and the potential at all points in the ground will remain unchanged. Therefore, the assumption of a line electrode is valid to the extent that a stake has the shape of a prolate ellipsoid of revolution. Actually, the shape of a pointed stake is reasonably close to that of a hemi-ellipsoid. In any event, the assumption of a line electrode is considerably better than that of a point electrode for computing potentials in the vicinity of the electrode. In this connection it is noted that a given line of finite length is the limiting case of one family of confocal prolate spheroids.

In order to compare the field of a vertical-line electrode with that of a point electrode, we consider only two principal directions, a horizontal direction along the x-axis—for example, radially out from the electrode along the xy-plane—and the vertical direction along the z-axis. Table 1 contains the data from which we draw our conclusions.

Most electrical prospecting is concerned with the potential difference between a given pair of points. Such a potential difference is the integral of the gradient between these two points. Therefore, although the potential is given in table 1, it is the gradient upon which attention should be focused.

The values of the potential and the gradient, for which x is specified, are for any horizontal radial line

TABLE 1.—*Comparison of the electric-current fields due to a vertical-line electrode of unit length (b=1) and a point electrode at the origin*

[If the total current I passing into the ground is 2π amperes, if the resistivity of the medium is 1 ohm-meter, and if the stake is 1 meter long, the potentials listed are in volts and the gradients listed are in volts per meter. Error in assuming point electrode, when line electrode is actually used, is expressed as a percentage of values for the line electrode]

Axis—		Vertical-line electrode		Point electrode		Error in assuming point electrode	
x	z	Potential (volts)	Potential gradient (volts per meter)	Potential (volts)	Potential gradient (volts per meter)	Potential (percent)	Potential gradient (percent)
On surface							
1	0	0.8814	0.7071	1.0000	1.0000	13.46	41.42
2	0	.4812	.2236	.5000	.2500	3.91	11.81
3	0	.3275	.1054	.3333	.1111	1.77	5.41
4	0	.2475	.0606	.2500	.0625	1.01	3.13
5	0	.1987	.0392	.2000	.0400	.65	2.04
6	0	.1659	.0274	.1667	.0278	.48	1.46
7	0	.1247	.0155	.1250	.0156	.24	.65
10	0	.0998	.00995	.1000	.0100	.20	.51
Below surface							
0	2	0.5493	0.3333	0.5000	0.2500	8.98	24.99
0	3	.3466	.1250	.3333	.1111	3.84	11.12
0	4	.2554	.0667	.2500	.0625	2.12	6.30
0	5	.2028	.0417	.2000	.0400	1.38	4.08
0	6	.1683	.0286	.1667	.0278	.95	2.80
0	8	.1257	.0159	.1250	.0156	.56	1.92
0	10	.1003	.0101	.1000	.0100	.30	.99
0	12	.0835	.00699	.0833	.00694	.24	.71

on the surface of the earth. By examining the potential, we would be led to believe that the field of a driven stake is approximated by the field of a point source (within one-half of 1 percent taken as a standard) at a horizontal distance from the stake equal to six times the length of the stake. However, when we consider the gradient, as we should do when using potential differences, we find that the field of the stake does not approach that of a point source except at horizontal distances from the stake of 10 times its length. On the other hand, we must go much farther than that in the vertical direction—values for which z is specified—before finding the same degree of approximation. This information should form a guiding background for those who wish to work with very small electrode separations or those who are examining geologic structures which are buried to a depth of the order of 10 times the depth to which the electrodes are driven.

In connection with the above discussion, we point out that the practice of balancing electrode resistances during resistivity measurements has no justification in theory. The important characteristic of electrode resistance is its distribution and not necessarily its magnitude. Regardless of the shape of the electrode and the manner in which the current enters the ground, there is some distance from the electrode beyond which the current can be assumed to be originating from a

point source. Since most of the theory of electrical prospecting is predicated on the assumption of a point source and a point sink, this theory is valid only in the regions far enough from the electrodes that the basic assumption is valid. Moreover, in the regions where the assumption is valid, the potential differences in isotropic media are dependent only on the geometry of the electrode configuration and the magnitude of the energizing current; the potential differences and consequently the apparent resistivities are completely independent of the magnitude and distribution of the resistances in the immediate vicinity of the electrodes. Small objects of very high resistivity in the immediate vicinity of the current electrode or poor stake contacts do necessitate greater voltages to be impressed to produce a sufficiently large energizing current; but once the required current is obtained, the current distribution in the region where the point-current-electrode assumption is valid is affected negligibly by these small irregularities adjacent to the current electrodes.

CURRENT SOURCE AND SINK ON THE SURFACE OF A HOMOGENEOUS EARTH

CURRENT LINES AND EQUIPOTENTIALS

In resistivity prospecting there must always be at least two current electrodes in contact with the earth, one as a source and the other as a sink. In order to understand even the minor complications of electrical prospecting, we must investigate the normal flow of current in a homogeneous isotropic earth. We will first study the pattern of the equipotentials, from which the current lines of flow can be obtained by drawing perpendiculars thereto; we will then study quantitatively the current flowing through the earth.

By using equation 2, assuming that the current I flows into the ground at C_1 and out at C_2, and by writing the distances from C_1 and C_2 in terms of the rectangular coordinates shown in figure 3, we find that the potential at any point $P(x, y, z)$ is given by

$$U = \frac{I\rho}{2\pi}\left\{\frac{1}{\left[\left(x-\frac{3a}{2}\right)^2+y^2+z^2\right]^{1/2}}-\frac{1}{\left[\left(x+\frac{3a}{2}\right)^2+y^2+z^2\right]^{1/2}}\right\} \quad (4)$$

or, more simply, by

$$U = \frac{I\rho}{2\pi}\left(\frac{1}{R_1}-\frac{1}{R_2}\right), \quad (5)$$

where R_1 and R_2 are the distances from each current stake, respectively, to the measuring point.

The equipotential surfaces are defined by equation 5 by making U equal to a constant and are surfaces of revolution of the fourth order about the line of electodes. The potential and current distribution in a vertical
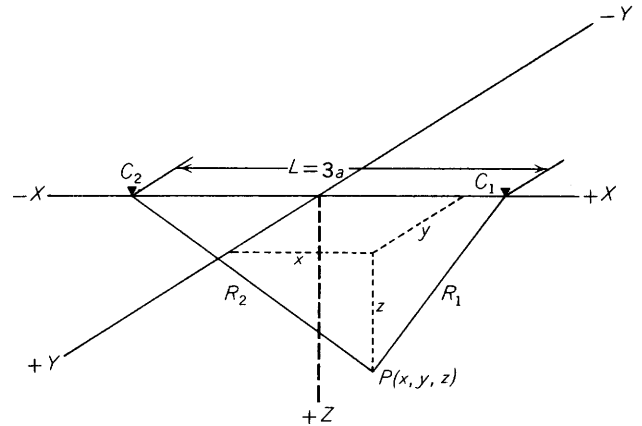
FIGURE 3.—Diagram showing source of current C_1 and sink C_2 on the surface of the earth, and conventions of coordinate system and symbols used.

plane passing through the line of electrodes is shown in figure 4. The potential and current distribution on the horizontal surface of the earth can be obtained by rotating this same diagram about the line of electrodes so that a complete pattern is obtained on both sides of the line of electrodes; the pattern shown in figure 4 represents half of the surface pattern that will result. The current lines of flow in figure 4 represent the surfaces of spindles each of which carry one-tenth of the total current I; the potential drop between successive equipotential lines is constant.

The values of the potential along the line of electrodes for a point source and sink on the surface of a homogeneous earth are shown in curve A, figure 5. Very rapid changes in potential occur near the electrodes; in the remaining broad central region, the potential is comparatively small and its slope is gentle and rather uniform (see fig. 5). The uniformity of the slope can be judged by comparison of the potential curve with the straight line which has been drawn tangent to that curve at its midpoint.

For comparison, the corresponding values around a single-point current electrode are shown in curve B of the same figure. For the two electrodes, the values of the potential are always less and the potential gradient greater, especially in the central region, than for the single electrode. At a distance of L (which equals the distance between C_1 and C_2) to the right of electrode C_1 and along the extension of the line of electrodes, the value of the potential with two electrodes present is exactly half the value of the potential with only the single electrode C_1 present.

DEPTH OF CURRENT PENETRATION

We will investigate the problem of the depth of current penetration in a homogeneous isotropic earth in terms of the distance L (which equals $3a$) between the
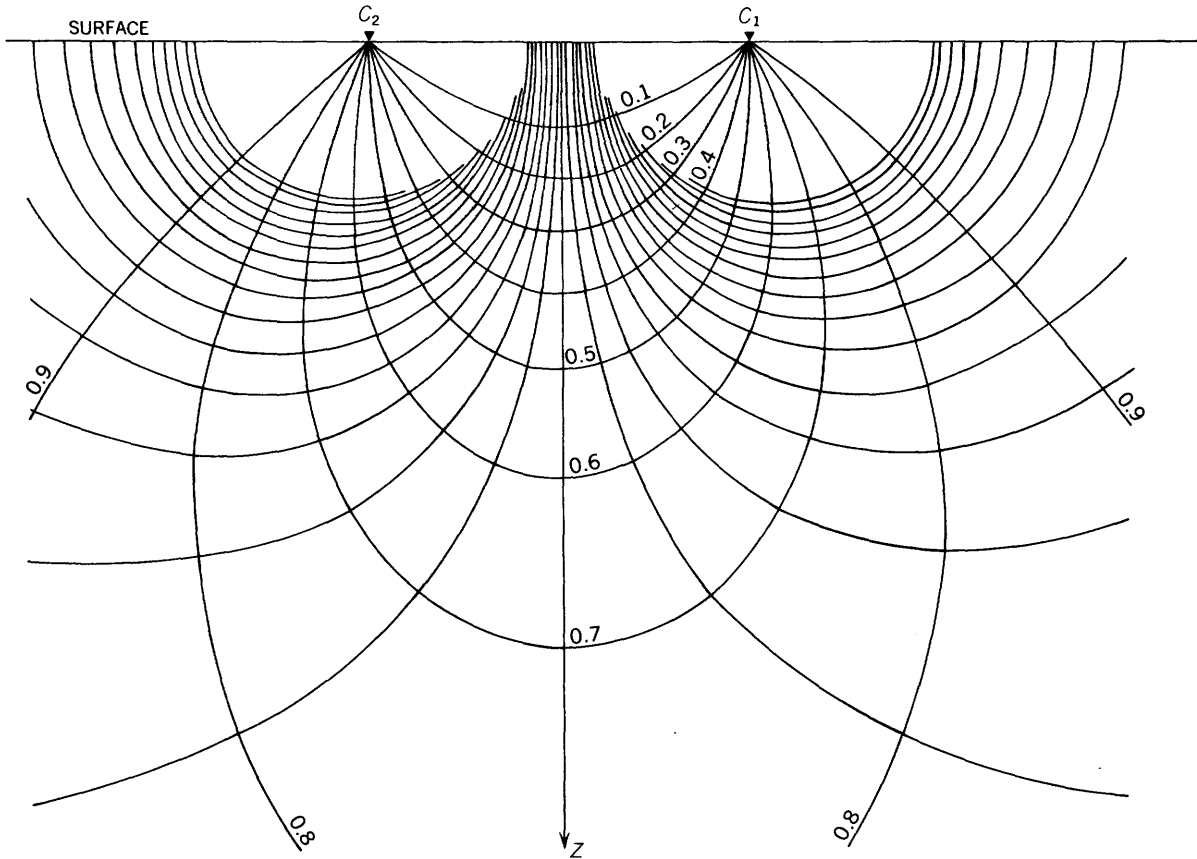
FIGURE 4.—Potential and current distribution in a vertical plane along the line of electrodes. Current lines of flow represent the surfaces of spindles each of which carries one-tenth of the total current. The potential drop between successive equipotential lines is constant. Adapted from Stefanesco (1929).

two current electrodes (fig. 3). The problem will be studied from two points of view: (1) the current density in various parts of the field is computed and (2) the total amount of current that penetrates certain regions of the earth is determined. In both, we note that current density is a vector quantity and that its x-component is given by

$$J_x = -\frac{1}{\rho} \frac{\partial U}{\partial x} \qquad (6)$$

where ρ is the resistivity of the medium and U is the electric potential. Since the components of a vector are scalars, the x-component of the total current density at a point may be found by adding algebraically the x-components of the current densities due to each of the electrodes taken separately.

Using the expression for the potential given in equation 4 and the conventions given in figure 3, it is seen that the x- and z-components of current density at point $P(x, y, z)$ are

$$J_x = \frac{I}{2\pi} \left\{ \frac{x-3a/2}{\left[\left(x-\frac{3a}{2}\right)^2+y^2+z^2\right]^{3/2}} - \frac{x+3a/2}{\left[\left(x+\frac{3a}{2}\right)^2+y^2+z^2\right]^{3/2}} \right\}, \qquad (7)$$

$$J_z = \frac{Iz}{2\pi} \left\{ \frac{1}{\left[\left(x-\frac{3a}{2}\right)^2+y^2+z^2\right]^{3/2}} - \frac{1}{\left[\left(x+\frac{3a}{2}\right)^2+y^2+z^2\right]^{3/2}} \right\}. \qquad (8)$$

It is fundamental that the current densities in homogeneous ground in the problem are independent of the true resistivity of the ground, although, as has already been pointed out, the potential does depend on the true resistivity of the ground.

Figure 6 shows the values of the x-component of the current density (J_x) along two vertical lines, one passing through the positive current electrode C_1 (curve A), and the other along the z-axis midway between C_1 and C_2 (curve B). For this example, the current I is one ampere and the current electrodes are separated a distance $L=30$ meters. Current densities for other values of the parameters may be obtained easily from these curves, together with a consideration of the manner in which the parameters enter equations 7 and 8. For example, if L were made 60 meters, the scale on the abscissa of figure 6 would need to be doubled also, and the scale on the ordinate would need to be reduced by a factor of 4. The x-component of the current density.
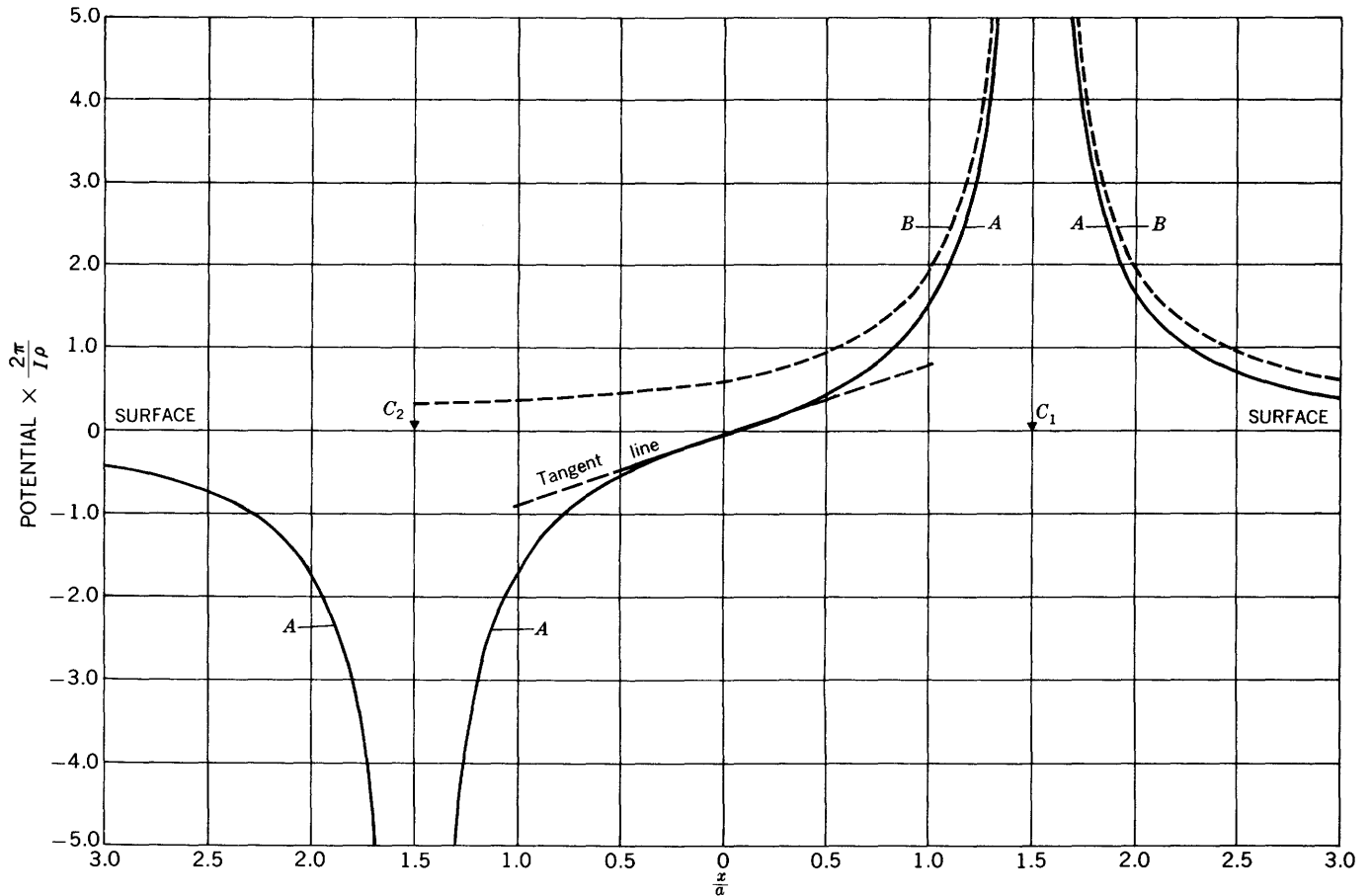
FIGURE 5.—Diagram showing comparison of values of potential (*A*) about a point source C_1 and sink C_2 on the surface of a homogeneous earth and (*B*) about a single point electrode C_1, with C_2 removed to infinity.

J_z, at the surface along the *y*-axis for any specific value of *y* is equal to the J_x value of the same value of *z* given in curve *B* (fig. 6); this fact results from symmetry of the lines of current flow about the line of electrodes C_1C_2. The current density J_x at any point along the *z*-axis midway between C_1 and C_2 can be shown to be $J_x = I_0 \sin^3 \phi$, where ϕ is half the angle subtended by the line of electrodes at the point. I_0 equals $-4I/(\pi L^2)$ and is the current density at the surface midway between C_1 and C_2; and L is the distance between C_1 and C_2.

For comparison purposes the *z*-component of the current density along the vertical line through C_1 (curve *C*, fig. 6) and the *x*-component of the current density on the surface along the horizontal *x*-axis (curve *D*, fig. 6) are shown; for a depth (curve C') or distance (curve D') less than 10 meters only, a change in scale of plotting the ordinate value (see inset) is used for these two curves to facilitate the plotting and comparison. The *z*-component of the current density either along the surface of the ground in the *xy*-plane or at depth at any point in the *yz*-plane is obviously zero.

It should be emphasized that the current densities in most of the region under investigation are very small. This fact must be borne in mind when one considers the theory of electrical prospecting.

The total amount of current which penetrates the assumed homogeneous earth to a given depth can best be studied by determining how much total current passes at various depths through an imaginary vertical plane midway between current electrodes C_1 and C_2 and perpendicular to the line of electrodes. This imaginary vertical plane coincides with the *yz*-plane (fig. 3) and extends to infinity in the $+y$, $-y$, and $+z$ directions. On this plane, $x=0$, and equation 7 becomes

$$J_x]_{x=0} = -\frac{12Ia}{\pi[9a^2+4r^2]^{3/2}} = -\frac{4IL}{\pi[L^2+4r^2]^{3/2}} \qquad (9)$$

where $r = \sqrt{y^2+z^2}$ and is the distance to a given point from the midpoint of the line of electrodes. The negative sign in equation 9 merely indicates that the current flows from right to left (from C_1 to C_2) with the convention used. To get the total current I_1 flowing above a given depth z_1, we integrate the current density over
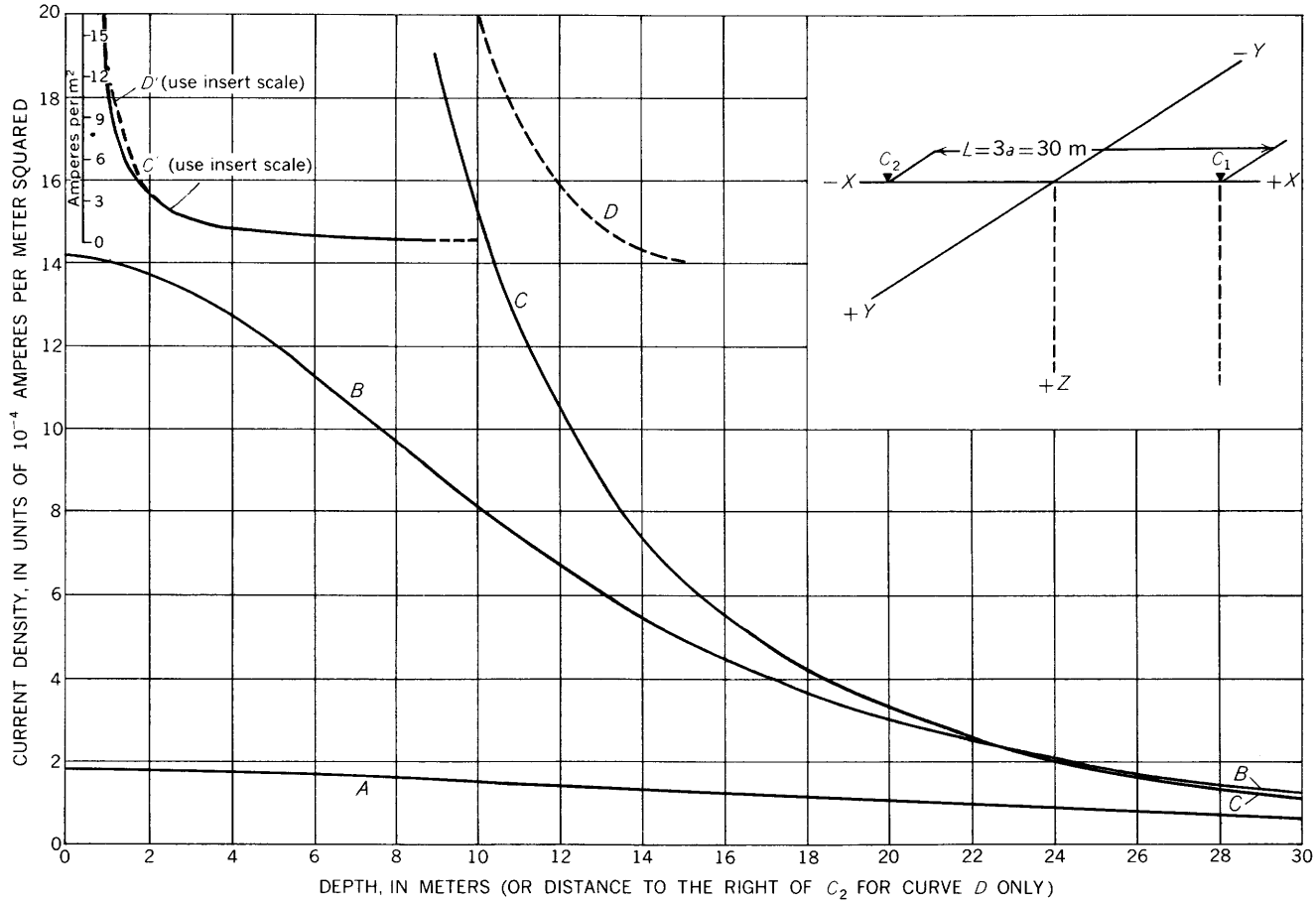
FIGURE 6.—Current densities along various vertical and horizontal lines. Curve A represents J_x on the vertical line through C_1; curve B represents J_x on the vertical line (z-axis) midway between current electrodes C_1 and C_2; curve C represents J_z on the vertical line through C_1; curve D represents J_x on the horizontal line (x-axis). Current I flowing between C_1 and C_2 is 1 amp; $L=30$ m.

the given vertical plane down to that certain depth:

$$i_1 = 2 \int_0^{z_1} \int_0^{\infty} J_x \Big]_{x=0} dy\,dz.$$

By carrying out the integration and expressing the total current I_1 down to depth z_1 as a fraction of the total current I passing between the electrodes, we obtain:

$$\frac{I_1}{I} = -\tan^{-1}\left(\frac{2z_1}{L}\right). \tag{10}$$

A plot of this relationship is given on curve A in figure 7. An analogous plot of the solution of this problem was first published, in slightly different form, by Weaver (1928).

The total amount of current I_1 that flows across this same vertical yz-plane within a radial distance r_1 of the midpoint of the line of electrodes can be obtained in the same manner, except that the integration is carried out in terms of r:

$$I_1 = \int_0^{r_1} J_x \Big]_{x=0} dr.$$

By carrying out the integration and expressing the total current I_1 within a radial distance r_1 as a fraction of the total current passing between the electrodes, we obtain:

$$\frac{I_1}{I} = 1 - \frac{3a/2}{\sqrt{\frac{9a^2}{4} + r_1^2}} = 1 - \frac{L/2}{\sqrt{\left(\frac{L}{2}\right)^2 + r_1^2}}. \tag{11}$$

A plot of this relationship is given on figure 7, curve B.

Relative to an imaginary horizontal plane, only half of the current penetrates to a depth greater than half of the distance between the current electrodes. Thirty-seven percent of the total current passes completely above a plane at a depth equal to the electrode separation a, and 70.5 percent passes above a plane at a depth equal to the distance between the current electrodes—that is, three times the electrode separation.

Within an imaginary horizontal cylinder whose axis coincides with the line of electrodes, exactly two-fifths of the total current remains within a cylinder whose radius is equal to two-thirds the distance between the current electrodes. Thus, any small inhomogeneity that lies near the line of electrodes can easily obscure
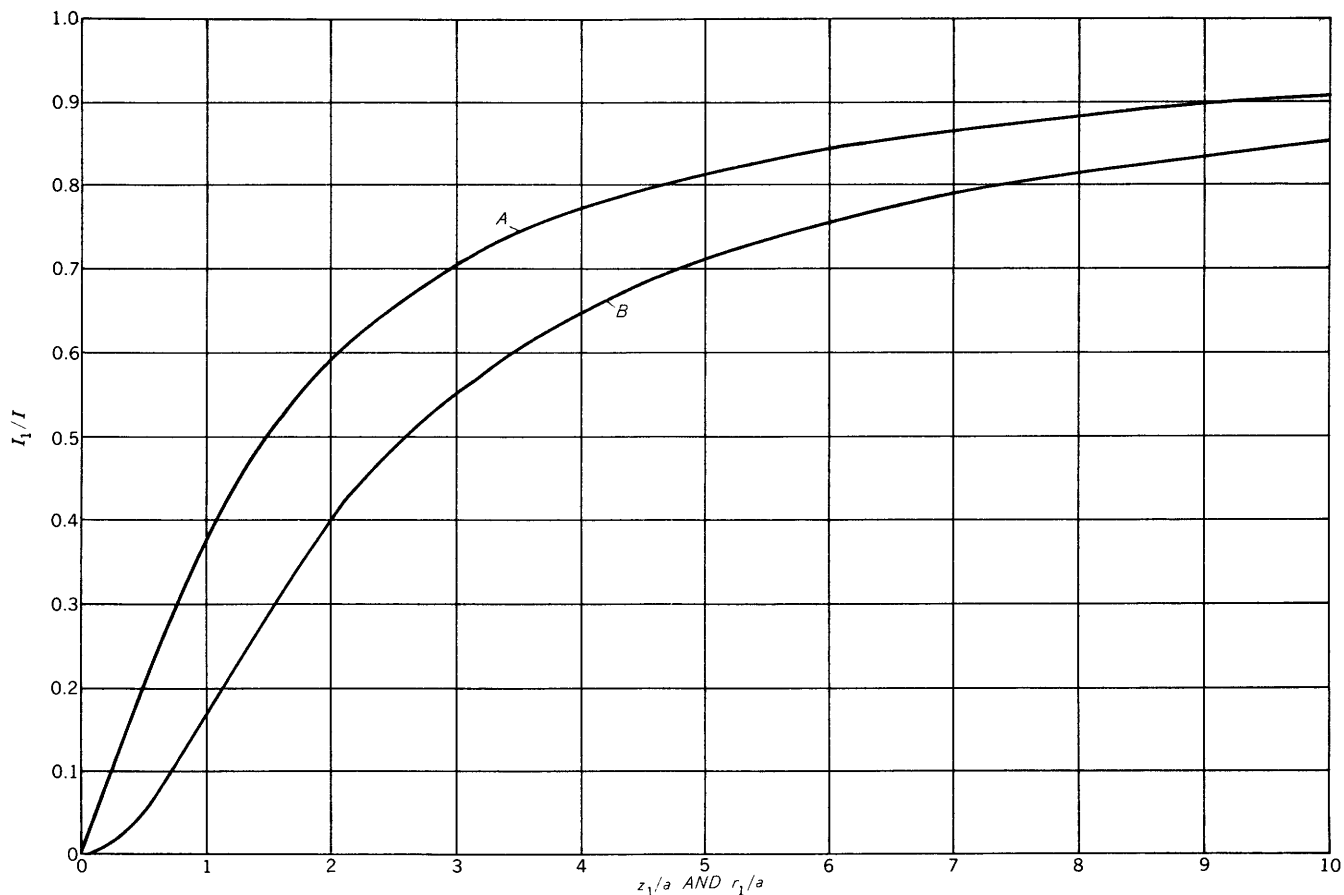
FIGURE 7.—Fraction of total current I which passes completely (A) above a horizontal plane of depth z_1, and (B) within a horizontal cylinder whose axis coincides with the line of electrodes and whose radius is r_1. Horizontal distance between current electrodes, $L=3a$.

the effect of a comparatively large inhomogeneity far removed from the configuration.

For two parallel infinitely long current line electrodes located at the surface of an assumed homogeneous earth, the fractional amount of current I_1/I that passes completely above a plane at depth z_1 is also given by equation 10 and curve A in figure 7, provided that here I_1 represents the current crossing a vertical strip of the yz-plane 1 meter wide extending from the surface to a depth of z_1 meters, and the line electrodes are parallel to and equidistant from the y-axis (Peters and Bardeen, 1930, p. 26). Although this particular analogy exists, the patterns of the equipotentials and current lines of flow for the line-electrode problem differ from that of the point-electrode problem and is treated further in the next section.

UNIFORM FIELD

When the two current electrodes are widely separated, the field in the region midway between the electrodes is effectively uniform—that is, the current lines are nearly parallel and uniform in density. It follows

that the equipotential lines here are also nearly parallel and uniformly spaced. The degree to which the uniformity extends in depth in this central region is evidenced in curve B in figure 6, which shows that the current density decreases only about 5 percent below the midpoint surface value at a depth equal to one-tenth the distance between the current electrodes. The same values apply along the y-axis at the surface of the earth.

The departure of the nonhomogeneous field due to two electrodes at the surface of the earth from a truly homogeneous field has been computed by Huber (1949). He charted the values of the fractional difference $\delta=(U-U_0)/U_0$ through a vertical cross section taken along the line of electrodes, where U is the value of the true potential and U_0 is the value of the potential with the assumption of a homogeneous field (see fig. 8). He showed that at the surface, where the potential measurements are ordinarily taken, the charted error in assuming a homogeneous field rather than the true field is about 10 percent and 20 percent, respectively, at distances of about $l/3$ and $2l/5$ from

the midpoint between electrodes, where l is the distance from the midpoint to either of the two current electrodes.

NATURAL EARTH CURRENTS

The electrical prospector must always contend with extraneous electric currents, which consist of telluric currents, natural local currents, and currents derived from industrial sources. All are detected by observation of the potential difference between two electrodes embedded in the earth.

Telluric currents flow in fairly uniform sheets over large areas; their exact cause is still in doubt. Telluric currents change continually in magnitude and direction with component periods varying from less than a second to many days. Qualitatively, these variations are related to the corresponding variations in the geomagnetic field. The principal variation, which is daily, has a normal maximum amplitude of a few tens of millivolts per kilometer. Disturbances, such as those due to magnetic storms, display amplitudes as much as 30 times the normal in middle latitudes and 150 times normal in high latitudes. Extremely large earth currents flow during thunderstorms, but they are more random and more localized than normal telluric currents.

Steady local currents, of much larger magnitude than telluric currents, are produced by strong electro-chemical reactions in the earth—for example, oxidation of that part of a sulfide deposit lying above the water table, in contrast to the inactive part lying below the water table, causes current to flow along the surface of the earth toward the zone of oxidation. Potential differences above 500 millivolts in 100 feet have been observed. The same type of differential electrochemical reaction in the corrosion of buried pipes causes the flow of currents that may be used to detect the centers of corrosion.

Artificial direct currents of large but variable magnitude are caused by the ground returns of electrical installation as, for example, electric railroads. Alternating currents of comparatively low and unpredictable magnitude are associated with power lines; frequencies of sixty cycles per second, and its odd harmonics, predominate.

Several excellent electrical-prospecting techniques use these natural earth currents. However, since this paper is concerned only with resistivity interpretation, we are interested in natural currents only insofar as they influence resistivity measurements. It is obvious that natural earth currents will interfere with resistivity prospecting if they are great enough. If the natural currents flow in the same direction as the applied current, the observed potential difference is too high; if the natural currents oppose the applied current, the observed potential difference is too low.
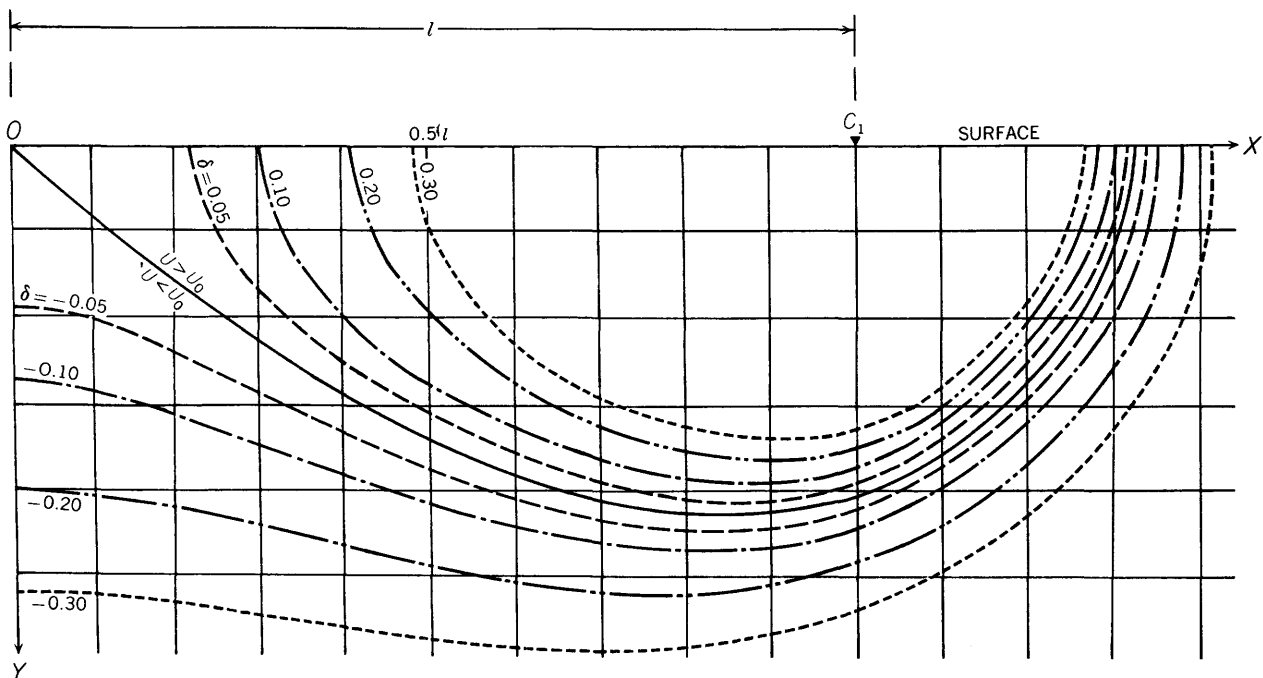
FIGURE 8.—Diagram showing values of fractional difference $\delta = (U - U_0)/U_0$ through a vertical cross section taken along the line of electrodes, where U is the value of the true potential and U_0 is the value of the potential of a homogeneous field. Adapted from Huber (1949) by permission of Springer-Verlag, Vienna, Austria.

There are two commonly used ways to overcome this difficulty. The most obvious way is to take two readings of the potential difference: first, with the current flowing in one direction and then with the current flowing in the opposite direction. The average of these two values is in principle the true value. If the natural currents or the spontaneous electrode potentials are varying with periods which are comparable in magnitude to the time required for a complete set of measurements, this technique is unsatisfactory. For example, in the far north, earth currents associated with the aurora borealis sometimes make the application of this method practically impossible. Similar difficulties are often encountered near facilities that use direct current, such as mines using direct-current tramming operations. If, however, the variations are of relatively high frequency or if the earth currents are comparatively constant, this technique works very well.

The second and surer method of eliminating the effect of natural earth currents is to use commutated direct current instead of continuous direct current. The potential-measuring circuit is also commutated, with provisions for an additional gap between commutator segments so that under normal field conditions the potential electrodes are connected only after the current transients have ceased; also the potential circuit is opened before the current circuit. Measurements are then made just as they are when continuous direct current is used. In effect, this method carries out instrumentally the averaging process which the previous method requires to be done manually. This double-commutator technique is known in the literature as the Gish-Rooney method. This method fails if the earth currents have essentially the frequency as the commutating rate used. The method will also lead to errors if the capacity of the rocks in the area is sufficiently large so that the current transients do not cease before the potential electrodes are connected.

EQUIPOTENTIAL METHOD

The earliest attempts at prospecting with applied electric currents were made by studying the potential distribution in the ground (Schlumberger, 1920b). Several variations of this method are available. When two driven stakes are used for current electrodes, one can measure the potential along a line connecting the electrodes in order to prepare a potential profile. It has been shown that in homogeneous ground, such a profile exhibits very rapid changes in potential within a distance from each stake equal to about one-tenth of the distance between the electrodes; in the remaining broad central region, the potential is comparatively small and its slope is very gentle (see fig. 5).

If the electrodes are separated by a comparatively great distance, the field in the vicinity of one of the electrodes is little affected by the second electrode or by the environment of the second electrode. Therefore, except for the restrictions due to the electrode being a stake, the field in the immediate vicinity of an electrode can be treated as though the electrode were a single point source acting alone. The nature of this field in a homogeneous earth was discussed on pages 30 to 34. It was shown that the equipotential surfaces all would be hemispheres with their centers at the point electrode. Thus, the equipotential lines at the surface of the earth would be concentric circles. The practice is to map these equipotential lines, either by measuring potentials at the points of a grid and contouring, or by actually tracing equipotential lines using some sort of a null measurement. Any inhomogeneities in the vicinity of the electrode are indicated as distortions in the concentric circles.

It has been pointed out that when the current electrodes are widely separated, the field in the region midway between the electrodes is effectively uniform. It is common practice to map equipotential lines in this region where the field is comparatively uniform, in search for conditions which might upset that uniformity.

Another system, which provides parallel equipotential lines in homogeneous ground, uses as electrodes two long parallel wires grounded at frequent intervals or continuously along their lengths. The field in this system differs from the "inverse square" fields of a point source in that it gives rise to a "logarithmic" potential if the electrodes are assumed to be infinitely long. As above, it is customary to map the equipotential lines between the line electrodes. The assumption of infinitely long electrodes is valid, except near the ends of the current line electrodes, if the line electrodes are long with respect to their separation.

Where the earth consists of zones of different resistivities instead of being homogeneous, the potential distribution is affected. The theoretical calculations of this new distribution, for certain special cases when point electrodes are assumed, are a large part of the remaining sections of this paper. However, such calculations for the most part are usually prohibitively difficult. In the present section, we restrict ourselves to general statements.

Suppose, for example, that in the region of otherwise essentially uniform current density where the equipotential lines are being mapped, there is buried a mass of material which is more conducting than the surrounding material. We can understand better what happens in this example if we assume that the foreign body is perfectly conducting. The current lines tend to concentrate through the buried body, which is raised

to some constant potential throughout. In the vicinity of the foreign body all equipotential surfaces except one pass around the body and are more closely spaced than normal in the adjacent country rock where the current enters and leaves the body. In other regions, where current lines are nearly parallel to the boundaries of the body, the equipotential lines are more sparsely disposed than normal. In regions far from the foreign body, the disturbance diminishes and becomes negligible.

If the foreign body is a better conductor than the country rock but is not perfectly conducting, the same generalizations apply except that there is some potential drop through the body. If the foreign body is less conducting than the country rock, a similar set of rules are established, based on the fact that current is directed away from the disturbing body. It is found, however, that for the same geometry and the same resistivity contrast there is a greater anomaly percentagewise where the foreign body is more conducting than the country rock than where it is more insulating.

The interpretation of equipotential maps and potential profiles is largely empirical. Successful interpretation depends upon a sound knowledge of potential fields and previous experience on the part of the interpreter, as well as upon a careful consideration of the general geological features of the area being studied.

The disposition of the equipotential lines is much less sensitive to disturbances due to foreign bodies in the earth than is the potential gradient. Therefore, the potential profile enjoys one advantage over the equipotential map in that changes in the potential gradient—that is, changes in slope of the potential profile curve—are more evident on the potential profile than on the equipotential map. Since the gradient—or the potential difference, which are related to the gradient—is the principal ingredient in the measurement of apparent resistivity, the resistivity techniques are in general superior to the simple potential studies discussed above. Only in a few special mining problems are the potential techniques superior because of the greater speed which they offer.

RESISTIVITY METHOD

CONCEPT OF APPARENT RESISTIVITY

In any prospecting method it is useful and sometimes imperative that some index be devised to describe the data taken. The most important characteristic of such an index is that it should normalize the data and thus facilitate the comparison of data which may have been taken in widely separated areas and under a wide variety of conditions. The index most commonly used in electrical prospecting is called "apparent resistivity."

The basic principle of defining an apparent resistivity is as follows. For any given arrangement of electrodes,

we consider first the electric field that would be expected with the given configuration in homogeneous ground. We note that, even for a given current and in spite of the homogeneous ground, the quantity we wish to measure varies greatly from one part of the field to another. This quantity may be either potential gradient or the potential itself measured with respect to the potential at some fixed point. So we proceed to derive a mathematical expression for this quantity—potential or potential gradient—in terms of the current, the actual resistivity of the assumed uniform medium, and the geometry of the electrode configuration. Then we solve this equation for the resistivity in terms of the potential or potential gradient, the applied current, and the interelectrode distances. This particular combination of these quantities then becomes the desired index— apparent resistivity—when the measurements are made over heterogeneous ground. The apparent resistivity is, therefore, a function not only of the region in which the measurements are made but also of the geometry of the electrode configuration used.

The most important part of this definition is the adjective "apparent." The apparent resistivity usually falls within the range of true resistivities of the materials within the ground over which measurements are made. Due to anomalous "pseudofocusing" effects, however, the apparent resistivity sometimes rises above or falls below the true resistivities of all of the materials present. This effect can readily be seen in many of the albums of theoretical apparent-resistivity curves to be presented later.

In order to illustrate the above abstract discussion, we refer to figure 9 in which a generalized configuration of electrodes is shown. We assume that the ground is homogeneous with a true resistivity of ρ ohm-meters and that a potential difference of V volts exists between the potential electrodes P_1 and P_2 when I amperes flow between the current electrodes C_1 and C_2. The interelectrode distances are as shown in the diagram and are expressed in meters. V is readily calculated
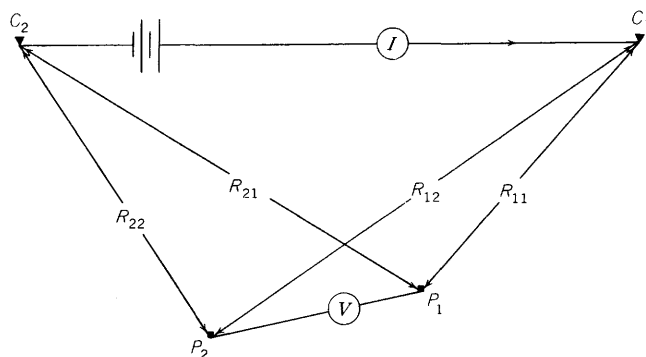
FIGURE 9.—A general configuration of electrodes. Plan view, with all electrodes at the surface of the earth.

by means of equation 2. The technique is to calculate the potential at P_1 due to both C_1 and C_2 taken separately, and then to add these two potentials to get the total. The same process is applied at P_2. The desired potential difference is then obtained by subtracting the second value from the first. This procedure is known as the "method of superposition" and will be used in all the more complex numerical cases which follow. Remembering that the current at C_2 is negative, we have:

$$V = \frac{I\rho}{2\pi} F(R\text{'s}), \qquad (12)$$

where $F(R\text{'s})$ is a simple function of the interelectrode distances. This function was designated the "form factor" by Roman (1951, p. 174).

Whether the earth is homogeneous or heterogeneous, we are still able to make a measurement of the potential difference. Moreover, V, I, and the R's may always be related in this manner if some constant, which has the dimensions of resistivity, is introduced where ρ appears in equation 12. As this new constant or index for inhomogeneous earth is not related in a simple manner to the actual resistivities present, but has the dimensions of resistivity, we choose to call it the apparent resistivity. Therefore, solving equation 12 for ρ and appending the subscript "a" to denote its new "apparent" character, we get for the apparent resistivity:

$$\rho_a = 2\pi \frac{V}{I} \Big/ F(R\text{'s}). \qquad (13)$$

This is one of the fundamental equations of resistivity prospecting. For several different configurations in which potential differences V are measured in the field, equations of this form are used to compute the apparent resistivity, even though it is realized that the ground being surveyed is heterogeneous. The observed field curve is then compared with theoretical-resistivity curves derived from this same type of equation.

Because the potential difference V is merely the line integral of the potential gradient from one electrode to the other, the apparent resistivity ρ_a is in a sense a function of the average gradient between the potential electrodes. Because this averaging process tends to subdue the anomalous values of the gradient that indicate abnormal geologic conditions, the best configuration is the one with the shortest distance between potential electrodes, other things being equal. This point will be illustrated below in the descriptions of the common electrode configurations. This particular advantage of the shortest distance between potential electrodes must be compromised with the disadvantage arising from the fact that the smaller the potential measuring base, the smaller and more difficult to measure is the potential difference.

If the same current I is passed between P_1 and P_2 (fig. 9), the potential difference between C_1 and C_2 is identical to that previously obtained between P_1 and P_2. Hence, the apparent resistivity is unchanged by this interchange of electrodes. Strange as the above statement may seem at first, this "principle of reciprocity" can be proven rigorously for any electrode configuration, even when the ground is heterogeneous. The only necessary assumption is that Ohm's law in its three-dimensional form applies to the flow of current in the earth.[2] Not only is the principle very useful in simplifying computations of theoretical-resistivity data, but it also can serve a useful purpose in planning a resistivity survey. To show the solid theoretical foundation of the theorem of reciprocity, as well as its possible limitations in electrical field work, we summarize briefly Wenner's analysis of this important topic.

Wenner (1912, p. 563) stated the theorem of reciprocity as follows:

In any conductor or system of conductors having four terminals 1, 2, 3, and 4 selected in any way, the drop in potential from 1 to 2 caused by a current entering at 3 and leaving at 4 is equal to the drop in potential from 3 to 4 caused by an equal current entering at 1 and leaving at 2.

In 1847 Kirchoff had given this theorem for a network of linear conductors. In 1853 Helmholtz had developed the theorem theoretically for an isotropic and homogeneous nonlinear conductor. Helmholtz had also considered the case of a conductor having two parts of different conductivities, and had tested the relation experimentally on a carbon cylinder 3.5 inches long and 2 inches in diameter; in this work electrical connections were made by means of four small quantities of mercury held in place by paper rings, and the currents compared by reading the deflections of a galvanometer. Rosen (1887) extended the proof of this theorem to include the case of nonhomogeneous and nonisotropic conductors. Searle (1911) gave two proofs of the theorem, one by Heaviside and one by Bromrich, both of which are somewhat similar to that given by Rosen (Wenner, 1912, p. 564). Wenner (1912) extended the theorem to the case of an alternating current in both isotropic and nonisotropic conductors. He emphasized, however, that the theorem of reciprocity has limitations: (1) the theorem assumes that the conductor is free from sources of current, such as thermoelectromotive forces, the Hall, and similar effects; (2) it assumes that in the conductor

there are at least three axes in each element of volume along which the current flows parallel to the potential gradient, and

---

[2] Some workers (Lee, 1939b) have suggested that under certain circumstances the flow of current in the ground is nonlinear and does not obey Ohm's law. If they are correct, the principle of reciprocity would not hold under the same circumstances. We suggest that one direct test of the nonlinearity theory would be to test rigorously the principle of reciprocity under a great variety of geologic conditions.

either that these three axes are mutually perpendicular, or the conductivities to current along each of the three axes are equal, or the conductivities to current along each of the two axes are equal and these two axes are both perpendicular to the third;

(3) in order that the theorem be applicable for alternating current, the total mutual inductance between the two circuits must be taken into consideration; and (4) the effect of electrostatic capacity has not been considered. Even to this day, these serious limitations of the theorem of reciprocity have apparently not been more clearly stated than by Wenner in 1912; and, indeed, his warning has often gone unheeded when adapting the theorem to actual field conditions, where the assumptions for its validity often do not hold.

ELECTRODE CONFIGURATIONS

With his background of measurements of the resistivity of blocks of metal with the four-electrode method, Wenner (1915) was the first to establish a system for the measurement of the resistivity of earth materials

A, Wenner configuration

B, Lee configuration

C, Asymmetrical Wenner configuration

D, Asymmetrical Lee configuration

E, Schlumberger configuration

F, Lögn configuration

FIGURE 10.—Various electrode configurations to be studied in this work.

in place. He proposed the use of four electrodes, spaced along a line and with equal interelectrode distances (fig. 10A). Current is passed into the earth through the two outer electrodes, designated C_1 and C_2, and the potential difference is measured between the two inner electrodes, designated P_1 and P_2. Throughout this study, we use the convention of letting the subscript "1" indicate the easternmost (or northernmost) electrode of a given pair, where geographical positions are involved. This convention has long been used in the field by the U.S. Geological Survey and others.

The electrode separation—the distance between adjacent electrodes—is designated "a" meters. Therefore, the interelectrode distances are $R_{11}=R_{22}=a$ and $R_{21}=R_{12}=2a$ (figs. 9 and 10A). Substituting these values into equation 13 leads at once to the conclusion that the apparent resistivity for the Wenner configuration is

$$\rho_a = 2\pi a \frac{V}{I}. \tag{14}$$

An electrode system used widely in the U.S. Geological Survey is the Lee "partitioning" configuration (fig. 10B). It differs from the Wenner configuration in that a third potential electrode P_0 is placed at the center of the configuration. Potential differences are measured between the pairs P_1-P_0 (that is, V_{10}) and P_0-P_2 (that is, V_{02}). Apparent resistivities are then derived on the basis of these potential differences, as was done in the case of the Wenner configuration. They are

$$\rho_1 = 4\pi a \frac{V_{10}}{I} \quad \text{and} \quad \rho_2 = 4\pi a \frac{V_{02}}{I}. \tag{15}$$

Thus ρ_1 is the apparent resistivity on the right-hand side of the partitioning plane—which is an imaginary vertical plane perpendicular to the line electrodes at P_0—and ρ_2 is the apparent resistivity on the left-hand side of this plane.

The reciprocity theorem is applied to the Wenner configuration by passing current through the two inner electrodes, at the same time measuring the potential difference between the two outer electrodes. If the reciprocity theorem is applied to the Lee configuration, all three central electrodes must be made current electrodes and they must be used in pairs corresponding to the potential-electrode pairs mentioned above; the potential difference would always be measured between the two outer electrodes.

In general, the Lee configuration holds a distinct advantage over the Wenner configuration. In particular, for detailed surveys over areas of special interest, the Lee configuration offers greater anomalies and closer definition of geologic boundaries. The reason for this
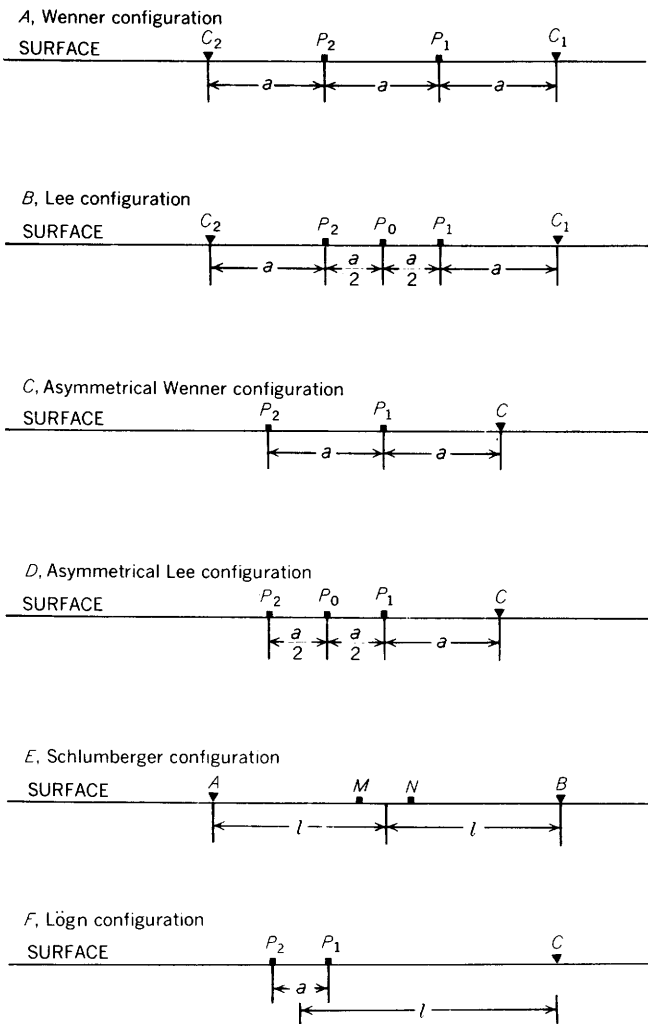
superiority lies in the fact that with the Lee configuration the potential difference is measured between two points which are only half as far apart as are the corresponding points in the Wenner configuration. The principle involved was discussed in the paragraph immediately following equation 13.

In order to reduce to a minimum the amount of work required in a field survey, let us inquire whether it is possible, in getting sufficiently large anomalies, to leave one of the current electrodes fixed at some point far removed from the other electrodes. Several asymmetrical configurations of this sort have been proposed but, since the principles involved are the same in all such cases, we will discuss only two. These particular configurations are chosen for study because theoretical resistivity curves can be readily constructed for them from data already computed for the electrode configurations described above.

If we remove C_2 to infinity in the Wenner configuration, we get what we shall call the asymmetrical Wenner configuration (fig. 10C). Other authors have referred to this system as the "unsymmetrical method" (Jakosky, 1950, p. 518) and the "double equidistant probe method" (Heiland, 1940, p. 710). In this case, the interelectrode distances are $R_{11}=a$, $R_{12}=2a$, and $R_{21}=R_{22}=\infty$. Therefore, the apparent resistivity is given by:

$$\rho_a = 4\pi a \frac{V}{I}.$$

The second asymmetrical configuration is similar to the first and is obtained by removing C_2 to infinity in the Lee configuration. We shall call this arrangement the asymmetrical Lee configuration (fig. 10D). Reference to this sort of arrangement has been made in the literature in connection with the potential-drop-ratio method (Heiland, 1940, p. 747) to be discussed later. For this configuration ρ_1 and ρ_2 are represented by different expressions:

$$\rho_1 = 6\pi a \frac{V_{10}}{I} \text{ and } \rho_2 = 12\pi a \frac{V_{02}}{I}.$$

In the theoretical work to follow in this paper, both of these asymmetrical configurations are studied to determine their relationships to the corresponding symmetrical configurations—that is, to study the effect of the second current electrode. One effect of the second current electrode can be observed by studying figure 5: for the same power expenditure or for the same current strength used, the measured potential differences in the region between the two electrodes are much greater (about double) when two current electrodes are included in the configuration than when only one is used. The larger these potential differences are, the easier it is to measure them accurately.

In the discussion of equipotential lines and maps we stated that changes in the gradient are much easier to recognize and to interpret than anomalies in the potential itself. At least two currently used electrode configurations take advantage of this fact: the Schlumberger configuration, and the "one-electrode configuration" (Lögn, 1954), which we here designate the Lögn configuration.

The Schlumberger electrode configuration (Chastenet de Géry and Kunetz, 1956; Compagnie Générale de Géophysique, 1955) consists of two current electrodes, A and B, and two potential electrodes, M and N, all along a straight line (fig. 10E). The potential electrodes are placed symmetrically about the midpoint between A and B and are kept sufficiently close together so that the electric field E between them can be considered constant. In practice, the separation between the potential electrodes M and N is always less than one-fifth the separation between the current electrodes A and B, and is usually kept less than one-tenth this separation. In computing the apparent resistivities from field measurements, the exact relative locations of the four electrodes is taken into account. The formula used for the apparent resistivity is

$$\rho_a = K \frac{\Delta V}{I},$$

where ΔV is the potential difference between the potential electrodes, and the geometrical term is

$$K = \frac{2\pi}{\left(\frac{1}{\overline{AM}} - \frac{1}{\overline{AN}}\right) - \left(\frac{1}{\overline{BM}} - \frac{1}{\overline{BN}}\right)}.$$

Because of symmetry, it is readily shown that

$$K = \frac{\pi l^2}{\overline{MN}},$$

where l is the distance from the midpoint of the configuration to either current electrode A or B. Thus the apparent resistivity is

$$\rho_a = \frac{\pi l^2}{\overline{MN}} \cdot \frac{\Delta V}{I}. \tag{16}$$

In order to construct theoretical curves for the Schlumberger configuration, the apparent resistivity is computed from the electric field E existing midway between the two current electrodes. Because $E = \Delta V / \overline{MN}$ approximately and is exactly the magnitude of the electric intensity—that is, the component of the gradient along the line of electrodes—at this midpoint when $\overline{MN}$ becomes infinitesimally small, another appropriate equation for the apparent resistivity,

which is obtained by making this substitution in equation 16, is

$$\rho_a = \pi l^2 \frac{E}{I}.$$

In order to obtain comparable data in the field, the potential electrodes would need to be infinitesimally close together. Discrepancies, arising from the fact that the actual distance $\overline{MN}$ is not infinitesimally small, usually do not exceed 2 or 3 percent, provided $\overline{MN}$ does not exceed $2l/5$ in accordance with the field techniques adopted by the Schlumberger organization in using this configuration.

The only vertical profiling field technique described in the literature to date for the Schlumberger configuration of electrodes is an expanding-type technique in which either the distance between the current electrodes or that between the potential electrodes is increased; but only a single set of electrodes is increased between successive measurements. This technique is in marked contrast with the regular vertical profiling technique with the Wenner or Lee configuration, in which both the potential and current electrodes are usually moved simultaneously, except in difficult areas. For the Schlumberger configuration, potential electrodes are moved only once out of every four or five changes of the current electrodes. Thus, for the five or six different values of $\overline{AB}$ in the interval from 100 to 800 meters, $\overline{MN}$ would have the fixed value of about 20 meters. In the following interval for $\overline{AB}$ up to 4,000 meters, $\overline{MN}$ would have a fixed value of about 100 meters. Both values of $\overline{MN}$ are usually used for some readings in the transition from one interval to the next.

The principal advantage in the Schlumberger technique is that the influence of local inhomogeneities close to the potential electrodes can be clearly located on the apparent-resistivity curves. These effects are shown by the differences between the results obtained with the same $\overline{AB}$ and different $\overline{MN}$'s. On the other hand, these local heterogeneities do not appreciably alter the shape of those arcs of the resistivity curves which have been obtained with a given $\overline{MN}$; they only displace the arcs as whole units. This fact often allows one to make a correction and to trace the diagram which would have been obtained in a laterally homogeneous earth. The Schlumberger configuration apparently sacrifices accuracy, which comes from measuring larger potential differences, for good definition, which comes from measuring potential differences between closely spaced potential electrodes.

The Lögn (1954) configuration, or "one-electrode configuration" (fig. 10F), which is the asymmetrical form of the Schlumberger configuration, also takes advantage of the principle of measuring changes in gradient. The potential difference ΔV is measured between two potential electrodes that are moved with constant electrode separation along lines passing through the single current electrode. The distance between the potential electrodes is assumed to be small in comparison with the distance from them to the single fixed current electrode. The second current electrode is placed effectively at infinity, and, therefore, has no effect on ΔV.

The expression for the apparent resistivity as measured with the Lögn configuration is easily obtained by doubling the corresponding expression for the Schlumberger configuration, to get

$$\rho_a = \frac{2\pi l^2}{a} \cdot \frac{\Delta V}{I}$$

where a is the distance between the potential electrodes.

HORIZONTAL AND VERTICAL PROFILING

Any of the above configurations can be used in one of two techniques, which are called horizontal profiling and vertical profiling. In horizontal profiling the electrode separation is maintained at some constant value and the whole configuration is moved along a traverse with readings being taken usually at regular intervals. A large part of the theoretical data to be presented later will be devoted to the results obtained in horizontal profiles over various types of geologic structures.

In vertical profiling, the center of the electrode configuration is fixed, and measurements are made for successively larger values of the electrode separation. Because a greater portion of the current penetrates deeper when the electrodes are moved farther apart, it is reasoned that the data also give more information about deeper geological conditions. A large number of papers have been published on how to determine the depth to horizontal beds by this method; some of these papers are reviewed in a later section. In addition, the effects of such structural features as dipping beds and vertical faults on vertical profiles are given in this paper.

The above two techniques result in a series of graphs. In horizontal profiling the apparent resistivity is plotted as a function of the position of the electrode configuration on the ground. Usually, the position of a given measurement, designated the "station," is taken as the point midway between the two potential electrodes. For the Lee configuration, this rule leads to a peculiarity because the position in the field, or station, is normally recorded as the point P_0 midway between the current electrodes. The plotted values of ρ_1 and ρ_2 are, therefore, offset from the recorded position of the station by a distance of $a/4$ to the east and west,

respectively, of P_0 for a traverse bearing east or by the same distance to the north and south, respectively, for a traverse bearing north. This method is designated the "offset method" of plotting horizontal profiles taken with the Lee configuration. In vertical profiling the apparent resistivity is plotted against electrode separation, and there are no special difficulties.

Yet a third representation of electrical prospecting data is found in the equiresistivity map, which is very useful as a reconnaissance tool. The resistivity is recorded on a map at each position where data are taken in horizontal profiling with some given electrode separation. The map is then contoured with lines along which the resistivity is a constant. The contour interval is chosen to fit the prevailing conditions. Although this map forms a very effective picture of the progress of a survey if it is kept current, it has one failing of which the inexperienced interpreter must be warned. The apparent resistivity varies according to the orientation of the line of electrodes and thus the fact that the data were taken along a series of parallel traverses tends to flavor the resulting map. Anomalies are abnormally elongated in the direction in which the traverses are run; and, multiple anomalies occur even though their cause is one geologic feature only.

WELL LOGGING

In electrical well logging, two standard electrode configurations are used. The first is the "normal configuration" (fig. 11), in which we essentially measure the potential at point M located a fixed distance $\overline{AM}$ from a single current electrode A as the pair of elec-

Normal configuration   Lateral configuration
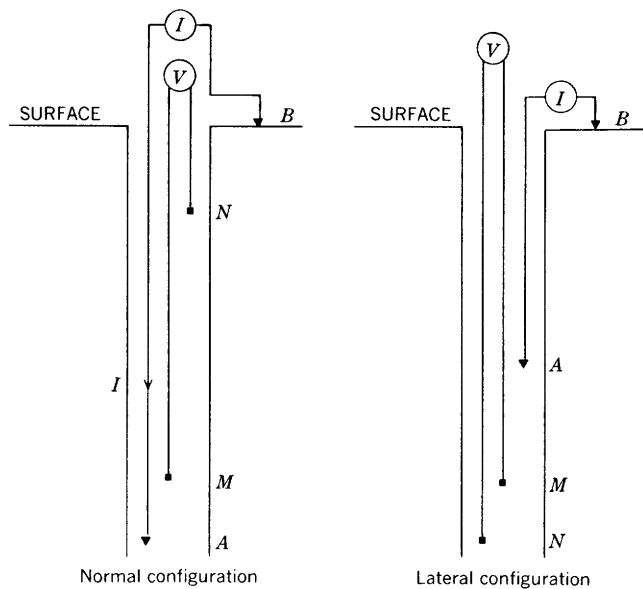
FIGURE 11.—Standard well-logging configurations, using notation of Schlumberger and others (1932).

trodes is moved up the hole. To alleviate induction effects in the measuring circuit, the reference potential electrode N is also placed in the hole but at a distance $\overline{AN}$ that is sufficiently greater than the distance $\overline{AM}$, so that the effect of potential changes at N can be neglected. The second current electrode B is effectively at infinity. If tne resistivity of the drilling mud is neglected, the apparent resistivity based on this configuration is

$$\rho_a = 4\pi \overline{AM}\frac{V}{I},\qquad (17)$$

where V is the potential difference between M and N and I is the current flowing between A and B. The relationship of this configuration to simple potential mapping about a point electrode is obvious. If such an electrode configuration were used on the earth's surface, the apparent resistivity defined on the basis of equation 2, is given by

$$\rho_a = 2\pi R\frac{V}{I}.$$

The difference between this expression and that given in equation 17 lies only in an additional factor of two, which appears in this equation. The reason for the difference is that the current I flowing outward from the current electrode in the hole flows throughout all space; whereas in surface prospecting the current I from the surface current electrode is restricted to a semispace, thus doubling the resulting potential difference V.

In the $\overline{AMN}$ lateral configuration (fig. 11), the two potential electrodes M and N are placed close together and at a relatively great distance from the current electrode A. The second current electrode B is placed at the earth's surface as it was in the normal configuration. This configuration with fixed electrode spacing is moved up the hole as readings are taken. The apparent resistivity is given by the expression.

$$\rho_a = 4\pi \frac{(\overline{AM})(\overline{AN})}{(\overline{MN})}\frac{V}{I}.\qquad (18)$$

Either of the asymmetrical configurations described above for surface resistivity work is comparable in principle to the lateral configuration used in well-logging work, and the equations for the apparent resistivity of the former can be derived by substituting the appropriate interelectrode distances into equation 18 and replacing the factor of "four," by "two," as discussed above. Moreover, the same remarks apply to Lögn's one-electrode configuration if the distance $\overline{MN}$ is small enough so that $\overline{AM}$ and $\overline{AN}$ can be considered equal.

Therefore, it can be said that the $\overline{AMN}$ lateral device essentially measures a gradient.

In review, we note that the only essential difference between electrical well logging and surface electrical prospecting lies in the restriction of the current to a semispace in surface prospecting. It follows then that much of the theoretical development to be presented herein for electrical prospecting will be applicable to problems encountered in electrical well logging, if the borehole and invaded-zone effects are neglected. Conversely, the many excellent papers which have already been published in the field of well logging, if they do not take into account the effects of the borehole, can be adapted to the use of certain electrode configurations in electrical prospecting. The most common problem encountered in well logging is that of horizontal beds which are cut perpendicularly. These correspond to outcropping vertical beds, vertical faults, or vertical dikes in surface prospecting. Another region of correspondence lies in regularly shaped bodies which may be penetrated by boreholes. The corresponding situation in surface electrical prospecting would be filled sinks which have the same regular shapes. Dipping beds in well logging cannot be compared with similarly dipping beds that crop out at the surface.

POTENTIAL-DROP-RATIO METHOD

Although we are concerned here principally with resistivity interpretation, our treatment will be extended in some cases to potential-drop-ratio methods for two reasons. First, we desire to show how the basic mathematics that was originally intended for resistivity studies can be used to equal advantage in potential-drop-ratio studies. Secondly, we will prove theoretically what other workers have known intuitively or have shown experimentally—namely, that for some problems potential-drop-ratio methods, by giving sharper anomalies, have the same advantages over resistivity methods that the latter have over potential-mapping methods.

Under the subject of potential-drop-ratio methods, we will discuss three separate types. The first is the method which was called the potential-drop-ratio (PDR) method by its originators, Lundberg and Zuschlag (1931); the second is the Resistolog method; and the third is a technique of using ratios of apparent resistivities. It will be shown that all these techniques are the same in principle and that no single one has an advantage over the others except, perhaps, in the ease with which it is applied. Finally, we mention briefly the possibility of taking successive differences rather than successive ratios.

In resistivity methods the convenient index used as a diagnostic parameter is called apparent resistivity;

and, because it has the dimensions of resistivity, it has units of ohm-meters, as used in this paper (Kelly, 1932a). The corresponding index in the PDR method is the ratio between two potential differences, and is therefore dimensionless. The electrode arrangement normally used in PDR measurements is shown in figure 12A. Three potential electrodes are spaced at equal

A

B
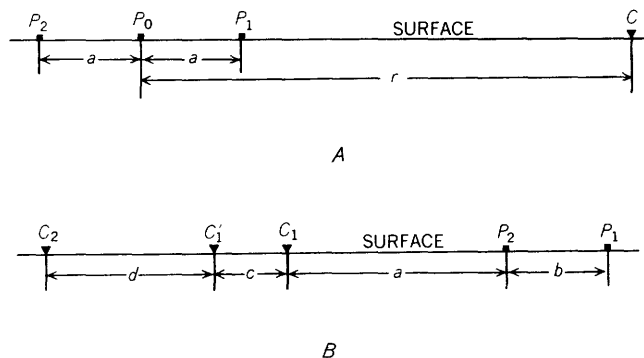
FIGURE 12.—Electrode configurations. (A), Configuration commonly used in potential-drop-ratio measurements. (B), Configuration for the Resistolog method.

intervals along a line passing through a single current electrode. The electrode spacing between the potential electrodes is designated a and the distance from the central potential electrode to the current electrode is designated r. The second current electrode is placed effectively at infinity, usually along a line perpendicular to the line of the other electrodes.

In PDR surveying the potential differences V_{10} and V_{02} are measured and their ratio taken. If the ground is perfectly homogeneous, the potential differences are calculated by means of equation 12. We find that

$$V_{10}=\frac{I\rho a}{2\pi r(r-a)} \text{ and } V_{02}=\frac{I\rho a}{2\pi r(r+a)}.$$

Therefore, their ratio for homogeneous ground is

$$V_{10}/V_{02}=\frac{r+a}{r-a}.$$

In order to normalize the PDR data, in practice the actual potential ratios are usually multiplied by the normalizing factor $(r-a)/(r+a)$, which is always less than one and gradually approaches one as r becomes large in comparison with the spacing a. Thus the PDR index for homogeneous ground is unity. In practice, it is unusual actually to measure the potential differences and then take the ratio. Instead, a specially calibrated bridge circuit is used to indicate the ratio directly when the bridge is balanced. Either direct current or low-frequency alternating current can be used. One specially designed bridge of this sort is

called Racom (Lundberg and Zuschlag, 1931). The
values of the measured ratio must then be multiplied
by the normalizing factor to obtain the PDR index
value.

In the PDR method, either a constant-spacing or an
expanding-electrode system is used. In either system
the current electrode C (fig. 12A) is usually kept fixed
and the potential electrodes moved by prescribed
amounts during a series of measurements. In the
constant-spacing technique, the separation a between
the three potential electrodes is kept constant as they
are all moved together, thus varying r only. In this
case the normalizing factor $(r-a)/(r+a)$ is usually
different for each new setting of the potential electrodes.

In the expanding-electrodes system, measurements
are taken at increasing electrode spacings with the
ratio a/r kept fixed. For convenience, r is made equal
to $3a$ so that the normalizing factor $(r-a)/(r+a)$ is
equal to 1/2. This normalizing factor gives a PDR index
of unity for homogeneous ground, as before. This
electrode configuration for the expanding-electrode
system is consequently identical to the asymmetrical
Lee configuration discussed earlier as one of the con-
figurations in resistivity methods.

The constant-spacing and expanding-electrode tech-
niques in the PDR method are somewhat analogous to
horizontal and vertical profiling techniques, respec-
tively, in the resistivity method. It should be empha-
sized, however, that the results obtained with the PDR
and resistivity methods as ordinarily used are quite
different, except for certain particular configuration
and geologic situations, and that the analogy is gener-
ally more apparent than real.

The electrode configuration for the Resistolog method,
invented by West and Beacham (1944), comprises three
current electrodes and two potential electrodes (fig.
12B). Current is first passed through C_1 and C_2, the
potential difference is measured between P_1 and P_2,
and a corresponding apparent resistivity is computed.
The same procedure is repeated when current is passed
through C_1' and C_2, and the ratio of the first apparent
resistivity to the second is computed. Taking the
ratio of successive resistivities has the same effect as the
normalizing factor used in the PDR method, in that
the ratio is unity for homogeneous ground. Because
West and Beacham were interested in depth determi-
nations for nearly horizontal bedding only, their
surveying technique consisted only of taking sets of
measurements at increasing values of a. Thus, their
technique is somewhat analogous to vertical profiling
techniques in the resistivity method. The authors
claim that their Resistolog method tends to cancel the
effect of near-surface inhomogeneities and enables the

prospector to explore at greater depths than is possible
with other techniques.

The Resistolog method is in principle a potential-
drop-ratio method and has no more potentialities
than the PDR or other such methods. In order to
show this relationship between the Resistolog and PDR
methods, let us apply the reciprocity theorem to the
Resistolog method as proposed by its authors. To do
this, we always pass current through electrodes P_1 and
P_2, measure the potential differences successively be-
tween the electrode pairs $C_1 C_2$ and $C_1'C_2$, calculate the
corresponding apparent resistivities, and take the ratio
of the first apparent resistivity to the second. This
final ratio would of course be equal to the ratio obtained
with the regular Resistolog technique.

The Resistolog method differs from the PDR method
in two major respects. First, in the PDR method, the
potential measurements are usually made essentially
within the potential field of one current electrode only
(Koenigsberger, 1930b, used two current electrodes),
the second electrode being situated effectively at
infinity; whereas in the Resistolog method—even in its
original form, shown in figure 12B—the effect of the
second current electrode must always be taken into
account. Because the potential measurements are
always made outside the current base, the presence of
the second current electrode produces the undesirable
effect of reducing the potential differences that are
measured. It is, therefore, reasonable to suspect that
a more detailed study would indicate that the sensi-
tivity of the system is similarly reduced in comparison
with the PDR method.

The second difference is more easily recognized in the
reciprocal version of the system—that is, after the
reciprocity theorem is applied to figure 12B as discussed
above. The PDR method compares potential differ-
ences over successive segments of the traverse; whereas
the Resistolog method effectively compares potential
differences over two segments of the traverse, one of
which completely includes the second but is not much
different. It follows, therefore, that one can expect
anomalies from the Resistolog method to be smaller
than anomalies from the PDR method. This second
difference is actually related to the first difference and,
if C_2 were removed to infinity, the disadvantage of the
Resistolog method relative to the PDR method would
be reduced to a minimum.

The authors of the Resistolog method have claimed
that their method eliminates the effect of near-surface
inhomogeneities in the vicinity of the potential elec-
trodes P_1 and P_2. Assuming that this claim is true,
as seems reasonable, there remains for consideration
the effects of the similar inhomogeneities in the vicinity
of the current electrodes C_1 and C_1'. Although such

inhomogeneities near the current electrodes certainly would not be eliminated, their effects would be subdued in a Resistolog profile, since the current electrodes are not moved while the data for a single profile are taken.

The third separate technique included for comparison under the topic of the potential-drop-ratio method is an adaptation of the regular Lee configuration, and the results comparable to those obtained by the PDR method. In particular, the technique consists of taking the ratios of the two Lee apparent resistivities "over adjacent ground," the ratio of the two Lee apparent resistivities "over the same ground," and the corresponding differences in apparent resistivities. The technique was suggested by Lee and Hemberger (1946) to enhance the fault-detection properties of the Lee configuration when the horizontal-profiling technique is used.

Lee and Hemberger (1946) designate as the "ratio of apparent resistivities over adjacent ground" the ratio ρ_2 to ρ_1 as these two quantities are measured at any given station. As previously noted for the asymmetrical Lee configuration, it is easily seen that the Lee-Hemberger technique of plotting the regular Lee apparent-resistivity data leads to a technique which, with one exception, is identical with the expanding-electrode technique of the PDR method, if the vertical-profiling technique with the regular Lee partitioning method is used. With the Lee configuration, the second current electrode tends to double the measured potential difference and thus facilitate accurate measurements. The question of whether the second current electrode also leads to more diagnostic data will be made the subject of a later section. When the Lee-Hemberger plotting is used, the horizontal-profiling technique with the regular Lee configuration is comparable in minor respects with the constant-spacing technique of the PDR method; yet the methods are different in major respects because of both the presence of the second current electrode for the Lee configuration and the variable distances of r for the constant-spacing PDR technique.

When the regular Lee configuration is used in horizontal profiling, the interval between adjacent stations along a traverse is usually $a/2$, where a is the electrode separation. If the configuration is being moved from west to east along the traverse, the positions of P_2 and P_0 at a given station are identical with the positions of P_0 and P_1, respectively, at the previous station. For this case, Lee and Hemberger designate as the "ratio of apparent resistivities over the same ground" the ratio of ρ_2 for a given station to ρ_1 for the previous station.

The ratio of apparent resistivities over adjacent ground yields a much more pronounced anomaly than the ratio of apparent resistivities over the same ground. Whereas the values of ρ_2 and ρ_1 often vary widely at a given station, the value of ρ_2 for one station usually approximates closely the value of ρ_1 for the previous station—assuming, as before, that the configuration is being moved from west to east—, even when the apparent resistivity is varying rapidly from point to point along the traverse. Thus, the resistivity ratios over adjacent ground are more valuable in prospecting than those over the same ground.

In order to give equal emphasis to ratios greater than 1 and to ratios less than 1, it is advisable to plot resistivity ratios or potential-drop ratios on logarithmic scales. For horizontal profiles the distance along the ground is best plotted on a linear scale, but on vertical profiles it is sometimes advantageous to plot the electrode separation on logarithmic scales also.

Lee and Hemberger (1946) also suggested the possibility of using the differences between ρ_1 and ρ_2 for the Lee configuration when horizontal profiling is used. The differences are usually found to be about as helpful as resistivity ratios over adjacent ground. A comparison of the two methods in specific examples will be made the subject of a later section. With the ordinary PDR configurations, the use of differences between potential drops would be more difficult to normalize and will not be considered.

CALCULATION OF THEORETICAL-RESISTIVITY CURVES

We will now outline the general considerations in solving problems in electrical prospecting and calculating theoretical-resistivity curves. The exact solution of such problems requires the use of three-dimensional considerations.

In addition to the direct procedure used in this treatise to solve general problems in electrical prospecting, any other standard means of solving differential equations are also acceptable. Transform theory, for example, forms a powerful tool for the solution of differential equations; and, although we do not use transform theory in this paper, it has been used by many authors to solve problems in electrical prospecting. For example, Slichter (1934) used Bessel transforms in the study of horizontal bedding, and Skal'skaya (1948) used a special Fourier-Bessel transform to solve the general problem of dipping beds.

The calculation of exact theoretical resistivity curves is extremely complex for most regularly shaped bodies and almost impossible for irregularly shaped bodies. There is, therefore, a great need for the development of methods of approximation that will yield helpful—though not necessarily exact—solutions of resistivity problems.

There are many ways in which an exact solution can be approximated. Actually, whenever we assume that a geologic body has a regular geometric form, we have already made an approximation. A cruder approximation is the assumption that the body has a shape even simpler than the nearest shape which is amenable to an exact solution; for example, to choose a sphere instead of a spheroid. The most obvious and commonly used approximation is to consider a very resistant body to have infinite resistivity or a very conducting body to have zero resistivity. The advantage of these assumptions is that the problems are usually easier to solve when one of the materials is either perfectly conducting or perfectly insulating.

Another form of approximation is the use of an image solution for a problem in which such a solution is not exactly applicable. See pages 51 to 62 for image solutions for problems in which the solutions are exact in some cases and approximate in others, and pages 48 to 50 and page 55 for outlines of logarithmic potential, which can be used to advantage in approximating solutions. Pages 50 to 51 present methods of plotting theoretical-resistivity curves.

The presentation of the theorems and the mathematics in this and later sections is designed to be descriptive and practical. Thus, extensive mathematical development is kept to a minimum, and proofs of equations used for starting points are included only when they serve to illustrate certain principles or when they do not appear elsewhere in accessible literature.

THE EXACT SOLUTION

In potential theory as applied to electrical prospecting, we distinguish between two types of potential: Newtonian potential, in which the potential in a homogeneous medium varies inversely as the distance from a point source causing the potential, and logarithmic potential, in which the potential varies logarithmically as the distance from a line source causing the potential. The logarithmic potential falls under the classification of two-dimensional problems and can be used with advantage in some problems as an approximation to three-dimensional problems; this is discussed on pages 48 to 50 and page 55. The Newtonian potential, which is used to solve an electrical prospecting problem exactly and may be classed as a truly three-dimensional problem, is discussed in the present section.

The basic problem in the theory of electrical prospecting is one of determining the values of the potential in the vicinity of a single point source of current when that source is in the vicinity of any one of a large variety of geologic discontinuities. The reduction of the problem to this simplicity is made possible by the principle of superposition. When the potential at a point

in space is influenced by two or more sources, the total potential at that point can be computed by algebraic addition of the separate potentials due to each of the sources considered as though each one were acting alone. Since a sink is no more than a negative source, the above reference to "sources" may also be interpreted to mean "sinks" or "combinations of sinks and sources."

After we compute the total potential at each of the potential electrodes due to all the current electrodes in a given configuration, we then can easily find the potential differences that are necessary for the computation of the apparent resistivity. The same reasoning applies to calculate potential-drop ratios or other quantities used in direct-current methods of prospecting.

A second general and useful principle is that of reciprocity. If we compute the potential at point A due to a current source at point B, we obtain the same solution that we would obtain if we were to compute the potential at point B due to a current source located at point A. We have already shown the significance of the reciprocity theorem when it is applied to specific electrode configurations. This theorem is general and is independent of the nature of the media surrounding, or between, the two points A and B. The main restriction is that the reciprocity theorem applies only when the flow of current is according to linear differential equations such as Laplace's equation. It has never been shown for certain that this restriction has ever been violated in practical field problems and, therefore, it is safe to apply the reciprocity theorem until its limitations are better defined for such field problems.

This theorem is especially useful in facilitating the reduction of numerical computations. Moreover, theoretical expressions for potential functions should always be checked to ascertain that they have the properties required by the reciprocity theorem.

Except for the image theory used on pages 51 to 62 for special problems, only one standard procedure is used in the solution of the problems presented in this treatise. Any departure from this procedure is only apparent and is due to special properties of the functions concerned. In general, the development of the main mathematical discussion in this treatise is subdivided according to the four steps outlined below.

The first step in the solution of resistivity problems is to select the proper coordinate system. We must be able to describe the existing boundaries in the idealized geologic situation in terms of the variables chosen. Preferably, these boundaries should be described as surfaces over which one of the three variable coordinates remains constant. Also, the

surface of the earth must be similarly described. Since no current flows across it, the earth's surface is usually chosen as a plane of symmetry in the co-ordinate system used. Only when studying the effect of topographic features on an electrical survey do we find it convenient to use surfaces other than planes of symmetry to represent the earth's surface. A description of the more useful coordinate systems is given on pages 62 to 75.

The second step in the solution of resistivity problems is to establish the proper form of Laplace's equation in the coordinate system which we prefer and to obtain the solutions to the equation. From our assumption that the flow of direct current depends on the resistance of the earth, it can be shown that the potential satisfies Laplace's equation. The forms of Laplace's equation in various coordinate systems and their general solutions are given on pages 62 to 75.

The third step in the solution of resistivity problems consists of finding the necessary expansion of the recip-rocal distance from the point current source to the point at which the potential is to be calculated. This expansion of the reciprocal distance, which is the keystone of the present method, is carried out either in terms of an infinite series or an integral. In order to apply the boundary conditions that govern the special solution to any problem, this expansion must contain the orthogonal functions that are chosen for the general solution. The development of the neces-sary expansions is given on pages 75 to 82.

The fourth, and final, step in the solution of each problem involves adapting the general solution to the special requirements of the problem by application of the boundary conditions. In each case, this step is shown in the section where the individual problem is discussed. The five boundary conditions are enum-erated below.

1. As the point source is approached from any direc-tion on the earth's surface, the potential must become infinite as $I\rho/2\pi R$, where I is the current flowing into the ground, ρ is the true resistivity of the ground in which the electrode is placed, and R is the distance from the electrode. This property is most conveniently implemented by forming the solution as the sum of the above term $I\rho/2\pi R$ plus a correction term that is required to remain finite everywhere except at the current source. It is this property which necessitates the expansion of the reciprocal distant $(1/R)$.

2. At great distances from the source the potential must vanish as $1/R$. In most general solutions there is usually one term that becomes infinite as the argument becomes infinite. This property necessitates discarding such terms when the

solution is to be applicable in a region that extends to infinity.

3. The potential must be continuous at all points in space except at the current source. This property applies equally well, and is especially important, at boundaries where there are discontinuities in electrical properties.

4. The normal component of current density $(1/\rho)\partial U/\partial n$, at the boundaries mentioned in the previous condition, must be continuous across the boundaries.

5. The solution must remain finite everywhere, except at real sources and sinks. In other words, the solution must not introduce poles (infinite values of the potential) in the electric field where poles do not physically exist. This difficulty is usually avoided by discarding those parts of the general solution which become indeterminate either at infinity, where the potential should vanish, or in other parts of the field, where the potential should remain finite.

It should be noted that the solution of a specific problem involves any function which satisfies the governing differential equation and all boundary conditions. One way of finding the solution is to specialize the general solution, if that solution can be found, by dropping those terms which do not satisfy the imposed conditions. Other methods may be found for specific problems.

Once the formal mathematical solution for a given problem has been found, the solution becomes the basis for arithmetic computations in order to obtain the data for useful graphs and charts. For each station and for each electrode separation, it is necessary to compute the potential U at each potential electrode due to each current electrode. For this purpose, if the current at C_1 is I, the current at C_2 is $-I$; allowance must be made for the change in sign. All computa-tional operations up to this point are conveniently organized into a work sheet, which is too bulky to include here. Of course, if automatic computing machines are used, the data are stored in a more convenient form such as on tape or on cards. Finally, the computed potentials U are transferred to a master work sheet, such as the one shown in figure 13, from which the apparent resistivities or other desired quanti-ties are computed. In the particular sample shown, the sheet is used to compute the apparent resistivities for the Lee and Wenner configurations for a horizontal profile over a filled sink shown in the upper part of figure 13.

In this table, x is the distance of P_0 from the center of the sink; r_0 is the distance from the center of the sink to either C_1 or C_2, as the case may be; and r is

FIGURE 13.—Sample master computation sheet with an explanation of the symbols used.
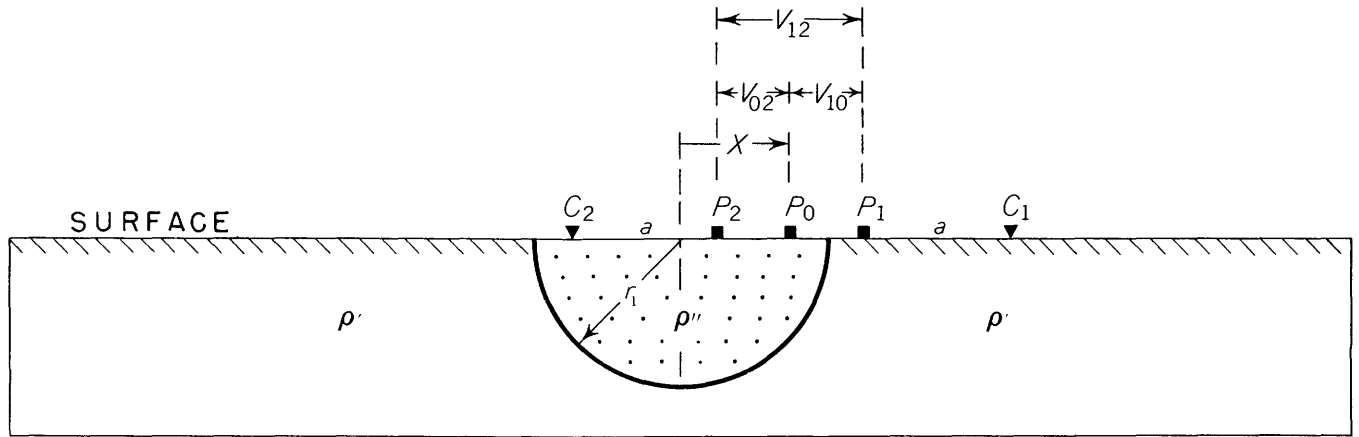
1	2	3	4	5	6	7	8	9	10	11	12	13	14	15	16	17	18	19	20
	Potentials due to C_2							Potentials due to C_1									Wenner $\rho_a = V_{12}$	Lee $\rho_1 = 2V_{10}$	Lee $\rho_2 = 2V_{02}$
		at P_2		at P_0		at P_1			at P_2		at P_0		at P_1						
X	r_0	r	U	r	U	r	U	r_0	r	U	r	U	r	U	V_{10}	V_{02}			
0	1.5	0.5	4.02	0	3.33	0.5	2.97	1.5	0.5	2.97	0	3.33	0.5	4.02	1.05	1.05	2.10	2.10	2.10
.1	1.4	.4	4.16	.1	3.47	.6	3.09	1.6	.4	2.85	.1	3.21	.6	3.89	1.06	1.05	2.11	2.12	2.10
.3	1.2	.2	4.52	.3	3.80	.8	3.40	1.8	.2	2.66	.3	3.01	.8	3.68	1.07	1.07	2.14	2.14	2.14
.5	←								etc	→									

the distance from the center of the sink to P_1, P_0, or P_2, as the case may be. The necessary potential differences are obtained by combining correctly the appropriate potentials—remembering that the current at C_2 is negative. For example, V_{10} is the potential difference between P_1 and P_0, and is found by adding columns 6 and 15, and subtracting columns 8 and 13. V_{02} is obtained by adding columns 4 and 13, and subtracting columns 6 and 11.

When the potential differences have been computed, equations 14 and 15 are applicable to compute the apparent resistivities. As the current was chosen as $I = 2\pi$ and the electrode separation a as unity, the last step is almost trivial. As is nearly always possible, these quantities have been chosen such that for the right-hand side of the Lee configuration, the apparent resistivity ρ_1 (column 19) is twice V_{10}; whereas, for the other side, the apparent resistivity ρ_2 (column 20) is twice V_{02}. The apparent resistivity ρ_a (column 18) as determined by the Wenner configuration is actually the average of these two, and is calculated most easily by adding columns 16 and 17.

LOGARITHMIC POTENTIAL

Logarithmic potentials are applicable to the solution of two-dimensional problems and are particularly useful as approximations to the exact solution of three-dimensional problems. By using logarithmic potentials, two-dimensional problems are comparatively easy to solve by using a conformal transformation, which is a powerful mathematical tool. At least one author has already published theoretical resistivity curves based on two-dimensional analysis with conformal transformations (Kiyono, 1950c). It is, therefore, desirable to investigate the degree of approximation to a three-dimensional solution that can be expected from a two-dimensional solution.

The first step in the comparison is to examine how the electric field due to an infinite-line current electrode in an infinite medium differs from that due to a point source in the same medium. For such a line source of strength I amperes per meter length, an expression for the potential due to this line source can be obtained by the same technique as that used on pages 27 to 28 to obtain the potential due to a point source in a homogeneous medium for the three-dimensional problem.

We first construct a cylindrical shell whose axis coincides with the line source of current. The radius of the shell is r, and the thickness of the shell is dr. The whole current I must pass outward through the shell. Therefore, by applying Ohm's law to the shell, the potential drop across the shell is given by

$$dU = \left(\frac{\rho dr}{2\pi r}\right) I.$$

As in the three-dimensional problem, the potential at any point in space is obtained by integrating over the region of radius r. The integration is more complicated in this problem, however, than in the three-dimensional problem because of the logarithm that appears in the present integration. In the three-dimensional problem, the potential is referred to a value of zero at an infinite value of r. In the present problem, an infinite potential is obtained if we integrate to an infinite value of radius r. Therefore, all potentials are referred to the potential at some arbitrary, finite, value of r, which we designate r', and we then integrate from r' to r. The potential at a distance r from the line source is then given by

$$U = \frac{I\rho}{2\pi} \ln \frac{r'}{r}. \tag{19}$$

If the line electrode is placed on the surface of the ground, so that all the current is confined to a half-space, equation 19 becomes

$$U = \frac{I\rho}{\pi} \ln \frac{r'}{r}. \tag{20}$$

To understand how the logarithmic potential for homogeneous ground differs from the Newtonian potential, it is unnecessary to plot a graph of the potential against r. A comparison of the equations for the two potentials shows that the Newtonian potential is equal to one-half the slope (gradient) of the logarithmic potential. In the region of interest, the gradient of the Newtonian potential is numerically smaller than the Newtonial potential itself and, therefore, smaller than the gradient of the logarithmic potential. Even with this information, however, the comparative behavior of the apparent resistivity curves is difficult to predict.

The degree of approximation afforded by a horizontal resistivity profile based on logarithmic potential is indicated in the comparison of the corresponding curves for the Wenner configuration over a vertical fault (fig. 14). The logarithmic approximation in figure 14
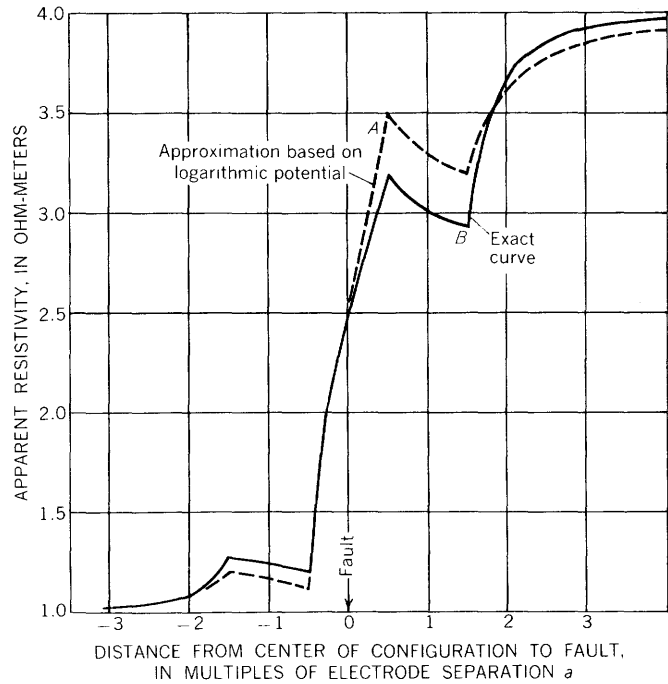
FIGURE 14.—Comparison of (A) a logarithmic approximation with (B) an exact horizontal resistivity profile made with the Wenner configuration over a vertical fault.

assumes that the potential electrodes are point electrodes and that the current electrodes are infinite-line electrodes lying on the earth's surface and oriented parallel to the strike of the fault. The current strength is I amperes per meter of length of the line electrode. Curve A was computed from equations 26, page 54, and curve B was computed from equations 27, page 55.

The important points of comparison are seen in figure 14. First, the peaks and troughs occur at the same positions on the traverse for both curves. This property is significant because usually the positions and character of the breaks in the curves are the most diagnostic features that can be found in the observed field curves for comparison with the theoretical curves. Secondly, the anomalies are always in the same direction but less pronounced on the logarithmic curve. In this particular problem, each of the apparent resistivities can be considered to consist of the regional value (ρ', for example) plus a correction term; the correction term for the three-dimensional problem is the derivative of the two-dimensional problem with respect to x.

For many problems in prospecting with direct current a logarithmic approximation is adequate qualitatively.

Logarithmic potentials can be used for this purpose, however, only when the traverse is in a vertical plane of symmetry; and herein lies a serious limitation of the logarithmic approximation. Examples in which logarithmic potential can be used as an adequate approximation include a traverse perpendicular to the strike of any body that is infinitely long in a horizontal direction and a traverse passing through the center of a filled hemispherical sink.

METHODS OF PLOTTING

To be most useful, the theoretical data should be plotted in the same way as the field data. For data taken with symmetrical configurations, there is no particular problem when only one quantity is to be plotted as a function of distance along a traverse. For example, a given value of the apparent resistivity as measured with the Wenner configuration in horizontal profiling is plotted at the midpoint of the configuration where the measurement is made. The same technique is used with the Schlumberger and other similar symmetrical configurations.

For data taken with asymmetrical configurations, however, there is no clear-cut "midpoint of the configuration;" and the apparent resistivity for these configurations is therefore usually plotted at a point midway between the two potential electrodes which are used in making the measurement. A similar problem exists for the Lee configuration, because each separate determination of the resistivity on either side of the partitioning plane is made in essence with an asymmetrical configuration. The same rule is therefore applied. With the Lee configuration, each value of the apparent resistivity is plotted at the midpoint of the pair of potential electrodes that are used in making a given measurement. The Lee configuration requires more care in plotting than do the others, because there are two values of the apparent resistivity for each station—that is, for each position of the midpoint of the whole configuration. Since the data are usually recorded as a function of the station position, ρ_1 must be plotted offset from the station a distance of $a/4$ towards potential electrode P_1, and ρ_2 for the same station must be plotted offset from the station a distance of $a/4$ towards potential electrode P_2.

For the plotting of vertical profiles there is no similar problem. The apparent resistivity is always plotted as a function of the electrode separation, in accordance with the manner in which the electrode separation is defined for the given configuration.

The choice of the best type of coordinates (linear or logarithmic) for plotting the resistivity data is complex, and different types of coordinates are used for different types of plotting. For the plotting of vertical re-

sistivity profiles logarithmic plotting for both the apparent resistivity and the electrode separation is preferable. The great advantage of logarithmic plotting for vertical profiles is illustrated on pages 90 to 101.

For the plotting of horizontal resistivity profiles linear scales are always used for the distances along the traverse and are usually used for the apparent resistivity. Logarithmic scales are used for the apparent resistivity on horizontal profiles only when they are needed to keep the amplitude of the graph under control in areas of great resistivity contrasts. A logarithmic scale tends to subdue the very high resistivities and accentuate the smaller changes.

For the plotting of potential-drop ratios or similar quantities, logarithmic plotting is advantageous, even for horizontal profiles. The reason lies in the fact that, for these quantities, the range of ratios from zero to one is exactly as important as the range from one to infinity. This equivalence is not apparent on a linear scale but is quite evident on a logarithmic scale.

In most of the following work in this treatise, the theoretical curves are presented as continuous smooth curves. But in field work, even if the geologic situation were ideal, the curves would not be smooth, because there is always a finite distance between adjacent stations at which measurements are taken. The usual practice is to plot the observed field values of apparent resistivity, or other quantity, at a position corresponding to the station as explained above, and then to connect adjacent points by straight lines. If the points were connected by the most reasonable continuous curve, we would find that even in the ideal case the characteristic points on the curve would not match the corresponding points on the theoretical curve. To emphasize this characteristic feature in resistivity field data, we introduced the concept of the "theoretical field plot" (Cook and Van Nostrand, 1954, p. 774).

The theoretical field plot consists of a series of discrete points taken from the continuous theoretical curve and connected by straight lines. The distance between successive points corresponds to the distance between successive stations along the traverse with which the theoretical curve is to be compared. An infinite number of theoretical field plots can obviously be drawn from a given continuous theoretical resistivity curve, each new theoretical field plot depending upon where the stations fall with respect to the disturbing body.

Figure 15 illustrates the extreme differences that can exist between a continuous resistivity curve and a theoretical field plot. The dashed line represents a continuous theoretical Wenner horizontal resistivity profile over a vertical fault between materials with resistivity values of 1 and 5 ohm-meters, respectively.
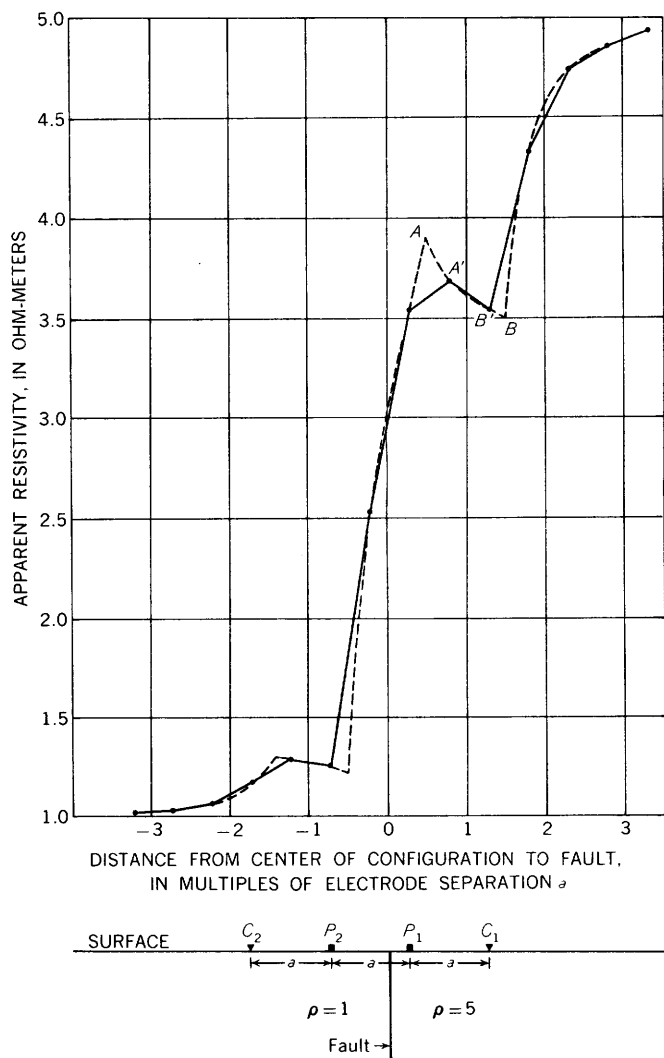
FIGURE 15.—Wenner horizontal resistivity profile over a vertical fault. Comparison of a theoretical field plot (solid line) and a continuous theoretical-resistivity curve (dashed line).

The solid line is one of the many possible theoretical field plots for the given continuous theoretical horizontal profile. The spacing between adjacent stations is $a/2$, which is the minimum interval between stations that is normally used in the field with the Wenner configuration. It is readily seen that, if the stations in a field survey perchance fall in the appropriate positions with respect to the fault, the plot of the actually observed field data would bear much more similarity to the theoretical field plot than to the continuous theoretical curve.

The particular theoretical field plot shown in figure 15 is chosen because it illustrates a maximum divergence from the original appearance of the continuous theoretical curve. The sharp maximum A in the continuous curve is subdued in its counterpart A' on the theoretical field plot. A more serious effect is that the

peak is shifted to the right a distance equal to three-tenths of the electrode separation. The shift of a pronounced peak in relation to the fault trace is of fundamental importance because the peaks are often used to locate the surface trace of the fault exactly. The minimum B is similarly shifted to the left, so that the horizontal distance between the maximum A' and the minimum B' is much less than one would expect from a casual examination of the continuous curve. The peak to the left of the fault is similarly affected, but is less important because of its lower amplitudes.

When using the Wenner configuration, many geophysicists make the interval between stations equal to the electrode separation. In this case, the small amount of character that is left in the theoretical field plot shown would ordinarily not be recognizable in the observed field data. Such a loss is most important when the character of the curve is being used to help ascertain the possible strike and dip of the fault. This and other aspects of theoretical field plots are discussed in detail on pages 116 to 118 where specific examples are introduced and explained.

APPLICATIONS OF THE IMAGE THEORY

As early as 1845, Sir William Thomson used the theory of electrical images for the solution of certain problems in electrostatics (Thomson, 1884, p. 144). Later, the image theory was used and extended by Maxwell and others, principally in its application to electrostatic problems.

The earliest theoretical solutions to direct-current electrical prospecting problems were based on the theory of electrical images. Image theory was applied successfully to the problems of horizontal bedding (Hummel, 1929c, d and Roman, 1931), vertical faults (Tagg, 1930), vertical dikes (Hedström, 1932), buried spheres (Peters and Bardeen, 1930), and certain special cases of inclined bedding (Aldredge, 1937). It will be shown in certain special problems to follow that harmonic solutions to Laplace's equation can be manipulated to yield terms that are identifiable with single images or with an infinite series of images.

It has been rigorously shown that the applicability of the theory of images is strictly limited (Keller, 1953). For problems in direct-current prospecting, the image theory is applicable only to horizontally bedded formations, to vertical faults and dikes, to dipping faults (or dipping beds) only when the lower formation is perfectly conducting or perfectly insulating and when the dip is restricted to certain angles (Van Nostrand and Cook, 1955), and to buried conducting spheres. For some problems, the image theory has proved useful even though it did not lead to exact solutions (Unz,

1953). In each such problem the degree of approximation must be worked out.

In the present section, we give examples of the solutions of each of the above problems in electrical prospecting that are amenable to exact solutions by the theory of images. The principal purpose of this section is to provide some simple theory for students and others who do not care to delve into the more complex mathematics required to solve the general problems. The subject is therefore developed from its basis in the simplest problems to its use in the more complex problems.

All the problems treated here, which deal with point electrodes near certain discontinuities, are also solvable by image theory if the electrodes are considered to be infinitely long and oriented parallel to the assumed discontinuity. Most of these problems were solved by Peters and Bardeen (1930); however, the very limited use of line electrodes does not make it worth while to include the solutions here. Moreover, the limitations on solvable problems with line electrodes are the same as those with point electrodes.

The approximate solutions that can be obtained by image theory for some problems are discussed in other sections (for example, p. 188–191).

VERTICAL FAULT

The vertical fault is one of the most useful geologic structures to study and, fortunately, one of the simplest structures to treat from a mathematical viewpoint. Before we introduce a specific configuration of electrodes, we will first investigate the field due to a point source of current at the surface in the presence of the fault. Figure 16 is a plan view of the fault with the current source C, of strength I, to the right. The
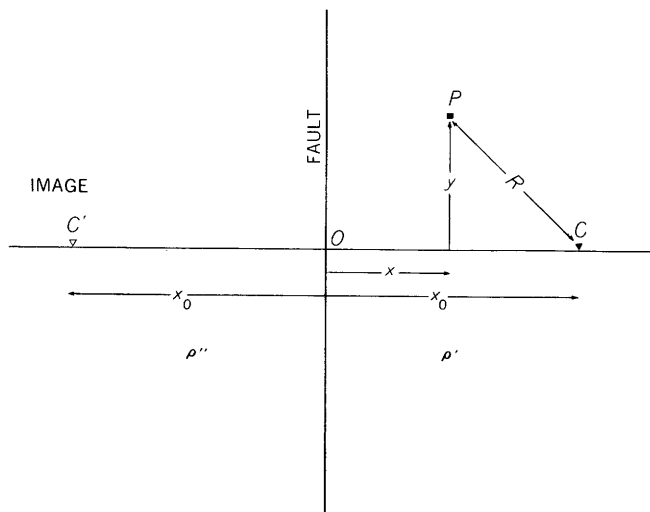
FIGURE 16.—Plan view of a point source of current in the vicinity of a vertical fault. Current electrode is C and potential electrode is P.

material to the right of the fault has resistivity ρ' and that to the left of the fault has resistivity ρ''. We measure distances from O; x is positive to the right, y positive upward, and z positive into the paper. We will arrive at our solution by assuming that the field to the right of the fault can be described in terms of the original current source of strength I and an image of strength I' equidistant on the opposite side of the fault. Applying the equation for a point source to the original source and to its image, we find that the potential at point P to the right of the fault is

$$U_{1A} = \frac{I\rho'}{2\pi\sqrt{(x_0-x)^2+y^2+z^2}} + \frac{I'\rho'}{2\pi\sqrt{(x_0+x)^2+y^2+z^2}}. \quad (21)$$

We tentatively ascribe the field to the left of the fault to a single image of strength I'' located at the position of the original source as though all media were of resistivity ρ''. The potential to the left of the fault is then

$$U_{2A} = \frac{I''\rho'}{2\pi\sqrt{(x_0-x)^2+y^2+z^2}}. \quad (22)$$

We now subject our assumptions to the boundary conditions. If the assumptions are invalid, some sort of an absurdity will result; if the assumptions are valid, the boundary conditions will lead to the correct values of the images I' and I'' in terms of the quantities given in the problem. All the conditions except two have already been satisfied when we set up the problem. The first condition to be satisfied is to make the two potential functions equal at the fault plane ($x=0$). Secondly, we must cause the normal component of the current density $\left(\dfrac{1}{\rho}\dfrac{\partial U}{\partial x}\right)$ to be equal on both sides of the fault. These conditions lead, respectively, to the following equations:

$$I+I'=I''$$

and

$$\rho''(I-I')=\rho'I''.$$

Solving these equations simultaneously, we learn that the images were correctly assumed and have the values given by

$$I' = +\frac{\rho''-\rho'}{\rho''+\rho'}I = +kI$$

and

$$I'' = (1+k)I,$$

where k is defined by the first of these equations as $(\rho''-\rho')/(\rho''+\rho')$ and is commonly called the "reflection factor" (originally so named by Roman, 1933). In later work, when more than two resistivities are involved, this reflection factor will be labelled k_{21} to distinguish it from other reflection factors

When the values of the images are replaced in equations 21 and 22, we get for the potential functions,

$$U_{1A} = \frac{I\rho'}{2\pi}\left[\frac{1}{R} + \frac{k}{\sqrt{(x_0+x)^2+y^2+z^2}}\right]$$

$$U_{2A} = \frac{I\rho'}{2\pi R}(1+k)$$

(23)

The symbol "R" refers as usual to the distance without regard to sign from the point source to the point where the potential is to be calculated. Note that in each of these functions the potential consists of a term $\left(\frac{I\rho'}{2\pi R}\right)$ due to the point source alone plus a correction factor. Note also the subscript notation for the potential, which may seem complex here but which is very useful in more complicated cases to be illustrated later. The subscript A indicates that the current source lies in the region of resistivity ρ'; the subscript B indicates that the current source is located in the region of resistivity ρ''; the subscript 1 labels the potential in the first region; and the subscript 2 denotes the potential in the second region. These subscripts are used in the appropriate combinations.

An optical analogy facilitates an understanding of the application of image theory for this problem. The analogy is based on the fact that the fault plane can be regarded physically as a partially silvered mirror whose reflecting property (k) is dependent upon the degree of silvered surface (resistivity contrast). To an observer at point P (fig. 16) in the same medium as the light source C, the intensity observed is that due to the source itself plus that due to the image C'; because the image is virtual, this added light—if k is positive—can be thought of as merely reflected from the partially silvered mirror. To the observer at point P' in the medium different from that containing the light source, the light source is seen dimly—if k is positive—and the light intensity is dependent on the reflecting property (k) of the mirror. This optical analogy, though helpful in this simple problem, must be used cautiously, as it fails in many of the more complicated problems of electrical prospecting.

Two special cases are of interest and, in elementary discussions, are usually treated before the above general case. If the material to the left of the fault is perfectly conducting, $k = -1$ and the image becomes equal in strength to the original source, but of opposite sign. The potential to the right of the fault is

$$U_{1A} = \frac{I\rho'}{2\pi}\left[\frac{1}{R} - \frac{1}{\sqrt{(x_0+x)^2+y^2+z^2}}\right],$$

(24)

and that to the left is everywhere zero. We have the identical result if the boundary plane is itself a perfectly

conducting sheet and is embedded in material of the same resistivity on both sides.

If the material to the left of the boundary plane is perfectly insulating, $k = +1$ and the image is identical to the original source both in magnitude and sign. The potential to the right of the fault is

$$U_{1A} = \frac{I\rho'}{2\pi}\left[\frac{1}{R} + \frac{1}{\sqrt{(x_0+x)^2+y^2+z^2}}\right].$$

(25)

Obviously, no current can pass into the region of infinite resistivity. However, we note that in this problem there remains a potential in the region where there is no current. This potential is not real and could not be measured. It arises when we use the second boundary condition; this leads in this limiting case to division of zero by zero, which is not allowed. If the boundary plane is a perfectly insulating sheet and the material on either side has the same resistivity, the potential to the right of the boundary plane is the same as when $k = +1$. It can be shown by a more complicated limiting process that the potential is zero everywhere to the left of the insulating plane. This problem can be used to obtain an approximate correction for a vertical cliff.

We may now calculate the apparent resistivity for any given electrode configuration in the vicinity of the fault. We will consider, for example, the Wenner configuration when it is oriented perpendicular to the strike of the fault (fig. 17). Now we may specialize equations 23 by setting $y = z = 0$. Further, we must also use the corresponding potential functions when the current electrodes pass to the opposite side of the fault. These may be obtained by interchanging the
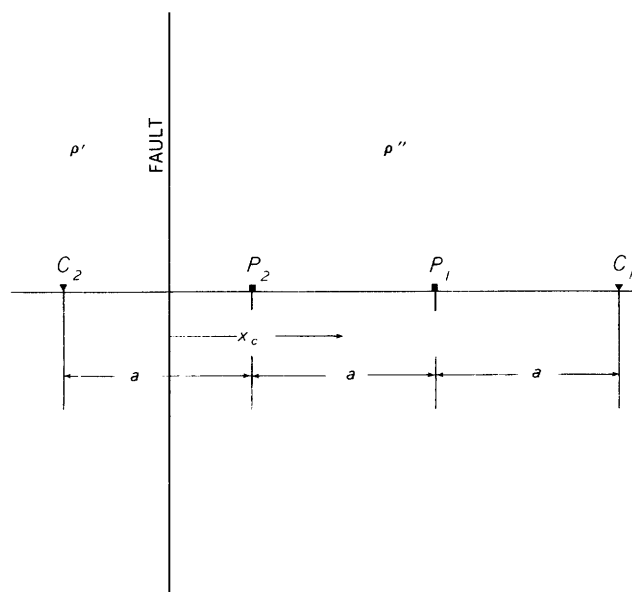
FIGURE 17.—Plan view of the Wenner configuration oriented perpendicular to a vertical fault.

roles of ρ' and ρ'' in equations 23. The four potential functions which we require are

$$U_{1A}=\frac{I\rho'}{2\pi}\Big[\frac{1}{R}+\frac{k}{x_0+x}\Big] \qquad U_{2A}=\frac{I\rho'}{2\pi R}(1+k)$$

$$U_{1B}=\frac{I\rho''}{2\pi R}(1-k) \qquad U_{2B}=\frac{I\rho''}{2\pi}\Big[\frac{1}{R}+\frac{k}{x_0+x}\Big].$$

It should be borne in mind that, in U_{2B}, x and x_0 are both negative numbers. In all these equations the reflection factor k remains equal to $(\rho''-\rho')/(\rho''+\rho')$. Also, it should be noted that in figure 16 the regions of resistivity ρ' and ρ'' are on the right- and left-hand side, respectively, of the fault; whereas in figure 17 the regions of resistivity ρ' and ρ'' are on the left- and right-hand side, respectively.

Owing to the variety of potential functions that apply when the electrodes occupy different positions with respect to the fault, the apparent-resistivity function assumes five different forms, each applicable to a different range of the ratio x_c/a. As shown in figure 17, x_c is the horizontal distance between the fault plane and the midpoint of the Wenner configuration in a direction perpendicular to the strike of the fault; x_c is positive in the same sense as x was defined above as positive. We will derive only one of these forms and then merely write down the others. The procedure is to calculate the total potential at each of the potential electrodes due to the combined effects of both current electrodes, then to determine the potential difference and use it in the formula for apparent resistivity for the Wenner configuration. These steps are carried out here only for illustrative purposes. Whereas it is possible in the example to write a closed expression for the apparent resistivity, it will be extremely complicated to do so in the more complex cases to be treated in later sections. The steps which are performed algebraically in the example will be carried out only numerically in the more complicated cases. The principles are the same for both.

Let us consider the case in which the fault lies between C_2 and P_2 (fig. 17). The potentials at P_1 and P_2 due to C_1 require the use of U_{2B}; the potentials at these electrodes due to C_2 require the use of U_{2A}. We write x_0, x, and R in terms of x_c and a in order to use the potential functions as they are written. Then, the potential at P_1 due to C_1 is

$$\frac{I\rho''}{2\pi}\Big[\frac{1}{a}+\frac{k}{2(x_c+a)}\Big].$$

Similarly, the potential at P_1 due to C_2 is

$$\frac{(-I)(1-k)\rho'}{2\pi(2a)},$$

or

$$\frac{-I\rho''(1+k)}{2\pi(2a)}.$$

By adding these two expressions, we find that the total potential at P_1 is

$$\frac{I\rho''}{2\pi}\Big[\frac{1}{2a}-\frac{kx}{2a(x_c+a)}\Big].$$

By similar reasoning, we find that the total potential at P_2 is

$$\frac{I\rho''}{2\pi}\Big[-\frac{1}{2a}-\frac{2kx_c}{a(2x_c+a)}\Big].$$

We then subtract the second from the first to get the potential difference between P_1 and P_2:

$$V_{12}=\frac{I\rho''}{2\pi a}\Big[1+\frac{kx_c(2x_c+3a)}{2(x_c+a)(2x_c+a)}\Big].$$

The expression for the apparent resistivity (the fourth equation listed in the group of equations 26) is now easily obtained by substituting this potential difference into equation 14. The corresponding expressions which are valid in other ranges of x_c may be found in the same way. We have then

$$\left.\begin{array}{l}-\dfrac{3a}{2}>x_c \\[2mm] \qquad \dfrac{\rho_a}{\rho'}=1+\dfrac{3ka^3x_c}{(x_c{}^2-a^2)(4x_c{}^2-a^2)} \\[4mm] -\dfrac{a}{2}>x_c>-\dfrac{3a}{2} \\[2mm] \qquad \dfrac{\rho_a}{\rho'}=1-\dfrac{kx_c(2x_c-3a)}{2(x_c-a)(2x_c-a)} \\[4mm] \dfrac{a}{2}>x_c>-\dfrac{a}{2} \\[2mm] \qquad \dfrac{\rho_a}{\rho'}=\dfrac{1}{1+k}\Big[1+k^2+\dfrac{ka(x_c+ak)}{(x_c{}^2-a^2)}\Big] \\[4mm] \dfrac{3a}{2}>x_c>\dfrac{a}{2} \\[2mm] \qquad \dfrac{\rho_a}{\rho'}=\dfrac{1-k}{1+k}\Big[1+\dfrac{kx_c(2x_c+3a)}{2(x_c+a)(2x_c+a)}\Big] \\[4mm] x_c>\dfrac{3a}{2} \\[2mm] \qquad \dfrac{\rho_a}{\rho'}=\dfrac{1-k}{1+k}\Big[1+\dfrac{3ka^3x_c}{(x_c{}^2-a^2)(4x_c{}^2-a^2)}\Big]\end{array}\right\}, \qquad (26)$$

As is customary, the apparent resistivity is expressed as the ratio ρ_a/ρ'; the right side of the equation contains only the resistivity contrast expressed as the reflection factor $k=(\rho''-\rho')/(\rho''+\rho')$. In this way, a given resistivity curve may be adapted to any problem, for which the resistivity contrast is correct, simply by correct labeling of the scales. For the same reason, it is also customary to express distances by one of the two

ratios, a/x_c or x_c/a, according as the expression is to be used for vertical profiling or for horizontal profiling, respectively. It should be emphasized that these equations are valid only for values of k lying between $+1$ and -1, and not for the end values themselves. The reason lies in the assumptions about the potentials in forming the equations.

The above reasoning can also be applied to obtain apparent-resistivity expressions for other electrode separations or potential-drop ratios. None of these are reproduced here. Derivation of these other expressions makes a useful exercise for students and others who want to impress upon themselves the superposition theorem and the other principles involved.

In the previous discussion the traverse is perpendicular to the strike of the fault. If the traverse crosses the fault at an angle, other considerations must be made. In figure 18, the unprimed distances are those which appear in equation 23. However, since distances are normally measured along the traverse, it is necessary to transform the equations using the unprimed dis-

tances to a set using the primed distances. The relationship is easily established from geometric considerations:

$$\begin{cases} y = (x_0' - x') \cos \alpha \\ x_0 = x_0' \sin \alpha \\ x = x' \sin \alpha. \end{cases}$$

To obtain apparent-resistivity expressions along the traverse which cuts the fault at an angle, it is necessary to derive expressions analogous to equations 26, but which are based on equations 23 as modified by the above transformations. For example, the first of equations 26 would become, in this case,

$$\frac{\rho_a}{\rho'} = 1 + \frac{3ka^3 x_c}{(x_c^2 - a^2)(4x_c^2 - a^2)\sin^3 \alpha}.$$

On page 49 we compared a "two-dimensional" horizontal profile with the corresponding "three-dimensional" horizontal profile (fig. 14). The logarithmic potentials which were necessary in preparing the two-dimensional curve can easily be adapted from the problem discussed above. Consider the example of a line electrode placed on the surface of the ground and oriented parallel to the fault plane, as in fig. 16. The only modifications required to transform equations 23 properly are to interpret I as current per unit length, to change the factor 2π to π in the denominator, and to change the reciprocal distances to logarithmic terms. The new expressions are

$$U_{1A} = \frac{I\rho'}{\pi}\left[\ln \frac{x_0}{\sqrt{(x_0-x)^2+z^2}} + k \ln \frac{x_0}{\sqrt{(x_0-x)^2+z^2}}\right].$$

$$U_{2A} = \frac{I\rho'}{\pi}(1+k) \ln \frac{x_0}{\sqrt{(x_0-x)^2+z^2}} \qquad (27)$$

For convenience, the potential of the fault trace is chosen always to be zero. To obtain resistivity equations comparable to equations 26, for example, we follow the procedures used to get equations 26 but base our calculations on potential functions like those given by equations 27.

DIPPING FAULT OR BED

For a dipping fault or bed, the image theory can yield an exact solution under restricted conditions only. First, the lower bed must be either perfectly conducting or perfectly insulating; second, the angles of dip are restricted to certain special values only; and third, the solutions are valid only on the downdip side of the fault trace.

If the lower bed has infinite resistivity, the problem may be solved by images for a dip of 60°. A dip of 45° is the largest for which the problem can be solved when the lower bed is either perfectly conducting or perfectly
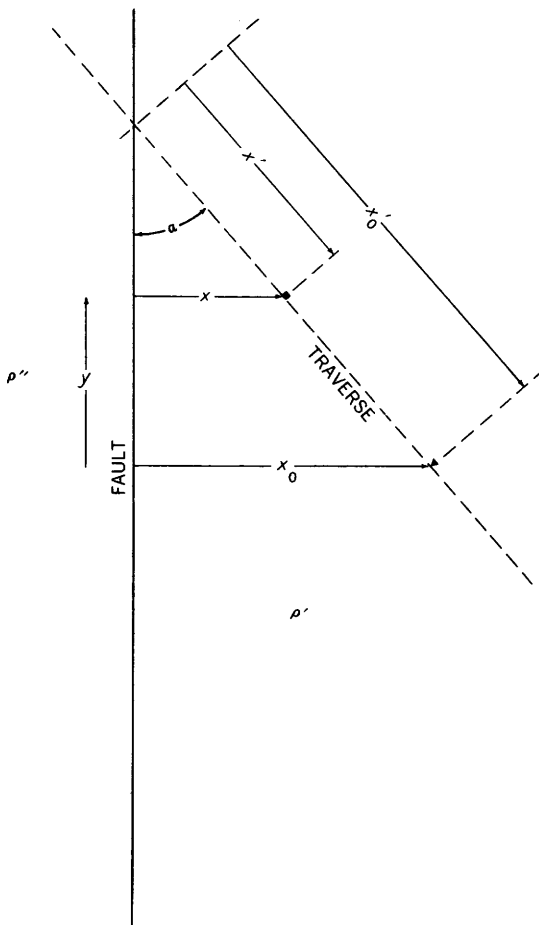
FIGURE 18.—Plan view showing a traverse crossing a vertical fault at an angle α.
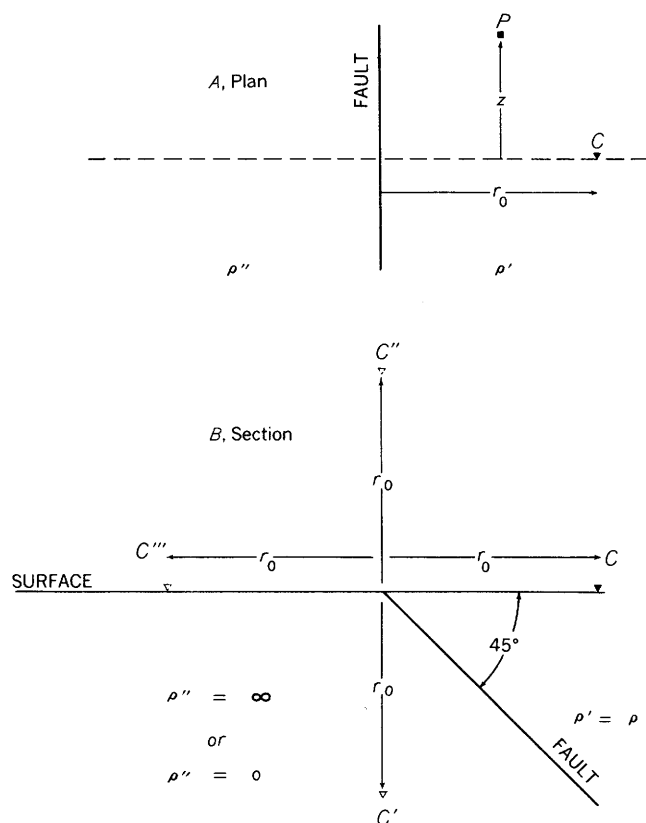
FIGURE 19.—*A*, Plan view of current and potential electrodes *C* and *P* near trace of a dipping fault, showing symbols used. *B*, Cross-sectional view of a current electrode *C*, together with its images, near a fault dipping 45°.

insulating. Assuming a problem with this angle of dip (fig. 19), let us consider first the case in which the lower medium is perfectly insulating. A point current electrode *C* is placed near the fault, and we wish to establish a set of images which will satisfy the boundary conditions. In this case the only boundary conditions are that no current should flow either across the fault plane (because the bottom bed is perfectly insulating) or across the surface of the earth. A current *I* flows into the ground from the current electrode.

In order that no current will cross the fault plane, it is necessary to establish an image of strength *I* at *C'*. However, the image at *C'* has the undesirable effect of causing a current to cross the earth's surface. This new effect is offset by a second image of strength *I* at *C''*. The current which *C''* causes to cross the fault plane is in turn counterbalanced by yet a third image of strength *I* at *C'''*. The original electrode and its three images now form complete symmetry in the electric field both about the fault plane and about the surface of the earth. Thus, no current crosses either of these planes, and the boundary conditions are satisfied. The potential at points on the earth's surface to the

right of the fault is now given by the sum of the potentials due to the electrode and its three images:

$$U=\frac{I\rho}{2\pi}\left[\frac{1}{\sqrt{(r_0-r)^2+z^2}}+\frac{2}{\sqrt{r_0^2+r^2+z^2}}+\frac{1}{\sqrt{(r_0+r)^2+z^2}}\right], \quad (28)$$

where the symbolism from figure 19 has been used. Since images *C'* and *C''* are of the same strength and at the same distance from the point at which the potential is to be computed, they produce equal contributions and have been combined in the second term.

Let us consider next the second case, also shown in figure 19, in which the lower fault block is perfectly conducting. The boundary conditions which must be satisfied are that no current crosses the earth's surface, and the fault plane remains at zero potential. We must select a set of images which is symmetrical about the earth's surface but antisymmetrical about the fault plane. The only change that must be made in the previous solution is to reverse the signs of the images at *C'* and *C''*. Therefore, the potential at *P* in this instance is

$$U=\frac{I\rho}{2\pi}\left[\frac{1}{\sqrt{(r_0-r)^2+z^2}}-\frac{2}{\sqrt{r_0^2+r^2+z^2}}+\frac{1}{\sqrt{(r_0+r)^2+z^2}}\right]. \quad (29)$$

Equations 28 and 29 would also result if the fault plane were either a perfectly insulating or perfectly conducting sheet, respectively, and were enclosed on both sides by material of a single uniform resistivity.

We can learn from the above example why the image theory cannot be used to solve problems in which the current electrode is on the updip side of the fault trace. Suppose, for example, that the fault plane in figure 19 is a perfectly insulating sheet, that the surrounding material on both sides has a single, uniform resistivity, and that the current electrode is placed in the position of *C'''*. We have shown that the image arrangement must be symmetrical both about the fault plane and about the earth's surface, in order that no current will cross either of these planes. Thus, the image theory with the current electrode to the left of the fault plane leads to the same distribution of images—if the source is also included in this set—as we had when the source was on the downdip side of the fault trace. This fact alone leads us to suspect that the solution is wrong, but there is a stronger reason yet. To be valid in any part of the region, the solution must be valid in all of the region to the left of the fault plane—in other words, in the lower fault block. However, our image solution has created a mathematical pole at *C'*, in the region where the potential function is to be determined and where there is no real pole. This violates one of the potential boundary conditions and, therefore, the solution is invalid. Whenever the image

theory fails in the case of dipping beds, it is for the same reason: poles are created in regions where there should be none.

It was pointed out that, when image theory is applicable to a dipping fault problem in which the lower formation is perfectly insulating, the distribution of images is such that they are symmetrically disposed both with respect to the earth's surface and to the contact plane. Also, there must be a finite number of images. Since all the images lie on a circle whose center is at the fault trace and which passes through the original source, such a distribution is possible only when the angle of dip is a submultiple of π. With this fact in mind, we are able to write a general equation for the potential for any such dip. Let the angle of dip $\alpha = \pi/n$, where n is any integer. Then the potential is given by:

$$U = \frac{I\rho}{2\pi} \sum_{i=0}^{i=n-1} \frac{1}{\sqrt{r_0^2 + r^2 - 2r_0 r \cos(2i\alpha) + z^2}}, \quad (30)$$

where the term for $i=0$ is that due to the original source itself. The same notation is used here as was used above.

If the lower bed is perfectly conducting, the set of images must be symmetrical about the earth's surface but antisymmetrical about the fault plane. Owing to the more complicated conditions, the validity of the image theory is more restricted and only dip angles which are submultiples of $\pi/2$ can be treated. Let the angle of dip α equal $\pi/2m$, where m is any integer. Then, the potential is given by

$$U = \frac{I\rho}{2\pi} \sum_{i=0}^{i=2m-1} \frac{(-1)^i}{\sqrt{r_0^2 + r^2 - 2r_0 r \cos(2i\alpha) + z^2}}, \quad (31)$$

where again the term for $i=0$ is that due to the original source itself.

Equations 30 and 31 can be derived only by inductive reasoning. The validity of the equations for any specific value of dip can readily be verified by the method used to derive equations 28 and 29. The general equations then follow from an examination of the special forms for several successive values of m and n. We note that equations 24 and 25 are also special cases of these general equations.

These equations are useful in the computation of resistivity or potential-drop-ratio curves along any traverse for either vertical profiling or horizontal profiling. The only restriction is that their validity ceases as soon as any electrode crosses to the updip side of the fault trace. Thus, if figure 17 is considered to represent the Wenner configuration in the vicinity of the trace of a fault dipping to the right, a horizontal traverse could be constructed for all values of x greater than $3a/2$. When x becomes less than $3a/2$, however,

C_2 is on the updip side of the fault trace and the image solutions are not exactly valid.

VERTICAL DIKE

We have seen how a single image can be used to solve the problem of a vertical fault. In certain special cases of the dipping-fault problem, we showed solutions in which a multiplicity of images were used. Now we introduce the problem of the vertical dike to illustrate the use of an infinite series of images.

Let us consider a single vertical dike of width b and resistivity ρ'' in a country rock of resistivity ρ' (fig. 20). For convenience, distances are measured from the original current source as the reference point. To the right of the source z is positive and, to the left, negative; r is always positive whether measured above or below the source. To solve the problem by images, it is necessary to establish three potential functions which are labeled U_{1A}, U_{2A}, and U_{3A} for the regions to the left of the dike, within the dike, and to the right of the dike, respectively. Each term in these functions is due to the original source or an image.

We consider first the set of images which arise from reflections of the original source in the first boundary. The resulting terms in the potential functions correspond to those for a single discontinuity as given in equation 23. Since U_{3A} applies to the third region which is also to the right of the boundary, we will assume that the complementary image at C affects U_{3A} as well as U_{2A}. Therefore, we have

$$U_{1A} = \frac{I\rho'}{2\pi} \left[\frac{1}{R} + \frac{k}{\sqrt{(2z_1 - z)^2 + r^2}} + \cdots \right]$$

$$U_{2A} = \frac{I\rho'}{2\pi} \left[\frac{(1+k)}{R} + \cdots \right] \quad \quad (32)$$

$$U_{3A} = \frac{I\rho'}{2\pi} \left[\frac{(1+k)}{R} + \cdots \right]$$

We consider next the images that arise from reflection of the original source in the second boundary—that is, the boundary at the right. We assume that an image exists at each point where an optical image would exist if we were getting multiple reflections of light from the two internal faces of the dike after the light has once entered the dike through the boundary at the left. The positions of these images and the successions of reflections are indicated in figure 20. We see that the positions of all of the images to the right of the dike can be expressed as $z = 2z_2 + 2nb$, where n is the number of the image in the set as they are counted outward from the dike, starting with zero. For the images to the left of the dike, $z = -2nb$. Since a potential function cannot contain artificial poles in its region of validity, we assume that the images to the right of the dike affect only U_{1A} and U_{2A} and that the
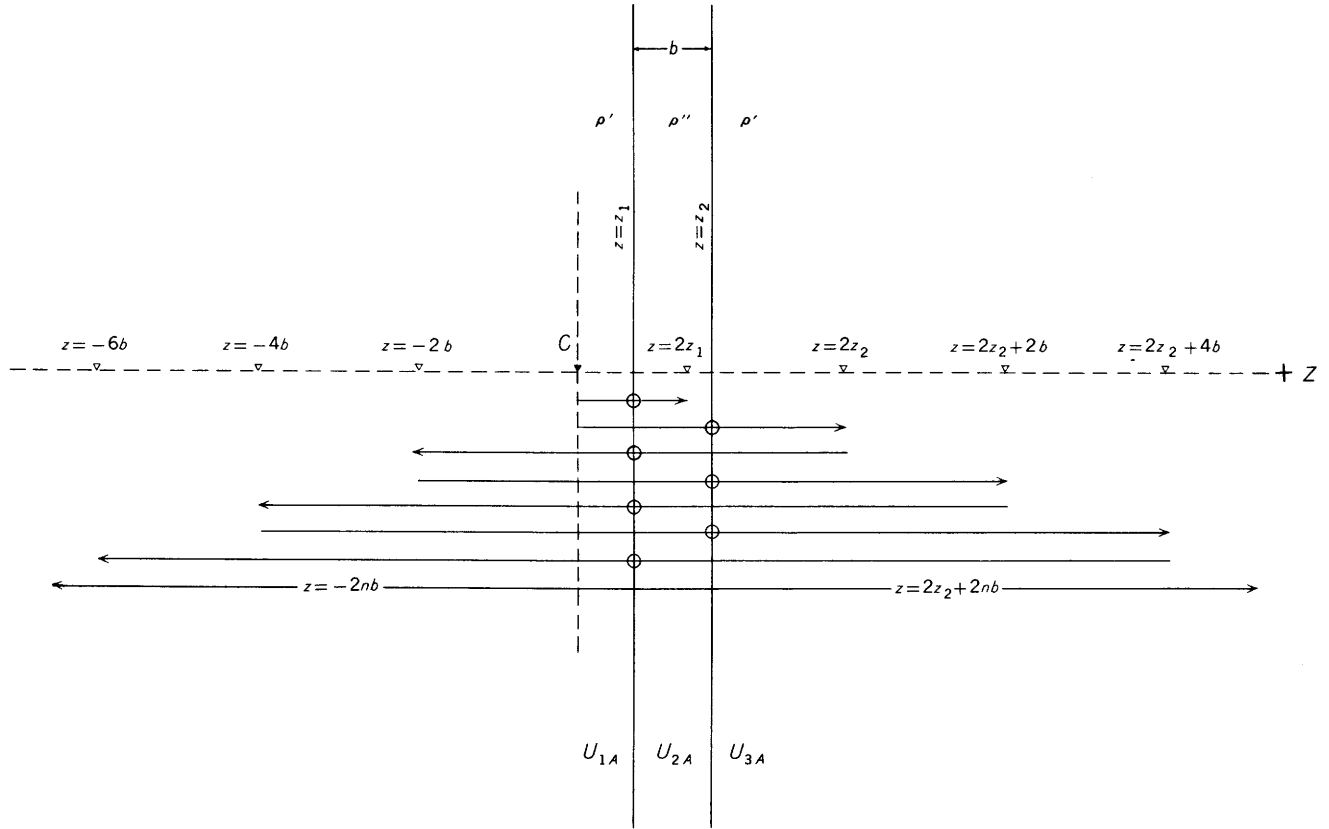
FIGURE 20.—Plan view showing a point source of current C, together with its images, in the vicinity of a vertical dike of width b. Arrows indicate the order of reflection and the small circles indicate the reflecting surface for any given reflection.

images to the left affect only U_{2A} and U_{3A}. Except for the first image in each set, each image in both sets will be the result of the reflection of some previous image across each boundary; in one of these reflections, the strength of the image will be multiplied by k at each reflection. Therefore, we will further assume that the dependence of all image strengths upon n is given by the factor $(k^2)^n$. The above assumptions give us the following forms of the potential function:

$$U_{1A}=\frac{I\rho'}{2\pi}\left[\frac{1}{R}+\frac{k}{\sqrt{(2z_1-z)^2+r^2}}+A\sum_{n=0}^{\infty}\frac{(k^2)^n}{\sqrt{(2nb+2z_2-z)^2+r^2}}\right]$$

$$U_{2A}=\frac{I\rho'}{2\pi}\left[B\sum_{n=0}^{\infty}\frac{(k^2)^n}{\sqrt{(2nb+2z_2-z)^2+r^2}}+C\sum_{n=0}^{\infty}\frac{(k^2)^n}{\sqrt{(2nb+z)^2+r^2}}\right]$$

$$U_{3A}=\frac{I\rho'}{2\pi}D\sum_{n=0}^{\infty}\frac{(k^2)^n}{\sqrt{(2nb+z)^2+r^2}}$$

In U_{2A} and U_{3A}, it should be noted that $1/R$ corresponds to the term in the set of image distances given by $z=-2nb$, where $n=0$. Thus, we have absorbed the terms introduced by U_{2A} and U_{3A} in equation 32 into the series

$$(k^2)^n/\sqrt{(2nb+z)^2+r^2}.$$

Application of the image theory is somewhat of a trial-and-error method, but any false assumption that is made in setting up the potential functions will lead to an absurdity when the boundary conditions are applied to determine the constants A, B, C, and D. From the boundary condition that the current must be continuous across the first boundary, we see that

$$\frac{1}{R}+\frac{k}{\sqrt{z_1^2+r^2}}+A\sum_{n=0}^{\infty}\frac{(k^2)^n}{\sqrt{[2(n+1)b+z_1]^2+r^2}}$$

$$=B\sum_{n=0}^{\infty}\frac{(k^2)^n}{\sqrt{[2(n+1)b+z_1]^2+r^2}}+C\sum_{n=0}^{\infty}\frac{(k^2)^n}{\sqrt{(2nb+z_1)^2+r^2}},\quad (33)$$

where $R=\sqrt{z_1^2+r^2}$ for points on this boundary. In equation 33, we have used the relationship that $z_2=z_1+b$. If we write the zeroth term of the second summation on the right explicitly and if we then substitute a new summation index $m=n-1$, we have

$$\frac{1+k}{\sqrt{z_1^2+r^2}}+A\sum_{n=0}^{\infty}\frac{(k^2)^n}{\sqrt{[2(n+1)b+z_1]^2+r^2}}=B\sum_{n=0}^{\infty}\frac{(k^2)^n}{\sqrt{[2(n+1)b+z_1]^2+r^2}}$$

$$+\frac{C}{\sqrt{z_1^2+r^2}}+C\sum_{m=0}^{\infty}\frac{(k^2)^{m+1}}{\sqrt{[2(m+1)b+z_1]^2+r^2}}.\quad (34)$$

Since this relationship holds for every value of r, it has to hold separately for each value of n. In this respect m in the last term is included with n in the other terms because both are summation indices, and what we label them is therefore trivial. From equation 34, we obtain the following equations:

$$\begin{cases} 1+k=C \\ A=B+k^2C. \end{cases} \quad (35)$$

When we apply the same boundary condition at the second boundary, we get

$$B\sum_{n=0}^{\infty}\frac{(k^2)^n}{\sqrt{(2nb+z_2)^2+r^2}}+C\sum_{n=0}^{\infty}\frac{(k^2)^n}{\sqrt{(2nb+z_2)^2+r^2}}$$
$$=D\sum_{n=0}^{\infty}\frac{(k^2)^n}{\sqrt{(2nb+z_2)^2+r^2}}, \quad (36)$$

whence

$$D=B+C. \quad (37)$$

By making the normal component of the current density continuous across the second boundary, we find that

$$D=\frac{\rho''}{\rho'}(C-B).$$

Equations 35, 36, and 37 constitute a simultaneous system from which we can determine A, B, C, and D. The second boundary condition need not be applied at the first boundary, as is usually done to get the proper number of simultaneous equations, because we have in effect already set down one equation when we assumed the power dependence of the image strengths on n. Solving the equations, we get

$$\begin{cases} A=-k(1-k^2) \\ B=-k(1+k) \\ C=1+k \\ D=1-k^2 \end{cases}$$

so that the final forms of the potential functions are

$$U_{1A}=\frac{I\rho'}{2\pi}\left\{\frac{1}{R}+\frac{k}{\sqrt{(2z_1-z)^2+r^2}}-k(1-k^2)\sum_{n=0}^{\infty}\frac{k^{2n}}{\sqrt{(2nb+2z_2-z)^2+r^2}}\right\}$$

$$U_{2A}=\frac{I\rho'}{2\pi}(1+k)\left\{\sum_{n=0}^{\infty}\frac{k^{2n}}{\sqrt{(2nb+z)^2+r^2}}-k\sum_{n=0}^{\infty}\frac{k^{2n}}{\sqrt{(2nb+2z_2-z)^2+r^2}}\right\}$$

$$U_{3A}=\frac{I\rho'}{2\pi}(1-k^2)\sum_{n=0}^{\infty}\frac{k^{2n}}{\sqrt{(2nb+z)^2+r^2}}. \quad (38)$$

The same technique could have been used to get similar equations for the dike if it had different materials on either side or for a brecciated zone associated with a fault. However, these general cases are discussed in a later section on the more direct approach

of harmonic analysis. The same statement is true of solutions when the source is within the dike instead of outside. The same general technique is also applicable to the problem of a horizontally stratified earth.

PERFECTLY CONDUCTING MASSES WITH CURVED BOUNDARIES

Problems involving some perfectly conducting bodies with curved boundaries are amenable to solution by the image theory. Examples are the hemispherical sink, the buried sphere, and the corresponding cylindrical bodies when line electrodes are used parallel to the cylindrical axis. However, problems involving the same bodies, if perfectly insulating, are not amenable to solution by the image theory. Solutions of Laplace's equation must be used to deal with similar bodies when such bodies present arbitrary resistivity contrasts or are perfectly insulating.

HEMISPHERICAL SINK

Image theory is applicable to a sink which approximates the shape of a hemisphere and is filled with a perfectly conducting material (fig. 21). We com-
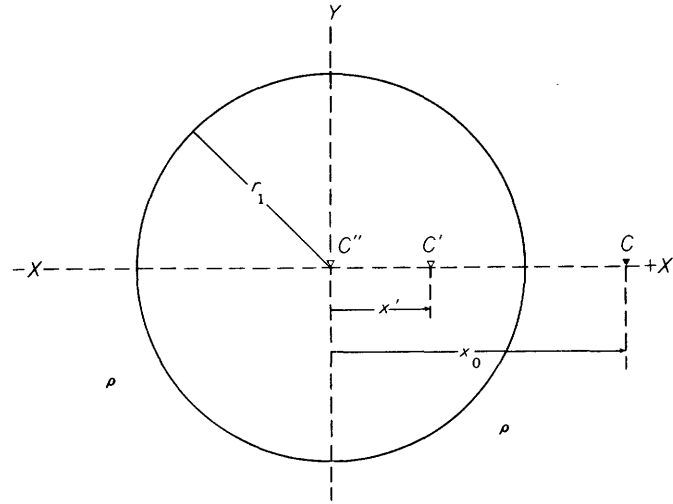
FIGURE 21.—Plan view showing a point source of current C near a hemispherical sink filled with a perfectly conducting material. The z-axis is positive, vertically downward into the paper.

mence the solution in the same manner as for the vertical fault. In this case, however, we know neither the strength nor the position of the images that are assumed to exist. Let us first assume that a single image of C, designated as C' in the diagram, will be sufficient to solve the problem. Initially, we will try to satisfy only one boundary condition—namely, that the boundary of the hemisphere be kept at zero potential. Since the whole hemisphere is perfectly conducting, this condition implies that the whole hemisphere is kept at zero potential.

The potential on the boundary of the hemisphere due to the original source is

$$\frac{I\rho}{2\pi}\left[\frac{1}{\sqrt{x_0{}^2-2x_0x+r_1{}^2}}\right]$$

and that due to the single image is

$$\frac{I'\rho}{2\pi}\left[\frac{1}{\sqrt{x'^2-2x'x+r_1{}^2}}\right].$$

The total potential on the boundary of the hemisphere will be zero only if these two potentials are equal everywhere on the boundary. If we square both quantities, and make certain rearrangements, we have

$$I'^2(x_0{}^2-2x_0x+r_1{}^2)=I^2(x'^2-2x'x+r_1{}^2).$$

This relationship must hold for all values of x over the surface of the hemisphere, a condition which is satisfied only if

$$I'^2(x_0{}^2+r_1{}^2)=I^2(x'^2+r_1{}^2)$$

and

$$I'^2x_0=I^2x'.$$

Thus, we have two equations and two unknowns. Solving, we learn that

$$\begin{cases} I'=-\dfrac{r_1}{x_0}I \\[2mm] x'=\dfrac{r_1{}^2}{x_0}. \end{cases}$$

The values of I' and x' are obtained with the assumption that the boundary is kept at zero potential. However, it is obvious that a conducting hemisphere in the field of a point source of current would be raised to some potential other than zero. The value of this potential can be obtained by using the principle of reciprocity. If a current I were flowing outward from the hemisphere, the field outside would appear to originate from a point source located at the center of the hemisphere. Therefore, the potential at C would be $\dfrac{I\rho}{2\pi x_0}$. In the reciprocal situation of our problem, therefore, the potential of the hemisphere due to a current source at C must also be $\dfrac{I\rho}{2\pi x_0}$. The surface of the hemisphere can be raised uniformly to this potential if a second image of strength $\dfrac{r_1}{x_0}I$ is placed at C'', the center of the hemisphere.

A second way to arrive at this result would be to realize that there must be no net flow of current into or out of the hemisphere. Therefore, we must add an image within the hemisphere, equal in strength but opposite in sign to the first image. The only possible position of the second image, in order that it will have

the same effect over the whole hemispherical surface, is the center of the hemisphere.

The problem is now solved. The potential outside the hemisphere is due to three things: the original electrode, an image at C', and a second image at the center of the hemisphere. The potential function on the surface of the earth outside the hemisphere is

$$U=\frac{I\rho}{2\pi}\left[\frac{1}{\sqrt{(x_0-x)^2+y^2}}-\frac{r_1}{x_0\sqrt{\{(r_1{}^2/x_0)-x\}^2+y^2}}+\frac{r_1}{x_0\sqrt{x^2+y^2}}\right]. \quad (39)$$

BURIED SPHERE

The problem of the buried conducting sphere is one of the most complicated problems that can be solved with the theory of images. To solve this problem, we start, as in the simpler hemisphere problem above, by assuming that the buried sphere will initially be maintained at zero potential (fig. 22). A system of rectangular coordinates is oriented with the z-axis positive downward, the x-axis positive to the right, and the y-axis positive out of the paper. As in the previous problem, an image must be placed at C_1 to keep the sphere at zero potential. C and C_1 are inverse points with respect to the sphere—that is, they bear the same relation to each other that the corresponding points do in figure 21. The existence of an image at C_1 upsets the condition that no current may cross the surface of
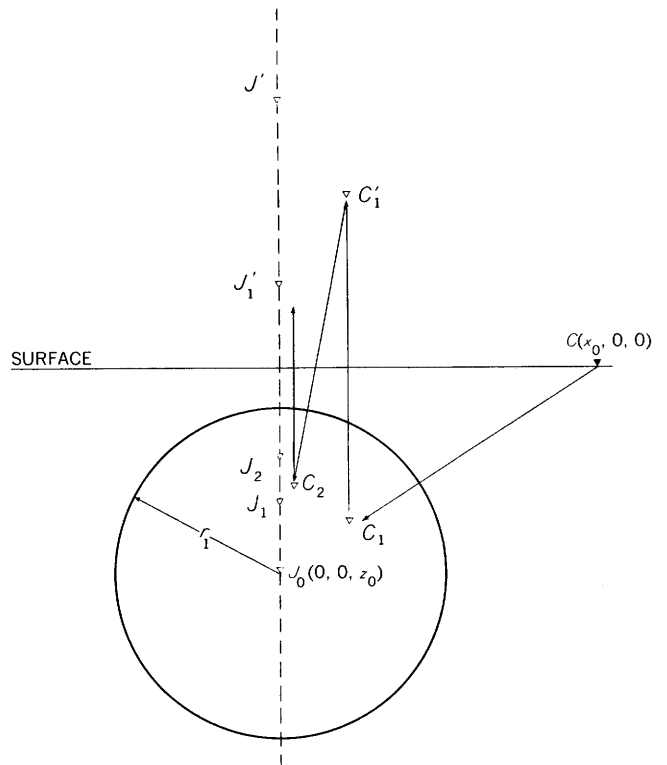
FIGURE 22.—Cross-sectional view showing a point source of current C and its images, near a buried perfectly conducting sphere.

the earth ($z=0$). Therefore, we must place a second image at C_1', where C_1' is as far above the surface of the earth as C_1 is below. The new image now upsets the boundary conditions on the surface of the sphere and a third image must be placed at the point inverse to C_1'. This process is repeated until an infinite series of images is established. All the images lie in the plane $y=0$. The problem now is to establish the locations and strengths of the images.

The strength of a given image above the earth's surface is the same as that of the corresponding image within the sphere. Using the results of the above hemisphere problem, the strength of a given image within the sphere can be obtained from the strength of the image giving rise to it. For example, if the current strength of the original source is I, the strength of the image at C_1 is

$$I_1 = -\frac{r_1 I}{\sqrt{x_0^2 + z_0^2}}.$$

Since C_1 is the inverse point of C, its location is given by

$$x_1 = \frac{x_0 r_1^2}{x_0^2 + z_0^2}$$

and

$$z_1 = z_0 \left(\frac{x_0^2 + z_0^2 - r_1^2}{x_0^2 + z_0^2}\right).$$

The image at C_1' has the same strength as that at C_1 and its position is given by coordinates as $x=x_1$ and $z=-z_1$. To determine the strength I_2 and position of the image at C_2 in terms of the strength I_1 and position of the image at C_1, consider the general relationship between a given image and the image within the sphere immediately preceding the given image. Thus, I_2 and I_1 could as easily refer to I_n and I_{n-1}, respectively. The strength I_2 is given as

$$I_2 = -\frac{r_1 I_1}{\sqrt{x_1^2 + (z_0 + z_1)^2}}.$$

It can be seen from the diagram that $\sqrt{x_{n-1}^2 + (z_0 + z_{n-1})^2} > z_0 > r_1$. Therefore, the strengths of succeeding images will form a converging set of numbers and the sum of their effects will be a convergent series. The position of C_2 can be determined from the fact that C_2 is the point inverse to C_1'. We find that

$$x_2 = \frac{x_1 r_1^2}{x_1^2 + (z_0 + z_1)^2}$$

and

$$z_2 = z_0 - \frac{(z_0 + z_1) r_1^2}{x_1^2 + (z_0 + z_1)^2}.$$

In order that there will be no net flow of current out of the buried sphere, we place at the center of the sphere a complementary image whose strength is the negative sum of all of the image strengths in the first series of images within the sphere. This image is $J = -\sum_{n=1}^{\infty} I_n$. The image J at the center of the sphere causes current to cross the earth's surface, and we are therefore obliged to place an image J' of equal strength at the point $z=-z_0$. The new image J' in turn upsets the boundary condition at the surface of the sphere and thus leads to a new series of all of images which lie on the vertical line passing through the center of the sphere. By reasoning similar to that used above, it can be shown that the successive images are

$$\begin{cases} J_r = -\frac{r_1 J}{2 z_0} \text{ at } z = \frac{2 z_0^2 - r_1^2}{2 z_0} \\ J_2 = \frac{r_1 J}{2 z_0^2 - r_1^2} \text{ at } z = z_0 \left(\frac{4 z_0^2 - 3 r_1^2}{4 z_0^2 - r_1^2}\right) \end{cases}$$

and so on.

This second series of images has now created a net flow of current from the sphere. Therefore, we must place at the center of the sphere a second complementary image whose strength equals the sum of the strengths of all of the images in the second set within the sphere. This second complementary image leads to a third series of images whose positions on the z-axis are identical to the positions of the images in the second set. The third set of images leads to yet a third complementary image at the center of the sphere, and this process is repeated until we finally have an infinite number of complementary images built up in this way. It can be shown that the sum of all of these complementary images is also a convergent series.

Finally, the total potential at a point on the earth is given by the sum of the effects of all of the images. We note that each image within the sphere gives rise, by reflection in the earth's surface, to an image above that surface. Since both images in a given pair have the same strength and are equidistant from the surface, we double the effect of the images within the sphere and discard those above the earth's surface.

The total potential at a point $P(x, y, 0)$ on the earth's surface is then given by

$$U = \frac{\rho}{2\pi} \left\{ \frac{I}{R} + 2 \sum_{n=1}^{\infty} \frac{I_n}{\sqrt{(x_n - x)^2 + y^2 + z_n^2}} \right.$$
$$\left. + 2 \sum_{n=0}^{\infty} \frac{J_n}{\sqrt{x^2 + y^2 + z_n'^2}} + \ldots \right\} \quad (40)$$

where such images as I_n and J_n, and their positions are calculated as indicated above. Although it is complicated to write down these expressions explicitly, it is a straightforward matter to compute them numerically step-by-step.

BURIED CYLINDER AND SEMICIRCULAR TROUGH

The above solution may be applied equally well to the field due to a line current electrode parallel to a

buried perfectly conducting cylinder whose axis is in turn parallel to the y-axis. The only modification in the above development is to set $y=0$, to consider the current strength to be amperes per unit length of the electrode, and to convert the reciprocal distances to logarithmic terms. The images are similarly line electrodes. The same comments apply to the semi-circular trough when compared to the hemispherical sink discussed earlier.

The problem of a point current electrode near a buried cylinder cannot be solved by image theory. However, it is interesting to note what happens when we erroneously assume that an image solution is valid. For example, let us consider a point source in the vicinity of a trough of semicircular shape (fig. 23). The true resistivity of the country rock is ρ and that of the material in the trough is sufficiently low to be considered zero. The distance from the axis of the trough is r, the distance along the axis of the trough perpendicular to the paper is z, and ϕ is the angle measured as shown in the diagram.

Commencing as we did with the hemispherical sink problem discussed earlier in this section, we assume that an image of strength I' exists at the point $(r', 0, 0)$ as shown in the diagram. Then, the potential over the surface $r=r_1$ due to the image must be equal in magnitude but opposite in sign to that due to the original source. Thus,

$$\frac{I\rho}{2\pi\sqrt{(r_0 \cos \phi - r_1)^2 + z^2}} = \frac{I'\rho}{2\pi\sqrt{(r' \cos \phi - r_1)^2 + z^2}}.$$

Squaring both sides of the equation, we get

$$I'^2(r_0^2 \cos^2 \phi - 2r_0r_1 \cos \phi + r_1^2 + z^2)$$
$$= I^2(r'^2 \cos^2 \phi - 2r_1r' \cos \phi + r_1^2 + z^2).$$

This relationship must be valid for all values of ϕ and z if the assumption of an image solution is correct. However, in order to be valid for all values of z, it is necessary that $I = \pm I'$. In order to be valid for all values of ϕ, it is necessary that $I'^2r_0^2 = I^2r'^2$, which con-

tradicts the first condition. This contradiction shows that a single image is not sufficient to satisfy the boundary conditions. We would encounter similar contradictions if we tried to solve the problem with a series of images.
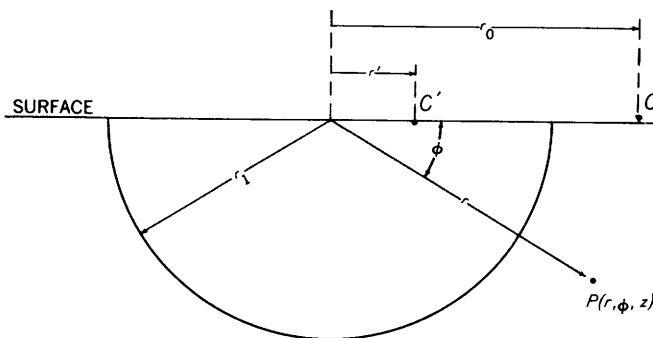
USEFUL COORDINATE SYSTEMS

In order to attack the potential problems which are the basis of theoretical studies in electrical prospecting, we try to choose a coordinate system in which an existing boundary can be described in terms of the constancy of only one of the three variables. We describe here a number of coordinate systems which can be used in electrical prospecting problems. All these systems will fall into two categories. The first and most important group contains systems that are formed by rotating some two-dimensional coordinate system about a "polar" axis. The second group contains systems that are cylindrical, that is, formed by projecting some two-dimensional coordinate system infinitely in a direction perpendicular to the plane of the original system. Some coordinate systems fall into both groups. It is seen, for example, that the system commonly called cylindrical coordinates can be formed by rotating a plane two-dimensional rectangular system about one of the original axes or by projecting a plane polar coordinate system perpendicularly to the plane of the original coordinates. With few exceptions, the systems which are not of the rotational type lead to mathematical development beyond the scope of this treatise.

If we assume, as we do, that the flow of current is ohmic in nature, it follows that the potential satisfies Laplace's equation. Therefore, in addition to describing the coordinate systems, we include the corresponding differential elements and Laplace's equations. We also solve Laplace's equation in the coordinate systems. Usually there will be more than one general solution for each form of Laplace's equation.

The general solution for each equation must contain sets of functions which possess two properties—those of orthogonality and completeness. We assume the second property when the first has been shown or given. However, we define both properties here so that the terms may be used with understanding later.

The term "orthogonality" comes originally from vector analysis (Pipes, 1946, p. 379). If two vectors are orthogonal (or perpendicular), their scalar product vanishes. This fact is expressed mathematically as:

$$\vec{A_1} \cdot \vec{B_1} = A_x B_x + A_y B_y + A_z B_z = 0.$$

If the vectors have n dimensions instead of the usual three, they are said to be orthogonal if

$$A_1 B_1 + A_2 B_2 + \ldots + A_n B_n = \sum_{i=1}^{n} A_i B_i = 0.$$

FIGURE 23.—Cross-sectional view of a point charge of current in the vicinity of a perfectly conducting trough of semicircular shape.

We consider now that the vectors exist in a space of infinite dimensions such that their components are continuously distributed. Then the summation becomes an integral, the summation index becomes a variable of integration, and the condition for orthogonality is

$$\int_0^s A(x)\,B(x)\,dx = 0.$$

We will now carry the analogy into the realm of functions. Let there be given a set of functions $f(x)$ which are characterized by some parameter which can assume discrete values. We designate by n and m two of the possible values of the parameter. The functions are said to be orthogonal to one another if

$$\int_0^s f_n(x)f_m(x)\,dx = 0$$

if n does not equal m. The integration is over the entire range of x.

The above fact can best be illustrated by a familiar set of orthogonal functions. We set $f_n(x)$ equal to sin (nx) and $f_m(x)$ equal to sin (mx). It can be verified by any table of integrals that

$$\int_0^{2\pi} \sin nx \sin mx \, dx = 0$$

if n and m are not equal. Therefore, the sine functions sin (nx) form an orthogonal set if n is restricted to integral values.

A set of functions is "complete" if an arbitrary function $g(x)$, satisfying the same boundary conditions as the functions of the set, can be expanded in the form

$$g(x) = \sum_{n=1}^{\infty} A_n f_n(x),$$

where the A_n's are constant coefficients (Pipes, 1946, p. 380). Thus, it is seen that the sine functions alone do not constitute a complete set because an arbitrary function cannot in general be expanded in terms of sine functions alone; cosine terms must also be included. Thus,

$$g(x) = \sum_{n=0}^{\infty} \{ A_n \sin nx + B_n \cos nx \}$$

which is recognized as the Fourier series.

The common basis for all useful coordinate systems is a generalized system of orthogonal curvilinear coordinates. We will study this system first. We will then find it more convenient to arrive at the specific systems by specializing the general system. We assume from the start that the reader is already familiar with the rectangular coordinate system in three dimensions and we will refer to that system as an example from time to time.

GENERALIZED COORDINATES

Let there be three families of surfaces, each family consisting of a set of nonintersecting curved surfaces. The families are related to each other in that any given surface of one family intersects perpendicularly all of the members of the other two families. Further, let these three families of surfaces be characterized by the parameters u_1, u_2, and u_3, respectively. Thus, any point in space may be described uniquely if one specifies the values of u_1, u_2, and u_3, which label the three mutually perpendicular surfaces that intersect at that point. The most common system of this type is the rectangular coordinate system in which the three families of surfaces are mutually perpendicular planes and the variables are x, y, and z.

In order to perform differential operations in generalized coordinates, it is necessary that the rates of change be calculated with respect to each of the three coordinates. We commence by considering two points, one specified by the coordinates u_1, u_2, and u_3, and the second given by $u_1 + du_1$, u_2, and u_3, where du_1 is arbitrarily small. We may reach the second point from the first by passing along the intersection of the surfaces for which u_2 and u_3 are given constants. The distance between the two points as measured along this intersection is given by $h_1 du_1$. The factor h_1 is a geometrical characteristic of the system; it is usually not a constant but can be calculated easily from geometrical considerations. If the geometry is too complex and the surfaces can be described analytically in rectangular coordinates, h_1 can be calculated from the relationship:

$$h_1^2 = \left(\frac{\partial x}{\partial u_1}\right)^2 + \left(\frac{\partial y}{\partial u_1}\right)^2 + \left(\frac{\partial z}{\partial u_1}\right)^2 \qquad (41)$$

The proportionality factors h_2 and h_3 are related similarly to the variables u_2 and u_3. The three elements of length in generalized coordinates are $dL_1 = h_1 du_1$, $dL_2 = h_2 du_2$, and $dL_3 = h_3 du_3$. It follows then that all the proportionality factors in rectangular coordinates are equal to unity and the three elements of length are dx, dy, and dz, respectively.

The elements of volume and area can now be established in terms of the above increments of length. Since any three coordinate surfaces are mutually perpendicular in the vicinity of the point at which they intersect, an element of volume has the shape of a rectangular parallelepiped. Its volume is the product of the three elements of length. A given element of area is one side of the parallelepiped, whence the area is the product of the two appropriate edges. A given element of area is specified by assigning to it a subscript which corresponds to the variable that changes in a direction perpendicular to the correspond-

ing face of the parallelepiped. The elements of volume and of area in generalized coordinates are:

$$\begin{cases} dv = h_1 h_2 h_3 du_1 du_2 du_3 \\ ds_1 = h_2 h_3 du_2 du_3 \\ ds_2 = h_1 h_3 du_1 du_3 \\ ds_3 = h_1 h_2 du_1 du_2. \end{cases}$$

One of the most important quantities of a potential field is the gradient. In contrast to the potential U, which is a scalar quantity, the potential gradient ∇U is a vector. By definition, the component of the gradient in a given direction is the space rate of change of the potential in that direction. Thus, the three principal components of the gradient in generalized coordinates are:

$$(\nabla U)_1 = \frac{1}{h_1} \frac{\partial U}{\partial u_1},$$

$$(\nabla U)_2 = \frac{1}{h_2} \frac{\partial U}{\partial u_2},$$

and

$$(\nabla U)_3 = \frac{1}{h_3} \frac{\partial U}{\partial u_3}.$$

The Laplacian operator ∇^2 is a scalar operator which may be defined as the divergence of a gradient. Hence, it is necessary to investigate the divergence before an expression for the Laplacian can be established. We begin by applying the divergence theorem,

$$\int \nabla \cdot V dv = \int V \cdot \overline{ds}, \tag{42}$$

to an elementary volume. In equation 42, V is any vector with the three scalar components V_1, V_2, and V_3, corresponding respectively to the three coordinates u_1, u_2, and u_3. The divergence of V is written mathematically as $\nabla \cdot V$. Within the elementary volume, the value of the divergence does not vary appreciably from its value at the center and its actual value may be replaced by its value at the center as an average. By removing $\nabla \cdot V$ from under the integral sign, we get for the left side of equation 42:

$$\nabla \cdot V \int dv = (\nabla \cdot V) \int (h_1 h_2 h_3 du_1 du_2 du_3). \tag{43}$$

The integral on the right side of equation 42 is a sum over the six faces of the elementary parallelepiped. If u_1 is the coordinate of the center of the element of volume, one of the faces is formed by the surface at $u_1 + du_1/2$ and the opposing face is formed by the surface at $u_1 - du_1/2$. We note at this point that the elementary cross-sectional area ds_1 may vary from one part of the elementary volume to another, because h_2 and h_3 may be functions of u_1. If $V_1 h_2 h_3 du_2 du_3$ is the scalar product of the vector V and the cross-sectional area at the

center section, the contribution to the integral from the two u_1 faces is given by:

$$\left\{ \left[h_2 h_3 V_1 + \frac{\partial (h_2 h_3 V_1)}{\partial u_1} \frac{du_1}{2} \right] - \left[h_2 h_3 V_1 - \frac{\partial (h_2 h_3 V_1)}{\partial u_1} \frac{du_1}{2} \right] \right\} du_2 du_3$$

$$= \frac{\partial (h_2 h_3 V_1)}{\partial u_1} du_1 du_2 du_3.$$

The remaining two pairs of faces make similar contributions so that we get for the right side of equation 42:

$$\left[\frac{\partial (h_2 h_3 V_1)}{\partial u_1} + \frac{\partial (h_1 h_3 V_2)}{\partial u_2} + \frac{\partial (h_1 h_2 V_3)}{\partial u_3} \right] du_1 du_2 du_3. \tag{44}$$

By equating 43 and 44, we finally get for the divergence in generalized coordinates:

$$\nabla \cdot V = \frac{1}{h_1 h_2 h_3} \left[\frac{\partial (h_2 h_3 V_1)}{\partial u_1} + \frac{\partial (h_1 h_3 V_2)}{\partial u_2} + \frac{\partial (h_1 h_2 V_3)}{\partial u_3} \right]. \tag{45}$$

The Laplacian operator may now be obtained by setting $V = \nabla U$ and by making use of the components of the gradient as written above:

$$\nabla^2 U = \frac{1}{h_1 h_2 h_3} \left[\frac{\partial}{\partial u_1} \left(\frac{h_2 h_3}{h_1} \frac{\partial U}{\partial u_1} \right) + \frac{\partial}{\partial u_2} \left(\frac{h_1 h_3}{h_2} \frac{\partial U}{\partial u_2} \right) \right.$$

$$\left. + \frac{\partial}{\partial u_3} \left(\frac{h_1 h_2}{h_3} \frac{\partial U}{\partial u_3} \right) \right]. \tag{46}$$

In the following discussion, we will obtain the necessary expressions for the various coordinate systems which we will use later. The method will be to determine the correct factors h_1, h_2, and h_3, and then to use these values to specialize the above general expressions. For example, we pointed out above that all of the proportionality factors in rectangular coordinates are equal to unity. We can, therefore, write down immediately the Laplacian in rectangular coordinates:

$$\nabla^2 U = \frac{\partial^2 U}{\partial x^2} + \frac{\partial^2 U}{\partial y^2} + \frac{\partial^2 U}{\partial z^2}. \tag{47}$$

SPHERICAL COORDINATES

Aside from the rectangular coordinate system, the most widely used systems are spherical and cylindrical coordinates. In spherical coordinates (fig. 24), the three families of surfaces are a set of concentric spheres, a family of right cones, and a set of half-planes. The centers of the concentric spheres is the origin of the system. The spheres are characterized by the parameter r, which is the radius of the sphere and which varies from zero to infinity. The equation of a given sphere in rectangular coordinates is $x^2 + y^2 + z^2 = r^2$. The vertices of the family of cones lie at the origin and their axes all lie along the z-axis which is known as the polar axis. The parameter θ is the angle formed between the positive z-axis and a generatrix of a given cone. Thus, θ can vary from zero to π. The angle θ is related to rectangular coordinates by the expressions
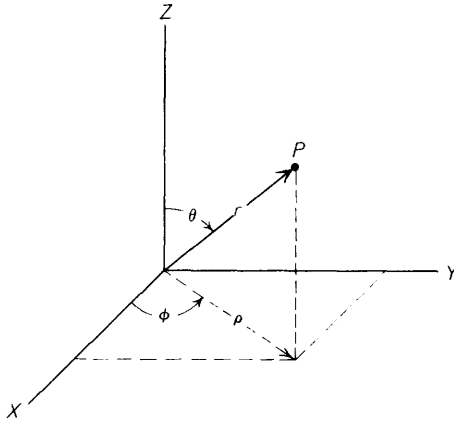
FIGURE 24.—Spherical coordinates.

$\sin\ \theta=\sqrt{x^2+y^2}/\sqrt{x^2+y^2+z^2}$ and $\cos\ \theta=z/\sqrt{x^2+y^2+z^2}$. The half-planes intersect in the polar axis and are characterized by the angle ϕ measured from the positive x-axis to a given plane. The angle ϕ can range from zero to 2π or sometimes from $-\pi$ to $+\pi$. The relationship between ϕ and rectangular coordinates is given by $\sin\ \phi=y/\sqrt{x^2+y^2}$ and $\cos\ \phi=x/\sqrt{x^2+y^2}$. The inverse relationship between rectangular and spherical coordinates is given by $x=r\cos\phi\sin\theta$, $y=r\sin\phi\sin\theta$, and $z=r\cos\theta$.

The proportionality factors for the spherical coordinate system are most easily determined from geometrical considerations. Let us consider the point P shown in figure 24. If the point is moved an infinitesimal distance along the radius vector, θ and ϕ being constant, the distance moved is dr. If, however, the point is moved an infinitesimal distance with ϕ and r kept constant, the distance moved is $rd\theta$. If the point is moved with θ and r held constant, the distance moved is $r\sin\ \theta d\phi$. Thus, we have determined the proportionality factors to be:

$$h_r=1,\ h_\theta=r,\ \text{and}\ h_\phi=r\sin\ \theta.$$

Thus, the elements of volume and of area in spherical coordinates are:

$$\begin{cases} dv=r^2\sin\ \theta d\theta d\phi dr \\ ds_r=r^2\sin\ \theta d\theta d\phi \\ ds_\theta=r\sin\ \theta d\phi dr \\ ds_\phi=rd\theta dr. \end{cases}$$

The components of the gradient are:

$$(\nabla U)_r=\frac{\partial U}{\partial r},\ (\nabla U)_\theta=\frac{1}{r}\frac{\partial U}{\partial \theta},\ \text{and}\ (\nabla U)_\phi=\frac{1}{r\sin\ \theta}\frac{\partial U}{\partial \phi}.$$

The Laplacian is:

$$\nabla^2U=\frac{1}{r^2}\frac{\partial}{\partial r}\left(r^2\frac{\partial U}{\partial r}\right)+\frac{1}{r^2\sin\ \theta}\frac{\partial}{\partial \theta}\left(\sin\ \theta\frac{\partial U}{\partial \theta}\right)+\frac{1}{r^2\sin^2\ \theta}\frac{\partial^2U}{\partial \phi^2}.$$

Equating the Laplacian to zero, we arrive at Laplace's equation in spherical coordinates:

$$\frac{\partial}{\partial r}\left[r^2\frac{\partial U}{\partial r}\right]+\frac{1}{\sin\ \theta}\frac{\partial}{\partial \theta}\left[\sin\ \theta\frac{\partial U}{\partial \theta}\right]+\frac{1}{\sin^2\ \theta}\frac{\partial^2U}{\partial \phi^2}=0.\quad(48)$$

This equation will be solved, as will other differential equations to follow, by separation of variables. We first assume a solution in the form of $U=R(r)\Theta(\theta)\Phi(\phi)$, where each of the factors is a function of a single variable only. When we divide each term in equation 48 by U and then substitute the assumed form of the solution, we get:

$$\frac{1}{R}\frac{d}{dr}\left[r^2\frac{dR}{dr}\right]+\frac{1}{\Theta\sin\ \theta}\frac{d}{d\theta}\left[\sin\ \theta\frac{d\Theta}{d\theta}\right]+\frac{1}{\Phi\sin^2\ \theta}\frac{d^2\Phi}{d\phi^2}=0.\quad(49)$$

We see that the first term contains only the variable r and that the second two terms contain only the angles θ and ϕ. Therefore, if the sum of these terms is to vanish for all values of the variables, the sum of the second and third terms must equal the negative of the first term, which in turn must equal some constant. For convenience, we choose that constant to be $n(n+1)$, whence we get for the differential equation in r:

$$\frac{d}{dr}\left[r^2\frac{dR_n}{dr}\right]-n(n+1)R_n=0.$$

The subscript n is appended to R because there will obviously be a separate solution for each value of n chosen. This equation is transformed by the substitution, $r=e^v$, into an equation that is easily solved by the methods of ordinary differential equations. The solution is

$$R_n=A_nr^n+B_nr^{-n-1}.\quad(50)$$

If we multiply each term in equation 49 by $\sin^2\ \theta$, we can show similarly that the resulting term involving only ϕ must equal a constant. For convenience, we choose this constant to be $-m^2$, whence we arrive at the equation,

$$\frac{d^2\Phi_m}{d\phi^2}+m^2\Phi_m=0.\quad(51)$$

The subscript m is appended to Φ for the same reason that the subscript n was used above. This equation is a standard equation from ordinary differential equations, and its solution is known to be

$$\Phi_m=C_m\cos\ m\phi+D_m\sin\ m\phi.\quad(52)$$

Any real physical problem requires that its solution be single valued. In the present case specifically, this requirement means that we should get the same solution whenever we increase the angle ϕ by 2π. This condition can be satisfied in the above solution only if m is an integer. Further, we will always choose our coordinate systems such that the source lies on the plane

$\phi=0$. This fact imposes the condition that the resulting potential functions will be even functions of the angle ϕ. As we lose no generality by this device, we will include in our general solution only the cosine term from equation 52. Because the cosine term is an even function of m, we will further restrict m to positive integral values.

Since most of the coordinate systems used in this paper are systems of revolution, the factor $\cos m\phi$ will appear in the corresponding solutions of Laplace's equation. In such cases, there will be no need to repeat the above development.

When we substitute m and n into equation 49, we get

$$\frac{1}{\sin\theta}\frac{d}{d\theta}\left[\sin\theta\,\frac{d\Theta_{mn}}{d\theta}\right]+\left[n(n+1)-\frac{m^2}{\sin^2\theta}\right]\Theta_{mn}=0. \quad (53)$$

This equation is known in the literature as the associated Legendre equation (Pipes, 1946, p. 322 ff.). Its solution is

$$\Theta_{mn}=E_{mn}P_n{}^m(\cos\theta)+F_{mn}Q_n{}^m(\cos\theta). \quad (54)$$

The term $P_n{}^m(\cos\theta)$ in the solution is called the associated Legendre polynomial of the first kind. When n is an integer and $|u|\le1$, this polynomial is defined by the relationship,

$$P_n{}^m(u)=(1-u^2)^{m/2}\frac{d^mP_n(u)}{du^m}, \quad (55)$$

where $P_n(u)$ is the Legendre polynomial defined by

$$P_n(u)=\sum_{s=0}^{r}(-1)^s\frac{(2n-2s)!}{2^n(s!)(n-s)!(n-2s)!}u^{n-2s}, \quad (56)$$

or

$$P_n(u)=\frac{1}{2^n n!}\frac{d^n(u^2-1)^n}{du^n}. \quad (57)$$

In equation 56, r is either $n/2$ or $(n-1)/2$ whichever is an integer. From the first definition, it is seen that $P_n{}^m(\cos\theta)$ is zero if $m>n$. We specify that n must be an integer in order to obtain a set of functions which are orthogonal over the spherical surfaces, because it can be shown that

$$\int_{-1}^{1}P_n{}^m(u)P_{n'}{}^m(u)du=\frac{2}{2n+1}\frac{(n+m)!}{(n-m)!}.$$

The term $Q_n{}^m(\cos\theta)$ in equation 54 is called the associated Legendre function of the second kind. Since $\cos\theta$ is either plus or minus one at some point in all regions in which our solution is of value, and since $Q_n{}^m(\cos\theta)$ becomes infinite at such points, we may drop this term from our solution.

The above solutions have all been derived for specific values of m and n. The general solution is the sum

of all of the special solutions. Therefore, the first general solution of Laplace's equation (48) in spherical coordinates is

$$U=\sum_{n=0}^{\infty}\sum_{m=0}^{n}[A_{mn}r^n+B_{mn}r^{-n-1}]P_n{}^m(\cos\theta)\cos m\phi. \quad (58)$$

A_{mn} and B_{mn} are arbitrary constants which depend upon m and n and which must be determined from the boundary conditions of the special problem to which this solution may be applied. As we have pointed out already, n is a positive integer which may range from zero to infinity, and m is a positive integer which ranges from zero to n.

Equation 58, which is the first solution of Laplace's equation 48, in spherical coordinates, is actually only one of a large number of possible solutions. As we have stated, that particular solution was chosen because it afforded a set of functions that are orthogonal over the spherical surfaces. Sets of functions which are orthogonal over other surfaces are possible if different forms of n and m are chosen. For example, if we substitute $ip-1/2$ for n in the above equations, we will have a set of functions that are orthogonal over the surfaces of the cones in spherical coordinates. In this complex expression for n, $i=\sqrt{-1}$ and p is a real number which may vary through all possible values from negative to positive infinity. The details of the solution follow closely those given above. We will first look at the effect of the substitution on R. Equation 50 now becomes

$$R_p=A(p)r^{ip-\frac{1}{2}}=\frac{A(p)}{\sqrt{r}}e^{ip\,\ln\,r}. \quad (59)$$

Since p takes on both positive and negative values, there is no longer a need to write down terms analogous to both terms in equation 50.

Equation 59 thus gives a second orthogonal set of functions over the conal surfaces, the functions $\cos m\phi$ constituting the first set. However, the expression of orthogonality is somewhat different from the previous case because we are now dealing with the continuous parameter p. We obtain this form of orthogonality through a knowledge of the Dirac delta function $\delta(p-p')$ (Pipes, 1946, p. 535), which is also known as the impulse function. As we have written it, p' is a specific fixed value of the variable p. The delta function equals zero when its argument is not zero but becomes infinite as its argument approaches zero. This infinity is such that the definite integral of the delta function from negative to positive infinity is equal to unity. A further property of the delta function is stated in the following form:

$$\int_{-\infty}^{\infty}f(p)\delta(p-p')dp=f(p'). \quad (60)$$

As applied to the present problem, one means of expressing this function is given by

$$\delta(p-p')=\frac{1}{2\pi}\int_0^\infty e^{i(p-p')\ln r}\frac{dr}{r},\qquad(61)$$

where p and p' are specific values of the set of parameters. That the expression on the right has the necessary properties can be verified by letting $r=e^v$ and then by directly testing the resulting expression.

The factor $\cos m\phi$ from equation 52 is unchanged by the substitution except that the integer m is no longer restricted and may vary from zero to infinity. However, the associated Legendre functions which form the solutions to equation 53 are affected. We now choose a solution to that equation in the form

$$\Theta_m(p)=E_m(p)\,P^m_{ip-\frac{1}{2}}(\cos\theta)+F_m(p)\,P^m_{ip-\frac{1}{2}}(-\cos\theta).$$

A valid definition of the Legendre function of order $ip-\frac{1}{2}$ is given in terms of the hypergeometric series (Hobson, 1931, p. 187):

$$P^m_{ip-\frac{1}{2}}(\cos\theta)=F\left(\frac{1}{2}-ip,\frac{1}{2}+ip;1;\frac{1-\cos\theta}{2}\right).\qquad(62)$$

Since m is an integer, the corresponding associated Legendre function is defined by equation 55. For later convenience, we have chosen $P^m_{ip-\frac{1}{2}}(-\cos\theta)$ instead of $Q^m_{ip-\frac{1}{2}}(\cos\theta)$ as the second independent solution of equation 53. This choice is a valid one whenever the order of the Legendre functions is not an integer. The associated Legendre function $P^m_{ip-\frac{1}{2}}(-\cos\theta)$ is defined equally well by equations 55 and 62 if $\cos\theta$ is replaced by $-\cos\theta$. An examination of equation 62 reveals that $P^m_{ip-\frac{1}{2}}(\cos\theta)$ becomes infinite when θ approaches π and that $P^m_{ip-\frac{1}{2}}(-\cos\theta)$ is infinite when $\theta=0$. These functions cannot be used in the regions where they become infinite.

This property of the component functions of the solutions to Laplace's equation is an observed empirical fact. When two of the component functions form orthogonal sets over a given surface, that surface partitions space into regions in which the separate parts of the third component are valid potential functions. In the immediately preceding case, R and Θ form sets of functions which are orthogonal over the conal surfaces. These same surfaces then separate space into regions in which

$$P^m_{ip-\frac{1}{2}}(\cos\theta)$$

and

$$P^m_{ip-\frac{1}{2}}(-\cos\theta)$$

are separately valid.

Finally, combining the above results, we get for the second general solution of Laplace's equation (48) in spherical coordinates:

$$U=\frac{1}{\sqrt{r}}\sum_{m=0}^\infty\cos m\phi\int_{-\infty}^\infty [A_m(p)\,P^m_{ip-\frac{1}{2}}(\cos\theta)$$

$$+B_m(p)\,P^m_{ip-\frac{1}{2}}(-\cos\theta)]e^{ip\ln r}\,dp.\qquad(63)$$

We use an integration over p instead of a summation because this parameter varies continuously. The functions $P^m_{ip-\frac{1}{2}}(\cos\theta)$ and $P^m_{ip-\frac{1}{2}}(-\cos\theta)$ are sometimes referred in the literature as cone functions; and the general solution of Laplace's equation given by equation 63 can, therefore, be considered as given in terms of these cone functions in spherical coordinates.

CYLINDRICAL COORDINATES

In cylindrical coordinates, the three sets of surfaces are a family of coaxial cylinders whose axis is the z-axis, a family of planes perpendicular to the z-axis, and a family of half-planes which intersect in the z-axis. The radius of any given cylinder is r, which may vary from zero to infinity and is related to rectangular coordinates by $x^2+y^2=r^2$. The planes perpendicular to the z-axis are identical with the xy-planes of rectangular coordinates. Therefore, z equal to a constant designates one of this family. The family of half-planes which intersect in the z-axis are characterized by the angle ϕ and are identical with the corresponding set of half-planes previously described in spherical coordinates. The inverse relationships are $x=r\cos\phi$, $y=r\sin\phi$, and $z\equiv z$. Cylindrical coordinates can be pictured in figure 24, if r is considered to be the perpendicular distance from the point P to the polar axis—that is, the projection of the r in spherical coordinates on the xy-plane. The diagram is labeled to show z and the angle ϕ is identical in both systems.

The proportionality factors of cylindrical coordinates, which are found geometrically as were those in spherical coordinates, are

$$h_r=1,\ h_\phi=r,$$

and

$$h_z=1.$$

It follows then that the elements of volume and area are

$$\begin{cases} dv=r\,dr\,d\phi\,dz \\ ds_r=r\,d\phi\,dz \\ ds_\phi=dr\,dz \\ ds_z=r\,d\phi\,dr. \end{cases}$$

The three components of the gradient are

$$(\nabla U)_r=\frac{\partial U}{\partial r},\ (\nabla U)_\phi=\frac{1}{r}\frac{\partial U}{\partial\phi},\ \text{and}\ (\nabla U)_z=\frac{\partial U}{\partial z}.$$

Laplace's equation in cylindrical coordinates becomes

$$\nabla^2 U = \frac{1}{r}\frac{\partial}{\partial r}\left(r\frac{\partial U}{\partial r}\right)+\frac{1}{r^2}\frac{\partial^2 U}{\partial \phi^2}+\frac{\partial^2 U}{\partial z^2}=0. \tag{64}$$

We commence the solution of this equation by assuming a solution in the form $U=R(r)Z(z)\Phi(\phi)$. $R(r)$ is a function only of r, $Z(z)$ is a function only of z, and $\Phi(\phi)$ is a function only of ϕ. If we substitute this expression in equation 64 and manipulate the terms, the new equation can be written as

$$\frac{1}{rR}\frac{d}{dr}\left(r\frac{dR}{dr}\right)+\frac{1}{r^2\Phi}\frac{d^2\Phi}{d\phi^2}+\frac{1}{Z}\frac{d^2Z}{dz^2}=0. \tag{65}$$

As the last term contains only z, and the first two terms contain only r and ϕ, it follows that the sum of the first two terms is equal to the negative of the third term which in turn must be equal to a constant. For convenience, we let this constant be λ^2 so that we get for the differential equation in z:

$$\frac{d^2Z}{dz^2}-\lambda^2 Z=0. \tag{66}$$

This equation is comparable to equation 51 except that it leads to exponential or hyperbolic functions instead of circular functions. Therefore, the solution is

$$Z_\lambda = A(\lambda)e^{\lambda z}+B(\lambda)e^{-\lambda z}. \tag{67}$$

There is no restriction on λ except that it be a real number; it may range from zero to infinity. If we desired to do so, we could let λ range from negative to positive infinity; in which case, we could discard the second term in this solution.

In equation 65, we could similarly isolate the part of the equation which contains only ϕ and set it equal to $-m^2$. This step leads to the solution $\Phi_m=\cos m\phi$ as discussed in the paragraph following equation 52. When we substitute the parameters λ and m back into equation 65, we find, after rearrangement, the final equation which must be solved:

$$r^2\frac{d^2R}{dr^2}+r\frac{dR}{dr}+(\lambda^2r^2-m^2)R=0. \tag{68}$$

This equation is known in the literature as Bessel's differential equation (Pipes, 1946, p. 307 ff.). The solutions of this equation are the Bessel functions, of which we require only the first kind $J_m(\lambda r)$ in our problems to follow. The second independent solution of equation 68 is the Bessel function of the second kind, $Y_m(\lambda r)$, which is unacceptable because it becomes infinite whenever $r=0$. A valid definition of the Bessel function of the first kind is

$$J_n(u)=\sum_{s=0}^{\infty}\frac{(-1)^s}{(s!)(n+s)!}\left(\frac{u}{2}\right)^{n+2s} \tag{69}$$

The most general solution of a differential equation consists of the sum of all special solutions. Therefore, upon combining the separate results from above, we get for the first general solution of Laplace's equation (64) in cylindrical coordinates:

$$U=\sum_{m=0}^{\infty}\cos m\phi\int_0^{\infty}[A_m(\lambda)e^{\lambda z}+B_m(\lambda)e^{-\lambda z}]J_m(\lambda r)d\lambda. \tag{70}$$

Equation 70 gives a solution which is valuable when boundary surfaces are the set of planes characterized by constant z. However, to work with boundaries which are formed by the half planes of constant ϕ, we must look for another form of the solution. We get the necessary solutions when we change both λ and m from real to pure imaginary numbers. We will commence by changing λ to it in equations 66 and 68. Since we will arbitrarily choose our coordinates so that the source lies in the plane $z=0$, we need retain only the part of the solution which is an even function of z. Thus, in the new solution, equation 67 is changed to read

$$Z_t=A(t)\cos tz.$$

In equation 52, we let m become is so that the solution in ϕ is either exponential or hyperbolic. For reasons given previously, we desire a solution which is an even function of ϕ. This is best obtained by choosing the hyperbolic form of the solution in ϕ and by retaining only the hyperbolic cosine. Moreover, anticipating the results in a later section (p. 77 to 78), we recognize that it will be more convenient if we use the angles $\pi\pm\phi$ instead of ϕ itself. Therefore, the present solution comparable to equation 52 is

$$\Phi_s=C(s)\cosh(\pi+\phi)+D(s)\cosh(\pi-\phi).$$

Finally, we must modify the solution of equation 68 which has become Bessel's equation with pure imaginary parameters. The solution $K_{is}(tr)$ is known as a modified Bessel function or a wedge function and is defined through the relationships (Morgan, 1947),

$$K_{is}(u)=\frac{i\pi}{2\sinh s\pi}[I_{is}(u)-I_{-is}(u)] \tag{71}$$

or

$$K_{is}(u)=\int_0^{\infty}e^{-u\cosh t}\cos st\,dt, \tag{72}$$

where

$$I_{is}(u)=e^{\pi s/2}J_{is}(u)=\sum_{m=0}^{\infty}\frac{1}{\Gamma(m+1)\Gamma(is+m+1)}\left(\frac{u}{2}\right)^{is+2m} \tag{73}$$

The implied definition of the ordinary Bessel function in equation 71 is consistent with equation 69 when the order is an integer. $K_{is}(tr)$ vanishes as r approaches

infinity; as r approaches zero, this function oscillates as $\cos\left(s \ln \dfrac{tr}{2}\right)$ (Smythe, 1950, p. 199). $I_{ts}(tr)$ is a second independent solution of equation 68, but it becomes infinite as r becomes infinite. Since all regions of interest contain infinite values of r, this second solution can be discarded.

The second general solution of Laplace's equation 64 in cylindrical coordinates now takes the form

$$U=\int_0^\infty \cos tz\, dt \int_0^\infty [A(s,\,t)\,\cosh s(\pi+\phi)$$
$$+\,B(s,\,t)\,\cosh s(\pi-\phi)]K_{is}(tr)ds. \quad (74)$$

We will require yet a third general solution to Laplace's equation in cylindrical coordinates. As in the previous case, we let $\lambda=it$ so the dependence of the third solution on z is the same as that of the second solution, given by equation 74. However, we retain the same dependence on ϕ that we had in the first solution given by equation 70. Therefore, for dependence on r, we seek solutions of equation 68 when λ is a pure imaginary number and when m is a positive integer or zero. Two independent solutions of equation 68 are the modified Bessel functions which are defined by

$$K_\nu(t)=\frac{\pi}{2\sin\nu\pi}\,[I_{-\nu}(t)-I_\nu(t)], \quad (75)$$

where

$$I_\nu(t)=e^{\frac{-i\nu\pi}{2}}\,J_\nu(it). \quad (75A)$$

$I_m(tr)$ becomes infinite as r becomes very large, and $K_m(tr)$ becomes infinite on the cylindrical axis where $r=0$. These conditions dictate the regions in which the solutions are valid.

We now have the third general solution to Laplace's equation in cylindrical coordinates:

$$U=\sum_{m=0}^{\infty}\cos\,m\phi\int_0^\infty \cos tz\,[A_m(t)I_m(tr)+B(t)_mK_m(tr)]dt. \quad (76)$$

This solution is useful when the boundaries are cylindrical in shape. We will find the solution of value in studying the anomalous effect of a filled channel, a pipe, or a long ditch on an electrical survey.

PROLATE SPHEROIDAL COORDINATES

A prolate spheroidal coordinate system (fig. 25) comprises the three orthogonal families of surfaces: prolate spheroids, hyperboloids of two sheets, and planes intersecting in the z-axis. The common foci of all the hyperboloids, which coincide with the common foci of all the ellipsoids, lie at the points $z=+b$ and $z=-b$. The parameter of the spheroids, η, varies from one to infinity. For $\eta=1$, the spheroid is degenerate
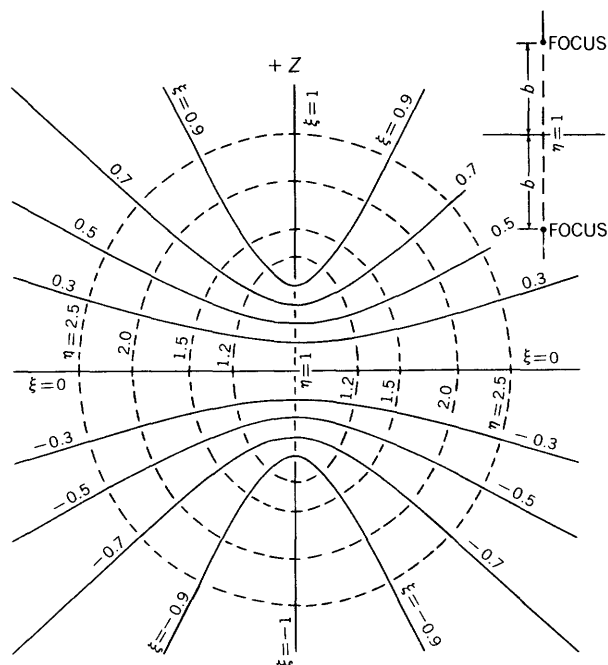
FIGURE 25.—Prolate spheroidal coordinates. Surfaces of constant third dimension are azimuthal planes through the vertical z-axis.

and consists of the segment of line connecting the points $z=+b$ and $z=-b$. For large values of η, the spheroids approach a spherical shape. The parameter of the hyperboloids, ξ, varies from -1 to $+1$. The portion of the z-axis for $z>b$ coincides with $\xi=1$ and that for $z<-b$ coincides with $\xi=-1$. The surface for $\xi=0$ corresponds to the xy-plane in rectangular coordinates. The complete prolate spheroidal coordinate system is obtained by rotating about the z-axis the diagram in figure 25. Therefore, the third variable is the angle ϕ which is identical to the corresponding angle in spherical coordinates.

The ellipsoids in prolate spheroidal coordinates are described by the equation, $z^2/b^2\eta^2+(x^2+y^2)/b^2(\eta^2-1)=1$, where η characterizes a given one of the family of ellipsoids. The hyperboloids are given by the equation, $z^2/b^2\xi^2-(x^2+y^2)/b^2(1-\xi^2)=1$. These two equations may be considered as serving to express η and ξ in terms of rectangular coordinates. The inverse transformations are given by $x=b\sqrt{(1-\xi^2)(\eta^2-1)}\,\cos\,\phi$, $y=b\sqrt{(1-\xi^2)(\eta^2-1)}\,\sin\,\phi$, and $z=b\eta\xi$.

Owing to the obvious complexity of the geometry in prolate spheroidal coordinates, it is more satisfactory to derive the proportionality factors through the use of equation 41. We will determine h_η in this manner. In order to do this, we use the inverse transformations given above. The necessary derivatives are

$$\frac{\partial x}{\partial\eta}=b\eta\sqrt{\frac{1-\xi^2}{\eta^2-1}}\,\cos\,\phi,\ \ \frac{\partial y}{\partial\eta}=b\eta\sqrt{\frac{1-\xi^2}{\eta^2-1}}\,\sin\,\phi,\ \text{and}\ \frac{\partial z}{\partial\eta}=b\xi.$$

We get h_η upon substitution of these derivatives into equation 41. The other factors are similarly derived so that we have

$$h_\eta = b\sqrt{\frac{\eta^2-\xi^2}{\eta^2-1}}, \quad h_\xi = b\sqrt{\frac{\eta^2-\xi^2}{1-\xi^2}}, \text{ and } h_\phi = b\sqrt{(\eta^2-1)(1-\xi^2)}.$$

It follows then that the elements of volume and area in prolate spheroidal coordinates are:

$$\begin{cases} dv = b^3(\eta^2-\xi^2)d\eta d\xi d\phi \\ ds_\eta = b^2\sqrt{(\eta^2-\xi^2)(\eta^2-1)}d\xi d\phi \\ ds_\xi = b^2\sqrt{(\eta^2-\xi^2)(1-\xi^2)}d\eta d\phi \\ ds_\phi = \frac{b^2(\eta^2-\xi^2)}{\sqrt{(\eta^2-1)(1-\xi^2)}}d\eta d\xi. \end{cases} \quad (77)$$

The three components of the gradient are

$$(\nabla U)_\eta = \frac{1}{b}\sqrt{\frac{\eta^2-1}{\eta^2-\xi^2}}\frac{\partial U}{\partial\eta}, \quad (\nabla U)_\xi = \frac{1}{b}\sqrt{\frac{1-\xi^2}{\eta^2-\xi^2}}\frac{\partial U}{\partial\xi},$$

and

$$(\nabla U)_\phi = \frac{1}{b\sqrt{(\eta^2-1)(1-\xi^2)}}\frac{\partial U}{\partial\phi}. \quad (78)$$

The Laplacian is

$$\nabla^2 U = \frac{1}{b^2(\eta^2-\xi^2)}\left\{\frac{\partial}{\partial\eta}\left[(\eta^2-1)\frac{\partial U}{\partial\eta}\right]+\frac{\partial}{\partial\xi}\left[(1-\xi^2)\frac{\partial U}{\partial\xi}\right] \right. \\ \left. +\frac{\eta^2-\xi^2}{(\eta^2-1)(1-\xi^2)}\frac{\partial^2 U}{\partial\phi^2}\right\}.$$

In prolate spheroidal coordinates, Laplace's equation is

$$\frac{\partial}{\partial\eta}\left[(\eta^2-1)\frac{\partial U}{\partial\eta}\right]+\frac{\partial}{\partial\xi}\left[(1-\xi^2)\frac{\partial U}{\partial\xi}\right]+\frac{\eta^2-\xi^2}{(\eta^2-1)(1-\xi^2)}\frac{\partial^2 U}{\partial\phi^2}=0. \quad (79)$$

As in previous forms of Laplace's equation, the variables in this equation may be separated by the assumption of a solution in the form, $U=H(\eta)G(\xi)\Phi(\phi)$. In terms of the new variables, equation 79 becomes

$$\frac{1}{H}\frac{d}{d\eta}\left[(\eta^2-1)\frac{dH}{d\eta}\right]+\frac{1}{G}\frac{d}{d\xi}\left[(1-\xi^2)\frac{dG}{d\xi}\right] \\ +\frac{\eta^2-\xi^2}{(\eta^2-1)(1-\xi^2)}\frac{1}{\Phi}\frac{d^2\Phi}{d\phi^2}=0. \quad (80)$$

The first step in the solution of the equation as it now stands is to set the term involving Φ equal to $-m^2$ so that the ϕ dependence of the potential is given by $\cos m\phi$ as it was in equation 58. When $-m^2$ is substituted back into equation 80, it is found that H and G both satisfy an equation of the same form. For G, the equation is

$$\frac{d}{d\xi}\left[(1-\xi^2)\frac{dG}{d\xi}\right]+\left[n(n+1)-\frac{m^2}{1-\xi^2}\right]G=0, \quad (81)$$

which is a form of the associated Legendre equation. For H, the equation is

$$\frac{d}{d\eta}\left[(\eta^2-1)\frac{dH}{d\eta}\right]-\left[n(n+1)+\frac{m^2}{\eta^2-1}\right]H=0, \quad (82)$$

which is the form the associated Legendre equation takes when the independent variable is larger than unity. Thus, the dependence of the solution upon η and ξ is given by

$$H = A_{mn}P_n{}^m(\eta) + B_{mn}Q_n{}^m(\eta)$$

$$G = C_{mn}P_n{}^m(\xi) + D_{mn}Q_n{}^m(\xi),$$

where $P_n{}^m(x)$ and $Q_n{}^m(x)$ are the associated Legendre functions of the first and second kinds, respectively.

In these expressions, both m and n are integers and $m \le n$. Either equation 56 or equation 57 is a valid definition of the Legendre polynomial for all possible values of the argument when n is an integer. Equation 55 is a valid definition of the associated Legendre polynomial when the argument is less than unity. However, when the argument is greater than unity, as is η, we prefer to define the associated Legendre polynomial as

$$P_n{}^m(u) = (u^2-1)^{\frac{m}{2}}\frac{d^m P_n(u)}{du^m} \quad (83)$$

because this definition avoids imaginary values when m is odd. When results from other sources have been taken into this paper, or have been compared with results derived herein, definitions have been changed to conform to the above equations. It is noted that the two definitions differ only by the constant factor, i^m, and thus it is not inconsistent that they both be valid definitions.

For the Legendre function of the second kind, one may write (Hobson, 1931, p. 90)

$$Q_n(u) = 2^n\sum_{s=0}^{\infty}\frac{(n+s)!(n+2s)!}{s!(2n+2s+1)!}u^{-n-2s-1}. \quad (84)$$

The associated functions of the second kind may be defined by equations 55 and 83 if the corresponding Q's replace the P's in the equations as they are now written. In all regions of interest, there are points at which $Q_n{}^m(\xi)$ becomes infinite. Therefore, this function may be omitted from the general solution.

The first general solution of Laplace's equation 79 in prolate spheroidal coordinates is, then,

$$U = \sum_{n=0}^{\infty}\sum_{m=0}^{n}[A_{mn}P_n{}^m(\eta)+B_{mn}Q_n{}^m(\eta)]P_n{}^m(\xi)\cos m\phi. \quad (85)$$

The above solution of Laplace's equation in prolate spheroidal coordinates contains functions that are orthogonal over the ellipsoidal surfaces.

We now desire a general solution that contains functions orthogonal over the hyperboloidal surfaces.

In order to gain insight into this problem, we first examine the relation between prolate spheroidal coordinates and spherical coordinates. In order to make the comparison, we return to the transformation equations from prolate spheroidal coordinates to spherical coordinates which can be obtained by comparing both of these to rectangular coordinates. We find that $r = b\sqrt{\eta^2 + \xi^2 - 1}$ and $\cos\theta = \eta\xi/\sqrt{\eta^2 + \xi^2 - 1}$.

Let us see what happens to the second of these relationships as η becomes large. We have $\lim\limits_{\eta \to \infty} \cos\theta = \xi$, which indicates that far from the origin the hyperbolic surfaces approach asymptotically the conal surfaces of spherical coordinates. Hence, it is inferred that the dependence of our present solution upon ξ should be the same as the dependence of equation 63 upon $\cos\theta$. In that equation we have a solution which contains functions orthogonal over the surfaces of the cones; in the present solution we want functions which are orthogonal over the hyperbolic surfaces asymptotic to these cones.

Therefore, we change n in equation 81 to $ip - 1/2$. Since $n(n+1)$, or $-p^2 - 1/4$ in this case, occurs in both equations 81 and 82, the order of the associated Legendre functions must be the same whether the argument is ξ or η. In considering the appropriate solution for H, it is noted the $P^m_{ip-1/2}(\eta)$ and $P^m_{ip-1/2}(-\eta)$ are independent solutions of the differential equation for the same reason given in the discussion of the cone functions. However, as previously noted, $P^m_{ip-1/2}(-\eta)$ becomes infinite as η approaches unity. Since η equals unity within any region bounded only by hyperboloids of the set for which ξ serves as the parameter, this function is discarded from the solution at once. The function $P^m_{ip-1/2}(\eta)$ is called the hyperboloid function to distinguish it from the cone functions in which the argument is less than unity.

Throughout the range of η, the hyperboloid function may be defined by (Magnus and Oberhettinger, 1949, p. 56)

$$P_{ip-1/2}(\eta) = \left(\frac{\eta+1}{2}\right)^{ip-1/2} F\left(\frac{1}{2} - ip, \frac{1}{2} - ip, 1; \frac{\eta-1}{\eta+1}\right) \quad (86)$$

when m is equal to zero. An integral expression for the same function is given as (Hobson, 1931, p. 451)

$$P_{ip-1/2}(\eta) = \frac{2}{\pi}\cos \pi p \int_0^\infty \frac{\cos px}{(2\cosh x + 2\eta)^{1/2}}\, dx. \quad (87)$$

As m is a positive integer, the associated function may be defined by equation 83.

A general solution to Laplace's equation in prolate spheroidal coordinates may now be written. It is necessary to sum over m from zero to infinity. The parameter p varies continuously, requiring an integral over all possible positive values; negative values of p

are not required because the solution is an even function of p. The second general solution of Laplace's equation 79 in prolate spheroidal coordinates is

$$U = \sum_{m=0}^{\infty} \cos m\phi \int_0^\infty [A_m(p)\, P^m_{ip-1/2}(\xi)$$
$$+ B_m(p)\, P^m_{ip-1/2}(-\xi)]\, P^m_{ip-1/2}(\eta)\, dp \quad (88)$$

and contains functions which are orthogonal over the hyperbolic surfaces as we desire.

OBLATE SPHEROIDAL COORDINATES

Oblate spheroidal coordinates (fig. 26) are formed by the families of orthogonal surfaces that are oblate
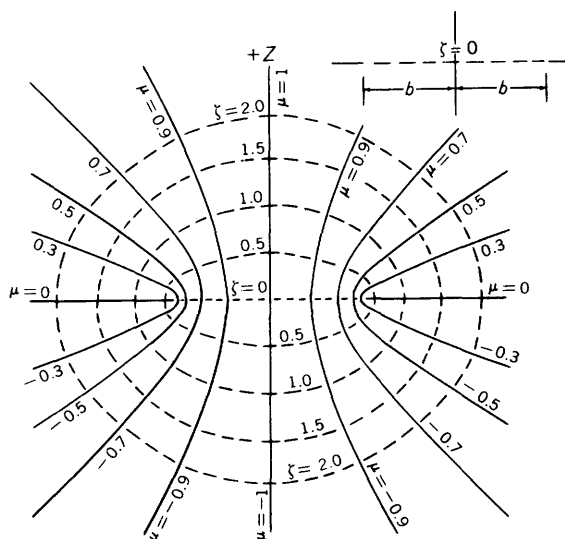
FIGURE 26.—Oblate spheroidal coordinates. Surfaces of constant third dimension are azimuthal planes through the vertical z-axis.

spheroids, hyperboloids of one sheet, and half-planes intersecting in the z-axis. The spheroidal parameter ζ varies from zero to infinity. Instead of a pair of foci, as in prolate spheroidal coordinates, a focal circle of radius b lies in the xy-plane. The points for which $\zeta = 0$ lie in the xy-plane within the focal circle. For large values of ζ, the spheroids approach spheres as in prolate spheroidal coordinates. The parameter of the hyperboloids μ ranges from -1 to $+1$. Points for which $\mu = -1$ lie on the negative z-axis, and points for which $\mu = +1$ lie on the positive z-axis. For the entire xy-plane outside the focal circle, $\mu = 0$. As in the prolate spheroidal case, the entire system is obtained by rotating the two-dimensional system (fig. 26) about the z-axis.

The spheroids in oblate spheroidal coordinates are described by the equation $\dfrac{x^2+y^2}{b^2(1-\mu^2)} - \dfrac{z^2}{b^2\mu^2} = 1$, where μ is given for a specific member of the family of ellip-

soids. The hyperboloids are given by the equation $\frac{x^2+y^2}{b^2(1+\zeta^2)}+\frac{z^2}{b^2\zeta^2}=1$. These two equations serve to express ζ and μ in terms of rectangular coordinates. The inverse transformations are given by $x=b\sqrt{(1+\zeta^2)(1-\mu^2)}$ $\cos\,\phi$, $y=b\sqrt{(1+\zeta^2)(1-\mu^2)}\,\sin\,\phi$, and $z=b\zeta\mu$.

Once again it is more satisfactory to use equations of the type of 41 to derive the proportionality factors. The necessary derivatives are easily obtained from the inverse transformations given above, so that we have:

$$h_\zeta=b\sqrt{\frac{\zeta^2+\mu^2}{\zeta^2+1}},\ h_\mu=b\sqrt{\frac{\zeta^2+\mu^2}{1-\mu^2}},\ \text{and}\ h_\phi=b\sqrt{(\zeta^2+1)(1-\mu^2)}.$$

The elements of volume and area are:

$$\begin{cases} dv=b^3(\zeta^2+\mu^2)d\zeta d\mu d\phi \\ ds_\zeta=b^2\sqrt{(\zeta^2+\mu^2)(\zeta^2+1)}\,d\mu d\phi \\ ds_\mu=b^2\sqrt{(\zeta^2+\mu^2)(1-\mu^2)}\,d\zeta d\phi \\ ds_\phi=\dfrac{b^2(\zeta^2+\mu^2)}{\sqrt{(\zeta^2+1)(1-\mu^2)}}\,d\zeta d\mu. \end{cases}$$

The three components of the gradient are:

$$(\nabla U)_\zeta=\frac{1}{b}\sqrt{\frac{\zeta^2+1}{\zeta^2+\mu^2}}\,\frac{\partial U}{\partial\zeta},\ (\nabla U)_\mu=\frac{1}{b}\sqrt{\frac{1-\mu^2}{\zeta^2+\mu^2}}\,\frac{\partial U}{\partial\mu},$$

and

$$(\nabla U)_\phi=\frac{1}{b\sqrt{(\zeta^2+1)(1-\mu^2)}}\,\frac{\partial U}{\partial\phi}.$$

The Laplacian is:

$$\nabla^2U=\frac{1}{b^2(\zeta^2+\mu^2)}\left\{\frac{\partial}{\partial\zeta}\left[(\zeta^2+1)\,\frac{\partial U}{\partial\zeta}\right]+\frac{\partial}{\partial\mu}\left[(1-\mu^2)\,\frac{\partial U}{\partial\mu}\right]\right.$$
$$\left.+\frac{\zeta^2+\mu^2}{(\zeta^2+1)(1-\mu^2)}\,\frac{\partial^2 U}{\partial\phi^2}\right\}.$$

In oblate spheroidal coordinates, Laplace's equation is

$$\frac{\partial}{\partial\zeta}\left[(\zeta^2+1)\,\frac{\partial U}{\partial\zeta}\right]+\frac{\partial}{\partial\mu}\left[(1-\mu^2)\,\frac{\partial U}{\partial\mu}\right]+\frac{\zeta^2+\mu^2}{(\zeta^2+1)(1-\mu^2)}\,\frac{\partial^2 U}{\partial\phi^2}=0.$$

We note the similarity between this equation and the corresponding equation 79 in prolate spheroidal coordinates. The previous equation may be converted to the present one if we make the following transformations:

$$\begin{cases} \xi\rightarrow\mu \\ \eta\rightarrow i\zeta. \end{cases} \tag{89}$$

Hence, we conclude that the solutions for prolate spheroids can be converted to the corresponding solutions for oblate spheroids through the same transformations. In addition, we must multiply the prolate spheroidal solutions by i to get the corresponding oblate spheroidal solutions. Therefore, we will not give separate proofs for the solutions applying to oblate spheroids, but will write them down directly by making the above substitutions in the solutions that apply

to prolate spheroids. The same relation obviously exists, except for the multiplication by i, between solutions for the hyperbolic surfaces in the two systems. However, this fact is of little value because the hyperboloids of one sheet in oblate spheroidal coordinates do not approximate any common geologic structure.

BIPOLAR COORDINATES

Bipolar coordinates, as they appear in cross section, are shown in figure 27. If the right half of figure 27 is rotated about the polar axis, it will generate two orthogonal families of surfaces; the third required family is the set of half-planes whose common intersection is the polar z-axis. The azimuthal angle ϕ is the parameter of this set of planes.

Bipolar coordinates may be related to spherical coordinates in the following way. Let us assume a point P with coordinates r and θ in a spherical coordinate system whose origin A is located at the point $z=b$ on the z-axis in a reference rectangular coordinate system (fig. 27). We then construct a circular arc AA' with a radius of $2b$ and with its center B at the point $z=-b$. We now locate a point P', on the line BP, such that $BP':2b=2b:BP$. The point P' is said to be inverse to the point P with respect to the circle AA'. The above proportionality relationship, together with the existence of the common angle ABP, establishes that triangle ABP is similar to triangle $P'BA$. It follows that angle $AP'B$ equals angle PAB, whence we see that $\tau=\pi-\theta$, where τ is defined as the angle subtended by the line AB at the point P'. This relationship between τ and θ depends only on the fact that P and P' are inverse points. Therefore, if we define a surface which is the locus of the inverse points (corresponding to P') of all points (corresponding to P) on the cone represented by a given value of θ, that surface will be one in which τ is also a constant.

In the cross section shown, this surface appears as the segment $AP'DB$ of a circle. We can determine the equation of the circle from the geometry of figure 27B. The distance CD is the radius of the circular arc whose center is at the point C. The line CE is drawn perpendicular to the line DB and thus bisects it. The steps in the proof are:

$$\angle ODB=\frac{\tau}{2}$$

$$\overline{DE}=\frac{1}{2}\,\overline{DB}=\frac{1}{2}\,b\,\csc\,\frac{\tau}{2}$$

$$\overline{CD}=\overline{DE}\,\sec\,\frac{\tau}{2}=\frac{b}{2}\,\sec\,\tau/2\,\csc\,\frac{\tau}{2}=b\,\csc\,\tau$$

$$\overline{OD}=b\,\cot\,\frac{\tau}{2}$$

$$\overline{OC}=b\left(\csc\,\tau-\cot\,\frac{\tau}{2}\right)=b\,\cot\,\tau.$$
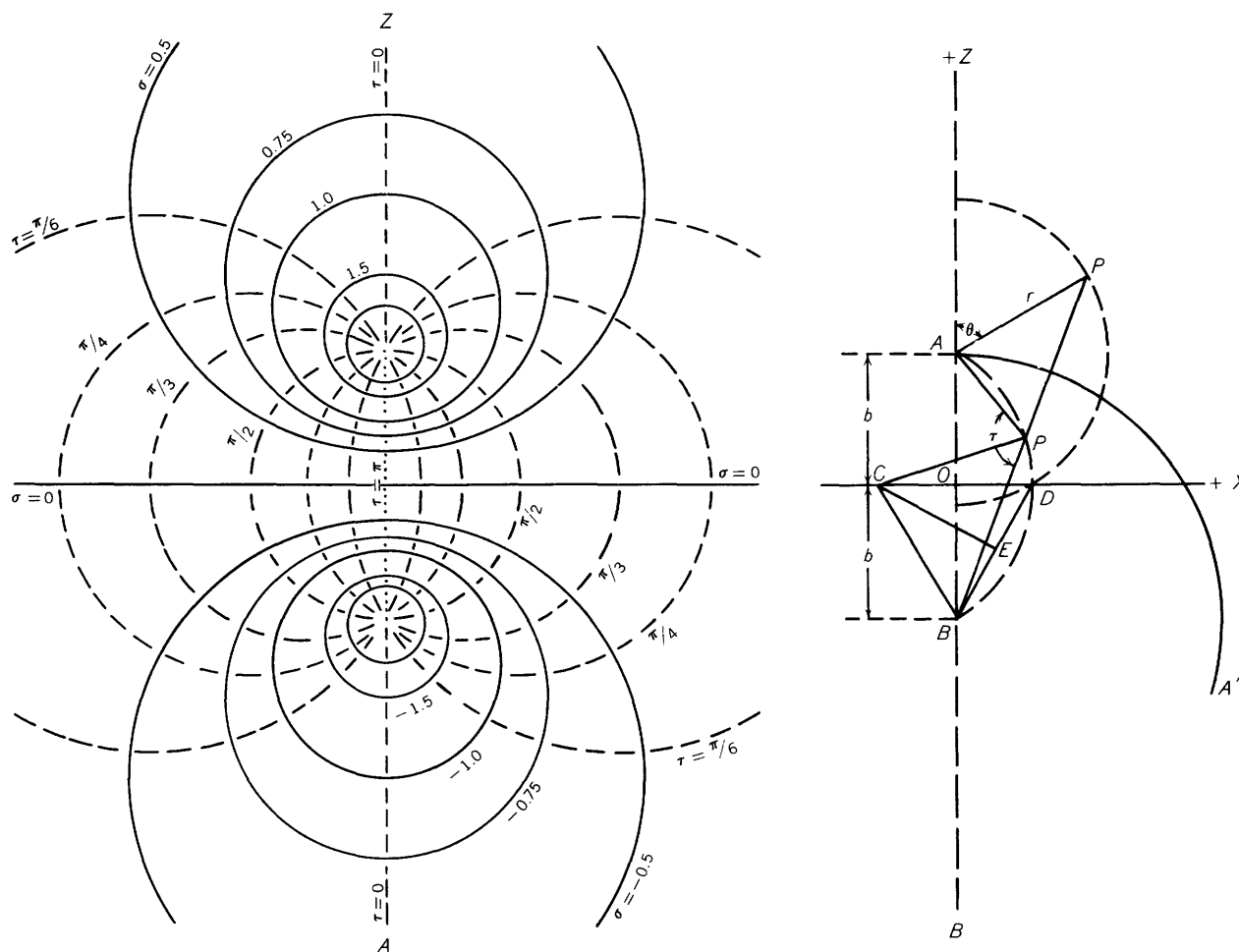
Therefore, the equation of the circular arc is $(\sqrt{x^2+y^2}-b \cot \tau)^2+z^2=b^2 \csc^2 \tau$. It should be realized that this is not the equation for a surface over which τ is constant, because the axis of rotation is the line AB and not a line through C. These surfaces are surfaces of degree four, which Hobson (1931, p. 449) calls spindles. The smallest sphere which can possibly pass through the two points $z=b$ and $z=-b$ has its center at the origin and is the surface $\tau=\pi/2$. The portion of the polar axis for $z>b$ and for $z<-b$ is the two-segment line $\tau=0$. That portion of the polar axis which lies between the points $z=b$ and $z=-b$ is the locus of points for which $\tau=\pi$.

The equation for the sphere over which σ is constant can be obtained by relating r through the inversion process to the coordinates x, y, and z. From the similarity of triangles ABP and $P'BA$, we have $r:2b= AP':BP'$. We arbitrarily define our new variable as

$$\sigma=\ln\left(\frac{r}{2b}\right)=\ln\left(\frac{AP'}{BP'}\right).$$

When we substitute the values $r/2b=e^\sigma$, $(BP')^2= (b+z)^2+x^2+y^2$, and $(AP')^2=(b-z)^2+x^2+y^2$, square both sides, and rearrange the terms, we finally get the equation for the circle of constant σ : $x^2+y^2+(z- b \coth \sigma)^2=b^2 \csch^2 \sigma$. The first pole is located at the point on the polar axis for which $z=b$ and, at this point, σ is positive and infinite. The spheres surrounding this point increase in radius as σ decreases until finally the equatorial xy-plane is the surface upon which σ is everywhere zero. At the second pole, where $z=-b$, σ is negatively infinite. The progressively larger spheres surrounding this point represent increasing values of σ.

The following transformations from bipolar coordinates to rectangular coordinates can readily be verified by substitution into the above equations:

$$x=\frac{b \sin \tau \cos \phi}{\cosh \sigma-\cos \tau}, \ y=\frac{b \sin \tau \sin \phi}{\cosh \sigma-\cos \tau}, \text{ and } z=\frac{b \sinh \sigma}{\cosh \sigma-\cos \tau}. \quad (90)$$

If we combine the transformation for z with the equation for a circle of constant σ, we get the special trans-

formation equation which will be of use later:

$$x^2+y^2+z^2=b^2\,\frac{\cosh\,\sigma+\cos\,\tau}{\cosh\,\sigma-\cos\,\tau}.\qquad(91)$$

It is seen that equation 91 represents a sphere with its center at the origin, if one side or the other is set equal to a constant.

It is again more satisfactory to use equations of the type of 41 to derive the proportionality factors. We obtain the necessary derivatives from the inverse transformations of equations 90. The proportionality factors are

$$\begin{cases} h_\sigma=\dfrac{b}{\cosh\,\sigma-\cos\,\tau}\\[2mm] h_\tau=\dfrac{b}{\cosh\,\sigma-\cos\,\tau}\\[2mm] h_\phi=\dfrac{b\,\sin\,\tau}{\cosh\,\sigma-\cos\,\tau}. \end{cases}$$

The elements of volume and area are then found to be

$$\begin{cases} dv=\dfrac{b^3\,\sin\,\tau\;d\tau d\sigma d\phi}{(\cosh\,\sigma-\cos\,\tau)^3}\\[2mm] ds_\sigma=\dfrac{b^2\,\sin\,\tau d\tau d\phi}{(\cosh\,\sigma-\cos\,\tau)^2}\\[2mm] ds_\tau=\dfrac{b^2\,\sin\,\tau d\sigma d\phi}{(\cosh\,\sigma-\cos\,\tau)^2}\\[2mm] ds_\phi=\dfrac{b^2 d\sigma d\tau}{(\cosh\,\sigma-\cos\,\tau)^2}. \end{cases}\qquad(92)$$

The three components of the gradient are:

$$\begin{cases} (\nabla U)_\sigma=\dfrac{(\cosh\,\sigma-\cos\,\tau)}{b}\dfrac{\partial U}{\partial\sigma}\\[2mm] (\nabla U)_\tau=\dfrac{(\cosh\,\sigma-\cos\,\tau)}{b}\dfrac{\partial U}{\partial\tau}\\[2mm] (\nabla)U_\phi=\dfrac{(\cosh\,\sigma-\cos\,\tau)}{b\,\sin\,\tau}\dfrac{\partial U}{\partial\phi}. \end{cases}\qquad(93)$$

The Laplacian is:

$$\nabla^2 U=\frac{(\cosh\,\sigma-\cos\,\tau)^3}{b\,\sin\,\tau}\left\{\frac{\partial}{\partial\sigma}\left[\frac{\sin\,\tau}{(\cosh\,\sigma-\cos\,\tau)}\frac{\partial U}{\partial\sigma}\right]\right.$$
$$\left.+\frac{\partial}{\partial\tau}\left[\frac{\sin\,\tau}{(\cosh\,\sigma-\cos\,\tau)\partial\tau}\right]+\frac{1}{\sin\,\tau\,(\cosh\,\sigma-\cos\,\tau)}\frac{\partial^2 U}{\partial\phi^2}\right\}.$$

In bipolar coordinates Laplace's equation is

$$\frac{\partial}{\partial\sigma}\left[\frac{\sin\,\tau}{\cosh\,\sigma-\cos\,\tau}\frac{\partial U}{\partial\sigma}\right]+\frac{\partial}{\partial\tau}\left[\frac{\sin\,\tau}{\cosh\,\sigma-\cos\,\tau}\frac{\partial U}{\partial\tau}\right]$$
$$+\frac{1}{\sin\,\tau\,(\cosh\,\sigma-\cos\,\tau)}\frac{\partial^2 U}{\partial\phi^2}=0.\qquad(94)$$

A separation of variables in equation 94 can be effected through a change of the dependent variable. To this end, we let

$$U=\sqrt{\cosh\,\sigma-\cos\,\tau}\;W$$

whence the differential equation assumes the form:

$$\frac{\partial^2 W}{\partial\sigma^2}+\frac{1}{\sin\,\tau}\frac{\partial}{\partial\tau}\left(\sin\,\tau\,\frac{\partial W}{\partial\tau}\right)+\frac{1}{\sin^2\,\tau}\frac{\partial^2 W}{\partial\phi^2}-\frac{W}{4}=0.$$

The variables in the new equation may now be separated by the assumption of a solution in the form of $W=S(\sigma)T(\tau)\Phi(\phi)$. In terms of the component dependent variables, the new equation becomes:

$$\frac{1}{S}\left[\frac{d^2S}{d\sigma^2}-\frac{1}{4}\right]+\frac{1}{T\,\sin\,\tau}\frac{d}{d\tau}\left[\sin\,\tau\,\frac{dT}{d\tau}\right]+\frac{1}{\Phi\,\sin^2\,\tau}\frac{d^2\Phi}{d\phi^2}=0.\quad(95)$$

An examination of this differential equation reveals that two parts of the equation may be equated to separate constants. The first of these is the part which is dependent upon the angle ϕ and which leads to the function Φ_m introduced in equation 52. The part of the equation which involves S may independently be equated to a second constant which we choose to be of the form $n(n+1)$. This step leads to the equation

$$\frac{d^2S}{d\sigma^2}-\left[n(n+1)+\frac{1}{4}\right]S=0$$

which, through the methods of ordinary differential equations, leads to

$$S_n=C_n e^{(n+1/2)\sigma}+D_n e^{-(n+1/2)\sigma}.$$

This solution in terms of exponentials is preferred to the form involving hyperbolic functions because the former facilitates application of the solution to regions in which σ becomes either positively or negatively infinite.

When the constants $-m^2$ and $n(n+1)$ are introduced into equation 95, we obtain the final differential equation which must be solved:

$$\frac{1}{\sin\,\tau}\frac{d}{d\tau}\left[\sin\,\tau\,\frac{dT}{d\tau}\right]+\left[n(n+1)-\frac{m^2}{\sin^2\tau}\right]T=0.$$

This equation is recognized as the ordinary associated Legendre equation (equation 53) for which the solution is:

$$T=E_{mn}P_n{}^m\,(\cos\,\tau)+F_{mn}Q_n{}^m\,(\cos\,\tau).$$

All regions in which this solution is useful contain points at which τ is either zero or π. Since the associated Legendre function of the second kind becomes infinite at such points, it may be excluded even from what we consider to be the general solution.

In the above solutions, the parameters m and n have their most common properties; that is, n is an integer which may assume any positive value and m is an integer which varies from zero to n.

When we assemble the various component parts, we obtain for the general solution of Laplace's equation 94 in bipolar coordinates:

$$U=\sqrt{\cosh \sigma - \cos \tau} \sum_{n=0}^{\infty} \sum_{m=0}^{n} [A_{mn}e^{(n+1/2)\sigma}$$

$$+ B_{mn}e^{-(n+1/2)\sigma}]P_n^m (\cos \tau) \cos m\phi. \quad (96)$$

EXPANSIONS OF THE RECIPROCAL DISTANCE

The key to the present method of solving potential problems involving a point source of current is the expansion of the reciprocal of the distance R between the point source and the point at which the potential is to be computed. This expansion must be in terms of the functions which make up the appropriate solutions of Laplace's equation. Such an expansion is necessary in order to apply the boundary condition that the normal component of the current density must be continuous across any boundaries present in the problem. This particular condition is more complicated than the other boundary conditions because it involves a derivative of the potential. An alternate approach to the problem would be to apply Gauss's theorem to a surface surrounding the point source separately in each problem. This technique is usually more laborious than the one to be used.

The quantity $1/R$ is a solution of Laplace's equation. This fact may be reasoned qualitatively by noting that R is the only variable in the expression for the potential when a point source is placed in a homogeneous medium. Since the potential function is a solution of Laplace's equation, it follows that $1/R$ is also a solution. The fact may also be readily verified if we substitute an expression for the reciprocal of a distance into Laplace's equation in any specific coordinate system.

We will now use several techniques to obtain expansions, in order that a student trying to attack a new problem will have various avenues of approach. In principle, any expansion could be obtained by any of the methods presented, but for a given expansion there is usually a preferred technique. One of the methods will be the application of Gauss's theorem to a surface surrounding the point source in a homogeneous medium. We will thereby demonstrate the equivalence of the technique used herein to solve the resistivity problems, with the alternate technique of applying Gauss's theorem in every problem.

The following discussion takes on an aspect of pure mathematics, more so than other parts of this treatise. We believe that the expansions to be developed are an essential part of the solution of resistivity problems. The reader may take for granted the results obtained herein, and turn immediately to the sections where the results are used and which apply more to field problems.

ASSOCIATED LEGENDRE POLYNOMIALS

One of the most useful theorems stems from the expansion of the reciprocal distance in spherical coordinates. Let us consider two points, P_0 located at $(r_0, \theta_0, 0)$ in the meridian plane and P located at some point (r, θ, ϕ) not in the meridian plane (fig. 24). For simplicity, we assume that $r_0 > r$. Moreover, we let the angle between the radius vectors to these two points be labeled γ. We commence our development by applying the cosine law to the triangle formed by P, P_0, and the origin. We can write that $R^2 = r_0^2 + r^2 - 2r_0 r \cos \gamma$, whence the reciprocal distance may be written as

$$\frac{1}{R}=\frac{1}{r_0}\left[1+\left(\frac{r}{r_0}\right)^2 - 2\left(\frac{r}{r_0}\right) \cos \gamma\right]^{-1/2}. \quad (97)$$

We now expand the expression on the right side by the binomial theorem:

$$\frac{1}{R}=\frac{1}{r_0}\left\{1+\left(-\frac{1}{2}\right)\left(\frac{r}{r_0}\right)\left[\frac{r}{r_0}-2 \cos \gamma\right]\right.$$

$$+\left(-\frac{1}{2}\right)\left(-\frac{3}{2}\right)\left(\frac{1}{2!}\right)\left(\frac{r}{r_0}\right)^2\left[\frac{r}{r_0}-2 \cos \gamma\right]^2$$

$$\left.+\left(-\frac{1}{2}\right)\left(-\frac{3}{2}\right)\left(-\frac{5}{2}\right)\left(\frac{1}{3!}\right)\left(\frac{r}{r_0}\right)^3\left[\frac{r}{r_0}-2 \cos \gamma\right]^3+ \ldots \right\}.$$

Since the series in this expression is absolutely convergent, we are at liberty to rearrange the terms as we see fit. Therefore, we choose to rearrange the terms in order of ascending powers of r/r_0 as follows:

$$\frac{1}{R}=\frac{1}{r_0}\left\{1+\frac{r}{r_0} \cos \gamma+\left(\frac{r}{r_0}\right)^2\left(\frac{3}{2} \cos^2 \gamma-\frac{1}{2}\right)\right.$$

$$\left.+\left(\frac{r}{r_0}\right)^3\left(\frac{5}{2} \cos^3 \gamma-\frac{3}{2} \cos \gamma\right)+ \ldots \right\}. \quad (97A)$$

We see that each separate power of r/r_0 is multiplied by a factor which is a polynomial in $\cos \gamma$. They are the Legendre polynomials, which have previously been defined and discussed in connection with the solutions of Laplace's equation. Actually, it would be permissible to use equation 97A as a generating function to define the Legendre polynomials and then to show under which conditions they satisfy Laplace's equation. Therefore, we may write equation 97A as:

$$\frac{1}{R}=\frac{1}{r_0}\left\{P_0(\cos \gamma)+\frac{r}{r_0}P_1 (\cos \gamma)\right.$$

$$\left.+\left(\frac{r}{r_0}\right)^2 P_2(\cos \gamma)+\left(\frac{r}{r_0}\right)^3 P_3 (\cos \gamma)+ \ldots \right\}$$

where $P_n (\cos \gamma)$ denotes the Legendre polynomial of

order n. The expansion which we seek is written in the abbreviated form:

$$\frac{1}{R}=\frac{1}{r_0}\sum_{n=0}^{\infty}\left(\frac{r}{r_0}\right)^n P_n\left(\cos\gamma\right). \qquad (98)$$

In order to introduce into the expansion the coordinates θ and ϕ, we will use inductive reasoning. We first note a theorem from solid geometry:

$$\cos\gamma=\cos\theta_0\cos\theta+\sin\theta_0\sin\theta\cos\phi. \qquad (99)$$

We next write down several expressions for sine and cosine functions, using trigonometric identities, the definitions for the Legendre polynomials inferred in equation 97A, and the definition for the associated Legendre polynomials given by:

$$P_n{}^m\left(\cos\theta\right)=\sin^m\theta\,\frac{d^m P_n\left(\cos\theta\right)}{d\left(\cos\theta\right)}. \qquad (100)$$

For example,

$$\cos\theta=P_1\left(\cos\theta\right)$$
$$\sin\theta=-P_1{}^1\left(\cos\theta\right)$$
$$\sin^2\theta=(1/3)\,P_2{}^2\left(\cos\theta\right)$$
$$\cos^2\theta=1-(1/3)\,P_2{}^2\left(\cos\theta\right)$$
$$\sin\theta\cos\theta=-(1/3)\,P_2{}^1\left(\cos\theta\right)$$
$$\cos^2\phi=(1/2)(1+\cos 2\phi).$$

It follows that

$$P_0\left(\cos\gamma\right)=1$$
$$P_1\left(\cos\gamma\right)=\cos\gamma=\cos\theta_0\cos\theta+\sin\theta_0\sin\theta\cos\phi$$
$$\qquad=P_1\left(\cos\theta_0\right)P_1\left(\cos\theta\right)+P_1{}^1\left(\cos\theta_0\right)P_1{}^1\left(\cos\theta\right)\cos\phi$$
$$P_2\left(\cos\gamma\right)=(3/2)\cos^2\gamma-1/2$$
$$\qquad=(3/2)(\cos^2\theta_0\cos^2\theta+2\cos\theta\sin\theta_0\cos\theta\sin\theta\cos\phi$$
$$\qquad\qquad\qquad+\sin^2\theta_0\sin^2\theta\cos^2\phi)-1/2$$
$$\qquad=P_2\left(\cos\theta_0\right)P_2\left(\cos\theta\right)+2(1/3!)\,P_2{}^1\left(\cos\theta_0\right)P_2{}^1\left(\cos\theta\right)\cos\phi$$
$$\qquad\qquad\qquad+2(1/4!)\,P_2{}^2\left(\cos\theta_0\right)P_2{}^2\left(\cos\theta\right).$$

Although the desired expansion is not obvious from these three terms, it would become clear if we were to calculate expressions for $P_n\left(\cos\gamma\right)$ for one or two more values of n. Therefore, we finally arrive at the conclusion that

$$P_n\left(\cos\gamma\right)=P_n\left(\cos\theta_0\right)P_n\left(\cos\theta\right)$$

$$+2\sum_{m=0}^{n}\frac{(n-m)!}{(n+m)!}\,P_n{}^m\left(\cos\theta_0\right)P_n{}^m\left(\cos\theta\right)\cos m\phi. \qquad (101)$$

This equation is designated the "addition theorem" for Legendre polynomials. Substituting this expression into equation 98, we obtain the expansion for $1/R$ in terms of the associated Legendre polynomials:

$$\frac{1}{R}=\frac{1}{r_0}\sum_{n=0}^{\infty}\left(\frac{r}{r_0}\right)^n\sum_{m=0}^{n}(2-\delta_{0m})\frac{(n-m)!}{(n+m)!}\,P_n{}^m\left(\cos\theta_0\right)$$

$$\times P_n{}^m\left(\cos\theta\right)\cos m\phi. \qquad (102)$$

Note the introduction of the kronecker delta δ_{0m} which assumes the value of unity when $m=0$ and the value zero when $m\neq 0$. This device enables us to write both terms in equation 101 as a single term.

An important special case exists when the source lies on the polar axis. Then $\theta_0=0$ and $\cos\theta_0=1$. The associated Legendre polynomials of argument unity are all zero unless $m=0$ in which case they are equal to unity. Therefore, we may drop from equation 102 all terms for which $m\neq 0$.

$$\frac{1}{R}=\frac{1}{r_0}\sum_{n=0}^{\infty}\left(\frac{r}{r_0}\right)^n P_n(\cos\theta). \qquad (103)$$

Another way of obtaining this same expression is simply to note that in this special case $\gamma=\theta$, whence equation 98 becomes equivalent to equation 103.

If r were greater than r_0, these two distances would simply change roles in equations 102 and 103. This symmetry in the coordinates of the two points is an expression of the reciprocity theorem; we will always use this property to test the validity of our expansions.

BESSEL FUNCTIONS OF ZERO ORDER

The development of the following expansion is based upon the fact that the quantity $1/R$ is itself a solution of Laplace's equation. A possible solution of Laplace's equation in cylindrical coordinates is taken from equation 70 by discarding the first term in brackets, by letting $B_m(\lambda)$ be unity, and then by introducing the constant factor λ^n

$$\cos m\phi\int_0^{\infty}e^{-\lambda z}J_m(\lambda r)\lambda^n d\lambda.$$

In this integral, we make the substitutions, $z=\rho\cos\theta$, $r=\rho\sin\theta$, and $\lambda\rho=k$, so that the expression becomes

$$\frac{\cos m\phi}{\rho^{n+1}}\int_0^{\infty}e^{-k\cos\theta}J_m(k\sin\theta)k^n dk.$$

In this section, we temporarily denote by ρ the radius vector in spherical coordinates, in order to distinguish it from the corresponding quantity in cylindrical coordinates. This is the only instance in this paper when there is a possibility of such ambiguity in the use of ρ.

In reality, the above substitutions are a transformation from cylindrical coordinates to spherical coordinates, so that the resulting expression is a solution of Laplace's equation in spherical coordinates. Since ρ and ϕ do not appear in the integrand, it follows that the integral must equal $A_{mn}P_n^m$ (cos θ), which from equation 58 is also known to be a solution of Laplace's equation in spherical coordinates. A_{mn} is a constant, depending only on the parameters m and n, and therefore may be evaluated at some special value of θ. We have then

$$\int_0^\infty e^{-k \cos \theta} J_m(k \sin \theta) k^n dk = A_{mn}P_n^m (\cos \theta). \quad (104)$$

From the definitions 55 and 56, we see that $P_n^m(\cos \theta)$ is zero when $\theta = 0$. Likewise, from equation 69, we learn that $J_m(k \sin \theta)$ is also zero when $\theta = 0$. If we divide both sides of equation 104 by $\sin^m \theta$, which also vanishes when $\theta = 0$, we obtain ratios which are finite. We evaluate the resulting ratio when $\theta = 0$ and get

$$\frac{1}{2^m m!} \int_0^\infty e^{-k} k^{m+n} dk = A_{mn} \frac{(-1)^m (n+m)!}{2^m m! (n-m)!}.$$

The integral on the left is by definition the gamma function of $(n+m+1)$ or $(n+m)!$ so that we can immediately solve to get

$$A_{mn} = (-1)^m (n-m)!$$

whence

$$\int_0^\infty e^{-\lambda z} J_m(\lambda r) d\lambda = \frac{(-1)^m (n-m)! P_n^m(\cos \theta)}{\rho^{n+1}}. \quad (104A)$$

This relationship is valid when $z \geq 0$ for all ranges in which $J_m(\lambda r)$ and $P_n^m(\cos \theta)$ are valid functions. The expansion which we are seeking is obtained from equation 104A for the special case in which $m = n = 0$ and is given by

$$\frac{1}{R} = \frac{1}{\rho} = \frac{1}{\sqrt{r^2 + z^2}} = \int_0^\infty e^{-\lambda z} J_0(\lambda r) d\lambda. \quad (105)$$

If we had been working in the realm of negative z in the above development, we would simply have used the factor $e^{\lambda z}$ instead of $e^{-\lambda z}$.

Carrying this sort of reasoning further, it has been shown (Gray and others, 1931, p. 101) that a second expansion of the same type may be written as

$$\frac{1}{R} = \frac{2}{\pi} \int_0^\infty \cos \lambda z K_0(\lambda r) d\lambda, \quad (106)$$

where $K_0(\lambda r)$ is a modified Bessel function of zero order.

MODIFIED BESSEL FUNCTIONS

One addition theorem for modified Bessel functions may be written in the form (Gray and others, 1931, p. 101),

$$K_0[\lambda \sqrt{r_0^2 + r^2 - 2r_0 r \cos \phi}]$$
$$= \sum_{m=0}^\infty (2 - \delta_{0m}) K_m(\lambda r_0) I_m(\lambda r) \cos m\phi. \quad (107)$$

In the application to which we will later put this addition theorem, it will be necessary to have it in the form of an integral. Obviously, r and r_0 are both real and, for the purposes of the discussion, we assume that $r < r_0$.

The summation on the right side of equation 107 may be transformed into an integral through a consideration of the following contour integral:

$$\oint \frac{\cos s(\pi - \phi)}{\sin s\pi} K_s(\lambda r_0) I_s(\lambda r) ds. \quad (108)$$

The path of integration in the s-plane will consist of the imaginary axis, indented to the right of the origin, and an infinitely large semicircle to the right of the imaginary axis. The integrand vanishes on the large semicircle and, thus, that part of the path makes no contribution to the integral. As the radius of the indentation at the origin tends to zero, the integral over that part of the path approaches $iK_0(\lambda r_0)I_0(\lambda r)$. Finally, the only undetermined part of the integration is that over the imaginary axis.

We are able to evaluate the contour integral directly by means of the residue theorem. We note that the only poles in the integrand of the expression 108 lie along the real axis at points where s is an integer. Therefore, the integral equals $-2\pi i$ times the sum of these residues or

$$-2\pi i \sum_{m=1}^\infty \frac{1}{\pi} \cos m\phi K_m(\lambda r_0) I_m(\lambda r).$$

If we write out the integral as the sum of the parts over the path as outlined above, we have the expression,

$$-\int_{-\infty}^\infty \frac{\cosh s(\pi - \phi)}{\sinh s\pi} K_{is}(\lambda r_0) I_{is}(\lambda r) ds + iK_0(\lambda r_0) I_0(\lambda r).$$

Equating these two expressions, we are able to express the summation on the right side of equation 107 in terms of an integral as required. Moreover, by using the definition of equation 72, we are able to reduce the integration over both positive and negative values of s to an integration over only positive values of s. Thus, we obtain for the integral form of the addition theorem:

$$K_0[\lambda \sqrt{r_0^2 + r^2 - 2r_0 r \cos \phi}] = \frac{2}{\pi} \int_0^\infty \cosh s(\pi - \phi) K_{is}(\lambda r_0) K_{is}(\lambda r) ds. \quad (109)$$

To obtain the expansion which has been the purpose of the above development, we substitute in equation 106 the expression on the right side of equation 109 for that on the left side. The desired expansion is then

$$\frac{1}{R}=\frac{4}{\pi^2}\int_0^\infty \cos \lambda z d\lambda \int_0^\infty \cosh s(\pi-\phi)K_{is}(\lambda r_0)K_{is}(\lambda r)ds. \quad (110)$$

The derivation of equation 110 depends upon ϕ being greater than 0 and less than 2π. If such is not so, the only change in the expression would be a change from $-\phi$ to $+\phi$ whenever this quantity appears in the equation. The reason for this restriction can be seen from an examination of the contour integration which was performed above.

We will also be able to use the following expansion obtained by substituting the right side of equation 107 into the expansion given by equation 106.

$$\frac{1}{R}=\frac{2}{\pi}\sum_{m=0}^\infty (2-\delta_{0m})\cos m\phi \int_0^\infty \cos tzK_m(tr_0)I_m(tr)dt. \quad (111)$$

In equation 111, it is assumed that $r_0>r$. If $r>r_0$, the roles of these two quantities will be interchanged.

SPHEROIDAL FUNCTIONS

The Legendre polynomials used to expand the reciprocal distance in a previous section are a special case of the general associated Legendre functions. In the present section, we desire to obtain expansions in terms of certain other types of associated Legendre functions which form orthogonal sets of functions over the spheroids in both prolate and oblate spheroidal coordinates. In order to accomplish these expansions, we will apply Gauss's theorem to a point source of current located within a homogeneous medium and within the framework of one of these two coordinate systems.

In prolate spheroidal coordinates, let a point source of strength I be located at the point $(\eta_0, \xi_0, 0)$. There is no loss of generality in choosing the meridian plane $\phi=0$ such that it contains the source. Moreover, this choice is convenient in that it restricts the expression for the potential to even functions of ϕ. Therefore, there need be no sine term in the general solution to Laplace's equation, which now is written (equation 85) as:

$$U=\sum_{n=0}^\infty \sum_{m=0}^n [A_{mn}P_n^m(\eta)+B_{mn}Q_n^m(\eta)]P_n^m(\xi) \cos m\phi,$$

where $P_n^m(\eta)$ is the associated Legendre function of the first kind and $Q_n^m(\eta)$ is the associated Legendre function of the second kind. $P_n^m(\xi)$ is the same associated Legendre polynomial which was used previously.

It is now necessary to examine $P_n^m(\eta)$ and $Q_n^m(\eta)$ to learn whether they behave properly throughout the range of their arguments in this problem. Such relationships are well known (Smythe, 1950, p. 1471-53);

both functions are continuous within the limits of their respective arguments. For argument zero, both functions remain finite; for argument unity, $P_n^m(\eta)$ remains finite but $Q_n^m(\eta)$ becomes infinite; and, for increasingly large argument, $P_n^m(\eta)$ becomes infinite while $Q_n^m(\eta)$ vanishes as the inverse $(n+1)$ power of the argument. In view of these facts, it becomes desirable to divide space into two regions, the first for which $1\leq\eta\leq\eta_0$ and a second for which $\eta_0\leq\eta<\infty$. Then, in the first region, where both η and ξ are sometimes unity, the potential has the form:

$$U_1=\sum_{n=0}^\infty \sum_{m=0}^n A_{mn}P_n^m(\eta)P_n^m(\xi) \cos m\phi. \quad (112)$$

In the second region, where η extends to infinity, the potential may be written in the form:

$$U_2=\sum_{n=0}^\infty \sum_{m=0}^n A_{mn}Q_n^m(\eta)P_n^m(\xi) \cos m\phi. \quad (113)$$

At the common boundary between these two regions, it is necessary that the potential be continuous; from which condition it is seen that:

$$B_{mn}=\frac{P_n^m(\eta_0)}{Q_n^m(\eta_0)} A_{mn}=\psi_n^m(\eta_0)A_{mn},$$

where the symbol which has been introduced is defined in the equation itself.

For a second boundary condition, consider the current which originates at the source. This source is now considered to be "smeared out" uniformly over a very small area on the surface $\eta=\eta_0$, keeping the average values of the coordinates as given above for the point source. If one now constructs a surface enclosing this area Δs, the total current which flows outward through the enclosing surface is simply equal to I.

In order to enclose the source in the present problem, two nonintersecting surfaces are used, one being the spheroid $\eta=\eta_0-\epsilon$ and the other being the spheroid $\eta=\eta_0+\epsilon$. The increment ϵ is chosen to be so vanishingly small that it can be neglected in evaluating the various functions on the two surfaces. Using the expressions of equation 78 for the component of the gradient normal to the surfaces, the current density outward from the volume enclosed by the two spheroids is calculated to be:

$$-\frac{1}{\rho}\{(\nabla U_2)_\eta-(\nabla U_1)_\eta\}_{\eta=\eta_0}$$

$$=\frac{1}{b\rho}\sqrt{\frac{\eta_0^2-1}{\eta_0^2-\xi^2}}\sum_{n=0}^\infty \sum_{m=0}^n A_{mn}\Psi_n^m(\eta_0)P_n^m(\xi) \cos m\phi, \quad (114)$$

where the symbol introduced is given by:

$$\Psi_n^m(\eta_0)=P_n'^m(\eta_0)-\psi_n^m(\eta_0)Q_n'^m(\eta_0) \quad (115)$$

and the primes indicate differentiation of a given function with respect to its own argument.

We now multiply both sides of equation 114 by $P_{n'}^{m'}(\xi)$ cos $m'\phi$ where these primes indicate specific integers in the sets of m and n. We consider first the integral of the left side of the equation over the whole surface of the spheroid $\eta=\eta_0$. The value of the integrand, which is the current density outward from the surface, is zero everywhere on the surface except over the area Δs. Thus, $P_{n'}^{m'}(\xi)$ cos $m'\phi$ may be given its value at the coordinates of the source and may then be removed from under the integral sign. As the only contribution to the current flow out of the bounded region occurs in the immediate vicinity of Δs, the remaining integral equals the total current I. Therefore, we have reduced the left side of equation 114 to $IP_{n'}^{m'}(\xi_0)$.

Integration of the right side of equation 114 over the surface of the spheroid is facilitated by the application of the orthogonality properties of the functions involved. These are:

$$\int_0^{2\pi} \cos m\phi \cos m'\phi d\phi = \frac{2\pi\delta_{mm'}}{2-\delta_{0m'}}$$ (116)

$$\int_{-1}^{1} P_n^{m'}(\xi) P_{n'}^{m'}(\xi) d\xi = \frac{2(n'+m')!\delta_{nn'}}{(2n'+1)(n'-m')!}.$$ (117)

The correct element of area in this case is given by equation 77. We first integrate with respect to ϕ, to show that all terms vanish if m does not equal m', and then we integrate with respect to ξ to eliminate all terms for which n does not equal n'. We get for the right side of the equation

$$\frac{b(\eta_0^2-1)}{\rho} A_{mn}\Psi_n^m(\eta_0)\left(\frac{2\pi}{2-\delta_{0m'}}\right)\frac{2(n'+m')!}{(2n'+1)(n'-m')!}.$$

Equating the results of the above operation, dropping the primes on m and n, and solving the resulting equation, we find that

$$A_{mn} = \frac{I\rho}{2\pi}\frac{(2-\delta_{0m})(2n+1)(n-m)!}{b(\eta_0^2-1)(n+m)!}\frac{P_n^m(\xi_0)}{\Psi(\eta_0)}.$$ (118)

It is now desirable to eliminate the derivatives from $\Psi(\eta_0)$. The associated Legendre functions $P_n^m(\eta)$ and $Q_n^m(\eta)$ both satisfy the same equation so that we have

$$\begin{cases}\frac{d}{d\eta}\left[(\eta^2-1)\frac{dP_n^m(\eta)}{d\eta}\right]-\left[n(n+1)+\frac{m^2}{\eta^2-1}\right]P_n^m(\eta)=0 \\ \frac{d}{d\eta}\left[(\eta^2-1)\frac{dQ_n^m(\eta)}{d\eta}\right]-\left[n(n+1)+\frac{m^2}{\eta^2-1}\right]Q_n^m(\eta)=0.\end{cases}$$

We multiply the first equation by $Q_n^m(\eta)$ and the second by $P_n^m(\eta)$, subtract the second from the first, and manipulate the terms to get

$$\frac{d}{d\eta}\{(\eta^2-1)[Q_n^m(\eta)P_n'^m(\eta)-P_n^m(\eta)Q_n'^m(\eta)]\}=0,$$

from which it follows immediately that

$$(\eta^2-1)[Q_n^m(\eta)P_n'^m(\eta)-P_n^m(\eta)Q_n'^m(\eta)]=C_{mn}.$$ (119)

The development has been general in the sense that it applies for all values of η. The value of C_{mn} may be most easily determined by investigating the relationship in the limit as η becomes infinite. For this purpose we must use the following asymptotic relationships:

$$\begin{cases}\lim_{\eta\to\infty} P_n^m(\eta) = \frac{(2n)!}{2^n n!(n-m)!}\eta^n \\ \lim_{\eta\to\infty} P_n'^m(\eta) = \frac{(2n)!}{2^n(n-1)!(n-m)!}\eta^{n-1} \\ \lim_{\eta\to\infty} Q_n^m(\eta) = \frac{(-1)^m n!(n+m)!2^n}{(2n+1)!}\eta^{-(n+1)} \\ \lim_{\eta\to\infty} Q_n'^m(\eta) = \frac{(-1)^{m+1}(n+1)!(n+m)!2^n}{(2n+1)!}\eta^{-(n+2)}.\end{cases}$$ (120)

When we substitute these asymptotic values into equation 119, we get

$$C_{mn} = (-1)^m\frac{(n+m)!}{(n-m)!}$$

whence the new expression which we seek is

$$\Psi_n^m(\eta_0) = \frac{(n+m)!(-1)^m}{(n-m)!(\eta_0^2-1)Q_n^m(\eta_0)}.$$ (121)

Finally, we combine equations 112, 113, 114, 118, and 121 to get the potential functions:

$$U = \frac{I\rho}{4\pi}\sum_{n=0}^{\infty}\sum_{m=0}^{n}\frac{(2-\delta_{0m})(2n+1)}{b(-1)^m}$$
$$\times\left[\frac{(n-m)!}{(n+m)!}\right]^2 P_n^m(\xi_0)P_n^m(\xi)\frac{Q_n^m(\eta_0)P_n^m(\eta)}{P_n^m(\eta_0)Q_n^m(\eta)}\cos m\phi.$$ (122)

Note that equation 122 combines both equations 112 and 113. When two functions occur in a column, the upper one applies when $\eta_0>\eta$ and the lower one when $\eta_0<\eta$. This result is consistent with the expression for the reciprocal distance in prolate spheroidal coordinates calculated by Hobson (1931, p. 422). In order to convert this expression to one which involves only the reciprocal distance, we have only to compare equation 122 with the expression for the potential due to a point source in an infinite medium of resistivity ρ:

$$U = \frac{I\rho}{4\pi R}.$$

We then see that the expansion of the reciprocal distance in prolate spheroidal coordinates is

$$\frac{1}{R} = \frac{1}{b}\sum_{n=0}^{\infty}\sum_{m=0}^{n}\frac{(2-\delta_{0m})(2n+1)}{(-1)^m}$$
$$\times\left[\frac{(n-m)!}{(n+m)!}\right]^2 P_n^m(\xi_0)P_n^m(\xi)\frac{Q_n^m(\eta_0)P_n^m(\eta)}{P_n^m(\eta_0)Q_n^m(\eta)}\cos m\phi.$$ (123)

The above considerations may be applied in the same manner to the expansion of the reciprocal distance

in oblate spheroidal coordinates, for which the desired expansion is

$$\frac{1}{R}=\frac{i}{b}\sum_{n=0}^{\infty}\sum_{m=0}^{n}\frac{(2-\delta_{0m})(2n+1)}{(-1)^{m}}$$

$$\times\left[\frac{(n-m)!}{(n+m)!}\right]^{2}\frac{Q_{n}{}^{m}(i\zeta_0)P_{n}{}^{m}(i\zeta)}{P_{n}{}^{m}(i\zeta_0)Q_{n}{}^{m}(i\zeta)}\,P_{n}{}^{m}(\mu_0)P_{n}{}^{m}(\mu)\,\cos m\phi \quad (124)$$

where $i=\sqrt{-1}$.

A SECOND EXPANSION IN ASSOCIATED LEGENDRE POLYNOMIALS

One expansion of the reciprocal distance in bipolar coordinates can be executed simply by transforming the reciprocal distance from rectangular coordinates into bipolar coordinates. We start with

$$R^2=(x_0-x)^2+(y_0-y)^2+(z_0-z)^2$$
$$=(x_0{}^2+y_0{}^2+z_0{}^2)+(x^2+y^2+z^2)-2(x_0x+y_0y+z_0z).$$

As we have done previously, we arbitrarily choose the median plane $\phi=0$ such that it contains the reference point P_0. Therefore, y_0 is also zero. If we substitute expressions of the type in equation 91 for the first two groups and of the type in equations 90 for the third group, we find that

$$R^2=2b^2\left[\frac{\cosh\sigma_0\cosh\sigma-\sinh\sigma_0\sinh\sigma-\cos\tau_0\cos\tau-\sin\tau_0\sin\tau\cos\phi}{(\cosh\sigma_0-\cos\tau_0)(\cosh\sigma-\cos\tau)}\right]$$
$$=\frac{2b^2[\cosh(\sigma_0-\sigma)-\cos\gamma]}{(\cosh\sigma_0-\cos\tau)(\cosh\sigma-\cos\tau)}$$

where

$$\cos\gamma=\cos\tau_0\cos\tau+\sin\tau_0\sin\tau\cos\phi.$$

If we change the hyperbolic cosine of $(\sigma_0-\sigma)$ into its exponential form and solve for the reciprocal distance, we obtain

$$\frac{1}{R}=\frac{e^{-(\sigma_0-\sigma)/2}}{b}\,(\cosh\sigma_0-\cos\tau_0)^{1/2}$$
$$\times(\cosh\sigma-\cos\tau)^{1/2}[1+e^{-2(\sigma_0-\sigma)}-2e^{-(\sigma_0-\sigma)}\cos\gamma]^{-1/2}$$

The last term in brackets now has the same form as the term in brackets in equation 97. Therefore, we can write down the expansion immediately to correspond to equation 98:

$$\frac{1}{R}=\frac{e^{-1/2(\sigma_0-\sigma)}}{b}\,(\cosh\sigma_0-\cos\tau_0)^{1/2}$$
$$\times(\cosh\tau-\cos\tau)^{1/2}\sum_{n=0}^{\infty}e^{-n(\sigma_0-\sigma)}P_n\,(\cos\tau).$$

Taking into consideration the value of $\cos\tau$ given above and the additional expansion in equation 101, we get the expansion of the reciprocal distance in bipolar coordinates:

$$\frac{1}{R}=\frac{1}{b}\,(\cosh\sigma_0-\cos\tau_0)^{1/2}\,(\cosh\sigma-\cos\tau)^{1/2}\sum_{n=0}^{\infty}e^{-(n+1/2)(\sigma_0-\sigma)}$$

$$\times\sum_{m=0}^{n}(2-\delta_{0m})\frac{(n-m)!}{(n+m)!}\,P_{n}{}^{m}\,(\cos\tau_0)P_{n}{}^{m}\,(\cos\tau)\,\cos m\phi. \quad (125)$$

In the development of equation 125, we have assumed that $\sigma_0>\sigma$. If the reverse is true, these quantities simply exchange their roles in the expansion.

CONE FUNCTIONS

We will obtain an expansion of $1/R$ in terms of cone functions by using a special kind of boundary condition (Van Nostrand, 1954) which may be expressed mathematically in the following equation:

$$\int_s \bar{n}\cdot\nabla\left(\frac{1}{R}\right)ds=-4\pi, \quad (126)$$

where $\bar{n}$ is the unit vector normal outward to the element of surface ds and $n\cdot\nabla(1/R)$ is the component of $\nabla(1/R)$ taken normal to that element of area. A second way to express the above relation is to say that $\bar{n}\cdot\nabla(1/R)$ ds is the negative of the element of solid angle subtended at the point P_0, from which R is measured, by the given element of area. Obviously, the integral taken over any surface surrounding the reference point P_0 is equal to the negative of the total solid angle 4π subtended by a sphere. This technique in principle is the same as that used in the derivation of equation 123. The above relationship is applied to a purely geometric problem as Gauss's theorem was previously applied to a potential problem.

As before, R is the distance between the reference point $P_0(r_0,\,\theta_0,\,0)$ and a second point $P(r,\,\theta,\,\phi)$. We commence by writing down two potential functions based on the general solution of Laplace's equation in terms of cone functions in spherical coordinates given by equation 63:

$$\frac{1}{R_1}=\frac{1}{\sqrt{r}}\sum_{m=0}^{\infty}\cos m\phi\int_{-\infty}^{\infty}AP_{ip-\frac{1}{2}}^{m}\,(\cos\theta_0)P_{ip-\frac{1}{2}}^{m}(-\cos\theta)e^{ip\,\ln\,r}\,dp$$

$$\frac{1}{R_2}=\frac{1}{\sqrt{r}}\sum_{m=0}^{\infty}\cos m\phi\int_{-\infty}^{\infty}AP_{ip-\frac{1}{2}}^{m}(-\cos\theta_0)P_{ip-\frac{1}{2}}^{m}\,(\cos\theta)e^{ip\,\ln\,r}\,dp$$

where the first equation applies when $\theta_0\geq\theta$ and the second when $\theta_0\leq\theta$. A is an arbitrary function of p which also depends on the value of m. The form of these expressions has been so chosen that they are equivalent on the surface of the cone $\theta=\theta_0$.

In the application of equation 126 to the present problem, the central point is P_0. Points on the surface, over which the integration is to be performed, are represented by P. In order to enclose P_0 in this problem, we used two nonintersecting surfaces, one being the cone $\theta=\theta_0-\delta$ and the other being the cone $\theta=\theta_0+\delta$, plus a segment of a sphere at infinity. Obviously, inte-

gration over the part of the enclosing surface at infinity has no effect on the result.

The increment δ is chosen to be so vanishingly small that it can be neglected in evaluating the various functions over the two remaining surfaces. Over the first cone, the first expression for $1/R_1$ must be used; whereas over the second cone, the second formula for $1/R_2$ must be used. For any element of area on one surface, there is a corresponding element, which may be considered to have the same coordinates, on the opposing surface; the only difference is that the normal unit vector is oppositely directed in the two cases. Thus, for any specified coordinates, the total element of solid angle subtended at P_0 is given by

$$\left[\left(\nabla \frac{1}{R_1}\right)_\theta - \left(\nabla \frac{1}{R_2}\right)_\theta\right]_{\theta=\theta_0}$$

$$= \frac{\sin \theta_0}{r^{3/2}} \sum_{m=0}^{\infty} \cos m\phi \int_{-\infty}^{\infty} A\, [P_{ip-\frac{1}{2}}^m (\cos \theta_0) P_{ip-\frac{1}{2}}'^m(-\cos \theta_0)$$

$$+ P_{ip-\frac{1}{2}}^m(-\cos \theta_0) P_{ip-\frac{1}{2}}'^m (\cos \theta_0)]\, e^{ip\,\ln r}\, dp. \quad (126A)$$

From a more general relationship (Snow, 1942, p. 54), it can be shown that the quantity in brackets on the right side of the equation is given by

$$P_{ip-\frac{1}{2}}^m(-\cos \theta_0) P_{ip-\frac{1}{2}}'^m (\cos \theta_0) + P_{ip-\frac{1}{2}}^m (\cos \theta_0) P_{ip-\frac{1}{2}}'^m(-\cos \theta_0)$$

$$= \frac{-2(-1)^m \Gamma(\frac{1}{2}+ip+m)}{\pi \sin^2 \theta_0 \Gamma(\frac{1}{2}+ip-m)} \cosh \pi p.$$

The next step is to multiply both sides of the equation by $\dfrac{e^{-iq\,\ln r}}{r^{\frac{1}{2}}} \cos n\phi$, where n and q are specific numbers in the sets of m and p, respectively. Then, we integrate over all values of ϕ and r. First, consider the left side of the equation. The only region in which the quantity in brackets, if appreciably different from zero, is in the immediate vicinity of P_0, a region so small that the coordinates of all the points included can be considered to be the same as those of P_0. Thus, $\dfrac{e^{-iq\,\ln r} \cos n\phi}{\sqrt{r}}$ can be given its value at P_0 and can then be removed from under the integral sign as a constant. The remaining integral is exactly that represented on the left side of equation 126. Therefore, the total result is

$$\frac{-4\pi e^{-iq\,\ln r_0}}{\sqrt{r_0}}.$$

Introducing the expression for an element of area and integrating over the angle ϕ to eliminate the terms for which m does not equal n, we get for the expression on the right side of equation 126A:

$$-\frac{8\pi(-1)^m}{2-\delta_{0m}} \int_{-\infty}^{\infty} A\, \frac{\Gamma(\frac{1}{2}+ip+m)}{\Gamma(\frac{1}{2}+ip-m)}\, \cosh p\pi\, dp\, \frac{1}{2\pi}\int_0^{\infty} e^{i(p-q)\,\ln r}\, \frac{dr}{r}.$$

$$\quad (127)$$

We can evaluate the integral 127 by comparing it to equations 60 and 61. The integral becomes

$$-\frac{8\pi(-1)^m}{2-\delta_{0m}}\, A\, \frac{\Gamma(\frac{1}{2}+iq+m)}{\Gamma(\frac{1}{2}+iq-m)}\, \cosh q\pi.$$

Rejoining the two sides of equation 126A, we solve the resulting equation to get

$$A = \frac{(2-\delta_{0m})\,(-1)^m}{2}\, \frac{\Gamma(\frac{1}{2}+ip-m)}{\Gamma(\frac{1}{2}+ip+m)}\, \frac{e^{-ip\,\ln r_0}}{\sqrt{r_0}}\, \text{sech } p\pi.$$

Therefore, the expansion which we are seeking is

$$\frac{1}{R_1} = \frac{1}{2\sqrt{r_0 r}} \sum_{m=0}^{\infty} \frac{(2-\delta_{0m})}{(-1)^m} \cos m\phi \int_{-\infty}^{\infty} \frac{\Gamma(\frac{1}{2}+ip+m)}{\Gamma(\frac{1}{2}+ip-m)}\, \text{sech } \pi p$$

$$\times P_{ip-\frac{1}{2}}^m(+\cos \theta_0)\, P_{ip-\frac{1}{2}}^m(-\cos \theta)\, e^{ip\,\ln \frac{r}{r_0}} dp. \quad (128)$$

Since the entire coefficient of $e^{ip\,\ln \frac{r}{r_0}}$ is an even function of p, the imaginary part of the expansion vanishes during the integration and the real part is double what it would be if p varied only from zero to infinity. Therefore, we may write the final form of the expansion of the reciprocal distance in terms of cone functions in spherical coordinates

$$\frac{1}{R_1} = \frac{1}{\sqrt{r_0 r}} \sum_{m=0}^{\infty} \frac{(2-\delta_{0m})}{(-1)^m} \cos m\phi \int_0^{\infty} \frac{\Gamma(ip+\frac{1}{2}-m)}{\Gamma(ip+\frac{1}{2}+m)}\, \text{sech } p\pi$$

$$\times P_{ip-\frac{1}{2}}^m(+\cos \theta_0)\, P_{ip-\frac{1}{2}}^m(-\cos \theta)\, \cos\left(p \ln \frac{r}{r_0}\right) dp. \quad (129)$$

Also, in order to facilitate computations based on equation 129, it is sometimes convenient to use the following identity (Hobson, 1931, p. 447):

$$\frac{\Gamma(ip+\frac{1}{2}+m)}{\Gamma(ip+\frac{1}{2}-m)} = (-1)^m \left[p^2+\frac{1}{4}\right]\left[p^2+\frac{9}{4}\right] \cdots \left[p^2+\frac{(2m-1)^2}{4}\right].$$

The cone functions discussed above were introduced in connection with problems in electrostatics by Mehler (1868). However, the validity of these solutions has long been in doubt because of the apparent singularity in them at the origin (Hobson, 1931, p. 448). Van Nostrand [3] has shown on the other hand that the singularity at the origin does not exist in fact. Qualitatively, this can be explained because $\cos$ $(p \ln r/r_0)$ oscillates so rapidly as either r or r_0 approach zero that the integral approaches zero in such a way as to keep the whole expression finite.

HYPERBOLOID FUNCTIONS

In order to develop an expansion of the reciprocal distance in terms of hyperboloid functions, we use the fact that prolate spheroidal coordinates approach

spherical coordinates in the limit as $\eta \to \infty$ or as $b \to 0$. We will write down an assumed solution, based on our knowledge of potential functions, and then will require that it approach the known solution for the expansion in cone functions as $b \to 0$. We commence with the general solution to Laplace's equation which is given in equation 88. We let $U = 1/R$. Since we have already shown that $\lim_{\eta \to \infty} \xi = \cos \theta$, we expect that our solution has the same dependence on ξ that equation 128 has on $\cos \theta$. Further, from the principle of reciprocity, we know that the dependence of the solution on η_0 will be the same as its dependence on η. Since the general solution already contains the factor $P^m_{ip-\frac{1}{2}}(\eta)$, the reciprocity condition is satisfied if we also include the factor $P^m_{ip-\frac{1}{2}}(\eta_0)$. Therefore, we assume a solution in the form of

$$\frac{1}{R} = \sum_{m=0}^{\infty} \cos m\phi \int_0^{\infty} A P^m_{ip-\frac{1}{2}}(\xi_0) P^m_{ip-\frac{1}{2}}(-\xi) P^m_{ip-\frac{1}{2}}(\eta_0) P^m_{ip-\frac{1}{2}}(\eta) dp \tag{130}$$

when $\xi_0 \geq \xi$. A is an arbitrary function whose dependence on m and p will be determined by the limiting process.

One possible definition of the associated Legendre function of order ν and degree μ is

$$P^{\mu}_{\nu}(\eta) = \frac{\sin (\nu+\mu)\pi \Gamma(\nu+\mu+1)}{2^{\nu+1} \cos \nu\pi \Gamma(\nu+\frac{3}{2})\Gamma(\frac{1}{2})} (\eta^2-1)^{\mu/2}\eta^{-\nu-\mu-1}$$

$$\times F\left(\frac{\nu+\mu+2}{2}, \frac{\nu+\mu+1}{2}; \nu+\frac{3}{2}; \frac{1}{\eta^2}\right) + \frac{2^{\nu}\Gamma(\nu+\frac{1}{2})}{\Gamma(\nu-\mu+1)\Gamma(\frac{1}{2})}$$

$$\times (\eta^2-1)^{\mu/2}\eta^{\nu-\mu} F\left(\frac{\mu-\nu+1}{2}, \frac{\mu-\nu}{2}; \frac{1}{2}-\nu; \frac{1}{\eta^2}\right) \tag{131}$$

where our functions fit the requirements of the definition (Magnus and Oberhettinger, 1949, p. 64). We recall that $\lim_{b \to 0} \eta = \frac{r}{b}$ and we note that the hypergeometric functions become unity as η becomes infinite. Therefore, using equation 131, we may write the limiting form of $P^m_{ip-\frac{1}{2}}(\eta)$ as

$$\lim_{b \to 0} P^m_{ip-\frac{1}{2}}(\eta) = \frac{1}{\sqrt{\eta}} [B\eta^{-ip} + C\eta^{ip}] = \frac{1}{\sqrt{\eta}} [Be^{-ip \ln \eta} + Ce^{ip \ln \eta}]$$

where

$$B = \frac{-(-1)^m \cosh p\pi \Gamma(ip+\frac{1}{2}+m)}{2^{ip+\frac{1}{2}}i \sinh p\pi \Gamma(ip+1)\Gamma(\frac{1}{2})},$$

$$C = \frac{2^{ip-\frac{1}{2}}\Gamma(ip)}{\Gamma(ip+\frac{1}{2}-m)\Gamma(\frac{1}{2})}, \text{ and } \eta = \frac{r}{b}. \tag{132}$$

We have also that

$$\lim_{b \to 0} P^m_{ip-\frac{1}{2}}(\eta_0) P^m_{ip-\frac{1}{2}}(\eta) = \frac{1}{\sqrt{\eta_0\eta}} [B^2 e^{-ip \ln (\eta_0\eta)} + C^2 e^{ip \ln (\eta_0\eta)}$$

$$+ BC(e^{ip \ln \eta_0/\eta} + e^{-ip \ln \eta_0/\eta})] = \frac{1}{\sqrt{\eta_0\eta}} \{ (C^2+B^2) \cos [p \ln (\eta_0\eta)]$$

$$+ i(C^2-B^2) \sin [p \ln (\eta_0\eta)] + 2BC [\cos (p \ln \eta_0/\eta)] \}.$$

A corollary of the Riemann-Lebesgue theorem (Carslaw, 1930, p. 358) states that

$$\lim_{\mu \to \infty} \int_a^b f(x) \frac{\sin}{\cos} (\mu x) dx = 0$$

where the sine and cosine terms appearing in a column means that either of them may be used in the equation. Therefore, we see that in the limit as η gets infinitely large, the terms containing $\cos [p \ln (\eta_0\eta)]$ and $\sin [p \ln (\eta_0\eta)]$ vanish during the integration over p. We are then left for consideration only the term $\cos [p \ln (\eta_0/\eta)]$. We now write the limiting form of the integral in equation 130, introducing the substitutions from equations 132 at the same time:

$$\lim_{b \to 0} \frac{1}{R} = \frac{b}{\pi\sqrt{r_0 r}} \sum_{m=0}^{\infty} (-1)^m \cos m\phi \int_0^{\infty} \frac{\cosh p\pi \Gamma(\frac{1}{2}+ip+m)}{p \sinh p\pi \Gamma(\frac{1}{2}+ip-m)}$$

$$\times A P^m_{ip-\frac{1}{2}}(\xi_0) P^m_{ip-\frac{1}{2}}(-\xi) \cos \left(p \ln \frac{r}{r_0}\right) dp.$$

In order that this equation be identical with equation 129 as we require, we see that

$$\frac{b(-1)^m}{\pi} \frac{\cosh p\pi \Gamma(\frac{1}{2}+ip+m)}{p \sinh p\pi \Gamma(\frac{1}{2}+ip-m)} A$$

$$= \frac{(-1)^m(2-\delta_{0m})}{\cosh \pi p} \frac{\Gamma(\frac{1}{2}+ip-m)}{\Gamma(\frac{1}{2}+ip+m)}. \tag{133}$$

Solving this equation for A and substituting it in equation 130, we get for the desired expansion of the reciprocal distance in terms of hyperboloid functions:

$$\frac{1}{R} = \frac{\pi}{b} \sum_{m=0}^{\infty} (2-\delta_{0m}) \cos m\phi \int_0^{\infty} \frac{p \tanh p\pi}{\cosh p\pi} \frac{\Gamma^2(\frac{1}{2}+ip-m)}{\Gamma^2(\frac{1}{2}+ip+m)}$$

$$\times P^m_{ip-\frac{1}{2}}(\xi_0) P^m_{ip-\frac{1}{2}}(-\xi) P^m_{ip-\frac{1}{2}}(\eta_0) P^m_{ip-\frac{1}{2}}(\eta) dp. \tag{134}$$

If $\xi_0 < \xi$, the role of these two quantities would be reversed in the above expansion.

PLANE PARALLEL BOUNDARIES

In this section we develop the fundamental equations that are used in the three following major sections. The discussion involves principally the mathematical treatment of the problem of one of several parallel layers of rocks—whether they be oriented vertically or horizontally. The solution is unique and novel in that it is general and is valid for any number of layers. Special forms of the solution are given in the later sections, where they are applied to particular problems in electrical prospecting. This general development is also used as a vehicle to introduce the use of boundary conditions in the solution of potential problems.

THE GENERAL PROBLEM

We commence the general problem by assuming that all of space is divided into a large but finite number of regions each of which is bounded by parallel planes (fig. 28). Two of these regions, which extend to infinity, are here designated exterior regions. The remainder of the regions are here designated interior regions. All the regions have different values for the resistivity and thickness.
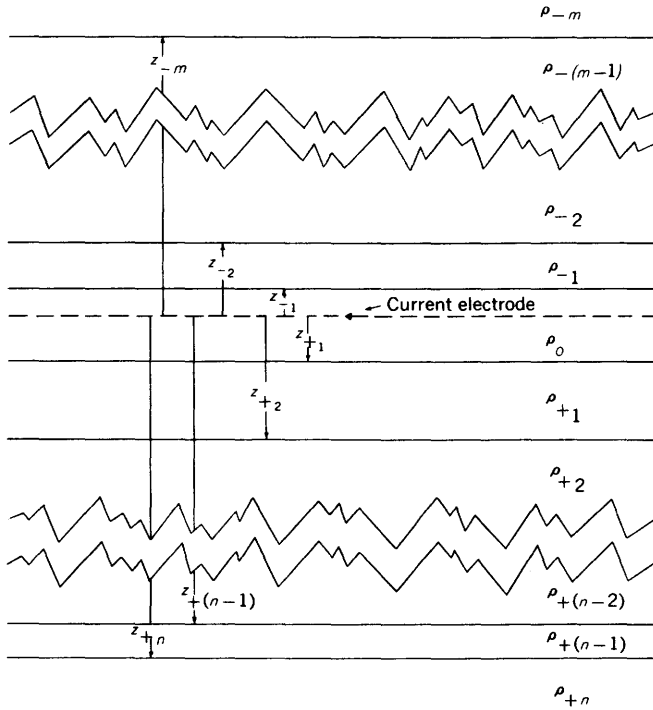
FIGURE 28.—Cross section showing a point source of current within a system containing an arbitrary number of layers of different resistivities.

The next step is to place a point source of current within one of the interior regions. This point source then is made the origin of a cylindrical coordinate system in which the xy-planes are parallel to the plane boundaries between the regions of different resistivity and the z-axis is perpendicular to these boundaries. Each of the boundaries is now describable in terms of a single value of z. The regions are next labeled to distinguish one from another. The region in which the source is located is designated as the zeroth region, and its resistivity is designated as ρ_0. Then, starting from the zeroth region and working in the direction of positive z, we designate the successive resistivities by ρ_{+1}, ρ_{+2}, ρ_{+3}, . . ., and ρ_{+n}. Starting from the zeroth region and working in the direction of negative z, we designate the successive resistivities by ρ_{-1}, ρ_{-2}, ρ_{-3}, . . ., and ρ_{-m}. It is evident that the total number of layers including both exterior regions is $n+m+1$. The problem is now to determine the

potential distribution in each of these regions due to current flowing outward from the point source of current at the origin.

The solution of Laplace's equation which is useful in this problem is that given by equation 70. As the point source is on the polar axis, there can be no dependence upon the angle ϕ. Therefore, equation 70 can be specialized for the present purposes by letting $m=0$:

$$U=\int_0^\infty [A_\lambda e^{\lambda z}+B_\lambda e^{-\lambda z}]J_0(\lambda r)d\lambda. \tag{135}$$

In each of the regions into which all of space has been divided, we assume that the potential function is the sum of $\dfrac{I\rho_0}{4\pi R}$, which we already know satisfies Laplace's equation and can be expressed in the form of equation 135 (see equation 105), plus a correction term in the form of equation 135. The solution of the problem depends on the determination of the arbitrary constants A and B.

We first focus our attention on two beds within the section on the positive side of the z-axis. We label them with the indices j and $j+1$. We note that j can assume any value from zero to $n-1$. In each of these regions there is a potential function which in general includes both exponential terms in the general solution. Therefore, we can write

$$\left. \begin{aligned} U_j&=\frac{I\rho_0}{4\pi}\left\{\frac{1}{R}+\int_0^\infty [A_je^{\lambda z}+B_je^{-\lambda z}]J_0(\lambda r)d\lambda\right\}\\ U_{j+1}&=\frac{I\rho_0}{4\pi}\left\{\frac{1}{R}+\int_0^\infty [A_{j+1}e^{\lambda z}+B_{j+1}e^{-\lambda z}]J_0(\lambda r)d\lambda\right\} \end{aligned} \right\}. \tag{136}$$

The present object, which is to determine the arbitrary constants A_j and B_j in terms of A_{j+1} and B_{j+1}, can be accomplished by using the boundary conditions that the potential and the normal component of the current density must both be continuous across the boundary $z=z_{j+1}$ between the two formations.

When the two potential functions (equation 136) are equated at the boundary the following equation is obtained:

$$\int_0^\infty [A_je^{\lambda z_{j+1}}+B_je^{-\lambda z_{j+1}}]J_0(\lambda r)d\lambda$$
$$=\int_0^\infty [A_{j+1}e^{\lambda z_{j+1}}+B_{j+1}e^{-\lambda z_{j+1}}]J_0(\lambda r)d\lambda. \tag{137}$$

The boundary condition concerning the continuity of the normal component of the current density is written as

$$\frac{1}{\rho_{j+1}}\frac{\partial U_{j+1}}{\partial z}=\frac{1}{\rho_j}\frac{\partial U_j}{\partial z}$$

in this case. Before applying this boundary condition, we must substitute for $1/R$ its expansion in terms of exponentials and Bessel functions of zero order. This expansion is given by equation 105. After making the substitution and taking the necessary derivatives, we obtain the second equation:

$$\rho_{i+1} \int_0^\infty [A_i e^{\lambda z_{i+1}} - (1+B_i)e^{-\lambda z_{i+1}}]J_0(\lambda r)d\lambda$$

$$= \rho_i \int_0^\infty [A_{i+1} e^{\lambda z_{i+1}} - (1+B_{i+1})e^{-\lambda z_{i+1}}]J_0(\lambda r)d\lambda. \quad (138)$$

It should be noted that the other three boundary conditions listed in the previous section have not really been neglected. By choosing the form of the solution such that it contains $1/R$ explicitly, we assured that the solution would become infinite properly at the point source. We had already assured that the solution would remain finite in any finite region when we discarded the Bessel functions of the second kind from equation 70. The condition that the solution must remain finite at infinity will be used below when we indicate how to determine the arbitrary constants in the exterior regions.

As equations 137 and 138 are valid for all values of r, it follows that the corresponding integrands must also be equal. These equations then reduce to

$$\left. \begin{array}{l} A_i e^{\lambda z_{i+1}} + B_i e^{-\lambda z_{i+1}} = A_{i+1}e^{\lambda z_{i+1}} + B_{i+1}e^{-\lambda z_{i+1}} \\[2mm] A_i \rho_{i+1} e^{\lambda z_{i+1}} - B_i \rho_{i+1}e^{-\lambda z_{i+1}} \\[1mm] \quad = A_{i+1}\rho_i e^{\lambda z_{i+1}} - B_{i+1}\rho_i e^{-\lambda z_{i+1}} + (\rho_{i+1}-\rho_i)e^{-\lambda z_{i+1}} \end{array} \right\} \cdot \quad (139)$$

Equations 139 can now be solved as a set of simultaneous equations in A_j and B_j to obtain the desired relationships:

$$\left. \begin{array}{l} A_i = \dfrac{1}{2\rho_{i+1}} [(\rho_{i+1}+\rho_i)A_{i+1} + (\rho_{i+1}-\rho_i)(B_{i+1}+1)e^{-2\lambda z_{i+1}}] \\[3mm] B_i = \dfrac{1}{2\rho_{i+1}} [(\rho_{i+1}-\rho_i)(A_{i+1}e^{2\lambda z_{i+1}}-1) + (\rho_{i+1}+\rho_i)B_{i+1}] \end{array} \right\} \cdot \quad (140)$$

These relationships are used in the following manner. First, it is noted that $A_{+n}=0$ because z goes to infinity in the positive exterior region; setting $A_{+n}=0$ assures that the solution will remain finite everywhere in that region. Equations 140 are then used to calculate $A_{+(n-1)}$ and $B_{+(n-1)}$ in terms of B_{+n}. These equations are then used repeatedly to calculate the arbitrary coefficients for succeeding layers, that is, for decreasing values of j. When calculation has been made for the zeroth region and we wish to calculate A_{-1} and B_{-1}, equations 140 are simply altered by changing the subscripts appropriately:

$$\left. \begin{array}{l} A_{-(i+1)} = \dfrac{1}{2\rho_{-i}} [(\rho_{-i}+\rho_{-(i+1)})A_{-i} + (\rho_{-i}-\rho_{-(i+1)})(B_{-i}+1)e^{-2\lambda z_{-i}}] \\[3mm] B_{-(i+1)} = \dfrac{1}{2\rho_{-i}} [(\rho_{-i}-\rho_{-(i+1)})(A_{-i}e^{2\lambda z_{-i}}-1) + (\rho_{-i}-\rho_{-(i+1)})B_{-i}] \end{array} \right\}$$

$$(141)$$

The arbitrary coefficients for the regions of negative z are then calculated by repeated application of equations 141. When we finally try to calculate A_{-m} and B_{-m}, we find two equations and three unknowns. At this point, we introduce once again the condition that the potential must remain finite at infinity. Since z goes to negative infinity in this exterior region, we see that $B_{-m}=0$ in order to satisfy this boundary condition. Hence, we are now left with only two unknowns, A_{-m} and B_{+n}, together with two simultaneous equations. The final step is to solve these equations for A_{-m} and B_{+n}.

In any given problem in the indirect method of interpretation, the numerical values of the assumed thicknesses and resistivities of the beds will be known. Therefore, it is generally preferable to introduce these numerical values step by step as the coefficients are calculated, especially if the number of regions were very large. However, in the following example, the coefficients are calculated by using only symbols for the thicknesses and resistivities.

APPLICATION OF THE GENERAL SOLUTION

As an example of the application of the solution, let us examine the potential field due to a point source of current situated in an exterior region of a space that is divided into three regions (fig. 29). For simplicity, let
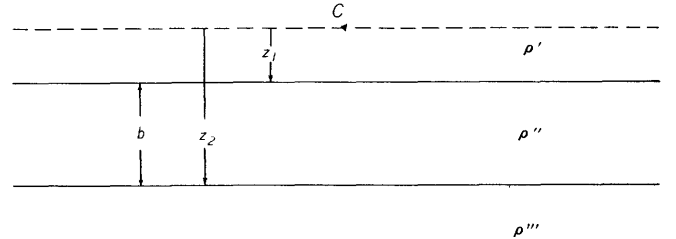
FIGURE 29.—Cross section showing a point source of current within an exterior region of a system containing three parallel layers of different resistivities.

all the regions be positive regions with resistivities $\rho_0=\rho'$, $\rho_1=\rho''$, $\rho_2=\rho'''$ respectively; the source, which is designated as the origin, is in the region of resistivity ρ'; and the boundaries are labeled as $z=z_1$ and $z=z_2$, as in the general problem. The thickness of the central region is $z_2-z_1=b$.

Three potential functions must now be determined. They have the forms

$$\left. \begin{array}{l} U_{1A} = \dfrac{I\rho'}{4\pi} \left\{ \dfrac{1}{R} + \int_0^\infty [A_1 e^{\lambda z} + B_1 e^{-\lambda z}]J_0(\lambda r)d\lambda \right\} \\[3mm] U_{2A} = \dfrac{I\rho'}{4\pi} \left\{ \dfrac{1}{R} + \int_0^\infty [A_2 e^{\lambda z} + B_2 e^{-\lambda z}]J_0(\lambda r)d\lambda \right\} \\[3mm] U_{3A} = \dfrac{I\rho'}{4\pi} \left\{ \dfrac{1}{R} + \int_0^\infty [A_3 e^{\lambda z} + B_3 e^{-\lambda z}]J_0(\lambda r)d\lambda \right\} \end{array} \right\} \cdot \quad (142)$$

The problem is to determine the A's and B's in these functions.

Since z becomes negatively infinite in the region of resistivity ρ' and positively infinite in the region of resistivity ρ''', it is immediately apparent that $B_1 = A_3 = 0$. This fact follows from the boundary condition that the potential must remain finite at infinity.

Equations 140 can now be used to determine A_2 and B_2 in terms of B_3. Thus we have

$$A_2 = \frac{\rho_3 - \rho_2}{2\rho_3} (B_3 + 1)e^{-2\lambda z_2}$$
$$B_2 = \frac{\rho_3 + \rho_2}{2\rho_3} B_3 - \frac{\rho_3 - \rho_2}{2\rho_3} \qquad (143)$$

When the second of equations 140 is applied to the boundary $z = z_1$ and the above expressions are substituted for A_2 and B_2, the following equation results:

$$(\rho_2 - \rho_1) \left[\frac{(\rho_3 - \rho_2)}{2\rho_3} (B_3 + 1)e^{-2\lambda b} - 1 \right]$$
$$+ \frac{(\rho_2 + \rho_1)}{2\rho_3} [(\rho_3 + \rho_2)B_3 - (\rho_3 - \rho_2)] = 0. \quad (144)$$

The only unknown in equation 144 is B_3. The equation is then solved to find that

$$B_3 = \frac{k_{32} + k_{21}(1 + k_{32}) - k_{21}k_{32}e^{-2\lambda b}}{1 + k_{21}k_{32}e^{-2\lambda b}}$$

where

$$k_{ij} = \frac{\rho_i - \rho_j}{\rho_i + \rho_j}.$$

When the expression for B_3 is substituted into equations 143, A_2 and B_2 are immediately shown to be

$$A_2 = \frac{k_{32}(1 + k_{21})e^{-2\lambda z_2}}{1 + k_{21}k_{32}e^{-2\lambda b}}$$
$$B_2 = \frac{k_{21} - k_{21}k_{32}e^{-2\lambda b}}{1 + k_{21}k_{32}e^{-2\lambda b}}.$$

Finally, A_1 is determined by substituting A_2 and B_2 into the first of equations 140. We find that

$$A_1 = \frac{[k_{21} + k_{32}e^{-2\lambda b}]e^{-2\lambda z_1}}{1 + k_{21}k_{32}e^{-2\lambda b}}.$$

In this particular problem, when the expressions for A_1, A_2, B_2, and B_3 are substituted into the potential functions, U_{2A} and U_{3A} are simplified in form if the expansion for $1/R$ (equation 105) is combined with the other integrals given in equations 142. Using this fact, we have as the three potential functions

$$U_{1A} = \frac{I\rho'}{4\pi} \left[\frac{1}{R} + k_{21} \int_0^\infty \frac{e^{-\lambda(2z_1-z)}J_0(\lambda r)}{1 + k_{21}k_{32}e^{-2\lambda b}} d\lambda \right.$$
$$\left. + \int_0^\infty \frac{k_{32}e^{-\lambda(2z_2-z)}J_0(\lambda r)}{1 + k_{21}k_{32}e^{-2\lambda b}} d\lambda \right]$$
$$U_{2A} = \frac{I\rho'}{4\pi} (1 + k_{21}) \left[k_{32} \int_0^\infty \frac{e^{-\lambda(2z_2-z)}J_0(\lambda r)}{1 + k_{21}k_{32}e^{-2\lambda b}} d\lambda \right. \qquad (145)$$
$$\left. + \int_0^\infty \frac{e^{-\lambda z}J_0(\lambda r)}{1 + k_{21}k_{32}e^{-2\lambda b}} d\lambda \right]$$
$$U_{3A} = \frac{I\rho'}{4\pi} (1 + k_{21})(1 + k_{32}) \int_0^\infty \frac{e^{-\lambda z}J_0(\lambda r)}{1 + k_{21}k_{32}e^{-2\lambda b}} d\lambda$$

It can be shown that these expressions are equivalent to the summations resulting from infinite series of images. As the summations are actually more useful in computational work, we will derive the series and hence demonstrate the equivalence. As an example, consider first U_{3A}. The first step in the transformation of the integral is to expand the denominator of the integrand by the binomial theorem:

$$[1 + k_{21}k_{32}e^{-2\lambda b}]^{-1} = \sum_{n=0}^\infty (k_{21}k_{23})^n e^{-2n\lambda b}, \qquad (146)$$

where it is noted that $k_{23} = -k_{32}$.

The potential function may now be written as

$$U_{3A} = \frac{I\rho'}{4\pi} (1 + k_{21})(1 - k_{23}) \sum_{n=0}^\infty (k_{21}k_{23})^n \int_0^\infty e^{-\lambda(2nb+z)} J_0(\lambda r) d\lambda.$$

Let us now consider the expansion for $1/R$ shown in equation 105. Each of the integrals for a specific value of n in the above summation is the expansion of the quantity $1/\sqrt{(2nb+z)^2 + r^2}$. Therefore, .the total potential is represented as an infinite sum:

$$U_{3A} = \frac{I\rho'}{4\pi} (1 + k_{21})(1 - k_{23}) \sum_{n=0}^\infty \frac{(k_{21}k_{23})^n}{\sqrt{(2nb+z)^2 + r^2}}. \qquad (147)$$

In a similar fashion, we can transform the other two potential functions into analogous forms:

$$U_{1A} = \frac{I\rho'}{4\pi} \left\{ \frac{1}{R} + k_{21} \sum_{n=0}^\infty \frac{(k_{21}k_{23})^n}{\sqrt{(2nb+2z_1-z)^2 + r^2}} \right.$$
$$\left. - k_{23} \sum_{n=0}^\infty \frac{(k_{21}k_{23})^n}{\sqrt{(2nb+2z_2-z)^2 + r^2}} \right\}$$
$$\qquad\qquad\qquad\qquad\qquad\qquad\qquad\qquad (148)$$
$$U_{2A} = \frac{I\rho'}{4\pi} (1 + k_{21}) \left\{ \sum_{n=0}^\infty \frac{(k_{21}k_{23})^n}{\sqrt{(2nb+z)^2 + r^2}} \right.$$
$$\left. - k_{23} \sum_{n=0}^\infty \frac{(k_{21}k_{23})^n}{\sqrt{(2nb+2z_2-z)^2 + r^2}} \right\}$$

It can be seen that the problem in figure 20 differs from that in figure 29 only in that figure 20 involves a half space while figure 29 involves an infinite space. Thus, if the above solutions can be related to images, we should be able to identify these solutions with those given in the treatment of the image theory (equations 38). In order to demonstrate the equivalence of the two sets of solutions, let us specialize the present problem to conform to the previous problem by noting that $\rho''' = \rho'$. It follows that $k_{21} = k_{23} = k$. Making these changes directly in equations 147 and 148, we get

$$U_{1A}=\frac{I\rho'}{4\pi}\left\{\frac{1}{R}+k\sum_{n=0}^{\infty}\frac{k^{2n}}{\sqrt{(2nb+2z_1-z)^2+r^2}}\right.$$

$$\left.-k\sum_{n=0}^{\infty}\frac{k^{2n}}{\sqrt{(2nb+2z_2-z)^2+r^2}}\right\}$$

$$U_{2A}=\frac{I\rho'}{4\pi}(1+k)\left\{\sum_{n=0}^{\infty}\frac{k^{2n}}{\sqrt{(2nb+z)^2+r^2}}\right.$$

$$\left.-k\sum_{n=0}^{\infty}\frac{k^{2n}}{\sqrt{(2nb+2z_2-z)^2+r^2}}\right\}$$

$$U_{3A}=\frac{I\rho'}{4\pi}(1-k^2)\sum_{n=0}^{\infty}\frac{k^{2n}}{\sqrt{(2nb+z)^2+r^2}}$$

$$(149)$$

U_{2A} and U_{3A} above are identical to the corresponding expressions in equations 38, except for the extra factor 2 appearing in the above expressions. This factor of two is related to the difference in the problem as described above.

U_{1A} above may also be shown to be equivalent to the previous image solution. We commence by rewriting the second term as:

$$\frac{k}{\sqrt{(2z_1-z)^2+r^2}}+k\sum_{n=1}^{\infty}\frac{k^{2n}}{\sqrt{(2nb+2z_1-z)^2+r^2}}=\frac{k}{\sqrt{(2z_1-z)^2+r^2}}$$

$$+k(k^2)\sum_{n=0}^{\infty}\frac{k^{2n}}{\sqrt{(2nb+2z_2-z)^2+r^2}}. \quad (150)$$

The new summation in equation 150 can now be added to the second summation in U_{1A} (equation 149) to get

$$U_{1A}=\frac{I\rho'}{4\pi}\left\{\frac{1}{R}+\frac{k}{\sqrt{(2z_1-z)^2+r^2}}-k(1-k^2)\sum_{n=0}^{\infty}\frac{k^{2n}}{\sqrt{(2nb-2z_2-z)^2+r^2}}\right\}$$

$$(151)$$

which is identical to the corresponding solution obtained directly by image theory.

HORIZONTAL BEDDING

From the viewpoint of the theorist, horizontal bedding has been given by far the greatest attention in electrical prospecting for two reasons. First, the mathematics for the horizontal-bed problem is relatively simple. Secondly, the problem of determining the depth to horizontal or nearly horizontal beds is of great economic importance in petroleum exploration and in ground-water and engineering problems. Consequently, many theoretical and field investigations have been made that evaluate the usefulness of various electrical methods to the solution of the horizontal-bed problem. The electrical theory for horizontal bedding has had much more success in ground-water and engineering problems, which usually involve finding the thickness of overburden or finding the depth to a shallow key horizon, than in petroleum-exploration problems which usually involve key horizons at relatively great depth.

The three schools of thought on prospecting for horizontal beds have been termed the curve-matching, the empirical, and the direct-interpretation schools (Mooney, 1954a). The curve matchers assume a geological situation and construct a theoretical resistivity curve based upon that assumption. Although these assumed conditions and theoretical curves can be organized into charts to cover a wide range of conditions even before the field work is done, this method is essentially one of trial and error. We highly endorse the curve-matching method, and we therefore describe it in detail in this section.

Workers of the empirical school first obtain their field curves. If there is good geological control, they relate the salient features of the curves to known geological contacts. Such features consist of maxima, minima, inflection points, and incongruous breaks in the curves. They then try to follow the geological contacts away from the region of control by observing the behavior of the resistivity curves in the new regions. This procedure is fairly dependable if there is enough geological control available. Another empirical method is to examine the series of field curves for "breaks" which seem to persist in all the curves. The interpreter then attributes these breaks to some horizontal discontinuity in resistivity at a depth corresponding to the electrode separation at which the break occurs. Although such breaks are completely outside the bounds of present theory, it must be said in defense of the empirical school that some excellent results have been obtained with this method. Many such breaks, however, are probably due to lateral or near-surface resistivity effects. The possibility does exist that we will eventually find some nonohmic flow of current which can explain a certain fraction of the observed breaks.

Certain other empirical methods, such as that given by Moore (1944), are also unfounded in theory and are usually limited in application to the special situations for which they were derived. Although the bibliography contains many references to these empirical methods, we will devote little space to them.

The direct-interpretation school, which was started by the work of Slichter (1933), involves the use of the measured-resistivity data in a mathematical operation to determine directly the horizontal layering which gave rise to the data. This method of approach is outlined here.

THEORY

The original solutions to horizontal-bedding problems were obtained by applying the theory of images directly (Hummel, 1928b, c, d). Later, other workers applied the solutions of differential equations to the same problems and showed that their solutions were equiv-

alent to those obtained directly by the method of images (Stefanesco and others, 1930). We will specialize the solutions that were obtained in the previous section for the general problem. In particular we will show how the solutions to the previous general problem can be applied to the less general problem of a large number of horizontal beds with arbitrary thicknesses and arbitrary resistivities. We will then give the special solutions for the two- and three-layer problems.

If we place the current electrode in the upper surface of the ρ_0 layer, as shown in figure 28, and if we make infinite the values of such resistivities as ρ_{-1}, ρ_{-2}, we then have a situation similar to a layered earth (fig. 30). The z-axis is positive downward with the origin at the source. The coordinate of the earth's surface is $z=0$.
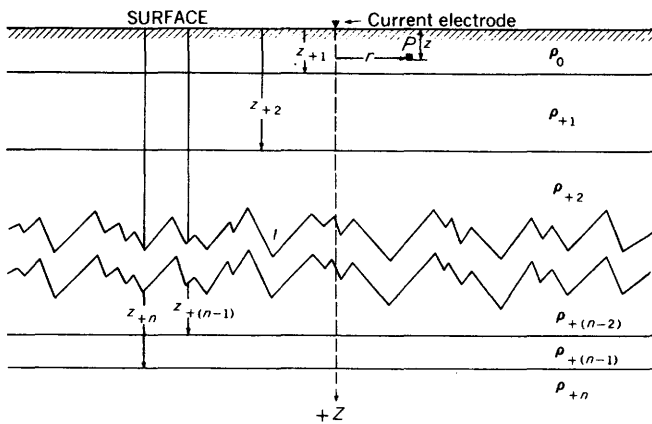
FIGURE 30.—General layered earth with any number of beds of different resistivities and thicknesses.

The potential functions still have the form of equations 136. Equations 140 are still valid for this less general problem; and they can be used in the same way as explained in the section on plane parallel boundaries, except in evaluating the potential function in the uppermost layer, where the potential function must be such that no current crosses the earth's surface because the air above has infinite resistivity. This boundary condition is satisfied, as may be readily verified by setting $\dfrac{\partial U_0}{\partial z}=0$ when $z=0$, if A_0 is made equal to B_0.

As we are usually interested only in A_0 in horizontal-bedding problems, some time can be saved in computations if equations 140 are solved for A_{j+1} and B_{j+1}. In the inverted form, these equations become

$$\begin{cases} A_{j+1}=\dfrac{1}{2\rho_j}\left[(\rho_{j+1}+\rho_j)A_j-(1+B_j)(\rho_{j+1}-\rho_j)e^{-2\lambda z_{j+1}}\right]\\ B_{j+1}=\dfrac{1}{2\rho_j}\left[(\rho_{j+1}-\rho_j)(1-A_je^{2\lambda z_{j+1}})+(\rho_{j+1}+\rho_j)B_j\right]. \end{cases} \quad (152)$$

In any given problem these equations can be used in a repetitive manner, starting with A_0. For the

bottom bed, we solve for A_n in terms of A_0 and set the expression equal to zero, because the $e^{+\lambda z}$ term must be removed if the solution is to remain finite at infinity. After solving the resulting equation for A_0, we can then solve for any of the other coefficients needed.

Slichter (1933) wrote down in a generalized form all the equations arising from the boundary conditions in an n-layer problem, and then solved the equations by the method of determinants. The evaluation of Slichter's determinants by the method of minors is identical step by step to the evaluation of the arbitrary constants by the repetitive use of equation 152.

The solution of the two-layer problem (fig. 31) is obtained by adapting the general forms to this problem. In particular, we must obtain expressions for the potential due to the point source of current in each of the two layers. These potentials initially have the form

$$\begin{cases} U_0=\dfrac{I\rho_0}{2\pi}\left\{\dfrac{1}{R}+\displaystyle\int_0^\infty A_0[e^{\lambda z}+e^{-\lambda z}]J_0(\lambda r)\,d\lambda\right\}\\ U_1=\dfrac{I\rho_0}{2\pi}\left\{\dfrac{1}{R}+\displaystyle\int_0^\infty B_1e^{-\lambda z}J_0(\lambda r)\,d\lambda\right\}. \end{cases}$$
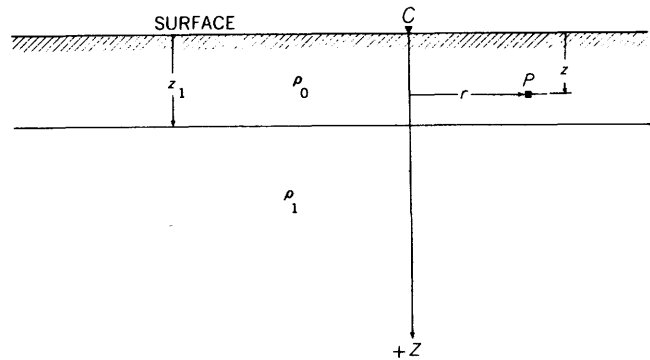
FIGURE 31.—A point source of current over a two-layer earth.

In choosing the forms for the potentials, we have already provided that U_1 must remain finite at infinity and that no current must cross the earth's surface. We have also altered the multiplying factor to $I\rho_0/2\pi$ because we know that it is the correct factor for a point source on the surface of a homogeneous earth (eq. 2); this factor controls the value of the potential at points very close to the source. We now use equations 152 to obtain the arbitrary constants A_0 and B_1. In our application, $j=0$. We merely put A_0 in place of both A_j and B_j in the expression for A_{j+1} and then set this expression equal to zero:

$$A_1=0=\dfrac{1}{2\rho_0}[(\rho_1+\rho_0)A_0-(1+A_0)(\rho_1-\rho_0)e^{-2\lambda z_1}].$$

Solving for A_0, we get

$$A_0=\dfrac{k_{10}e^{-2\lambda z_1}}{1-k_{10}e^{-2\lambda z_1}}.$$

Since we now know A_0, we can solve immediately for B_1, using the second of equations 152.

Thus, the potential functions are found to be

$$\begin{cases} U_0 = \frac{I\rho_0}{2\pi} \left\{ \frac{1}{R} + k_{10} \int_0^\infty \frac{e^{-2\lambda z_1}[e^{\lambda z} + e^{-\lambda z}]}{1 - k_{10}e^{-2\lambda z_1}} J_0(\lambda r) d\lambda \right\} \\ U_1 = \frac{I\rho_0}{2\pi} \left\{ \frac{1}{R} + k_{10} \int_0^\infty \frac{(1 + e^{-2\lambda z_1})e^{-\lambda z}}{1 - k_{10}e^{-2\lambda z_1}} J_0(\lambda r) d\lambda \right\}. \end{cases} \quad (153)$$

Many of the practical solutions used as the basis for theoretical resistivity curves in the literature are based on the theory of images (for example, Roman, 1934). Equations 153 can be reduced to the image solutions by the method used to get equations 148. Following this method, we write down the expansion (eq. 146):

$$[1 - k_{10}e^{-2\lambda z_1}]^{-1} = \sum_{n=0}^\infty k_{10}^n e^{-2n\lambda z_1} \quad (154)$$

whence

$$\begin{cases} U_0 = \frac{I\rho_0}{2\pi} \left\{ \frac{1}{R} + k_{10} \sum_{n=0}^\infty k_{10}^n \int_0^\infty e^{-2\lambda(n+1)z_1}[e^{\lambda z} + e^{-\lambda z}]J_0(\lambda r) d\lambda \right\} \\ U_1 = \frac{I\rho_0}{2\pi} \left\{ \frac{1}{R} + k_{10} \sum_{n=0}^\infty k_{10}^n \int_0^\infty e^{-2\lambda n z_1}(1 + e^{-2\lambda z_1})e^{-\lambda z}J_0(\lambda r) d\lambda \right\}. \end{cases} \quad (155)$$

When we apply the expansion from equation 105, we finally get

$$\begin{cases} U_0 = \frac{I\rho_0}{2\pi} \left\{ \frac{1}{R} + k_{10} \sum_{n=0}^\infty \frac{k_{10}^n}{\sqrt{[2(n+1)z_1 - z]^2 + r^2}} \right. \\ \left. \qquad + k_{10} \sum_{n=0}^\infty \frac{k_{10}^n}{\sqrt{[2(n+1)z_1 + z]^2 + r^2}} \right\} \\ U_1 = \frac{I\rho_0}{2\pi} \left\{ \frac{1}{R} + k_{10} \sum_{n=0}^\infty \frac{k_{10}^n}{\sqrt{[2nz_1 + z]^2 + r^2}} \right. \\ \left. \qquad + k_{10} \sum_{n=0}^\infty \frac{k_{10}^n}{\sqrt{[2(n+1)z_1 + z]^2 + r^2}} \right\}. \quad (156) \end{cases}$$

Usually we are interested in values of the potential function at points on the earth's surface only. Therefore, the useful equation is finally obtained by letting $z = 0$ in equation 156:

$$U_0(z=0) = \frac{I\rho_0}{2\pi} \left\{ \frac{1}{R} + 2k_{10} \sum_{n=0}^\infty \frac{k_{10}^n}{\sqrt{4(n+1)^2 z_1^2 + r^2}} \right\}. \quad (157)$$

Thus, equation 157 represents the potential on the surface of a two-layer earth due to a point source of current also located on the earth's surface. Equation 157 can be manipulated easily into the forms which various authors have obtained using the theory of images. It is the equation useful for computations, especially when k is negative—that is, when the underlying bed is the more conducting.

Equations for the three-layer problem and for other multilayer problems can be computed in the same manner from the general equations. The expression for A_0 in the three-layer case is developed in a later section on direct interpretation (eq. 169).

Using the above results, we can now study the current penetration between two current electrodes in a two-layer medium in a manner somewhat analogous to our study of the depth of current penetration in homogeneous ground. The results will help refute the contention that the effective depth of current penetration in a two-layered medium equals the electrode separation a in the Wenner configuration; the results will also indicate the importance of the so-called "blanketing effect" of high resistivity contrasts.

In determining the potential distribution due to more than one electrode, the principle of superposition enables us to study the effect of each electrode taken separately and then later to add these effects in order to determine the effect of the configuration of electrodes as a whole. As the same principle applies in the present problem, we will consider first the current distribution due to a single electrode only, and next the current distribution due to two electrodes. It should be cautioned that because we are dealing with vectors, algebraic addition can be used only when we are considering the corresponding scalar components of a number of vectors.

Remembering that the x-component of current density (eq. 6) is $J_x = -\frac{1}{\rho} \frac{\partial U}{\partial x}$, we obtain the total current ΔI flowing across any given yz-plane below a depth z':

$$\Delta I = \int_0^{z'} \int_{-\infty}^\infty \left[-\frac{1}{\rho} \frac{\partial U}{\partial x} \right] dy\, dz. \quad (158)$$

The present problem differs from the one discussed previously in that we now must consider two separate derivatives and two separate resistivities. Consequently, there are many ways to study the problem. We will choose only one of these approaches. Specifically we will investigate the amount of current that enters the lower bed only; and we will therefore need to consider the current density in the lower bed only. By manipulating the second series in the expression for U_1 in equation 156, it can be shown that:

$$U_1 = \frac{I\rho_0}{2\pi} (1 + k_{10}) \sum_{n=0}^\infty \frac{k_{10}^n}{\sqrt{(2nz_1 + z)^2 + r^2}},$$

where $r^2 = x^2 + y^2$. The necessary derivative in this case is

$$\frac{\partial U_1}{\partial x} = -\frac{I\rho_0 x}{2\pi}(1 + k_{10}) \sum_{n=0}^\infty \frac{k_{10}^n}{[(2nz_1 + z)^2 + x^2 + y^2]^{3/2}}.$$

Substituting this derivative into equation 158, we get the total amount of current flowing in the lower bed

through any given yz-plane (specified by assigning the value of x):

$$\Delta I = \frac{I\rho_0 x}{2\pi\rho_1}(1+k_{10}) \sum_{n=0}^{\infty} k_{10}^n \int_{z_1}^{\infty}\int_{-\infty}^{\infty} \frac{dydz}{[(2nz_1+z)^2+x^2+y^2]^{3/2}}.$$

We integrate first with respect to y:

$$\Delta I = \frac{I\rho_0 x}{\pi\rho_1}(1+k_{10}) \sum_{n=0}^{\infty} k_{10}^n \int_{z_1}^{\infty} \frac{dz}{(2nz_1+z)^2+x^2}$$

and then with respect to z:

$$\Delta I = \frac{I\rho_0}{\pi\rho_1}(1+k_{10}) \sum_{n=0}^{\infty} k_{10}^n \left[\frac{\pi}{2} - \text{arc tan}\,\frac{(2n+1)z_1}{x}\right]. \quad (159)$$

To determine the amount of current that enters the lower bed in the case of two current electrodes on the surface of a two-layer earth, we determine the amount of current that passes in the lower bed and through the plane bisecting the line of electrodes. The distance of this plane from one of the current electrodes is $3a/2$, where a is the electrode separation of the Wenner configuration. Thus, x in equation 159 becomes $3a/2$. Owing to symmetry, the amount of current that flows through the midplane will be the same from each current electrode. Since equation 159 is based on only one electrode, the expression which we seek is double that given above. Thus the current entering the lower bed, when expressed as a fraction of the total current, is

$$\frac{\Delta I}{I} = \frac{2\rho_0}{\pi\rho_1}(1+k_{10}) \sum_{n=0}^{\infty} k_{10}^n \left[\frac{\pi}{2} - \text{arc tan}\,\frac{2(2n+1)z_1}{3a}\right].$$

This expression can be simplified for computations by substituting for the arc tangent its series representation. Thus, we have

$$\frac{\Delta I}{I} = \frac{2\rho_0}{\pi\rho_1}(1+k_{10}) \sum_{n=0}^{\infty} k_{10}^n \sum_{m=0}^{\infty} \frac{(-1)^m}{2m+1}\left[\frac{3a}{2(2n+1)z_1}\right]^{2m+1} \quad (160)$$

Figure 32 represents the results of a computation based on equation 160. In this particular case, the depth to the second layer is made equal to one-half the distance between the current electrodes. The current penetrating the lower bed is given as a function of the resistivity contrast expressed in terms of k_{10}. The curve starts out, as it should, with no current entering the lower bed when that bed is perfectly insulating. For a homogeneous earth, one-half the total current penetrates the horizontal contact plane which we have chosen (see above). For the case of a perfectly conducting lower bed, only slightly less than three-quarters of the total current penetrates the lower bed. Using intuition alone, one might reason errone-
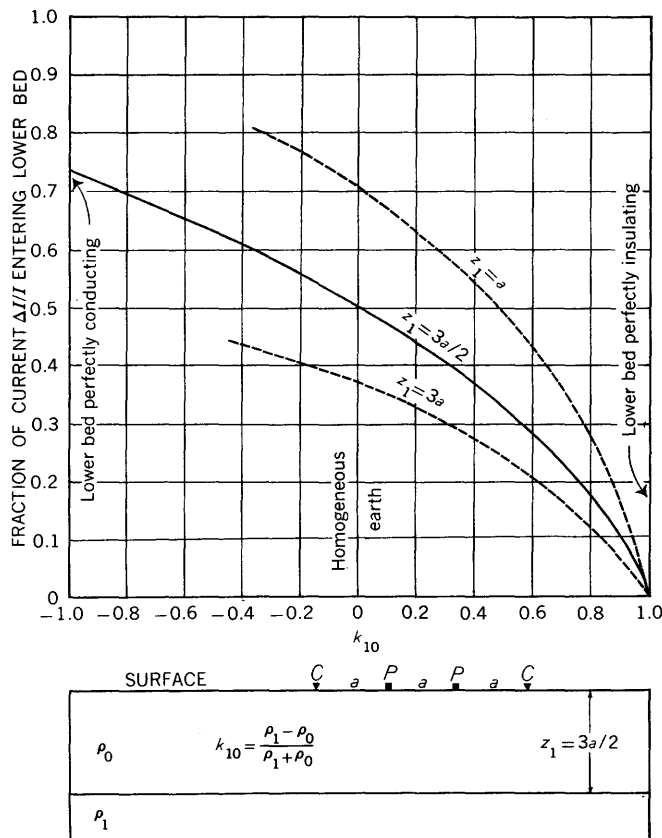
FIGURE 32.—The fraction $\Delta I/I$ of the total current I which passes into a bed whose depth equals one-half the distance L between the current electrodes.

ously that essentially all the current enters the lower bed.

We can also predict qualitatively what we can expect when the depth to the second layer is different from that assumed. We know the current penetration in homogeneous media. We know further that the general shape of the curve for any given depth of contact must be the same as the one shown. Using these two principles, we can easily sketch out the probable curves for other geometrical relationships. Two such curves have been indicated in figure 32 by dashed lines.

THEORETICAL CURVES

Our approach to the subject of theoretical curves of horizontal bedding problems is objective. Literally hundreds of apparent-resistivity curves have been published for the two-, three-, and four-layer cases (Mooney and Wetzel, 1956). Our principal objectives, therefore, are to digest and analyze the works of others on the horizontal-bed problems, and to give an evaluation of the best solutions available and the best methods to use in actual field problems. It should be emphasized that the key to the interpretation of the horizontal-bed problem lies in the recognition of the

practical limitations of the resistivity method to solve the problem.

The most serious limitation is one of depth. We normally find that the electrode separation in the Wenner configuration, for example, must be of the order of two or three times the depth to the beds of interest. Thus, even though current penetration can be obtained, the great electrode separations needed for the effects of deep layers to manifest themselves usually result in lateral effects superposed on the depth effects. Exceptions to this rule are rare in the field, and consequently the quantitative interpretation of horizontal-bed problems is usually restricted to relatively shallow depths.

Other limitations are sufficient resistivity contrasts and compatible thicknesses. Although the restrictions imposed by resistivity contrasts are fortunately not very stringent, the vast range of resistivities is not as important as it appears. As we found in the previous section on theory, the resistivity contrast invariably enters the problem in the form of the reflection factor $k_{ij} = (\rho_i - \rho_j)/(\rho_i + \rho_j)$. The absolute value of the reflection factor ranges only from zero to unity. If the resistivity of a given bed is twice that of a neighboring bed, the reflection factor is one-third—which is already one-third of its entire range. If the resistivity of a given bed is 5 times the resistivity of an adjacent bed, the reflection factor is two-thirds. As the resistivity contrast rises above this value of 5 to 1, the reflection factor increases very slowly toward unity. For all practical purposes, a resistivity contrast of the order to 10 to 1 gives an anomaly of the same order of magnitude as an infinite resistivity contrast. This rule applies to almost all types of structures.

The thicknesses of the beds also govern our approach to the problem of horizontal beds. For example, if there exist three layers and if the middle layer is of sufficient thickness, the three-layer problem can be solved by the successive use of methods normally applied to solve two-layer problems. As the thickness of the middle layer decreases, we find a stage in which the theoretical three-layer curves must be consulted; for an expanding electrode configuration, the effect of the bottommost bed appears in the apparent resistivity almost as soon as the effect of the middle layer. Finally, when the thickness of the middle layer becomes even smaller, the problem reduces to a simple two-layer case because the effect of the middle layer is no longer important at any electrode separation. It is obvious that the critical thicknesses of the middle layer in this hypothetical case are dependent on the resistivity contrasts.

A working knowledge of what can or cannot be accomplished with resistivity techniques for the hori-zontal-bed problem is predicated upon a practical viewpoint of the manner in which these parameters of depth, thicknesses, and resistivity contrasts are interrelated.

TWO-LAYER CASE

For the plotting of vertical resistivity profiles in horizontal-bed problems, logarithmic plotting for both the apparent resistivity and the electrode separation is preferable to linear plotting. When both the observed and theoretical curves are plotted on the same type of logarithmic paper, the effect of scale is eliminated; and once a satisfactory match between the observed and theoretical curves is made, the parameters can be determined. For the observed curves, the apparent resistivity ρ_a is plotted as the ordinate, and the electrode separation a is plotted as the abscissa. For the theoretical curves, the ratio of the apparent resistivity ρ_a to the true resistivity ρ_0 of the top layer is usually plotted as the ordinate, and the ratio of the electrode separation a to the thickness z_1 of the top layer is plotted as the abscissa; it is convenient to plot the theoretical curves on transparent material to facilitate curve matching.

Figure 33 shows a master set of such theoretical curves for the two-layer case (adapted from Roman, 1941). The values of the reflection factor k are shown for intervals of 0.1 between $+1.0$ and -1.0. The theoretical curves are applicable for either the Wenner or Lee configurations. Assuming that a satisfactory fit occurs between the observed apparent resistivity curve and one of the curves in figure 33, the following factors may be readily obtained when the curves are in superposition. (See fig. 34).

1. The reflection factor k, which equals $(\rho_1 - \rho_0)/(\rho_1 + \rho_0)$ is read immediately off the theoretical curve that fits the data. If an observed curve fits, but lies intermediate between the ones drawn on the master curves in figure 33, the estimated value of k can be obtained by interpolation from the chart.

2. The resistivity ρ_0 of the top layer is obtained by noting where the horizontal "resistivity index" line on the master chart intersects the axis of ordinates of the observed curve. This results from the fact that the resistivity index is the line (axis of abscissas) on the master chart representing $k=0$, which means that $\rho_a/\rho_0 = 1$, and consequently $\log \rho_a = \log \rho_0$. The fundamental reason for the validity of superposition in this manner, however, lies in the facts that $\log (\rho_a/\rho_0) = \log \rho_a - \log \rho_0$ and $\log (a/z_1) = \log a - \log z_1$ and because both $\log \rho_0$ and $\log z_1$ are constant. Thus the sliding of the master chart up and down, or back and forth to the right and left, does not affect the scale.

A

$C_2 \quad a \quad P_2 \quad a \quad P_1 \quad a \quad C_1$

ρ_0 z_1

ρ_1

k	ρ_1 / ρ_0
+1.0	∞
.9	19.00
.8	9.00
.7	5.67
.6	4.00
.5	3.00
.4	2.33
.3	1.86
.2	1.50
.1	1.22
.0	1.00

$k = \dfrac{\rho_1 - \rho_0}{\rho_1 + \rho_0}$

$\dfrac{\rho_a}{\rho_0}$

DEPTH INDEX

k POSITIVE

Perfect insulator

$k = 1.0$
0.9
0.8
0.7
0.6
0.5
0.4
0.3
0.2
0.1
$k = 0$

$\leftarrow$ RESISTIVITY INDEX

0.3 0.4 0.5 0.6 0.7 0.8 0.9 1.0 2 3 4 5

B

$\leftarrow$ RESISTIVITY INDEX

$k = \dfrac{\rho_1 - \rho_0}{\rho_1 + \rho_0}$

$C_2 \quad a \quad P_2 \quad a \quad P_1 \quad a \quad C_1$

ρ_0 z_1

ρ_1

$\dfrac{\rho_a}{\rho_0}$

k	ρ_1 / ρ_0
-0.0	1.00
- .1	.82
- .2	.67
- .3	.54
- .4	.43
- .5	.33
- .6	.25
- .7	.18
- .8	.11
- .9	.05
-1.0	.00

DEPTH INDEX

k NEGATIVE

$k = -0.1$
-0.2
-0.3
-0.4
-0.5
-0.6
-0.7
-0.8

Perfect conductor

-1.0
-0.9

$\dfrac{a}{z_1}$

0.3 0.4 0.5 0.6 0.7 0.8 0.9 1.0 2 3 4 5

FIGURE 33.—Apparent-resistivity curves for two-layer case, logarithmic plotting. (A) Positive and (B) negative values, respectively, of reflection factor k = $(\rho_1 - \rho_0)/(\rho_1 + \rho_0)$ Adapted from Roman (1941).
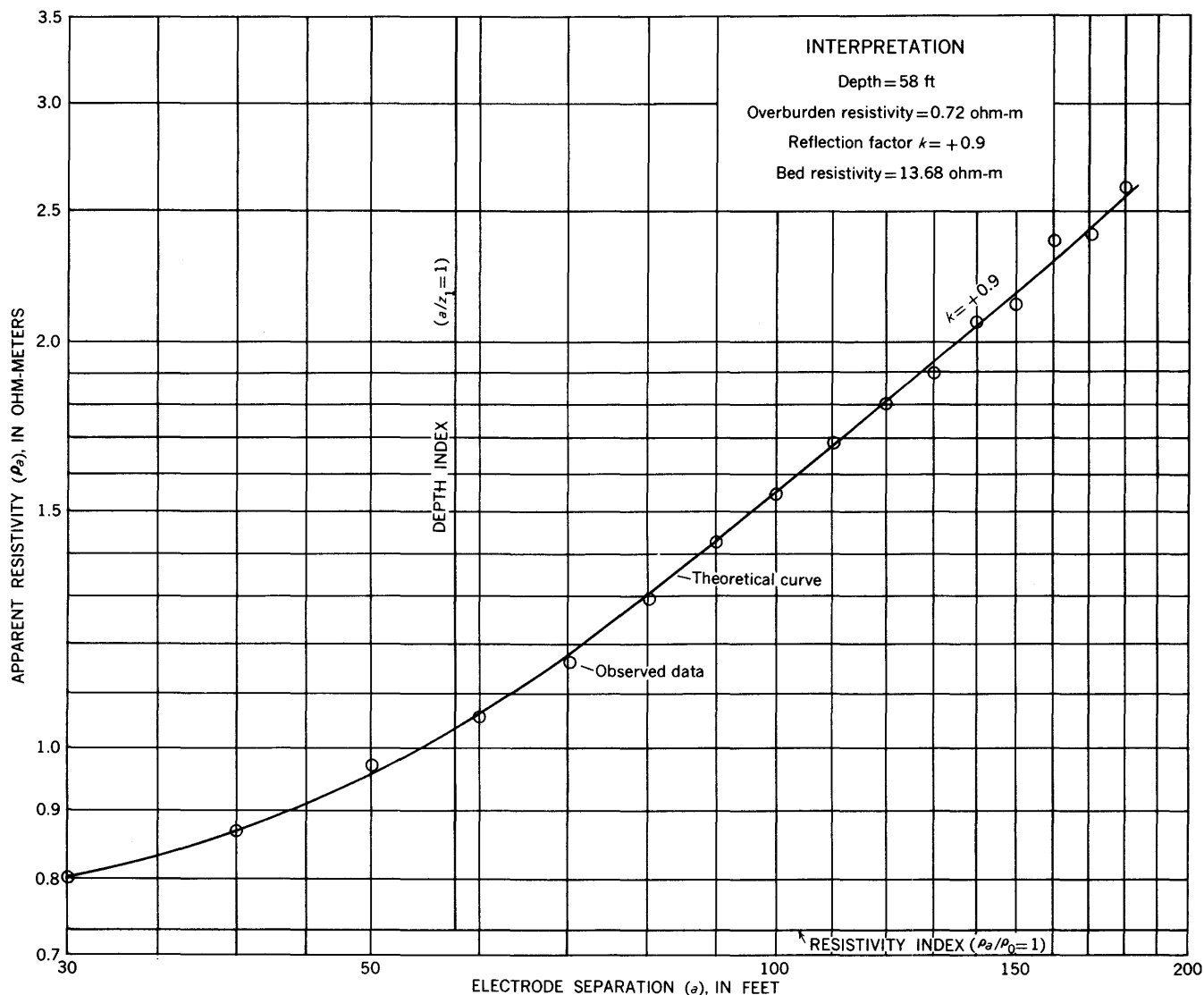
FIGURE 34.—Example of resistivity interpretation by curve matching, two-layer case, logarithmic plotting. Adapted from Irwin Roman (1952, unpublished data).

3. The depth z_1 to the bottom layer is obtained by noting where the vertical "depth index" line (axis of ordinates) on the master chart intersects the axis of abscissas (values of electrode separation a) on the observed curve. This results from the fact that the depth index is the line on the master chart representing log $(a/z_1)=0$, which means that $a/z_1=1$ and that, therefore, $a=z_1$. The fact that this electrode separation a is equal to the depth z_1 has nothing to do with the Gish-Rooney empirical rule mentioned earlier.

4. The resistivity ρ_1, of the bottom bed is determined directly from the relationship

$$\rho_1=\frac{1+k}{1-k}\rho_0.$$

In the example shown in figure 34, the values of the factors listed above are given in the diagram.

Though we recommend curve matching as the best procedure for quantitative resistivity interpretation, there are certain generalizations that assist the interpreter in making a preliminary analysis of observed apparent-resistivity curves for the two-layer case. The fact that larger anomalies are obtained for negative reflection factors than for positive reflection factors (see fig. 33) indicates that a bed of better conducting material at depth can be detected more readily than a poorly conducting one, other things being equal. The most valuable generalizations, however, apply to situations in which the resistivity of the bottom bed is assumed to be great, because usually the resistivity

does increase with depth. When the bottom bed in the two-layer case is a perfect insulator, the apparent-resistivity curve for a vertical profile gives a limiting straight-line curve which passes through the origin of coordinates (for linear plotting) and which has an inclination tan $\alpha=1.386$. A limiting straight line also occurs with logarithmic plotting. For this limiting case the limiting value of the slope will be reached when $a/z_1=1.5$; this is also approximately true for other resistivity contrasts that exceed about $\rho_1/\rho_0=10:1$. This property, which is important also in considering the analysis of three- and four-layer cases discussed later, implies that in a two-layer region in which the bottom bed is ten or more times resistive than the top bed, the configuration will need to be expanded to only about two or three times the suspected depth to obtain the thickness z_1 of the top layer. In addition, for large values of ρ_1/ρ_0, the apparent resistivity ρ_a is 1.5 times the true resistivity ρ_0 of the upper layer when $a=z_1$, that is, when the electrode separation is equal to the thickness of the top layer. As the true resistivity of the ordinary alluvium is usually much lower than that of the bedrock below it, a valuable indication of the depth of the bedrock can frequently be obtained by this relationship in simple two-layer, depth-to-bedrock problems. Of course, this assumes that a determination of ρ_0 can be obtained from the value of the apparent resistivity at small electrode separations.

In the two-layer problem the various rules for depth that depend upon the points of inflection of the apparent-resistivity curves have been shown by various investigators (Ehrenburg and Watson, 1931; Palmer and Hough, 1953) to be applicable to certain reflection factors only; each rule breaks down when applied universally. As the resistivity contrast is not generally known, it is therefore considered preferable— and usually just as fast—merely to compare the observed curve with the master logarithmic curves rather than to rely on the rules concerning inflection points.

Figure 35 shows the families of apparent-resistivity curves for the two-layer case when linear plotting is used (after Tagg, 1932). The curves are taken at intervals of k of 0.1 from $+1.0$ to -1.0. The ratio of the apparent resistivity ρ_a or conductivity σ_a to the true resistivity ρ_0 or conductivity σ_0, respectively, of the top layer is plotted as the ordinate on a linear scale; and, because the electrode separation a is known, the ratio of the thickness z_1 of the top layer to the electrode separation a is plotted as the abscissa on a linear scale. The curves are applicable for either the Wenner or Lee configurations. These linear curves are used today principally for the Tagg method of interpretation, which will be discussed in a later section.

Either the constant-electrode system or the expanding-electrode system of the potential-drop-ratio method can be used in studies of horizontal bedding. Figures 36 and 37 show the normalized potential-drop ratios for both these systems for different reflection factors.

For the constant-electrode system (fig. 36), the potential electrode separation a is taken as half the depth z_1 to the bottom layer. For a perfectly insulating bottom bed ($k=1$), the maximum value of the potential-drop ratio is about 1.3, and occurs when the distance r between center potential electrode P_0 and current electrode C equals about 1½ times the depth z_1. For smaller positive reflection factors, the potential-drop-ratio curves become flatter, and the maxima shift so slightly to the right that their position on the abscissa of the chart can be used as a valuable criterion of the depth for the two-layer case. For this reason, claims are made that the potential-drop-ratio method gives a faster interpretation of the depth for a two-layer problem than resistivity techniques, provided the reflection factor is positive (Heiland, 1940, p. 747). Additional potential-drop-ratio curves for different positive reflection factors and electrode separations than those in figure 36 are deemed necessary to substantiate these claims. For negative reflection factors (top bed is more resistive than bottom bed), it is seen from figure 36 that the potential-drop-ratio minima shift so much to the right that a curve-matching comparison with theoretical curves would be necessary for making reliable depth estimates.

For the expanding-electrode system making $r'=3a$ (fig. 37), the potential-drop-ratio maxima for positive reflection factors (bottom layer more resistive than top layer) occur when the distance between current electrode C and the nearest potential electrode P_1 is approximately equal to the depth of the bottom layer (Heiland, 1940, p. 748). For negative reflection factors no general rule can apparently be made.

MULTIPLE-LAYER CASE

The three-layer case comprises a top layer of thickness z_1, a middle layer of thickness d, and a bottommost layer at depth z_2 (z_2 is defined by the equation $z_2=z_1+d$) that theoretically extends to infinity (see fig. 38). As there are an infinite number of permutations and combinations of the factors of electrode separations, thicknesses of beds, and resistivity contrasts of the three beds, it is helpful in the analysis of the three-layer problem to first systematize the conventions and practices that will suffice for practical needs and at the same time keep the problem from being unwieldly Our conventions and reasonings for the three-layer case follow those of Wetzel and McMurry (1937)
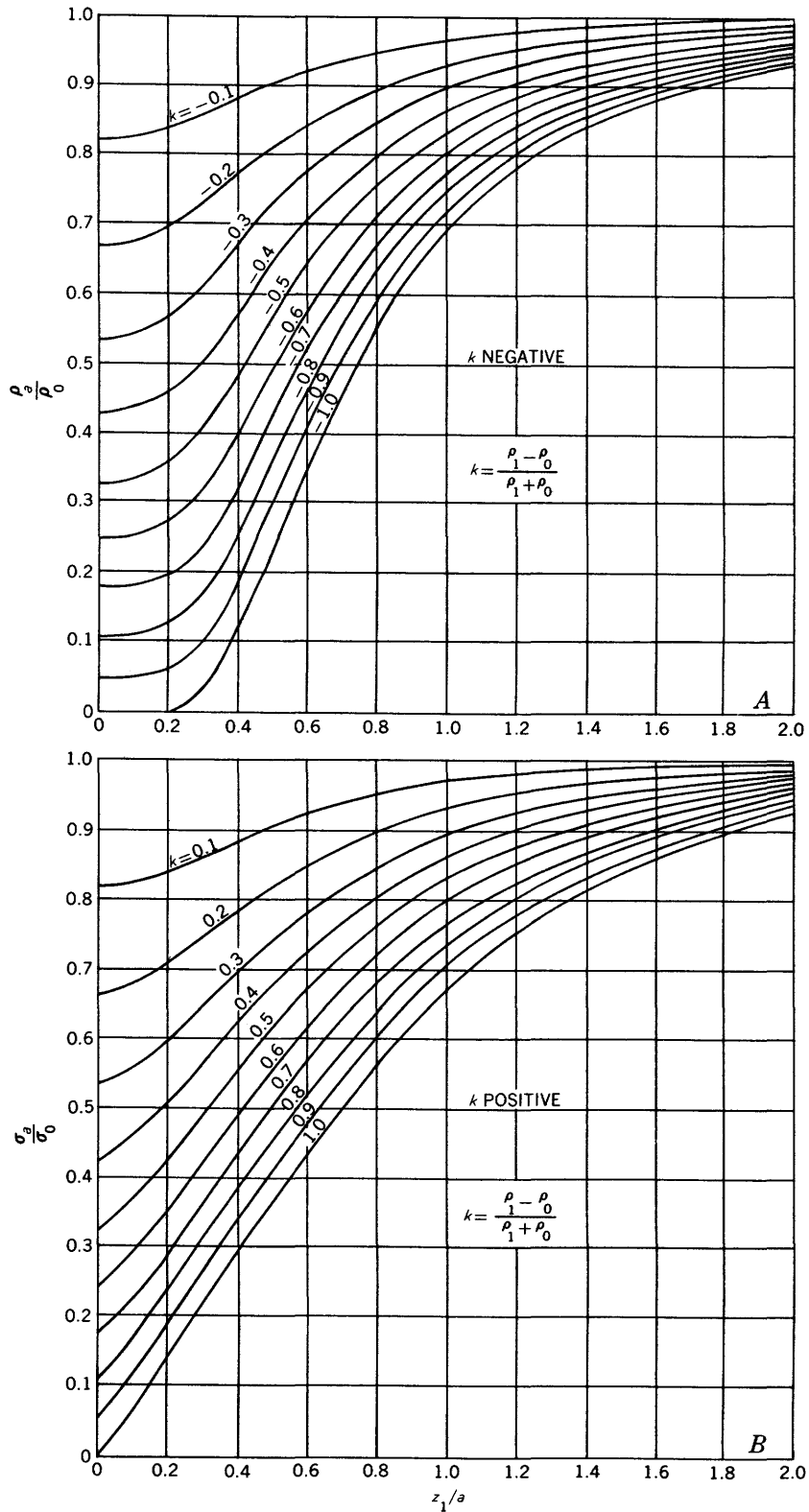
FIGURE 35.—(A) Apparent-resistivity (B) apparent-conductivity curves for Tagg interpretation of two-layer case, linear plotting; reflection factor k, (A) negative; and (B) positive. Adapted from Tagg (1932). Copyright by Am. Inst. Mining Metall. Engineers.
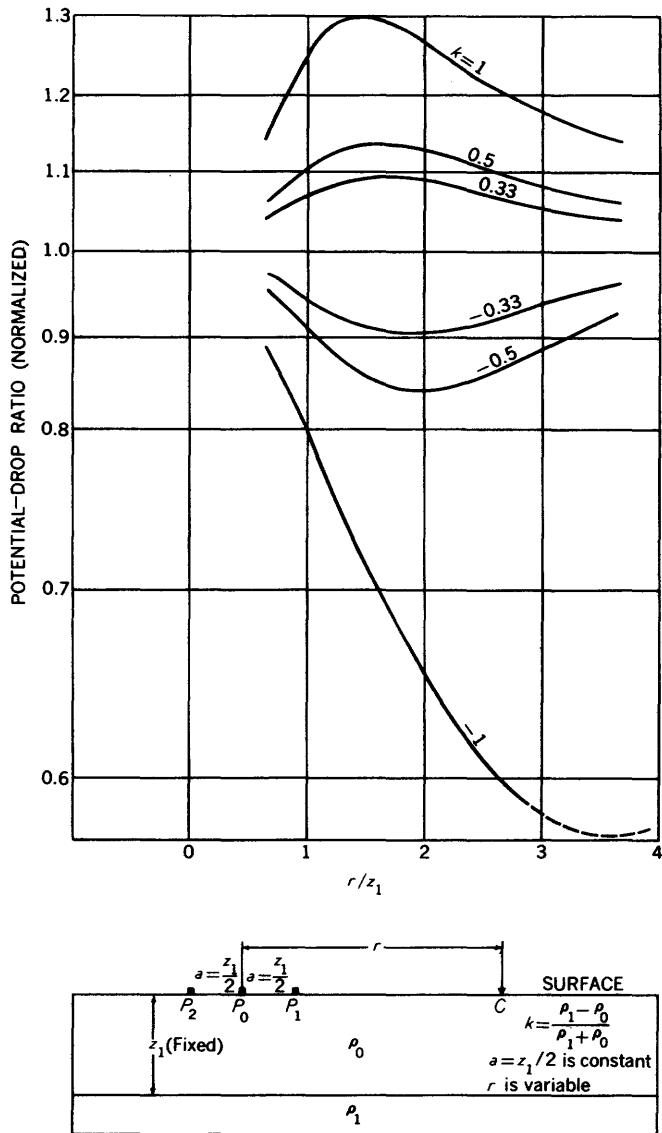
FIGURE 36.—Potential-drop ratios (normalized) for two-layer case, constant-electrode system for various reflection factors k. Electrode spacing $a = z_1/2$ is constant; r variable. Adapted from John Baird (1940, "Potential-drop ratios in the case of stratified medium," unpublished doctor's thesis, Colorado School of Mines Library).

FIGURE 37.—Potential-drop ratios (normalized) for two-layer case, expanding-electrode system, perfectly insulating bottom bed. Depth $z_1 = 18.5$ units; $r' = 3a$. Adapted from M. H. Jameson (1937, "Effect of dipping strata on potential-drop-ratio determinations," unpublished master's thesis, Colorado School of Mines Library).

with some modifications. The thickness z_1 of the top layer is always taken as our unit of length. Except in special cases, the assumed resistivity contrasts will be in ratios of $1/\infty$, $1/100$, $1/10$, $1/3$, $3/1$, $10/1$, $100/1$, and $\infty/1$. There are three main groups of possibilities concerning the resistivity of the middle bed in relation to that of the others: its resistivity may be higher than, lower than, or intermediate between the resistivities of the top and bottommost beds. The assumed thicknesses of the layers are either equal or are simple multiples of each other. Thin beds of thickness less than one unit will not be considered because, for all practical purposes, they will not be detectable in the field unless they are either nearly perfectly conducting

or perfectly insulating; and if they are so, they fall into the category of special limiting cases of the three-layer problem that can be recognized from the families of theoretical curves that will be shown later. It should be emphasized, however, that the presence of undetectable thin beds can still cause erroneous interpretations.

As in the two-layer case, logarithmic plotting is recommended, because it renders the shape of the curves independent of the field units used and allows the interpreter to become familiar with the curve trends. This is difficult to do if linear plots are used. Provided the three-layer assumption is correct and the beds are homogeneous, a unique solution is possible, as in the two-layer case; but to obtain a unique solution, the electrode configuration must generally be expanded to much larger electrode separations than for the two-layer case. Great care must also be used in obtaining the apparent resistivity for small electrode separations.

The best depth determinations that can ordinarily be expected with the resistivity method for the three-layer case is to within an accuracy of only 10 percent When reference is made to obtaining an "accurate" depth estimate in this paper, the inherent limitation of the method is still implied.

For the special three-layer cases in which the bottommost bed is either a perfect insulator or perfect conductor, the mathematics is greatly simplified, and the properties are therefore easily obtainable. When the bottommost layer is a perfect insulator, the asymptotic curve for large electrode separations passes through the origin of coordinates (for linear plotting), and its slope is identical to that for the two-layer case in which the bottom layer is a perfect insulator.

Figure 38 shows the effect on the apparent resistivity of varying ratios of the top-layer thickness z_1 to middle-layer thickness d for the Wenner or Lee configuration (Wetzel and McMurry, 1937). The ratios of resistivities are $\rho_0:\rho_1:\rho_2::1:1/3:1$. The ratio $z_1:d::0:8$ is identical to a two-layer case, and the ratio $z_1:d::8:0$ is the homogeneous case. Because for large separations the slopes of the curves approach that for the two-layer case, it is clear that a family of logarithmic two-layer curves can be used to obtain approximately the depth z_2 of the bottommost bed. The same is true in this case for the depth z_1.

Figure 39 shows the effect on the apparent resistivity of varying the resistivity ρ_1 of the middle layer, all other factors remaining constant (Wetzel and McMurry, 1937). The resistivities of the top and bottommost beds are equal, and $z_1:d::3:1$. All curves are asymptotic to the value $\rho_a/\rho_0=1$. In this case the logarithmic two-layer curves can be used to obtain approximately the thickness z_1 of the top layer, but they cannot be used to obtain the depth z_2 of the bottommost layer because the curves on the right-hand side of the diagram are not close enough to asymptotic values to allow the two-layer approximation to be applied.

Figure 40 shows the effect on the apparent resistivity of variations in the resistivity ρ_2 of the bottommost layer, all other factors remaining constant (Wetzel and McMurry, 1937). The fixed resistivities are such that $\rho_1=3\rho_0$, and $z_1:d::1:3$. The curve labeled $\rho_2=3\rho_0$ is for the two-layer case; and it fits the other curves so closely for abscissa values less than 3 that in this case also the thickness z_1 of the top layer can obviously be obtained approximately from the two-layer logarithmic curves for all resistivity contrasts involved.

Figure 41 shows the behavior of certain types of resistivity curves by comparing three-layer curve A for $z_1:d::4:4$ with various limiting curves. The resistivities for curve A are $\rho_0:\rho_1:\rho_2::1:10:1/3$; thus
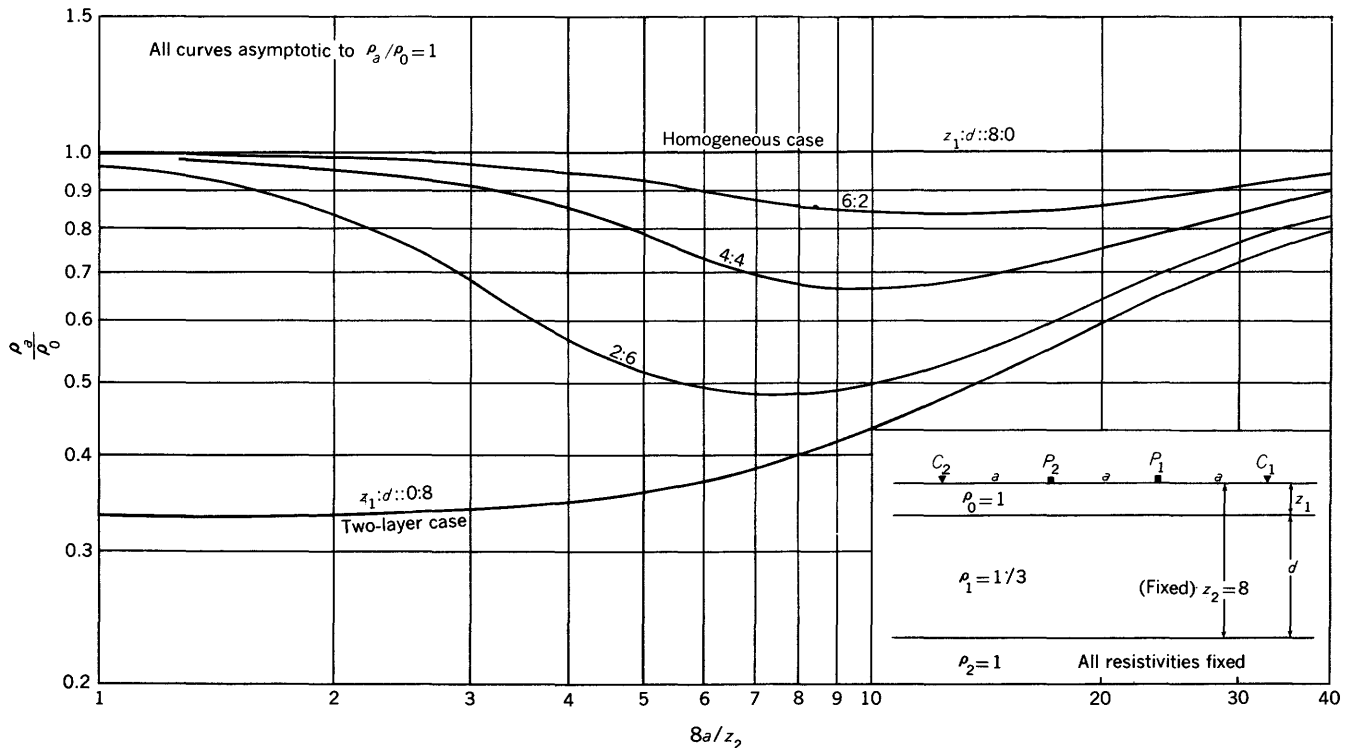
FIGURE 38.—Diagram of three-layer case showing the effect on the apparent resistivity ρ_a of varying ratios of top-layer thickness z_1 to middle-layer thickness d, Wenner or Lee configuration. $\rho_0:\rho_1:\rho_2::1:1/3:1$. Adapted from Wetzel and McMurry (1937).
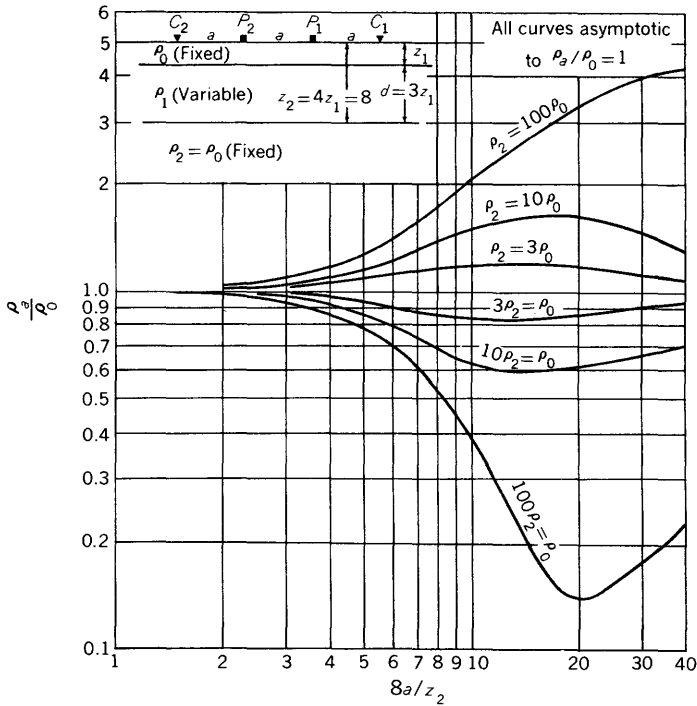
FIGURE 39.—Diagram of three-layer case showing the effect on the apparent resistivity ρ_a of varying resistivity ρ_1 of the middle layer, all other factors remaining constant, Wenner or Lee configuration; $z_1:d::3:1$; $\rho_0=\rho_2=1$. Adapted from Wetzel and McMurry (1937).
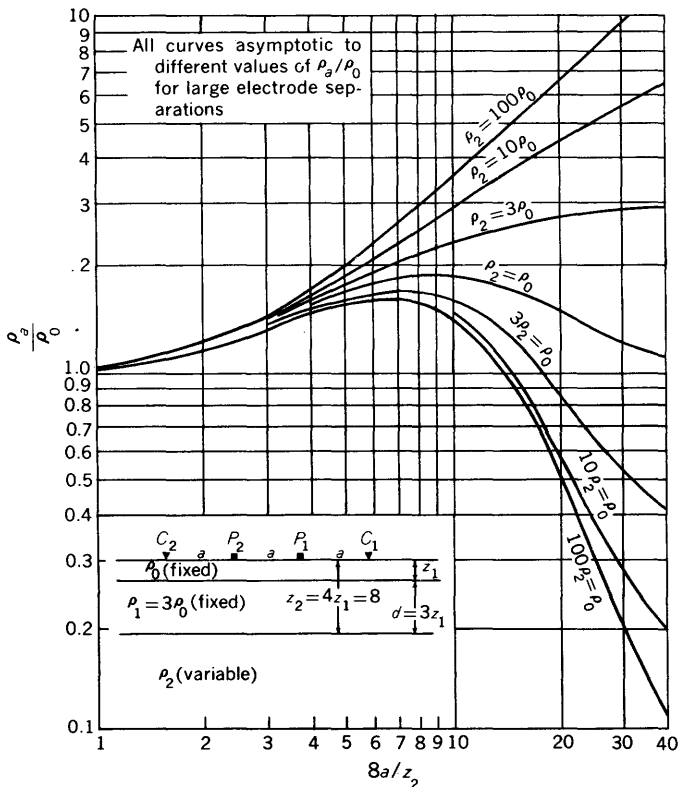
FIGURE 40.—Diagram of three-layer case showing the effect on the apparent resistivity ρ_a of variations in resistivity ρ_2 of bottommost layer, all other factors remaining constant, Wenner or Lee configuration; $z_1:d::1:3$; $\rho_0=1$; $\rho_1=3$. Adapted from Wetzel and McMurry (1937).
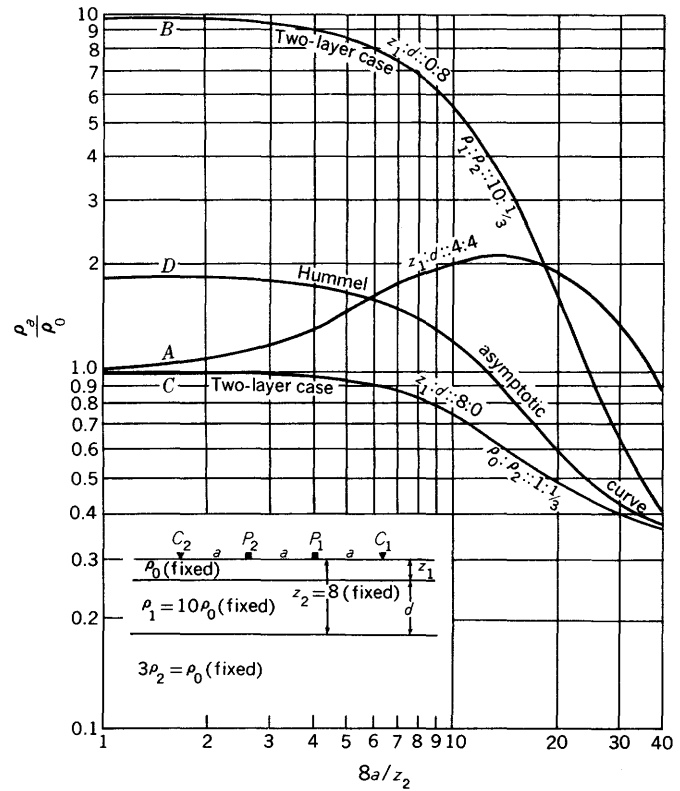
FIGURE 41.—Comparison of three-layer curve A with limiting two-layer curves B and C and Hummel asymptotic curve D (for the top layers only), Wenner or Lee configuration. $\rho_0:\rho_1:\rho_2::1:10:1/3$; various values of $z_1:d$. Adapted from Wetzel and McMurry (1937).

the resistivity of the middle layer is greater than that of either the top or bottommost layers, and the resistivity of the bottommost layer is least of all three. Asymptotic curve D is for the two-layer case in which the resistivities of the upper-two layers have been averaged according to Hummel's (1929 c, d) method. Curve A approaches this asymptotic curve for much larger electrode separations than shown in the figure. Within the region of the chart shown, however, this asymptotic value cannot be used as a guide in the analysis of curve A. In this example the logarithmic two-layer curves, therefore, cannot be used to obtain even approximately the depth z_2 to the bottommost layer. An attempt to do so in this example would involve a 400-percent error in the determination of depth z_2.

The mathematical expression for the apparent resistivity of the three-layer case reduces continuously to the expression for the two-layer case if either z_1 or d is allowed to approach zero. Applying this to our present example in figure 41, curve B is obtained when z_1 approaches zero, and curve C is obtained when d approaches zero. It should be emphasized that the apparent-resistivity curves B and C for the limiting two-layer cases are *not* envelopes for the families of three-layer curves similar to curve A, as might normally

be expected. In addition, it is possible for members of these multiple-layer resistivity curve families to cross; this fact makes the task of extrapolation of curve families difficult.

Figure 42 shows an example of the interpretation of a three-layer case by superposition of the logarithmic theoretical (solid lines) and hypothetical observed (dashed line) curves (Wetzel and McMurry, 1937). The family of theoretical curves are for fixed resistivities $\rho_0:\rho_1:\rho_2::1:3:10$ and for various values of $z_1:d$. The "resistivity index" line, which is defined as the axis of abscissas on the theoretical chart for which $\rho_a/\rho_0=1$, is extended to the left to intersect the ordinate value of ρ_a on the observed logarithmic chart; this gives the value of ρ_0, which in the present example is 33 ohm-centimeters. The fact that the observed curve matches a theoretical curve in this family, whose theoretical ratio is $\rho_0:\rho_1:\rho_2::1:3:10$ indicates that the field resistivity values are $\rho_0:\rho_1:\rho_2::33:99:330$. The "depth index" line, which is defined in the three-layer case as the electrode separation equal to the depth of the bottommost layer—that is, $a=z_2$—, corresponds in the Wetzel-McMurry charts with the abscissa point $8a/z_2=8$, and is found on the diagram to be $z_2=330$ feet. Finally the $z_1:d$ ratio is read by noting that the field curve lies about halfway between the theoretical curves whose ratios are 2:2 and 1:3; therefore, the

$z_1:d$ ratio for the field curve corresponds to about 3:5. Using the relationship $z_2=z_1+d$ and knowing that $z_2=330$ feet, we readily obtain the thickness of the top layer $z_1=124$ feet. The problem is thus completely solved.

The members of the Schlumberger school have pointed out the advantages of logarithmic curve matching and themselves have used it as a standard procedure for many years for both two- and three-layer problems. During 1933 to 1936 the Schlumberger organization in Paris, la Compagnie Générale de Géophysique, computed an album of 480 master curves for two- and three-layer cases that were recently published (Compagnie Générale de Géophysique, 1955). Figure 43 shows the values of the parameters used in the Schlumberger album and the generalized character of the apparent-resistivity curves in each category with the Schlumberger configuration. The resistivity ρ_2 of the bottommost layer is assumed to have only four separate values, namely, $\rho_2=0$, ρ_0, ρ_1^2/ρ_0, and ∞.

An example of one of the families of two- and three-layer curves for the Schlumberger configuration is shown in figure 44. The curves are plotted on logarithmic paper whose cycle is identical to that used for the field curves. For all curves the resistivities of the top, middle, and bottommost layers are, respectively, ρ_0; $\rho_1=\rho_0/39$; and $\rho_2=\infty$. The only differences in the
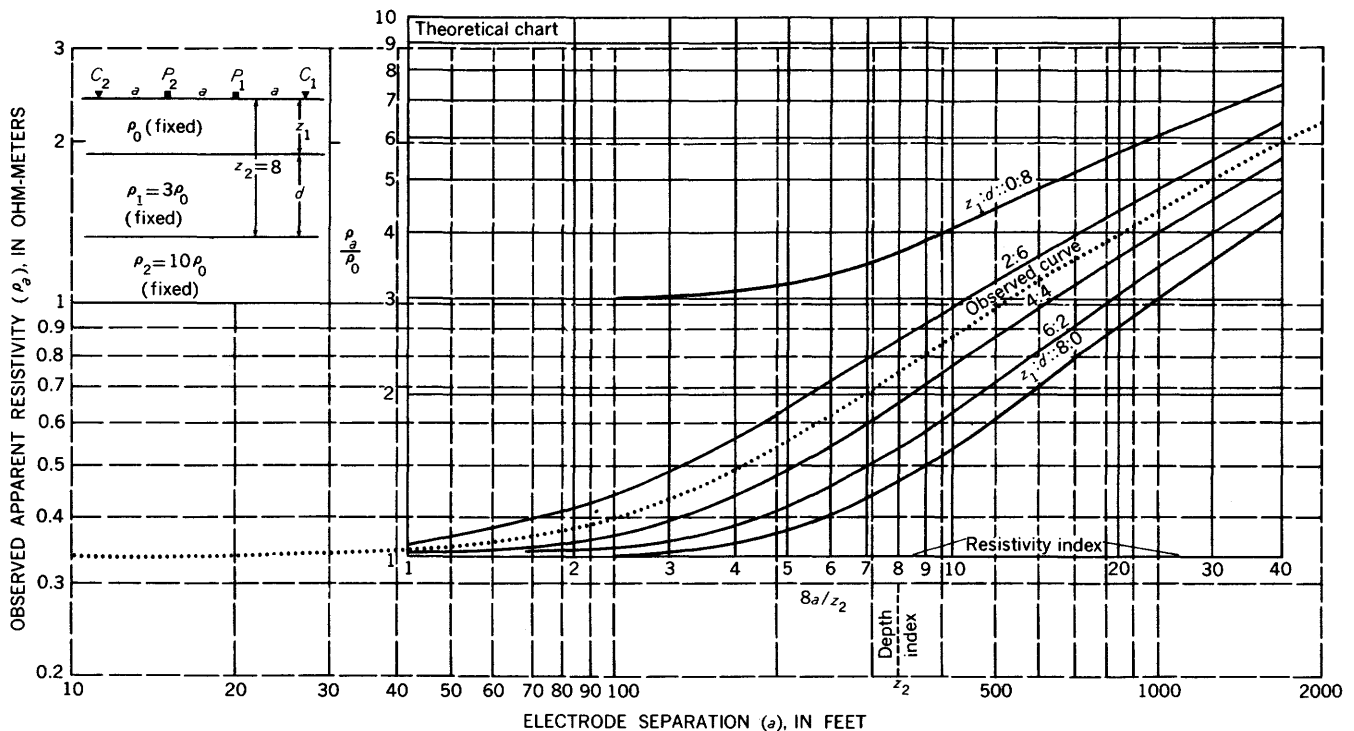
FIGURE 42.—Example of interpretation of three-layer case by superposition of logarithmic theoretical (solid lines) and hypothetical observed (dashed line) curves, Wenner or Lee configuration. $\rho_0:\rho_1:\rho_2::1:3:10$; various values of $z_1:d$; $z_2=8$ units (depth index). Adapted from Wetzel and McMurry (1937).

$\dfrac{AB}{2}$ — $\dfrac{AB}{2}$ — $\dfrac{MN}{AB} = \dfrac{1}{5}$

SURFACE B N ΔV O M A

ρ_0 z_1

ρ_1 d z_2

ρ_2

$\rho_2 =$	0	ρ_0	$\rho_1^?/\rho_0$	∞
$\rho_1 > \rho_0$				
$\rho_1 < \rho_0$				

$\dfrac{\rho_1}{\rho_0} = \dfrac{1}{39}, \dfrac{1}{19}, \dfrac{1}{9}, \dfrac{1}{4}, \dfrac{3}{7}, \dfrac{2}{3}, \dfrac{3}{2}, \dfrac{7}{3}, 4, 9, 19, 39$

$\dfrac{z_2 - z_1}{z_1} = 0^*, \dfrac{1}{9}, \dfrac{1}{5}, \dfrac{1}{3}, \dfrac{1}{2}, 1, 2, 3, 5, 9, 24, \infty^\star$

*Two-layer case: $z_1 = z_2 : d = 0$ ★ Two-layer case: $z_2 \gg z_1$

$\rho_{\text{TOP LAYER}}/\rho_{\text{BOTTOM LAYER}} = \rho_0/\rho_2$

LOG OF APPARENT RESISTIVITY (ρ_a)

LOG ($AB/2$)
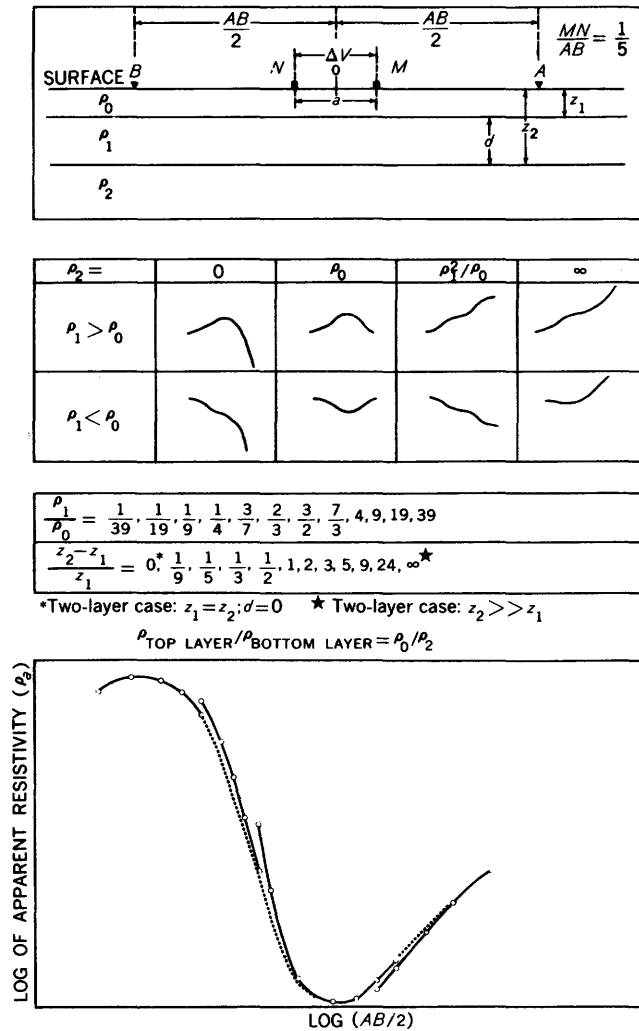
FIGURE 43.—Diagram showing values of parameters used in the Schlumberger album of 480 master two- and three-layer curves and the generalized character of the apparent-resistivity curves in each category for vertical profiles, Schlumberger configuration. Adapted from Compagnie Générale de Géophysique (1955).

curves are in the thicknesses of the layers. The two limiting curves are for the limiting two-layer cases. The apparent resistivity is plotted against $AB/2$, where AB is the distance between the current electrodes. The depth index is z_1, the thickness of the top layer. The $10z_1$ mark is included to indicate the dimensions of the logarithmic cycle used. The resistivity index is the horizontal line, which represents the value of ρ_0. The theoretical curves are matched with the logarithmically plotted observed field values for the Schlumberger configuration in a manner similar to that discussed previously for the Wenner and Lee configurations.

As pointed out on page 40, the French school—contrary to the Wenner procedure—has always chosen to take a vertical profile by increasing either the distance between the current electrodes or that between the potential electrodes, but only *one set at a time* between successive measurements. In order not to introduce the ratio between these two distances as an extra variable, all the calculations are made for an infinitely small value of the distance between the potential electrodes. If the ratio of the distance between the potential electrodes to that between the current electrodes does not exceed 1/5, it is sufficient to shift the points of the field curve in the negative direction of the distance axis (in the vertical profile) by an amount equivalent to a reduction of the distance by 0 to 6 percent depending on the case (Compagnie General de Geophysique, 1955, p. 1).

The principal advantage of this technique is that the influence of local inhomogeneities close to the potential electrodes can be clearly located on the apparent-resistivity curves. A schematic representation of this idea is shown in figure 45 (after Chastenet de Géry and Kunetz, 1956). The top diagram (fig. 45) contains three segments of curves, each of which represents data taken with one of three different values of the distance $\overline{MN}$ between the potential electrodes. Because a local inhomogeneity existed near one or both of the potential electrodes when $\overline{MN}$ had the second value used, segment B of the curve is displaced upward from the other two. Obviously, it is easy to connect segments A and C correctly by moving segment B downward to its correct position. The middle diagram (fig. 45) shows, for example, what might have been obtained with the Wenner configuration as it is normally used. The effect of the local inhomogeneity cannot be differentiated from the effects of deep horizontal discontinuities on the smooth Wenner curve.

The four-layer case comprises a top layer of thickness z_1 and resistivity ρ_0 and two successively deeper layers of respective thickness d_1 and d_2 whose bottoms lie at successive depths of z_2 and z_3, respectively, below the earth's surface (fig. 46). The bottommost layer, at depth z_3, is assumed to extend to great depth.

At the outstart, we repeat our contention that, except for ideal and very rare field problems, lateral variations interfere too much for the four-layer case analysis to be applied with much degree of certainty. In addition, there is a lack of uniqueness—from the practical point of view—in the four-layer case. Although we realize that much more time and experience must be had with the application of the four-layer curves to prove this statement conclusively, we will now show the characteristics of the four-layer case that lead us to this contention. In doing this, we will use some four-layer curves taken from the album of four-layer curves by Mooney and Wetzel (1956), which is the most comprehensive work of its type ever published for the resistivity method. This album is of great help in showing curve
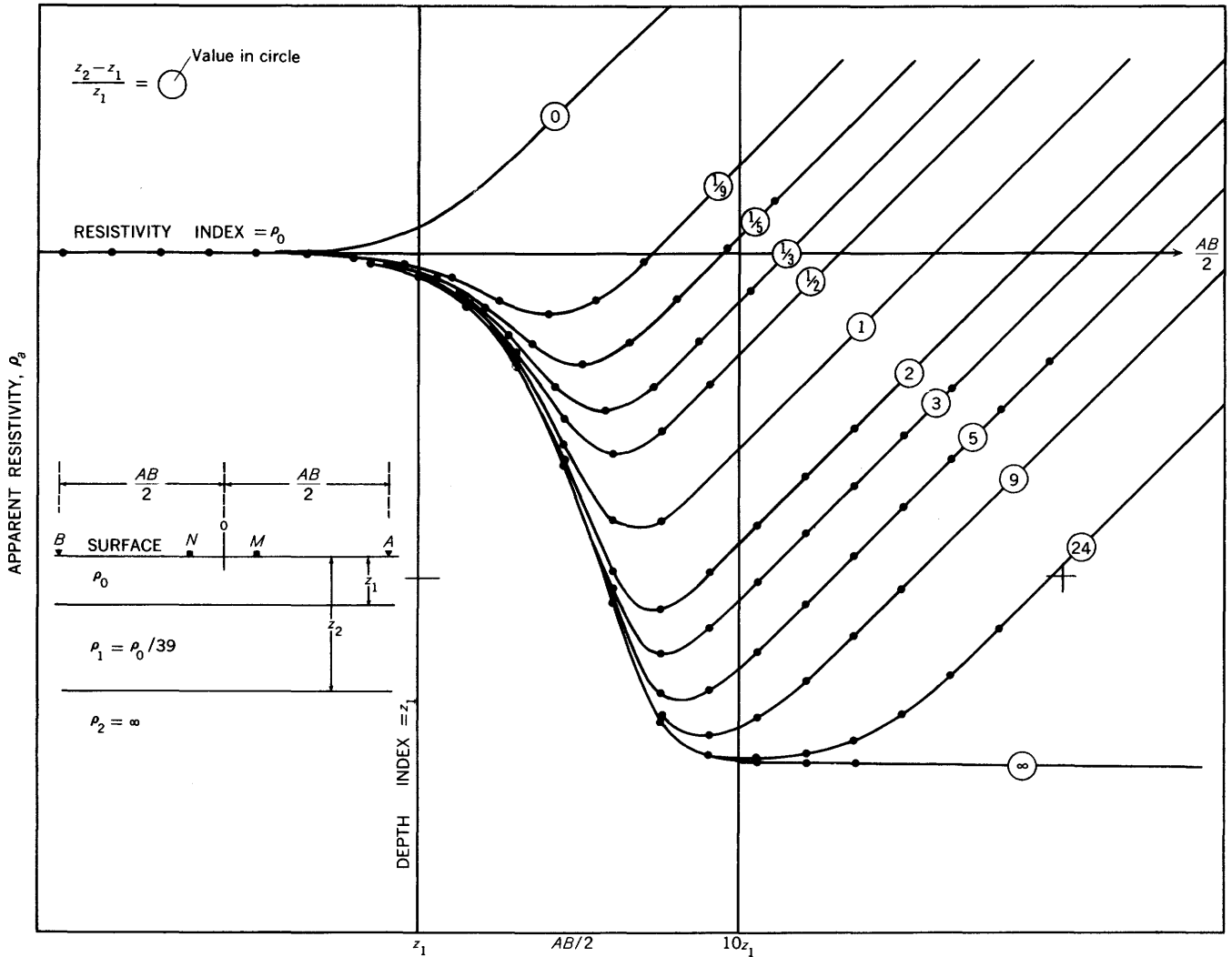
FIGURE 44.—Family of apparent-resistivity curves for two- and three-layer cases, Schlumberger configuration. Adapted from Compagnie Générale de Géophysique (1955).

trends that would be expected in ideal four-layer problems.

Figure 47 shows the large expansions of configuration necessary to distinguish three-layer curves (B, C, D, and F) from four-layer curves (A, E, and G; all curves from Mooney and Wetzel, 1956). In the example shown, the resistivities of the top two layers for the three-layer case are identical to those of the four-layer case (that is, $\rho_1 = 100 \ \rho_0$); the thickness z_1 of the top layer is the same in both cases; and z_2 for the three-layer case is made equal to z_3 for the four-layer case; in the four-layer case, the thickness of the third layer is one unit. As the configuration is expanded, there is essentially no resolution between the apparent-resistivity curves up to an electrode separation $a = 5z_3/3$; and the distinction between the curves is not marked until $a = 10z_3/3$ which corresponds to a distance equal to 3 1/3 times the depth z_3 to the bottommost layer.

Even at these large electrode separations the three-layer curves D and F are similar to the four-layer curve E and, considering "noise" effects of about 10 percent, would be difficult to distinguish with confidence in the field data. Many other examples of similarity between three- and four-layer curves can be cited from a study of the curves given by Mooney and Wetzel (1956). Still more similarities would be seen if additional thickness ratios and resistivity ratios had been taken. Consequently there is a nonuniqueness in the resistivity data that manifests itself strongly within the relatively small range of electrode separations that are practical in resistivity prospecting. Even though theoretically the curves would differ if the electrode separations are expanded far enough, there is a practical limit to this expansion in actual field work; and it is herein that the usefulness of the four-layer analysis is seriously limited.
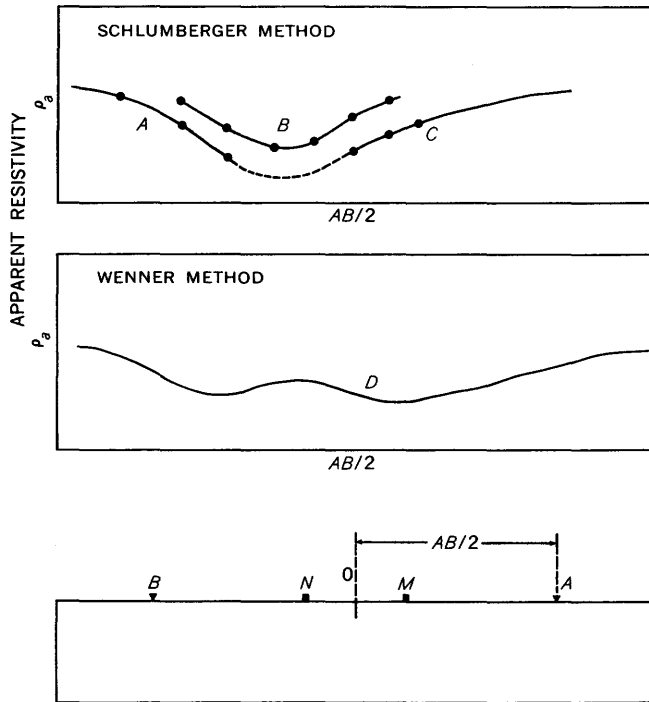
FIGURE 45.—Qualitative effect of inhomogeneity on apparent-resistivity curves. A, B, and C are segments of the Schlumberger curve; D is the Wenner curve. Adapted from Chastenet de Géry and Kunetz (1956).
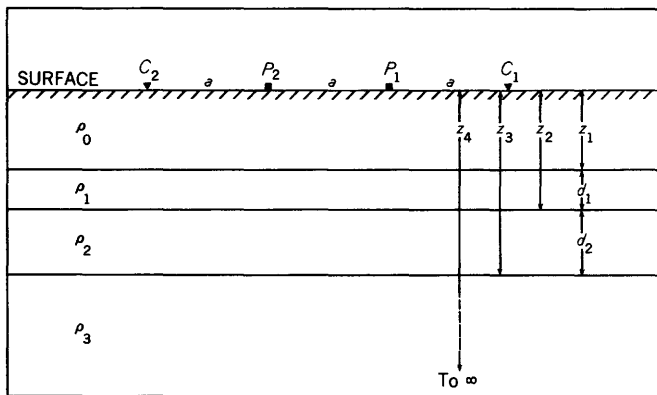
FIGURE 46.—Diagram of geologic cross section of four-layer case showing convention of symbols used.

Quite apart from minor "noise" effects due to minor local departures from homogeneity of any of the four layers—which would make difficult the distinction between curves D and E in figure 47, for example—are the more important lateral effects that often occur in the geologic section when the configuration is expanded to larger separations. These ordinarily amount to more than 10 percent; and they can therefore cause the observed apparent-resistivity curve to vary in such a direction and amount that a four-layer case might be suspected in an actual three-layer field problem. The departures caused by these major lateral effects in

some areas can be so large as to vitiate the effectiveness of a two- or three-layer analysis, let alone a four-layer analysis. There are field techniques available to detect these truly lateral effects—see, for example, the discussion of the technique for the Schlumberger configuration, page 40—and allowances can be made for them; but they impose on the field data a serious limitation for accurate depth estimates in multiple-layer cases.

PRACTICAL APPLICATIONS

In depth determination of "horizontal" layers, it is important to ascertain that the layering is indeed horizontal rather than dipping, and that major lateral effects are absent. This can be accomplished by taking two or more separate vertical profiles in different azimuths. The Lee partitioning method is particularily suited for this purpose, and is recommended by us. For this purpose some investigators, notably Spicer (1952 and 1955), use the Lee configuration and plot not only the regular Lee ρ_1 and ρ_2 values, but also the Wenner values as measured by computing the apparent resistivities from potential differences between the outer potential electrodes P_1 and P_2.

EMPIRICAL METHODS

Although their results cannot be explained on the basis of present theory assuming Laplace's equation, the empirical methods have long been used. The fact that testing has often borne out the correctness of the predictions based on empirical methods has established the method in the geophysical industry, and it is still in use today.

Figure 48 shows the observed vertical resistivity profiles for the determination of the depth to salt water with the Lee configuration at Kahului Fair Grounds, island of Maui, Hawaiian Islands (Swartz, 1940b). Here the lens of fresh water is buoyed up by the underlying salt water. On the basis of the characteristic downbreak at A (fig. 48) occurring at an electrode separation of 140 feet, it was predicted by Swartz prior to drilling that salt water would be encountered at a depth of 140 feet. The top of the salt water of approximate sea-water salinity was found at a depth of 141 feet, which was in surprisingly good accord with the predicted depth. The transition zone between fresh water and salt water occurred in the well over a vertical distance of only 22 feet, and Swartz attributes the success of the method in this area to this rather abrupt transition in resistivities. The possible causes of peaks B', C, and C' (fig. 48) were not discussed by Swartz. Because peak A' on the ρ_2 curve occurs at a value of the electrode separation (150 feet) that is exactly three times the value of the electrode separation (50 feet) at which peak B' occurs on the same
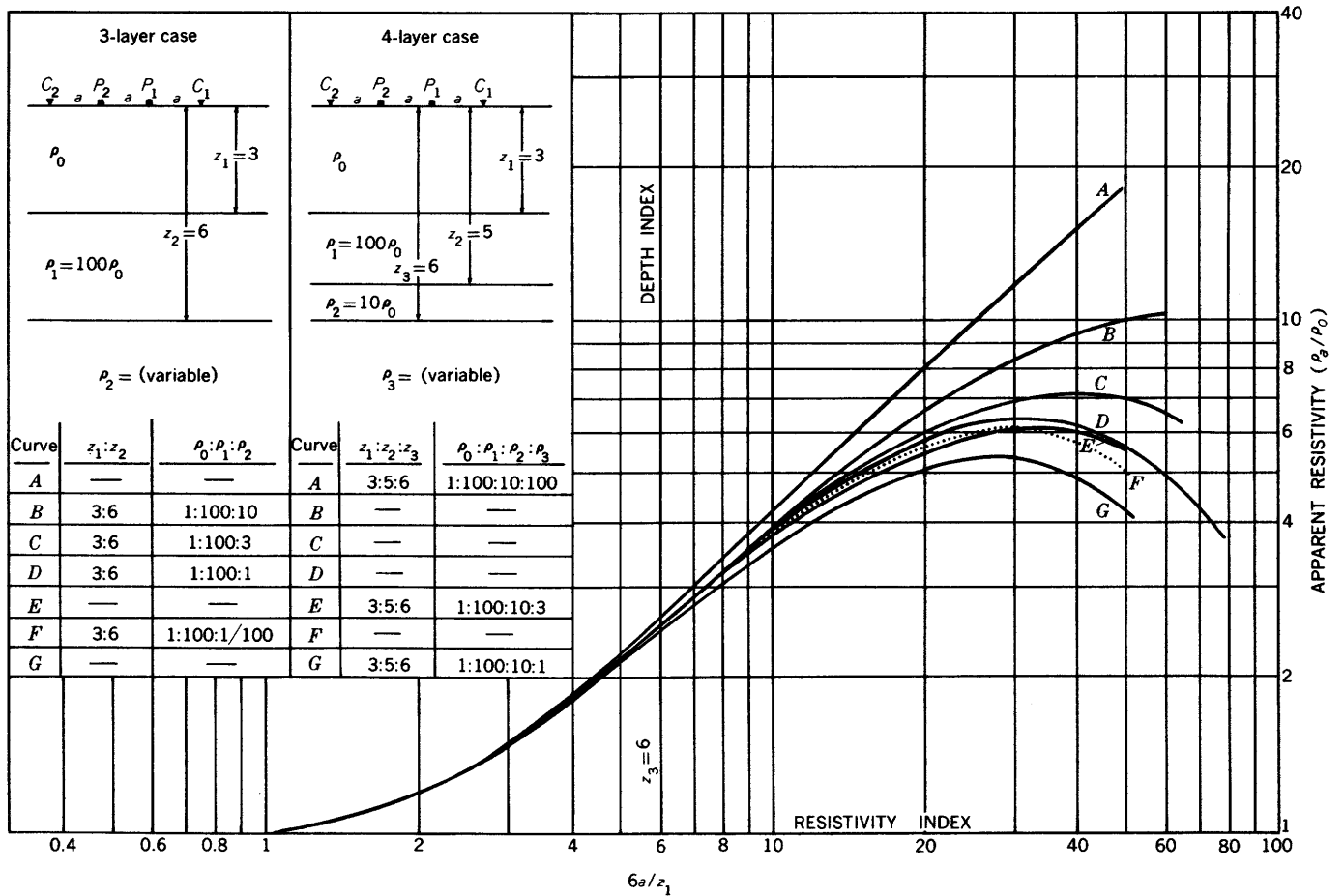
FIGURE 47.—Diagram showing large expansions of configuration necessary to distinguish three-layer apparent-resistivity curves (B, C, D, and F) from four-layer curves (A, E, and G), Wenner or Lee configuration. Note similarity of some three-layer curves (D and F) to four-layer curve E. Curves from Mooney and Wetzel (1956), "Potentials about a point electrode and apparent-resistivity curves for a two-, three-, and four-layer earth," by permission of Univ. Minnesota Press. Copyright 1956 by University of Minnesota.
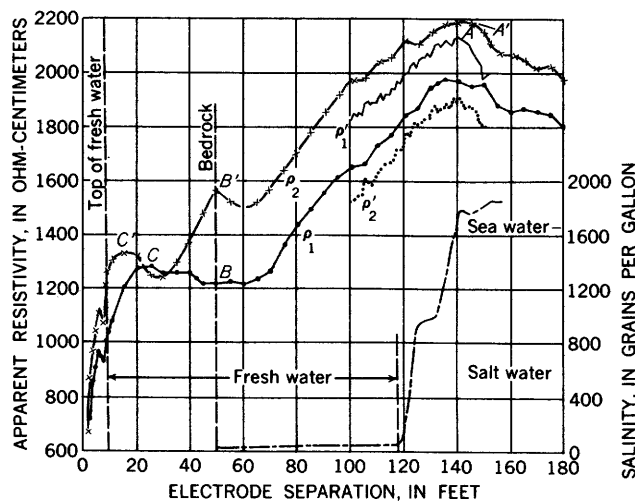
FIGURE 48.—Observed vertical resistivity profiles for determination of depth to salt water, Lee configuration, Kahului Fair Grounds, Maui, Hawaiian Islands. Interpretation by empirical method. Adapted from Swartz, (1940b).

curve, the logical question arises as to whether peak B' could occur as the current electrode crossed a truly lateral feature, and peak A' could occur as the potential electrode crossed the same feature. It can be observed from theoretical curves in plates 3, and 4, and figure 157 that truly lateral effects of this type would have caused the ρ_1 curve to have a peak at B also; such a peak was not observed, although data were carefully taken at small intervals. Therefore, the maxima in the four apparent-resistivity curves in the vicinity of A (fig. 48) are regarded by us as not caused by truly lateral effects, and are probably some unexplained manifestation of the salt water at depth.

On the island of Lanai, where similar salt-water problems occur, Swartz (1940b) obtained apparent-resistivity curves with characteristics like those of figure 48; and his depth predictions, which were based on the empirical method, were verified later by testing.

By using an analysis similar to the above, the geophysicists using empirical methods today will probably find it helpful to review their observed field curves with some of the theoretical curves of truly lateral effects given in this treatise. It is anticipated that some of the breaks on their curves can be attributed to truly lateral effects. Other significant breaks, especially if they accompany or define a major change in slope of the overall curve, if they cannot be explained by truly lateral effects or instrumental procedures, and if they do correlate with vertical resistivity contrasts, may be caused by effects not taken into account in our assumptions of the ohmic flow of current.

TAGG'S METHOD

Tagg's method employs a family of apparent-resistivity curves and apparent-conductivity curves for negative and positive reflection factors, respectively (see fig. 35). Tagg's method for depth determination for the two-layer case, utilizing these theoretical
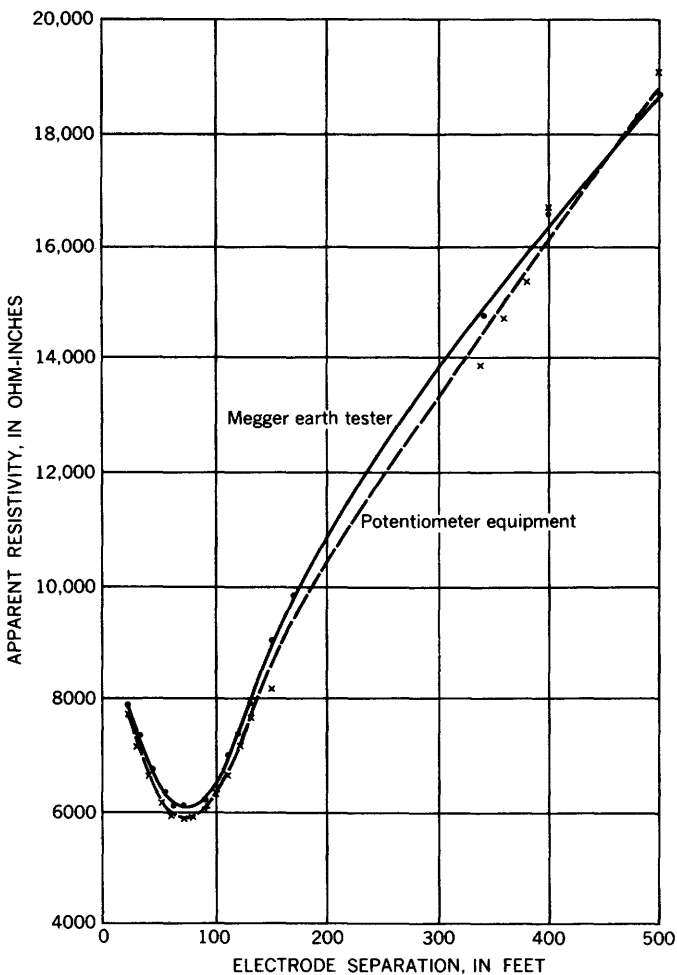
curves and the observed field curve (fig. 49, after Tagg, 1932) is as follows:

1. Apparent-resistivity measurements are taken for small, intermediate, and large electrode separations.
2. The apparent-resistivity measurements taken at small electrode separations are used first to determine as accurately as possible the true resistivity ρ_o (or conductivity σ_o) of the top layer. In the present example, the average value of ρ_o, based on the apparent-resistivity values up to electrode separations of 70 feet, was taken by Tagg as 6,703 ohm-inches.
3. Next, several apparent-resistivity values ρ_a (or apparent conductivity values σ_a, if k is positive) are selected for small, intermediate, and large electrode separations on the observed field curve. Using these values and the value of ρ_o (or σ_o) already obtained, the corresponding values of ρ_a/ρ_o (or σ_a/σ_o) are computed.
4. For each value of ρ_a/ρ_o (or σ_a/σ_o) and its accompanying value of a, a series of corresponding values of z_1/a for k intervals of 0.1 from -0.1 to -1.0 (or $+0.1$ to $+1.0$) are read off the curves in figure 35. Since the electrode separation a is known, the z_1/a values can be converted into a series of values of z_1. Thus for each value of the electrode separation, there is a series of corresponding values of z_1 and k. For our field example, the values for six electrode separations are listed in table 2. This table shows that for the value $k=0.7$ the depth values of z_1 remain practically constant, and that the value $z_1=142$ feet may be taken as the required depth to the high-resistive layer.
5. For each of the six separations used in the table, a plot of the k-versus-z_1 curve is made by reading these values from the table (see fig. 50, after Tagg, 1932). The six curves should theoretically intersect at a point, which then gives the unique solution of not only the thickness z_1 of the top layer, but also the reflection factor k. In the field example shown, the curves intersect at $z_1=142$ feet. The true depth in this case ranged from 145 feet to 150 feet. The most probable value of k is 0.702.
6. The true resistivity ρ_1 of the lower layer can then be calculated from the equation $\rho_1=\rho_0(1+k)/(1-k)$; in the example it is 38,280 ohm-inches.

When the logarithmic curve-matching method is used on this same field example, the resulting values are as follows: $k=0.7$; $\rho_0=6,720$ ohm-inches; $z_1=141$ feet; and $\rho_1=38,080$ ohm-inches (Roman, 1934, p. 193). These values are in excellent agreement with the values obtained by the Tagg method.

Theoretically, only two different electrode separations resulting in two intersecting curves are needed, if the true resistivity of the top layer has already been

TABLE 2.—*Tagg's method for determining values of* z_1 *and* k *for each electrode separation* a

[Data from Tagg (1932). Depth values (z_1) for $k=0.7$ show close agreement]

Electrode separation a (feet)	σ_a/σ_1	k=1		k=0.9		k=0.8		k=0.7		k=0.6	
		z_1/a	z_1	z_1/a	z_1	z_1/a	z_1	z_1/a	z_1	z_1/a	z_1
150	0.748	1.19	179	1.12	168	1.045	157	0.96	144	0.87	130.5
200	.625	.915	183	.850	170	.775	155	.700	140	.620	124
250	.544	.770	193	.705	176	.640	160	.565	141	.485	121
300	.483	.675	202	.610	183	.545	163	.478	143	.390	117
350	.441	.61	214	.545	191	.485	170	.41	144	.325	114
400	.407	.560	224	.500	200	.435	174	.36	144	.28	112

Electrode separation a (feet)	σ_a/σ_0	k=0.5		k=0.4		k=0.3		k=0.2		k=0.1	
		z_1/a	z_1	z_1/a	z_1	z_1/a	z_1	z_1/a	z_1	z_1/a	z_1
150	0.748	0.785	118	0.66	99	0.525	79	0.315	47		
200	.625	.525	105	.42	84	.26	52				
250	.544	.39	97.5	.27	67.5	.03	7.5				
300	.483	.295	74	.16	40						
350	.441	.226	78	.06	21						
400	.407	.17	68								

determined, and, of course, if the assumptions of the two layers are fulfilled and each layer is homogeneous and isotropic. In practice, several electrode separations (Tagg recommended at least three) are taken to ascertain that the assumed conditions essentially prevail, in which case the resulting triangle of error in the k-versus-z_1 plot is small and its center can be taken as the indicated depth z_1. If, on the other hand, the triangle of error is excessively large and the third (or more) k-versus-z_1 curve lies a great distance from the point of intersection of the first two similar curves, the structure being investigated is probably not of the simple two-layer type with the given assumptions, and the method is inapplicable.

To determine the thickness of the top layer only, it is not necessary to determine the resistivity of the top layer, provided auxiliary sets of special Tagg curves are available and provided that the values of the electrode separations (na) are taken at simple multiples or submultiples of a given electrode separation a. The reasoning used in this approach results from the property of the ratio of ρ_a/ρ_{na}, where ρ_a is the observed apparent resistivity at electrode separation a and ρ_{na} is the apparent resistivity at electrode separation na. It can be shown that

$$\frac{\rho_a}{\rho_{na}} = \frac{\sigma_{na}}{\sigma_a} = \frac{1+4F(a)}{1+4F(na)}$$

where $F(a)$ and $F(na)$ are functions of z_1/a and z_1/na, respectively, as well as of the reflection factor k. For any value of n—which is usually taken as 1.5, 2.0, 2.5, and 3.0—the values of ρ_{na}/ρ_a or σ_{na}/σ_a are calculated for any values of z_1/a and k; and sets of special master curves are plotted on linear scales in this way for both positive and negative reflection factors. For any single given value of n, a family of 10 curves is desirable for either positive or negative reflection factors by taking k at intervals of 0.1.

As an example, the ratio of the observed apparent resistivities ρ_{2a}/ρ_a for electrode separations $2a$ and a, respectively, is first calculated. Since in this case $n=2$, the set of auxiliary master curves for $n=2$ and, say, negative reflection factors, are used to obtain a series of corresponding values of z_1/a and k from inspection of the curves. Since a is known, these values are next
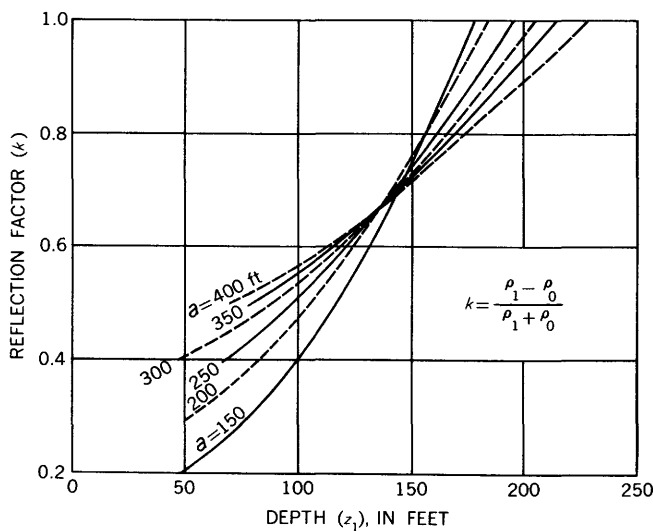
FIGURE 50.—Plots of reflection factor *k* versus depth z_1 for different electrode separations *a*, Tagg method of interpretation. Adapted from Tagg (1932). Copyright by Am. Inst. Mining Metall. Engineers.

converted into a series of corresponding values of z_1 and k. By taking other pairs of values of electrode separation, further sets of corresponding values of z_1 and k can be obtained. Just as for figure 50, these z_1-versus-k curves should theoretically intersect at a point to give the true values of z_1 and k. Thus the thickness z_1 of the top layer is determined without determining the resistivity of the top layer.

Tagg's method can also be adapted to solve the three-layer case by using either the technique in which the resistivity of the top layer is determined or the same techniques described in the previous paragraph. In either case, care must be taken not to choose electrode intervals close to the maximum or minimum of the three-layer apparent-resistivity curves, because at these points the observed field curves have a large departure from the theoretical curves.

COMPARISON OF THE LOGARITHMIC CURVE-MATCHING METHOD AND TAGG'S METHOD

From the standpoint of speed of application, the logarithmic curve-matching method apparently has a great advantage. For either method, at least one observed vertical resistivity profile and the theoretical curves or the underlying tables are needed. Although with Tagg's method it is theoretically possible, after taking a sufficiently large number of readings to obtain the resistivity of the top layer, to solve the problem completely by taking measurements for only *two* large electrode separations (Tagg recommended *three* to have one serve as a check on the other two), a *complete* observed profile for the Tagg method is desirable to show that a fit is possible. In either case, the conclusion should be checked by starting with the determined constants and calculating the theoretical values for the apparent resistivity from the tables or formulas. Without this check, the method of Tagg may lead to an interpretation without much foundation. The logarithmic method is more likely to eliminate poor interpretation.

For the true resistivity of the top layer, which is a key to each method—unless the more cumbersome method of using the auxiliary Tagg curves is used—Tagg's method assumes a value determined from small electrode separations and the conclusions are based on the value assumed. In the logarithmic method this resistivity is determined directly from the entire curve and hence may be a good starting point for the method of Tagg.

Each method will theoretically yield unique values of ρ_0, ρ_1, and z_1, if the ground conditions conform essentially to the assumption of two horizontal homogeneous layers. With the Tagg method the depth and reflection factor are determined by the common intersection of several curves; and, if the above assumption of ho-

mogeneous layers is not fulfilled—which is often true—this intersection is not well defined, because the common point spreads out, as into a triangle of error. A different value for the resistivity of the top layer may lead to a much better intersection, but this alone is not a valuable criterion. With the logarithmic method, under like conditions, there is often much choice in the fitting of the curves; and in such a case, a unique solution requires further knowledge. Apparently, the method of Tagg determines the reflection factor and the thickness of the top layer as accurately as the graph can be read; but this accuracy is only apparent, as a slight change in the assumed resistivity of the top layer may shift the intersection of the Tagg curves as much as the apparent indefiniteness of the matching in the logarithmic method (Roman, 1934).

Reliability is not assured, because both methods can lead to incorrect results if the assumption of the homogeneous two-layer case is not fulfilled. If the two methods can be made to furnish the same conclusion, it is likely that these conclusions will be useful as a geophysical interpretation. However, these methods, like most others, have an inherent ambiguity of interpretation unless there is a sufficient amount of geologic control, because of the possibility of anisotropic media giving the same observed resistivity profile. In general, the logarithmic method will eliminate impossible cases better than the Tagg method, but in both methods the results should be considered as an indicator rather than a fact.

If more than two layers are present, an intersection point of the curves is usually not found with the Tagg method, and thus not even an approximate depth may be obtained without selecting special parts of the curve for analysis. The logarithmic method is, in that respect, preferable, as it often permits a quick determination of the first interface even if a third layer is present at some greater depth; and it helps to point quickly to the possibility that a third layer is indeed present. Of course, if three layers are suspected, the Tagg method can be revised to allow for this possibility.

Several field examples are available in the literature in which comparisons of the logarithmic curve-matching and Tagg techniques are made for the two-layer case (see, for example, Roman, 1934). In those examples in which a clear-cut two-layer case exists, the results of the determinations of the various parameters with the two techniques usually agree with each other within a degree of accuracy that is sufficient for most fieldwork.

EXTENSION OF TWO-LAYER LOGARITHMIC CURVES TO THREE- AND FOUR-LAYER PROBLEMS

Two-layer logarithmic curves can often be used to solve three-layer problems approximately. This "principle of extension" (Watson and Johnson, 1938) is

predicated upon the fact that in problems involving more than two layers, for electrode separations large in comparison with the thickness of these two layers, the top two layers can be combined to give a composite resistivity (Hummel, 1929 c, d). Consequently for large electrode separations, the two top layers are considered as one layer, and the three-layer problem then reduces to a two-layer problem. Then the object is to find the depth z_2 of the two top layers taken together. For large electrode separations, the application of logarithmic curve-matching will give the values of z_2, the composite resistivity ρ_0' of the two top layers, and k'. But since $k' = (\rho_2 - \rho_0')/(\rho_2 + \rho_0')$, therefore, ρ_2 also can be determined.

Figure 51 shows an example of the use of logarithmic two-layer curves to solve a three-layer problem approximately (Watson and Johnson, 1938). In the upper diagram (fig. 51), the values of ρ_0, z_1, and $k = (\rho_1 - \rho_0)/(\rho_1 + \rho_0)$ are determined; and in the middle diagram (fig. 51) the values of z_2, ρ_0', and k' are determined.

Theoretically, according to the Hummel's principle of extension, the depth z_2 to the bottommost bed in the three-layer case can be determined from the logarithmic two-layer curves, provided the configuration is expanded far enough. This is not so, however, for the determination of the thickness z_1 in the three-layer case as the accuracy of the approximation obtained with the two-layer logarithmic curves depends on how near and how effective is the bottom layer. Studies by Watson and Johnson (1938) show that when the thickness of the top and middle layers (in the three-layer case) are equal or nearly equal to each other, the influence of the resistivity of the bottommost bed becomes so large even for small electrode separations that a good interpretation is not likely; in this unfavorable case, however, the interpretation is most favorable when the middle layer is either highly conductive or highly resistive in comparison with the top layer. When the thickness of the middle layer is less than that of the top layer, the chance for a good determination of the thickness of the top layer is even poorer. As the thickness of the middle layer increases compared to that of the top layer, the possibilities of a good determination increase; so that when the thickness of the middle layer is three or four times that of the top layer, a good two-layer approximation can be made, especially if ρ_1 is very much larger than ρ_0. However, the advantage gained in the determination of the thickness of the top layer due to a large resistivity ratio ρ_1/ρ_0 is offset by the larger electrode separations necessary for a correspondingly good interpretation of the depth to the bottommost layer.

In the determination of the depth to the bottommost layer, the accuracy of the two-layer approximation is greatly enhanced when the middle layer is the best conductor of the three layers involved. Even when the resistivity ratio ρ_0/ρ_1 is large, the accuracy of the two-layer approximation is good. When the middle layer is the better resistor of the two upper beds, however, very large expansions of the configuration are required to obtain the depth to the bottommost layer; and there are, therefore, practical and economic limitations to the expansions before lateral changes and topographic conditions vitiate the accuracy.

To summarize how logarithmic three-layer curves can be approximated by logarithmic two-layer curves, we note that a rule with few exceptions is that three-layer curves containing a minimum may be approximated by two-layer solutions with fair accuracy (Wetzel and McMurry, 1937, p. 335). For three-layer curves containing a maximum, the thickness of the top layer can usually be approximated by logarithmic two-layer curves, but the depth to the bottommost layer cannot generally be so approximated within feasible electrode separations. This, of course, applies to analytical as well as graphical approximations. It is important that an accurate value of the resistivity ρ_0 of the top layer be obtained and that the electrode configuration be expanded to as large values as is feasible.

Because the resistivity of rocks increases with depth in most areas due to the increasing compaction and decreasing porosity, the bottommost of the three layers is generally of higher resistivity than either of the two overlying layers, and a maximum in the apparent-resistivity curves is not obtained generally. Consequently the two-layer approximations using logarithmic theoretical curves can be made for most three-layer problems with the required accuracy. When the middle layer is of higher resistivity than either the top or bottommost layers and a maximum in the apparent resistivity curve is obtained, the logarithmic three-layer curves should usually be used to obtain the depth of the bottommost layer, but the two-layer approximation using logarithmic theoretical curves can generally be used with the required accuracy to obtain the thickness of the top layer. For all such two-layer approximations to three-layer cases, we strongly recommend the logarithmic plotting method rather than the various linear "successive approximations" methods suggested by Hummel (1929 c, d), Pirson (1934), Tagg (1935), and others.

DIRECT INTERPRETATION

The bulk of this treatise has been devoted to the development of characteristics of resistivity anomalies
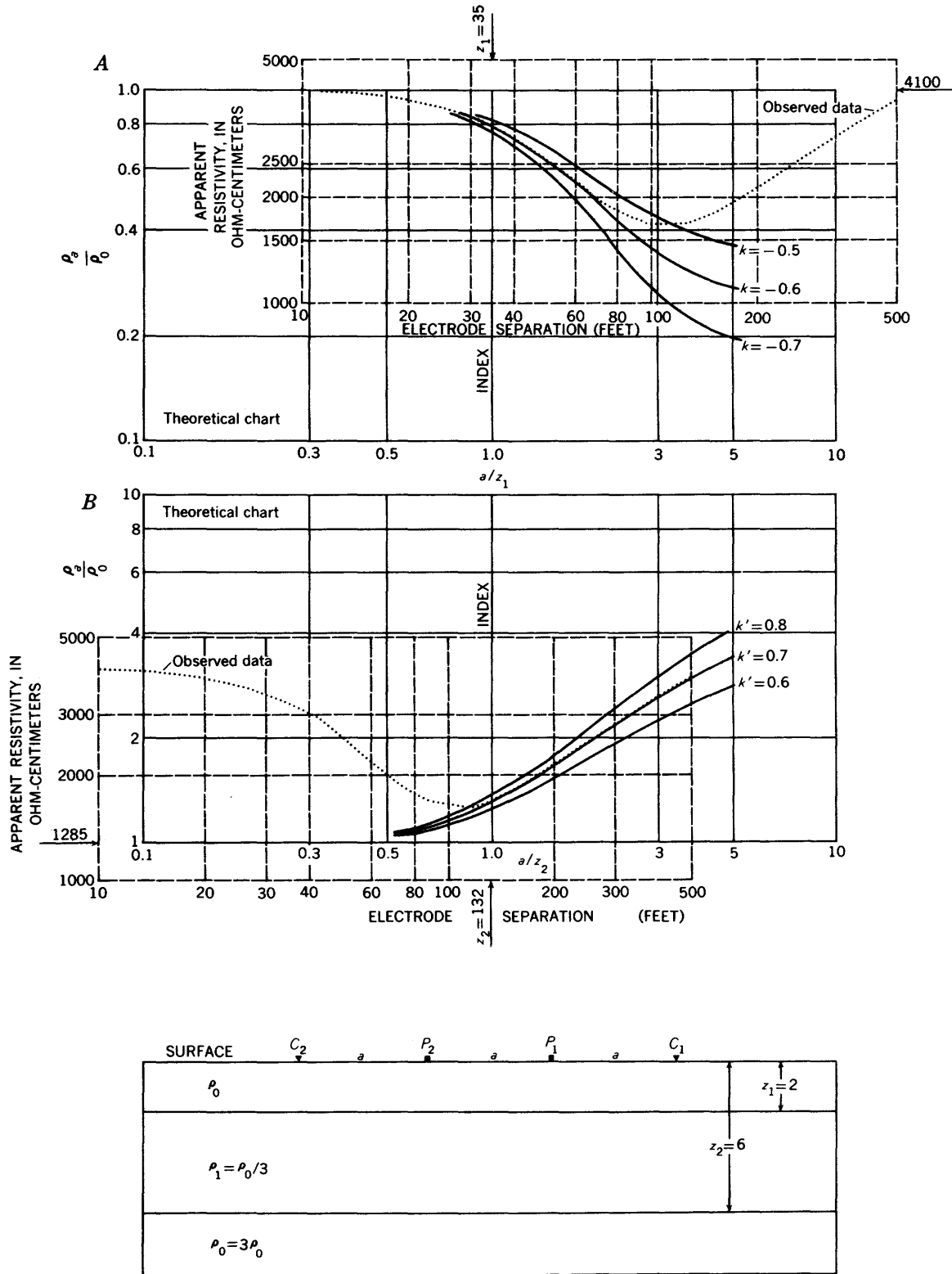
FIGURE 51.—Example of using logarithmic two-layer curves to solve a three-layer problem approximately, Wenner or Lee configuration. $z_1=2$; $z_2=6$; $\rho_0:\rho_1:\rho_2::1:1/3:3$.
Adapted from Watson and Johnson (1938).

which are recognizable in the field and which therefore assist in the interpretation of the results of a resistivity survey. To this point our approach has taken the form of trying to compare vertical profiles which are prepared from field data with families of type curves which are prepared ahead of the field work. In many instances one of the theoretical curves exactly fits the field curve and thus indicates uniquely the structure of near-surface part of the earth. In many of the other examples in this treatise, however, the theoretical curves are meaningful only insofar as the characteristic features of the curves can be used qualitatively to indicate the geological structures which give rise to the corresponding field curves.

By "direct interpretation" we mean a method in which the measured potentials or measured apparent resistivities are used in some mathematical process to determine directly the actual resistivity of the earth as a function of depth. The method to be described here is applicable only to horizontal-bedding problems. It is conceivable that an analogous technique could be developed for any resistivity distribution, but apparently no one has solved this problem. It should be emphasized that direct-interpretation techniques require a tremendous amount of computation time; and they will therefore probably be used only on occasional problems that require a great deal of attention or on surveys for which enough field data must be processed to make machine computations reasonable.

We commence our solution by assuming a single-current electrode on the surface of an earth in which the resistivity varies with depth. Temporarily we remain less precise than in previous sections about how the resistivity varies with depth. Moreover, we use the conductivity, $\sigma(z) = 1/\rho(z)$, for simplicity in the equations. The z in parentheses indicates merely that the conductivity is a function of depth. The cylindrical coordinate system is identical with that shown in figure 28; the positive polar axis ($+z$) is vertically downward.

As always, we assume the applicability of Laplace's equation. However, in the present section we must examine the origin of that assumption. All our work is in essence based on the divergence theorem, which states that the divergence of the electric field vanishes in regions where there are no charges, or—in this case—where there are no positive or negative electrodes. The electric field is defined as $-\sigma \nabla U$ so that the divergence theorem can be written as

$$\nabla \cdot \sigma(z) \nabla U = \nabla \sigma(z) \cdot \nabla U + \sigma(z) \nabla^2 U = 0. \quad (161)$$

This is the equation that must be solved in all electrical prospecting problems. However, whenever $\sigma(z)$ is constant, as is usually assumed in all discrete regions, equation 161 reduces to Laplace's equation, which we

have used. In the present problem, we specify that the conductivity varies with depth only. Therefore, we can simplify the first term of equation 161 so that the equation to be solved becomes

$$\sigma(z) \nabla^2 U + \frac{d\sigma(z)}{dz} \frac{\partial U}{\partial z} = 0.$$

In cylindrical coordinates, we can write

$$\sigma(z) \left[\frac{1}{r} \frac{\partial}{\partial r} \left(r \frac{\partial U}{\partial r} \right) + \frac{1}{r^2} \frac{\partial^2 U}{\partial \phi^2} + \frac{\partial^2 U}{\partial z^2} \right] + \frac{\partial \sigma(z)}{\partial z} \frac{\partial U}{\partial z} = 0. \quad (162)$$

This equation is to be compared with equation 64. Since we have done nothing to alter the terms containing the variable r, we may assume that the solution in the present problem has the same dependence upon r as the solution in the previous problem. We also note that symmetry requires that the solution be independent of the angle ϕ. Therefore, we assume a solution in the form of

$$U = \int_0^\infty Z(\lambda, z) J_0(\lambda r) d\lambda. \quad (163)$$

When we substitute this form of the solution into equation 162 and also take into account the fact that $J_0(\lambda r)$ satisfies Bessel's equation (equation 68), we find that

$$\frac{d}{dz} \left[\sigma(z) \frac{dZ}{dz} \right] - \lambda^2 \sigma(z) Z = 0. \quad (164)$$

The solutions of this equation have been examined in some detail (Morse and Feshbach, 1953, p. 725–726); and Slichter (1933) gave solutions of it for several problems of academic interest only, in which the resistivity varies in various continuous ways with depth. Our consideration here is restricted to the more practical problems in which the resistivity is a step-function of depth. Our approach is similar to that of Pekeris (1940) in that the conductivity $\sigma(z)$ is constant within any given medium. Thus, our consideration is restricted to those solutions of equation 164 after $\sigma(z)$ had been factored out. Equation 164 then reduces to equation 66, the solutions of which have previously been discussed in detail (see equation 67).

Let us now consider the potential on the earth's surface only; for this problem, equation 163 can now be written as

$$U(r, 0) = \int_0^\infty Z(\lambda, 0) J_0(\lambda r) d\lambda,$$

where $U(r, 0)$ is written to show that the potential is taken where $z = 0$ and is now a function of r only. $Z(\lambda, 0)$ has a comparable meaning. Multiplying both sides of the equation by $r J_0(\lambda_1 r)$ and integrating over r from zero to infinity, we obtain

$$\int_0^\infty U(r, 0) r J_0(\lambda_1 r) dr = \int_0^\infty Z(\lambda, 0) d\lambda \int_0^\infty r J_0(\lambda_1 r) J_0(\lambda r) dr. \quad (165)$$

The integral on the right side of equation 165 is known as the Fourier-Bessel integral (Morse and Feshbach, 1953, p. 766) and is equal simply to $Z(\lambda_1, 0)$. Since only λ_1 appears in the equation now, we are free to drop the subscript and thus obtain

$$Z(\lambda, 0) = \int_0^\infty U(r, 0) r J_0(\lambda r) d\lambda. \tag{166}$$

Equation 166 suggests that we can first measure the potential as a function of the distance from a single-current electrode, and then use this potential to determine $Z(\lambda, 0)$.

To investigate how a knowledge of $Z(\lambda, 0)$ leads to a unique picture of the subsurface resistivity distribution, we restrict our attention to horizontal bedding; we will use the three-layer problem to illustrate the technique. Beginning as we did to get equations 152, we write down a potential function for each of three media:

$$\begin{cases} U_0 = \dfrac{I\rho_0}{2\pi} \left\{ \dfrac{1}{R} + \int_0^\infty A_0 [e^{\lambda z} + e^{-\lambda z}] J_0(\lambda r) d\lambda \right\} \\[2mm] U_1 = \dfrac{I\rho_0}{2\pi} \left\{ \dfrac{1}{R} + \int_0^\infty [A_1 e^{\lambda z} + B_1 e^{-\lambda z}] J_0(\lambda r) d\lambda \right\} \\[2mm] U_2 = \dfrac{I\rho_0}{2\pi} \left\{ \dfrac{1}{R} + \int_0^\infty B_2 e^{-\lambda z} J_0(\lambda r) d\lambda \right\}. \end{cases} \tag{167}$$

From each of these expressions, we may write a function $Z(\lambda, z)$. Thus we have

$$\begin{cases} Z_0(\lambda, z) = \dfrac{I\rho_0}{2\pi} [A_0 e^{\lambda z} + (A_0 + 1) e^{-\lambda z}] \\[2mm] Z_1(\lambda, z) = \dfrac{I\rho_0}{2\pi} [A_1 e^{\lambda z} + (B_1 + 1) e^{-\lambda z}] \\[2mm] Z_2(\lambda, z) = \dfrac{I\rho_0}{2\pi} (B_2 + 1) e^{-\lambda z}, \end{cases} \tag{168}$$

where the subscript indicates the region in which the function is valid. To derive these functions, we had to expand $1/R$ in terms of Bessel functions (equation 105) in equation 167. Ultimately the function of prime interest is $Z_0(\lambda, z)$.

To obtain the arbitrary constant A_0, and eventually $Z_0(\lambda, z)$, we apply equations 152 repetitively. In the first application of equations 152, we note that $j=0$, $j+1=1$, and $B_0 = A_0$. Therefore, we obtain the relationships

$$\begin{cases} A_1 = \dfrac{1}{2\rho_0}(\rho_1 + \rho_0) A_0 - (1 + A_0)(\rho_1 - \rho_0) e^{-2\lambda z_1}] \\[2mm] B_1 = \dfrac{1}{2\rho_0}[(\rho_1 - \rho_0)(1 - A_0 e^{2\lambda z_1}) + (\rho_1 + \rho_0) A_0]. \end{cases}$$

The second application depends only upon A_2, which is zero from the boundary conditions. In this case $j=1$.

Therefore, we have

$$A_2 = 0 = \frac{1}{4\rho_0\rho_1} \{ (\rho_2 + \rho_1)[(\rho_1 + \rho_0) A_0 - (1 + A_0)(\rho_1 - \rho_0) e^{-2\lambda z_1}] $$
$$ - [2\rho_0 + (\rho_1 - \rho_0)(1 - A_0 e^{2\lambda z_1}) + (\rho_1 + \rho_0) A_0](\rho_0 - \rho_1) e^{-2\lambda z_2} \}$$

from which we can solve directly for A_0.

$$A_0 = \frac{k_{10} e^{-2\lambda z_1} + k_{21} e^{-2\lambda z_2}}{1 - k_{10} e^{-2\lambda z_1} - k_{21} e^{-2\lambda z_2} + k_{10} k_{21} e^{-2\lambda(z_2 - z_1)}}. \tag{169}$$

Finally, from equations 168 and 169, we obtain the desired function:

$$Z_0(\lambda, 0) = \left(\frac{I\rho_0}{2\pi}\right) \frac{1 + k_{10} e^{-2\lambda z_1} + k_{21} e^{-2\lambda z_2} + k_{10} k_{21} e^{-2\lambda(z_2 - z_1)}}{1 - k_{10} e^{-2\lambda z_1} - k_{21} e^{-2\lambda z_2} + k_{10} k_{21} e^{-2\lambda(z_2 - z_1)}}. \tag{170}$$

To investigate how to analyze $Z_0(\lambda, 0)$ to obtain the required parameters, let us first examine a function $f_1(\lambda)$, which we define as

$$f_1(\lambda) = \frac{Z_0(\lambda, 0) + 1}{Z_0(\lambda, 0) - 1} = \frac{1 + k_{10} k_{21} e^{-2\lambda(z_2 - z_1)}}{k_{10} e^{-2\lambda z_1} + k_{21} e^{-2\lambda z_2}}. \tag{171}$$

For very large values of λ, we find that

$$\lim_{\lambda \to \infty} f_1(\lambda) = \lim_{\lambda \to \infty} e^{2\lambda z_1}/k_{10}$$

or

$$\lim_{\lambda \to \infty} \ln f_1(\lambda) = \lim_{\lambda \to \infty} [2\lambda z_1 - \ln k_{10}]. \tag{172}$$

If $\ln f_1(\lambda)$ in equation 172 is plotted as a function of λ, the curve will approach asymptotically a line whose slope is twice the depth of the first interface and whose y-intercept is the negative logarithm of the corresponding reflection factor k_{10}.

In this same way we define a second function as

$$f_2(\lambda) = \frac{k_{10} e^{-2\lambda z_1} f_1(\lambda) - k_{10}}{1 - k_{10} e^{-2\lambda z_1} f_1(\lambda)} = \frac{k_{10} e^{+2\lambda(z_2 - z_1)}}{k_{21}} + k_{10}. \tag{173}$$

The reflection factor k_{10} is always less than one, which is small compared to the first term on the right, even for small values of λ. Therefore, if $\ln f_2(\lambda)$ is plotted as a function of λ, all the points will appear to lie on a straight line whose slope is twice the thickness of the second bed and whose y-intercept is $\ln (k_{10}/k_{21})$. Thus, by the above technique, all of the parameters of the problem have been determined from a knowledge of $Z_0(\lambda, 0)$. If the potentials in the vicinity of an isolated current electrode are measured as a function of the distance from the electrode, these potentials can be used in equation 166 to determine $Z_0(\lambda, 0)$.

If it is found in an actual analysis that the last step does not lead to a straight line for all values of λ, this fact indicates that the problem is one involving more than three layers. The procedure must then be repeated until the final boundary is reached. Pekeris

(1940)[4] has shown that the function to be used in locating the ith boundary is

$$f_i(\lambda) = \frac{k_{i-1}[e^{-2\lambda t_{i-1}}f_{i-1}(\lambda) - k_{i-1}k_{i-2}]}{k_{i-2} - k_{i-1}e^{-2\lambda t_{i-1}}f_{i-1}(\lambda)} \qquad (174)$$

where $k_i = (\rho_i - \rho_{i-1})/(\rho_i + \rho_{i-1})$ and $t_{i-1} = (z_i - z_{i-1})$ is the thickness of the $(i-1)^{th}$ bed. The preceding f's are to be formed from $f_1(\lambda)$ and $f_2(\lambda)$ as defined above. Equation 173 fits this definition equally well if we consider that the reflection factor at the earth's surface is 1. When $\ln f_i(\lambda)$ is plotted as a function of λ, the slope is the thickness of the corresponding bed and the y-intercept is $\ln k_{i-1}/k_i$.

In addition to the large amount of computations involved, one of the possible objections to the direct method of interpretation is the difficulty of measuring the potentials sufficiently accurately in the neighborhood of an isolated current electrode. The difficulty is especially serious for points at some distance from the electrode if the effects of greater depths are sought. This particular difficulty would be alleviated somewhat if the potentials obtained from Wenner-type measurements could be used in the above equations. It might also be convenient to make this sort of study in connection with a regular resistivity survey.

We will now show that the Wenner potentials can indeed be used for the direct method of interpretation with little modification of the equations. The potential difference between the two potential electrodes of the Wenner configuration can be expressed as

$$V = 2\int_0^\infty Z_0(\lambda, 0)[J_0(\lambda a) - J_0(2\lambda a)]d\lambda \qquad (175)$$

where a is the usual electrode separation. This simple result is obtained because the potential difference for this configuration is exactly twice the potential at one electrode. Further, the effect of the layering is exactly the same on the fields of both current electrodes; and, finally, the principle of superposition applies.

The integral containing the term $J_0(2\lambda a)$ in equation 175 can easily be converted to one containing $J_0(\lambda a)$ by a simple change of variables. Let λ become $\lambda/2$ in the integral involving the second term only, so that we have

$$V = \int_0^\infty [2Z_0(\lambda, 0) - Z_0(\lambda/2, 0)]J_0(\lambda a)d\lambda. \qquad (176)$$

The quantity in brackets takes the place of $Z_0(\lambda, 0)$ in the previous equations and V, which is a function of a, takes the place of $U(r, 0)$. The effect of these new

functions on the determinations of depth and thickness can be foreseen by inductive reasoning. We note first that λ occurs in $Z_0(\lambda, 0)$ only in combinations like $e^{-2\lambda z_i}$. For every term like $e^{-2\lambda z_i}$ in the quantity in brackets, there is a corresponding term $e^{-\lambda z_i}$. As the limits of large λ are taken, only these latter terms will persist. Therefore, we may conclude that the determinations using Wenner potentials will lead directly to thicknesses instead of double thicknesses, which are obtained by using the potentials about a single-current electrode. On the other hand, the information about the reflection factors is unchanged by using the Wenner potentials.

VERTICAL STRUCTURES

Vertical faults and fissures can be detected by direct-current prospecting methods under favorable field conditions. In the present section we point out the characteristic features of the plotted data that permit the detection of these geologic features with an accuracy that is sufficient in many mining and structural-geology problems.

The theoretical background for the problems of vertical faults and fissures was given in detail in the section "Applications of image theory" (p. 52 to 53) and is therefore not repeated here. The data for most of the curves in the present section were computed from equations of the type of equation 26. The equations for the potentials that are used—for example, those which were previously derived directly by the method of images on pages 57 to 59 are also found applicable to limiting cases of similar equations for the vertical-dike problem (p. 133 to 135).

In the present section, we study families of theoretical curves for different configurations over vertical faults and fissures. Field examples are included in many instances to prove the usefulness of the mathematics used and to illustrate how the salient features of the field curves are used to detect faults and fissures precisely.

In contrast with the study of the effects of horizontal beds in the previous section, the effects of vertical faults and fissures are lateral effects. Because these geologic features are usually assumed to crop out, abrupt discontinuities in slope of the charted curves are obtained as the configuration crosses the fault or fissure. This property is not observed in the theoretical curves for horizontal beds. Moreover, in faults and fissures, the sharp peaks in the curves will usually be somewhat subdued owing to soil cover over the bedrock. Mukhina (1950a) has worked out the theory of a fault covered with a conducting layer. However, the main principles can be gained from the simpler mathematical treatment.

---

[4] There are slight differences between our functions and those of Pekeris. Equation 174, for example, has obviously been adapted from that given by Pekeris to apply to the definitions of our functions.

PERFECTLY CONDUCTING OR INSULATING PLANES

A narrow fissure can sometimes be approximated by a vertical perfectly conducting or insulating plane, if the resistivity of the country rock is essentially the same on either side of the fissure. For example, a wet-clay gouge along a fault plane that cuts an otherwise high resistivity country rock may simulate a highly conducting plane; and, contrariwise, a thin vertical mass of gilsonite filling a fracture may simulate a highly insulating plane.

A study of the effect of perfectly conducting or insulating planes on different configurations facilitates a qualitative reasoning that is helpful to an understanding of more complex geologic features.

ASYMMETRICAL CONFIGURATIONS

The data obtained with asymmetrical configurations over vertical perfectly insulating or conducting planes is better understood by considering first the potentials that exist in the vicinity of such planes due to a single point current electrode (fig. 52). The charted potentials for the curves A and C in figure 52 are those obtained at potential electrode P_1, which is kept a constant distance a to the left of current electrode C_1, as these electrodes are moved across the surface along a traverse perpendicular to the planes. The value of the potential is plotted at the position of P_1.

For the perfectly conducting plane (fig. 52A), the potential values lie between zero and $I\rho/2\pi a$. Although the potential is zero when the plane straddles the

electrodes, there is no discontinuity in the potential values.

For the perfectly insulating plane (fig. 52B), the potential values lie between zero and $I\rho/\pi a$ which is twice the maximum value in the previous case. As before, the potential is zero when the plane straddles the electrodes; for all other electrode positions, however, the potential values are restricted between $I\rho/2\pi a$ and $I\rho/\pi a$ because of the discontinuity of potential values that occur as either of the electrodes cross the plane. The greater range in the potential values for the perfectly insulating plane than for the perfectly conducting plane causes greater apparent-resistivity anomalies to occur over the former for the ordinary configurations.

The asymmetrical methods, as previously pointed out, measure gradients in potential that are converted to apparent resistivities. For the vertical perfectly conducting or insulating planes, the general pattern of the apparent-resistivity anomaly that any specific asymmetrical configuration will give can be reasoned qualitatively by considering the gradient of the curves in figure 52 for the given configuration. As examples of the reasoning used, we will treat only the asymmetrical Wenner and asymmetrical Lee configurations; but the same reasoning can be applied to the other asymmetrical configurations.

The potential at P_2 (fig. 52A), lying a distance $2a$ to the left of a single current electrode C_1 in the vicinity of a vertical perfectly conducting plane, is given by
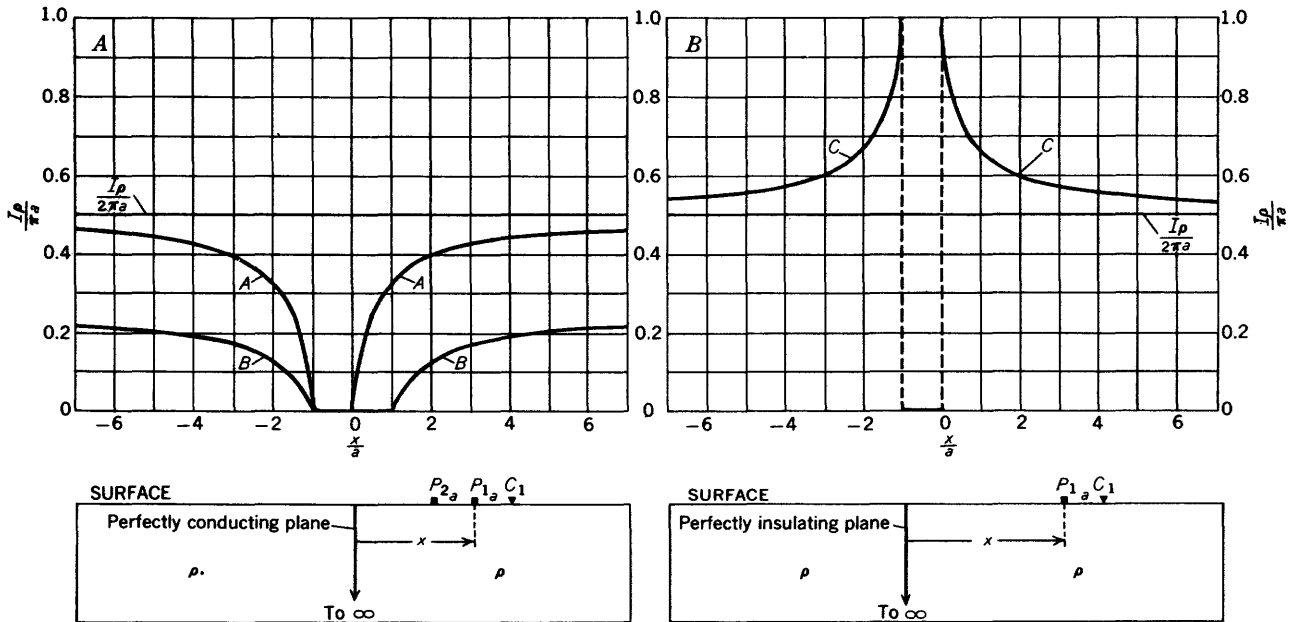
FIGURE 52.—Potentials at a distance a (electrode P_1) to the left of a single current electrode in the vicinity of (A) a vertical perfectly conducting plane (curve A) and (B) a vertical perfectly insulating plane (curve C). Potentials at a distance $2a$ (electrode P_2) to the left of a single current electrode in the vicinity of (A) a vertical perfectly conducting plane (curve B).

curve B, figure 52A. The value of the potential is plotted midway between electrodes C_1 and P_2; this position of plotting thus corresponds with the position of electrode P_1. For the asymmetrical Wenner configuration, the potential difference V between P_1 and P_2 for a given position of the configuration can be obtained by taking the differences directly from curves A and B, respectively (fig. 52A). The apparent resistivity for the asymmetrical Wenner configuration can then be obtained readily by multiplying V by $4\pi a/I$. A graphical solution could be obtained similarly for the apparent resistivity of the perfectly insulating plane. In fact, a graphical solution of such horizontal profile problems can be obtained by this method for any configuration; but it is generally more convenient and accurate to compute directly the numerical values of the potentials and apparent resistivities. This procedure was used to compute the curves now to be discussed.

Figure 53 shows the apparent-resistivity values along a horizontal profile across vertical perfectly conducting and insulating planes with the asymmetrical Wenner and asymmetrical Lee configurations. The apparent-resistivity values ρ_a/ρ are plotted as the ratio of the apparent resistivity ρ_a to the true resistivity ρ of the country rock. For both configurations, the apparent resistivity values are plotted at the position of potential electrode P_1, which is the electrode nearest to the current electrode C_1; in this respect our method of plotting departs from the more conventional method of plotting the apparent-resistivity value at the point midway between the two potential electrodes. Our method of plotting in this example, however, results in some of the breaks in the curves occurring at the position vertically over the planes.

The apparent-resistivity anomalies over the perfectly insulting plane are—as expected—larger than those over the perfectly conducting plane; also the former are discontinuous, whereas the latter are continuous. Over the perfectly insulting planes, the maximum apparent-resistivity values ρ_a/ρ are 4.0 for the asymmetrical Wenner configuration and 6.0 for the asymmetrical Lee configuration; the peaks occur as the potential electrode P_1 crosses the plane. As before, the minimum value is zero, and occurs when the plane straddles the P_1 and C_1 electrodes. Over the perfectly conducting plane, the maximum apparent resistivity values are 1.33 for the asymmetrical Wenner configuration and 1.50 for the asymmetrical Lee configuration.

The total relief of the apparent-resistivity anomalies are larger for the asymmetrical Lee configuration than for the asymmetrical Wenner configuration; yet in certain regions of the curves, the apparent-

resistivity anomalies are slightly smaller for the asymmetrical Lee configuration than for the symmetrical Wenner configuration, for example, as on the left side of the perfectly insulating plane. As the current electrode touches the perfectly insulating plane, however, the apparent resistivity for both configurations is equal to 2.0.

Many of the minor differences in apparent resistivity curves for the different configurations cannot be reasoned intuitively from the apparent-resistivity formulas. For example, the apparent-resistivity formula is $\rho_a = 4\pi a V/I$ for the asymmetrical Wenner configuration and $\rho_1 = 6\pi a V_{10}/I$ for the asymmetrical Lee configuration; but the functions V and V_{10} are nonlinear functions of the differences (gradients) of potential, and therefore difficult to reason intuitively without numerical computations.

LEE AND WENNER CONFIGURATIONS HORIZONTAL PROFILES

As an example of a symmetrical configuration along a horizontal resistivity profile crossing a vertical perfectly conducting or insulating plane, we use the Wenner and Lee configurations (fig. 54). The customary method of offset plotting is used for the Lee data; and the regular method of plotting is used for the Wenner data.

Because, as the configuration crosses the vertical plane, one or both of the current electrodes are always on the same side of the plane as one or both of the potential electrodes, the apparent resistivity for symmetrical configurations of this type never goes to zero, although it did so for the asymmetrical configurations.

For the perfectly insulating plane (fig. 54 A, B), the apparent-resistivity curves are discontinuous as each electrode crosses the plane, as for the asymmetrical configurations; the apparent-resistivity curves are piecewise continuous for the perfectly conducting plane.

The apparent-resistivity values for the symmetrical configurations are different from those for the asymmetrical configurations. Along some segments of the apparent-resistivity curves, however, where the relative positions of the electrodes and the resulting potential differences are identical for both the asymmetrical and symmetrical configurations, the corresponding apparent-resistivity values for the two configurations bear a simple relationship to each other. For the vertical perfectly insulating plane, for example, the symmetrical Wenner positions of electrodes P_2, P_1, and C_1, where C_2 lies to the left of the plane (fig. 54A), are such as to give apparent-resistivity values of 0.333 or greater (see lower right-hand segment of curve for $x/a = 1/2$ or greater in fig. 54A); whereas the corresponding asym-
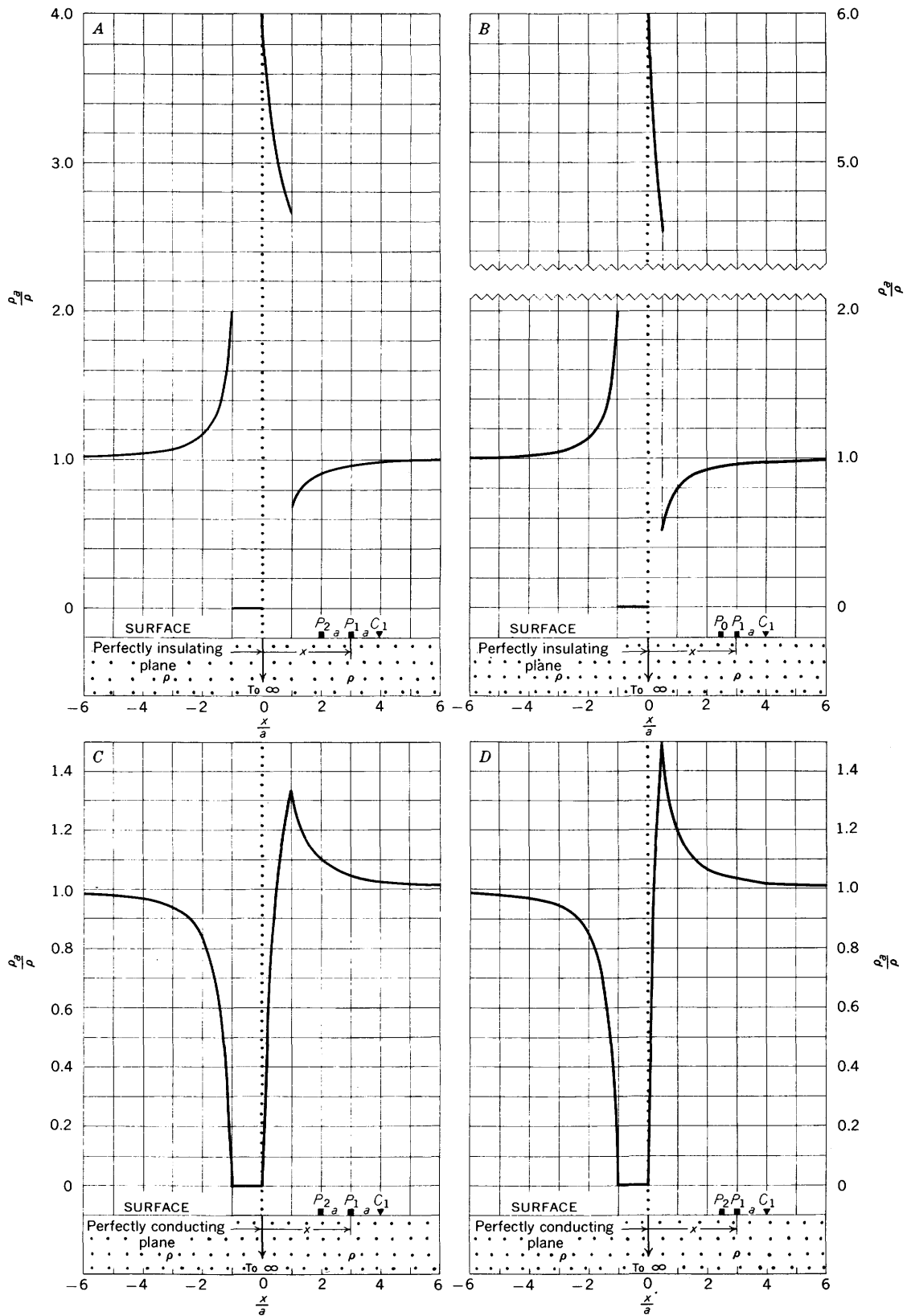
FIGURE 53.—Theoretical horizontal resistivity profiles across vertical perfectly conducting and insulating planes with (A and C) asymmetrical Wenner and (B and D) asymmetrical Lee configurations.
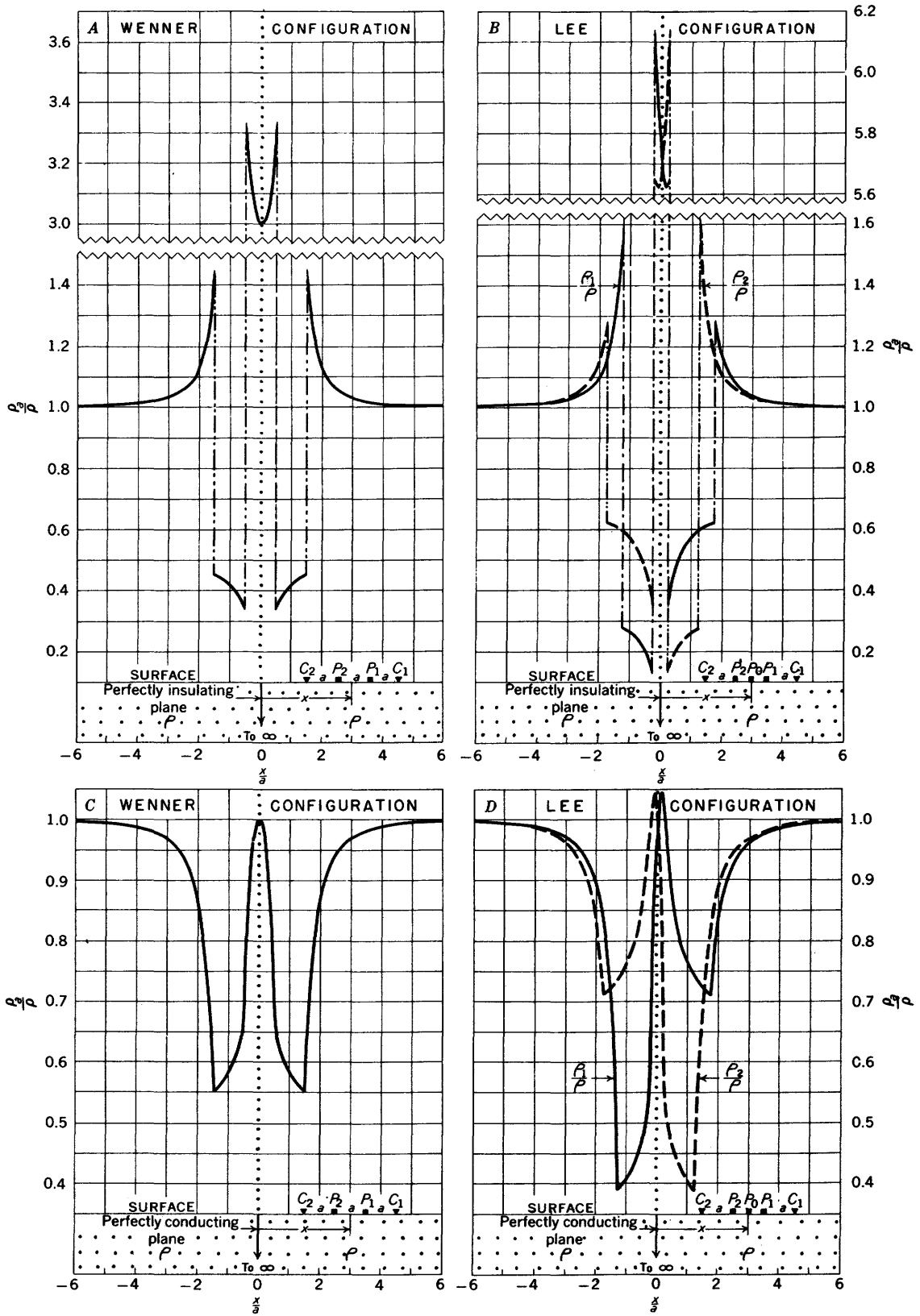
FIGURE 54.—Theoretical horizontal resistivity profiles across vertical perfectly conducting and insulating planes with the Wenner and Lee configurations. Diagrams (A) and (C) adapted from Howell, (1934). Copyright by Am. Inst. Mining Metall. Engineers.

metrical Wenner positions of the same electrodes P_2, P_1, and C_1 give apparent-resistivity values of 0.667 or greater (see right-hand segment of curve for $x/a = 1$ or greater in fig. 53A), although in these two cases the differences between potential electrodes P_1 and P_2 are identical. Actually, the apparent-resistivity value of the symmetrical positions is exactly half that of the asymmetrical positions because there is a difference of a factor of two in the two apparent-resistivity formulas.

Along other segments of the apparent-resistivity curves any relationship between the apparent-resistivity curves of the symmetrical configurations on the one hand and the asymmetrical configurations on the other hand is either obscure or absent. Many paradoxes exist, and the theoretical apparent-resistivity curves must be computed because their behavior is usually unpredictable.

For the perfectly insulating plane, a minimum in the central segment of the anomaly, with an apparent-resistivity value equal to three times that of the surrounding country rock, is obtained as the center of the Wenner configuration lies vertically over the plane (fig. 54A); the maximum apparent-resistivity value is less with the Wenner configuration than with the asymmetrical Wenner configuration. For a vertical perfectly conducting plane with the Wenner configuration (fig. 54C), a typical W-shaped curve is obtained, and an apparent-resistivity value equal to that of the surrounding country rock is obtained as the center of the configuration lies vertically over the plane; none of the apparent-resistivity values exceeds the true resistivity of the surrounding country rock.

The apparent-resistivity curves for the Lee configuration cross symmetrically at a point lying vertically above either the conducting or insulating planes, when the offset method of plotting is used (fig. 54B, D). For the perfectly insulating plane the maximum apparent-resistivity value is greater with the Lee configuration than with the asymmetrical Lee configuration; and the maximum apparent-resistivity values with the regular Lee configuration greatly exceed the true resistivity of the surrounding country rock.

For both the perfectly insulating and conducting planes the Lee anomalies are greater than the Wenner anomalies. This follows partly as a consequence of the fact that for such planes the asymmetrical Lee anomalies are greater than the asymmetrical Wenner anomalies.

The paradoxes and unpredictable behavior of the apparent-resistivity curves that have been emphasized for these horizontal profile examples are duplicated to some degree in most of the families of curves given in this treatise. Space permits our discussing only the most important characteristics of such curves, but
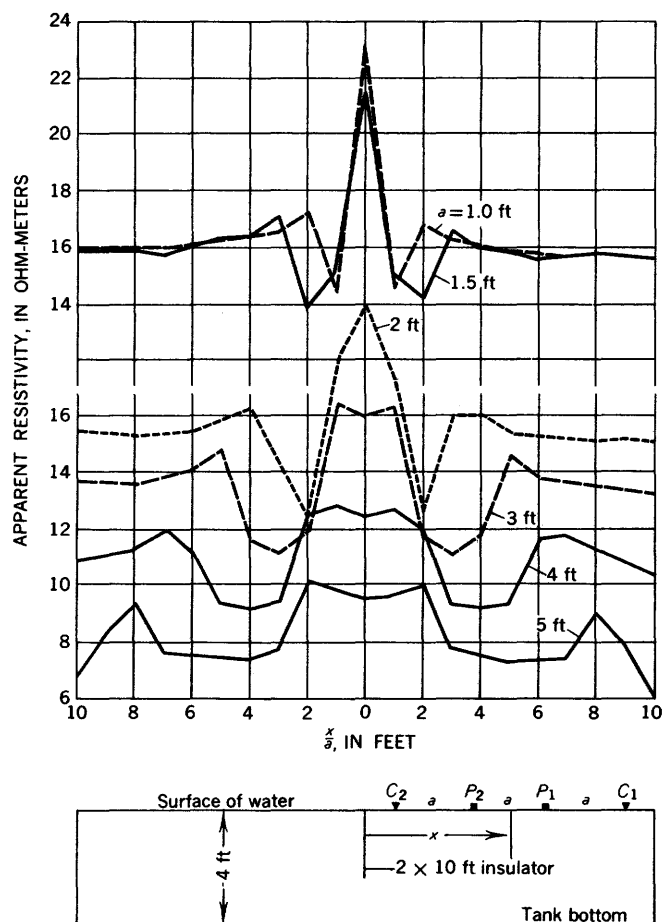
FIGURE 55.—Results of model study of horizontal resistivity profiles across a vertical insulating sheet. Adapted from Johnson, (1934). Copyright by Am. Inst. Mining Metall. Engineers.

with experience the varied characteristics of the theoretical curves become more important and meaningful to the interpreter of resistivity data.

Horizontal resistivity profiles with the Wenner configuration were taken over a vertical insulating sheet in model studies by Johnson (1934). Figure 55 shows the results of this study. The apparent-resistivity curves are comparable with those of figure 54A; but an exact comparison cannot be made because the depth extent of the insulating sheet used in the model work was short in comparison with the electrode separations used, and there was therefore a short-circuiting effect around the bottom of the sheet that gave a continuous curve rather than abrupt discontinuities in the curve.

Howell (1934) made brief model studies to test the validity of the theoretical curves similar to those in figure 54A, C for horizontal resistivity profiles with the Wenner configuration over both vertical conducting and insulating planes. His plotted points confirmed the theoretical curves within the experimental error of his models. Figure 117D (solid curve) in a later section
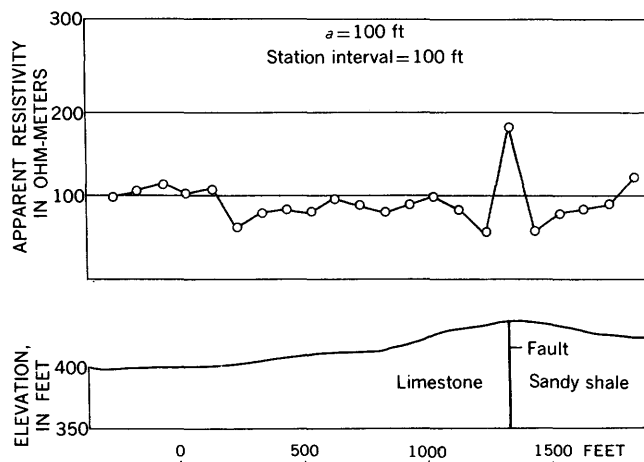
FIGURE 56.—Field example of a Wenner horizontal resistivity profile across a vertical fault zone that simulates an insulating sheet. Adapted from Hubbert (1932). Copyright by Am. Inst. Mining Metall. Engineers.

shows the results of a tank-model study of a horizontal resistivity profile across a vertical perfectly conducting plane (Heiland, 1932b). The W-shape of the curve and the fact that the central peak attains an apparent-resistivity value that is approximately equal to that of the tank fluid agree with the theoretical curve in figure 54C.

Figure 56 shows a field example of a Wenner horizontal resistivity profile across a vertical fault zone of high resistivity that simulates an insulating sheet (Hubbert, 1932; 1944, p. 85–86).

VERTICAL PROFILES

Because of their limited usefulness, the complete vertical resistivity profiles over vertical perfectly conducting and insulating planes are not given here. Part of these profiles for both the Lee and Wenner configurations are identical to part of the apparent-resistivity curves for $k=\pm1$ for a vertical fault (see fig. 59 and discussion of this figure).

FAULTS

The vertical fault is one of the most useful geologic structures to study. A thorough understanding of the anomalies obtained with different configurations in the vicinity of a vertical fault is also helpful in understanding the more complex anomalies obtained over the more complex geologic structures. Many of the key features found in the anomalies over the vertical fault are found also in the anomalies over other geologic structures, and thus are fundamental guides in the interpretation of resistivity data in general. Our treatment of the interpretation of resistivity data for faults is therefore more detailed than that for any other geologic features. The principles set forth here, however, will be used repeatedly throughout the remainder of the treatise.

It should be emphasized that the interpretation given here for a vertical fault applies equally well to any other geologic features that involve vertical or nearly vertical contacts between two media, of different resistivity, that extend for a considerable distance horizontally along the contact, as, for example, the vertical contact between a large igneous intrusion and the surrounding country rock.

LEE CONFIGURATION
HORIZONTAL PROFILES
CONTINUOUS THEORETICAL CURVES

The theoretical horizontal resistivity profiles for the Lee configuration over a vertical fault are given in plate 1 for values of k in steps of 0.1 from ±0.1 to ±0.9. The apparent-resistivity values are charted as the ratio of the apparent resistivity ρ_a to the resistivity ρ' of the rock lying on the left side of the fault. The offset method of plotting the Lee data is used; the ρ_1 and ρ_2 values are for the right- and left-hand sides, respectively, of the configuration.

Certain features of the apparent-resistivity curves that can be proved theoretically are the same irrespective of the resistivity contrast of the rocks on either side of the fault. One of the apparent-resistivity peaks attains a value equal to the resistivity of the rock on the high-resistivity side of the fault. The positions of the peaks, lows, and abrupt changes in slopes of the curves are the same in all the curves. The most pronounced peaks for both ρ_1/ρ' and ρ_2/ρ' on the high-resistivity side of the fault coincide in their horizontal position and lie a distance of $a/4$ from the fault trace in the direction of the high resistivity rock. If a continuous curve were obtained in the field, the position of such a vertical fault could be predicted accurately from these two peaks, if sufficient resistivity contrast exists and other factors, such as a small amount of overburden, are favorable. In the field, however, only discrete points along the curves are obtained; the distance between successive points depends on the station interval, which is usually $a/2$ or less for the Lee configuration. For a detailed interpretation of field data, it is therefore desirable to use the theoretical field plot.

THEORETICAL FIELD PLOTS

Various theoretical field plots obtained along a traverse taken perpendicular to the strike of the fault are shown in plate 2. The assumed resistivity contrast is $\rho''/\rho'=\frac{1}{4}$. The station interval in all the diagrams in this plate is constant, namely, $a/2$, which is the station interval usually used for the Lee configuration; and the same fault is crossed in each case. The offset method of plotting the Lee data is used; the ρ_1 and ρ_2 values are for the right- and left-hand sides, respectively, of the configuration. The only factor that

differs between the diagrams is the starting point along the traverse, which differs for each diagram. For example, the starting point of the configuration in plate 2A is such that for one of the stations along the horizontal profile, the center potential electrode P_0 is placed directly over the fault plane. The starting point of the configuration in plate 2B is a distance of $0.050a$ to the right of that for plate 2A, so that for one of the stations along the horizontal profile, the center potential electrode P_0 is placed a distance of $0.050a$ to the right of the fault plane. The numerical values of the distances from the fault plane to three decimal places arise in calculations for the station interval $a/2$, from different starting points.

For a horizontal resistivity profile in which center electrode P_0 falls on the fault plane (pl. 2A), the fault plane lies a distance of $0.250a$ to the right of peaks A and A', on the ρ_1 and ρ_2 curves,[5] respectively. Peak A attains an apparent-resistivity value equal to the regional value of the country rock to the left of the fault. As this is the only case in which peak A attains such a high value in a simple fault problem, this feature can be used in some cases to facilitate the location of the fault.

For a horizontal resistivity profile in which center electrode P_0 falls a distance of $0.050a$ to the right of the fault plane (pl. 2B), the fault plane lies a distance of $0.200a$ to the right of peaks A and A'. In this case peaks A and A' are lower than the corresponding peaks in plate 2A. Otherwise the curves are very similar to those in plate 2A, and distinguishing between them in the field data would be difficult.

When the center electrode P_0 falls a distance of $0.062a$ to the right of the fault plane (pl. 2C), a limiting case arises that divides the theoretical field plots into two families. A horizontal line $B'A'$ is obtained on the ρ_1 curve in the place where peak A' usually occurs. The peak at A on the ρ_2 curve is maintained, however, although it is lower than the corresponding peak in plate 2B. The fault plane lies a distance of $0.188a$ to the right of peak A and point A', and a distance of $0.688a$ to the right of point B'. Point B' occurs when center electrode P_0 lies a distance of $0.938a$ (that is, $x/a = -0.938$) to the left of the fault, and point A' occurs when center electrode P_0 lies a distance of $0.438a$ (that is, $x/a = -0.438$) to the left of the fault. The transition of peak A' in plate 2B to straight line $B'A'$ in plate 2C occurs, with increasing distance of P_0 away from the fault, as the result of a decrease in the apparent-resistivity value of point A' in plate 2B with a concomitant increase of the apparent-resistivity value of point B' in plate 2B; the final result is the straight line

$B'A'$ in plate 2C. For the resistivity contrast assumed, the horizontal line $B'A'$ provides a limiting case in two respects: first, the apparent-resistivity value of a peak in this part of the ρ_1 curve is never less than the apparent-resistivity value of ρ_1 for this horizontal line, as either the peak A' (pl. 2B) or peak B' (pl. 2D) will have higher values than this horizontal line; and second, in this case the fault lies as close as it ever can to a peak formed in this part of the ρ_1 curve, as no peak in this part of the ρ_1 curve can be formed closer than a distance of $0.188a$ to the left of the fault.

For a horizontal profile in which center electrode P_0 falls a distance slightly less than $0.062a$ to the right of the fault plane, horizontal line $B'A'$ changes to a line dipping to the left, so that point B' is lower than point A'.

For a horizontal profile in which center electrode P_0 falls a distance slightly greater than $0.062a$ to the right of the fault plane, horizontal line $B'A'$ changes to a line dipping to the right, so that point A' is lower than point B'. In this case point B' forms a peak with a gently dipping right flank, and the fault plane lies at a distance of approximately $0.688a$ (actually, slightly less than this value) to the right of this peak B'. It should be emphasized that this peak B' lies a distance of $0.500a$ to the left of peak A of the ρ_2 curve. Though this condition is not shown in the diagrams, it represents the limiting case for which peak B' is barely made manifest and in which the fault plane lies at a distance of approximately $0.688a$ to the right of the peak B'.

For a horizontal profile in which center electrode P_0 falls a distance of $0.100a$ to the right of the fault plane (pl. 2D), line $B'A'$ dips rather steeply to the right, so that well-defined peak B' is formed on the ρ_1 curve. Peak A persists on the ρ_2 curve, but it is much less pronounced on its left flank than in the previous cases. The fault plane lies a distance of $0.150a$ to the right of peak A and a distance of $0.650a$ to the right of peak B'. Thus, peak B' lies a distance of $0.500a$ to the left of peak A. This offset of peak B' on the ρ_1 curve with respect to peak A of the ρ_2 curve is a diagnostic feature that facilitates the location of the fault plane in some cases.

For a horizontal profile in which center electrode P_0 falls a distance of $0.115a$ to the right of the fault plane (pl. 2E), another limiting case arises. A horizontal line BA is formed on the ρ_2 curve in the place where peak A usually occurs. The peak at B' on the ρ_1 curve is maintained, and lies directly under point B on the ρ_2 curve. The fault plane lies a distance of $0.135a$ to the right of point A and a distance of $0.635a$ to the right of point B and peak B'. Point B occurs where center electrode P_0 lies a distance of $0.385a$ (that is, $x/a = -0.385a$) to the left of the fault, and point A

[5] For convenience the ρ_1/ρ' and ρ_2/ρ' curves in plate 2 are referred to as the ρ_1 and ρ_2 curves, respectively, in the present discussion.

occurs where center electrode P_0 lies a distance of $0.115a$ (that is, $x/a=+0.115$) to the right of the fault. The transition of peak A in plate $2D$ to straight line BA in plate $2E$ occurs with increasing distance of P_0 away from the fault as the result of a decrease in the value of point A in plate $2D$ with a concomitant increase of the value of point B in plate $2D$; the final result is the straight line BA in plate $2E$. For the resistivity contrast assumed, the horizontal line BA provides a limiting case in two respects: first, the apparent-resistivity value of a peak in this part of the ρ_2 curve is never less than the apparent-resistivity value of ρ_2 for this horizontal line, as either the peak A (pl. $2D$) or peak B (pl. $2B$) will have higher values than this horizontal line; and second, in this case the fault lies as close as it ever can to a peak formed in this part of the ρ_2 curve, as no peak in this part of the ρ_2 curve can be formed closer than a distance of $0.135a$ to the left of the fault.

For a horizontal profile in which center electrode P_0 falls a distance slightly less than $0.115a$ to the right of the fault plane, peak A, though not pronounced, is present as the line BA dips to the left, with point B lower than point A.

For a horizontal profile in which center electrode P_0 falls a distance slightly greater than $0.115a$ to the right of the fault plane, line BA dips to the right, with point A lower than point B, so that peak A loses its identity as a peak, and hereafter is designated as. point A. At the same time the value of point B rises to become peak B, though it is not pronounced in this case. The fault lies a distance of approximately $0.635a$ (actually, slightly less than this value) to the right of this peak B.

For a horizontal profile in which center electrode

P_0 falls a distance of $0.150a$ to the right of the fault (pl. $2F$), peak B, which is rather pronounced on the ρ_2 curve, takes the place of the former peak A. Thus a pronounced shift to the left takes place in the peak on the ρ_2 curve. The fault plane in this case lies a distance of $0.600a$ to the right of peaks B and B', which are now coincident. The apparent-resistivity value of peak B is greater than the apparent-resistivity value of the horizontal line BA in plate $2E$.

For horizontal profiles in which center electrode P_0 falls at distances greater than $0.150a$, but less than $0.500a$, to the right of the fault (pl. 2 G–L), the ρ_1 and ρ_2 curves are similar in character. The apparent-resistivity values of peaks B and B' increase steadily with increasing distance of center electrode P_0 from the fault. As shown in table 3, the distance between the fault plane and peaks B and B' is progressively less. In the limit, where center electrode P_0 falls at a distance of $0.500a$ to the right of the fault, the ρ_1 and ρ_2 curves become identical to those for plate $2A$, in which the electrode P_0 falls on the fault plane. Then the cycle repeats itself.

The analysis in table 3 applies for a resistivity contrast of 1 to 4 and for a station interval of $a/2$. A similar analysis, using the same station interval, but with different resistivity contrasts, would give somewhat different results, only with respect to the magnitude of the features that have been described; the positions of these features would remain the same.

CRITERIA FOR SELECTING THE APPROXIMATE LOCATION OF A FAULT

For a vertical fault with the higher-resistivity material lying to the left of the fault plane, the charac-

TABLE 3.—*Distance between vertical fault plane and points of discontinuity of slope on the ρ_1 and ρ_2 apparent-resistivity curves, Lee configuration (offset plotting)*

[Electrode separation, a; station interval, $a/2$; $\rho'/\rho''=4$. See pl. 2.]

Distance between center electrode P_0 and fault	Distance between fault and—		Remarks
	Peak on ρ_2 curve	Peak on ρ_1 curve	
$0.000a$	$0.250a$	$0.250a$	Peaks A and A' coincident.
$.050a$	$.200a$	$.200a$	Do.
$.062a$	$.188a$	$.688a$; $0.188a$	Horizontal line $B'A'$ on ρ_1 curve. Peak A and point A' coincident. Peak A' vanishes.
$.100a$	$.150a$	$.650a$	Peak B' offset $0.500a$ from peak A.
$.115a$	$.635a$; $0.135a$	$.635a$	Horizontal line BA on ρ_2 curve. Peak B' and point B coincident. Peak A vanishes.
$.150a$	$.600a$	$.600a$	Peaks B and B' coincident.
$.200a$	$.550a$	$.550a$	Do.
$.250a$	$.500a$	$.500a$	Do.
$.300a$	$.450a$	$.450a$	Do.
$.350a$	$.400a$	$.400a$	Do.
$.400a$	$.350a$	$.350a$	Do.
$.450a$	$.300a$	$.300a$	Do.
$.500a$	$.000a$; $0.500a$	$.000a$; $0.500a$	Cycle repeats here.

teristics of the peaks lying to the left of the fault usually offer the best criteria for determining the location of the fault.

If a continuous horizontal resistivity profile taken in the field is available, a vertical fault is located theoretically at a distance of $a/4$ from the main peaks (pl. 1), irrespective of the resistivity contrast. As continuous profiles are not usually available, however, other criteria based on the theoretical field plots are necessary.

Although criteria based on the theoretical field plots involve certain inherent margins of error, they nevertheless can be used as a guide in selecting the approximate location of a fault. The criteria apply to the peaks or other features that are characteristically found on the high resistivity, or in this case the left-hand side of the fault. The offset method of plotting the Lee data is used; the ρ_1 and ρ_2 values are for the right- and left-hand sides, respectively, of the configuration irrespective of whether the configuration is run from left to right, or vice versa. The criteria are (see also table 3):

1. If the peaks on both the ρ_1 and ρ_2 curves are not offset and are pronounced, with a steep gradient on the right side of the peaks, the fault lies a distance of approximately $0.20a$ to $0.50a$ to the right of the peaks. If, in addition, the value of the ρ_2 peak is approximately equal to the true resistivity of the higher-resistivity material to the left of the fault, the fault lies a distance of approximately $0.25a$ to the right of the ρ_2 peak.

2. If the peaks on both the ρ_1 and ρ_2 curves are not offset and are gentle, with a small gradient on the right side of the peaks, the fault lies a distance of approximately $0.50a$ to $0.64a$ to the right of the peaks.

3. If the peaks on the ρ_1 and ρ_2 curves are offset, the fault lies a distance of approximately $0.14a$ to $0.19a$ to the right of the peak on the ρ_2 curve.

4. If the peak on the ρ_2 curve is flat-topped, or nearly so, to form a plateau, the fault lies at a distance of approximately $0.14a$ to the right of the right edge of the plateau.

5. If the peak on the ρ_1 curve is flat-topped, or nearly so, to form a plateau, the fault lies at a distance of approximately $0.19a$ to the right of the right edge of the plateau.

Similar criteria apply where the high-resistivity medium lies to the right of the fault plane, but for such a case the ρ_1 and ρ_2 curves are the mirror image of those in plate 2.

The above criteria apply only to horizontal profiles taken perpendicular to the strike of a vertical fault with the Lee configuration using a station interval of $a/2$. They apply strictly only for a resistivity contrast of 1 to 4, but can be used to determine the approximate location of a vertical fault that separates two media with resistivity contrasts that are not 1 to 4. If the resistivity contrast is small, so that ρ'/ρ'' is only slightly greater than 1, the observed peaks are not sufficiently definitive to make a trustworthly analysis. Thus a sufficient resistivity contrast should exist, so that definitive peaks are obtained in the field data.

For the interpretation of field curves, the numerical results can be computed so that they are consistent with the estimated accuracy of the field data. We prefer to use the criteria given above, and round off the final estimates of the location of the fault. A careful analysis is justified only if good operating conditions prevail in the field, so that no great distortions in the field resistivity curves are present. As the analysis can break down completely unless the geologic conditions fulfill the assumptions that are made, caution should be used. The above criteria are no panacea for problem areas, in which more refined techniques, such as station intervals smaller than $a/2$, may be desirable.

TRAVERSES AT AN ANGLE TO THE FAULT

Figure $57B$ to E give theoretical horizontal resistivity profiles with the Lee configuration across a vertical fault. For a traverse at an angle of $60°$ to the fault (fig. $57C$), the position of the trace of the fault can be determined rather accurately with the Lee configuration under favorable field conditions, although the diminished height of the diagnostic peaks causes some loss of resolution. For traverses at small angles to the fault (figs. $57D$ and E), the position of the fault trace cannot be determined accurately because the diagnostic peaks are absent. The sharp resistivity escarpment obtained in crossing the fault even at these small angles, however, indicates that a major lateral resistivity change has been crossed by the configuration; and traverses more nearly perpendicular to the suspected strike of the fault can then be taken for determining more accurately the position of its trace.

Figure $57F$ to I show theoretical horizontal resistivity profiles across a vertical fault with the Wenner configuration along traverses taken at different angles to the fault. The assumed resistivity contrast is $\rho'/\rho''=4$. If the angle between the fault trace and the traverse is less than $60°$, the position of the fault trace probably could not be picked accurately under ordinary field conditions; although, of course, the resistivity escarpment would indicate the existence of a pronounced lateral change in resistivity of the rock.
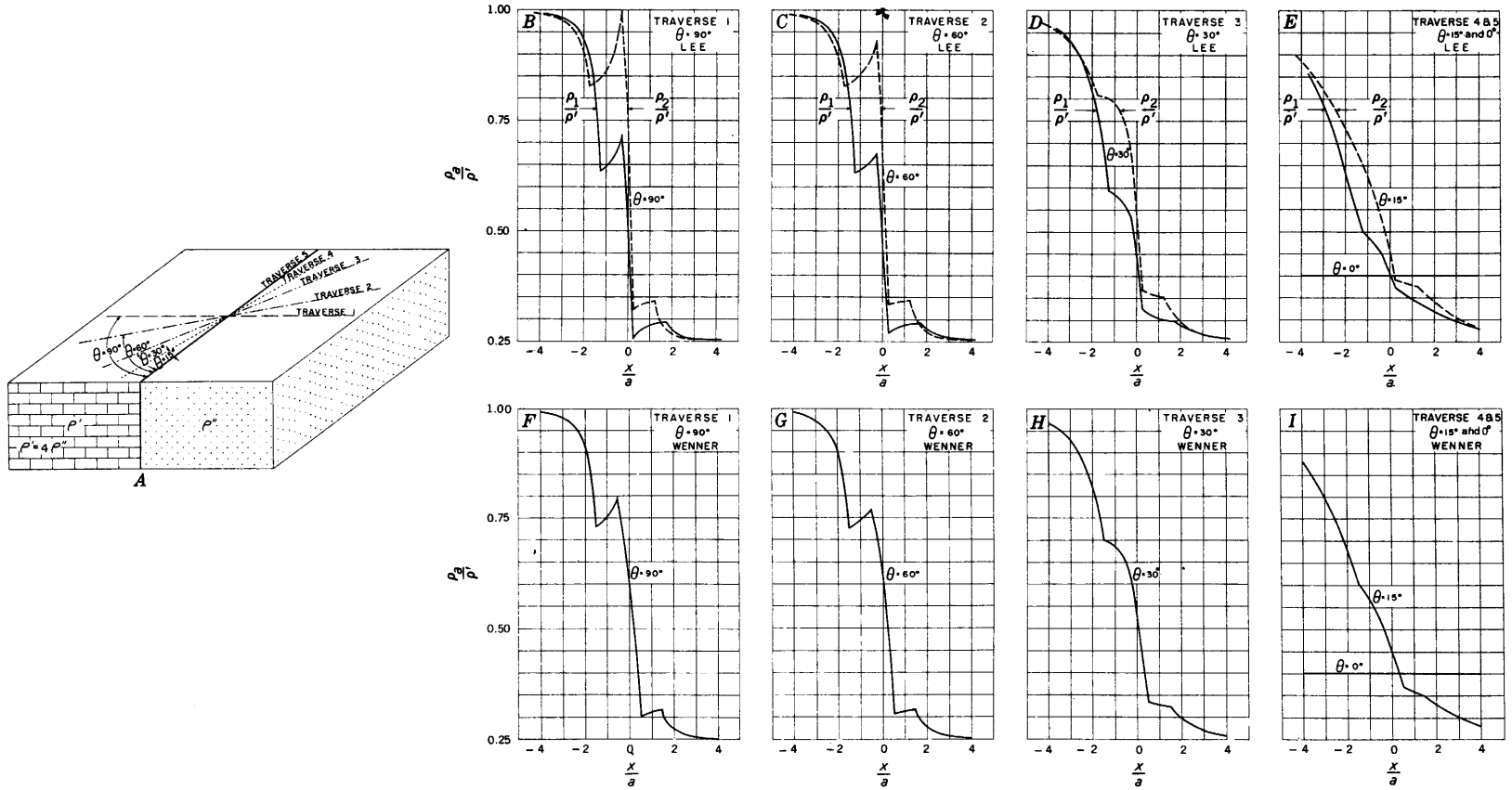
FIGURE 57.—Theoretical horizontal resistivity profiles across a vertical fault, (*B* to *E*) Lee configuration (offset plotting) and (*F* to *I*) Wenner configuration; traverses taken at different angles to the fault. $\rho'/\rho''=4$.
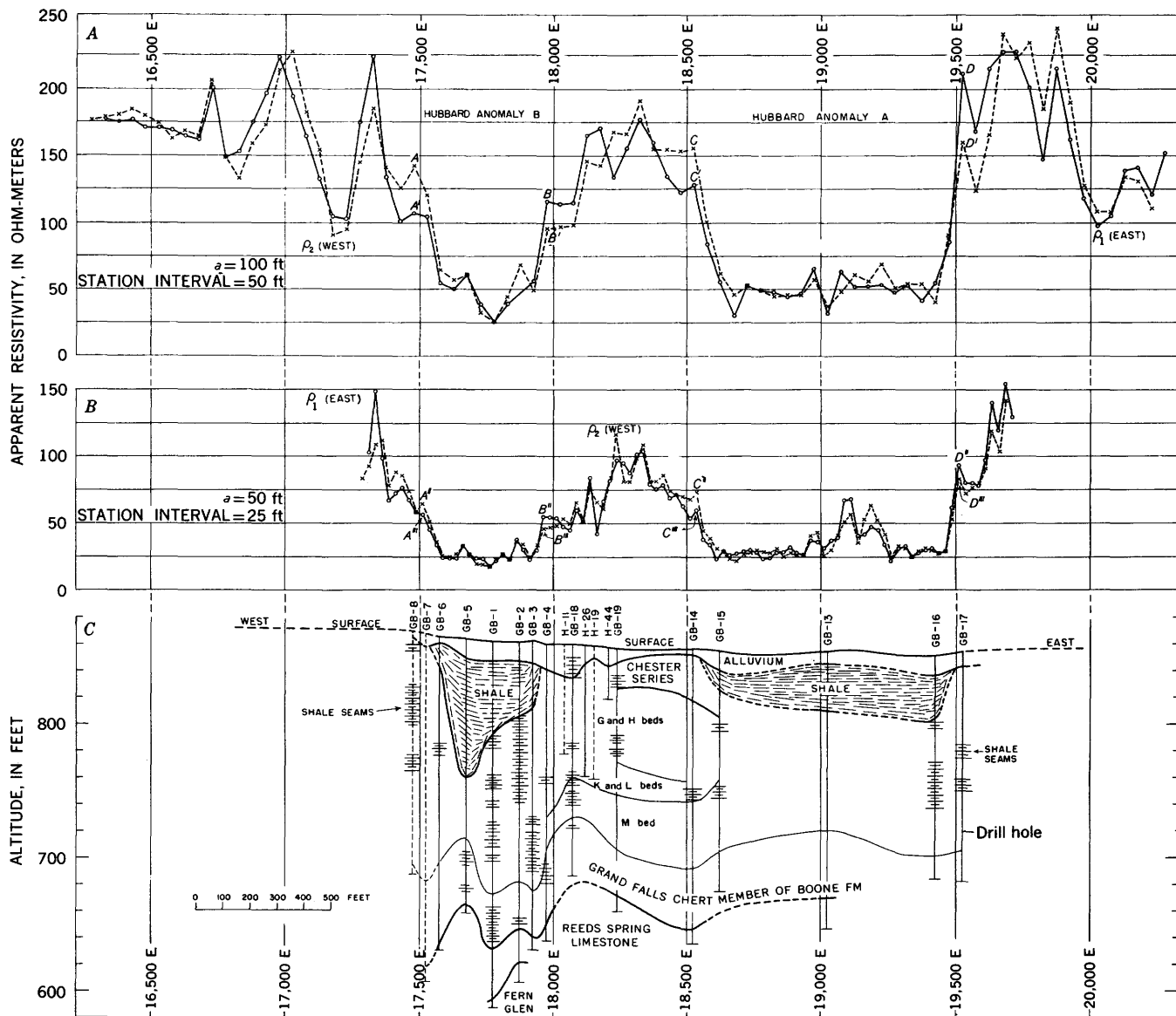
FIGURE 58.—A, B, Horizontal resistivity profiles across two shale sinks using Lee configuration (offset plotting) with electrode separations of (A) 100 feet and (B) 50 feet; (C), geologic cross section. Tri-State mining district, Cherokee County, Kans. Resistivity data and interpretations by K. L. Cook (1951-53); drill-hole data from Brichta and Ryan, 1958.

FIELD EXAMPLES

The best field examples of "fault" anomalies available to us for horizontal resistivity profiles with the Lee configuration are the anomalies that are found at the margins of shale sinks in the Tri-State lead-zinc mining district (Cook, 1951-54, unpublished data). Here the shale-limestone contacts—though not necessarily vertical and not faults in the usual sense because the sinks were formed principally by solution phenomena—are often so steep that the analysis and criteria of a vertical fault can be used successfully for picking many contacts in the ordinary application of the resistivity method in this district.

Field examples, as well as the use of the criteria for detecting the position of the fault trace, are given in figure 58. The letter designations of the peaks in the field curves are generally different from those in the theoretical curves in plate 2. Estimates of the location of the shale-limestone contacts based on the criteria given previously will be only approximate at best, as the assumptions are only partially realized in the examples considered. The fault plane does not extend to infinite depth, as assumed; the resistivity contrast may not be exactly 1 to 4; and some overburden exists in the field examples.

For an electrode separation of 100 feet and station interval of 50 feet (fig. 58A), the apparent resistivity is about 150 to 200 ohm-meters over the limestone country rock and about 50 ohm-meters or less over the shale areas. In the transition area near the west margin of the west sink, peak A, on the ρ_2 curve, has a gentle slope to the east and is somewhat similar to the theoretical field plot in plate 2F. Thus, the limestone-shale contact at the west margin of the sink theoretically lies as much as 0.60a, or 60 feet, to the east of peak A on the field curve. Point B, on the ρ_1 curve on the east side of the west sink, lies at the west edge of a resistivity plateau and is thus similar to the theoretical counterpart of plate 2E. Thus, the shale-limestone contact at the east margin of the sink theoretically lies a distance of about 0.014a, or about 14 feet, west of peak B in the field curve. By similar reasoning, point C, on the ρ_2 curve, constitutes the east edge of a resistivity plateau and indicates that the limestone-shale contact at the west edge of the east sink theoretically lies at a distance of about 0.14a, or about 14 feet, east of point C. Peak D, on the ρ_1 curve, near the east margin of the east sink, is pronounced and is coincident with peak D', on the ρ_2 curve; therefore the shale-limestone contact theoretically lies at a distance of 0.20a to 0.50a, or about 20 to 50 feet, west of peaks D and D'.

The contact can usually be picked more accurately if the station interval is made smaller so that the measured data approach more closely a continuous curve. For thick overburden, the electrode separation should be kept large; but for relatively thin overburden, as in the present example, the electrode separation was reduced when the station interval was made smaller.

For an electrode separation of 50 feet and station interval of 25 feet (fig. 58B), the apparent resistivity is about 80 to 100 ohm-meters over the limestone and about 25 ohm-meters over the shale. The same criteria as before are used on the peaks obtained along this repeat traverse, except that a is now 50 feet instead of 100 feet; and independent estimates of the location of the fault traces are then made by studying the new peaks on this traverse. When these new estimates are compared with the first ones given, the discrepancies involved are less than about 20 feet in this example.

For resistivity contrasts of 1 to 3 or more, the criteria, when used on a single Lee horizontal profile with the normal station interval of a/2, will usually result in the correct location of the fault trace within a few tens of feet when a=100 feet.

Thin uniform overburden tempers somewhat the size of the diagnostic peaks, but apparently does not greatly hinder the location of the fault trace. Experience to date (1956) indicates that as a rule for satisfactory results, the electrode separation for hori-

zontal profiles used to detect faults covered by alluvium overburden should be kept at least 5—and preferably 10 or more—times the suspected thickness of the overburden. The actual detectability of a buried fault, however, depends not only upon the depth of the overburden, but also upon the resistivity of the overburden in relation to the resistivity contrast of the materials on either side of the fault. This problem is treated on pages 268–274.

VERTICAL PROFILES

An under standing of the character of vertical resistivity profiles across a vertical fault is helpful in picking the fault contact when vertical-profile techniques are used for that purpose. In addition, a knowledge of the pattern of such profiles is desirable when depth studies by vertical-profile techniques are being made on assumed horizontal layers, because truly lateral effects sometimes occur unexpectedly, and the interpreter should be able to recognize them.

Vertical profiles taken across a vertical fault with the Lee configuration are shown in figure 59. The assumed reflection factors vary at intervals of 0.1 between +1.0 and −1.0. In each case, center electrode P_0 lies 2 units from the fault plane. For each diagram the curves are plotted in terms of the true resistivity of the medium on the left side of the fault, which is taken as unity in each diagram. This procedure facilitates obtaining the apparent resistivity in terms of specific units, such as ohm-meters, for an individual case in the field.

The point of discontinuity in slope in the vertical profiles can be used to locate the trace of a vertical fault at the surface, if the resistivity contrast is sufficiently great. For a station located over the high-resistivity material at a point lying 2 units to the left of the fault plane (fig. 59A), the apparent resistivity for small electrode separations is essentially equal to the true resistivity ρ'. As the electrode configuration is expanded, leaving potential electrode P_0 fixed, the apparent-resistivity values for both ρ_1 and ρ_2 decrease, with ρ_1 decreasing much more than ρ_2 until current electrode C_1 crosses the fault, at which point a discontinuity in slope occurs in each curve. As the configuration is expanded further, the apparent resistivity ρ_2 increases continuously and approaches asymptotically the true resistivity of the material to the left of the fault. At the same time the apparent resistivity ρ_1 increases until potential electrode P_1 crosses the fault trace, when a rather pronounced peak occurs in the ρ_1 curve only. As the configuration is expanded further, the apparent resistivity ρ_1 decreases continuously and approaches asymptotically the value of the material on the right side of the fault.
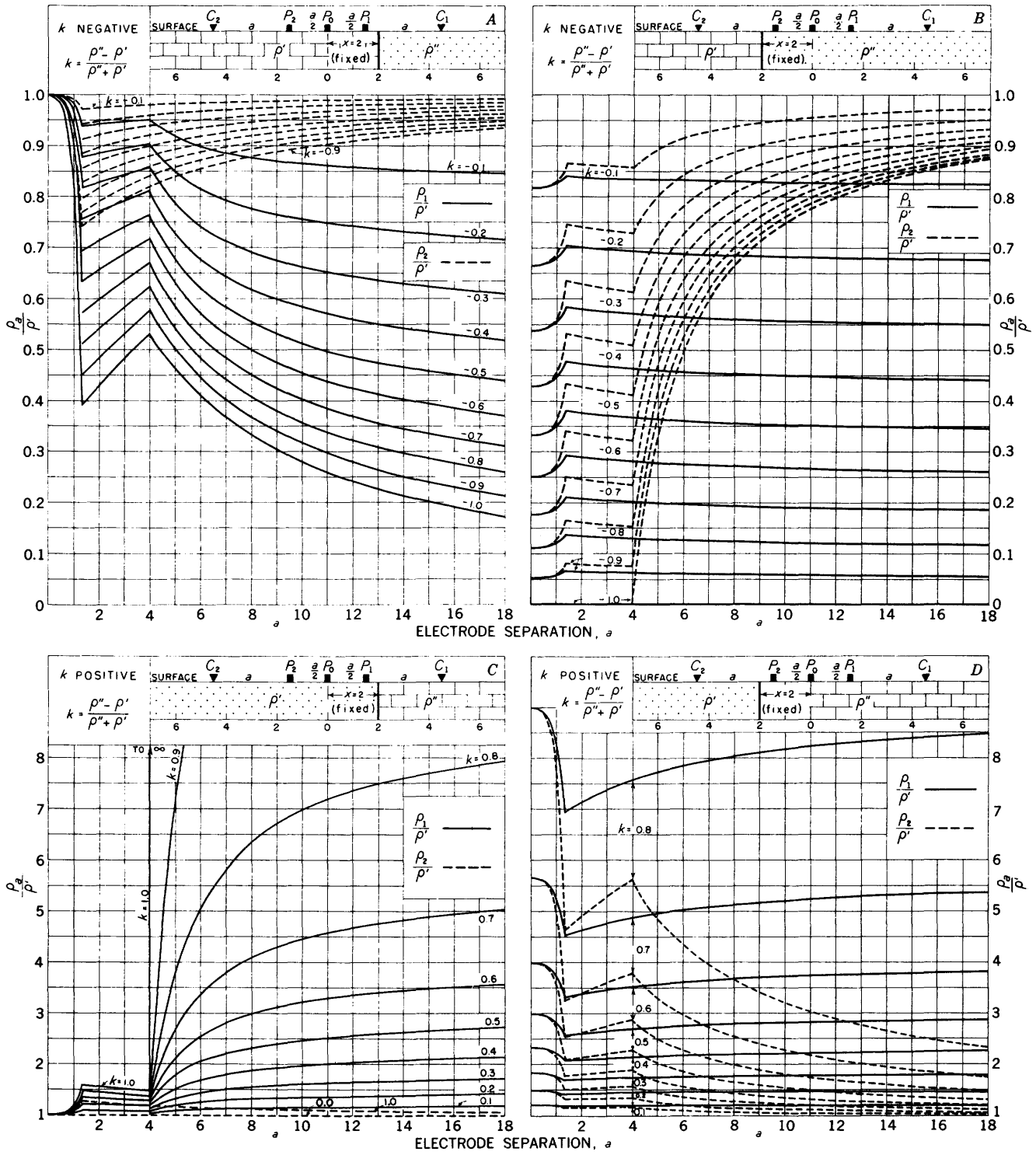
FIGURE 59.—Theoretical vertical resistivity profiles over an infinite vertical fault with center electrode P_0 a distance of 2 units from the fault, Lee configuration (offset plotting). Reflection factor k varies between +1.0 and −1.0.

Figure 59D can be used conveniently to obtain apparent-resistivity values at a station taken over the high-resistivity material lying on the right side of a fault. Here the ρ_2 curve shows two discontinuities in slope similar to the ρ_1 curve in figure 59A, and the ρ_1 curve shows a single discontinuity in slope similar to the ρ_2 curve in figure 59A.

For a station over the low-resistivity material at a point lying 2 units to the right of the fault plane (fig. 59B), the apparent resistivity for small electrode separations is essentially equal to the true resistivity ρ''. As the electrode configuration is expanded, leaving potential electrode P_0 fixed, the apparent resistivities ρ_1 and ρ_2 both increase, with ρ_2 increasing more than ρ_1, until current electrode C_2 crosses the fault trace, when a discontinuity in slope occurs in both curves. With increased expansion of the configuration, the apparent resistivity ρ_1 diminishes gradually and approaches asymptotically the value of the material on the right side of the fault. At the same time the apparent resistivity ρ_2 decreases, paradoxically, in spite of the fact that current electrode C_2 has entered the medium of higher true resistivity, until the point where potential electrode P_2 crosses the fault trace, at which point a sharp discontinuity in slope occurs in the ρ_2 curve. Further expansion of the configuration gives a sudden rise in apparent resistivity ρ_2, which increases continuously thereafter and approaches asymptotically the value of the true resistivity of the material on the left side of the fault.

Figure 59C can be used conveniently for a station taken over low-resistivity material on the left side of a fault. Here the ρ_1 curve shows two discontinuities in slope similar to the ρ_2 curve in figure 59B; and the ρ_2 curve, with its single discontinuity in slope, is similar to the ρ_1 curve for figure 59B.

Figures 59C and D represent an alternative method of plotting the same data in figures 59B and A, respectively, when ρ' and ρ'' are interchanged. Although the same concepts can be shown by using the two figures 59A and 59B only, it is found convenient in making field comparisons to have available the four complete sets of curves shown in figure 59.

The vertical resistivity profiles over perfectly conducting and insulating planes for both the Lee and Wenner configurations are identical to part of the apparent-resistivity curves for $k=\pm1$ in figure 59 for a vertical fault. In particular they are identical except for that part of the curves when one of the potential electrodes lies on the side of the fault opposite from that side containing the center of the whole configuration. The ρ_1/ρ' Lee curve for $k=+1.0$ in figure 59A, for example, gives also the correct apparent-resistivity
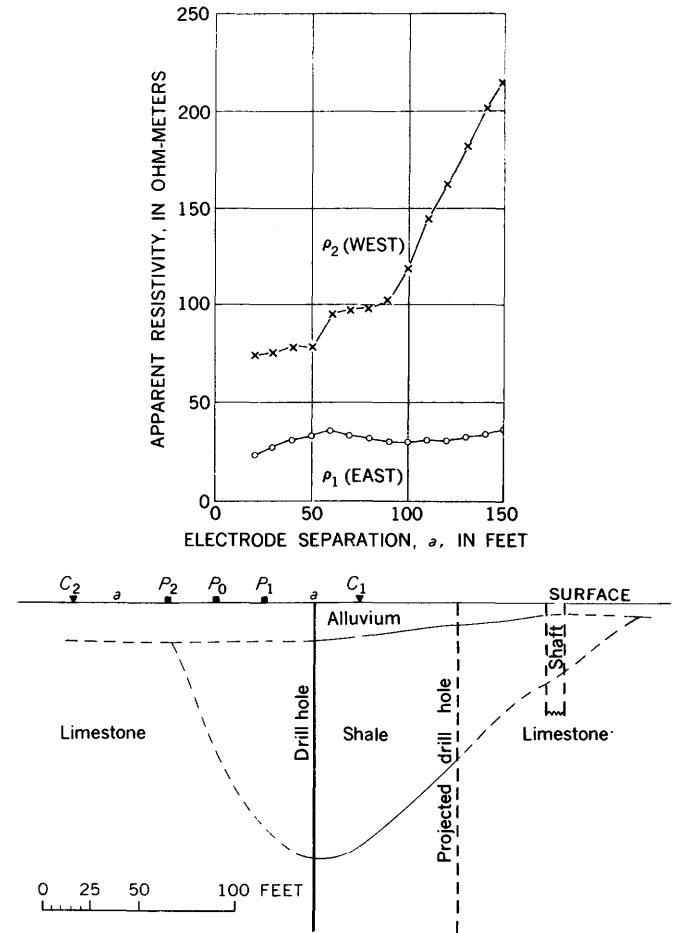
FIGURE 60.—Vertical resistivity profile for station near left edge of shale sink, Lee configuration. Tri-State mining district, Cherokee County, Kans. (Resistivity data and interpretations by K. L. Cook (1951–54); drill-hole data from Brichta and Ryan (1958).)

values for a vertical resistivity profile at a station lying 2 units to the left of a vertical perfectly conducting plane for electrode separations between $a=0$ and $a=4$ units. For larger values of a, the apparent resistivities can be readily calculated.

Figure 60 shows a fault-type vertical resistivity profile obtained near the left edge of a shale sink in the Tri-State lead-zinc mining district. Essentially all the observed effects are due to the steep limestone-shale contact at the left edge of the sink, as the right edge is too far away to affect greatly the apparent-resistivity values for small values of the electrode separation; the results, however, are tempered somewhat by the alluvium.

The abrupt change in slope of the ρ_2 curve at $a=50$ feet occurs as potential electrode P_2 crosses the inferred limestone-shale contact as shown in the geologic section. The location of the west edge of the shale, as inferred from this vertical profile, agrees well with its location as obtained independently from horizontal resistivity
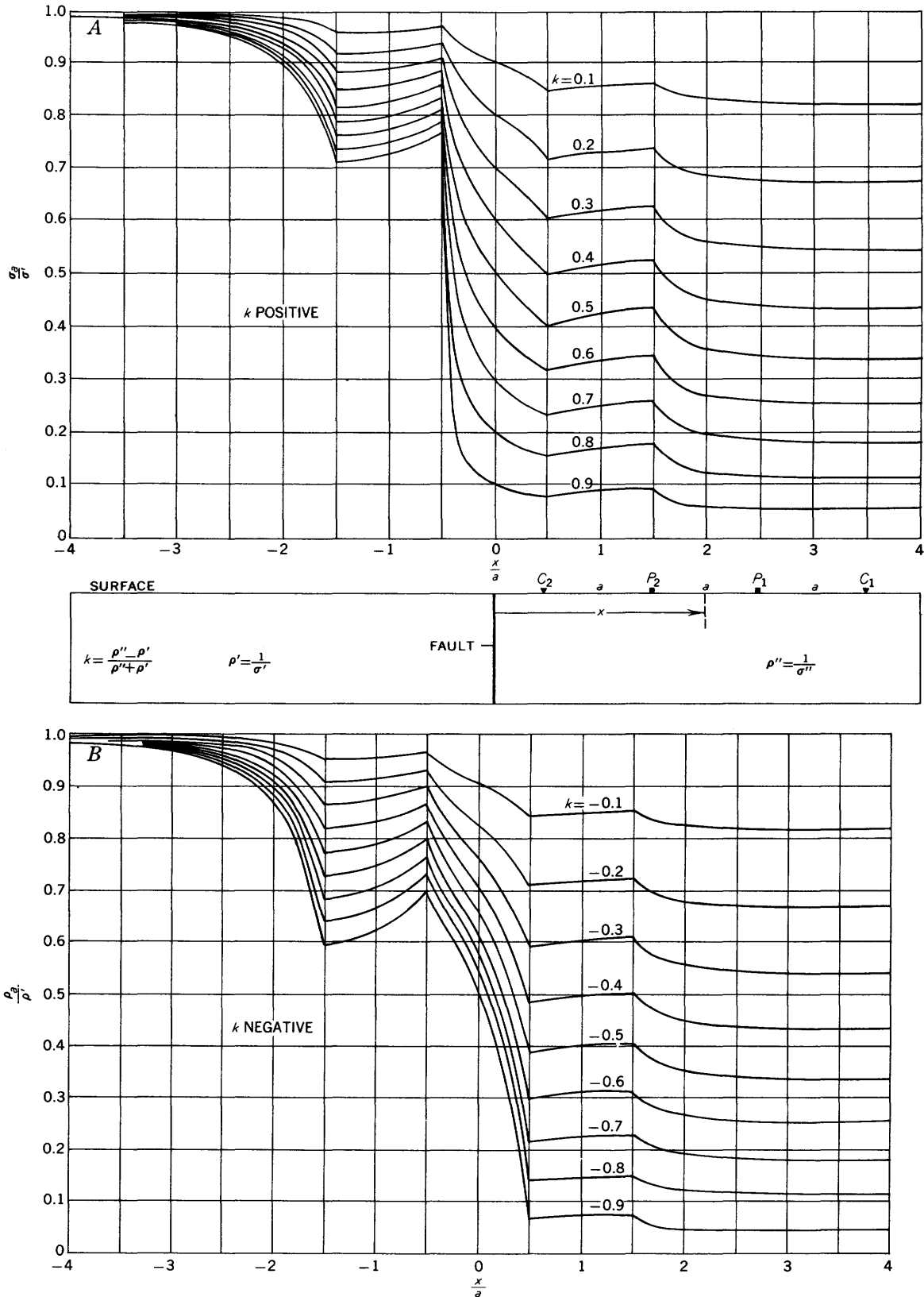
FIGURE 61.—Theoretical horizontal (A) conductivity and (B) resistivity profiles across a vertical fault, Wenner configuration. Traverse perpendicular to fault trace. Reflection factor k varies between (A) 0.1 and 0.9 and (B) −0.1 and −0.9. Adapted from Tagg (1930) by permission of Mining Magazine.

profiles. The cause of the second abrupt change in slope in the ρ_2 curve at $a=90$ feet is not known. The persistent low values of ρ_1 are in accord with the theoretical curves.

WENNER CONFIGURATION
HORIZONTAL PROFILES

Figure 61 (after Tagg, 1930) shows theoretical horizontal profiles across a vertical fault with the Wenner configuration along a traverse perpendicular to the fault trace. The values of k are taken at intervals of 0.1 for positive and negative values between -0.9 and $+0.9$. For positive values of k (fig. 61A), the ratio of the apparent conductivity σ_a to the true conductivity σ' of the material on the left side of the fault are plotted against x/a. For negative values of k (fig. 61B), the

FIGURE 62.—Comparison of observed and theoretical horizontal resistivity profiles across a vertical fault, Wenner configuration, with an electrode separation of (A) 15 meters and (B) 30 meters. Assumed reflection factor $k=-0.9$ and $\rho'=900$ ohmmeters. Adapted from Rothé and Rothé (1952).

ratio of the apparent resistivity ρ_a to the true resistivity ρ' of the material on the left side of the fault are plotted against x/a. A discontinuity in slope is obtained as each of the four electrodes cross the contact. As the configuration is moved from a medium of high resistivity on the left to one of low resistivity on the right (fig. 61B), the apparent resistivity increases paradoxically when the fault straddles electrodes C_1 and P_1.

For all resistivity contrasts, the principal diagnostic peak lies a distance of $a/2$ from the fault, and its value is always less than the true resistivity of the more resistive medium. If the apparent resistivity—rather than apparent conductivity—is always used, the fault lies this distance in a down-resistivity direction from the peak—that is, toward the lower resistivity medium.

Figure 62 shows field examples of observed horizontal resistivity profiles across a vertical fault with the Wenner configuration with electrode separations of 15 meters and 30 meters. The fault separates the Vosges Sandstone, of relatively high resistivity, from Oligocene marl, of relatively low resistivity. An observed pronounced peak lies northwest of the fault over the high-resistivity sandstone.

To compare the observed profiles with theoretical profiles, Rothé and Rothé (1952) computed theoretical horizontal resistivity profiles with the assumption that the reflection factor k is -0.9 and the true resistivity of the Vosges Sandstone is 900 ohm-meters. In making the comparison (fig. 62), Rothé and Rothé used a theoretical field plot with the assumption that the discrete station intervals were such that the electrodes in crossing the fault would lie vertically above the fault; and they then shifted their observed field curve correspondingly to obtain the best match between this particular field plot and the observed curve. They considered the match in figure 62B to be somewhat better than that in figure 62A, but still not entirely satisfactory. Our procedure of using several different theoretical field plots by trial and error as outlined in an earlier section would perhaps yield a slightly better match.

VERTICAL PROFILES

Figure 63 (after Tagg, 1930) shows theoretical vertical profiles across a vertical fault with the Wenner configuration along a traverse perpendicular to the fault trace. The values of k are taken at intervals of 0.1 for positive and negative values between -0.9 and $+0.9$. For positive values of k (fig. 63A), the ratio of the apparent conductivity σ_a to the true conductivity σ' of the material on the left side of the fault are plotted against a/x. For negative values of k (fig. 63B), the ratio of the apparent resistivity ρ_a to the true resistivity ρ' of the material on the left side of the fault are

FIGURE 63.—Theoretical vertical (A) conductivity and (B) resistivity profiles across a vertical fault, Wenner configuration. Reflection factor k varies between (A) 0.1 and 0.9 and (B) —0.1 and —0.9. Adapted from Tagg (1930) by permission of Mining Magazine.

plotted against a/x. A discontinuity in slope is obtained as the current and potential electrodes cross the contact.

For vertical resistivity profiles along traverses parallel to the trace of a vertical fault, families of theoretical curves are given by Tagg (1930) for values of k taken at intervals of 0.1 between -1.0 and $+1.0$. These curves indicate that the effect on the vertical profile is practically negligible when the distance of the configuration from the fault is four times the electrode separation. This fact can help serve as a guiding principle for profiles taken near the edge of a steep cliff for example.

LÖGN CONFIGURATION

The Lögn configuration (see p. 41) of electrodes uses potential electrodes sufficiently close together so that the measurement made is essentially the electric field or potential gradient at a point. The Schlumberger configuration is similar to the Lögn configuration in this respect, and thus its results should apply qualitatively to those expected from the Lögn configuration. In both configurations, the measurements made are fundamentally different from the measure-

FIGURE 64.—Horizontal resistivity profiles across vertical fault for different resistivity contrasts, Lögn configuration. Adapted from Lögn (1954).

ments of potential differences that are made with other electrode configurations such as the Wenner and Lee.

Figure 64 shows horizontal resistivity profiles with the Lögn configuration across a vertical fault for different resistivity contrasts (Lögn, 1954). The solid curves are for positive reflection factors and the dashed curves are for negative reflection factors. A discontinuity in the apparent-resistivity values occurs at the contact. In field practice discrete values are obtained; and an apparent-resistivity high or low occurs over the contact for a positive or negative reflection factor, respectively.

Figure 65. shows an observed horizontal resistivity profile across two vertical contacts in Meheia, near Kongsberg, Norway (Lögn, 1954). The three apparent-resistivity curves are drawn to an arbitrary scale for the three different fixed current-electrode locations, respectively, that are shown in the cross section. Here a great low-resistivity breccia zone about 230 meters in width lies between the younger Telemark Granite Gneiss on the west and the older Kongsberg-Bamle Granite Gneiss on the east. The pronounced peaks associated with the contacts were used to help trace the boundaries of the breccia, especially where the boundaries were covered with alluvium.

POTENTIAL-DROP-RATIO METHODS
LEE-HEMBERGER PLOTTING

We pointed out previously the analogy between the potential-drop-ratio method and the regular Lee configuration when the Lee-Hemberger plotting is used for the Lee data (Lee and Hemberger, 1946). Using the data for a vertical fault, we now investigate this problem in more detail to ascertain the best method of Lee-Hemberger plotting. In all these studies, only a horizontal profile will be considered. It is assumed that the configurations are moved from left to right and, in particular, from a medium of low resistivity ρ_A to one of higher resistivity ρ_B; the assumed resistivity contrast is $\rho_A/\rho_B=1/5$. It should be recalled that usually the different index numbers charted are obtained from the same data of potential differences and represent merely different ways of charting the ratios of the various combinations of potential differences or, actually, apparent resistivities. One of the main distinctions to observe is whether the data are plotted for a station interval of $a/2$, which is customary for the Lee configuration, or for a smaller station interval, such as $a/10$, which can be used for detailed investigations.

Figures 66 and 67 show the charts for the different index numbers. Although the charts are compiled to show specific comparisons of anomalies for station intervals of $a/2$ compared with station intervals of $a/10$,
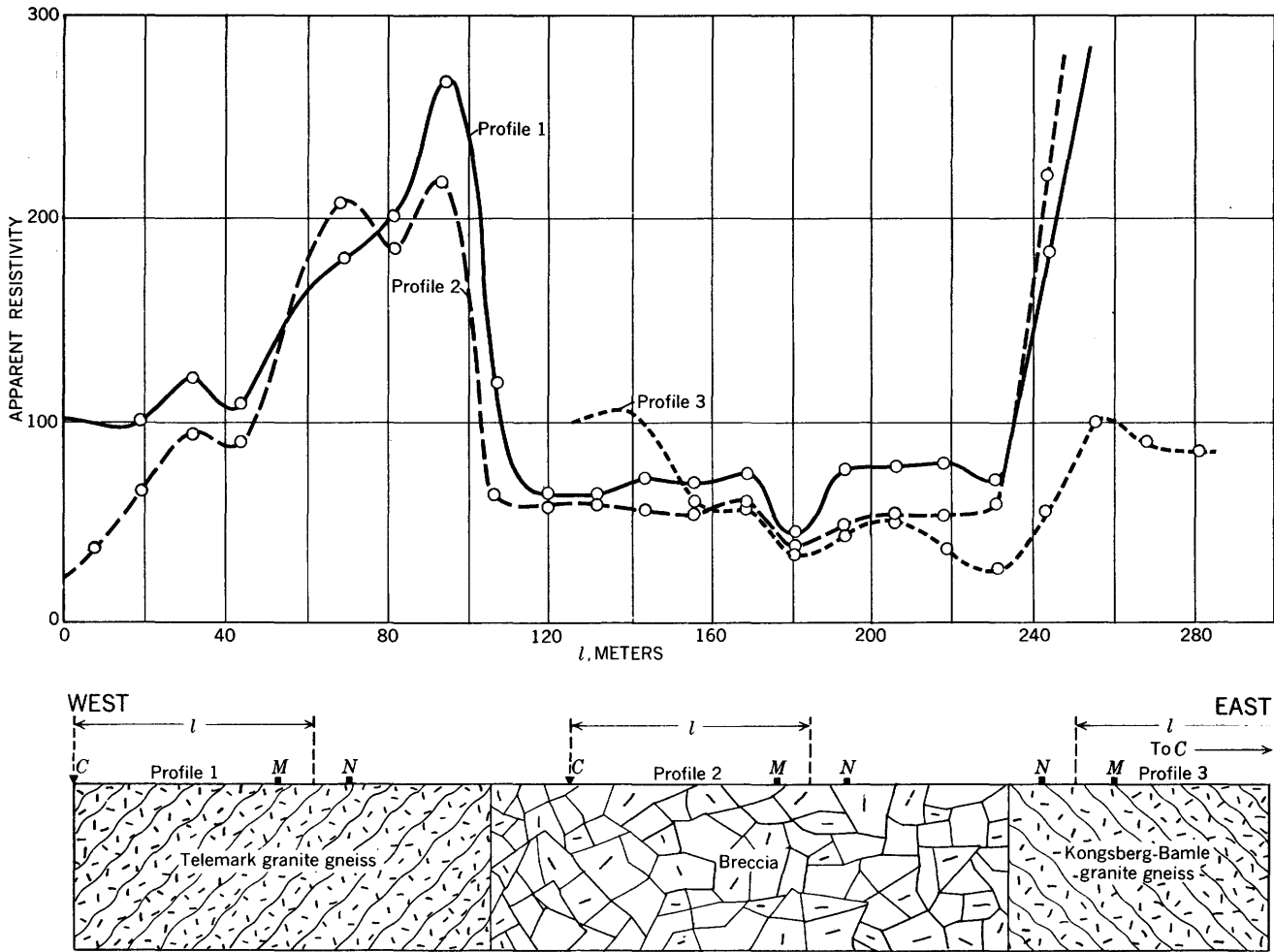
FIGURE 65.—Three observed horizontal resistivity profiles across two vertical contacts in Meheia, near Kongsberg, Norway, Lögn configuration. Adapted from Lögn (1954).

it is convenient to consider first all the index numbers charted for station intervals of $a/2$ in these two figures.

Figure 66A shows the "ratio of apparent resistivity over adjacent ground" (Lee and Hemberger, 1946), which is charted here as the ratio of ρ_1 to ρ_2 as these two quantities are measured at a given station (station interval of $a/2$). The value of this ratio, which is the "index number" in this case, is plotted at X, the position of the station. The index number reaches a maximum value of five at the fault trace, with a total relief of four; and this pronounced peak thus serves to indicate the position of the fault. It is shown below that this ratio yields the largest anomaly.

Figure 66C shows the "ratio of apparent resistivities over the same ground" (Lee and Hemberger, 1946), which is charted here as the ratio of ρ_1 for a given station to ρ_2' for the next station (station interval of $a/2$). The maximum index number, which is small, occurs as a minor peak.

Figure 67A shows the "ratio of apparent resistivity over adjacent ground in opposition to the traverse direction" (Lee and Hemberger, 1946), which is charted here as the ratio of ρ_2' for a given station to ρ_2 of the previous station (station interval of $a/2$). The index number attains a maximum value of about 3.4.

Figure 67B shows the "ratio of apparent resistivity over adjacent ground in the direction of traverse" (Lee and Hemberger, 1946), which is charted here as the ratio of ρ_1' for a given station to ρ_1 for the previous station (station interval of $a/2$). The index number attains a maximum value of about 3.6.

In detailed work, when the station intervals are made smaller than $a/2$, there are various ways of plotting the ratios of the apparent resistivities. In all the examples given, it is assumed that the station interval is $a/10$.
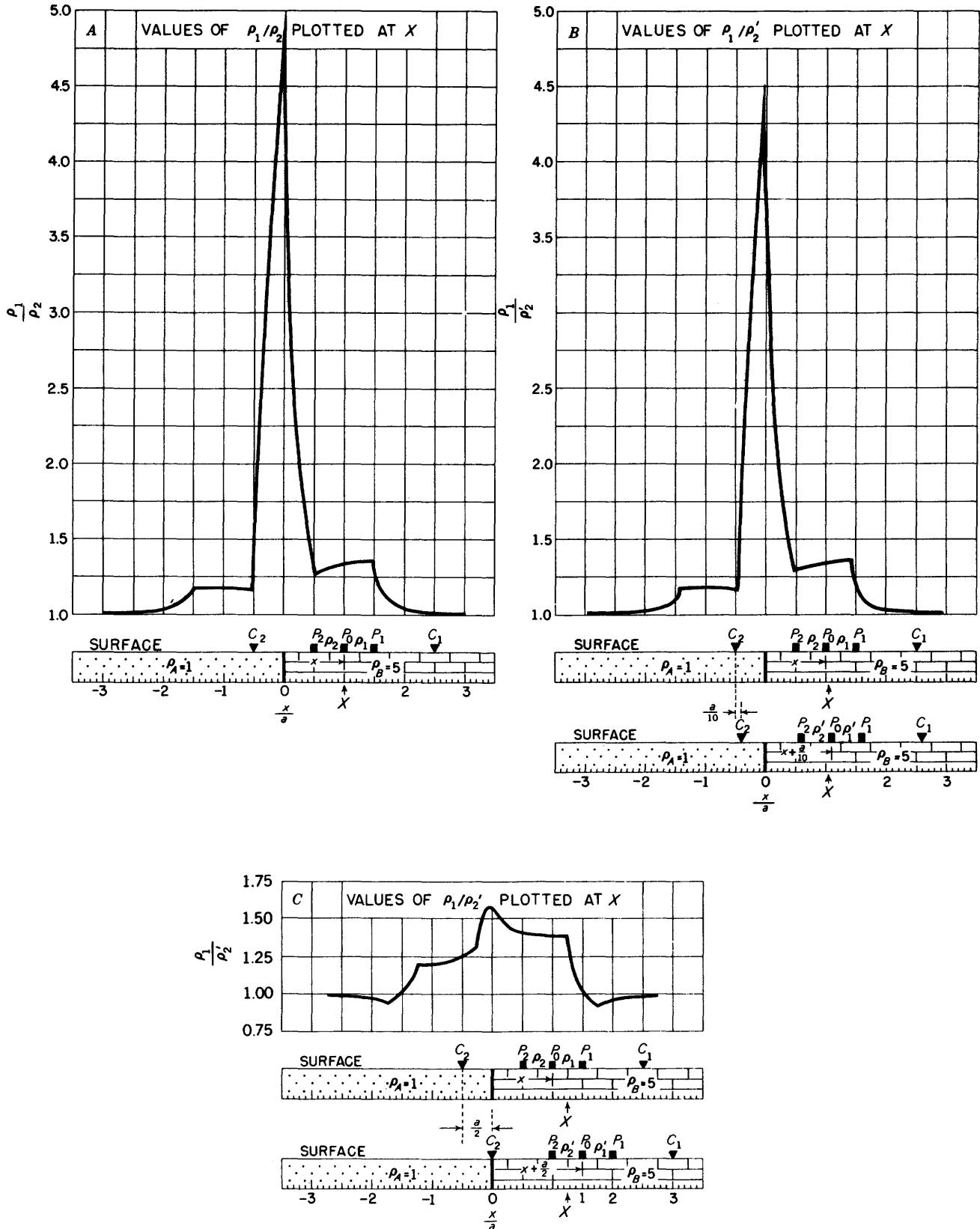
FIGURE 66.—Index numbers for Lee-Hemberger plotting of horizontal profiles across vertical fault, Lee configuration; ratios of apparent resistivity from both electrode pairs at the same or two successive stations. $\rho_A/\rho_B = 1/5$.
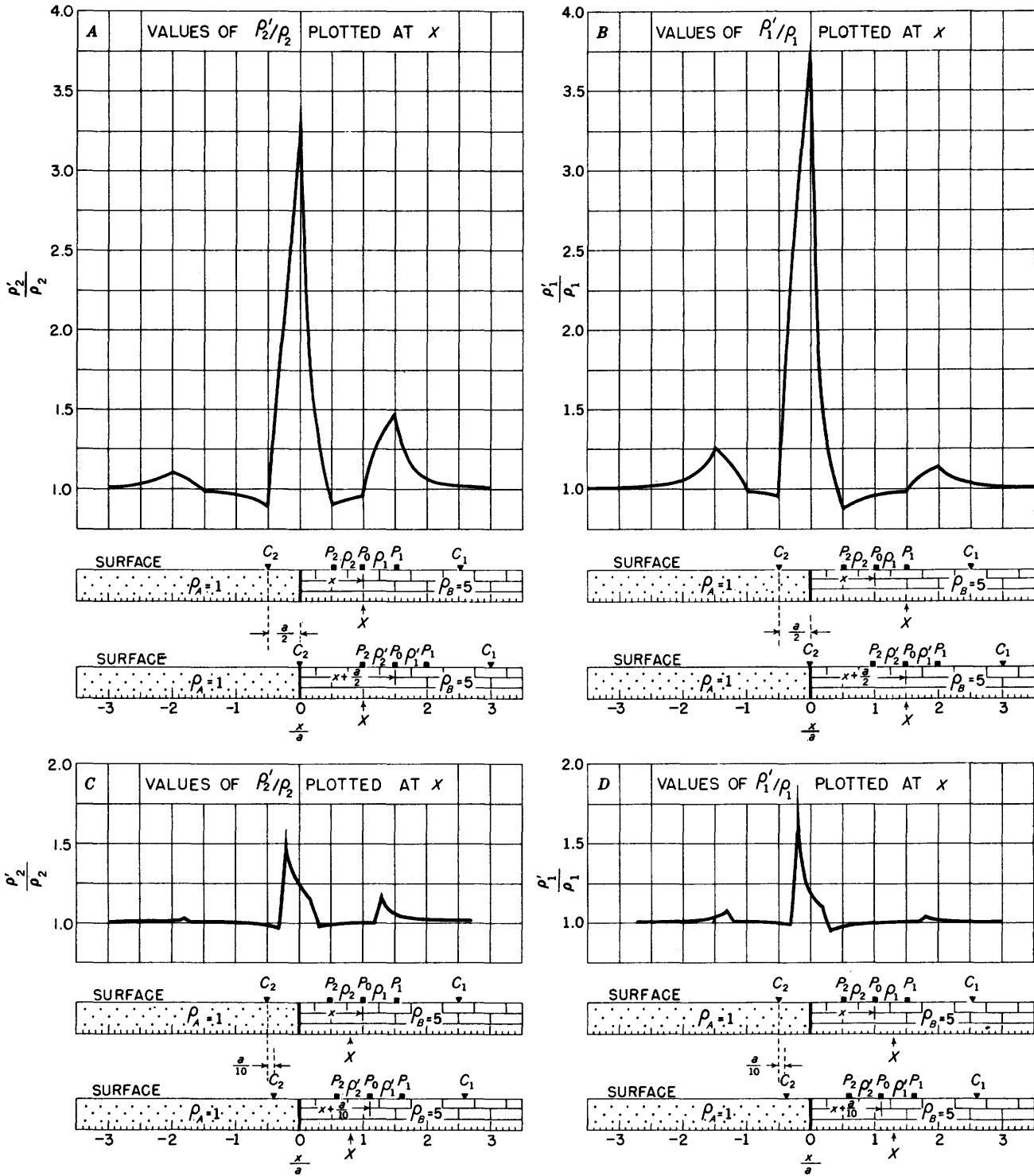
FIGURE 67.—Index numbers for Lee-Hemberger plotting of horizontal profiles across vertical fault, Lee configuration; ratios of apparent resistivity from the same electrode pairs at two successive stations. $\rho_A/\rho_B=1/5$.

Figure 67D shows the "ratio of apparent resistivity over adjacent ground with reduced overlap in the direction of traverse" (Lee and Hemberger, 1946), which is charted here as the ratio of ρ_1' for a given station to ρ_1 for the previous station (station interval of $a/10$). The maximum index number is small.

Figure 67C shows the "ratio of apparent resistivity over adjacent ground with reduced overlap in opposi-

tion to the traverse direction" (Lee and Hemberger, 1946), which is charted here as the ratio of ρ_2' for a given station to ρ_2 of the previous station (station interval of $a/10$). The maximum index number is small.

Another method of plotting, which was not mentioned by Lee and Hemberger (1946), is to chart the ratio of ρ_1 for a given station to ρ_2' for the next station, when a small station interval is used. Figure 66B shows the results of this method. The total relief of this anomaly is pronounced, though smaller than the anomaly obtained from the ratio of apparent resistivities over adjacent ground.

Of all these potential-drop-ratio methods of plotting with the Lee configuration, the ratio of apparent resistivities over adjacent ground, that is, the ratio of

ρ_1 to ρ_2 as measured at a given station (fig. 66A), yields a more pronounced anomaly than the other ratios considered; and this method is recommended as the best when these techniques of plotting ratios of apparent resistivities are used.

PLOTTING OF DIFFERENCES OF APPARENT RESISTIVITIES

Lee and Hemberger (1946, p. 12) also suggested the possibility of using the differences between ρ_1 and ρ_2 for the Lee configuration when horizontal profiling is used. The differences usually are found to be about as helpful as the resistivity ratios over adjacent ground. Figure 68 shows curves for various differences of apparent resistivities for Lee horizontal profiles across a vertical fault. All curves are for the same fault with a resistivity contrast $\rho_A/\rho_B=\frac{1}{5}$; and, as before, the meas-
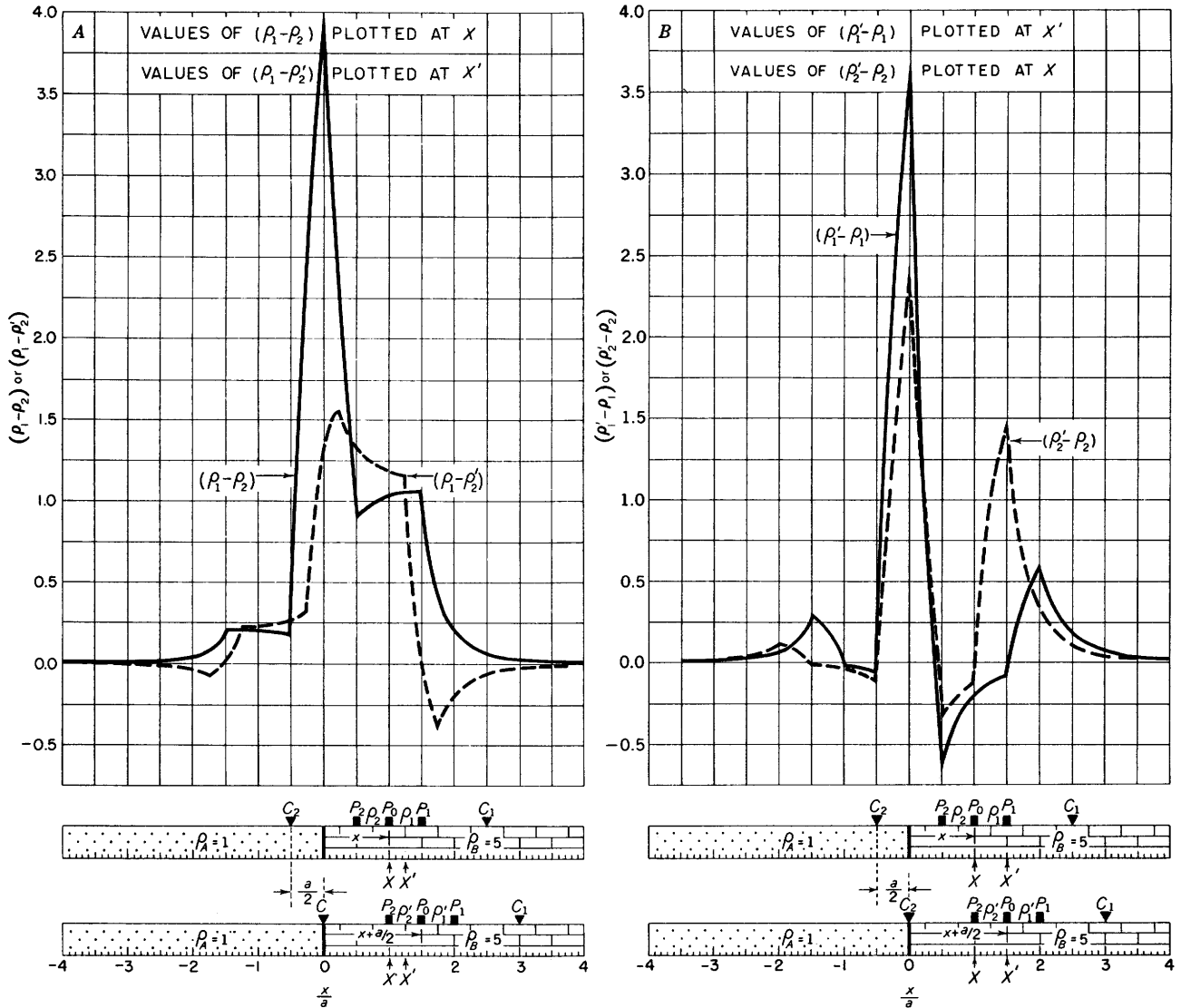
FIGURE 68.—Plotting of differences of apparent resistivities for horizontal profiles across vertical fault, Lee configuration. $\rho_A/\rho_B=1/5$.

urements are taken as the regular Lee configuration is moved in each case from left to right.

Figure 68A (solid curve) shows the difference between ρ_1 and ρ_2 for a given station, as suggested by Lee and Hemberger (1946). The difference attains a maximum value of four at the fault trace, with a total relief of four; and this pronounced peak thus serves to indicate the position of the fault. The anomaly is essentially identical on its left side but definitely less on its right side than the anomaly obtained over an identical fault using the ratio of apparent resistivities over adjacent ground; and on field data this difference method would be slightly inferior to the method of plotting ratios of apparent resistivities over adjacent ground.

The remaining curves in figure 68B show methods of taking differences in addition to that suggested by Lee and Hemberger. Except for the solid curve in figure 68A, which applies to continuous readings, all the curves in figure 68 are for station intervals of $a/2$. The dashed curve in figure 68A shows the difference between ρ_1 of a given station and ρ_2 of the next station. The solid curve in figure 68B shows the difference between ρ_1 of a given station and ρ_1 of the previous station. The dashed curve in figure 68B shows the difference between ρ_2 for a given station and ρ_2 of the previous station.

We summarize the method of plotting differences by stating that from a practical point of view, the plotting of the difference $\rho_1 - \rho_2$ for a given station will probably yield satisfactory results in detecting a vertical fault, but is slightly inferior to the method of plotting the ratio ρ_1/ρ_2 of apparent resistivities over adjacent ground.

ACCURACY OF DETECTION OF FAULT BY POTENTIAL-DROP-R ATIO METHODS

The Lee-Hemberger plotting of ratios of apparent resistivities or the plotting of differences of apparent resistivities inherently contain the same uncertainties of accurate detection of a vertical fault as the ordinary method of plotting apparent resistivities along a horizontal profile. The reason is that the data are taken at discrete points only.

Though either the Lee-Hemberger plotting or the plotting of differences of apparent resistivities brings out more sharply to the eye the existence of a lateral resistivity change by showing a pronounced peak, it should be emphasized that this manner of plotting fails to show the true resistivities on either side of the fault. In the ordinary method of plotting apparent resistivities, this feature is not sacrificed, and the abrupt change in apparent resistivity shows the experienced interpreter that an abrupt lateral resistivity change has occurred; and he then studies the finer features of the apparent-resistivity curves to detect the position of the fault within the accuracy of the data.

DIKES

The interpretation of resistivity data for vertical dikes is important for several reasons. First, the resistivity anomalies can be used to discover and delineate shallow dikes or dikelike features, provided the resistivity contrast is sufficiently great; these features include dikes, veins, and brecciated zones, all of which may be directly or indirectly related to mineral deposits. Secondly, a knowledge of the resistivity anomalies known to occur over dikes and dikelike features are helpful in recognizing and interpreting the lateral effects that often appear in the data for various types of surveys where depth estimates to horizontal layers are the chief objective. Thirdly, the theoretical resistivity anomalies that are obtained principally from surface measurements across dikes and brecciated zones can readily be converted to anomalies that would be obtained with the same configurations in a vertical well as the configurations cross horizontal formations.

In this section, we refer repeatedly to structures with vertical boundaries; but the conclusions apply equally well to structures with near-vertical boundaries. For all practical purposes, a boundary that is inclined as much as 30° from vertical would yield essentially the same results as the vertical boundaries that are assumed.

There is an equivalence, or near equivalence, between the resistivity anomalies over dikes and those over faults. A thorough understanding of the characteristics of anomalies over faults therefore greatly facilitates the interpretation of anomalies over dikes. For example, a wide dike causes an apparent-resistivity anomaly that is equivalent to two faults of reversed type. If either dike wall affects the profile near the other, the dike is narrow and the conclusions vary with the ratio of the dike width to the electrode separation.

THEORETICAL BACKGROUND

In the theory underlying electrical prospecting over dikes, we assume that a dike consists of a vertical slab of material, bounded by two parallel planes, and surrounded on both sides with a material whose resistivity is different from that of the dike itself (fig. 69). In order to make the solution as general as possible, we assume that the resistivity of the material on one side of the dike is different from that on the other side and that both differ from the resistivity of the dike material itself. In that way the solution also serves for problems in which two major zones of different resistivity are separated by a transition zone of a yet different resistivity. Examples are brecciated fault zones and metamorphosed zones.

If the dike assumes a horizontal position—strictly, a sill—it falls mathematically into the category of horizontal beds. If the dike is inclined, it falls mathematically into the category of dipping beds.

In the vertical-dike problem, we require a set of potential functions for each of three different cases—a set in which the current electrode is located in each of the three materials represented. The mathematics for the first case, when the current electrode is to the left of the dike, has already been given on pages 57 to 59, where we showed how to apply the set of general equations. If we compare figures 29 and 69, we can see immediately what must be done to make equations 145, 147, and 148 applicable to the present dike problem. Since the current in the previous problem emanated outward in all directions from the electrode and since the current in the present problem is restricted to a half space, the previous solutions will be valid if we simply change the previous factor $I\rho'/4\pi$ to the new factor $I\rho'/2\pi$. Thus, equations 145 can be converted into the potential functions in integral form where the current electrode lies to the left of the dike:

$$
\begin{cases}
U_{1A}=\dfrac{I\rho'}{2\pi}\left[\dfrac{1}{R}+k_{21}\displaystyle\int_0^\infty \dfrac{e^{-\lambda(2z_1-z)}J_0(\lambda r)}{1+k_{21}k_{32}e^{-2\lambda b}}\,d\lambda\right.\\
\qquad\qquad\left.+k_{32}\displaystyle\int_0^\infty \dfrac{e^{-\lambda(2z_2-z)}J_0(\lambda r)}{1+k_{21}k_{32}e^{-2\lambda b}}\,d\lambda\right]\\[2ex]
U_{2A}=\dfrac{I\rho'}{2\pi}\,(1+k_{21})\left[k_{32}\displaystyle\int_0^\infty \dfrac{e^{-\lambda(2z_2-z)}J_0(\lambda r)}{1+k_{21}k_{32}e^{-2\lambda b}}\,d\lambda\right.\\
\qquad\qquad\left.+\displaystyle\int_0^\infty \dfrac{e^{-\lambda z}J_0(\lambda r)}{1+k_{21}k_{32}e^{-2\lambda b}}\,d\lambda\right]\\[2ex]
U_{3A}=\dfrac{I\rho'}{2\pi}\,(1+k_{21})(1+k_{32})\displaystyle\int_0^\infty \dfrac{e^{-\lambda z}J_0(\lambda r)}{1+k_{21}k_{32}e^{-2\lambda b}}\,d\lambda.
\end{cases}\qquad(177)
$$

The same functions in series form are similarly converted from equations 147 and 148:

$$
\begin{cases}
U_{1A}=\dfrac{I\rho'}{2\pi}\left\{\dfrac{1}{R}+k_{21}\displaystyle\sum_{n=0}^\infty \dfrac{(k_{21}k_{23})^n}{\sqrt{(2nb+2z_1-z)^2+r^2}}\right.\\
\qquad\qquad\left.-k_{23}\displaystyle\sum_{n=0}^\infty \dfrac{(k_{21}k_{23})^n}{\sqrt{(2nb+2z_2-z)^2+r^2}}\right\}\\[2ex]
U_{2A}=\dfrac{I\rho'}{2\pi}(1+k_{21})\left\{\displaystyle\sum_{n=0}^\infty \dfrac{(k_{21}k_{23})^n}{\sqrt{2nb+z)^2+r^2}}\right.\\
\qquad\qquad\left.-k_{23}\displaystyle\sum_{n=0}^\infty \dfrac{(k_{21}k_{23})^n}{\sqrt{(2nb+2z_2-z)^2+r^2}}\right\}\\[2ex]
U_{3A}=\dfrac{I\rho'}{2\pi}(1+k_{21})(1-k_{23})\displaystyle\sum_{n=0}^\infty \dfrac{(k_{21}k_{23})^n}{\sqrt{(2nb+z)^2+r^2}}.
\end{cases}\qquad(178)
$$

Both z_1 and z_2 are positive numbers in equations 177 and 178.

The corresponding equations that are applicable when the current electrode lies within the second medium can also be derived from the same general considerations. Thus, we get

$$
\begin{cases}
U_{1B}=\dfrac{I\rho''}{2\pi}(1+k_{12})\left[\displaystyle\sum_{n=0}^\infty \dfrac{(k_{21}k_{23})^n}{\sqrt{(2nb-z)^2+r^2}}\right.\\
\qquad\qquad\left.-k_{23}\displaystyle\sum_{n=0}^\infty \dfrac{(k_{21}k_{23})^n}{\sqrt{(2nb+2z_2-z)^2+r^2}}\right]\\[2ex]
U_{2B}=\dfrac{I\rho''}{2\pi}\left[\dfrac{1}{R}+k_{21}k_{23}\displaystyle\sum_{n=0}^\infty \dfrac{(k_{21}k_{23})^n}{\sqrt{(2nb-2z_1+2z_2-z)^2+r^2}}\right.\\
\qquad\qquad-k_{23}\displaystyle\sum_{n=0}^\infty \dfrac{(k_{21}k_{23})^n}{\sqrt{(2nb+2z_2-z)^2+r^2}}\\
\qquad\qquad+k_{21}k_{23}\displaystyle\sum_{n=0}^\infty \dfrac{(k_{21}k_{23})^n}{\sqrt{(2nb-2z_1+2z_2+z)^2+r^2}}\\
\qquad\qquad\left.-k_{21}\displaystyle\sum_{n=0}^\infty \dfrac{(k_{21}k_{23})^n}{\sqrt{(2nb-2z_1+z)^2+r^2}}\right]\\[2ex]
U_{3B}=\dfrac{I\rho''}{2\pi}(1-k_{23})\left[\displaystyle\sum_{n=0}^\infty \dfrac{(k_{21}k_{23})^n}{\sqrt{(2nb+z)^2+r^2}}\right.\\
\qquad\qquad\left.-k_{21}\displaystyle\sum_{n=0}^\infty \dfrac{(k_{21}k_{23})^n}{\sqrt{(2nb-2z_1+z)^2+r^2}}\right].
\end{cases}\qquad(179)
$$
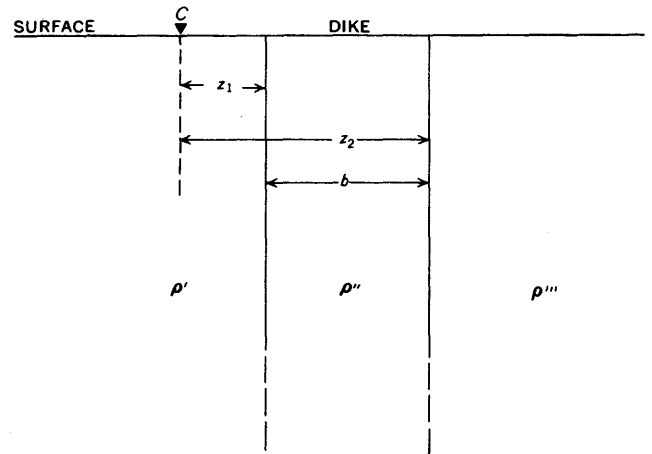
FIGURE 69.—Cross section showing a point source of current in the vicinity of a vertical dike bounded on either side by materials of different resistivities.

It is unnecessary to write down the corresponding equations when the current electrode is in medium three, because they could easily be obtained by simply reversing the conventions established for equations 178 above. For the sake of completeness, however, we include the third set of equations in the convention that has already been established. If the current

electrode lies within medium three (fig. 69), the potential functions are

$$U_{1c} = \frac{I\rho'''}{2\pi}(1+k_{21})(1+k_{23}) \sum_{n=0}^{\infty} \frac{(k_{21}k_{23})^n}{\sqrt{(2nb-z)^2+r^2}}$$

$$U_{2c} = \frac{I\rho'''}{2\pi}(1+k_{23}) \left[\sum_{n=0}^{\infty} \frac{(k_{21}k_{23})^n}{\sqrt{(2nb-z)^2+r^2}} \right.$$

$$\left. -k_{21} \sum_{n=0}^{\infty} \frac{(k_{21}k_{23})^n}{\sqrt{(2nb-2z_1+z)^2+r^2}} \right]$$

$$U_{3c} = \frac{I\rho'''}{2\pi} \left[\frac{1}{R} + k_{23} \sum_{n=0}^{\infty} \frac{(k_{21}k_{23})^n}{\sqrt{(2nb-2z_2+z)^2+r^2}} \right.$$

$$\left. -k_{21} \sum_{n=0}^{\infty} \frac{(k_{21}k_{23})^n}{\sqrt{(2nb-2z_1+z)^2+r^2}} \right]. \quad (180)$$

In establishing equations 179, we maintain the convention established in figure 69, namely that the z-axis is positive to the right of the current electrode and negative to the left. This convention requires that z_1 is actually a negative number because the boundary between mediums one and two is now to the left of the current electrode; z_2 is a positive number. In equations 180, both z_1 and z_2 are negative numbers because both boundaries are to the left of the current electrode.

The above equations are most commonly used for problems in which all the electrodes are on the surface of the ground along the z-axis. The equations are then considerably simplified because r is zero, and the square roots are eliminated from the denominators of all terms.

The above equations can be simplified for certain special problems. For the vertical dike, ρ' equals ρ''' in figure 69, and all of the equations are simplified by letting $k_{21}=k_{23}=k$. The situation in figure 69 reduces to a simple fault if ρ'' equals ρ'''. Then, $k_{21}=k$ and $k_{23}=0$, in which case the equations simplify to those given in a previous section for a simple fault.

In many cases the above functions, or preferably the resistivity functions themselves, can be reduced in complexity by appropriate approximations. For example, Lögn (1954) derived and evaluated approximation formulas for a thin vertical sheet; he found them to be of sufficient accuracy for most cases in the field. On the basis of these approximation formulas, he found that the apparent resistivity with the Lögn configuration across a conducting sheet is determined by the product of the conductivity and the thickness of the sheet; and the apparent resistivity with the Lögn configuration across an insulating sheet is determined by the product of the resistivity and the thickness of the sheet.

A brecciated zone of assumed uniform resistivity can be treated theoretically like a dike. A brecciated zone that lies in country rock whose resistivity is the same on either side of the zone can be treated as a dike of resistivity ρ'' in an otherwise uniform country rock of resistivity ρ' on either side of the dike; this problem is discussed later. A brecciated zone that lies along the contact of two media of unlike resistivity, however, is identical to the problem of a dike that lies similarly between two unlike media. This problem, which will be covered in this section, is more complicated numerically because there is no symmetry of the complete curves about the axis of the brecciated zone.

The brecciated zone is of practical importance in mining areas where a fault gouge or mineralized zone occurs along the fault zone or contact zone between two media of different resistivity.

Figure 70 shows the horizontal resistivity profiles with the Lee configuration across a brecciated zone of width $a/2$ for different resistivities of the brecciated zone. The ratio of the true resistivity ρ' of the country rock at the left of the brecciated zone to the true resistivity ρ''' of the country rock at the right of the brecciated zone is fixed at $1:5$ in all the diagrams. In terms of ρ' taken as unity, the assumed true resistivities of the brecciated zone are ∞, 10, 4, 3, 2, and 0. The apparent resistivity is plotted as the ratio of the apparent resistivity to the true resistivity of the material at the left of the brecciated zone.

For a perfectly insulating brecciated zone (fig. 70A), pronounced apparent-resistivity peaks in the ρ_1 and ρ_2 curves lie vertically over the axis of the zone. The height of the peak depends upon the resistivity of the country rock on either side of the zone and the width of the brecciated zone in terms of the electrode separation.

For a brecciated zone with a finite resistivity that is greater than the resistivity of the high-resistivity material to the right of the zone (fig. 70B), peaks in the ρ_1 and ρ_2 curves are obtained vertically over the axis of the zone. If the resistivity of the brecciated zone in the present example is 5 units, which is equal to the resistivity of the country rock to the right, the peak in the ρ_1 curve becomes equal to 5 and a typical single fault curve is obtained (not shown in fig. 70); and the peak lies a distance of $a/4$ to the right of the left edge of the brecciated zone.
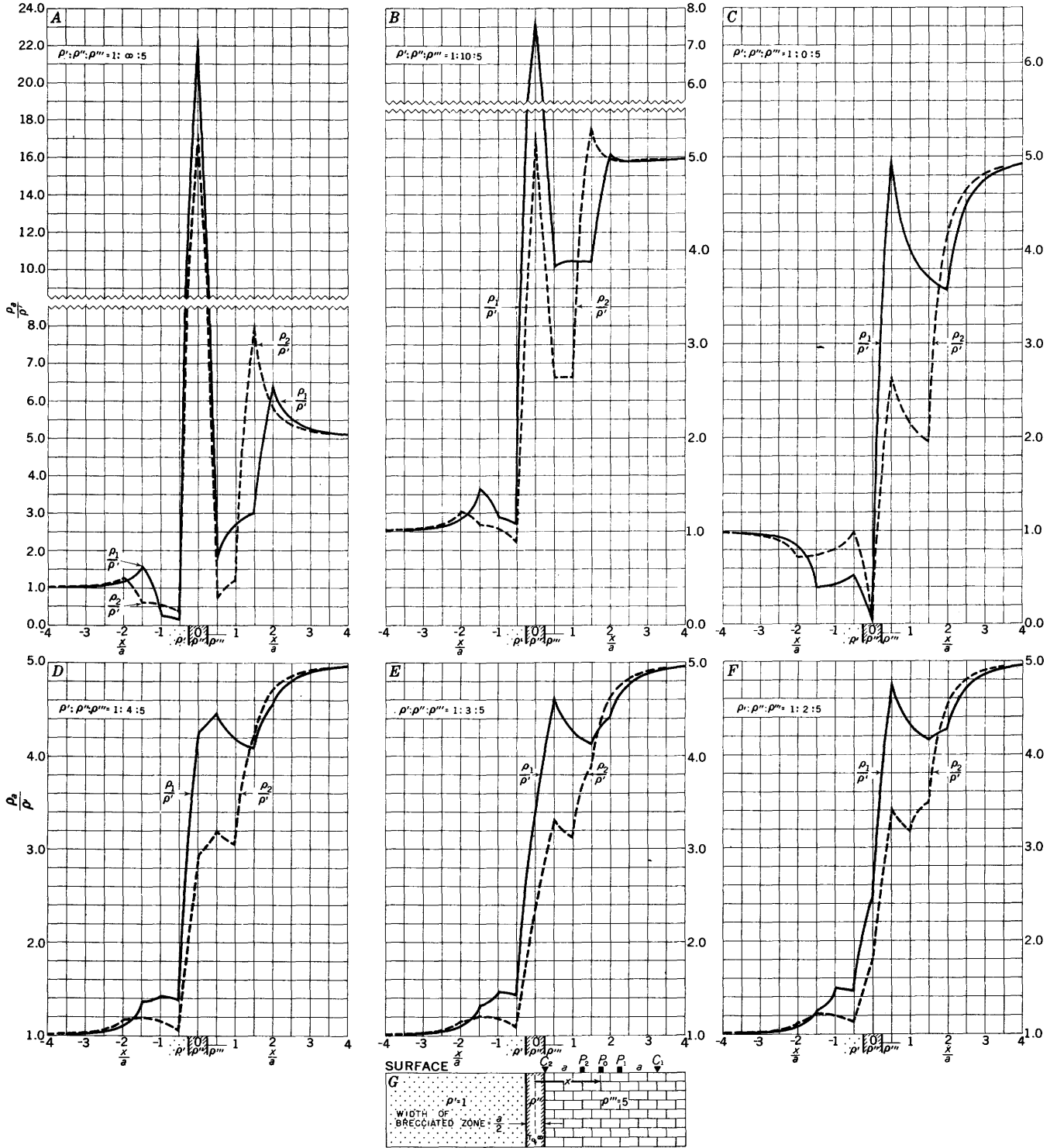
FIGURE 70.—Horizontal resistivity profiles across brecciated zone of different resistivities, Lee configuration (offset plotting).   For all diagrams $\rho'/\rho'''=1:5$ and width is $a/2$.

For a brecciated zone with a resistivity less than 5 units (figs. 70C, D, E, and F), a peak is obtained in both the ρ_1 and ρ_2 curves at a distance of $a/4$ to the right of the right edge of the zone.   Except for additional minor discontinuities in slope, the general shape of all these curves is similar to those over a single fault,   As the resistivity of the brecciated zone decreases, the height of the ρ_1 peak increases.   For a perfectly conducting brecciated zone (fig. 70C), the value of ρ_1 at the peak is equal to the true resistivity of the country rock at the

right of the zone; and the values of ρ_1 and ρ_2 are zero over the axis of the zone.

The theoretical curves indicate that under ordinary field conditions a conducting brecciated zone of width $a/2$ would probably not be detected if it occurred at the contact of two media with a resistivity ratio of $1:5$; and a high-resistivity brecciated zone would be detected only if its resistivity is considerably greater than the higher resistivity country rock on one of its sides. The effect of the low-resistivity breccia apparently subdues the peaks on the low-resistivity side of the fault and thus interferes with the exact determination of the location of the fault trace.

Figure 71 shows the corresponding horizontal resistivity profiles across the same brecciated zone with the Wenner configuration; the resistivity contrasts are identical to those in the previous examples. Because the apparent-resistivity values are plotted at the locations of the stations, no abrupt discontinuities in slope are observed over the axis of the brecciated zone. In general the anomalies are not as pronounced for the Wenner configuration as for the Lee configuration.

For a brecciated zone of infinite resistivity (fig. 71A), a recognizable anomaly is obtained with the Wenner configuration. For a brecciated zone whose true resistivity is 10 units (fig. 71B), the value of the peak
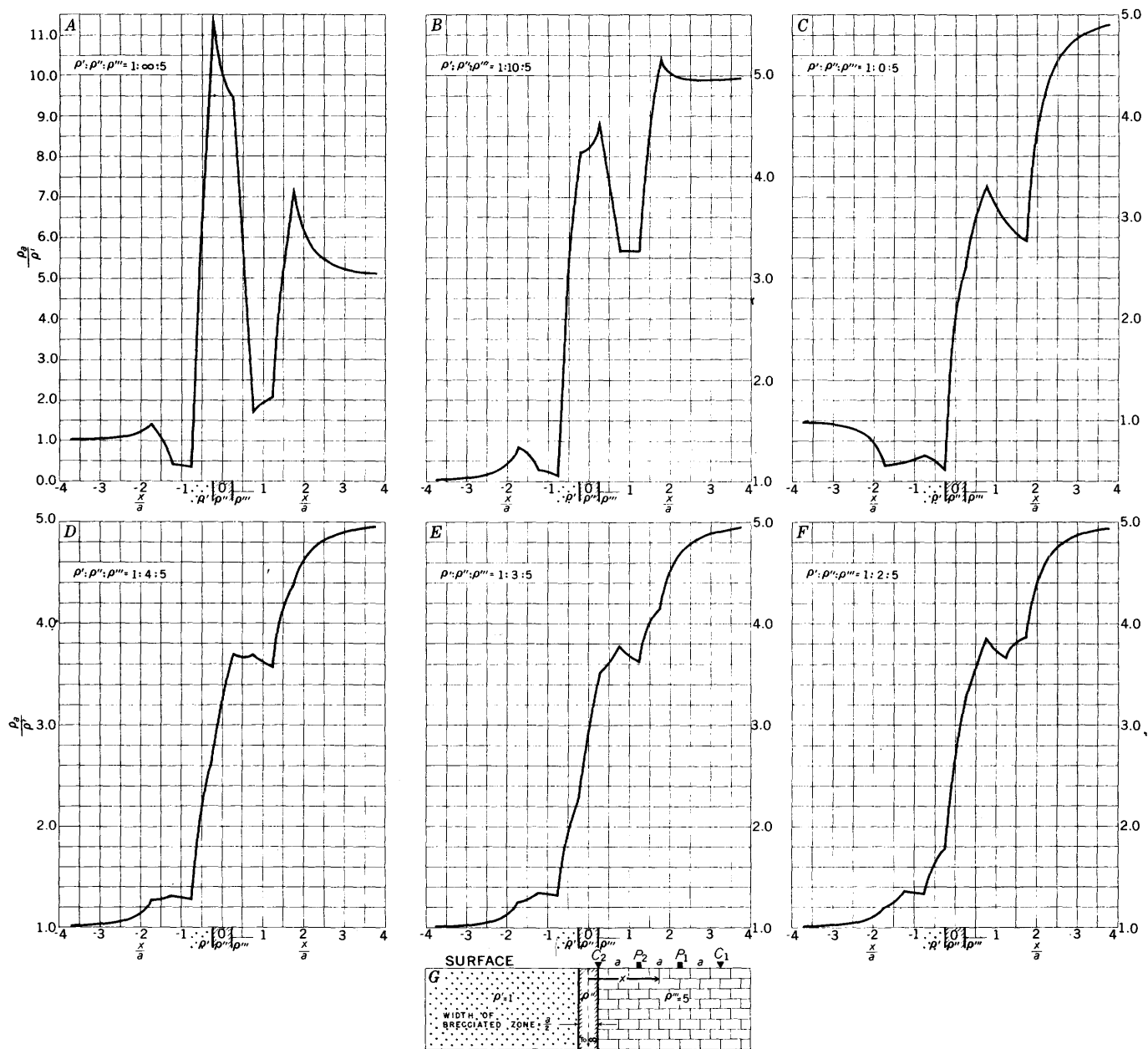
FIGURE 71.—Horizontal resistivity profiles across brecciated zone of different resistivities, Wenner configuration. For all diagrams $\rho'/\rho''' = 1/5$ and width is $a/2$.

over the right edge of the brecciated zone is less than the true resistivity of the medium to the right of the brecciated zone (5 units); this feature was not so for the Lee configuration. For brecciated zones with small resistivity (figs. 71 *C*, *E*, and *F*), the peak shifts to the right so that instead of occurring at the right edge of the brecciated zone (fig. 71*D*), it occurs a distance of $a/2$ to the right of the right edge of the brecciated zone. These peaks are similar to those obtained over a single fault; and it would be difficult to recognize in the field data in such cases any evidence of the brecciated zone as such; the additional minor discontinuities in slope are not sufficiently pronounced to be recognized in ordinary field data. The generalizations concerning the detectability of a brecciated zone, given above for the Lee configuration, apply also to the Wenner configuration.

Figures 72, 73, 74, and 75 show horizontal resistivity profiles with the Lögn configuration across thin vertical brecciated zones of different widths and resistivity contrasts (Lögn, 1954). In figures 72 and 73, the resistivity ρ'' of the country rock on the right is varied, and the other factors are held constant; the ratio ρ'/ρ''' is small ($\rho'/\rho'''=10$) in the former diagram and large

FIGURE 73.—Horizontal resistivity profiles across thin vertical brecciated zone of thickness $b=1$, Lögn configuration. ρ'' variable; $\rho'/\rho'''= 1,000$; $c=100$. Adapted from Lögn (1954).

FIGURE 72.—Horizontal resistivity profiles across thin vertical brecciated zone of thickness $b=1$, Lögn configuration. ρ'' variable; $\rho'/\rho'''=10$; $c=100$. Adapted from Lögn (1954).

($\rho'/\rho'''=1,000$) in the latter. In figures 74 and 75, the thickness b of the brecciated zone is varied; the resistivities are such that $\rho'=\rho''$ in both figures, and $\rho'/\rho'''=1,000$ in the former and $\rho'/\rho'''=1/1,000$ in the latter. The curves are discontinuous. Because of the small thickness of the vertical sheet, the true relationships are not shown in the curves as drawn. The apparent resistivities across the country rock on the right side of the brecciated zone are in all evaluated cases nearly zero, and the resistivity curves have two points of discontinuity, one at $l=c$, and the other at $l=c+b$. Figure 73 shows a "saturation" effect similar to that in the single fault problem, where the anomalies are not proportional to the resistivity variations. Figure 74 shows a similar saturation effect with respect to variation in the thickness of the sheet; the anomalies here are not proportional to the thickness of the sheet. Thus there is a resistivity saturation effect and a thickness saturation effect. Because of this feature, the Lögn configuration—according to Lögn—is very sensitive to small resistivity differences and to small thicknesses of brecciated zone. Each curve in figure 75 really has two discontinuity points, but these do not
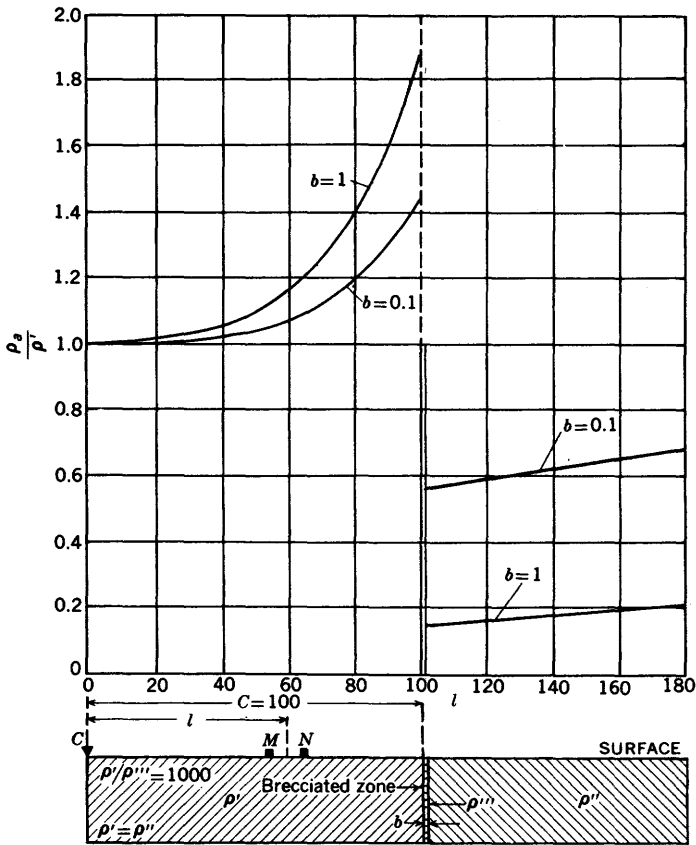
FIGURE 74.—Horizontal resistivity profiles across thin vertical conducting brecciated zone, Lögn configuration. Thickness b variable; $\rho'/\rho'''=1,000$; $\rho'=\rho''$; $c=100$. Adapted from Lögn (1954).
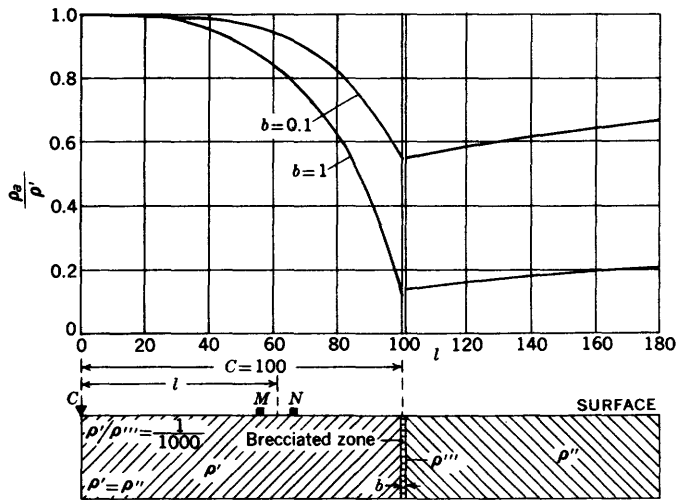
FIGURE 75. -Horizontal resistivity profiles across thin vertical insulating brecciated zone, Lögn configuration. Thickness b variable; $\rho'/\rho'''=1/1,000$; $\rho'=\rho''$; $c=100$. Adapted from Lögn (1954).

appear in the figure. The apparent resistivity in the insulating sheet is high; it almost reaches the value of $2\rho'$ (Lögn, 1954).

In the field the brecciated zone and the rocks on either side of it are generally covered with overburden. If this overburden has a resistivity of the same order of magnitude as the rocks, it has only a small influence on the current distribution and gives rise to small differences in the resistivity curves. Laboratory measurements made by Lögn on model sheets with their upper limits at a selected depth below the surface have shown that in these cases the resistivity curves are continuous curves with a maximum nearly coincident with the front of the sheet and a more indistinct minimum behind the sheet.

VERTICAL DIKES

The theoretical horizontal resistivity profile obtained over a vertical dike in homogeneous country rock of the same resistivity on either side of the dike depends not only upon the resistivity contrast between the dike and the country rock, but also upon the width of the dike. In this section we will study both Lee and Wenner horizontal profiles for various widths of the dikes in relation to the electrode separation. Usually, apparent-resistivity curves for both the Lee and Wenner configurations are given for reflection factors of ± 1.0, ± 0.8, ± 0.6, ± 0.4, and ± 0.2. The families of curves for positive values of the reflection factor are usually charted separately from those for negative values of the reflection factor. Many paradoxes occur, but space permits our pointing out only the most important features on the curves.

For positive reflection factors, the horizontal resistivity profiles across a dike of width $2a$ (figs. 76 and 77) show an apparent-resistivity peak within each of the edges of the dike and a paradoxical minimum zone in the region between the peaks; the bulk of the anomaly, however, has high-resistivity values over the central region above the dike. These features occur for both the Lee and Wenner configurations.

For the Lee configuration (fig. 76), the ρ_1 and ρ_2 curves cross at a point lying vertically above the axis of the dike; this property is always true for the subsequent Lee horizontal profiles across vertical dikes. For the Lee configuration, a peak in the ρ_1 curve lies a distance of $a/4$ inward from the left edge of the dike and is therefore similar to the ρ_1 peak found over the high-resistivity material when it lies to the right of a vertical fault. The apparent resistivity value of the ρ_1 peak for a dike of width $2a$ is somewhat lower, however, than that of the ρ_1 peak for a vertical fault for the same resistivity contrast because the low resistivity of the country rock on the other side of the dike manifests itself. For positive reflection factors of 0.8, 0.6, 0.4, and 0.2, for example, the values of the apparent resistivities for the ρ_1 peak are approximately 7, 3.4, 2.1,
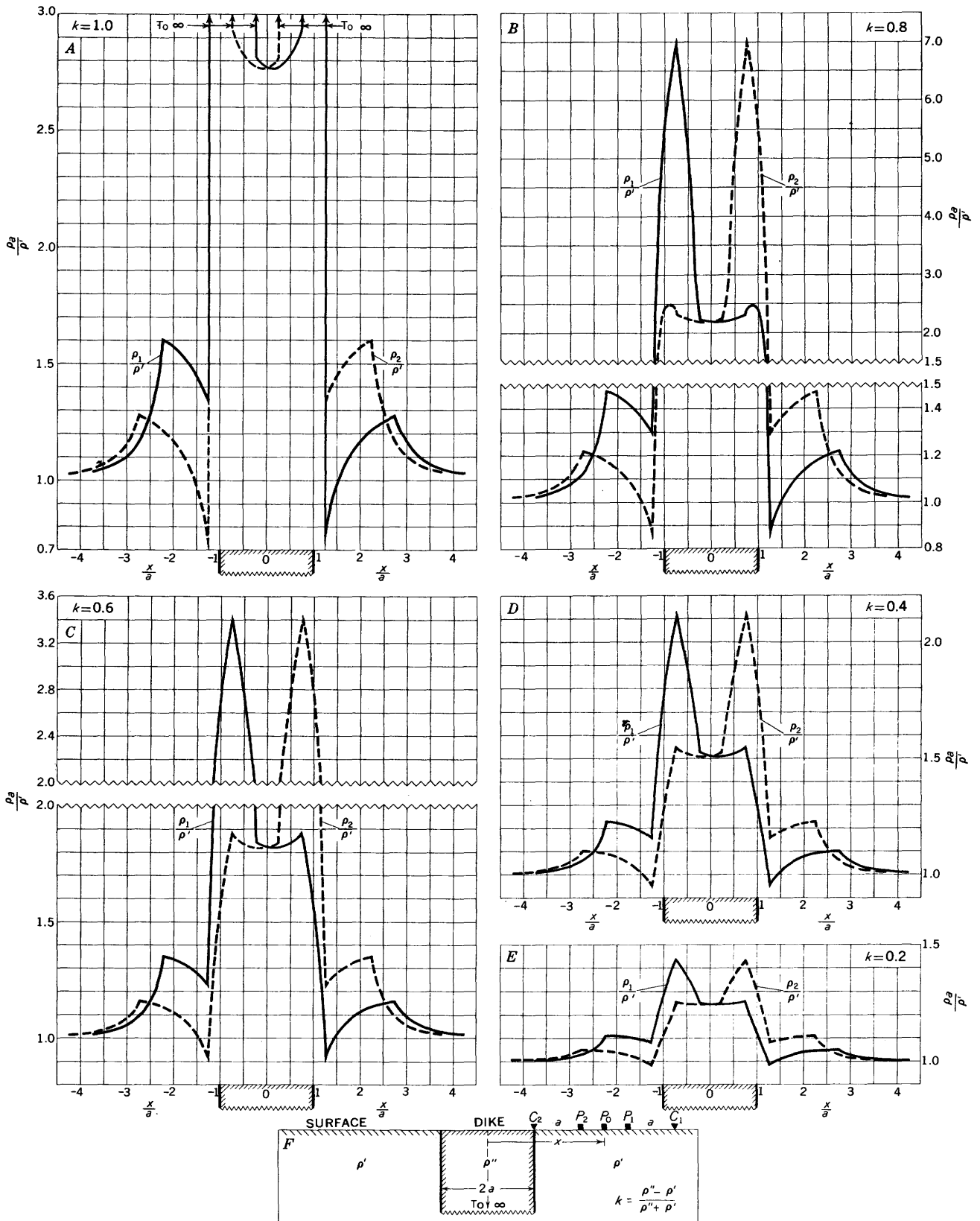
FIGURE 76.—Horizontal resistivity profiles across a vertical dike of width $2a$, Lee configuration (offset plotting); reflection factor $k=1.0$, 0.8, 0.6, 0.4, and 0.2.
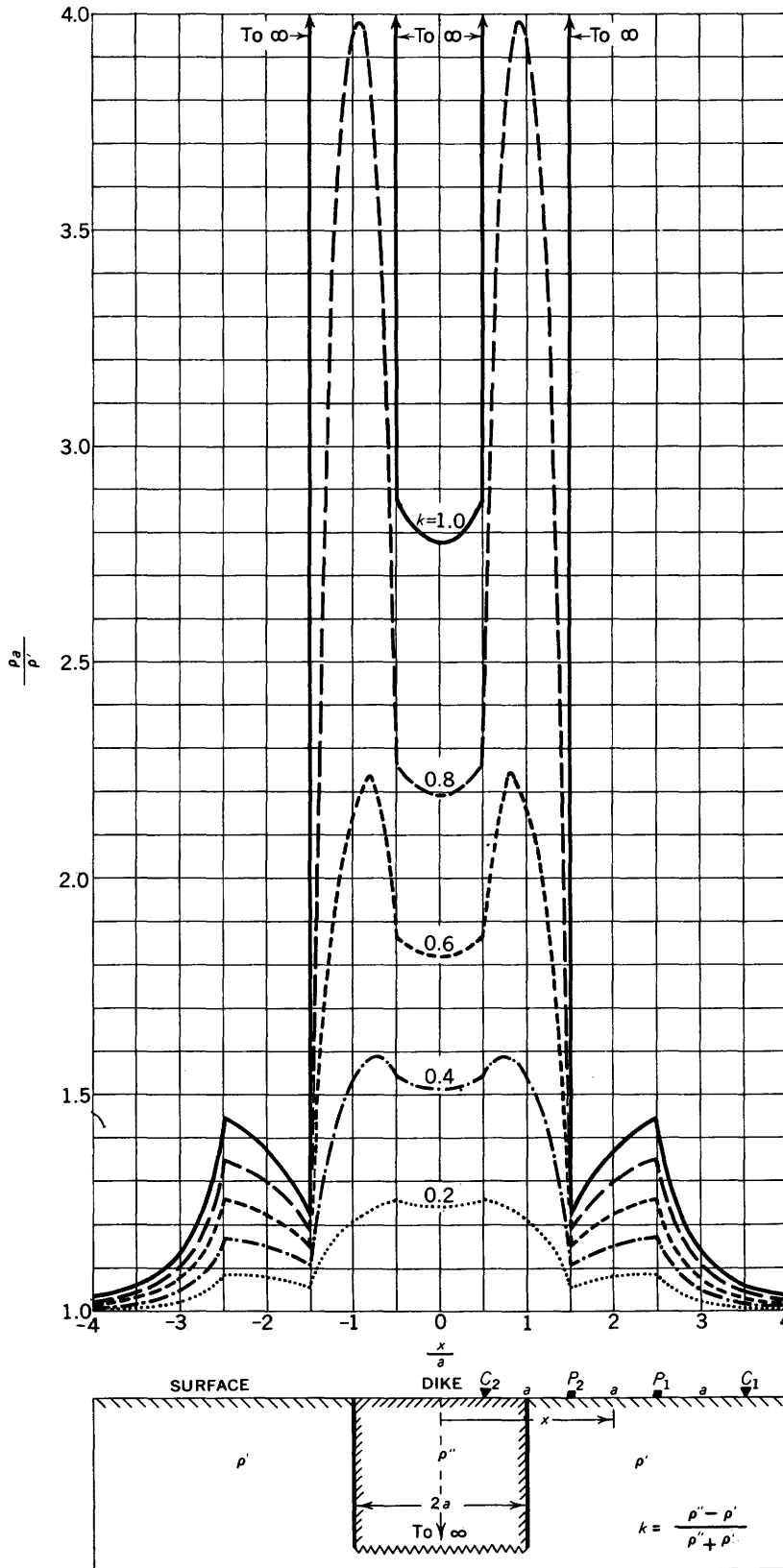
FIGURE 77.—Horizontal resistivity profiles across a vertical dike of width $2a$, Wenner configuration; reflection factor $k=1.0$, 0.8, 0.6, 0.4, and 0.2.

and 1.4 (fig. 76), respectively, for the dike and 9, 4, 2.3, and 1.5 (pl. 1), respectively, for a vertical fault. For the Lee configuration, similar reasoning can be applied to the corresponding peak in the ρ_2 curve, which lies a distance of $a/4$ inward from the right edge of the dike. It should be emphasized that for a dike of width $2a$, the ρ_1 peak near the left edge of the dike is accompanied by an insignificant peak in the ρ_2 curve at the corresponding horizontal location; and the ρ_2 peak near the right edge of the dike is similarly accompanied by an insignificant ρ_1 peak. For the continuous curve, the horizontal distance between the ρ_1 and ρ_2 peaks is equal to the width of the dike minus $a/2$. For the field curves for which stations are taken at discrete intervals, however, this width rule contains an inherent uncertainty that depends upon the station interval taken.

For the Wenner configuration (fig. 77), the horizontal position of the apparent-resistivity twin peaks shift toward the center of the dike for smaller resistivity contrasts. There is also a small but important peak that lies on either side of the main anomaly. For the continuous profile, the distance between these outer two peaks is equal to the width of the dike plus $3a$. Without knowledge of these major twin peaks for a single dike for both the Lee and Wenner configurations, they might be erroneously misinterpreted as being caused by two separate dikes; also the subsidiary peaks might be erroneously interpreted as separate dikes.

For negative reflection factors, the horizontal resistivity profiles across a dike of width $2a$ (figs. 78 and 79) show pronounced resistivity lows over the dike and a barely perceptible paradoxical maximum in the central region of the dike. The apparent-resistivity values rise slightly above one for the Lee configuration, if k is different from -1.0, but are always less than one in this example for the Wenner configuration. It is noteworthy that the Lee apparent-resistivity values rise above one even though the maximum value of the true resistivities involved in the example is one. We shall observe this paradox in many more theoretical, as well as field, curves in this treatise.

For both the Lee and Wenner configurations, the apparent-resistivity features near the edges of the dikes of width $2a$ are very similar to those found over a vertical fault, and the peaks bear the same horizontal relationship to the edges of the dike as they did for a fault. The apparent-resistivity values of the peaks, however, are in general different from those in the corresponding fault problem because of the effect of the country rock on the other side of the dike. For the continuous curves the horizontal distance between the peaks is equal to the width of the dike plus $a/2$ for the Lee configuration and the width of the dike plus a for the Wenner configuration. It should be emphasized

that for the field data, for which discrete stations only are taken, these rules for width estimates contain an inherent uncertainty that depends on the station intervals taken.

For dikes of width $2a$ that are perfectly insulating or conducting, the apparent resistivity with both the Lee and Wenner configuration attains a value of infinity or zero, respectively, over parts of the curves. This is not so for a dike of small or intermediate width.

The subsidiary apparent-resistivity peaks or lows, which occur far out on the flanks of both the Lee and Wenner curves for a dike, are helpful in detecting the existence and location of the dike. The peaks or lows are usually recognizable for dikes of high-resistivity contrast with the country rock, but unfortunately are usually obscured within the noise level —taken arbitrarily by us as 10 percent of the regional value—for dikes of small resistivity contrast.

Figure 80 shows horizontal resistivity profiles with the Lee and Wenner configurations across a vertical dike of width $1.5a$ for reflection factors of ±0.6. For positive reflection factors, the shapes of these apparent-resistivity curves are markedly different from the corresponding curves for a dike of width $2a$; yet for negative reflection factors, the shapes are similar to those for the dike of width $2a$. In particular for positive reflection factors, the Lee apparent-resistivity peaks for the same resistivity contrast are not as high as the dike of width $2a$ (compare figs. 76E and 80A); and the Wenner apparent-resistivity curve consists of a single broad peak centrally located over the axis of the dike and flanked on either side by two subsidiary peaks. The Wenner curve might be erroneously interpreted as a wide dike flanked by two thin dikes on each side. The curves in figure 80, all drawn at the same scale, provide an excellent comparison between the size of the Lee and Wenner anomalies. As usual, the Lee anomalies are more pronounced than the Wenner anomalies.

For positive reflection factors, the horizontal resistivity profiles with the Lee configuration across a dike of width a show a pronounced ρ_2 peak near the left edge of the dike and an equally pronounced ρ_1 peak near the right edge of the dike (fig. 81). On the continuous curve, the distance between the highest peaks on the ρ_2 and ρ_1 curves is equal to the width of the dike plus $a/2$; but this rule would be only approximately true for the distance between the observed peaks on a Lee field curve for which discrete station intervals were taken. As always, the ρ_1 and ρ_2 curves cross symmetrically at a point vertically over the axis of the dike. The two peaks observed in a field curve might erroneously be interpreted as two separate dikes; in this case the symmetrical crossing of the ρ_1 and ρ_2 curves, as well as the
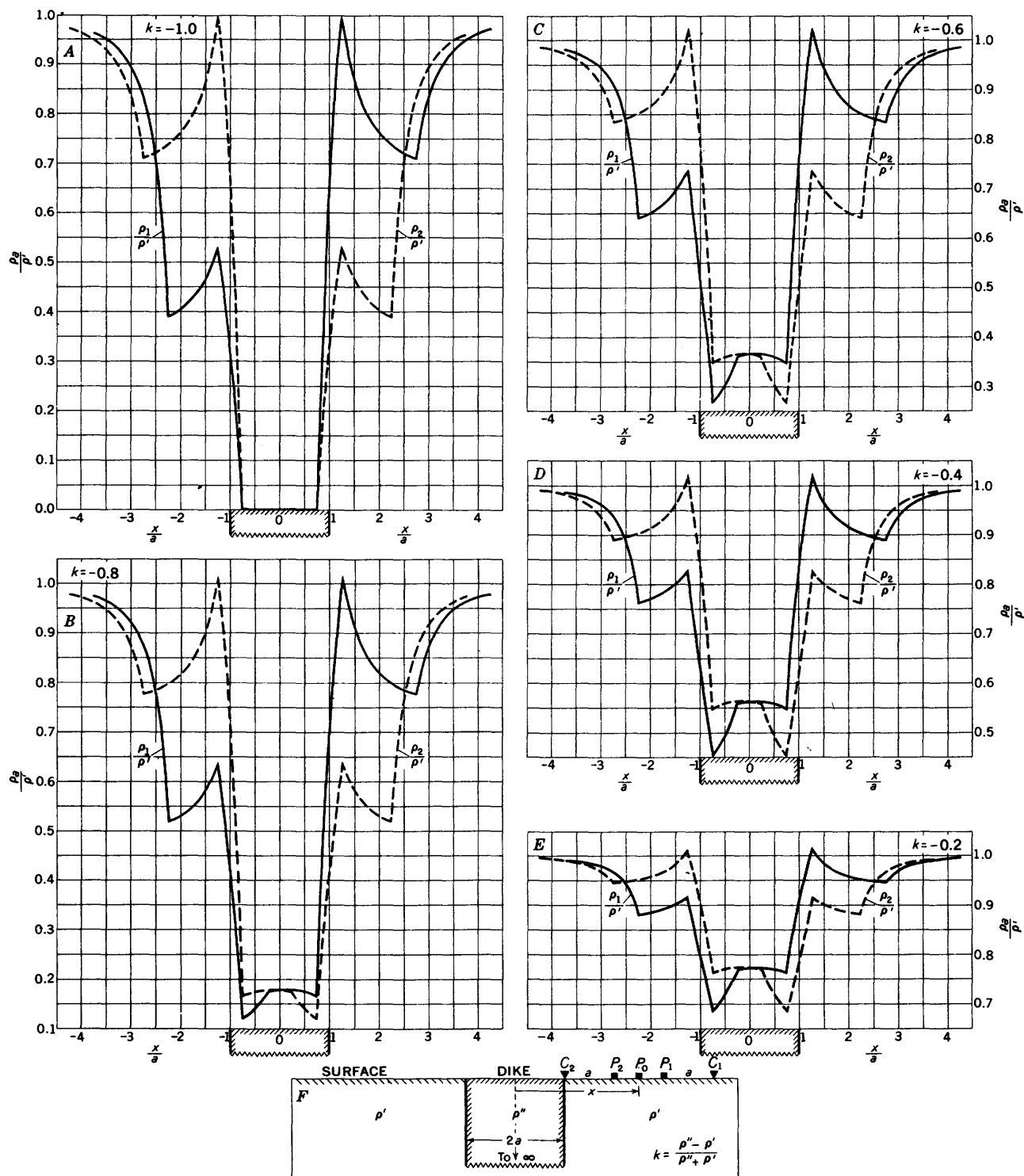
FIGURE 78.—Horizontal resistivity profiles across a vertical dike of width $2a$, Lee configuration (offset plotting); reflection factor $k = -1.0$, -0.8, -0.6, -0.4, and -0.2.
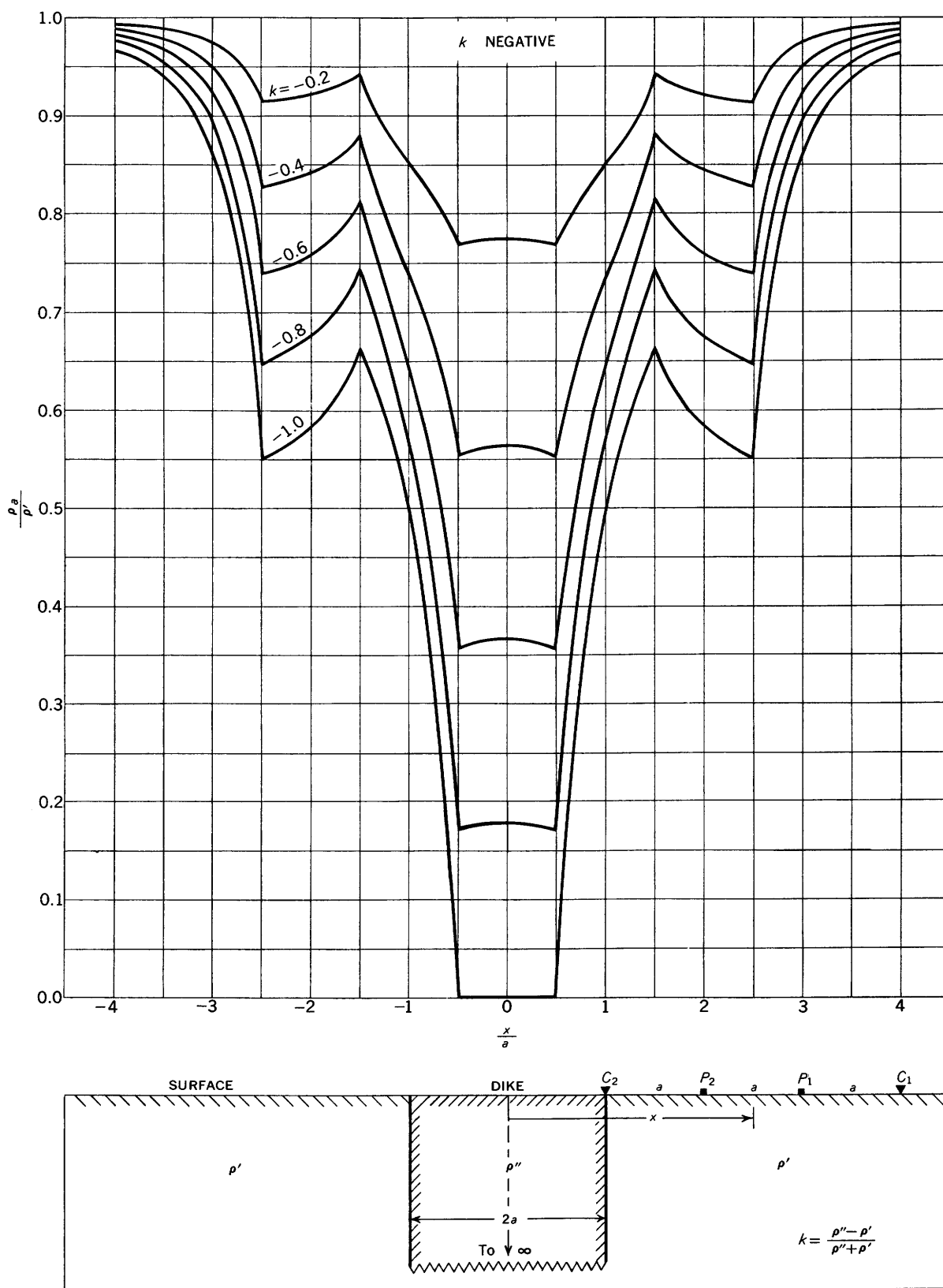
FIGURE 79.—Horizontal resistivity profiles across a vertical dike of width $2a$, Wenner configuration; reflection factor $k=-1.0$, -0.8, -0.6, -0.4, and -0.2.
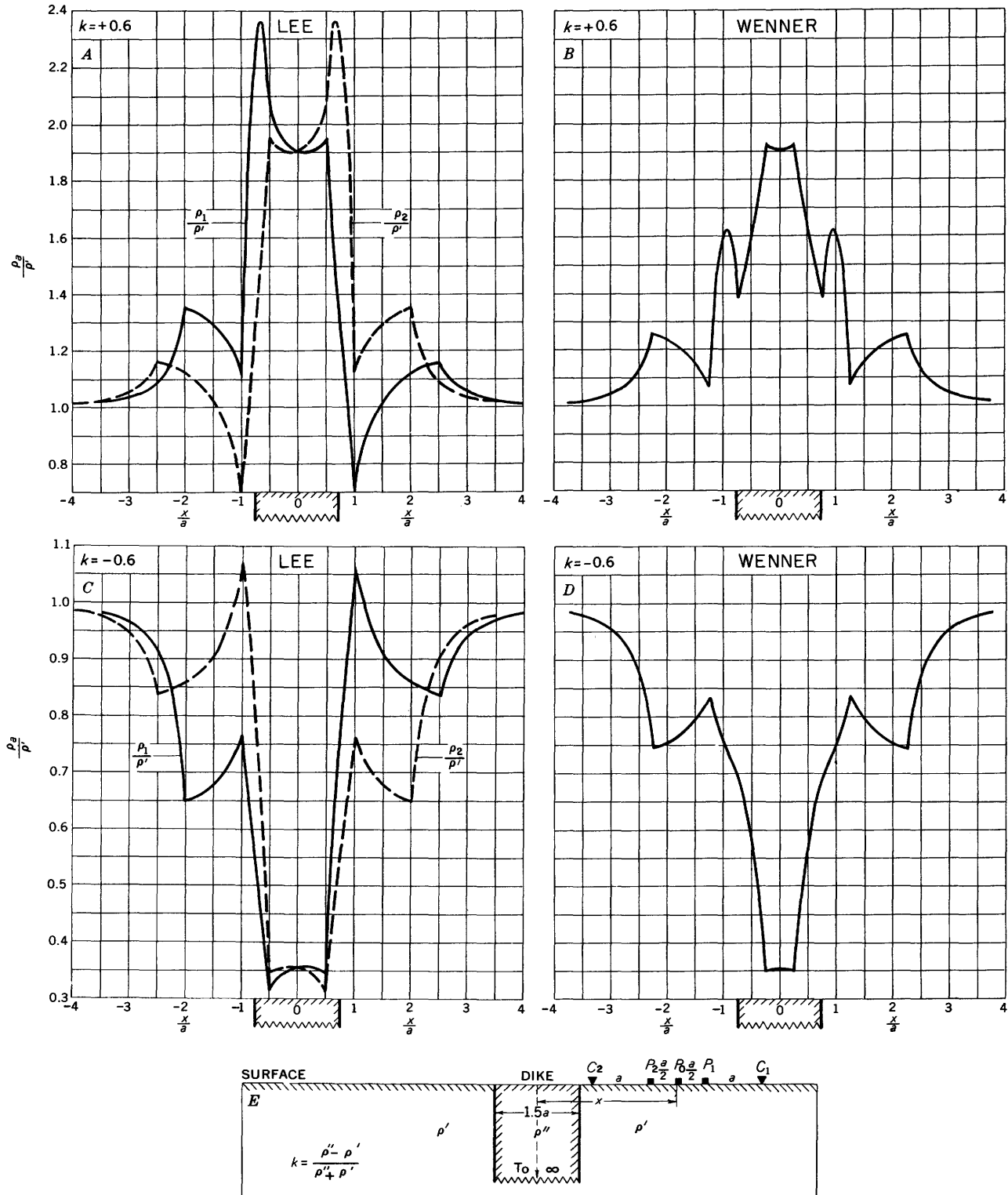
FIGURE 80.—Horizontal resistivity profiles across a vertical dike of width 1.5a, Lee configuration (offset plotting) and Wenner configuration; reflection factor k=±0.6.
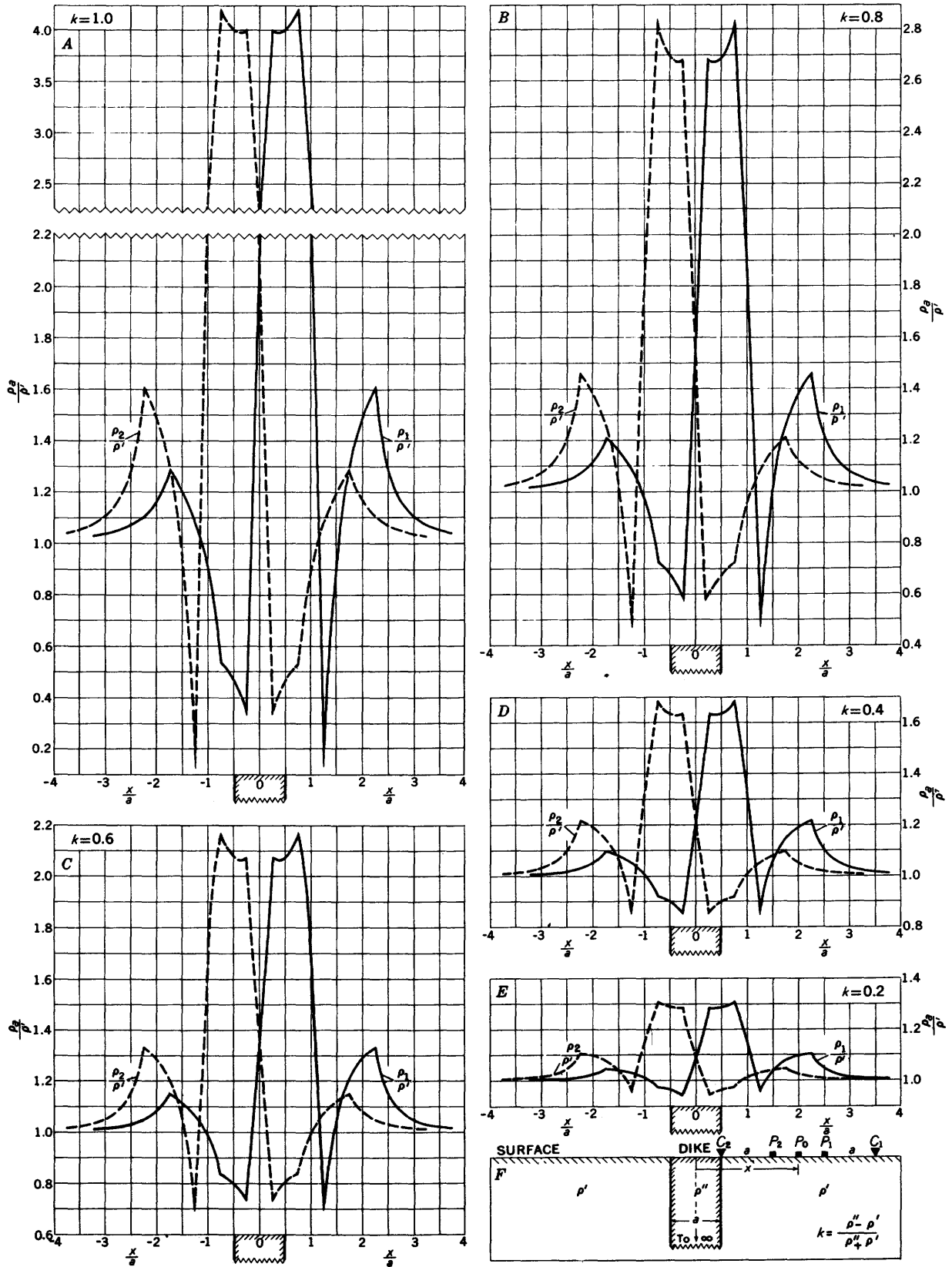
FIGURE 81.—Horizontal resistivity profiles across a vertical dike of width a, Lee configuration (offset plotting); reflection factor $k=1.0$, 0.8, 0.6, 0.4, and 0.2.

occurrence of the ρ_2 peak on the left and the ρ_1 peak on the right, are valuable criteria to use in analyzing the field anomaly. It should be noted that the feature of a ρ_2 peak on the left of the dike and a ρ_1 peak on the right of the dike of width a is directly opposite to the feature of a ρ_1 peak on the left and a ρ_2 peak on the right of the dike of width $2a$ (fig. 76B). For the dike of width $2a$, however, the bulk of the anomaly has high-resistivity values throughout the central region of the dike, whereas for the dike of width a the apparent-resistivity values are not universally high over the central region, especially directly over the axis of the dike. For the continuous curve the distance between the subsidiary ρ_2 peak lying to the left of the main anomaly and the subsidiary ρ_1 peak lying to the right of the main anomaly is equal to the width of the dike plus $7a/2$.

For positive reflection factors, the horizontal resistivity profiles with the Wenner configuration across a dike of width a show a pronounced W-shape (fig. 82). The highest peak lies vertically over the axis of the dike. The distance between the peaks flanking either side of the main anomaly is equal to the width of the dike plus $3a$.

For negative reflection factors, the horizontal resistivity profiles with the Lee configuration across a dike of width a show a pronounced minimum in the ρ_2 curve near the left edge of the dike and an equally pronounced minimum in the ρ_1 curve near the right edge of the dike (fig. 83). Paradoxically, the apparent-resistivity values of ρ_1 and ρ_2 exceed one near the left and right edges, respectively, of the dike, as center electrode P_0 touches the left and right edges, respectively. As always, the ρ_1 and ρ_2 curves cross symmetrically at a point lying vertically above the axis of the dike. For the continuous curve, the distance between the subsidiary ρ_2 low lying on the left flank and the subsidiary ρ_1 low lying on the right flank is equal to the width of the vein plus $7a/2$.

For negative reflection factors, the horizontal resistivity profiles with the Wenner configuration across a dike of width a show a pronounced minimum vertically above the axis of the dike (fig. 84). For a reflection factor of -0.2, the Wenner apparent-resistivity value exceeds one as one current electrode and one potential electrode simultaneously cross the opposite edges of the dike. This example is one of the relatively few cases for which the apparent-resistivity value for the Wenner configuration exceeds the value of the higher resistivity material, although this characteristic is commonly observed with Lee profiles over dikes—as has been pointed out.

For dikes of intermediate width comparable to the electrode separation or for widths less than the electrode separation, the maximum apparent-resistivity values are finite even though the dike is perfectly insulating or perfectly conducting. Thus the true resistivity of the country rock on the side of the dike opposite from the configuration manifests itself sufficiently to keep the apparent resistivities finite. For a dike of width a, the maximum apparent-resistivity value attainable with the Wenner configuration even for a perfectly insulating dike is only four times the true resistivity of the surrounding country rock (fig. 82). Comparable conclusions are true for a perfectly conducting dike. For thinner dikes the maximum apparent resistivity for positive reflection factors diminishes; and the minimum apparent resistivity for negative reflection factors increases.

Figure 85 shows the horizontal resistivity profiles with both the Lee and Wenner configurations across a vertical dike of width $0.6a$ for $k=\pm0.6$. For the positive reflection factor, the Lee curve is W-shaped. This W-shape is not observed on continuous Lee curves for dikes unless their width is considerably less than a. The W-shape for the Wenner curve over a dike of width $0.6a$ is similar to that for a dike of width a. For the Wenner configuration the top of the central peak of the W-shaped curve is paradoxically wider for a dike of width $0.6a$ than for a dike of width a, although the magnitude of the peak is much less for the width $0.6a$. For a negative reflection factor, a pronounced apparent-resistivity low occurs vertically above the axis of the vein for both the Lee and Wenner configurations.

Figures 86, 87, 88, and 89 show the horizontal resistivity profiles for both the Lee and Wenner configurations across a vertical dike of width $a/2$ for various resistivity contrasts. For positive reflection factors the outstanding feature of the apparent-resistivity curves for both the Lee and Wenner configurations is the W-shape of the curves. For the Lee configuration the most pronounced peaks and lows of the ρ_1 and ρ_2 curves lie vertically over the axis of the dike.

Figure 90 shows the horizontal resistivity profiles with both the Lee and Wenner configurations across a vertical dike of width $a/5$; the reflection factors are ±0.6. For the positive reflection factor, a typical W-shape is obtained with both the Lee and Wenner configurations; and the distance between the peaks that form either side of the main anomaly is equal to the electrode separation a minus the width of the dike. For the negative reflection factor, the anomaly obtained with the Lee configuration would probably be recognizable in the field data; but that obtained with the Wenner configuration might not be recognizable because of the paradoxical apparent-resistivity high occurring within the resistivity low directly over the dike. For
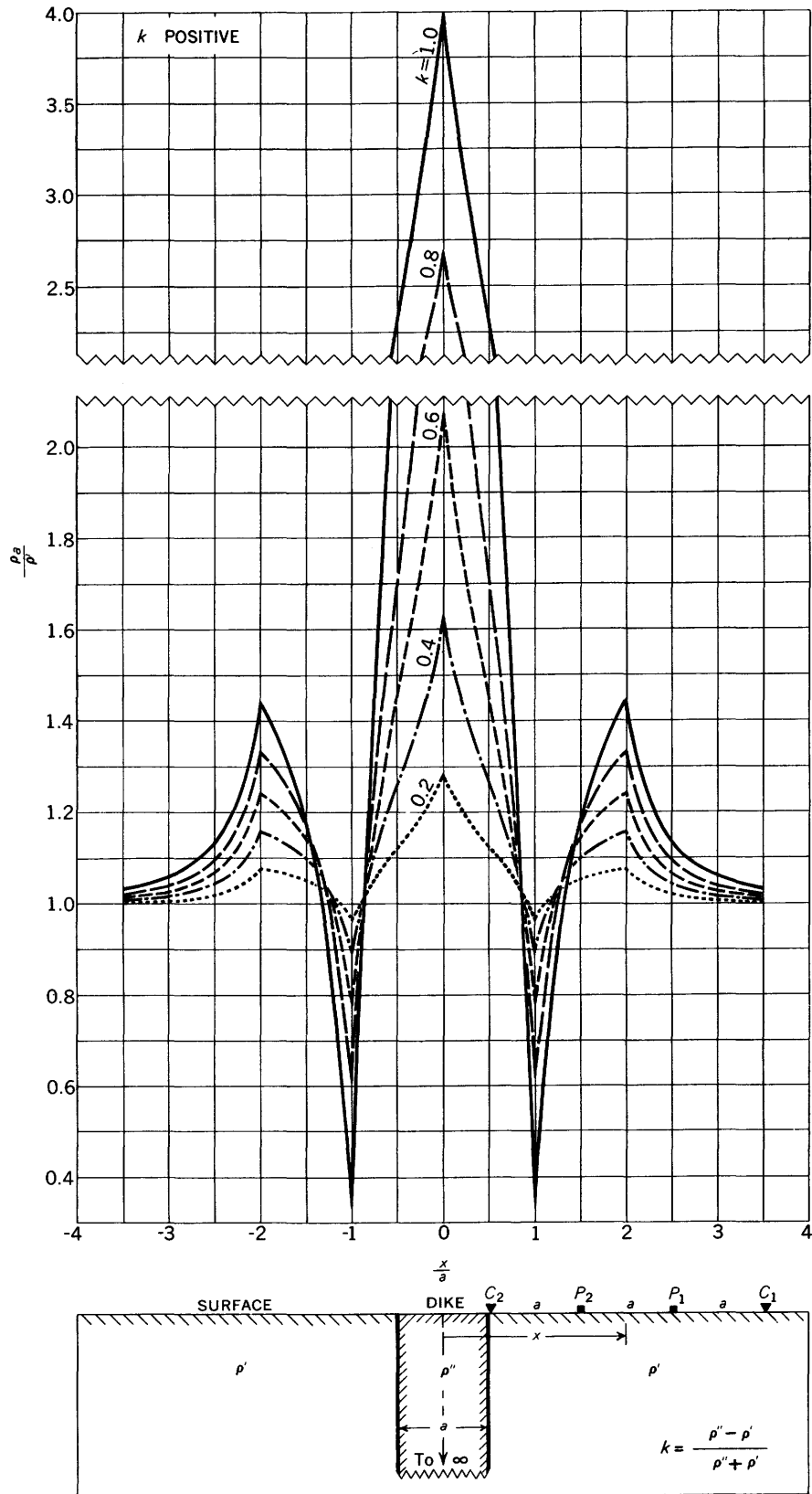
FIGURE 82.—Horizontal resistivity profiles across a vertical dike of width a, Wenner configuration; reflection factor k=1.0, 0.8, 0.6, 0.4, and 0.2.
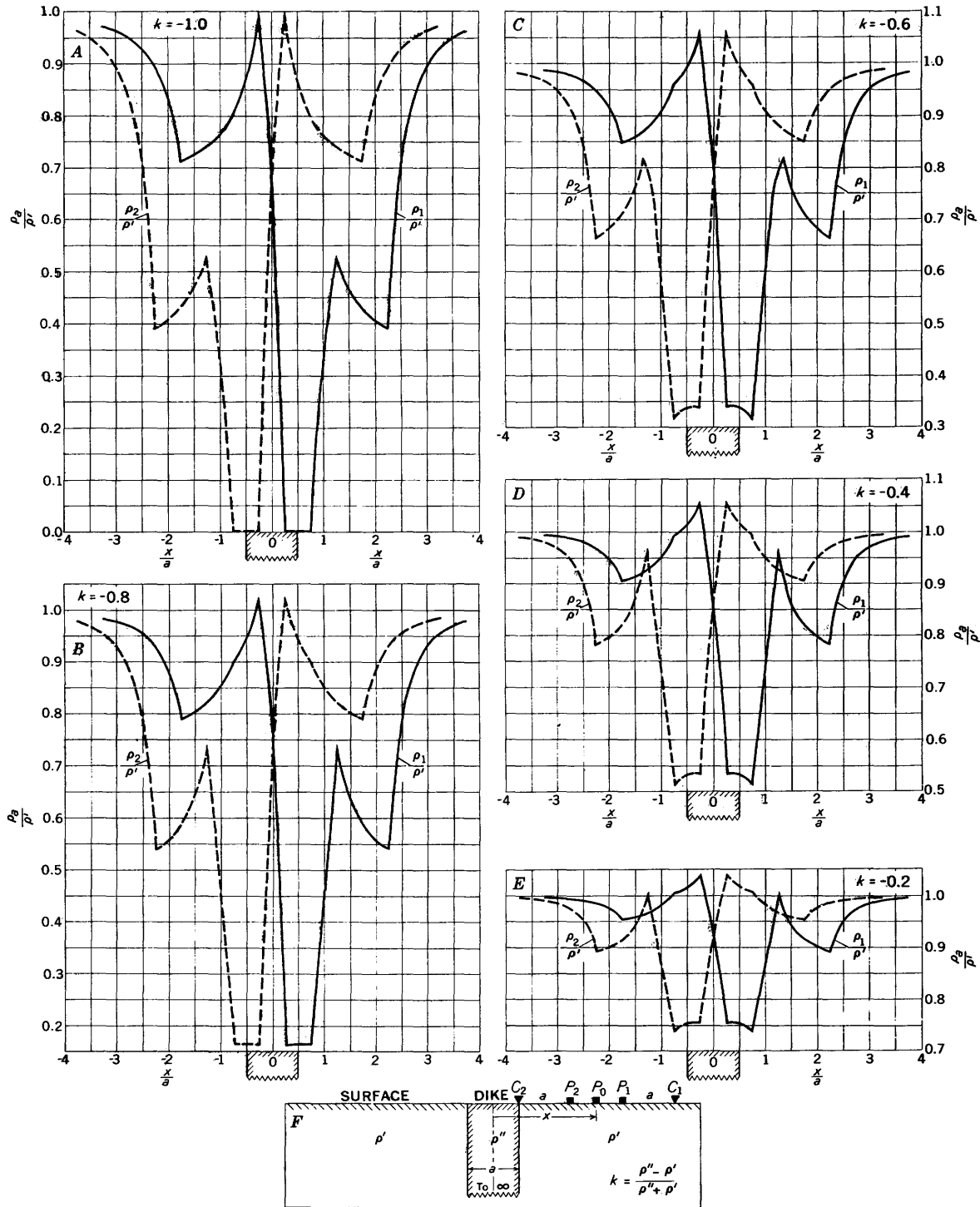
FIGURE 83.—Horizontal resistivity profiles across a vertical dike of width a, Lee configuration (offset plotting); reflection factor $k=-1.0$, -0.8, -0.6, -0.4, and -0.2.

either positive or negative reflection factors the anomalies might be erroneously interpreted as a multiple-dike system rather than as a single dike.

Figure 91 shows a comparison of horizontal resistivity profiles with the Wenner configuration across the same

vertical dike with different electrode separations (Onodera, 1949). For all curves, the width of the dike is 11 units, and the reflection factor is 0.9. For small electrode separations relative to the dike width, two pronounced peaks occur over and inside of the
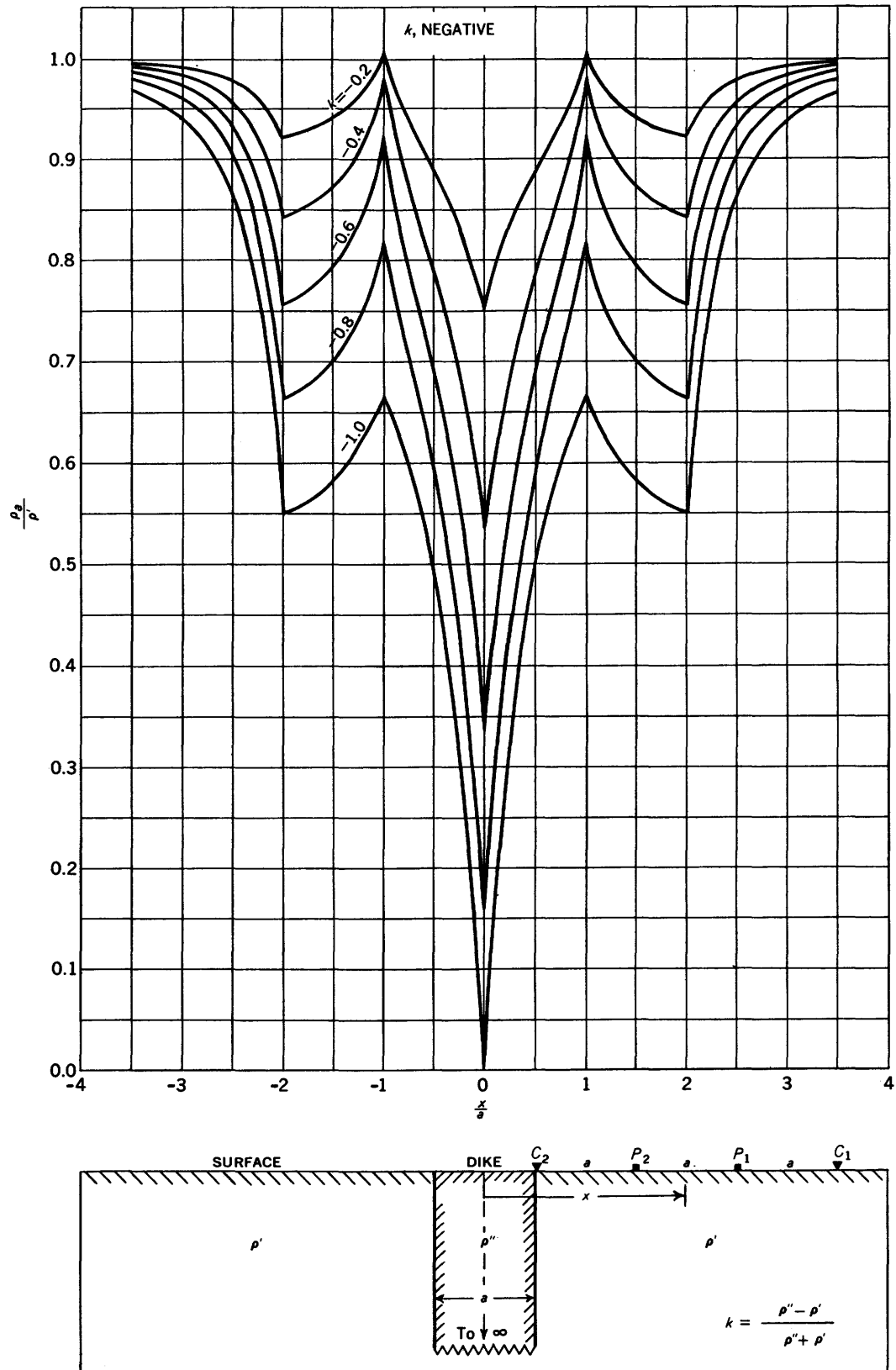
FIGURE 84.—Horizontal resistivity profiles across a vertical dike of width a, Wenner configuration; reflection factor $k = -1.0, -0.8, -0.6, -0.4,$ and -0.2.
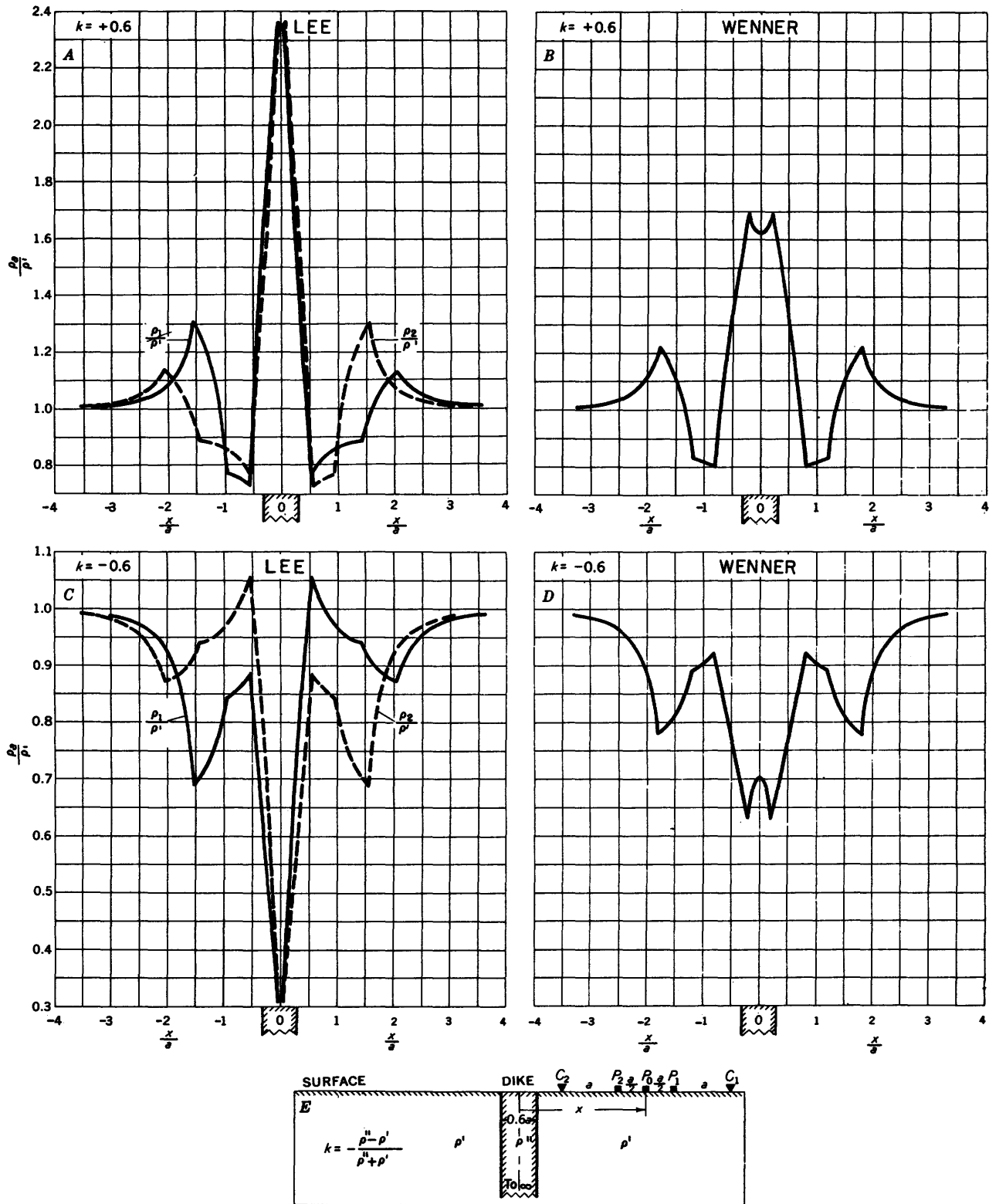
FIGURE 85.—Horizontal resistivity profiles across a vertical dike of width 0.6a, Lee configuration (offset plotting) and Wenner configuration; reflection factor k=±0.6.
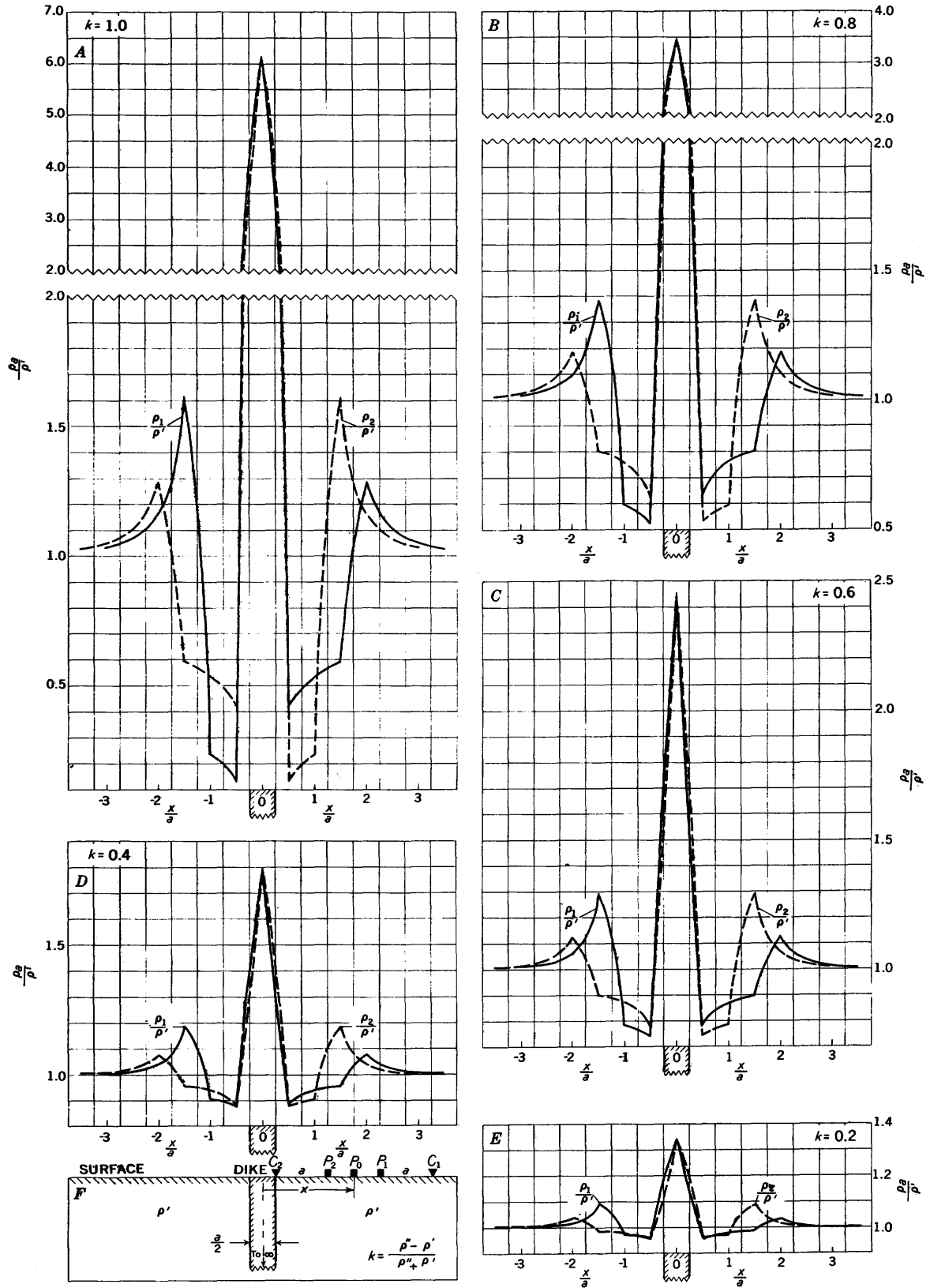
FIGURE 86.—Horizontal resistivity profiles across a vertical dike of width $a/2$, Lee configuration (offset plotting); reflection factor $k=1.0$, 0.8, 0.6, 0.4, and 0.2.
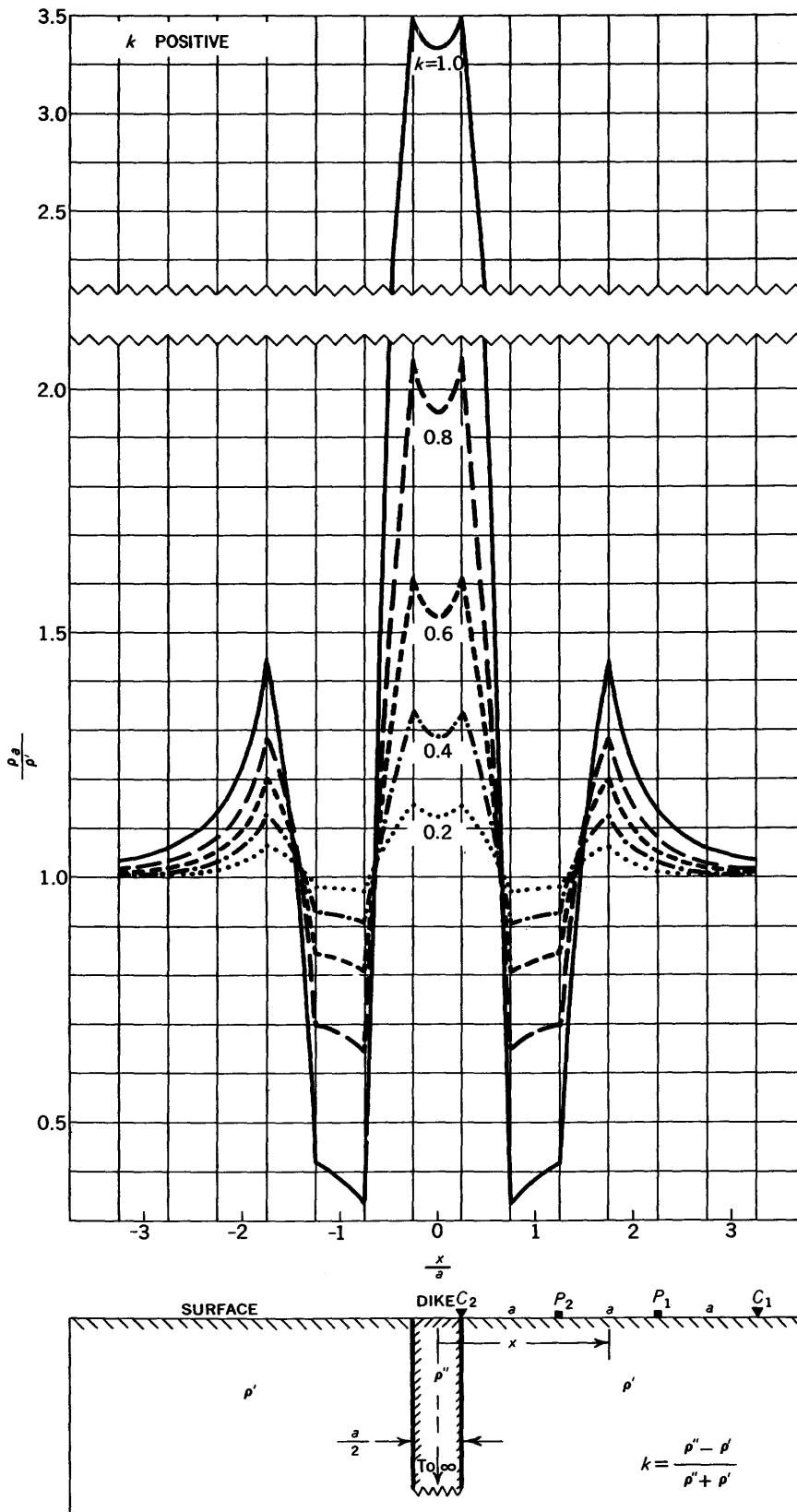
FIGURE 87.—Horizontal resistivity profiles across a vertical dike of width $a/2$, Wenner configuration; reflection factor $k=1.0$, 0.8, 0.6, 0.4, and 0.2.
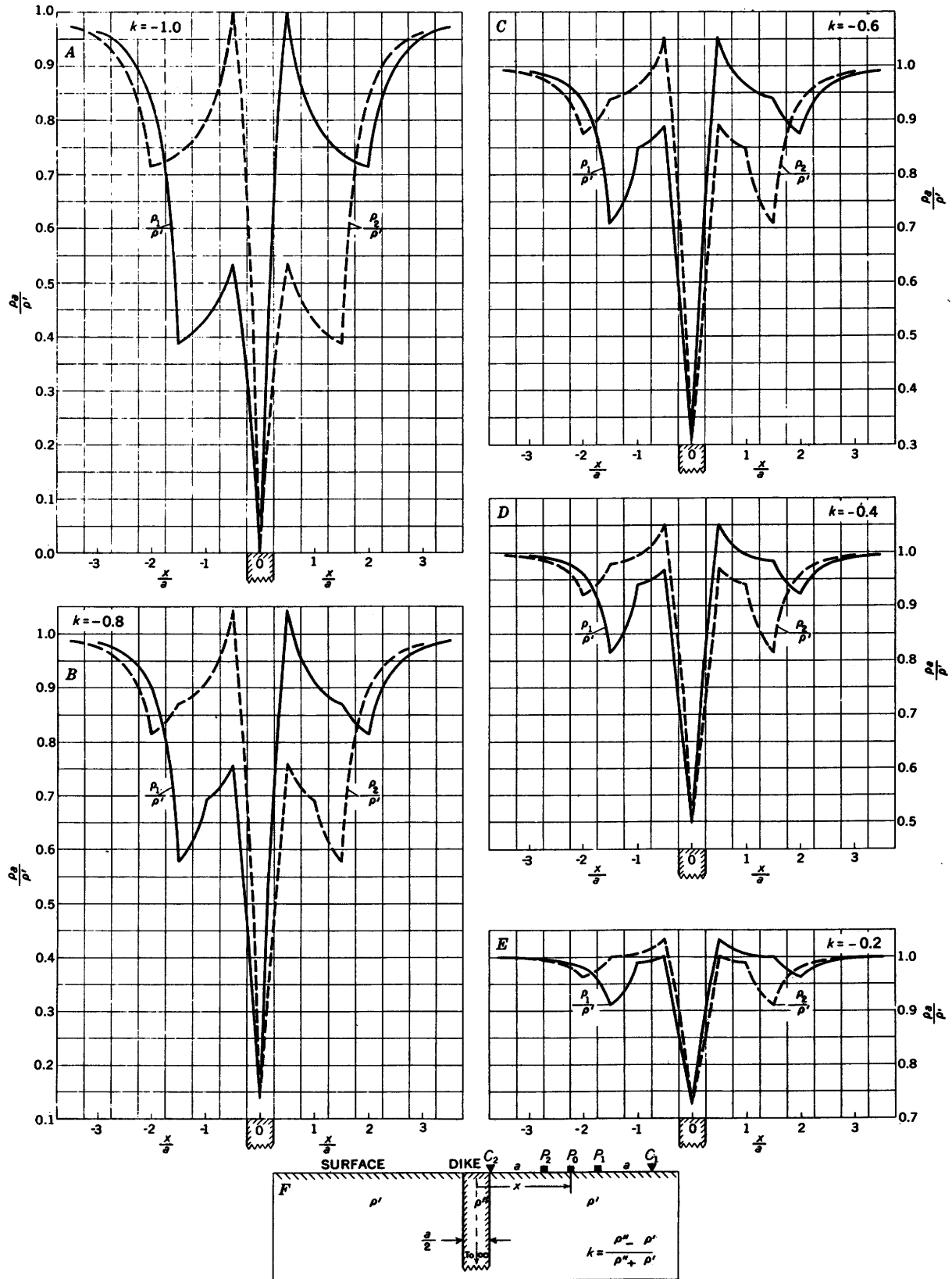
FIGURE 88.—Horizontal resistivity profiles across a vertical dike of width $a/2$, Lee configuration (offset plotting); reflection factor $k=-1.0$, -0.8, -0.6, -0.4, and -0.2.
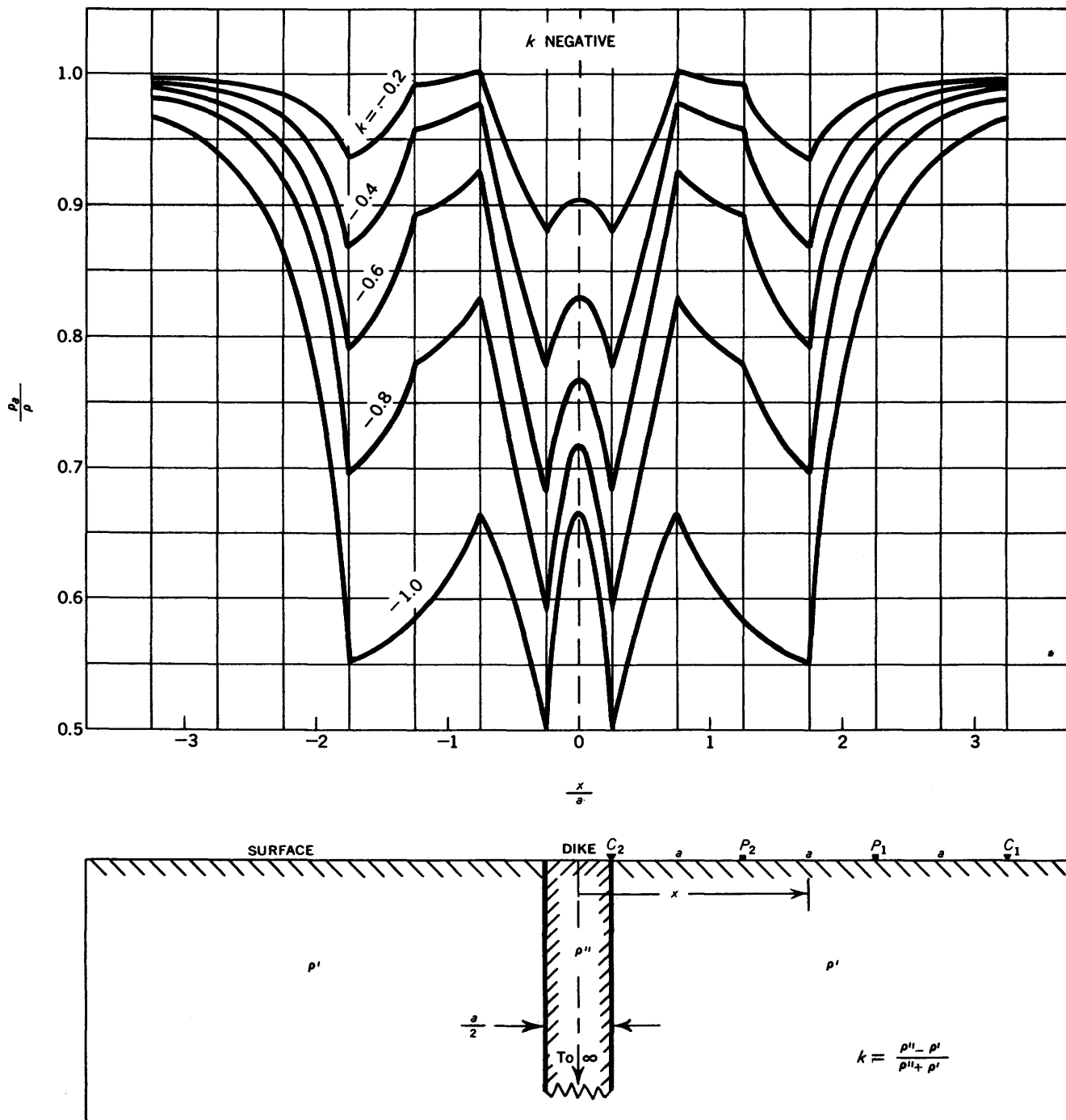
FIGURE 89.—Horizontal resistivity profiles across a vertical dike of width $a/2$, Wenner configuration; reflection factor $k = -1.0$, -0.8, -0.6, -0.4, and -0.2.

edges of the dike. For larger separations, these peaks migrate away from the axis of the dike and diminish in size. For a separation of the same order of magnitude as the width of the dike, the peaks become subsidiary peaks lying outside of the dike. Concomitantly, the apparent-resistivity high over the axis of the dike increases in size as the electrode separation is increased.

Several generalizations can be made for the horizontal resistivity profiles for both the Lee and Wenner configurations across vertical dikes.

1. For wide dikes —widths of $2a$ or more—the effects near the edges of the dikes are similar to those obtained over and adjacent to single faults; and the rules for detecting the trace of a vertical fault from a continuous
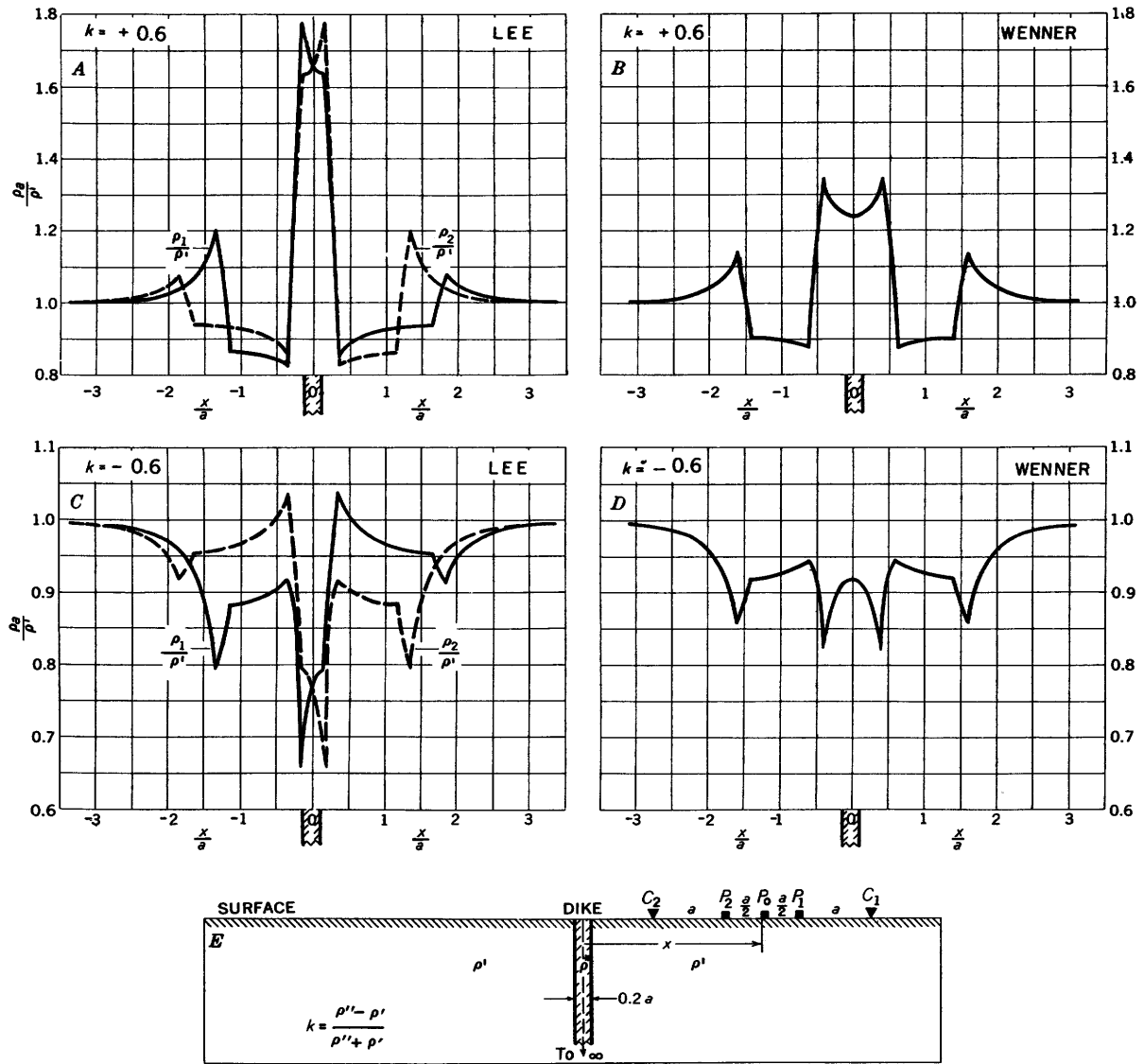
FIGURE 90.—Horizontal resistivity profiles across a vertical dike of width $a/5$, Lee configuration (offset plotting) and Wenner configuration; reflection factor $k=\pm0.6$.

profile can be used to detect the edges of a wide dike. The maximum and minimum apparent-resistivity values obtained in crossing a wide dike are somewhat different from the maximum and minimum values obtained in crossing a vertical fault, however, because the country rock on the other side of the dike manifests itself on the measurements. For detecting the edge of a vertical dike from field data taken at discrete station intervals, therefore, a separate analysis of the theoretical field plots for the dike curves must be made, because the theoretical field plots used for a vertical fault are not strictly applicable. The wider the dike, however, the more closely will the fault analysis of the theoretical field plots apply to the corresponding analysis of the theoretical field plots for a dike. By applying

the fault analysis to each side of the dike, its width can be estimated.

2. For the continuous curve the subsidiary (in size) but important apparent-resistivity peaks or lows that flank the main anomalies are helpful in determining the width of the dike. For the Lee configuration and with positive reflection factors, the distance between the subsidiary ρ_1 peak and the corresponding subsidiary ρ_2 peak is equal to the width of the dike plus $7a/2$. For the Wenner configuration with positive reflection factors, the distance between the subsidiary peaks is equal to the width of the dike plus $3a$. These same rules hold for the subsidiary apparent-resistivity lows that flank the main anomalies for negative reflection factors. When applying these rules, however, the uncertainty
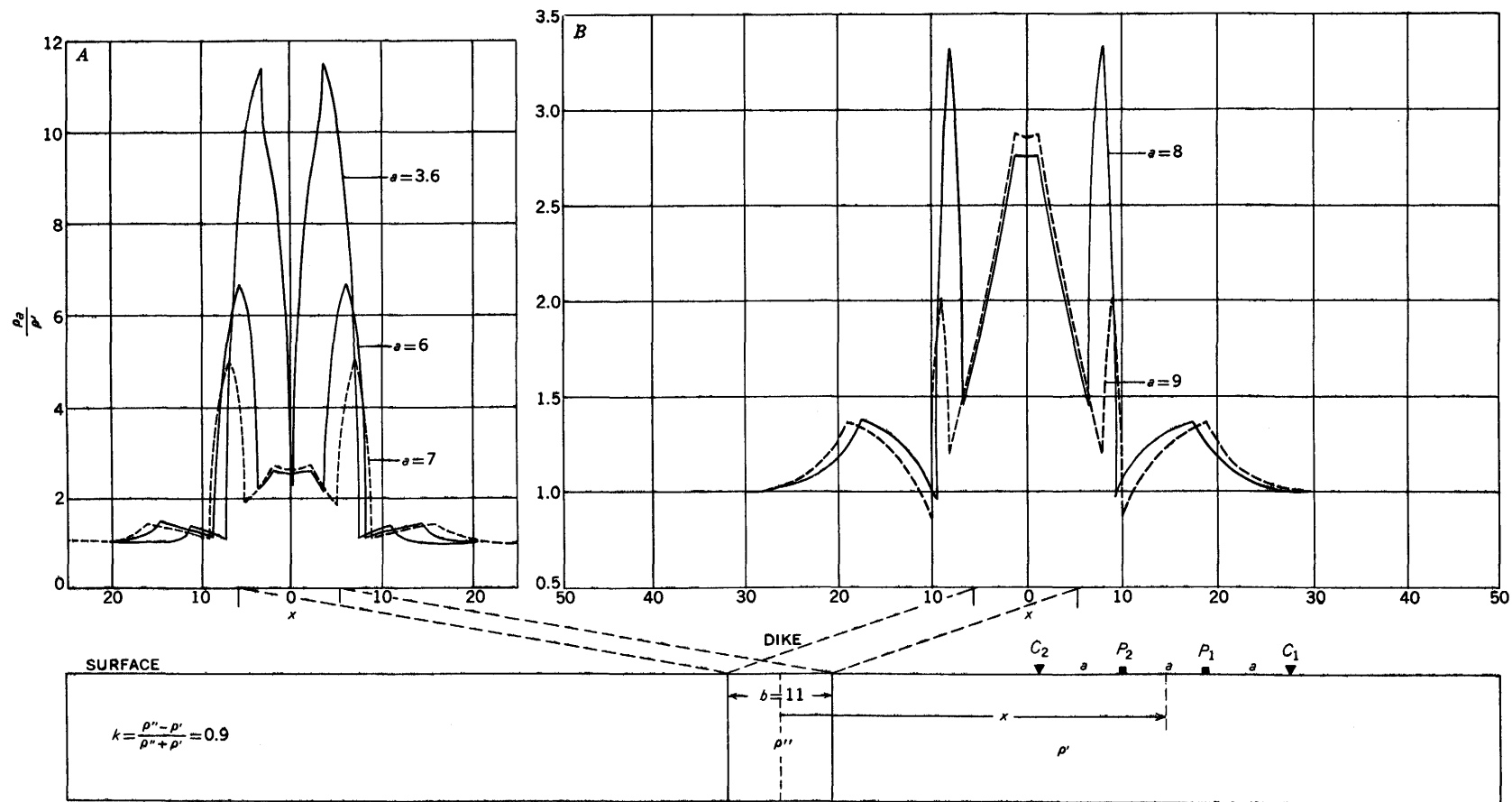
FIGURE 91.—Comparison of horizontal resistivity profiles across the same vertical dike with different electrode separations, Wenner configuration. For all curves, width of dike $b=11$, and reflection factor $k=0.9$. Adapted from Onodera (1949).

introduced by the fact that the field curve is not ordinarily a continuous curve must be taken into consideration.

3. With the Wenner configuration for positive reflection factors over dikes that are not as wide as the electrode separation, the distance between the edges of the steep resistivity plateau at the top of the main central anomaly is equal to the electrode separation a minus the width of the dike.

4. A single dike often gives multiple apparent-resistivity peaks that might be erroneously interpreted as two or more dikes rather than a single dike unless the interpreter is familiar with the various possibilities.

5. Many paradoxes of high and low apparent resistivities occur over and adjacent to a single dike.

6. For dikes with a width comparable to the electrode separation, a typical W-shape curve is obtained with the Wenner configuration, provided the reflection factor is positive; but the Lee profiles for this width are complicated for both positive and negative reflection factors.

7. For dikes with a width comparable to half the electrode separation, a typical W-shaped curve is obtained for both the Lee and Wenner configurations, if the reflection factor is positive.

8. The ρ_1 and ρ_2 curves of the Lee configuration (offset plotting) always cross symmetrically at a point lying vertically over the axis of a vertical dike, irrespective of whether the reflection factor is positive or negative.

9. For wide dikes, the apparent resistivity can attain very high or very low values when the true resistivity of the dike is either correspondingly high or low, respectively, in relation to the true resistivity of the country rock. For dikes of width comparable to the electrode separation, however, there is a maximum apparent resistivity attainable for positive reflection factors that is considerably lower than the true resistivity of the dike in comparison with that of the country rock. For still thinner dikes the maximum apparent resistivity for positive reflection factors diminishes. For a perfectly insulating dike, the maximum apparent resistivity diminishes as the dike is made thinner so that in the limit the maximum apparent-resistivity value reaches the value obtained over an infinite vertical perfectly insulating plane. Corresponding statements apply also to minimum values over dikes for negative reflection factors and for perfectly conducting dikes.

Figures 92 and 93 show observed horizontal resistivity profiles with the Lee configuration across two different quartz veins in Vance County, N.C. For both diagrams an electrode separation of 40 feet and station

interval of 20 feet was used. The quartz veins, in which tungsten minerals may occur, are of much higher resistivity than the surrounding country rock. The Sneed 1–B quartz vein (fig. 92), which is exposed in a trench near the traverse, shows a high apparent-resistivity peak approximately centrally located over the exposed vein. The two subsidiary peaks that lie along the flanks of the main resistivity high—the small ρ_1 peak to the left of the main resistivity high and the small ρ_2 peak to the right of the main resistivity high—are also manifestations of the Sneed vein; these subsidiary peaks resemble those observed in the theoretical profile in figure 90A. The point of crossing of the ρ_1 and ρ_2 curves lies about 10 feet west of the center of the vein as inferred from the exposure in the trench; this feature indicates either that the vein broadens in depth more to the west than to the east or that it dips west.

The Walker 5 quartz vein, known to exist with a width of 1 ft at the indicated position in the geologic cross section in figure 93, shows a pronounced resistivity high directly over the vein.

A Triassic diabase dike, which is known to exist approximately at the indicated position in the geologic cross section in figure 93, shows a resistivity low over the dike. In this district, resistivity lows are found over diabase dikes and are attributed to their content of iron-bearing minerals, which make the dikes more conductive than the surrounding country rock (MacCarthy and Shuler, 1948, unpublished data). The exact margins of the diabase dike in this example were not known and are inferred by us from the resistivity peaks that lie on either side of the dike and from the fact that the ρ_1 and ρ_2 curves theoretically cross at a point lying vertically over the axis of the dike. The inferred width of the dike is 90 feet, which slightly exceeds twice the electrode separation of 40 feet. The observed curve resembles somewhat the theoretical curves in figure 78E for a low-resistivity dike whose width is exactly twice the electrode separation.

Figures 94, 95, and 96 show observed horizontal resistivity profiles with the Lee configuration across inferred silicified limestone zones in the Tri-State lead-zinc mining district, Cherokee County, Kans. In all diagrams, the electrode separation is 100 feet, and the station interval is 50 feet. These silicified zones, which are vertical or steeply dipping, probably have been formed by silica-bearing solutions that infiltrated the vertical or steeply dipping fractures in fracture zones and later crystallized as silica and filled the fractures. The present low porosity and permeability of the silicified zones cause them to be impermeable to the ground water and hence to be of much higher resistivity than the surrounding limestone country rock.

Figure 94 shows an observed horizontal profile over a wide silicified zone. The pronounced ρ_1 and ρ_2 peaks on the left and right sides, respectively, of the main anomaly, and the subsidiary ρ_2 peak to the right of the main anomaly correspond with similar features on the theoretical curve for a dike of width $2a$ (fig. 76C). In this example, using the rule for the continuous curve that the width of the dike is equal to the distance between the pronounced ρ_1 and ρ_2 peaks (200 ft.) plus a/2 (50 ft.), the width of the zone is estimated as 250 feet; it should be recalled, however, that in this example there is an uncertainty in this width estimate of at least a few tens of feet, because a relative shift can occur in the position of the peaks on the field plot. The ρ_1 and ρ_2 curves cross at a point lying vertically over the inferred axis of the zone.

Figure 95 shows an observed horizontal profile over a silicified zone of intermediate width. The twin peaks

WEST   EAST
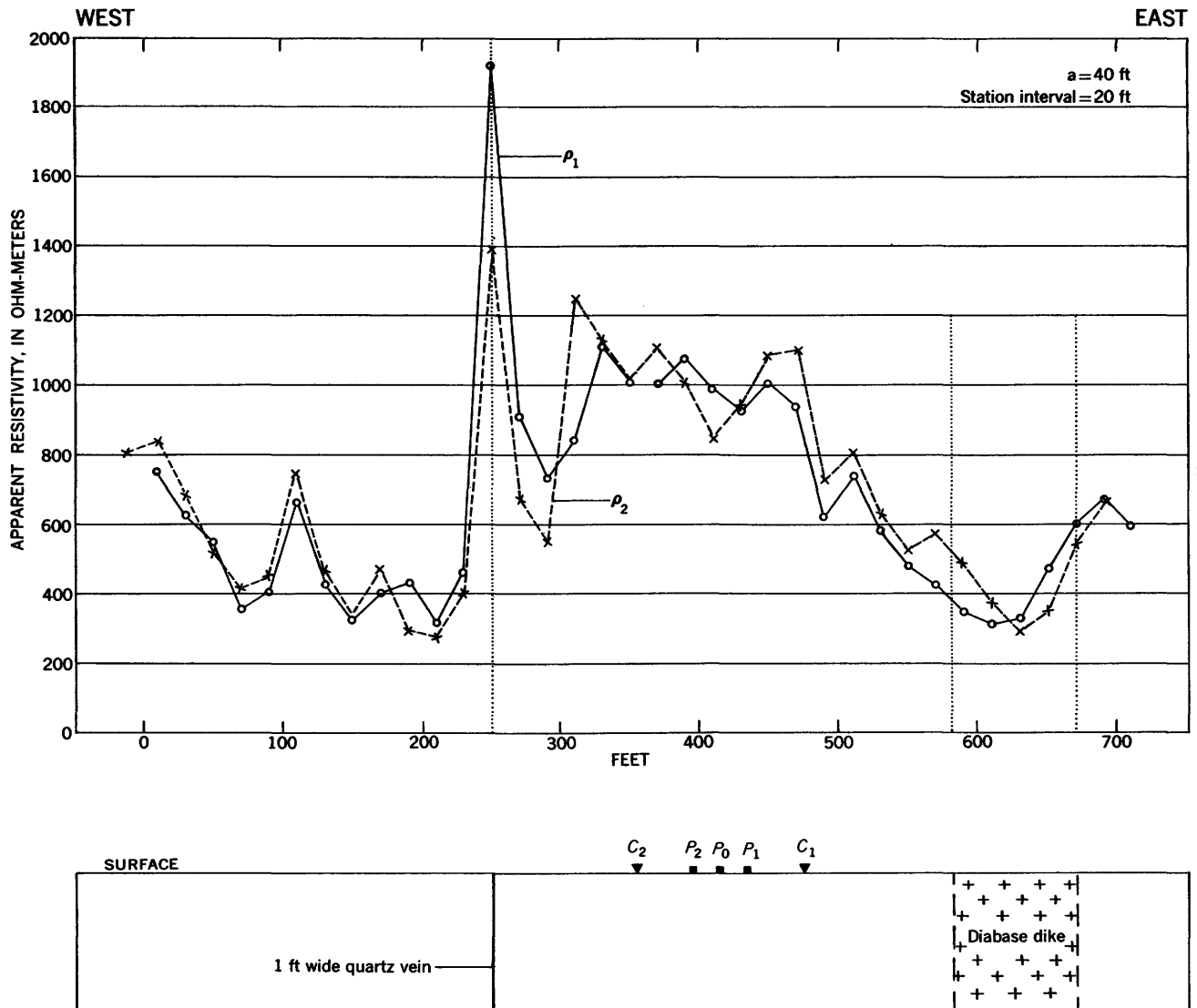
FIGURE 93.—Horizontal resistivity profile across Walker 5 quartz vein and exposed diabase dike, Vance County, N.C., Lee configuration (offset plotting). Electrode separation $a=40$ ft; station interval $=20$ ft.   G. R. MacCarthy and R. M. Shuler (1948, unpublished data).

over the main apparent-resistivity high, the subsidiary ρ_1 peak to the left of the main anomaly, and the subsidiary ρ_2 plateau to the right of the main anomaly are probably manifestations of a single silicified zone of dikelike form. The field curve is similar to the theoretical curve in figure $80A$ for a dike of width $1.5a$, although the ρ_1 and ρ_2 curves do not cross at the axis of the zone. The inferred width of the silicified zone is shown as $1.5a$ or 150 feet.

Figure 96 shows three observed horizontal resistivity profiles over three separate silicified zones of relatively small width that are in separate areas far removed from each other. Each shows a single sharp peak with subsidiary ρ_1 and ρ_2 peaks to the left and right, respectively, of the main peak in a manner similar to the

theoretical curves in figure $86C$. Because the distance between the ρ_1 and ρ_2 subsidiary peaks is equal to $3a$ in each case, the width of each of the silicified zones is probably of the order of magnitude of $a/2$, or 50 feet.

These field curves should be compared with not only the dike profiles given in this section but also similar profiles for near-surface buried dikelike features given in pages 268 to 272.

Figure 97 shows an observed horizontal resistivity profile with the Wenner configuration across a shear zone (right side of profile) and limestone fault block (left side of profile) (Hubbert, 1932, p. 16). The apparent resistivity curve over the shear zone is W-shaped and indicates that the true resistivity of the shear zone is higher than that of the surrounding country rock.
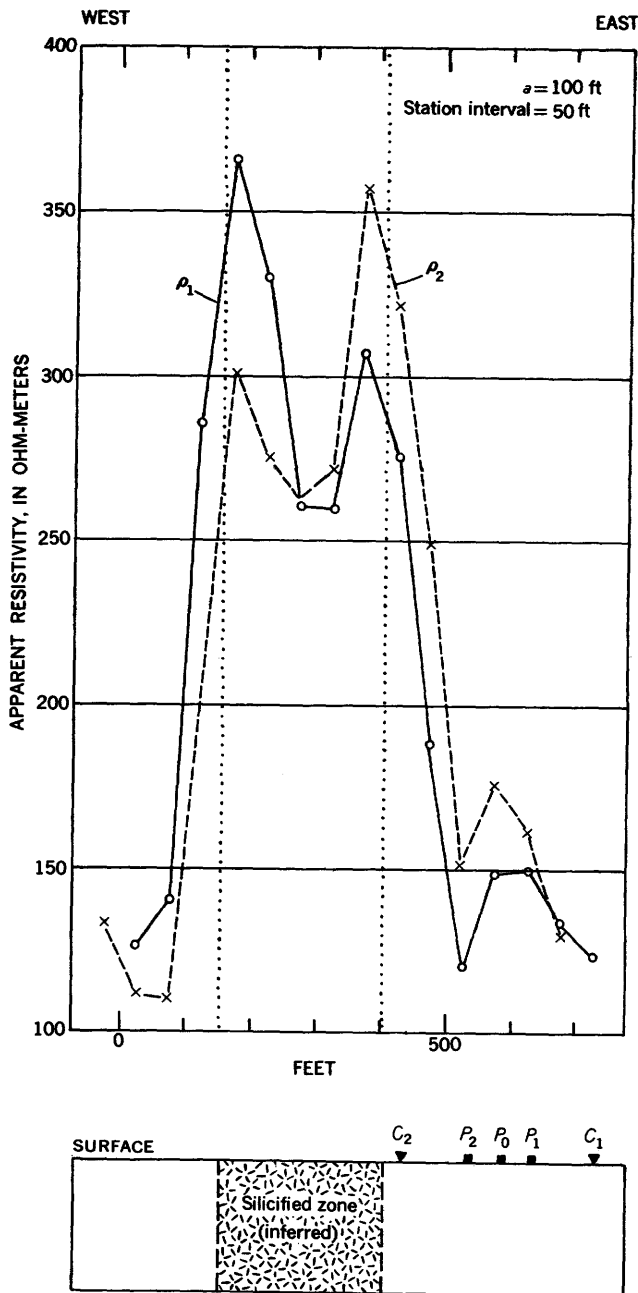
FIGURE 94.—Horizontal resistivity profile across inferred silicified limestone zone, Tri-State lead-zinc mining district, Cherokee County, Kans., Lee configuration (offset plotting). Electrode separation a=100 ft; station interval =50 ft. K. L. Cook (1951-54, unpublished data).

The observed curve is similar to the theoretical curve obtained over a thin dike (see fig. 90B) when it is realized that only a few points would be obtained on a theoretical field plot when station intervals of 100 feet are taken across such a thin dike. The apparent resistivity over the limestone block has a character similar to the theoretical curves over a wide dike (see fig. 77). The twin peaks occur, although they are not symmetrically placed relative to the center of the

limestone block; a definite subsidiary peak occurs on the right flank of the main anomaly, and a sloping resistivity plateau occurs on the left flank of the main anomaly.

Figure 98 shows observed horizontal resistivity profiles with the Wenner configuration across Bauerle's "reef," Busia gold field, Uganda (Way, 1944). The "reef" is a dikelike feature and is here designated a dike by us to avoid any misinterpretation by American readers. All the profiles were taken along the same traverse perpendicular to the strike of the dike in an area where the dike is known from trenching to be 10 feet in width and covered with 10 feet of overburden; the dike apparently extends to a depth of at least several tens or scores of feet. The resistivity of the dike is much greater than that of both the surrounding country rock and also the overburden material. Electrode separations of 10, 20, 30, 40, and 50 feet were taken; station intervals of 10 feet were maintained for all profiles. The observed profiles are similar to the model results obtained by Johnson over a vertical insulating sheet (see fig. 55) and the theoretical curves over dikes (see figs. 77, 82, 87, and 90B). As emphasized by Way, the main anomaly directly over the dike is flanked by a subsidiary peak on either side. As the electrode separation is increased relative to the width of the dike, the distance between these flanking subsidiary peaks increases, and the main anomaly tends to flatten and widen, with the formation of a small minimum at its top. Except for the absence of a minimum in curve D (fig. 98), the features observed in the field curves are in accord with the theoretical curves.

Figures 99 and 100 show horizontal resistivity profiles with the Wenner configuration across the Cowboy gilsonite vein, Uintah County, Utah. The gilsonite, a hydrocarbon material, is of higher resistivity than the surrounding country rock. The average width of the vein is between 10 and 20 feet. Figure 99 shows two profiles taken along the same traverse with different electrode separations and station intervals. For an electrode separation of 50 feet and station interval of 10 feet (fig. 99), a sharp pronounced apparent-resistivity high is flanked symmetrically by subsidiary resistivity highs on either side. Using the rule for the continuous curve that the distance between the subsidiary highs (in this case, 170 feet) is theoretically equal to the width of the vein plus 3a, we obtain a width of 20 feet, which is in accord with the order of magnitude of the known width. Although this rule strictly holds for a continuous curve, in the present case the station interval is so small that the uncertainty in the estimate is probably of the order of 10 feet.

For an electrode separation of 150 feet and a station interval of 30 feet (fig. 99B), a much broader resistivity
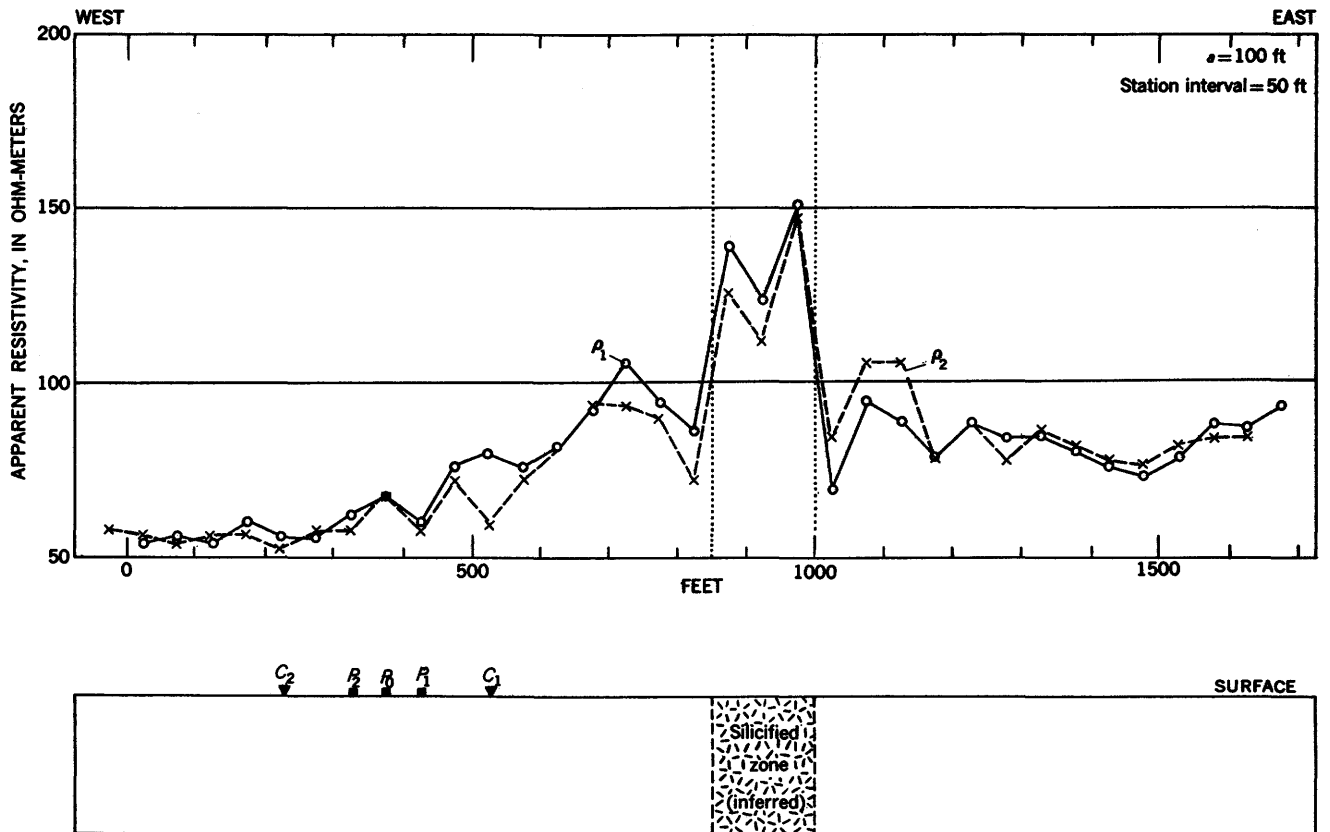
FIGURE 95.—Horizontal resistivity profile across inferred silicified limestone zone, Tri-State lead-zinc mining district, Cherokee County, Kans., Lee configuration (offset plotting). Electrode separation a=100 ft; station interval =50. K. L. Cook (1951-54, unpublished data).

high is observed. Using the rule for the continuous curve that the width of the dike is theoretically equal to the electrode separation (in this case, 150 feet) minus the width of the steep resistivity plateau on top of the resistivity high (in this case, 120 feet), we obtain a width estimate of 30 feet. This estimate of course contains a much greater uncertainty than the previous profile because 30-foot station intervals were used.

Figure 100 shows another horizontal resistivity profile with the Wenner configuration across the same vein at a different location from that in figure 99. The electrode separation is 150 feet, and the station interval is 50 feet. A pronounced apparent-resistivity high occurs over the vein; but the high is not as sharp as in the example in figure 99B with the same electrode separation.

Figure 101 shows a horizontal resitivity profile with the Wenner configuration across the Rainbow gilsonite vein, Uintah County, Utah. The average width of the vein is between 10 and 20 feet. The electrode separation a is 420 feet, and the station interval is 30 feet. A pronounced resistivity high is obtained over the vein. The vein is so narrow in relation to the electrode separation that a pronounced

peak similar to that over a perfectly insulating sheet (fig. 54A) is obtained. The rise in resistivity before the potential electrodes cross the outcrop indicates that the vein is probably wider below the surface than at the surface. The minor peak at the right indicates more broadening in that direction and probably a sharper contact. The rules for obtaining the width of the dike cannot be applied because its width at the outcrop is too small in relation to the electrode separation.

VERTICAL PROFILES

Vertical resistivity profiles can be used to detect and delineate vertical brecciated zones and dikes. In this section we investigate the effects of a vertical dike upon the vertical resistivity profiles with both the Lee and Wenner configurations. The effects observed are lateral effects. Therefore, the curves obtained are useful not only to detect vertical dikes in a region where they are expected, but also to permit the interpreter to recognize such truly lateral effects when they appear unexpectedly in field measurements over horizontal beds in depth determinations. This latter application is perhaps the more valuable of the two because techniques are superior to vertical
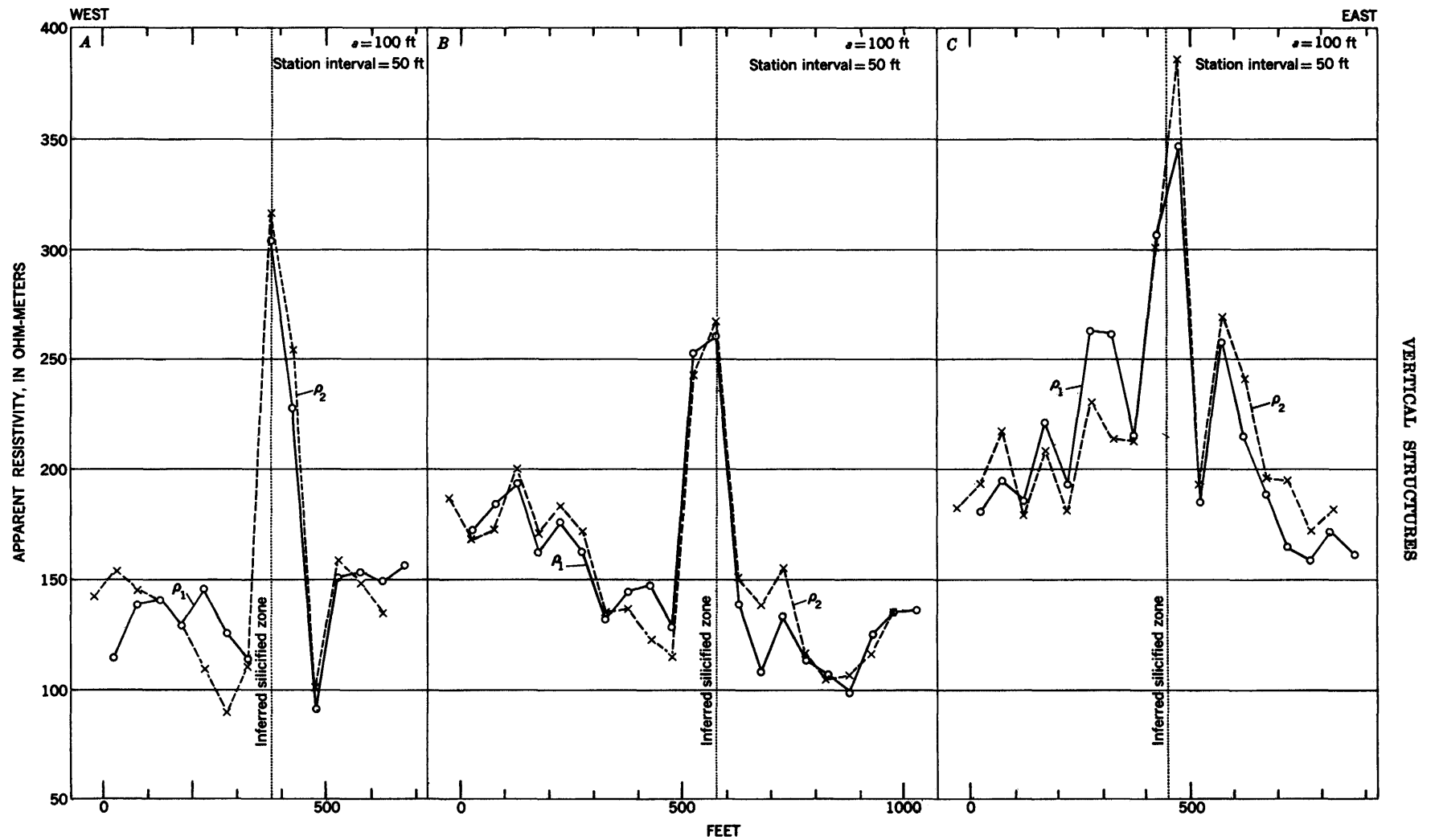
FIGURE 96.—Horizontal resistivity profiles across inferred silicified zones, Tri-State lead-zinc mining district, Cherokee County, Kans., Lee configuration (offset plotting). In each case, electrode separation *a*=100 ft, and station interval=50 ft. K. L. Cook (1951-54, unpublished data).
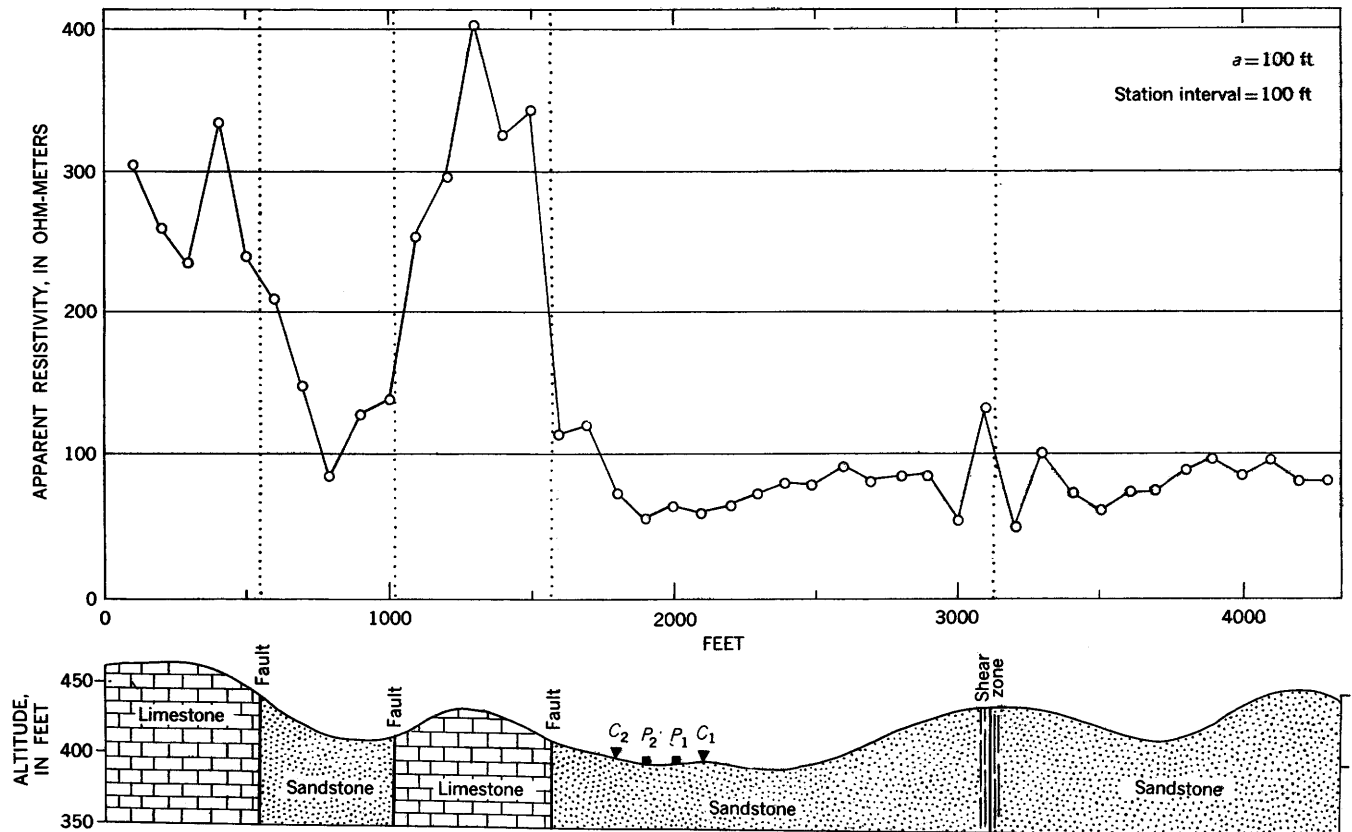
FIGURE 97.—Horizontal resistivity profile across shear zone and limestone fault block, in Illinois, Wenner configuration. Electrode separation *a*=100 ft; station interval =100 ft. Adapted from Hubbert (1932). Copyright by Am. Inst. Mining Metall. Engineers.

profiling techniques for the discovery and delineation of a dike.

Plates 3 and 4 show vertical resistivity profiles across a vertical dike of unit width b with both the Lee and Wenner configurations. The center of each configuration is taken at various distances from the dike: distances of $3b$, $2b$, and b from the left edge of the dike; at the left edge of the dike; and at the axis of the dike. Plate 3 shows the vertical resistivity profiles for a dike whose true resistivity is four times that of the surrounding country rock. In each case the ratio of the apparent resistivity to the true resistivity of the country rock is plotted for both the Lee and Wenner configurations against the ratio of the electrode separation a to the unit width b of the dike. This method of plotting permits the curves to be used for any width of dike.

Abrupt changes in slope of the apparent-resistivity curves occur as the electrodes cross the edges of the dike. In each diagram the particular electrode, or electrodes, that cross the edges are specified at the corresponding position of the abrupt change in slope of the apparent-resistivity curves.

For a dike whose true resistivity is greater than that of the country rock, for example, (pl. 3A), four abrupt changes in slope are obtained on the ρ_1 curve with the Lee configuration: a peak in the curve as current electrode C_1 crosses the left edge of the dike, a low as C_1 crosses the right edge, an abrupt increase as potential electrode P_1 crosses the left edge, and a peak as P_1 crosses the right edge. For the same dike, only two abrupt changes in slope occur on the ρ_2 curve: a peak as C_1 crosses the left edge, and an abrupt change in slope as C_1 crosses the right edge. Obviously neither current electrode C_2 nor potential electrode P_2 crosses any edges of the dike in this example. When the Wenner configuration is used at the same station for vertical profiles across the same dike (pl. 3K), similar abrupt changes in slopes of the apparent-resistivity curves occur at positions identical to those obtained with the Lee configuration. The Wenner anomalies are not as pronounced as the Lee anomalies. For any given value of electrode separation, the Wenner value of the apparent resistivity is the arithmetic mean of the ρ_1 and ρ_2 values of the apparent resistivity with the Lee configuration.
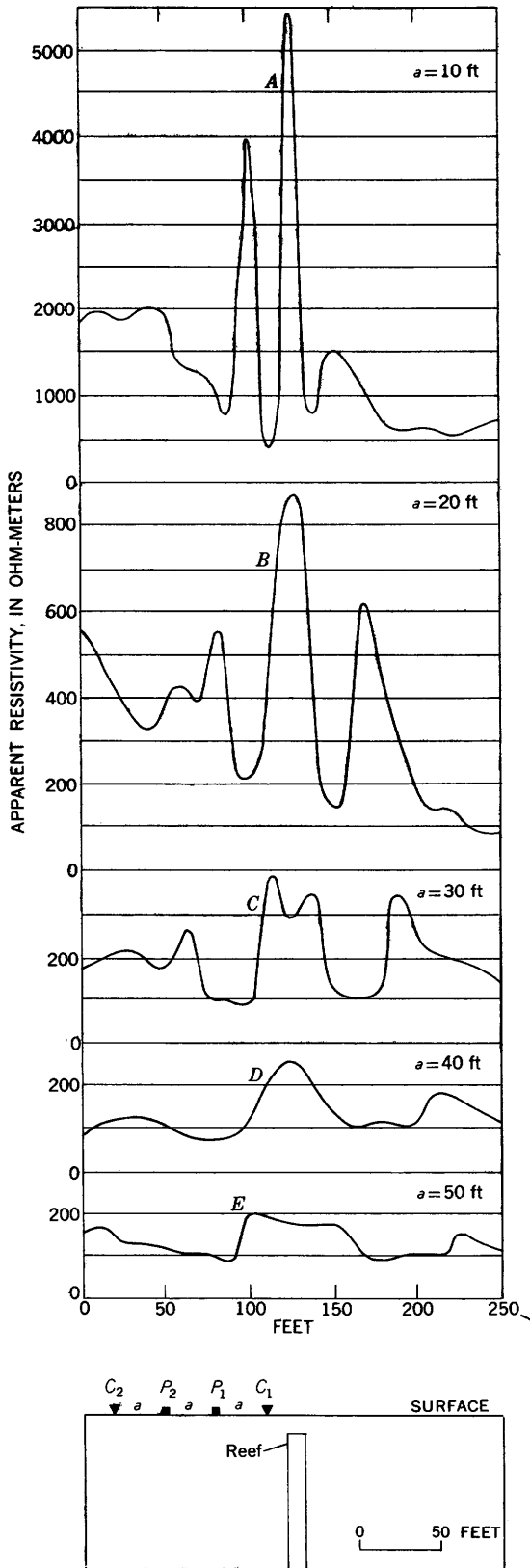
As the station is taken closer to the edge of the dike (pl. 3B, E, L, and M), the anomalies are much more pronounced, and the peaks are better defined. For a station with the center of the Lee configuration at the left edge of the dike, the values of ρ_1 and ρ_2 for very small electrode separations are 4 and 1, respectively (pl. 3D). As the configuration is expanded, both the ρ_1 and ρ_2 values decrease until current electrode C_1 crosses the right edge of the dike; then the ρ_1 values paradoxically increase rapidly to reach a peak as potential electrode P_1 crosses the right edge. For a station at the center of the vein, the apparent-resistivity curve for the Lee configuration (pl. 3D) is identical to that for the Wenner configuration (pl. 3O). Only one curve is obtained for the Lee configuration because all electrodes cross the edges symmetrically.

Plate 4 shows the corresponding vertical profiles across vertical veins whose resistivity is one-fourth that of the surrounding country rock. Except for the fact that apparent-resistivity lows are obtained instead of apparent resistivity highs, the generalizations made above apply identically to these curves. For a station with the center of the Lee configuration at the left edge of the dike (pl. 4D), the ρ_1 curve paradoxically decreases as the configuration is expanded after current electrode C_1 has crossed the right edge of the dike and until potential electrode P_1 crosses the right edge. For a station taken at the center of the dike for either the Lee or Wenner configurations (pl. 4E, and O), a peak is obtained as current electrodes C_1 and C_2 simultaneously cross the right and left edges, respectively. This peak is caused by the converging property of the current as it flows between current electrodes in a low-resistivity medium that is confined between media of higher resistivity. The current-converging property manifests itself especially as the current electrodes lie within the low-resistivity material and immediately adjacent to the wall of the dike.

Although the edges and hence the width of a dike can be obtained from vertical-profile measurements, it is generally faster and cheaper to determine the edges and width of the dike by horizontal-profile techniques.

Figure 102 shows an observed vertical profile across a high-resistivity steeply dipping quartzite bed in the Mountain City copper district, Elko County, Nev. (C. H. Sandberg and K. L. Cook, 1945, unpublished data). The traverse was taken in a due north direction, and the strike of the quartzite bed is probably about N. 80° W.; therefore, the traverse is within about 10° from being perpendicular to the strike of the bed. The quartzite bed, which is partly exposed, is believed to be overlain and underlain conformably with shale; in the immediate area of the traverse, however, neither the shale nor the shale-quartzite contact is exposed but

FIGURE 98.—Horizontal resistivity profiles across Bauerle's "reef" (dikelike feature) with various electrode separations, Busia gold field, Uganda, Wenner configuration. Adapted from Way (1944). Copyright by Am. Inst. Mining Metall. Engineers.
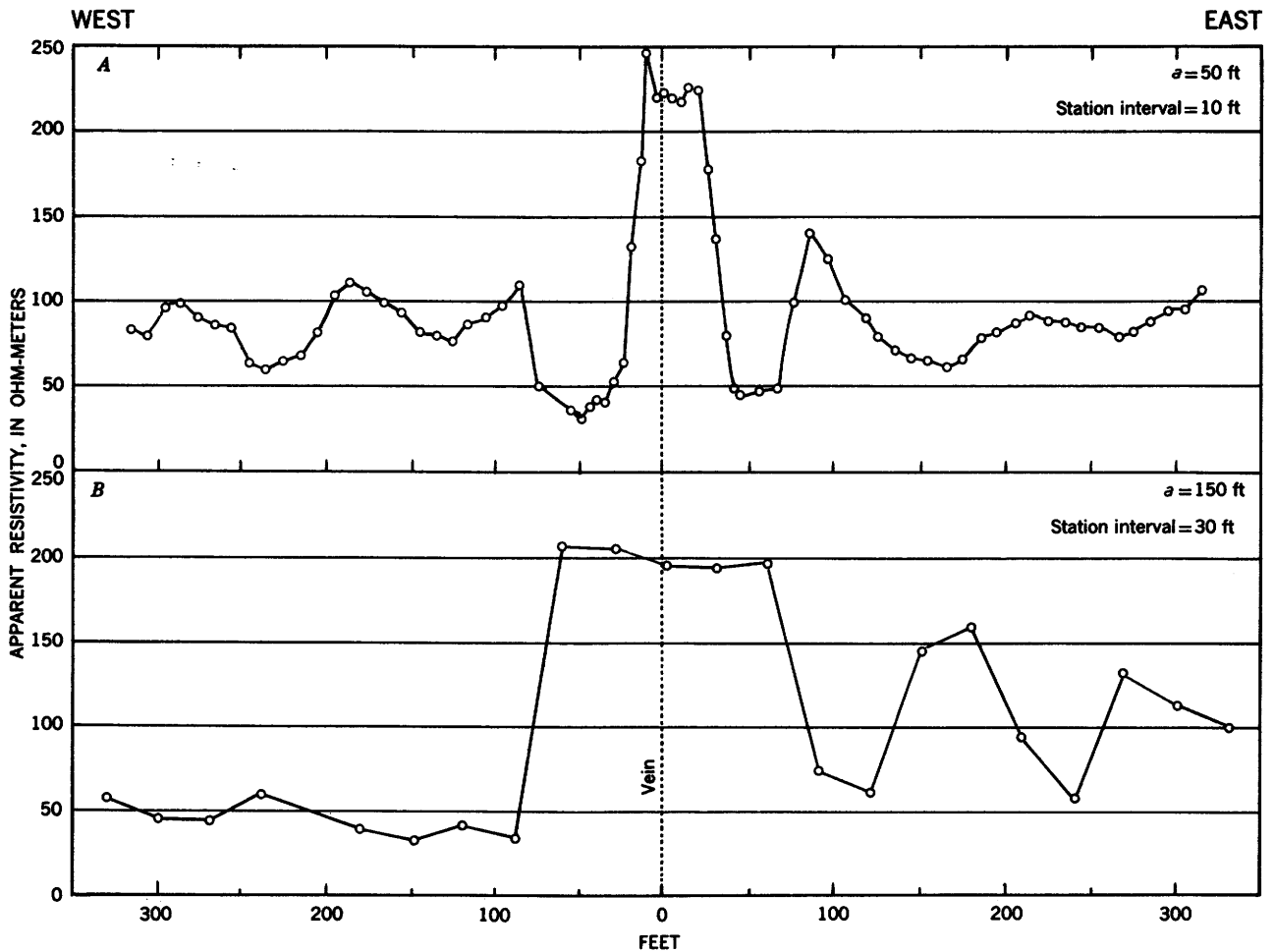
FIGURE 99.—Two horizontal resistivity profiles along same traverse across Cowboy gilsonite vein, Uintah County, Utah, with different electrode separations and station intervals, Wenner configuration. (A) Electrode separation a=50 ft; station interval=10 ft. (B) a=150 ft; station interval=30 ft. Data by LeRoy Scharon, released for publication through the courtesy of the Sinclair Research Laboratories, Tulsa, Okla.
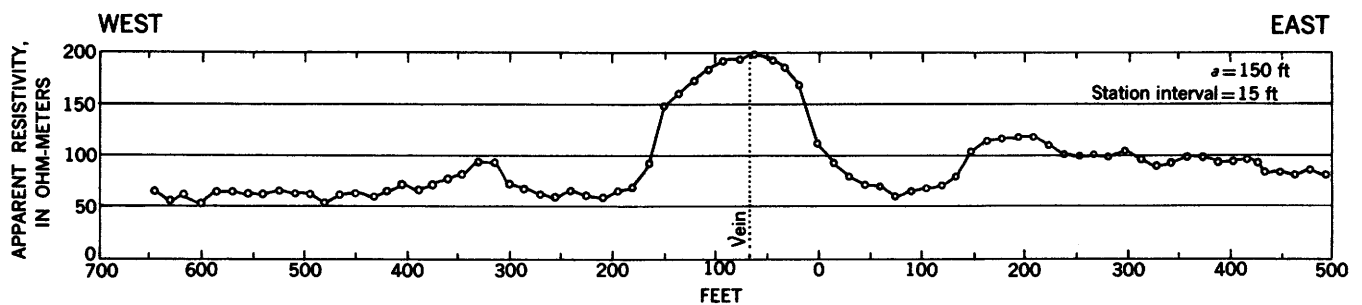
FIGURE 100.—Horizontal resistivity profile across Cowboy gilsonite vein, Uintah County, Utah, Wenner configuration. Electrode separation a=150 ft; station interval= 15 ft. Data by LeRoy Scharon, released for publication through the courtesy of the Sinclair Research Laboratories, Tulsa, Okla.

is covered with a thin veneer of alluvium. The observed apparent-resistivity curves are similar to the theoretical curves in plate 3C. Because the field data are for discrete points only rather than being a continuous curve, the estimates of the edges of the quartzite vein have an inherent uncertainty.

The discontinuity in slopes of the observed curves indicate that the quartzite bed is probably about 55 feet thick and that the south edge of the quartzite bed lies about 120 feet north of the resistivity station. Peak A in the ρ_1 curve occurs theoretically for a continuous curve as current electrode C_1 crosses the south
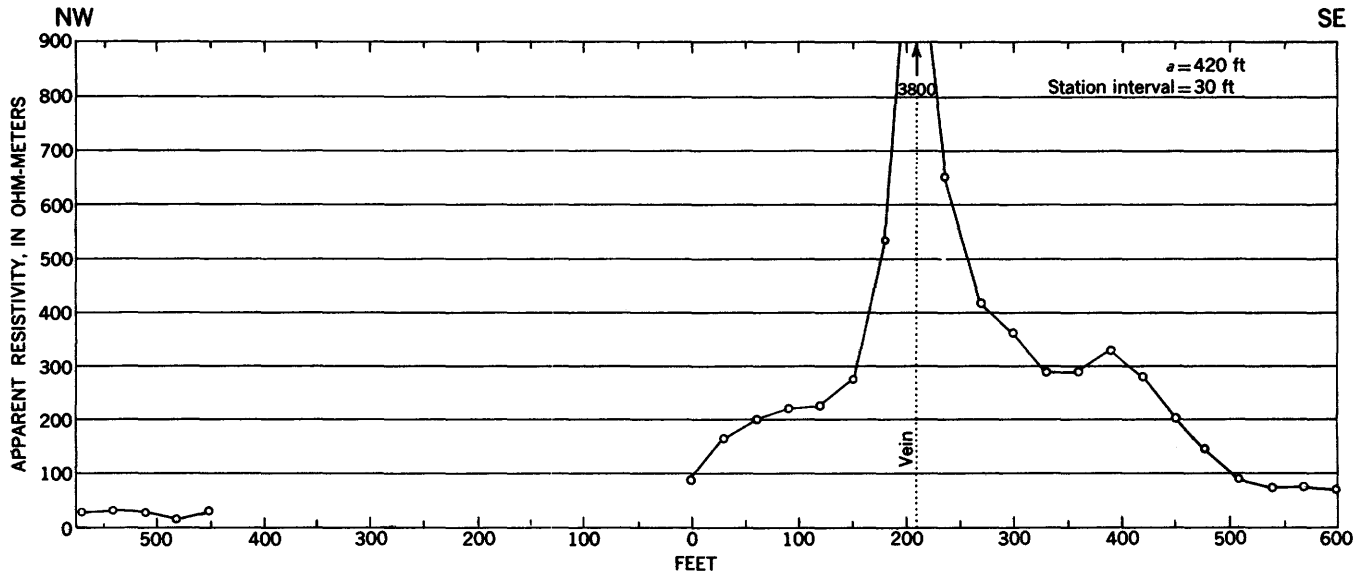
FIGURE 101.—Horizontal resistivity profile-across Rainbow gilsonite vein, Uintah County, Utah, Wenner configuration. Electrode separation a=420 ft; station interval =30 ft. Data by LeRoy Scharon, released for publication through the courtesy of the Sinclair Research Laboratories, Tulsa, Okla.

edge of the quartzite bed; since peak A occurs at an electrode separation $a=80$ feet, the south edge of the bed is drawn at a distance of $3a/2$, or 120 feet, north of the resistivity station in the geologic cross section in figure 102. The corresponding peak in the ρ_2 curve, which should theoretically occur for the same value of a, as does the ρ_1 peak, actually occurs in this example at a lower value of a, probably because of local effects. A sharp rise in the ρ_1 curve at point C occurs theoretically for a continuous curve as potential electrode P_1 crosses the south edge of the bed; in the present example, however, the ρ_1 values rise so steeply in this part of the ρ_1 curve that the point of discontinuous slope cannot be picked with confidence. Peak D in the ρ_1 curve occurs theoretically for a continuous curve as potential electrode P_1 crosses the north edge of the bed; since peak D occurs at an electrode separation $a=340$ feet, the north edge of the bed is tentatively considered to lie a distance of $a/2$, or 170 feet, north of the resistivity station. The apparent resistivity low at B occurs theoretically for a continuous curve as current electrode C_1 crosses the north edge of the bed; in the present example the low at B occurs at an electrode separation $a=120$ feet when current electrode C_1 is 180 feet north of the resistivity station and thus 10 ft north of the tentatively assigned position of the north edge of the quartzite bed as inferred from peak D. By taking an average of these two determinations, the position of the north edge of the quartzite bed is inferred to lie 175 feet north of the resistivity station, thus making the width of the bed equal to 55 feet; and the bed is so drawn in the geologic section in figure 102.

The agreement between the theoretical and observed curves is believed excellent in this field example.

POTENTIAL-DROP-RATIO TECHNIQUES

The advantages of potential-drop-ratio techniques in detecting vertical discontinuities have long been known. In this section we will show several typical potential-drop-ratio anomalies across vertical dikes and discuss them in relation to the resistivity anomalies obtained with conventional resistivity techniques. Anomalies will be shown for both the constant-spacing system and the expanding-electrode system.

The theoretical plots in this paper for the potential-drop-ratio method use a linear scale; there is an advantage, however, in plotting the data on semi-logarithmic paper.

CONSTANT-SPACING SYSTEM

Figure 103 shows the profiles with the constant-spacing system of the potential-drop-ratio (PDR) method across a vertical dike of width b. The reflection factors are $k=\pm 0.6$. The current electrode is fixed at various distances from the dike: distances of $3b$, $2b$, and b to the left of the left edge of the dike; at the left edge, and on the axis of the dike. The distance between the potential electrodes is kept fixed at a value of $b/2$ as all three potential electrodes are moved together, thus varying r only; where r is the distance between current electrode C_2 and center potential electrode P_0. On the charts the horizontal distance from current electrode C_2 to center potential electrode P_0 is shown on the abscissa in terms of the width of the dike b as unity so that these curves are
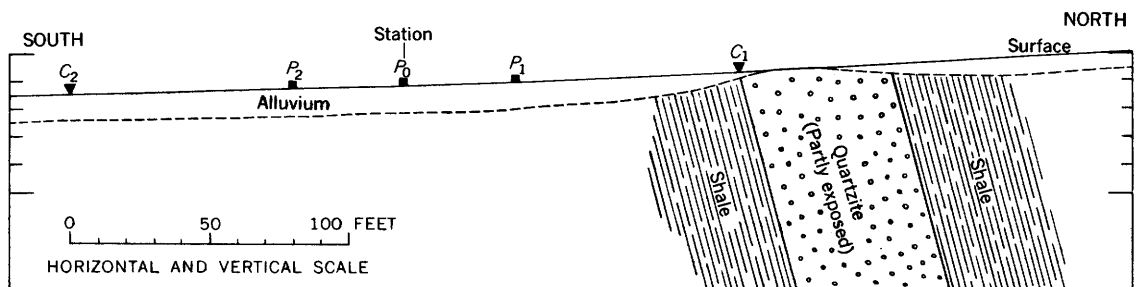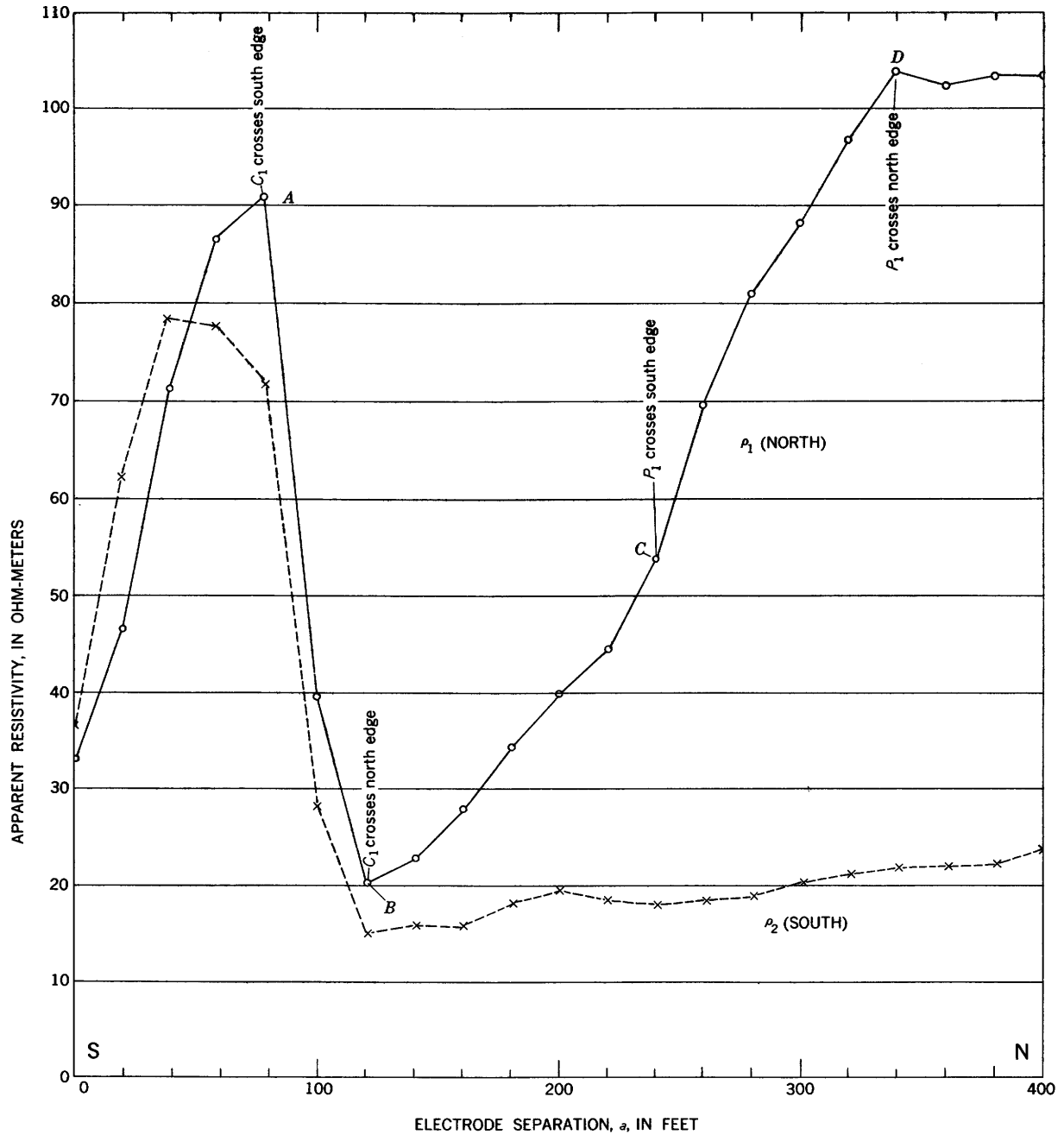
FIGURE 102.—Vertical resistivity profile across high-resistivity steeply dipping quartzite bed, Mountain City copper district, Elko County, Nev., Lee configuration. Adapted from C. H. Sandberg and K. L. Cook (1945), unpublished data.
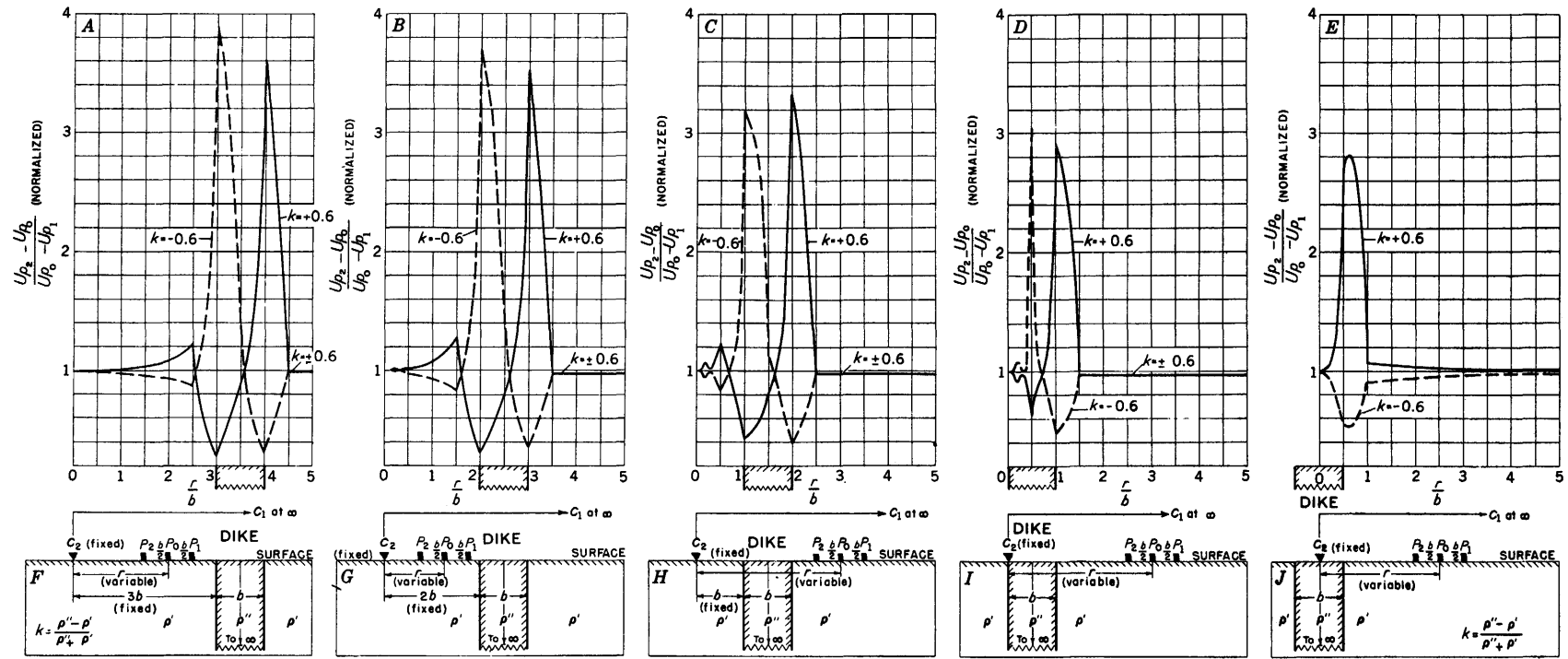
FIGURE 103.—Profiles with constant-spacing system of potential-drop-ratio method across a vertical dike of width b, with current electrode C_1 fixed at various distances from the dike. Data are normalized. Solid curves for reflection factor $k=+0.6$, and dashed curves for reflection factor $k=-0.6$.

independent of the scale used, although, of course, they apply only where the distance between the consecutive potential electrodes is equal to half the width of the dike. The data are plotted at the position of center potential electrode P_0. The normalized values of the potential drop ratio $(U_{P_2}-U_{P_0})/(U_{P_0}-U_{P_1})$, which are obtained by multiplying the actual theoretical potential-drop-ratio values by $(r-b/2)/(r+b/2)$, are plotted on the ordinate. The normalized potential-drop-ratio index for homogeneous ground is unity. In each case the solid curve applies for a dike whose true resistivity is higher than that of the surrounding country rock, and the dashed curve applies for a dike whose true resistivity is lower than that of the country rock.

For a dike that is a distance of $3b$ from the fixed current electrode and whose true resistivity is greater than that of the surrounding country rock (fig. 103A, solid curve), abrupt changes in slope are obtained as the potential electrodes cross the edges of the dike; and the points of these changes in slope can be used to determine the edges and width of the dike. The sharpest changes in the curve occur as potential electrode P_0 crosses the edges of the dike. A sharp pronounced PDR low coincides with the left edge of the dike, and a sharp peak coincides with the right edge of the dike; and obviously, for the continuous curve, the horizontal distance between these two features gives the width of the dike. The anomalies are pronounced. Whether a maximum or minimum is obtained at a specific edge of the dike depends on whether the fixed current electrode is placed to the left (as shown in fig. 103) or right of the dike. For the same dike that is a distance of $2b$ or b from the fixed current electrode (figs. 103B, C), the same generalizations apply. When the current electrode is placed at the left edge of the dike (fig. 103D), a PDR minimum is obtained over the axis of the dike and a peak over the right edge of the dike. When the current electrode is placed over the axis of the dike (fig. 103E), only a PDR maximum, which lies to the right of the right edge of the dike, is obtained. When current electrode C_2 lies at the left edge of the dike or over the country rock to the left of the left edge of the dike, the normalized PDR value is always equal to one in the region to the right of the dike when all potential electrodes lie over this region.

Paradoxically, the magnitude of the maximum and minimum observed PDR values decreases progressively as the fixed current electrode is placed nearer the dike. This property does not mean that a dike would be detected more easily by placing current electrode C_2 a distance of $3b$ rather than b from the dike, however, because the observed potential differences at great distances from C_2 are much more difficult to measure

accurately. Therefore, a dike is ordinarily easier to detect when current electrode C_2 is near the dike than when it is far removed, even though the theoretical PDR anomaly is somewhat smaller.

The same generalizations as those given above apply to a dike whose resistivity is less than that of the surrounding country rock (fig. 103A–E, dashed curves), except that the maxima and minima PDR values coincide with the left and right edges, respectively, of the dike. It is necessary to know whether the fixed current electrode lies to the left (as shown in fig. 104) or right of the dike in order to know whether the dike is of high or low resistivity relative to the country rock. The relative positions of the electrodes would of course be known in field operations.

Figure 104 shows the profiles with the constant-spacing system of the potential-drop-ratio method across a vertical dike of width b (Kiyono, 1950b). The resistivity contrasts are $\rho''/\rho'=1/10$ (fig. 104A) and $\rho''/\rho'=10$ (fig. 104B). The data are plotted on semilogarithmic paper. The convention of taking the potential-drop ratio in this case is the reverse of that shown in figure 103.

Figure 105 shows an observed profile with the constant-spacing system of the potential-drop-ratio method across an andesite dike of high resistivity near Lebong Donok gold mine, Sumatra (Hedström, 1932). The separation between the potential electrodes is 30 feet, and the station interval is 30 feet. The PDR data are normalized and plotted on semilogarithmic paper. The PDR anomaly shows a high peak on the left side of the dike and a sharp low on the right side; the curve crosses the normalized unity at a point lying over the central part of the dike. The anomaly curve is similar to that in figure 103A.

Figure 106 shows an observed profile with the constant-spacing system of the potential-drop-ratio method across the dikelike Falconbridge pyrrhotite orebody, Ontario, Canada (Heiland, 1942, p. 80). The data were obtained by surveying in two directions with a potential ratiometer (Swedish-American Racom method), which gives the ratio of potential differences in adjacent ground intervals. Data were taken in opposite direction from the two power electrodes for the "elimination" of surface anomalies, and the PDR data (curves A and B), were averaged to give curve C. The data were not normalized in this case; therefore, the physical property actually plotted is the potential gradient per unit distance (electric-field intensity). The potential gradient curve C shows a minimum in the middle of the profile, indicating a good conductor. The asymmetry of the average curve indicates the direction of dip.

Figure 107 shows an observed profile with the con-
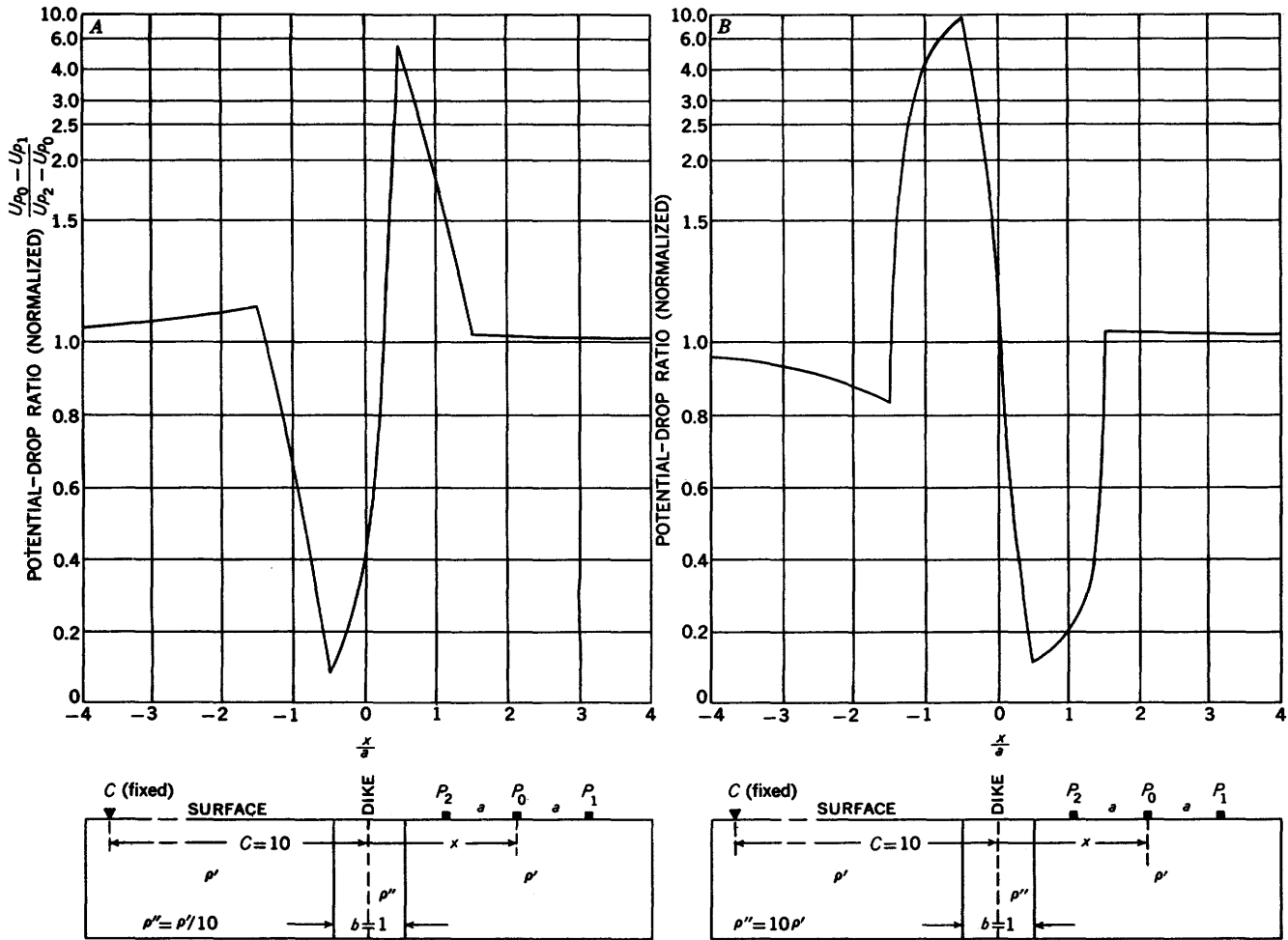
FIGURE 104.—Profiles with constant-spacing system of potential-drop-ratio method across a vertical dike of width b, with current electrode C_2 fixed at a distance of 10 units from axis of dike. Data are normalized. (A) Curve for $\rho''/\rho'=1/10$; (B) Curve for $\rho''/\rho'=10$. Adapted from Kiyono (1950b).

stant-spacing system of the potential-drop-ratio method across a graphite zone at the Graphite mine, Port Lincoln, South Australia (Broughton Edge and Laby, 1931, p. 118). The data are not normalized. The potential-gradient curve shows a minimum over the low-resistivity graphite zone; the small peaks on either side signify a crowding of the equipotential lines. On the basis of the electrical survey, a graphite body about 50 feet in width and dipping about 45° to 50° NW. was discovered.

Figure 108 shows a profile with the constant-spacing system of the potential-drop-ratio method across a quartz vein, in the Woodall area, McDuffie County gold belt, Georgia. The known width of the vein on the right side of the profile is at least 3 feet. The resistivity of the quartz veins is higher than that of the surrounding country rock. The distance between each of the three potential electrodes was 50 feet and the interval between stations was also 50 feet. The data plotted are actually the ratios of resistances

as measured with these electrodes rather than ratios of potential differences as such. A pronounced peak is obtained over the known vein.

EXPANDING-ELECTRODE SYSTEM

Figures 109, 110, 111, and 112 show profiles with the expanding-electrode system of the potential-drop-ratio method across a vertical dike of width b, which is taken as the unit of length. The assumed reflection factors in each case are $k=\pm 0.6$. Current electrode C_2 is taken at various fixed distances from the dike: distance of $3b$ (fig. 109), $2b$ (fig. 110), and b (fig. 111) to the left of the left edge of the dike; and on the axis of the dike (fig. 112). In the conventional expanding-electrode system, the electrode configuration is made identical to the asymmetrical Lee configuration because the normalizing factor is then always equal to one-half; this normalizing factor gives a PDR index of unity for homogeneous ground. The normalized values of the potential-drop-ratio values are plotted on the
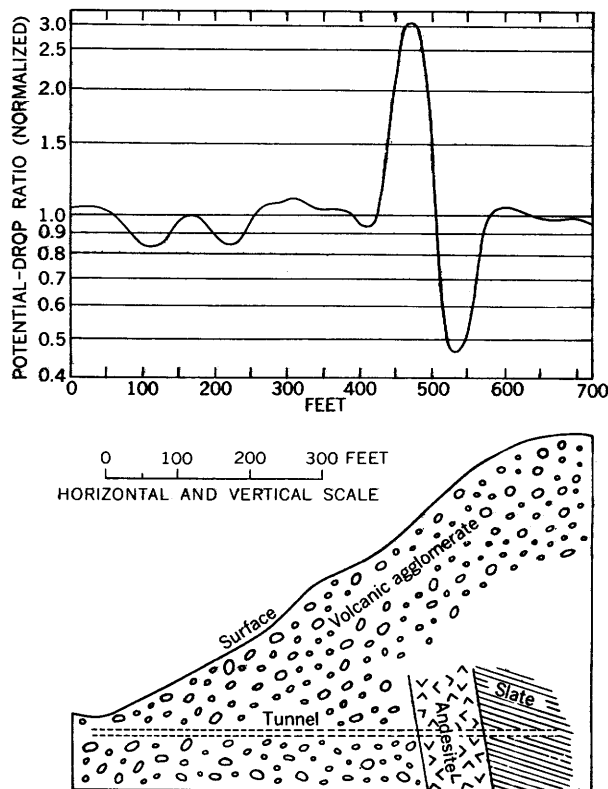
FIGURE 105.—Profile with constant-spacing system of potential-drop-ratio method across an andesite dike of high resistivity, near Lebong Donok gold mine, Sumatra. Separation between potential electrodes=30 ft; station interval=30 ft. Data are normalized. Adapted from Hedström (1932) by permission of The Mining Magazine.

ordinate. On the abscissa are plotted the values of the electrode separation a in terms of the width of the dike b as unity so that the curves are independent of the scale used, although, of course, they apply only where the current electrode lies a specified distance from the dike. The solid part of each profile curve applies when the configuration lies to the right of the current electrode; and the dashed part applies when the configuration lies to the left of the current electrode.

For a dike that is a distance of $3b$ from the fixed current electrode and whose true resistivity is greater than that of the surrounding country rock—that is, the positive reflection factor, is as shown in fig. 109A— abrupt changes in slope are obtained as the potential electrodes cross the edges of the dike; and the points of these changes in slope can be used to determine the edges and width of the dike. Whether a maximum or minimum is obtained at a specific point in relation to the edge of the dike depends on whether the fixed current electrode is placed to the left (figs. 109, 110, and 111) or right of the dike. When the current electrode lies closer to the dike (figs. 110A and 111A), the positions of the abrupt changes in relation to the dike are of course different in each case; and also the magnitude

of the PDR anomaly is somewhat larger than when the current electrode is farther removed from the dike. When the current electrode lies on the axis of the dike (fig. 112A), a sharp pronounced anomaly occurs, but it is confined to only a small distance horizontally; the peaks are so narrow that they might easily be missed unless the station spacing is small.

SUMMARY OF POTENTIAL-DROP-RATIO METHOD OVER DIKES

Potential-drop-ratio techniques give sharper anomalies over vertical dikes than do the conventional resistivity techniques.

All of the theoretical curves shown here are continuous curves. Because only discrete stations are usually taken in the PDR techniques as well as in resistivity techniques, the PDR method also contains inherent uncertainties of detecting the edges and estimating widths of dikes—as was true for resistivity methods. PDR anomalies are greater for dikes of good conductivity than for dikes with correspondingly poor conductivity.

DIPPING FAULTS AND BEDS

Having examined in detail the effects of horizontal bedding and vertical structures on resistivity data, we now study similar geological features that are neither strictly horizontal nor strictly vertical. In the present section we will show not only how to recognize dip in structures, but also how the dip may be measured quantitatively in some cases. The features on apparent-resistivity curves that are diagnostic of dipping faults and beds are so subtle that they are usually obscured in the normal fluctuations found in routine field surveys designed for purposes other than dip studies. Unfortunately no field examples of dip studies are available to us that portray the characteristics of dipping faults and beds which we regard as diagnostic in the theoretical curves.

In a previous section, "Applications of the image theory" (p. 51 to 62), we discussed the simplest cases of dipping faults and beds, in which image theory is applicable. As emphasized in that section, such solutions are restricted not only to infinite resistivity contrasts but also to certain finite angles. Moreover, the solutions are not applicable on the updip side of the surface trace of the dipping fault plane or dipping contact. In the present section we will develop the theory that enables us to calculate data for any resistivity contrast, for any angle of dip, and for any point in the vicinity of the dipping fault or dipping bed. These solutions are then used to compute data for the theoretical curves which are given. Because the mathematics for dipping beds in this section is the most difficult of the theory contained in this treatise, the nonmathematical reader may wish to omit the mathe-
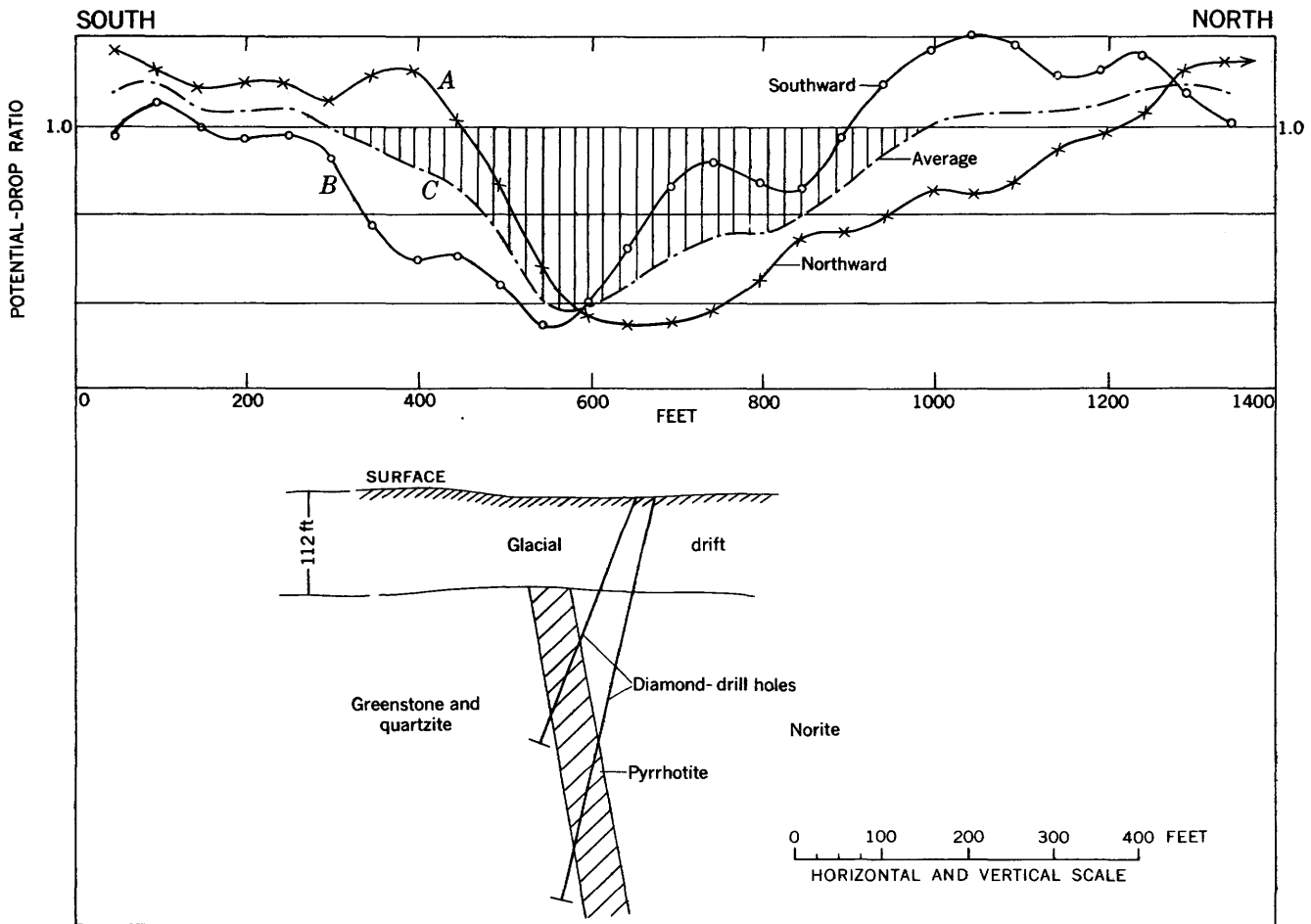
Figure 106.—Profile adapted from Lundberg by Heiland (1942, p. 80) showing constant-spacing system of potential-drop-ratio method across Falconbridge pyrrhotite orebody, Ontario, Canada. PDR data are not normalized.

matical part of this section and continue immediately to the discussion of the theoretical curves, which is understandable without a knowledge of the mathematics.

Our development is limited to the consideration of single interfaces between materials of different resistivity or of perfectly conducting separations between materials of the same resistivity. To our knowledge there are no exact theoretical curves that have been published to date (1964) for dipping dikes or for dipping beds involving more than one interface.

THEORY OF DIPPING FAULTS AND BEDS

The general theory of electrical prospecting over dipping faults and beds can be attacked in several ways. Tikhonov (1946) obtained a solution to the appropriate integral equations by means of successive approximations. Tyurkisher (1946) extended these solutions and showed that part of the solution reduced to a complete elliptic integral. Some approximate curves, based on Tikhonov's method, for dip angles of 30°

and 45° were published by Berel'kovskiy and Zubanov (1951). The theoretical work of this group culminated in the studies of Skal'skaya (1948), who obtained a complete solution to the problem for all possible angles of dip, following a modification of the procedure established by Grinberg (1940), in solving the corresponding electrostatic problem. Her method involves the use of a Fourier-Bessel type integral transformation.

In the following section we will solve the problem by the direct solution of the differential equation, following the method introduced by Maeda (1955). The general solution will then be transformed into a simpler form for certain cases useful for computations. The method introduced by Chastenet de Géry and Kunetz (1956) will be used. Since the limiting cases when the electrodes are alined along the fault trace are useful in determining the dip of the contact, these limiting cases will also be developed. Finally, we will develop the method of MacDonald (1895), which is useful for general angles of dip but for infinite-resistivity contrasts only.

WEST   EAST

Potential-electrode separation (a) = 50 ft

POTENTIAL VARIATION

1800   1600   1400   1200   1000   800

FEET

Current line electrode
at 4000 ft

Current line electrode
at zero →

P_3 P_2 P_1

SURFACE

Gneiss   Graphite lode   Schist
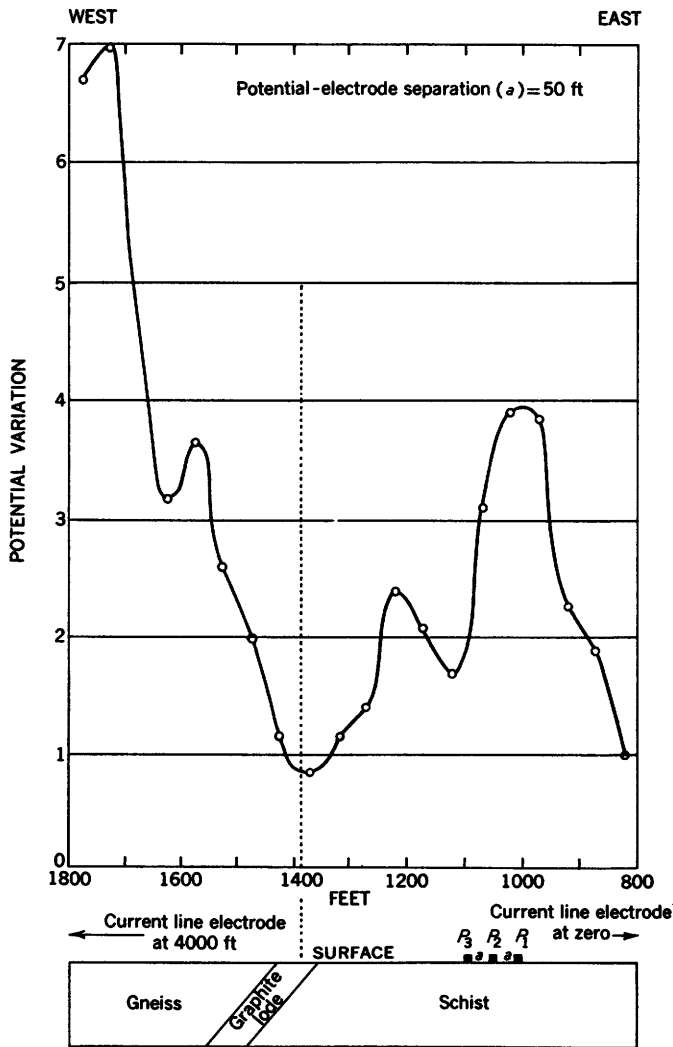
FIGURE 107.—Profile with constant-spacing system of potential-drop-ratio method across graphite zone, Graphite mine, Port Lincoln, South Australia. PDR data are not normalized. Adapted from Broughton Edge and Laby (1931).

A GENERAL SOLUTION

Let us consider a point source of current on the earth's surface in the vicinity of a dipping contact between two formations (fig. 113). This contact can be either the contact between two dipping beds or a fault plane separating different materials; in this discussion, we choose to refer to the contact as a fault plane. The resistivity of the material above the contact is ρ' and that of the material below the contact is ρ''. We choose a cylindrical coordinate system in which the fault trace is the z-axis and the origin is such that $z_0 = 0$ and $\phi_0 = 0$.

In this problem we require the solutions of Laplace's equation given by equation 74. In region 1, we can use the solution as it is written. However, since the function must be an even function of ϕ, it follows that

the two arbitrary constants must be equal. The potential must similarly be symmetrical about the plane $\phi = \pi$ in order that no current crosses that plane, whence we discard the form of the general solution containing cosh $s(\pi + \phi)$ in setting up a function for region 2. Thus, we have

$$U_{1A} = \frac{I\rho'}{2\pi} \left\{ \frac{1}{R} + \int_0^\infty \cos tz dt \int_0^\infty A[\cosh s(\pi + \phi) + \cosh s(\pi - \phi)] K_{is}(tr) ds \right\}$$

$$U_{2A} = \frac{I\rho'}{2\pi} \left\{ \frac{1}{R} + \int_0^\infty \cos tz dt \int_0^\infty B \cosh s(\pi - \phi) K_{is}(tr) ds \right\}. \quad (180A)$$

When we apply the condition $U_{1A} = U_{2A}$ at $\phi = \phi_1$, we get

$$A[\cosh s(\pi + \phi_1) + \cosh s(\pi - \phi_1)] = B \cosh s(\pi - \phi_1). \quad (181)$$

SOUTH   NORTH

Station interval = 50 ft
Potential-electrode separation (a) = 50 ft

POTENTIAL-DROP RATIO

0   100   200   300   400   500   600   700   800   900   1000   1100

FEET

P_3 P_2 P_1

SURFACE

Sandy stringers and quartz veinlets   Vein   13 veins   Vein
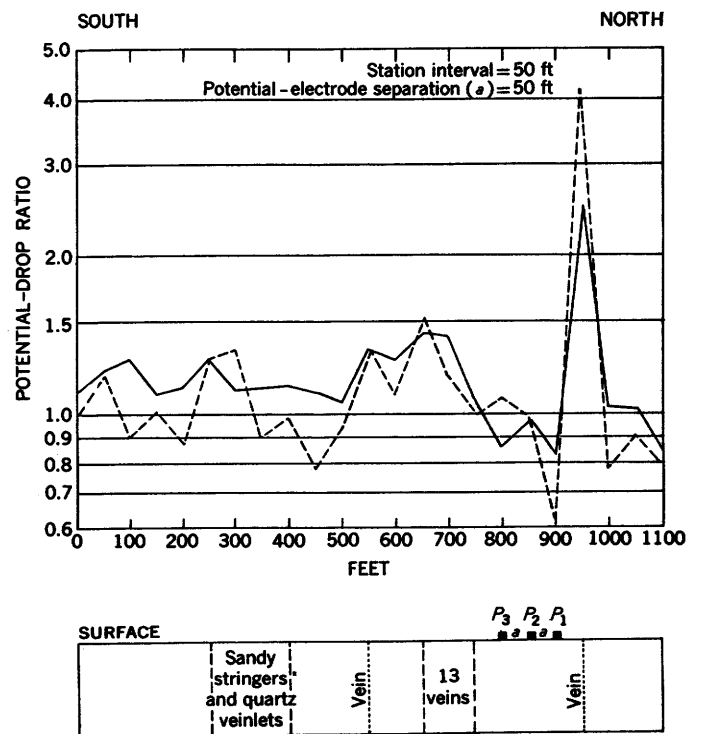
FIGURE 108.—Profile with constant-spacing system of potential-drop-ratio method across quartz vein, Woodall area, McDuffie County gold belt, Georgia. Data are not normalized. Known width of vein is at least 3 ft. Adapted from Kelly, Zuschlag, and Low (1934). Copyright by Am. Inst. Mining Metall. Engineers.

We then substitute the expansion for $1/R$ given by equation 110 and apply the condition that the normal component of current density must be continuous across the plane $\phi = \phi_1$. Thus, we get

$$A(1+k)[\sinh s(\pi + \phi_1) - \sinh s(\pi - \phi_1)] + B(1-k) \sinh s(\pi - \phi_1)$$

$$= \frac{8k}{\pi^2} \sinh s(\pi - \phi_1) K_{is}(tr_0). \quad (182)$$

FIGURE 109.—Profiles with expanding-electrode system of potential-drop-ratio method across a vertical dike of width b, with current electrode C_1 at a fixed distance $3b$ from the dike. Data are normalized. Reflection factors are $(A)k=+0.6$; $(B)k=-0.6$.
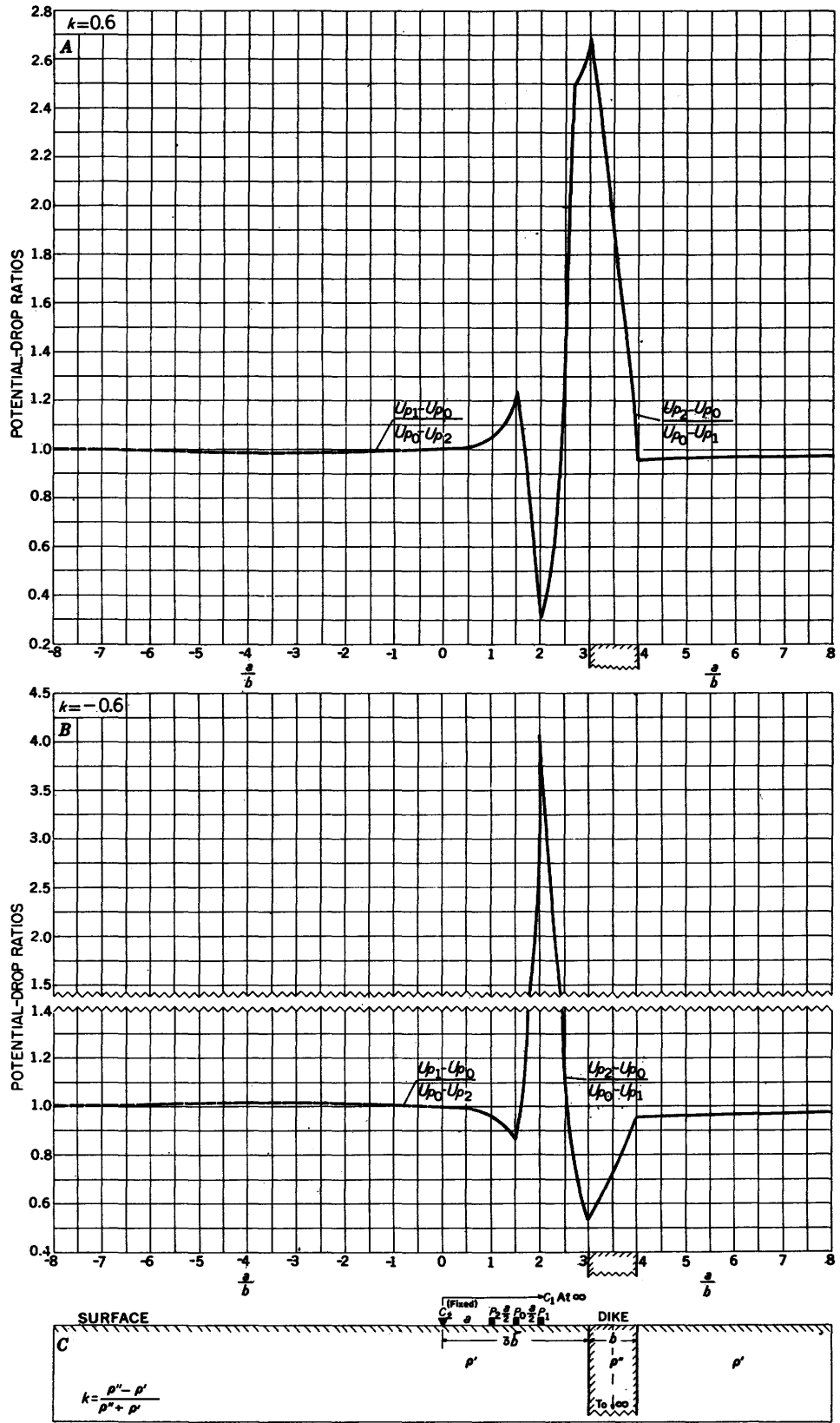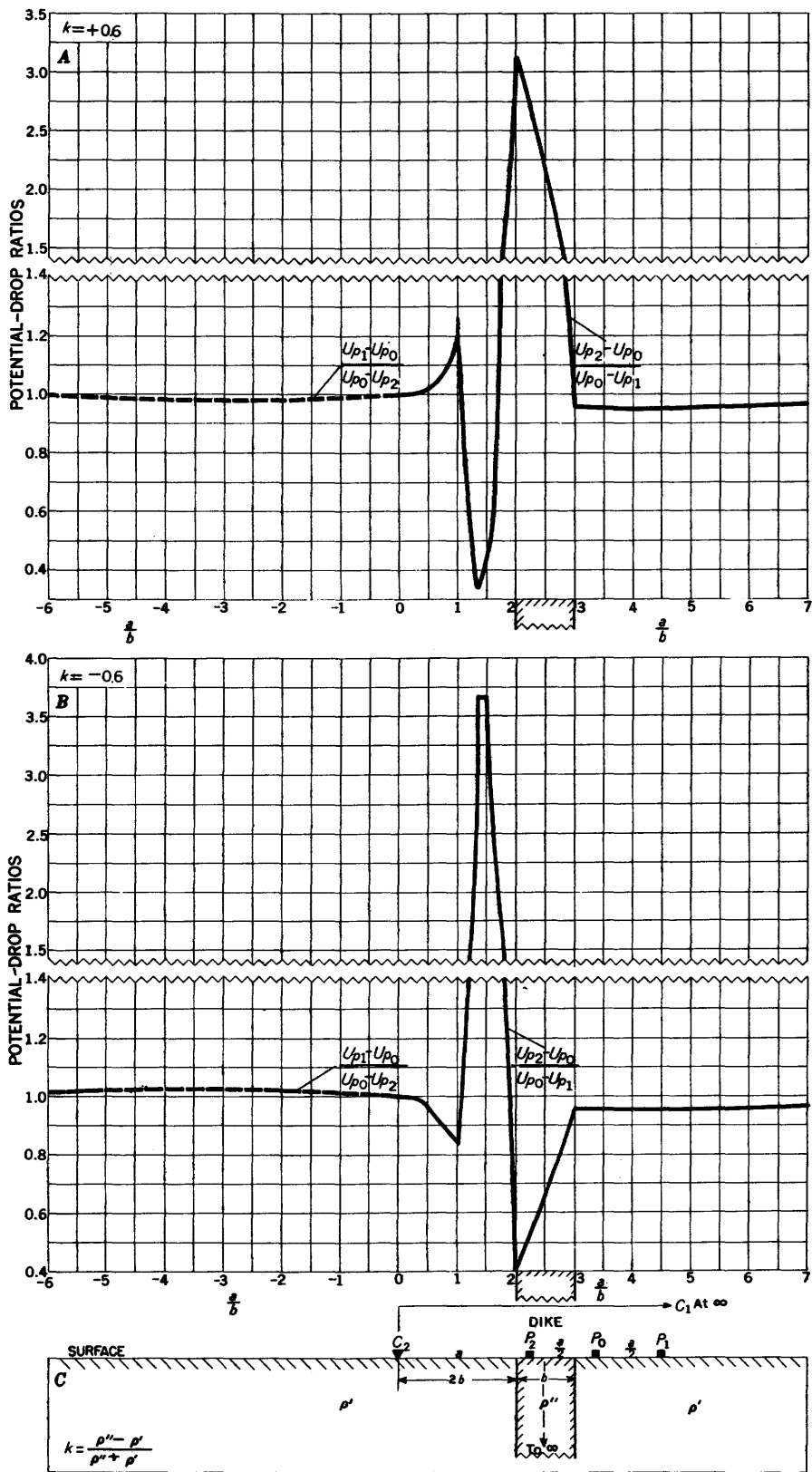
FIGURE 110.—Profiles with expanding-electrode system of potential-drop-ratio method across a vertical dike of width b, with current electrode C_2 at a fixed distance $2b$ from the dike. Data are normalized. Reflection factors are $(A) k = +0.6$; $(B) k = -0.6$.
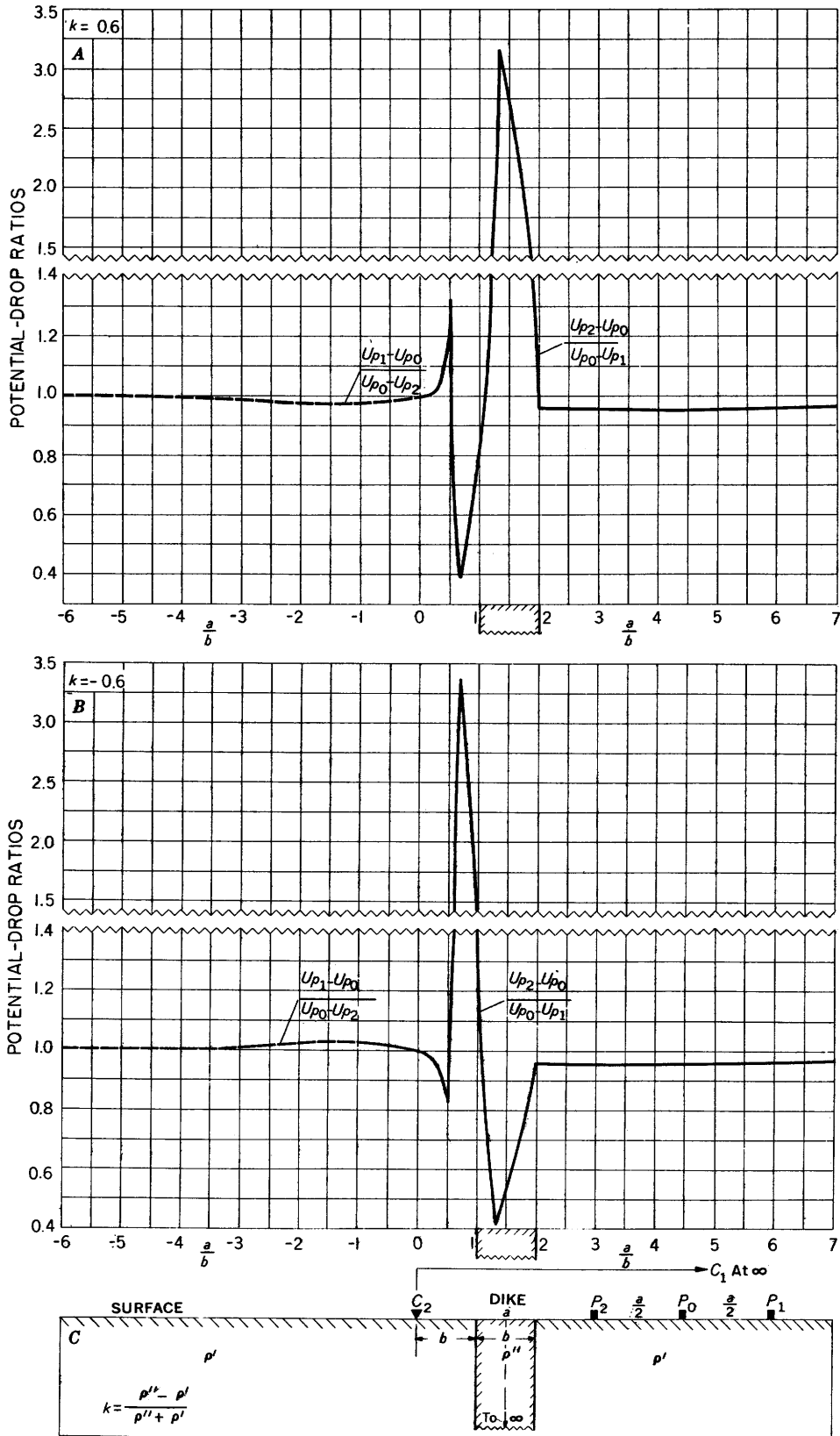
FIGURE 111.—Profiles with expanding-electrode system of potential-drop-ratio method across a vertical dike of width b, with current electrode C_1 at a fixed distance b from the dike. Data are normalized. Reflection factors are $(A) k = +0.6$; $(B) k = -0.6$.
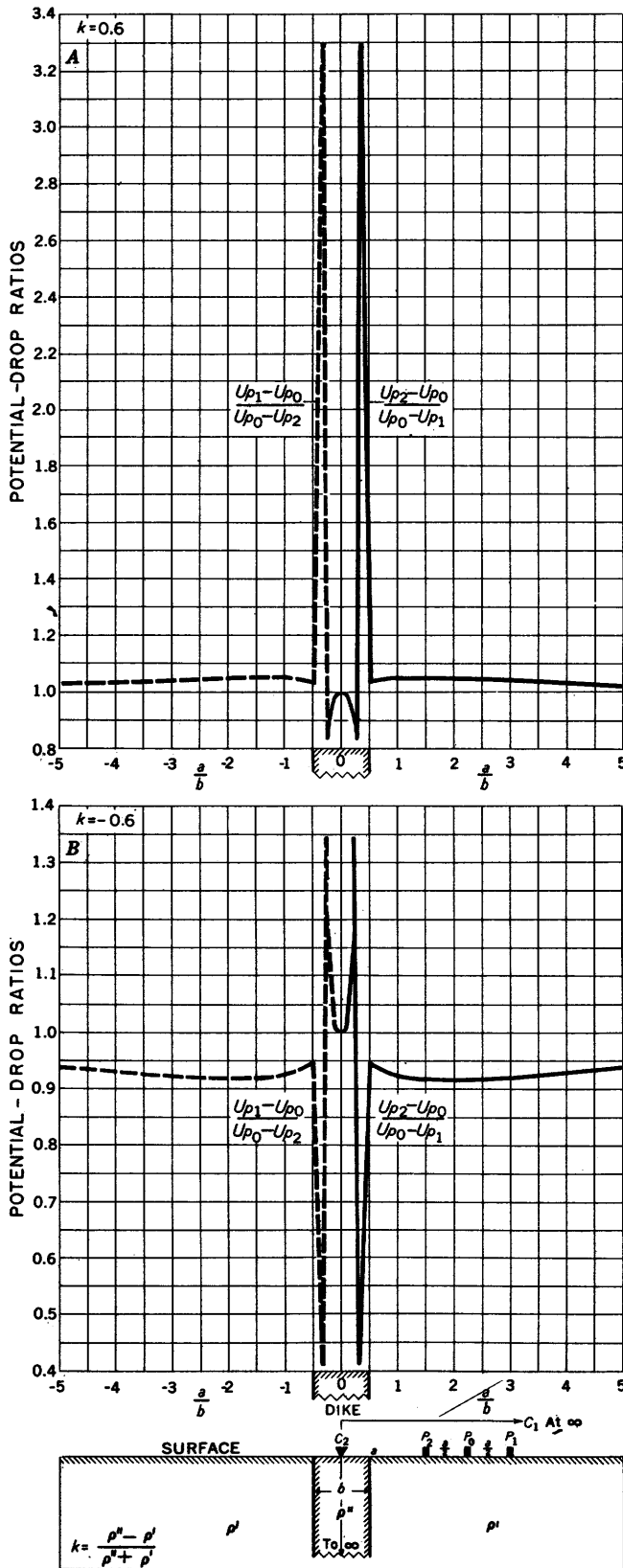
FIGURE 113.—Cross-sectional view of a point source of current C in the vicinity of a dipping fault.

We solve equations 181 and 182 as a set of simultaneous equations for A and B. Substituting these back into equations 180A, we finally get

$$U_{1A}=\frac{I\rho'}{2\pi}\left\{\frac{1}{R}+\frac{4k}{\pi^2}\int_0^\infty \cos tz\, dt\right.$$

$$\left.\times\int_0^\infty \frac{\sinh 2s(\pi-\phi_1)\cosh s\phi}{\sinh \pi s-k\sinh s(\pi-2\phi_1)} K_{is}(tr_0)K_{is}(tr)ds\right\}$$

$$U_{2A}=\frac{I\rho'}{2\pi}\left\{\frac{1}{R}+\frac{8k}{\pi^2}\int_0^\infty \cos tz\, dt\right.$$

$$\left.\times\int_0^\infty \frac{\cosh s\phi_1\sinh s(\pi-\phi_1)\cosh s(\pi-\phi)}{\sinh \pi s-k\sinh s(\pi-2\phi_1)} K_{is}(tr_0)K_{is}(tr)ds\right\}.$$

$$(183)$$

These expressions are the solutions for the general case of a point source of current in the vicinity of a dipping plane separating two materials with an arbitrary resistivity contrast. Obviously, the integrals do not lend themselves well to computations. However, Skal'skaya (1948) has shown that these equations, applied at points on the earth's surface only, can be simplified considerably when the angle of dip assumes certain values.

For example, let $\phi_1=\pi/4$ and consider only points on the earth's surface where $\cosh s\phi=1$. The hyperbolic terms in the integrand of U_{1A} can be manipulated so that

$$\frac{\sinh \frac{3\pi s}{2}}{\sinh \pi s-k\sinh \frac{\pi s}{2}}=2\cosh \frac{\pi s}{2}+k-\frac{1-k^2}{2\cosh \frac{\pi s}{2}-k}. \quad (184)$$

We see, by comparison with equation 110, that the integration which involves the first of the three terms on the right-hand side of equation 184 leads to the reciprocal of the distance $\sqrt{r_0^2+r^2+z^2}$. Thus the resulting contribution to the potential function may be attributed to an image of strength kI located at the point $(r_0, \pi/2, 0)$ and an image of equal strength located at the point $(r_0, 3\pi/2, 0)$. The second term in equation 184 may similarly be related to an image of strength k^2I located at the point $(r_0, \pi, 0)$. These three images correspond to the images which we used to get equation 28. If the lower bed were perfectly insulating $(k=1)$, the third term in equation 184 would vanish and U_{1A} would become identical to equation 28. There-

FIGURE 112.—Profiles with expanding-electrode system of potential-drop-ratio method across a vertical dike of width b, with current electrode C_1 fixed on the axis of the dike. Data are normalized. Reflection factors are $(A)k=+0.6$; $(B)k=-0.6$.

fore, we may regard the third term in equation 184 as leading to a correction to a solution which we would get to the problem on the basis of the image theory.

In order to reduce the integral involving the third term to one containing elementary functions, we make use of the following expansion:

$$\frac{1}{2\cosh u + 2\cos v} = \frac{1}{\sin v}\sum_{n=1}^{\infty}(-1)^{n+1}e^{-nu}\sin nv.$$

The interior integral then becomes

$$-(1-k^2)\int_0^{\infty}\frac{K_{is}(tr_0)K_{is}(tr)ds}{2\cosh \pi s/2 - k} = -\frac{(1-k^2)}{\sin \delta}\sum_{n=1}^{\infty}(-1)^{n+1}$$

$$\times \sin n\delta \int_0^{\infty}K_{is}(tr_0)K_{is}(tr)e^{-n\pi s/2}\,ds \quad (185)$$

where $\cos \delta = -k/2$. We now employ the integral theorem which states that

$$\int_0^{\infty}K_{is}(tr_0)K_{is}(tr)e^{-n\pi s/2}ds = \frac{n\pi}{2}\int_0^{\infty}\frac{K_0(t\sqrt{r_0^2+r^2+2r_0r\cosh s})}{s^2+n^2\pi^2/4}\,ds.$$

If we substitute $s = \frac{nu}{2}$, the integral on the right becomes

$$n\int_0^{\infty}\frac{K_0(t\sqrt{r_0^2+r^2+2r_0r\cosh \pi u/2})}{u^2+n^2}\,du.$$

We now draw upon another theorem which permits us to write

$$\sum_{n=1}^{\infty}(-1)^{n+1}\frac{n\sin n\delta}{n^2+u^2} = \frac{\pi}{2}\frac{\sinh \delta u}{\sinh \pi u},$$

whence equation 185 finally becomes

$$-(1-k^2)\int_0^{\infty}\frac{K_{is}(tr_0)K_{is}(tr)}{2\cosh \pi s/2 - k}\,ds$$

$$= \frac{1-k^2}{\sin \delta}\left(\frac{\pi}{2}\right)\int_0^{\infty}\frac{\sinh \delta u}{\sinh \pi u}K_0(t\sqrt{r_0^2+r^2+2r_0r\cosh \pi u/2})\,du.$$

The third term which we are trying to evaluate is now

$$-\frac{1-k^2}{\sin \delta}\left(\frac{\pi}{2}\right)\int_0^{\infty}\cos tz dt$$

$$\times \int_0^{\infty}\frac{\sinh \delta u}{\sinh \pi u}K_0(t\sqrt{r_0^2+r^2+2r_0r\cosh \pi u/2})\,du.$$

If we make use of equation 106, we may integrate over t to get

$$-\frac{1-k^2}{\sin \delta}\int_0^{\infty}\frac{\sinh \delta u}{\sinh \pi u}\frac{du}{\sqrt{r_0^2+r^2+z^2+2r_0r\cosh \pi u/2}}.$$

We have now reduced the potential function to one containing only elementary functions. We finally get U_{1A} by adding together the effect of the original source with its three images and the above correction term. We may similarly transform the above expression for U_{2A}. We can also solve for the potential functions when the current electrode is on the updip side of the

fault ($\phi_0 = \pi$) and can reduce those potential functions in the same manner. Therefore, we have the following potential functions, at the earth's surface, for an angle of dip of 45° and for an arbitrary resistivity contrast:

$$U_{1A} = \frac{I\rho'}{2\pi}\left\{\frac{1}{R} + \frac{2k}{\sqrt{r_0^2+r^2+z^2}} + \frac{k^2}{\sqrt{(r_0+r)^2+z^2}} - k(1-k^2)J(r_0, r, z)\right\}$$

$$U_{2A} = \frac{I\rho'}{2\pi}\left\{\frac{1+k}{R} + k(1+k)J(r_0, r, z)\right\}$$

$$U_{1B} = \frac{I\rho''}{2\pi}\left\{\frac{1-k}{R} + k(1-k)J(r_0, r, z)\right\}$$

$$U_{2B} = \frac{I\rho''}{2\pi}\left\{\frac{1}{R} - kJ(r_0, r, z)\right\} \quad (186)$$

where $\cos \delta = -k/2$ and

$$J(r_0, r, z) = \frac{1}{\sin \delta}\int_0^{\infty}\frac{\sinh \delta u\, du}{\sinh \pi u\sqrt{r_0^2+r^2+z^2+2r_0r\cosh \pi u/2}}.$$

Of the various forms of solutions presented in the literature, we prefer solutions of the type given in equations 183 for computations. The integral converges very rapidly and, as shown below it is not necessary to have tables of special functions available.

Whereas we can identify several terms in U_{1A} with images, we can similarly identify only one term in U_{2A} and none in U_{2B}. The reason is that the image theory cannot be used to solve any problems in which the electrodes are on the updip side of the fault. We recognize the one image appearing in U_{2A} as the one for the case when the fault is vertical.

Since $\rho''(1-k) = \rho'(1+k)$, U_{2A} is identical with U_{1B} just as the reciprocity theorem requires it to be.

Chastenet de Géry and Kunetz (1956) have shown that

$$K_{is}(tr_0)K_{is}(tr) = \int_0^{\infty}\cos \lambda s K_0(t\sqrt{r_0^2+r^2+2r_0r\cosh \lambda})d\lambda$$

from which equations 183 can be reduced to include only elementary functions. Using this relationship together with equation 106, we obtain

$$\frac{2}{\pi}\int_0^{\infty}\cos tz K_{is}(tr_0)K_{is}(tr)dt = \int_0^{\infty}\frac{\cos \lambda s\, d\lambda}{\sqrt{z^2+r_0^2+r^2+2r_0r\cosh \lambda}}. \quad (187)$$

Since the integral on the left of equation 187 appears in both U_{1A} and U_{2A}, we may now write these potentials in terms of elementary functions:

$$U_{1A} = \frac{I\rho'}{2\pi}\left\{\frac{1}{R} + \frac{2k}{\pi}\times\right.$$

$$\int_0^{\infty}\int_0^{\infty}\frac{\sinh 2s(\pi-\phi_1)\cosh s\phi \cos \lambda s}{[\sinh \pi s - k\sinh s(\pi-2\phi_1)]\sqrt{z^2+r_0^2+r^2+2r_0r\cosh \lambda}}\,dsd\lambda\right\}$$

$$U_{2A} = \frac{I\rho'}{2\pi}\left\{\frac{1}{R} + \frac{4k}{\pi}\times\right.$$

$$\int_0^{\infty}\int_0^{\infty}\frac{\cosh s\phi_1\sinh s(\pi-\phi_1)\cosh s(\pi-\phi)\cos \lambda s}{[\sinh \pi s - k\sinh s(\pi-2\phi_1)]\sqrt{z^2+r_0^2+r^2+2r_0r\cosh \lambda}}\,dsd\lambda\right\}.$$

Chastenet de Géry and Kunetz reduced these equations still further. For example, in U_{2A}, if we carry out one step of division in the integrand, we obtain a term which is the expansion of the reciprocal distance $1/R$. Thus, this function becomes

$$U_{2A} = \frac{I\rho'}{2\pi} \left\{ \frac{1+k}{R} + \frac{2k}{\pi} (1+k) \int_0^\infty \frac{\sinh s(\pi - 2\phi_1) \cosh s(\pi - \phi)}{\sinh \pi s - k \sinh s(\pi - 2\phi_1)} ds \right.$$

$$\left. \times \int_0^\infty \frac{\cos \lambda s}{\sqrt{z^2 + r_0^2 + r^2 + 2r_0 r \cosh \lambda}} d\lambda \right\}. \quad (188)$$

For U_{1A}, we must consider three separate forms. If ϕ_1 lies between $\pi/2$ and π, the function remains in the form given above. If ϕ_1 lies between 0 and $\pi/2$, we can perform N successive divisions within the integrand to obtain expressions which are found to be expansions of reciprocal distances. N is the integer lying between $\pi/2\phi_1$, and $\pi/2\phi_1 - 1$. These distances are related to the first N images that would be formed if we were seeking an image solution. The remainder then becomes the correction term to that image solution. The potential is written as

$$U_{1A} = \frac{I\rho'}{2\pi} \left\{ \frac{1}{R} + 2 \sum_{n=1}^{N} \frac{k^n}{\sqrt{z^2 + r_0^2 + r^2 - 2r_0 r \cos 2n\phi_1}} - \frac{2}{\pi} (1 - k^2) \right.$$

$$\int_0^\infty \frac{\sum_{n=1}^{N-1} k^n \sinh 2n\phi_1 s + k^N \sinh 2N\phi_1 s - k^{n-1} \sinh [2\pi - 2(N+1)\phi_1]s}{\sinh \pi s - k \sinh s(\pi - 2\phi_1)}$$

$$\left. \cosh s\phi ds \int_0^\infty \frac{\cos \lambda s}{\sqrt{z^2 + r_0^2 + r^2 + 2r_0 r \cosh \lambda}} d\lambda \right\}. \quad (189)$$

This equation is useful for arbitrary angles of dip when the current electrode is on the downdip side of the outcrop of the dipping contact.

In the special case when ϕ_1 is the Nth submultiple of $\pi/2$, the Nth image falls on the earth's surface, where $\phi = \pi$, and equation 189 reduces to

$$U_{1A} = \frac{I\rho'}{2\pi} \left\{ \frac{1}{R} + \frac{k^N}{\sqrt{z^2 + (r_0 + r)^2}} + 2 \sum_{n=1}^{N-1} \frac{k^n}{\sqrt{z^2 + r_0^2 + r^2 - 2r_0 r \cos 2n\phi_1}} \right.$$

$$- \frac{2}{\pi} (1 - k^2) \int_0^\infty \frac{\sum_{n=1}^{N-1} k^n \sinh 2n\phi_1 s \cosh s\phi}{\sinh \pi s - k \sinh s(\pi - 2\phi_1)} ds$$

$$\left. \times \int_0^\infty \frac{\cos \lambda s}{\sqrt{z^2 + r_0^2 + r^2 + 2r_0 r \cosh \lambda}} d\lambda \right\}. \quad (190)$$

If we let $\phi_1 = \pi/4$ so that $N = 2$ in equations 188 and 190, these equations reduce to the corresponding expressions given in equations 186 (Chastenet de Géry and Kunetz, 1956).

One method for measuring the dip of a fault plane depends on placing the current electrode on the surface trace of the fault (Sumi, 1953). In this application,

$r_0 = 0$. Skal'skaya (1948) showed that equations 183 reduce to the correct form when $r_0 = 0$; the proof is complicated, and it is easier to obtain the answer from first principles by using the same approach that we used to get equation 2.

If the current electrode in figure 113 lies on the surface trace of the fault, the geometry indicates that the current emanates radially outward from the electrode. The problem thus is reduced to one of determining what fraction of the total current flows into each of the two media. We first construct a hemispherical shell with its center at the origin. If the thickness of the shell is dR, then the potential drop across the shell is

$$dU = I' \left(\frac{\rho' dR}{2\phi_1 R^2} \right) = I'' \left(\frac{\rho'' dR}{2(\pi - \phi_1) R^2} \right), \quad (191)$$

where I' is the current flowing into the first medium and I'' is the current flowing into the second medium. We note that $R^2 = r^2 + z^2$. Equation 191 can be used to determine I'' in terms of I'. To determine the value of each of the current fractions, this relationship is then combined with the fact that the sum of the two fractions must equal the total current I. The desired currents are

$$I' = \frac{I\rho''\phi_1}{\rho'(\pi - \phi_1) + \rho''\phi_1}; \quad I'' = \frac{I\rho'(\pi - \phi_1)}{\rho'(\pi - \phi_1) + \rho''\phi_1}.$$

If these values of the currents are substituted into equation 191 and the equation is integrated from R to infinity, the potential at a distance R from the current electrode is

$$U = \frac{I\rho'\rho''}{2[\rho'(\pi - \phi_1) + \rho''\phi_1]R}. \quad (191A)$$

A SPECIAL SOLUTION

The qualitative effects of dipping beds can be obtained by studying the perfectly conducting plane. The mathematics can be derived by taking the limiting case of zero resistivity from the previously derived general solutions. However, we will solve the problem directly from first principles. Our solution is no more complicated than the other, and our development exemplifies a method which is used widely in electrostatics (MacDonald, 1895).

Figure 113 serves for our present purpose when we set $\rho'' = 0$ and $\rho' = \rho$. As in the previous section, the coordinates of the point source (the current electrode) are r_0, 0, and 0. We choose to make $r_0 < r_1$. We will temporarily put the following additional restrictions on the electric field: Two vertical conducting planes described by $z = z_1$ and $z = -z_1$, and a conducting cylinder described by $r = r_1$. The boundary conditions are that

the potential must be zero at $z=\pm z_1$, $\phi=\phi_1$, and $r=r_1$; no current can cross the earth's surface $\phi=0$; everywhere within this space the potential must remain finite except at the current electrode; and, the total current originating within the space is the sum (integration) of the elementary currents originating within each element of volume.

We use cylindrical coordinates in which Poisson's equation is

$$\frac{\partial^2 U}{\partial r^2}+\frac{1}{r}\frac{\partial U}{\partial r}+\frac{1}{r^2}\frac{\partial^2 U}{\partial\phi^2}+\frac{\partial^2 U}{\partial z^2}=-\rho i,$$

where i is the current-source density, which is a function of position. We will later make use of the fact that i is zero everywhere except in the vicinity of the current electrode.

A solution can be developed which is a Fourier series with respect to ϕ, namely,

$$U=\sum_n W_n(r,z)\cos\frac{n\pi\phi}{2\phi_1}.$$

The choice of the cosine term only insures that no current will cross the earth's surface, and restricting n to odd integers insures that the potential is zero at $\phi=\phi_1$. If we now substitute this assumed form of U into the differential equation preceding the last equation, we obtain

$$\sum_n\left[\frac{\partial^2 W_n}{\partial r^2}+\frac{1}{r}\frac{\partial W_n}{\partial r}-\frac{n^2\pi^2}{4r^2\phi_1^2}W_n+\frac{\partial^2 W_n}{\partial z^2}\right]\cos\frac{n\pi\phi}{2\phi_1}=-\rho i. \quad (192)$$

Because cylindrical functions can be expanded in terms of Bessel functions in a series comparable to a Fourier series, we assume that $W_n(r,z)$ has the form

$$W_n(r,z)=\sum_\lambda J_{n\pi/2\phi_1}(\lambda r)Z_{\lambda n}(z). \quad (193)$$

If $W_n(r,z)$—and consequently U—is to be zero over the surface $r=r_1$, it follows that λ is restricted to roots of the equation

$$J_{n\pi/2\phi_1}(\lambda r_1)=0.$$

The first of these values is $\lambda=0$. The summation in equation 193 is taken over all such roots. Substituting equation 193 into equation 192, we have

$$\sum_{n,\lambda}\left[\frac{\partial^2 Z_{\lambda n}}{\partial z^2}-\lambda^2 Z_{\lambda n}\right]J_{n\pi/2\phi_1}(\lambda r)\cos\frac{n\pi\phi}{2\phi_1}=-\rho i. \quad (194)$$

The term $(-\lambda^2 Z_{\lambda n})$ is obtained readily from the first three terms of equation 192 when we consider Bessel's equation (equation 68), which the Bessel function $J_{n\pi/2\phi_1}(\lambda r)$ satisfies.

We can also expand $Z_{\lambda n}(z)$ in a Fourier series of the form:

$$Z_{\lambda n}(z)=\sum_m A_{\lambda mn}\cos\frac{m\pi z}{2z_1}.$$

Once again we have chosen only the cosine term because the solution must remain symmetrical in z. Also, m is restricted to odd integers in order that the potential will vanish on the plane $z=z_1$. Substituting this expression into equation 194, we obtain

$$\sum_{\lambda,m,n}A_{\lambda mn}\left[\frac{m^2\pi^2}{4z_1^2}+\lambda^2\right]J_{n\pi/2\phi_1}(\lambda r)\cos\frac{n\pi\phi}{2\phi_1}\cos\frac{m\pi z_1}{2z_1}=-\rho i. \quad (195)$$

To determine $A_{\lambda mn}$, multiply both sides of equation 195 by

$$rJ_{n'\pi/2\phi_1}(\lambda r)\cos\frac{n'\pi\phi}{2\phi_1}\cos\frac{m'\pi z}{2z_1}\,dr\,d\phi\,dz$$

and integrate over the whole interior of the bounded space. The primes on the three indices indicate that specific values have been chosen from each of the three sets. We first consider the step-by-step integration of the left side of the equation. Using the relation given by equation 116, we obtain immediately the integrals over ϕ and z. We have, remembering that neither n nor m assumes the value zero,

$$\int_0^{\phi_1}\cos\frac{n\pi\phi}{2\phi_1}\cos\frac{n'\pi\phi}{2\phi_1}\,d\phi=\frac{\phi_1}{2}\delta_{nn'}, \quad (196)$$

and

$$\int_{-z_1}^{z_1}\cos\frac{m\pi z}{2z_1}\cos\frac{m'\pi z}{2z_1}\,dz=z_1\delta_{mm'}.$$

Equation 196 is valid because n assumes only odd values; if n were to assume random values, the equation would not always hold. An orthogonality relation exists between the Bessel functions (Watson, 1952, paragraphs 5–11) which permits us to integrate over r:

$$\int_0^{r_1}rJ_{n\pi/2\phi_1}(\lambda r)J_{n\pi/2\phi_1}(\lambda'r)dr=\frac{r_1^2}{2\lambda^2}J'^2_{n\pi/2\phi_1}(\lambda r_1)\delta_{\lambda\lambda'}.$$

This relation depends on λ's assuming discrete values that are roots of the equation $J_{n\pi/2\phi_1}(\lambda r_1)=0$. The prime on $J_{n\pi/2\phi_1}(\lambda r)$ indicates the derivative with respect to r.

Because of the orthogonality relation applied, the integrations above have eliminated all values of λ, n, and m except λ', n', and m'. Therefore, we can drop the primes and refer only to the original indices, remembering of course that there remains no summation.

Examining the integration over the right side of the equation, we find that the integrand vanishes everywhere except in the vicinity of the source because i is zero everywhere except in that neighborhood. In this small region where i is not zero, the other functions in the integrand can be considered to have approximately the same values that they have at the point source exactly. Therefore, they become constants and can be removed from under the integral sign. The r_0 must be retained within the integral to maintain the

element of volume $dv=r_0drd\phi dz$. Integrating i over the region in which it is finite, we obtain the total current flowing outward from the point source.

Combining the results of the above integration, we have in place of equation 195:

$$A_{\lambda mn}\left[\frac{m^2\pi^2}{4z_1^2}+\lambda^2\right]\frac{z_1\phi_1}{4\lambda^3}J'^2_{n\pi/2\phi_1}(\lambda r_1)=I\rho J_{n\pi/2\phi_1}(\lambda r_0). \quad (197)$$

Equation 197 is solved for $A_{\lambda mn}$, which when introduced into the expression for the potential, gives

$$U=\frac{4I\rho}{z_1\phi_1 r_1^2}\sum_{\substack{n=1\\ \text{odd values}\\ \text{only}}}^{\infty}\sum_{m=1}^{\infty}\sum_{\lambda=0}^{\infty}\frac{\lambda^3 J_{n\pi/2\phi_1}(\lambda r_0)}{\left[\frac{m^2\pi^2}{4z_1^2}+\lambda^2\right]J'^2_{n\pi/2\phi_1}(\lambda r_1)}$$

$$\times J_{n\pi/2\phi_1}(\lambda r)\cos\frac{n\pi\phi}{2\phi_1}\cos\frac{m\pi z}{2z_1}. \quad (198)$$

This expression can be simplified somewhat by noting the following identity:

$$\sum_{\substack{m=1\\ \text{odd}}}^{\infty}\frac{\lambda\cos\frac{m\pi z}{2z_1}}{\frac{m^2\pi^2}{4z^2}+\lambda^2}=\frac{z_1}{2}\frac{\cosh\lambda(2z_1-z)-\cosh\lambda z}{\sinh 2\lambda z_1}.$$

With this substitution, equation 198 becomes

$$U=\frac{2I\rho}{\phi_1 r_1^2}\sum_{\substack{n=1\\ \text{odd}}}^{\infty}\sum_{\lambda=0}^{\infty}\frac{\lambda J_{n\pi/2\phi_1}(\lambda r_0)}{J'^2_{n\pi/2\phi_1}(\lambda r_1)}J_{n\pi/2\phi_1}(\lambda r)$$

$$\times\cos\frac{n\pi\phi}{2\phi_1}\left[\frac{\cosh\lambda(2z_1-z)-\cosh\lambda z}{\sinh 2\lambda z_1}\right] \quad (199)$$

which is valid now only if z is positive.

This expression gives the potential only within the prism which we constructed, and it therefore represents only an intermediate solution to the problem. To obtain the desired solution it is necessary to remove the vertical conducting planes and the conducting cylinder that were introduced at the beginning. This end can be accomplished by letting r_1 and z_1 both become infinite. First letting z_1 become infinitely large, because taking its limit is straightforward, we obtain

$$U=\frac{2I\rho}{\phi_1 r_1^2}\sum_{\substack{n=1\\ \text{odd}}}^{\infty}\sum_{\lambda=0}^{\infty}\frac{\lambda J_{n\pi/2\phi_1}(\lambda r_0)}{J'^2_{n\pi/2\phi_1}(\lambda r_1)}J_{n\pi/2\phi_1}(\lambda r)e^{-\lambda z}\cos\frac{n\pi\phi}{2\phi_1}. \quad (200)$$

Next we consider the result on equation 199 when r_1 is made very large. The asymptotic behavior of the Bessel function is given by

$$\lim_{r_1\to\infty}J_{\frac{n\pi}{2\phi_1}}(\lambda r_1)=\lim_{r_1\to\infty}\sqrt{\frac{2}{\pi\lambda r_1}}\cos\left(\frac{n\pi^2}{4\phi_1}+\frac{\pi}{4}-\lambda r_1\right), \quad (201)$$

from which we can deduce the asymptotic behavior of its derivative (indicated by a prime)

$$\lim_{r_1\to\infty}J'_{n\pi/2\phi_1}(\lambda r_1)=\lim_{r_1\to\infty}\sqrt{\frac{2\lambda}{\pi r_1}}\sin\left(\frac{n\pi^2}{4\phi_1}+\frac{\pi}{4}-\lambda r_1\right). \quad (202)$$

Since the values of λ are by definition such that $J_{n\pi/2\phi_1}(\lambda r_1)=0$, it follows that the cosine term in equation 201 must be zero and that consequently the sine term in equation 202 must equal one. Further, if λ and $\lambda+\delta\lambda$ are successive roots of $J_{n\pi/2\phi_1}(\lambda r_1)=0$, for large values of r_1 we can state that $\delta\lambda=\pi/r_1$, and thus

$$\lim_{r_1\to\infty}r_1^2 J'^2_{n\pi/2\phi_1}(\lambda r_1)=\frac{2\lambda r_1}{\pi}=\frac{2\lambda}{\delta\lambda}.$$

In the limit as r_1 becomes very large, λ becomes infinitesimally small. Hence, the summation over λ becomes an integral and

$$U=\frac{I\rho}{\phi_1}\sum_{\substack{n=1\\ \text{odd}}}^{\infty}\cos\frac{n\pi\phi}{2\phi_1}\int_0^{\infty}e^{-\lambda z}J_{n\pi/2\phi_1}(\lambda r_0)J_{n\pi/2\phi_1}(\lambda r)d\lambda. \quad (203)$$

Equation 203 corresponds to the expression obtained by MacDonald for the electrostatic problem. However, since tables of these Bessel functions do not exist, we have carried the calculation further in order to expedite computations. We are most interested in the solution for a traverse crossing the inclined plane in a direction perpendicular to the strike. In this case, $z=0$ and $\phi=0$. Using a relationship developed by Watson (1952, p. 410), namely

$$\int_0^{\infty}J_{n\pi/2\phi_1}(\lambda r_0)J_{n\pi/2\phi_1}(\lambda r)d\lambda=\frac{1}{r}\left(\frac{r_0}{r}\right)^{\frac{n\pi}{2\phi_1}}$$

$$\times\frac{\Gamma\left(\frac{n\pi}{2\phi_1}+\frac{1}{2}\right)}{\sqrt{\pi}\,\Gamma\left(\frac{n\pi}{2\phi_1}+1\right)}F\left(\frac{n\pi}{2\phi_1}+\frac{1}{2},\frac{1}{2};\frac{n\pi}{2\phi_1}+1;\frac{r_0^2}{r^2}\right)$$

and substituting this expression into equation 203, we have the desired equation:

$$U=\frac{I\rho}{r\phi_1\sqrt{\pi}}\sum_{n=1}^{\infty}\left(\frac{r_0}{r}\right)^{\frac{n\pi}{2\phi_1}}\frac{\Gamma\left(\frac{n\pi}{2\phi_1}+\frac{1}{2}\right)}{\Gamma\left(\frac{n\pi}{2\phi_1}+1\right)}F\left(\frac{n\pi}{2\phi_1}+\frac{1}{2},\frac{1}{2};\frac{n\pi}{2\phi_1}+1;\frac{r_0^2}{r^2}\right). \quad (204)$$

This equation was used to compute the data for the curves in the next section. As throughout this section, we take only odd values of n.

$\Gamma(\ )$ is the gamma function and $F(\ )$ is the hypergeometric function. Equation 204 converges rapidly, especially when used to compute data for horizontal resistivity profiles, and therefore it is not as

formidable as it looks. It should be cautioned, however, that the equation preceding equation 204 is valid only when $r>r_0$; and that equation 204 is therefore valid only under the same condition. If $r_0>r$, we need only to interchange their roles to make equation 204 valid.

Both equations 203 and 204 are valid for any angle of dip between $\phi_1=0$ and $\phi_1=\pi$. For computations of potential when the potential electrode is on the updip side of the fault trace, our convention requires that the coordinate system be set up so that the current electrode has the coordinate $\phi_0=0$. This means that in this case, the angle ϕ_1 will be larger than 90°.

If the angle of dip has certain special values, the above solutions may be transformed into the corresponding image solutions which were given in the section on the image theory. If the angle of dip is not one of these special values, image theory is not applicable. We note further that U_{14} of equation 183 may also be transformed into equation 203 for this special case of perfect conductors.

EFFECT OF VERTICAL CLIFFS

The simplest example of topography which can be treated is a line along which the ground has a very steep slope, or, in the ideal case, a vertical cliff. If the survey is being conducted on the high side of the cliff and the electrode separation is much smaller than the height of the cliff, the potential field can be adequately described in terms of equation 25. If the electrode separation is comparable to the height of the cliff or is larger, a more sophisticated mathematics is required for the solution. The reason for the restriction on the problem is that the cliff has a finite height, whereas the usual solution assumes an infinite height. Although Kiyono (1952b) has published an approximate solution for this problem based on logarithmic potential, we know of no exact solution.

If the survey is being conducted at or near the foot of the cliff, the problem is also more complicated; but the problem can be solved by using the same mathematics as that used in the dipping-bed problem, provided the electrode separation is small in comparison with the height of the cliff. To solve the problem in cylindrical coordinates, the z axis is taken along the base of the cliff, the origin is chosen so that $z_0=0$, and the axes are oriented so that $\phi_0=0$ (fig. 114). For solutions of Laplace's equation given by equation 74, the expansion of $1/R$ given by equation 110 is used. In the derivation of equation 110 the only stipulation was that ϕ should lie between 0 and 2π. In the present problem the total angle involved is $3\pi/2$, and consequently only a single form of the expansion is needed. The angle ϕ is therefore always positive and varies clockwise from 0 to $3\pi/2$.
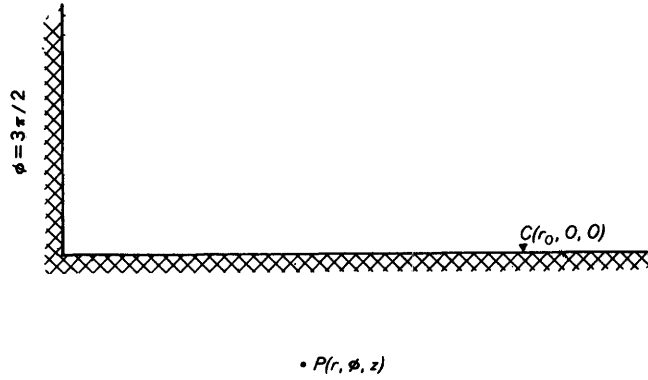
As there are no restrictions on the problem, the general solution can be used. In order to keep current from flowing across the surface of the earth, however, the two arbitrary constants must be made equal. Therefore, the general solution for the potential at point P (fig. 114) is

$$U=\frac{I\rho}{2\pi}\left\{\frac{1}{R}+\frac{4}{\pi^2}\int_0^\infty \cos tzdt \int_0^\infty A(s)[\cosh s(\pi-\phi)\right.$$
$$\left.+\cosh s(\pi+\phi)] K_{is}(tr_0)K_{is}(tr)ds\right\}, \quad (205)$$

where the form of the solution is chosen to conform to the known expression for $1/R$. The potential function in the air, where there is no current, can be ignored.

To satisfy the boundary condition that no current can flow across the vertical face of the cliff, it is necessary to obtain the derivative of the potential function with respect to ϕ, which is found to be

$$\frac{\partial U}{\partial \phi}=\frac{I\rho}{2\pi}\left(\frac{4}{\pi^2}\right)\int_0^\infty \cos tzdt\int_0^\infty \{-\sinh s(\pi-\phi)$$
$$+A[-\sinh s(\pi-\phi)+\sinh s(\pi+\phi)]\}K_{is}(tr_0)K_{is}(tr)sds.$$

By setting this derivative equal to zero at $\phi=3\pi/2$, the resulting equation can be solved immediately for $A(s)$. By substituting this value in equation 205, the final potential function is obtained:

$$U=\frac{I\rho}{2\pi}\left\{\frac{1}{R}-\frac{8}{\pi^2}\int_0^\infty \cos tzdt\right.$$
$$\left.\times\int_0^\infty \frac{\sinh \pi s/2 \cosh \pi s \cosh s\phi}{\sinh \pi s/2+\sinh 5\pi s/2} K_{is}(tr_0)K_{is}(tr)ds\right\}. \quad (206)$$

In this expression the two terms appearing in brackets in equation 205 have been combined. This solution is valid only when the electrode separation is small as compared to the height of the cliff. Similar solutions can be derived for cases in which the slopes are slanting rather than vertical and in which the electrodes are either on the high side or at the foot of the cliff.

The effect of a vertical cliff can be pronounced, as shown in the following field example. Figure 115
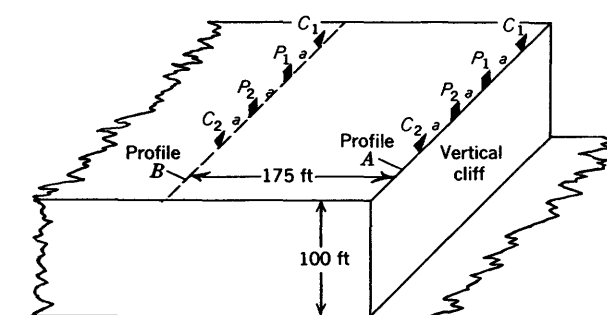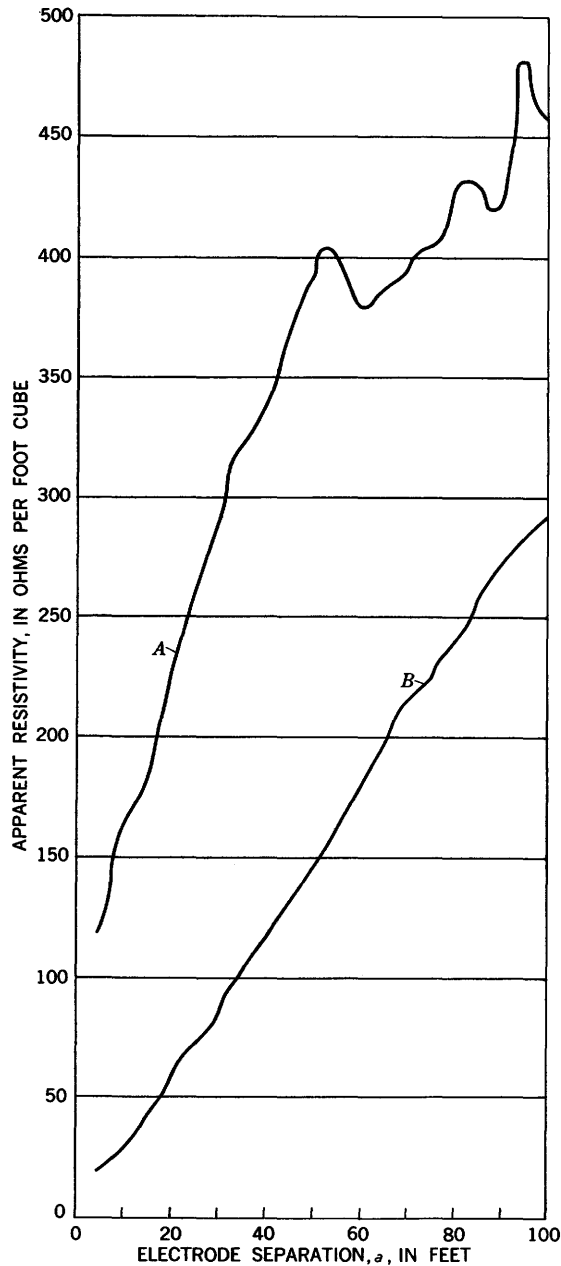
FIGURE 115.—Vertical resistivity profiles at top of and parallel to edge of vertical 100-foot cliff of Joachim Dolomite and Plattin Limestone, near Foley, Mo., Wenner configuration. Profile A taken within a few feet of the top edge of cliff; profile B taken 175 feet from the top edge of cliff. Adapted from Keller (1934).

shows observed vertical resistivity profiles with the Wenner configuration along traverses at the top of and parallel to the edge of a vertical 100-foot cliff of Joachim Dolomite and Plattin Limestone, near Foley, Mo. (Keller, 1934).

For small electrode separations the apparent resistivity is equal to the true resistivity of the rock. As the configuration is expanded, the volume effect of the void manifests itself, and gives an essentially straight-line apparent-resistivity curve. The erratic nature of curve A for large separations is probably caused by lateral effects.

DIPPING PERFECTLY CONDUCTING OR INSULATING PLANE

The dipping perfectly conducting or insulating plane simulates geologically a thin dipping fault zone in which the gouge material is either an excellent conductor or insulator, respectively, relative to the country rock on either side. The true resistivity of the country rock on one side of the fault plane is assumed to be equal to that on the other side; and the anomaly is therefore due solely to the gouge material.

Figure 116 shows the horizontal resistivity profiles with both the Lee and Wenner configurations across a perfectly conducting plane dipping 30°. As in the case for the vertical perfectly conducting plane (fig. 54), the curves for both the Lee and Wenner configurations are continuous. Rather than being symmetrically W-shaped, as for a vertical perfectly conducting plane, the overall shape of both the Lee and Wenner profiles is that of a letter "W" written asymmetrically and leaning to the right. For the Lee profile (fig. 116A), the ρ_2 curve attains a value of 1.3, which is much higher than the corresponding maximum value of ρ_2 for a vertical perfectly conducting plane; and similarly the ρ_2 curve attains a minimum that is much lower than the corresponding minimum value of ρ_2 for a vertical perfectly conducting plane.

RESULTS OF MODEL STUDIES

Figure 117 shows the results of tank-model studies with the Wenner configuration to determine the effect of dip on the apparent resistivity over a perfectly conducting sheet dipping at angles of 0°, 30°, 60°, and 90° (Heiland, 1932b).

For a vertical perfectly conducting plane (fig. 117D), the apparent-resistivity curve for the model is symmetrically W-shaped similar to the theoretical curve in figure 54C; and the value of the apparent resistivity at the top of the central peak is approximately equal to the true resistivity of the tank fluid. For a perfectly conducting plane with a 60° dip (fig. 117C), the "W" is somewhat asymmetrical, and the apparent resistivity value of the lower right part of the "W" is lower than
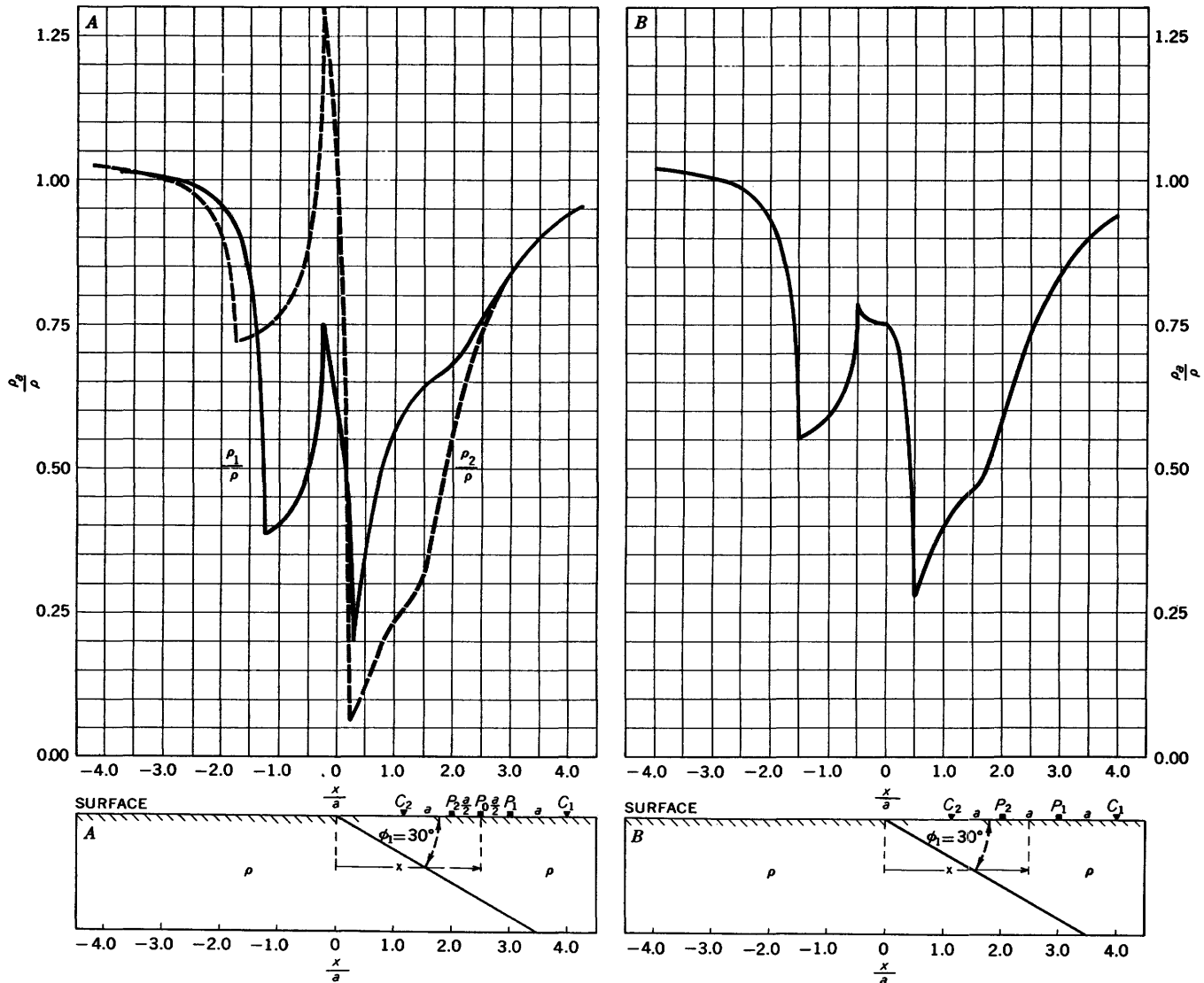
FIGURE 116.—Horizontal resistivity profiles across a perfectly conducting plane dipping 30°, (A) Lee configuration (offset plotting), and (B) Wenner configuration.

the corresponding part of the curve for a vertical plane.[6] For a dip of 30° (fig. 117B), the asymmetry of the curve is more pronounced, and the "W" leans to the right in a manner similar to that on the theoretical profile in figure 117B. The highest part of the peak in the central part of the "W" on a theoretical continuous curve lies a distance of $a/2$ to the left (that is, on the updip side) of the outcrop of the plane (fig. 117B). The peak in the model result as published by Heiland (1932b) lies downdip from the apex of the conducting sheet; but this peak should theoretically occur to the left of the apex of the sheet. The shift is apparently due to a drafting error; and in this diagram we therefore show the curve as published by Heiland and the same curve

shifted to the left to what we believe to be the approximately correct position. By independent reasoning that is discussed later, it also appears that the dashed curve should be shifted the same amount.

The dashed curves in figure 117, which are for transverse traverse profiles (Hubbert, 1932, p. 12), will be discussed in a later section.

SINGLE INCLINED DISCONTINUITY

POTENTIAL DISTRIBUTION

The solid curve in figure 118 shows the departure from the normal potential[7] due to two current electrodes placed over a bed with a 10 percent (slightly

[6] The extreme right-hand part of the curves was omitted from the published curves for some of the models.

[7] The departure from the normal potential is defined here as the difference between the value of the potential at a given point on the surface for homogeneous ground of resistivity ρ' and the value of the potential at the same point when the bed of resistivity ρ'' exists as a second layer.
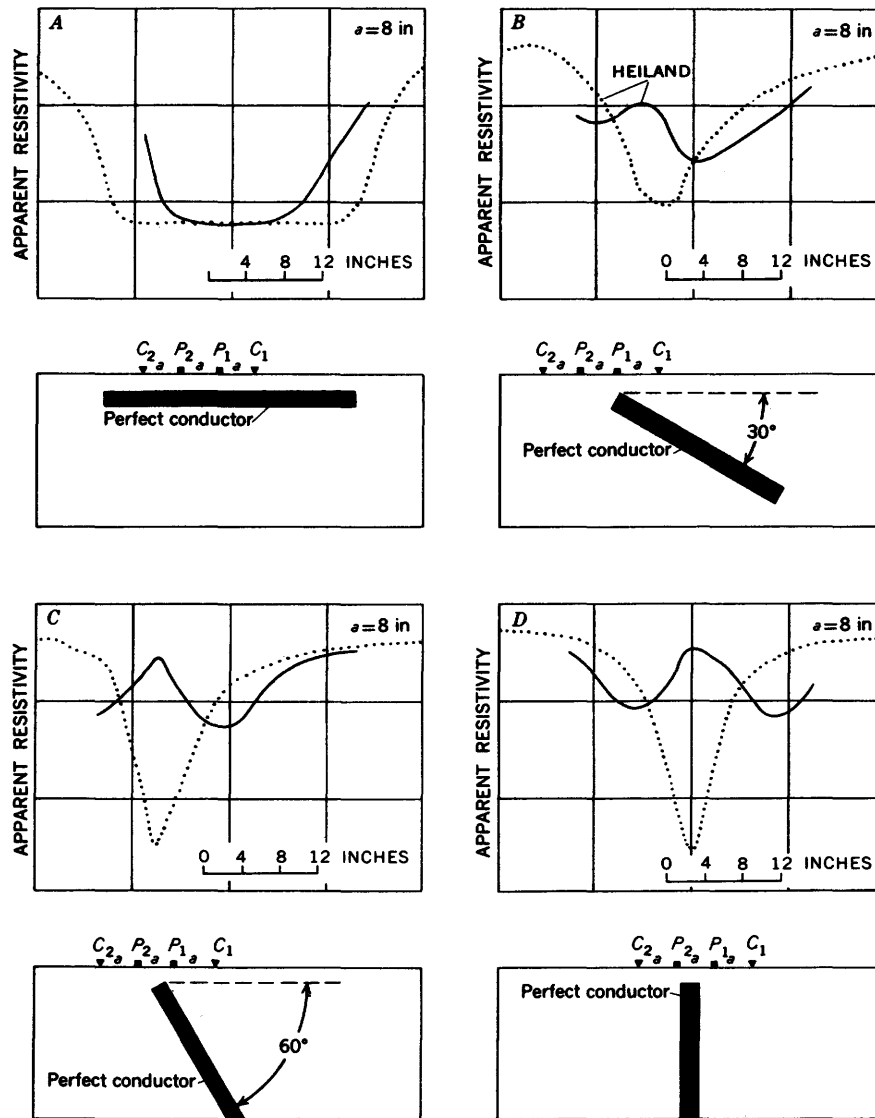
FIGURE 117.—Profiles over tank models with Wenner configuration showing effect of dip on apparent resistivity. Electrode separation a=8 in. for all curves. Solid curves are for horizontal profiles along traverses perpendicular to strike; dashed curves are for transverse traverse profiles with line of electrodes parallel to the strike. Angles of dip=0°, 30°, 60°, and 90°. Adapted and in part modified from Heiland (1932b).

less than 6°) dip where the resistivity of the lower bed is 10 times that of the upper bed (Weaver, 1928). There is lack of symmetry about the midpoint between the current electrodes. For comparison, the dashed curve in figure 118 shows the departure from the normal potential for a horizontal layer whose depth is the depth, namely, 60 feet, of the slanting layer at the midpoint between current electrodes C_1 and C_2. It is reasoned from these curves that the departure from the normal potential at the midpoint of the configuration along a traverse perpendicular to the strike of the sloping bed greatly exceeds the departure from the normal potential at the same midpoint of the same configuration along a traverse parallel to the strike of a sloping bed. The strike of the slanting layer therefore can be determined

theoretically by rotating the current electrodes about their midpoint until the potential at the midpoint is the mean potential; and information concerning the dip of the bed can then be determined from profiles taken along a traverse perpendicular to the strike.

Figure 119 shows the equipotential lines on the surface of the earth around a point source of current over a contact dipping 45° (Chastenet de Géry and Kunetz, 1956). The reflection factor is 0.8. The units of potential are arbitrary. Along the outcrop of the dipping contact, for arbitrary dip and resistivity contrast, the potential is given by equation 191A, which reduces to

$$U = \frac{3I\rho'}{2\pi R}.$$
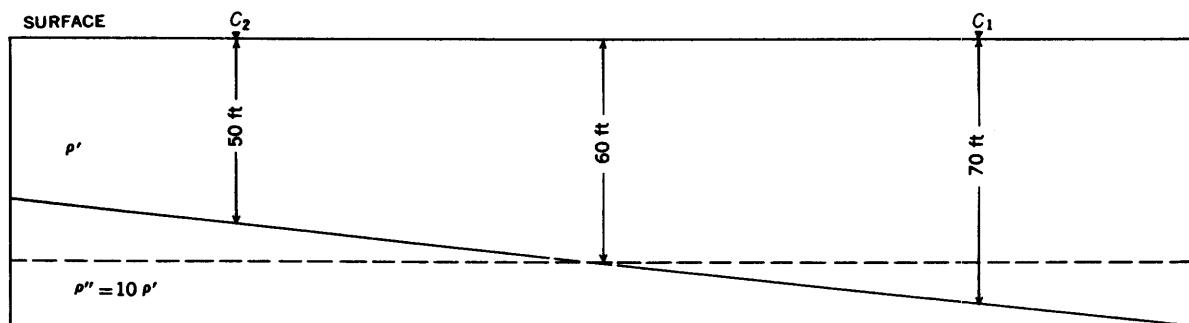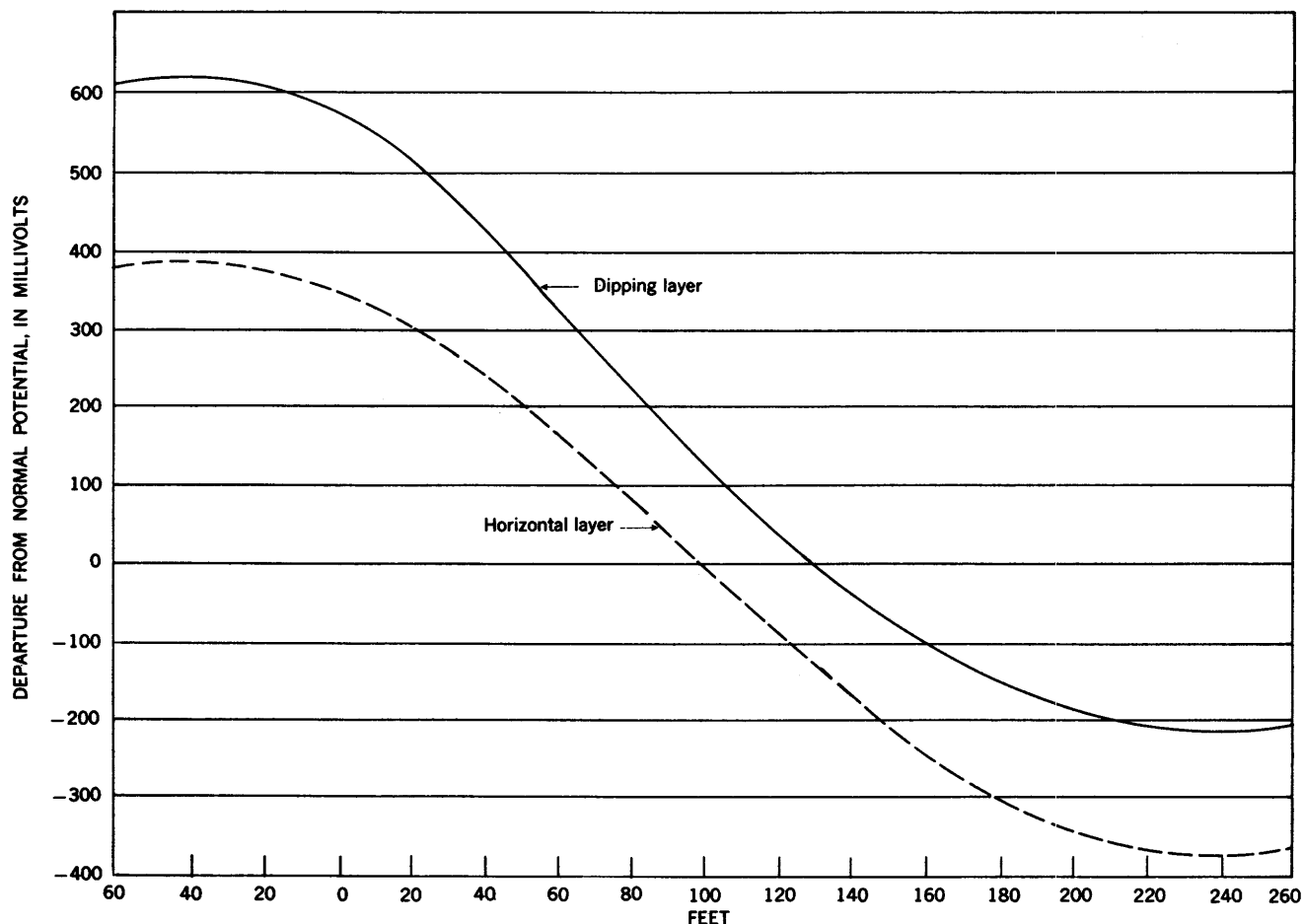
FIGURE 118.—Departure from normal potentials caused by a slanting layer (solid curve) and horizontal layer (dashed curve). Slope of dipping bed is 10 percent (slightly less than 6°); depth of horizontal bed=60 ft. $\rho''=10\rho'$. Adapted from Weaver (1928). Copyright by Am. Inst. Mining Metall. Engineers.

PROFILES PARALLEL TO THE STRIKE

In the dipping-bed problem the complexity of obtaining the potential at a point on the surface of the lower bed is much greater than that of obtaining the potential at a point on the surface of the upper bed. We have already shown that the former problem can never be solved exactly by images and that the latter problem can be solved exactly by images under very restricted conditions. In treating the resistivity anomalies over inclined faults or beds, we find it convenient therefore to discuss first the profiles obtained over the upper bed; we will discuss later the more difficult problems of profiles over the lower bed and profiles that cross the fault trace—the contact between the upper and lower bed. In examining the resistivity anomalies obtained over the upper bed, the easier
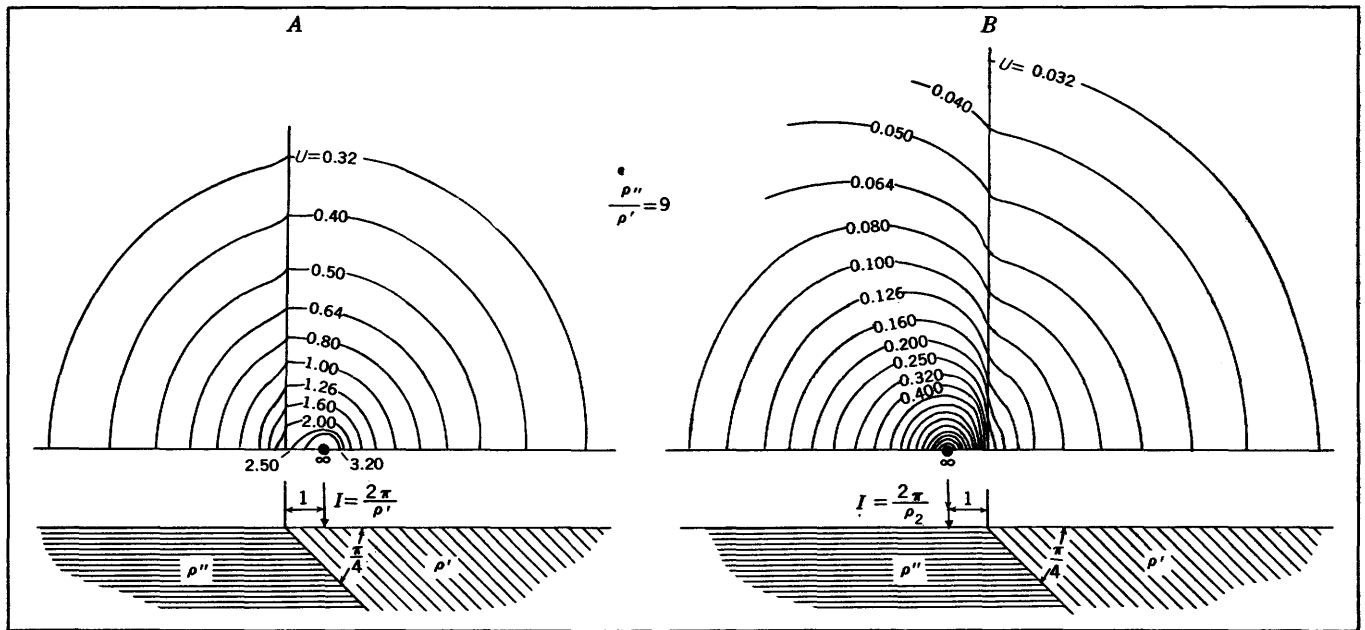
FIGURE 119.—Equipotential lines on surface of earth around a point source of current over a contact dipping 45°. Reflection factor $k=0.8$. Units of potential are arbitrary. Adapted from Chastenet de Géry and Kunetz (1956).

problem of profiles taken along traverses parallel to the strike is discussed first, then the more difficult problem of profiles taken along traverses perpendicular to the strike.

THEORETICAL CURVES BASED ON IMAGE THEORY

We have seen that the exact solution to the dipping-bed problem based on image theory is restricted to profiles over the upper bed only and to certain discrete angles of dip; also the bottom bed must be either perfectly conducting or insulating. In this section we will examine the theoretical curves that are based on image theory with these restrictions and also the approximations that are needed when the image theory is used in more general cases than the restricted ones just mentioned.

Unz (1953), who used image theory, was the first to present in English the exact apparent-resistivity curves as measured with the Wenner configuration in the upper formation and oriented parallel to the strike of the dipping beds. Figures 120 and 121 show the results of the analysis of the dipping-bed problem that can be made with the image theory (Unz, 1953).

For reflection factors $k=\pm 1$ (fig. 120), the diagrams for various dip angles ϕ_1 are exact, and their asymptotic values were checked by Unz. In these diagrams, h is the vertical distance from the line of electrodes to the contact between the two beds. For a perfectly insulating bottom bed (fig. 120), the asymptotic value for a horizontal bed ($\phi_1=0°$) is $(\rho_a/\rho')_{a/h=\infty}=\infty$; and, as expected, the slope of this straight line going to

infinity is 1.386. At a dip angle $\phi_1=90°$—that is, for a vertical fault—the value of ρ_a/ρ' remains constant at 2 for all values of the electrode separation; in this case the line of electrodes lies along the vertical fault trace and the apparent resistivity remains independent of the electrode separation. The fact that the apparent-resistivity curves for different dip angles cross each other at intermediate values of a/h is explained qualitatively by Unz by the varying share of the ρ' and ρ'' areas in carrying the bulk of the current. The asymptotic values of the different curves are given in figure 120.

For a perfectly conducting bottom bed (fig. 120), the apparent resistivity for all dip angles becomes zero as the line of electrodes comes nearer to the trace of the bed. Thus the asymptotic value is zero for all values of dip angle. Crossing of the apparent-resistivity curves occurs in this case, too, but not as pronouncedly as in the previous case. The curves shown in figure 120 are for angles that are submultiples of $\pi/2$ only.

Figure 120 shows that for a Wenner profile parallel to the strike and overlying the upper bed, the measurements are much more sensitive to changes in dip for a bottom bed that is perfectly insulating than for one that is perfectly conducting.

The vertical resistivity profiles for a perfectly insulating bed that dips at an angle different from a submultiple of π (for example, fig. 120) can be obtained from figure 121, which shows a plot of apparent-resistivity values as a function of the dip angle ϕ_1 for $k=$
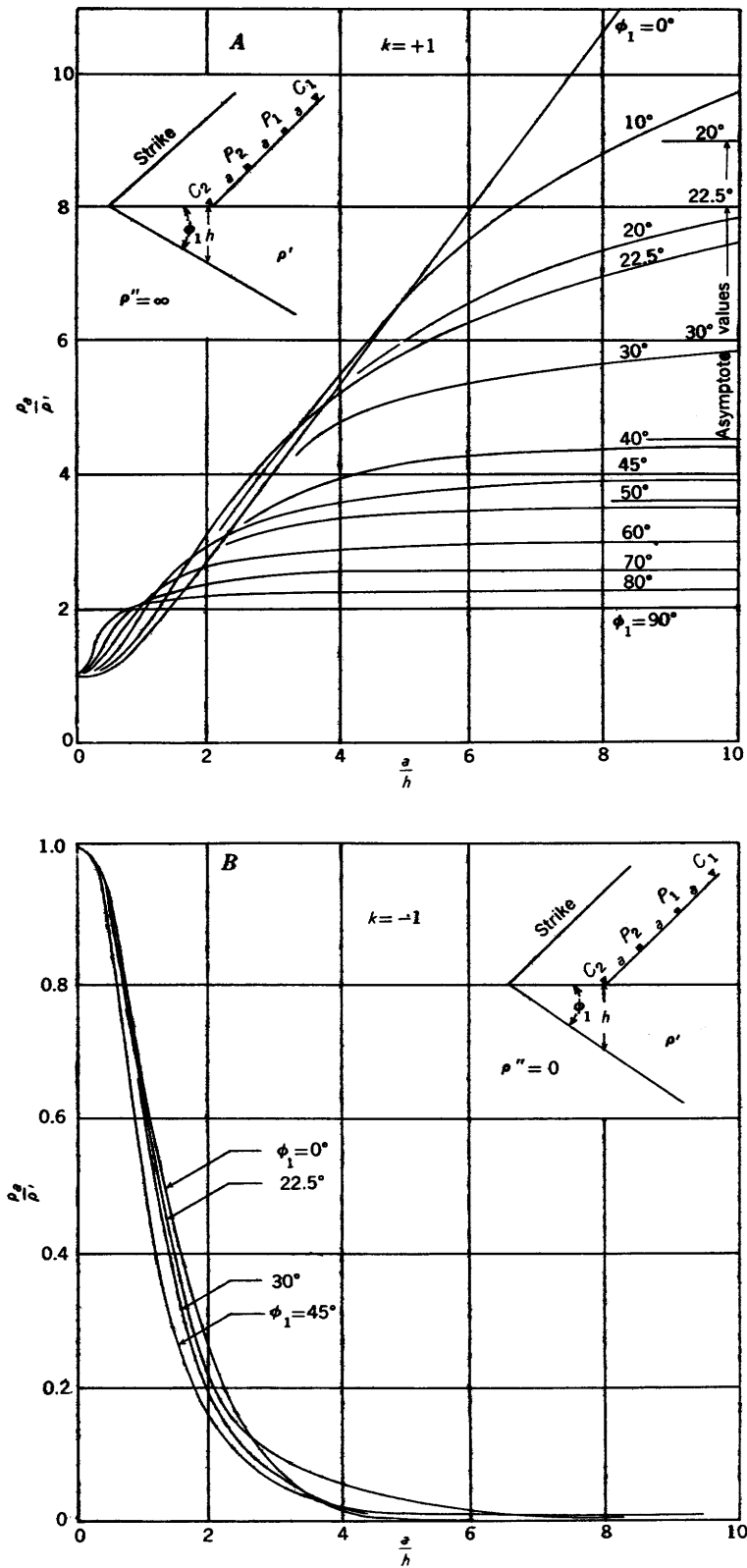
FIGURE 120.—Vertical resistivity profiles over upper bed along traverses parallel to strike of dipping bed for various angles of dip ϕ_1, Wenner configuration. Reflection factors, $k=\pm 1$. Adapted from Unz (1953).
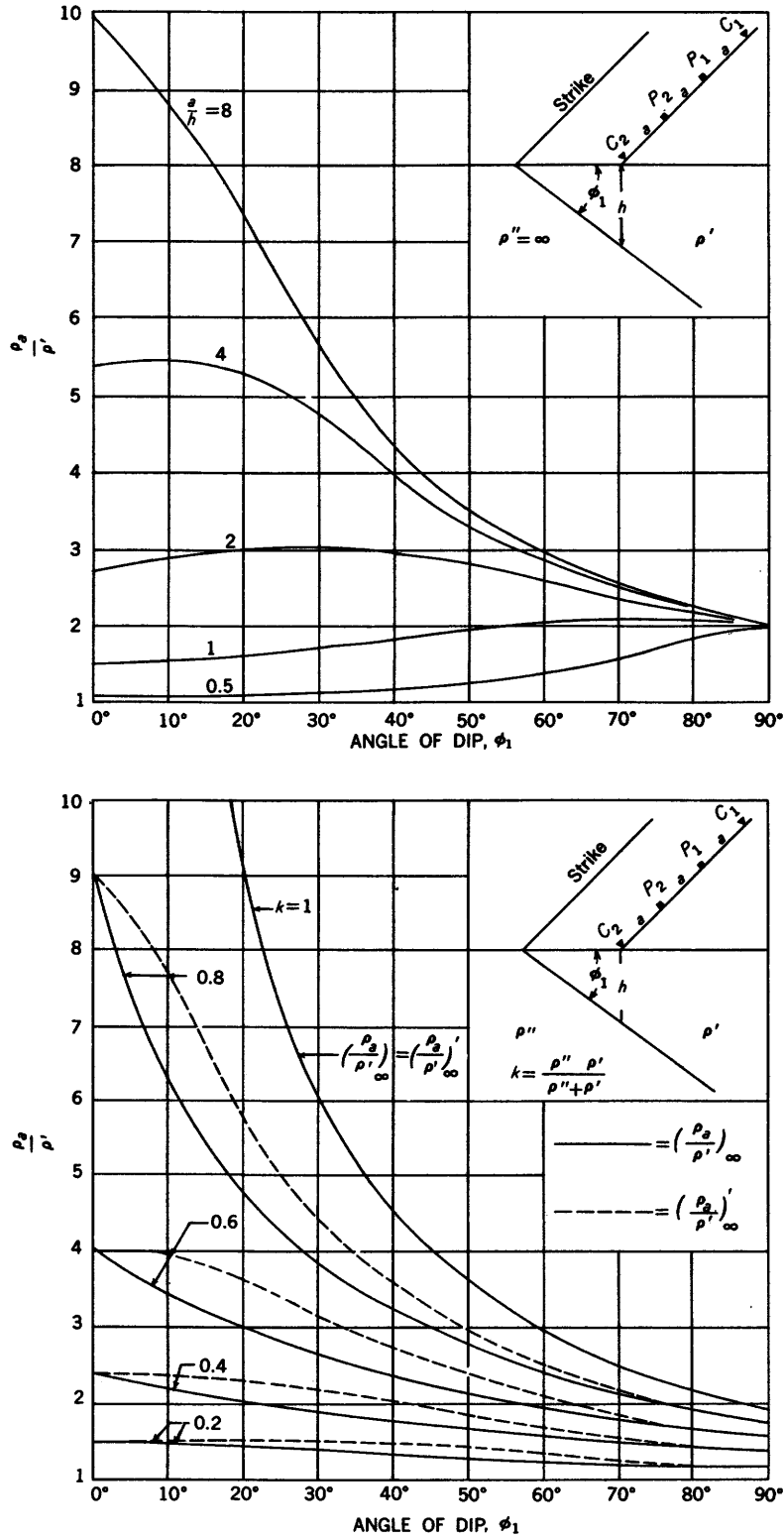
FIGURE 121.—Apparent-resistivity values for different angles of dip ϕ_1 for vertical resistivity profiles over upper bed along traverse parallel to strike of dipping bed, Wenner configuration. *Upper,* Values for reflection factor $k=+1$ for various electrode separations. Adapted from Unz (1953). *Lower,* Asymptotic value for positive values of reflection factor k. Solid curves are exact values; dashed curves are values as obtained from image theory. Adapted from Unz (1953).

+1. Unz obtained these curves by computing the exact apparent-resistivity values, using different values of the parameter a/h, for angles that are submultiple of π—for which the image theory, which he used, holds— and then connecting these exact points with a smooth curve. Thus he could take points off these curves and use them as exact apparent-resistivity values to chart the curves shown in figure 120 for angles that are different from the submultiples of π. In figure 121, all curves converge toward a single point for which $\rho_a/\rho'=2$ and $\phi_1=90°$—that is, for a vertical fault. The points of crossing of apparent-resistivity curves in figure 120 appear in figure 121 as points for which the ordinates are equal for a given value of a/h.

For dipping beds in which the reflection factor is different from either $+1$ or -1, Unz computed some approximate apparent-resistivity curves and tried to analyze the degree of approximation that the image theory affords toward the exact solution of the dipping-bed problem. He reasoned that for intermediate positive reflection factors, the maximum error resulting from the image theory occurs in the asymptotic values. Figure 121 shows the asymptotic values of apparent resistivity for different angles of dip for positive values of the reflection factor. The solid curves are exact values and the dashed curves are values as obtained from image theory. The errors for negative reflection factors are oscillatory and more involved.

Because every calculated curve using image theory for a dipping bed is exact for small values of a/h, and because its true asymptotic value is known for large values of a/h, Unz found it convenient to correct the apparent-resistivity curve obtained from image theory by modifying its asymptote only. A corrected reflection factor k' must be substituted in the equation to adapt its asymptote to the true value $(\rho_a/\rho')_{a/h}=0$.

We will discuss in the next section the accuracy attained by Unz in one of his approximate curves for a dipping bed with finite resistivity contrasts.

Šumi (1953), using elementary principles already given in a previous theoretical section of this section, computed and charted curves that can be used to obtain the angle of dip of a dipping bed or fault when the line of electrodes coincides with the outcrop of the horizontal contact (fig. 122). If the resistivities ρ' and ρ'' are known from other measurements in the region, a single measurement of the apparent resistivity ρ_a with the line of electrodes along the outcrop of the contact is theoretically sufficient to determine the angle of dip ϕ_1. As plotted by Šumi (fig. 122), a known value of ρ_a/ρ'' (on the abscissa) and ρ_a/ρ' (on the ordinate) determines the value of ϕ_1, which is plotted as parameter lines on the chart.

Figure 123 shows how the error of the determination of the angle of dip ϕ_1 depends on different resistivity contrasts and on the true angle of dip, when using the Šumi method. The chart is calculated on the assumption that the apparent resistivity is known exactly within ±5 percent.

Šumi's method is obviously one that can serve only in detailed work after the trace of the fault or dipping bed has been mapped rather accurately. Effects of the fault gouge, which is limited to a comparatively narrow zone, will generally be negligible at the large electrode separations used in this method.

THEORETICAL CURVES BASED ON HARMONIC ANALYSIS

Figure 124 shows the vertical resistivity profiles with the Wenner configuration over the upper bed along traverses parallel to the strike of perfectly insulating ($k=+1$) and conducting ($k=-1$) lower beds dipping at various angles (Maeda, 1951b).

Figures 125 and 126 show vertical profiles for the Wenner configuration over the upper bed along traverses taken parallel to the strike of beds of different resistivity contrasts and dipping at angles of 45° and 60°, respectively (Maeda, 1955). The ratio of the apparent resistivity to the true resistivity of the upper bed is plotted against a/h, where a is the electrode separation and h is the vertical distance from the line of electrodes to the contact between the two beds.

When the bottom bed is of lower resistivity than the upper bed (negative reflection factors), the apparent resistivity for a vertical resistivity profile parallel to the strike is rather insensitive to changes in dip; and it would be very difficult, with field data for such a profile, to distinguish between a dip of 60° and 45°. When the bottom bed is of higher resistivity than the upper bed (positive reflection factors), the apparent resistivity for such a profile is rather insensitive to changes in dip for small reflection factors but sensitive to changes in dip for large reflection factors; and it would probably be possible under ideal field conditions with large reflection factors to distinguish between a dip of 60° and 45°.

It should be emphasized that a vertical resistivity profile taken parallel to the strike of dipping beds is a weak field technique to determine the dip. More powerful techniques will be shown below.

Figure 127 shows vertical resistivity profiles with the Wenner configuration along traverses parallel to the strike of beds of finite resistivity contrasts ($\rho''/\rho'=10$ and $\rho''/\rho'=1/10$) and dipping at various angles (Huber, 1955). The graphs are plotted on logarithmic paper. Curves are given for angles of dip both less than and also greater than 90°; therefore, the curves apply when the line of electrodes lie on both the upper and lower beds.
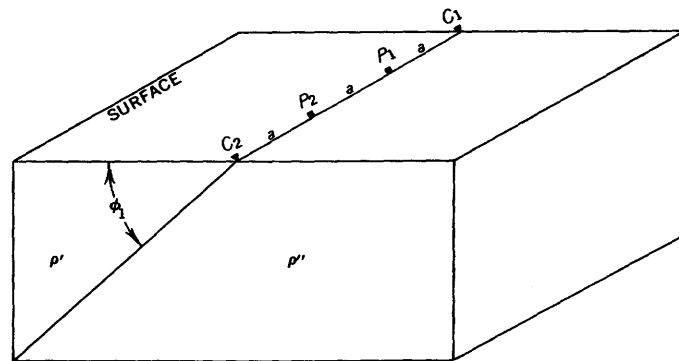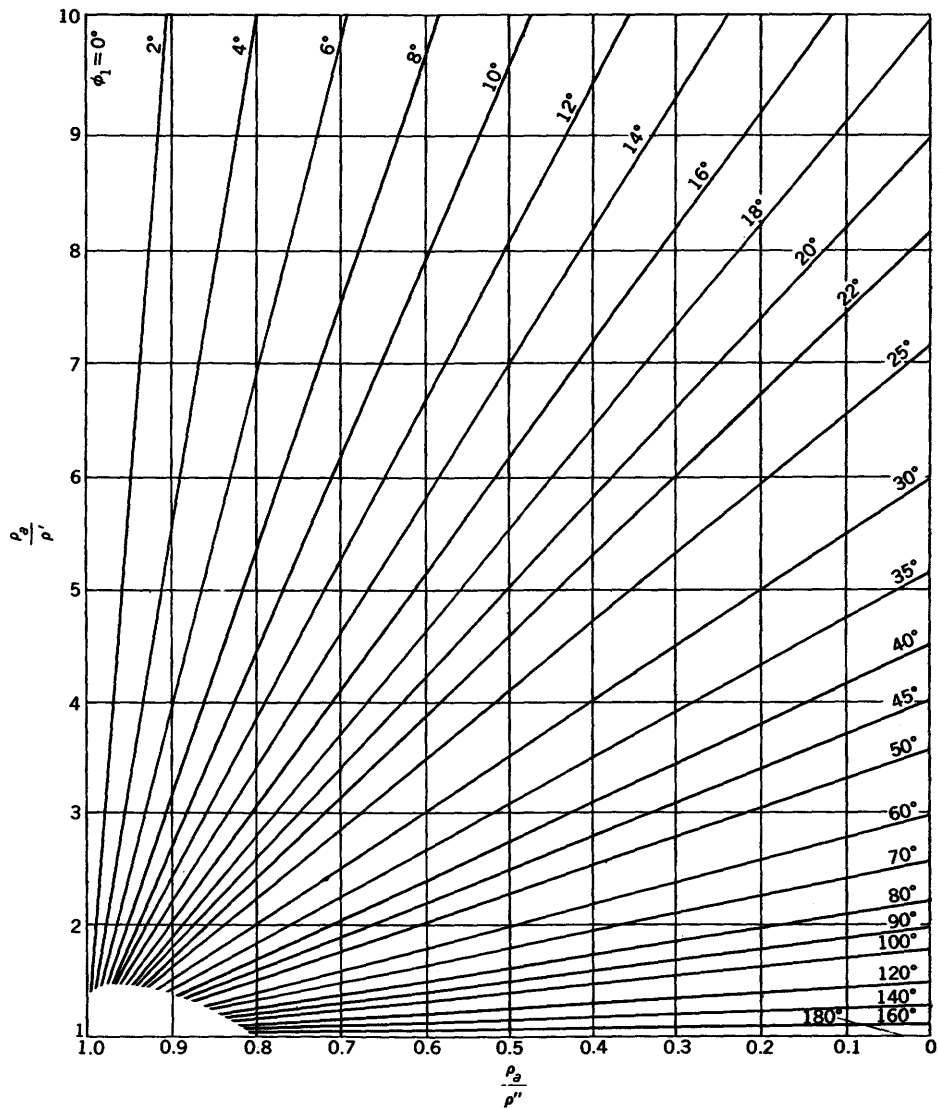
FIGURE 122.—Diagram for determination of angle of dip ϕ_1 of dipping bed when line of electrodes coincides with outcrop of contact, Wenner configuration. Adapted from Šumi (1953).
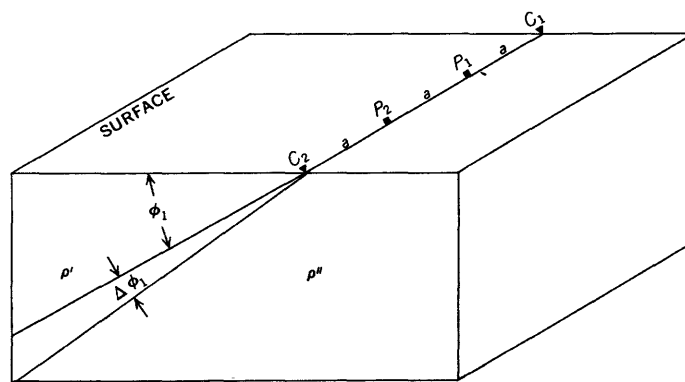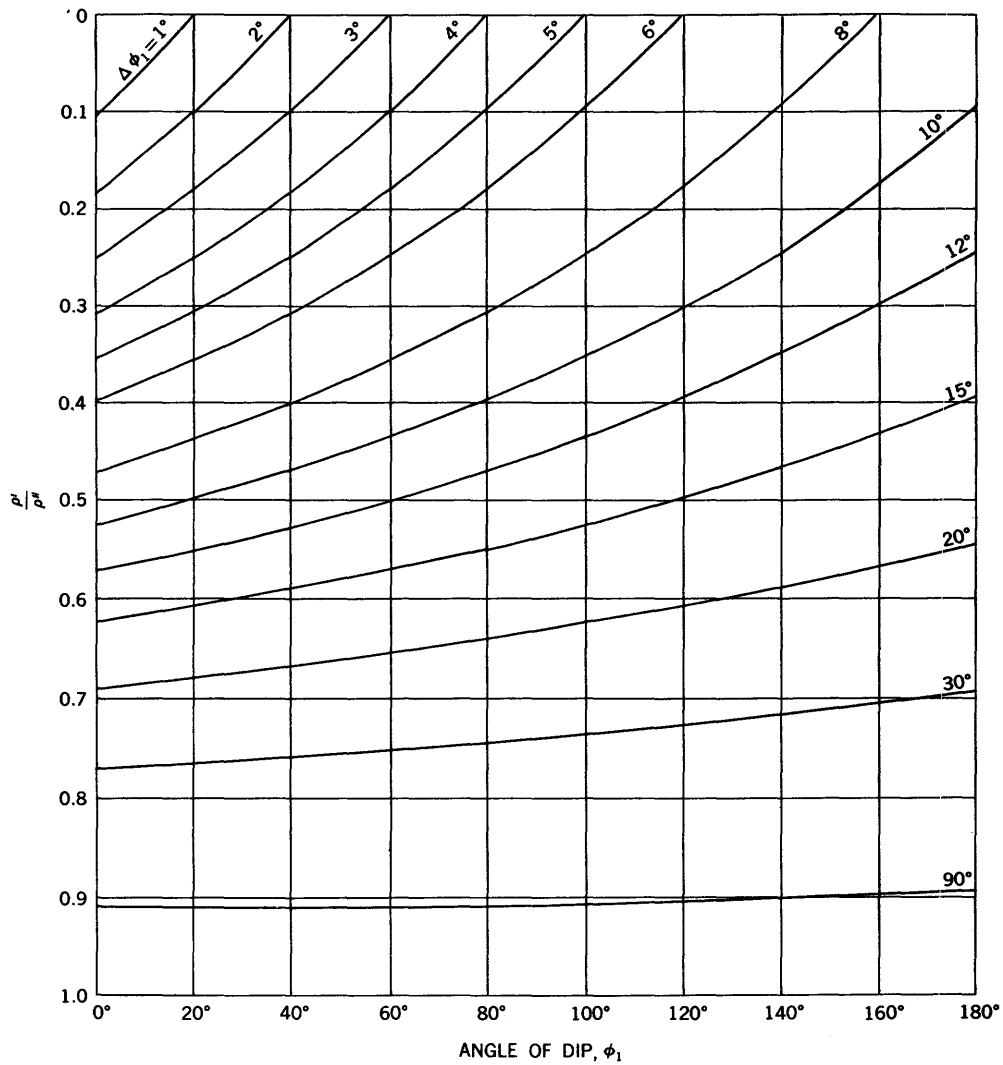
FIGURE 123.—Diagram showing the error in the determination of the angle of dip ϕ_1 of dipping bed for different angles of true dip and for different resistivity contrasts, when using the Šumi method. Apparent resistivity ρ_a is assumed known exactly within ±5 percent. Adapted from Šumi (1953).
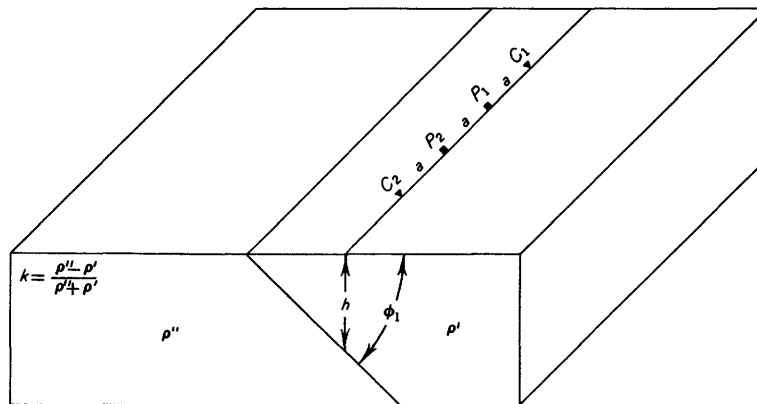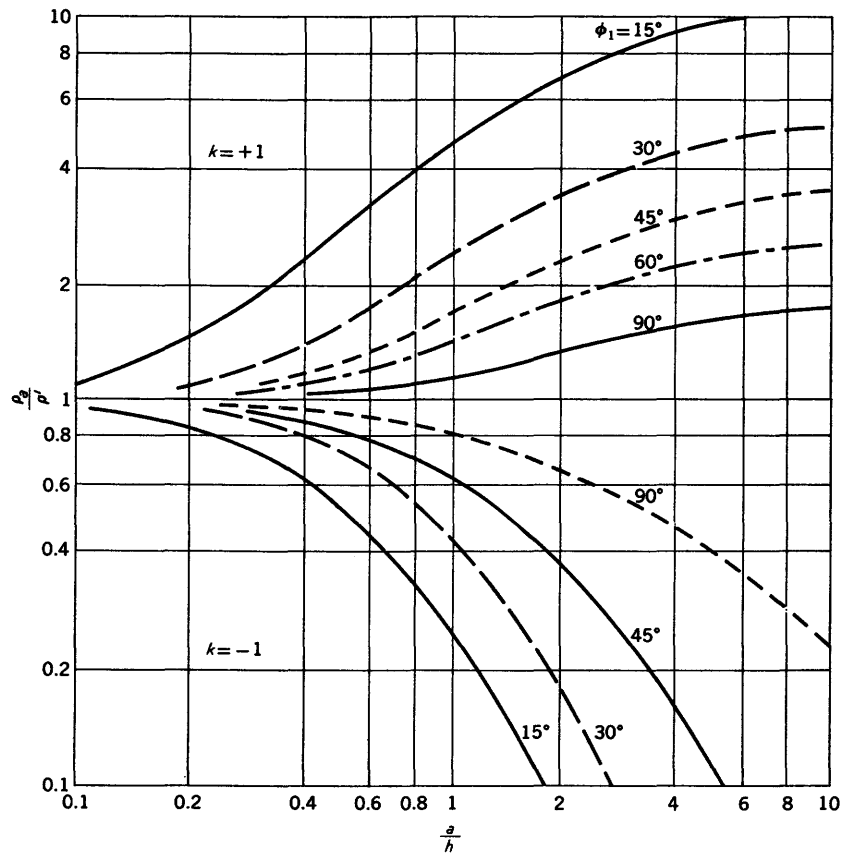
FIGURE 124.—Vertical resistivity profiles over upper bed along traverses parallel to strike of perfectly insulating $(k=+1)$ and conducting $(k=-1)$ lower beds dipping at various angles ϕ_1, Wenner configuration. Adapted from Maeda (1951b).

Figure 128 shows theoretical vertical resistivity profiles for the Schlumberger configuration over both the upper and lower beds along traverses parallel to the strike of a bed dipping 45° (Chastenet de Géry and Kunetz, 1956). Various resistivity contrasts are assumed. The abscissa of the graphs is the distance $\overline{AB}/2$. Electrode separations are measured in units of the distance from the outcrop of the dipping contact

to the line of electrodes. As would be expected, the effect of the dip is considerably less when the line of electrodes is on the updip side than when it is on the downdip side of the dipping contact.

The apparent resistivity is plotted in both cases as the ratio ρ_a/ρ', where ρ' is the true resistivity of the medium containing all the electrodes. If the resistivity were plotted instead on an absolute scale, the asymp-
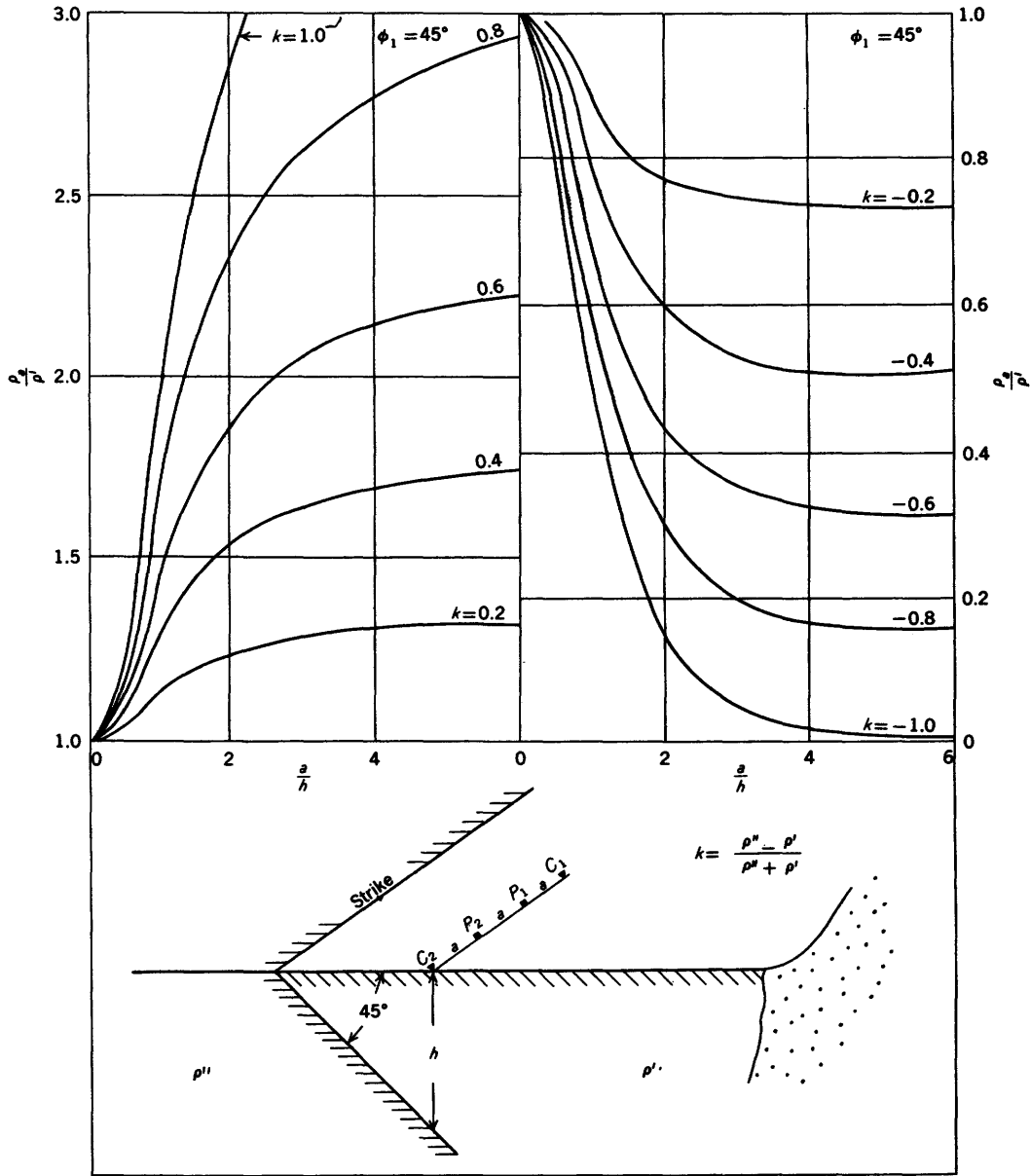
FIGURE 125.—Vertical resistivity profiles over upper bed along traverses parallel to strike of bed dipping 45°, Wenner configuration. Reflection factor $k = \pm 1.0$, ± 0.8, ± 0.6, ± 0.4, and ± 0.2. Adapted from Maeda, 1955.

totic values for large electrode separations would be the same, for a given resistivity contrast, regardless of which side of the contact the electrodes are placed. This statement is true only if the line of electrodes is oriented parallel to the strike of the contact. The reason is that the parallel component of the electric field must be continuous across the boundary. As the electrode separation increases, the configuration moves relatively closer to the boundary. Since ρ_a is here (for the Schlumberger configuration) calculated from the electric field, it follows that ρ_a must be the same on both sides of the fault when the configuration is parallel to the strike and the electrode separation is large.

COMPARISON OF APPARENT-RESISTIVITY CURVES

Figure 129 shows a comparison of the approximate apparent-resistivity profiles with the correct vertical profile for beds dipping at an angle of 45° (Van Nostrand and Cook, 1955). The resistivity contrast is 1 to 4; the upper set of curves represent the case in which the upper bed is more conducting, and the lower set the case in which the lower bed is more conducting. The Wenner configuration is alined parallel to the strike of the beds. The apparent resistivity is plotted against the electrode separation on logarithmic paper. The exact curves are based on equation 186. The integral was evaluated by Simpson's rule, dividing the intervals
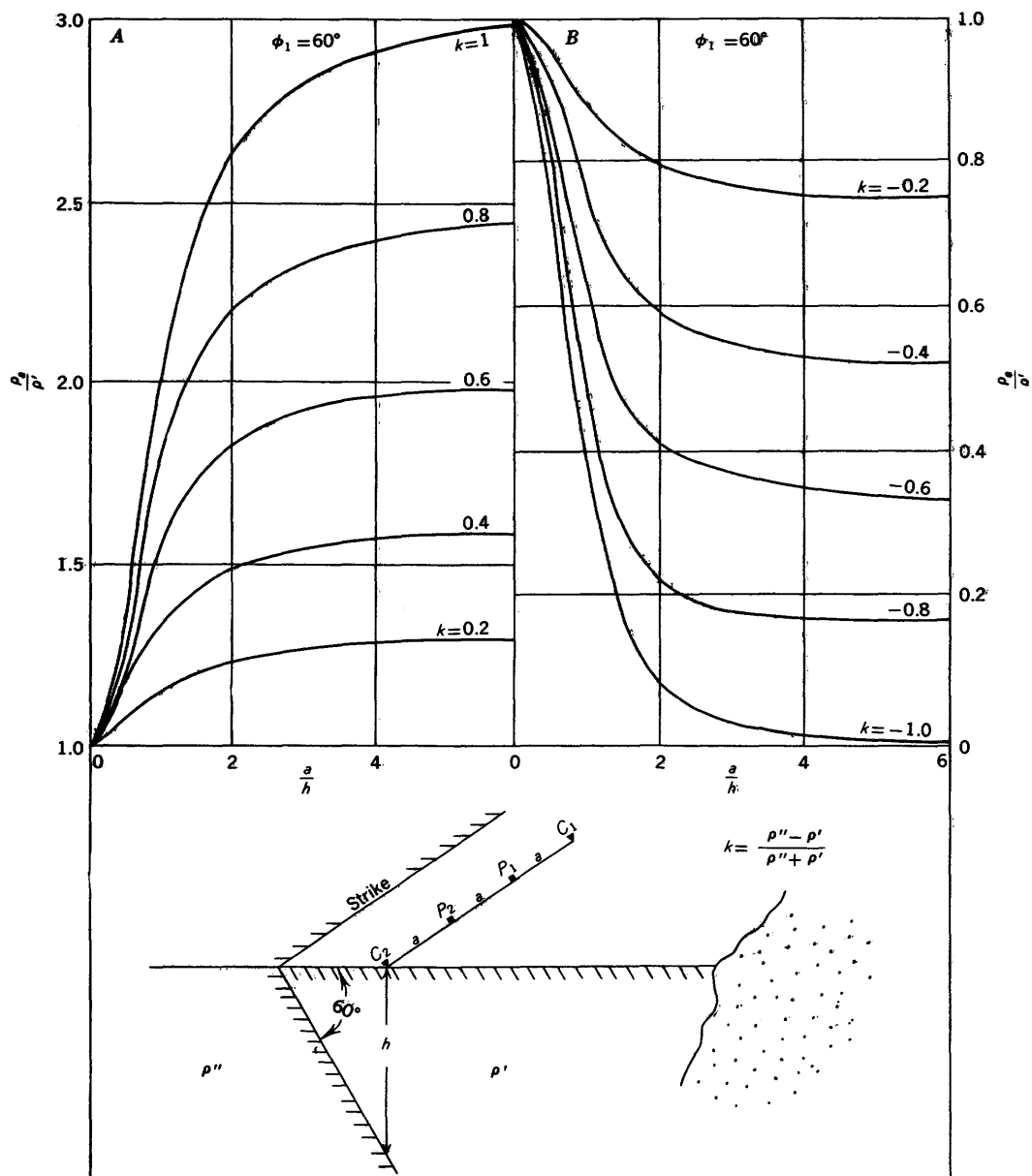
FIGURE 126.—Vertical resistivity profiles over upper bed along traverses parallel to strike of bed dipping 60°, Wenner configuration. Reflection factor $k=\pm1.0$, ±0.8, ±0.6, ±0.4, and ±0.2. Adapted from Maeda (1955).

$0 \leq s \leq 1$ and $1 \leq s \leq 4$ each into six parts. The remainder for $s > 4$ is negligible, being less than 0.05 percent. Computations for the approximate curves are based on equations given by the respective authors.

For $k = +0.6$, we see that Unz was correct in assuming that the maximum error in his raw curve was in its asymptotic value. His modified curve very closely approximates the true curve, displaying an error of only 3.5 percent at about $a=2$. The Aldredge curve, which is based on an unacceptable premise, is about as good as the Unz corrected curve. Unz's modified curves for

$k = -0.6$ contains a maximum error of about 15 percen at $a=2$. In this case Aldredge's approach leads to a negative apparent resistivity, which is possible in some cases of very complex geology but is impossible here.

We emphasize that this example, both with respect to the resistivity contrast and to the angle of dip if that angle is a submultiple of π, embodies about the maximum error possible in Unz's approximation (Unz, written communication). Therefore, errors in approximations for other angles or for other resistivity contrasts would at worst be only slightly larger than those shown
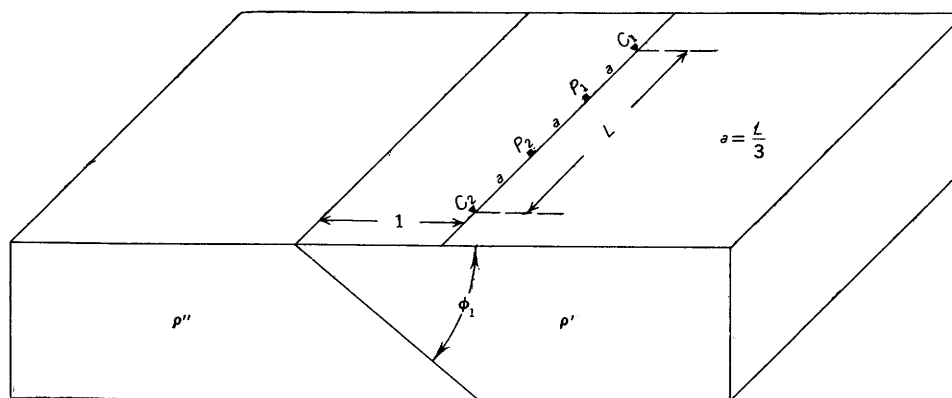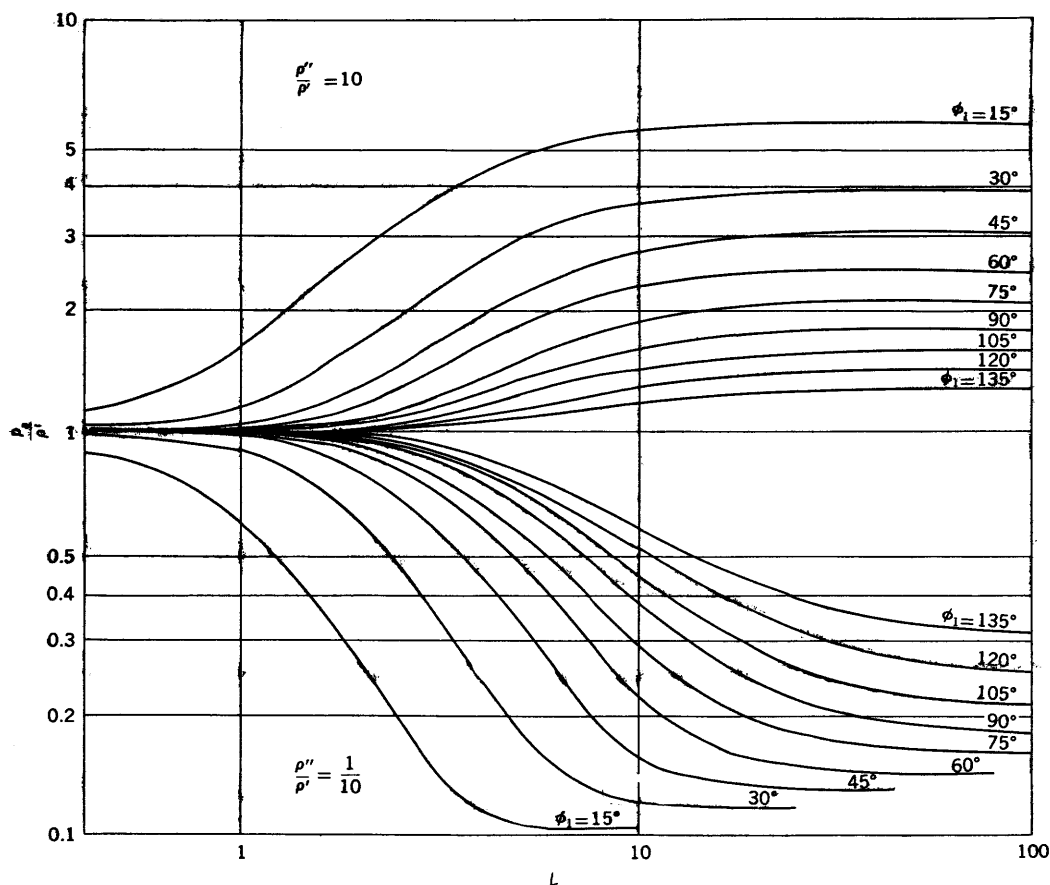
FIGURE 127.—Vertical resistivity profiles along traverses parallel to strike of beds of finite resistivity contrasts $(\rho''/\rho'=10$ and $\rho''/\rho'=$ $1/10)$ and dipping at various angles ϕ_1, Wenner configuration. Adapted from Huber (1955) by permission of Springer-Verlag, Vienna, Austria.

n this example and would probably be less. Of course, there would be no error when $k=\pm 1$, when $\phi_1=0°$, or when $\phi_1=90°$.

General conclusions, especially those concerning the accuracy of approximations applied to examples other than the one chosen, must await a more thorough study that includes variations of all the parameters, such as angle of dip, resistivity contrast, and orientation of the electrode configuration. Without exact numerical computations the quantitative influence of the parameters upon the character of the apparent-resistivity curves is often unpredictable. We emphasize that Unz's analysis is restricted to traverses lying in the upper bed and oriented parallel to the strike of the dipping beds.

$$k=\frac{\rho''-\rho'}{\rho''+\rho'}$$
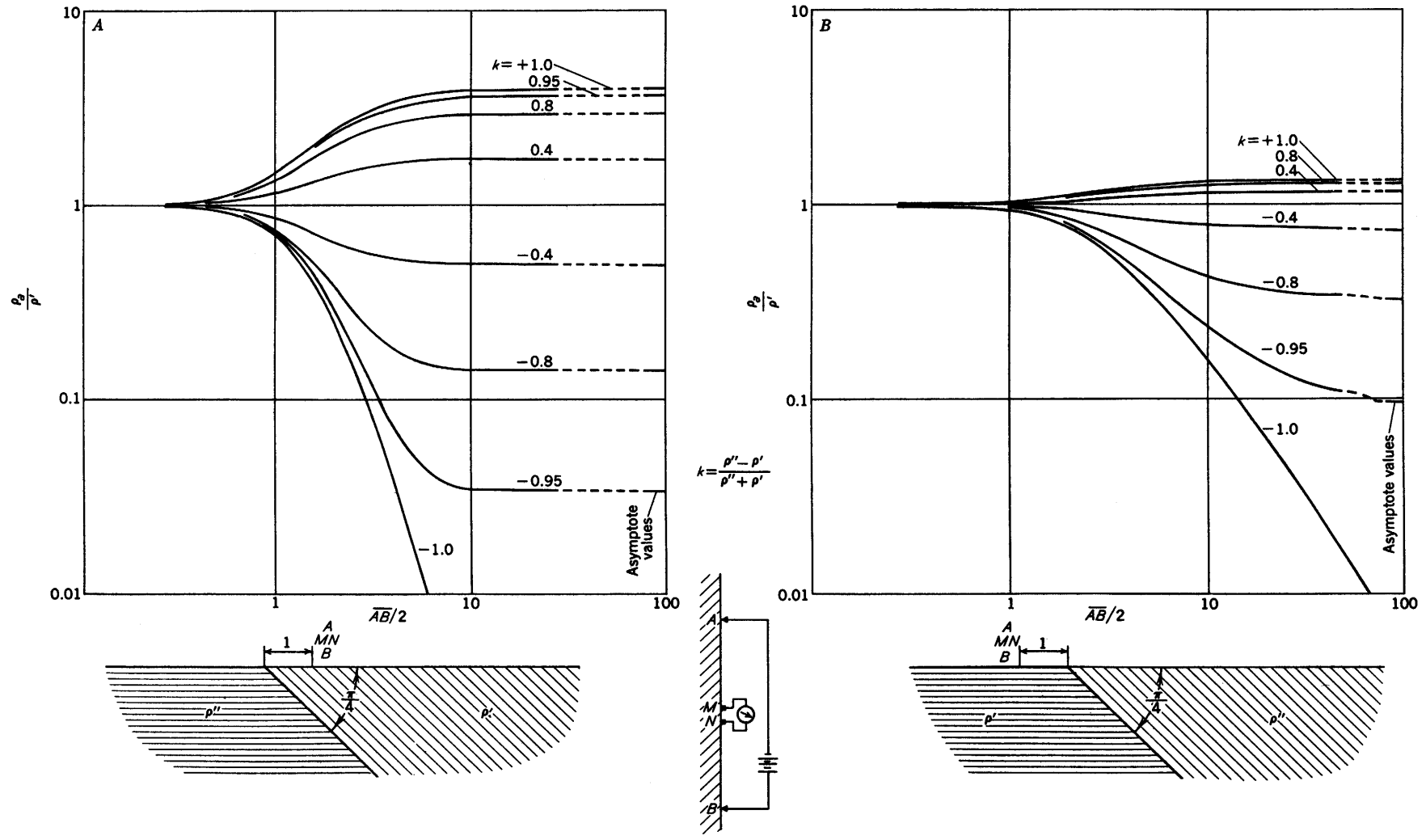
FIGURE 128.—Vertical resistivity profiles over (A) lower bed and (B) upper bed along traverses parallel to strike of bed dipping 45°, Schlumberger configuration. Various values of reflection factor k are assumed. (Adapted from Chastenet de Géry and Kunetz (1956)).
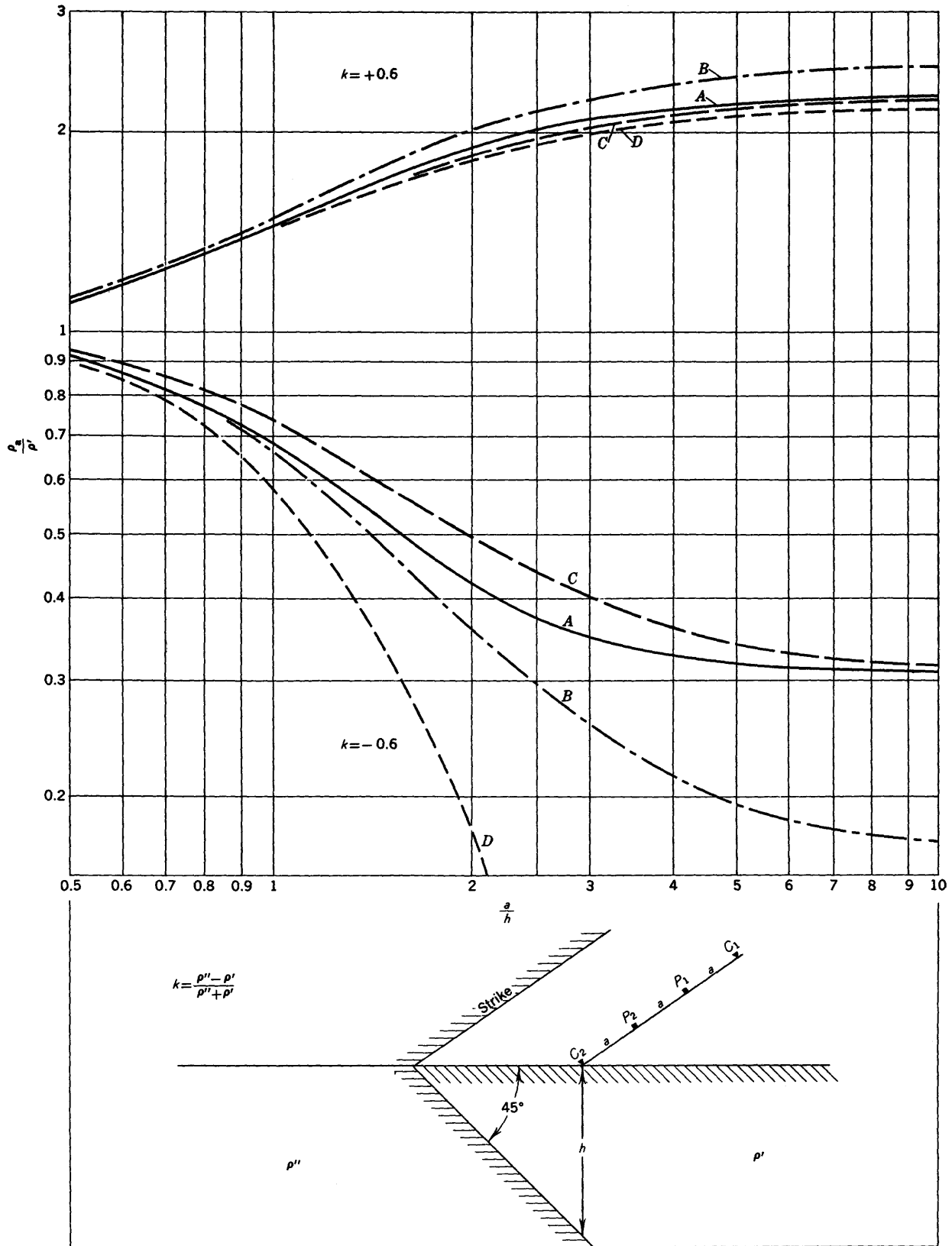
FIGURE 129.—Comparison of approximate vertical resistivity profiles (Wenner configuration) with exact curves for reflection factor $k=\pm0.6$, angle of dip $\phi_1=45°$, and with line of electrodes parallel to strike of dipping bed. (A) Exact curves based on Maeda (1955) and Skal'skaya (1948). (B) Unz (1953) preliminary curves based solely on images. (C) Unz (1953) corrected curves. (D) Aldredge (1937) curves. Adapted from Van Nostrand and Cook (1955).

His approximations seem to be adequate for positive reflection factors but are borderline for negative reflection factors. For positive reflection factors, the apparent-resistivity curves based on Aldredge's method warrant checking to ascertain the limits of their reliability in the case of profiles taken both parallel and perpendicular to the strike of the dipping beds.

RESULTS OF MODEL STUDIES

The dashed curves in figure 117 show apparent-resistivity values for profiles taken with the line of electrodes parallel to the strike of the dipping plane; the line of electrodes is moved so that it is always parallel to the strike as it crosses over and beyond the dipping plane. Hubbert (1932, p. 12) designated this type of profiling as a transverse traverse profile; it is not used commonly in resistivity prospecting. This type of a profile, from a strictly theoretical viewpoint, yields a theoretical apparent-resistivity curve that is identical to a vertical resistivity profile taken at a fixed distance from the trace of the plane along a traverse parallel to the strike of the plane. Although no theoretical curves for a vertical profile over a dipping perfectly conducting plane are available to us for comparison with the profiles obtained with the models, we can compare the right-hand part of the profiles over the models with the theoretical vertical profiles for the Wenner configuration along traverses parallel with the strike of the dipping bed, which are now available for dips of 45° and 60° (figs. 125 and 126). In this comparison, we must use only those curves for a reflection factor of -1.0; and our comparison will be limited to a study of the downdip side of the fault only, because the profiles over the bottom bed—which is of zero resistivity—are indeterminate. Moreover, the comparison must be an inverse one in which the large electrode separations in vertical profiling correspond to points at which the transverse traverse profile of Hubbert approaches the conducting sheet.

For a dip of 90° (dashed curve, fig. 117D) the apparent resistivity is a minimum, as the line of electrodes is vertically over the apex of the conducting sheet; the apparent resistivity does not go to zero, which would be so if the sheet were exposed, because the apex of the sheet is kept slightly submerged in the tank experiment. For a dip of 60° (dashed curve, fig. 117C), a minimum in the apparent resistivity occurs as the configuration crosses the apex of the conducting sheet. If the apex of the sheet were at the water level in the tank, a minimum of zero resistivity would be obtained, as the line of electrodes is positioned along this apex. For a dip of 30° (dashed curve, fig. 117B), the minimum is shifted farther downdip, as would be expected.

PROFILES PERPENDICULAR TO THE STRIKE

VERTICAL PROFILES THAT DO NOT CROSS THE CONTACT

Figure 130 shows vertical resistivity profiles with the asymmetrical Wenner configuration over the upper bed along a traverse perpendicular to the strike of both perfectly insulating ($k=+1$) and conducting ($k=-1$) lower beds dipping at various angles (Maeda, 1951b). The current electrode is closer to the outcropping trace of the contact than the potential electrodes. In each case, the current electrode is fixed and the electrode separation a is varied. All distances are with references to h taken as unity, where h is the vertical distance between the line of electrodes and the contact between the two dipping beds. The ratio of the apparent resistivity to the true resistivity ρ' of the upper bed is plotted on the ordinate.

Figure 131 shows the corresponding vertical resistivity profiles with the asymmetrical Wenner configuration when the current electrode is farther from the outcropping trace of the contact than the potential electrodes. (Maeda, 1951).

Figure 132 shows the vertical resistivity profiles with the asymmetrical Wenner configuration over the upper bed along a traverse perpendicular to the strike of beds dipping at 60°, 45°, and 30°; various values of the reflection factor are used (Maeda, 1955).

Figure 133 shows the vertical resistivity profiles with the Wenner configuration over the upper bed along a traverse perpendicular to the strike of both perfectly insulating and perfectly conducting lower beds ($k=\pm1.0$) dipping at various angles (Maeda, 1955). In each case, the current electrode nearest the surface trace is fixed and the electrode separation a is varied. All distances are with reference to the distance x taken as unity.

Figure 134 shows vertical resistivity profiles with the Wenner configuration along a traverse perpendicular to the strike of beds of finite resistivity contrasts ($\rho''/\rho'=10$ and $\rho''/\rho'=1/10$) and dipping at various angles (Huber, 1955). The profiles do not cross the contact. In figure 134 left, current electrode C_2, which is the electrode nearest the outcropping trace of the contact, remains fixed; and the expansion of the configuration is charted on the abscissa as the ratio $L=3a/d$, where d, the distance from the outcropping trace to C_2, is unity. In figure 134 right, current electrode C_1 remains fixed; and the expansion of the configuration is charted on the abscissa as the ratio $L/D=3a/D$, where D, the distance from the outcropping trace to C_1, is unity.
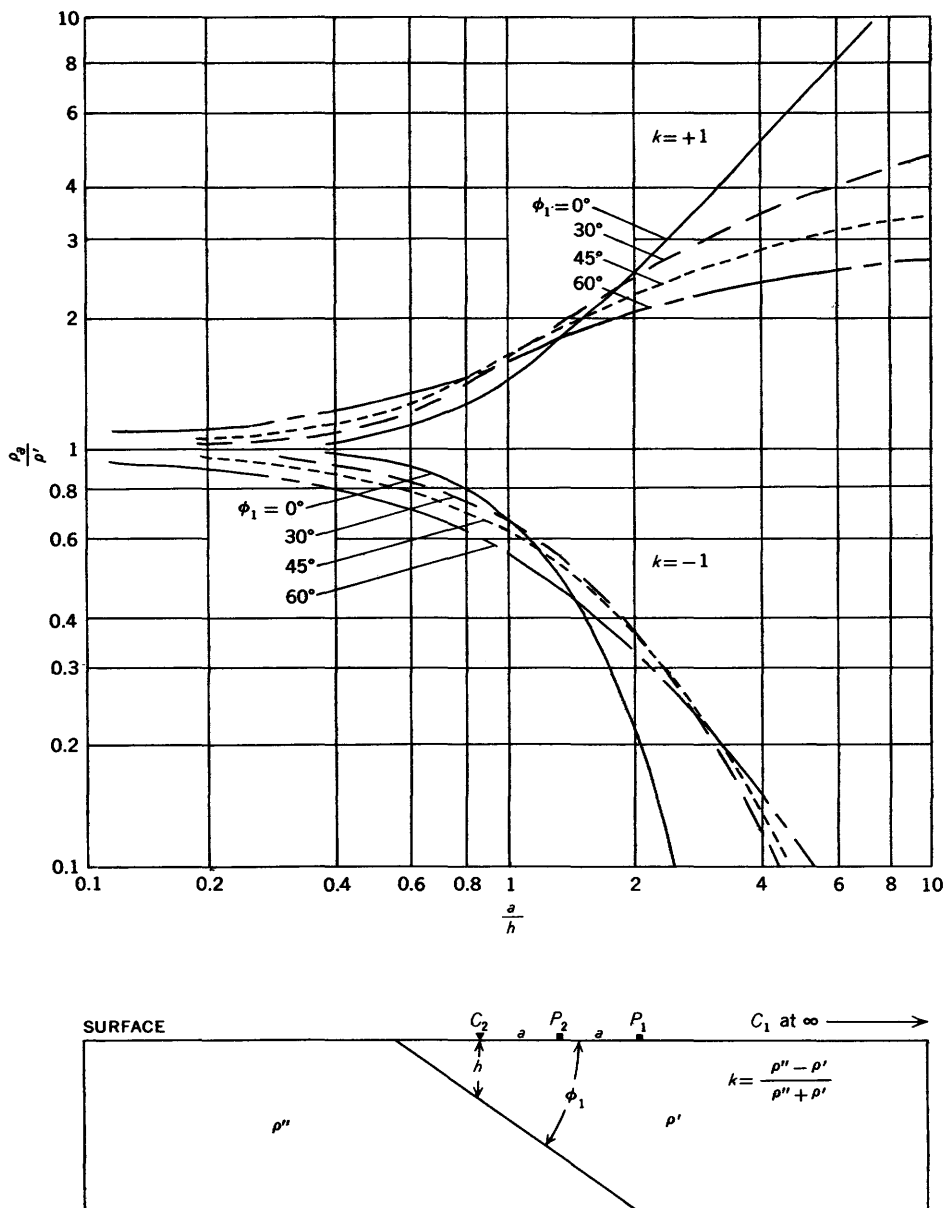
FIGURE 130.—Vertical resistivity profiles over upper bed along traverse perpendicular to strike of perfectly insulating (reflection factor $k=+1$, upper set of curves) and conducting ($k=-1$, lower set of curves) lower beds dipping at various angles ϕ_1, asymmetrical Wenner configuration. Current electrode is closer to outcropping trace of contact than potential electrodes. Adapted from Maeda (1951b).

PROFILES THAT CROSS THE CONTACT

HORIZONTAL PROFILES

Figure 135 shows horizontal resistivity profiles with both the Lee and Wenner configurations along a traverse perpendicular to the strike of a fault dipping 45°. The profiles cross the contact. The resistivity of the material on the left of the contact is four times that on the right.

For the Lee configuration (fig. 135A) the general appearance of the ρ_1 and ρ_2 curves is similar to that for

a vertical fault. For example, peaks A and A' lie a distance of $a/4$ from the outcrop of the trace of the inclined fault, as for the vertical fault. The important feature of great diagnostic value that distinguishes the inclined fault from the vertical fault in the present example is the high apparent-resistivity value of peak A in the ρ_2 curve. For a vertical fault, peak A theoretically has a value equal to that of the country rock (4 units in this case); in the present dipping-fault example, peak A has a value of about 4.5. (See pl. 1F
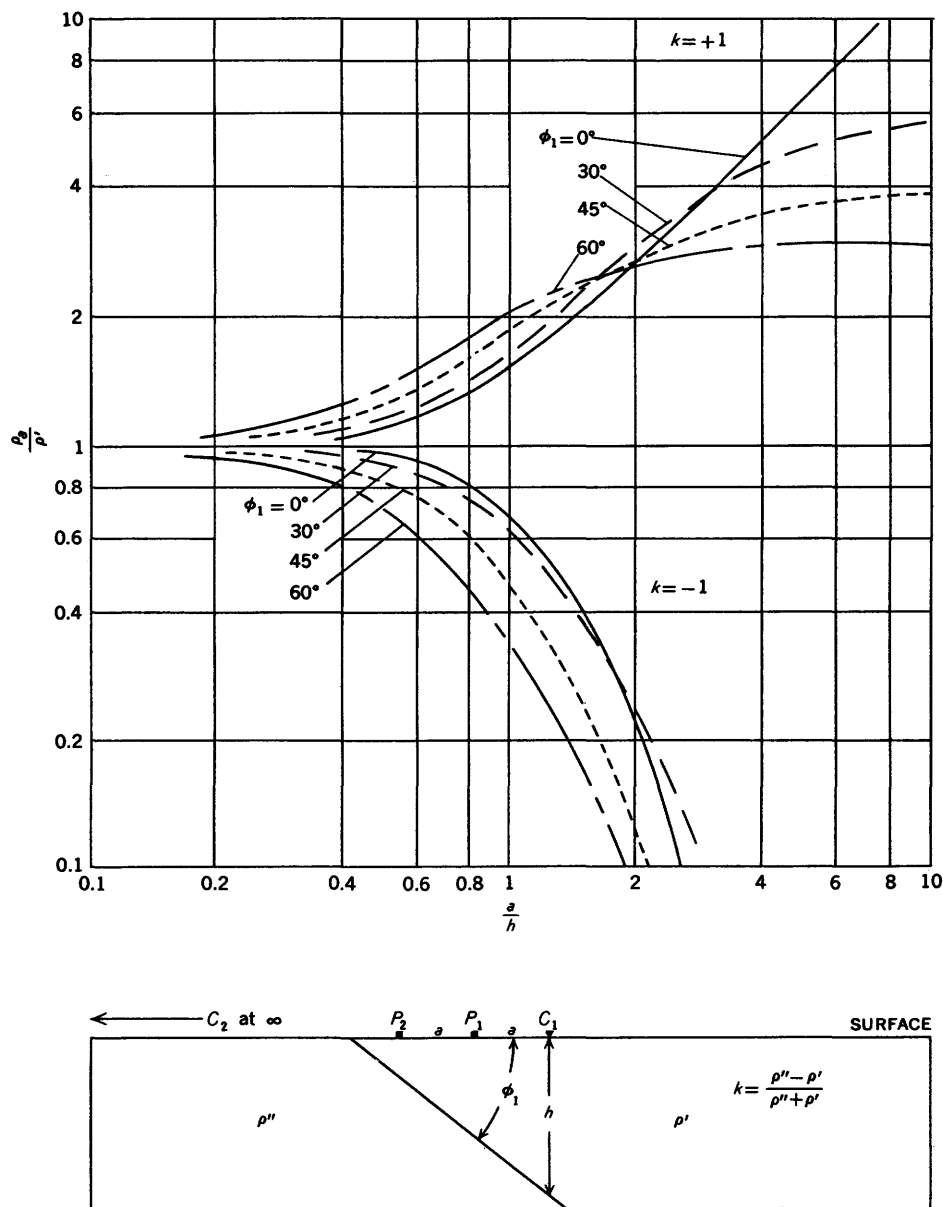
FIGURE 131.—Vertical resistivity profiles over upper bed along traverse perpendicular to strike of perfectly insulating ($k=+1$, upper set of curves) and conducting ($k=-1$, lower set of curves) lower beds dipping at various angles ϕ_1, asymmetrical Wenner configuration. Current electrode is farther from outcropping trace of contact than potential electrodes. Adapted from Maeda (1951b).

for comparison with vertical fault.) In addition, peak A' on the ρ_1 curve has a value of about 2.85 for a vertical fault with the same resistivity contrast and a value of about 3.6 for the dipping fault. Similarly the apparent-resistivity values of peaks B and B' in the ρ_2 and ρ_1 curves, respectively, are much higher for the dipping fault than the corresponding values for the vertical fault. Although this difference is not of great diagnostic value on field curves because it cannot be so readily recognized on this part of the curves, these

peaks at B and B' are of great academic importance because they represent the converging-current effect as current electrode C_2 lies near the outcrop of the fault plane. The same results would be obtained for beds dipping 45° and having a contact located where the fault plane is shown.

For the Wenner configuration (fig. 135B), peak A lies a distance of $a/2$ from the outcrop of the inclined fault trace, as for the vertical fault. Peak A is also
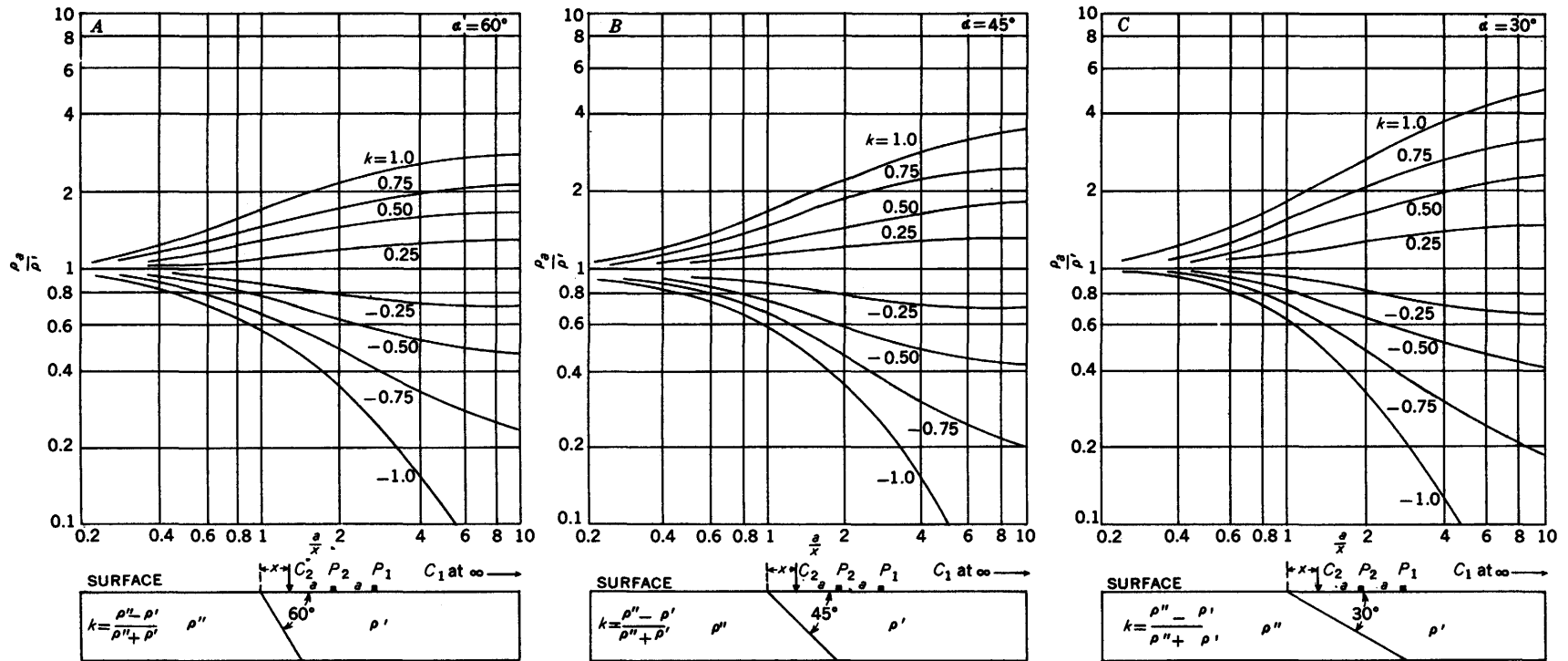
Figure 132.—Vertical resistivity profiles over upper bed along traverse perpendicular to strike of beds dipping at (A) 60°, (B) 45°, and (C) 30°, asymmetrical Wenner configuration. Reflection factor $k=\pm 1.0$, ± 0.75, ± 0.50, and ± 0.25. Adapted from Maeda (1955).
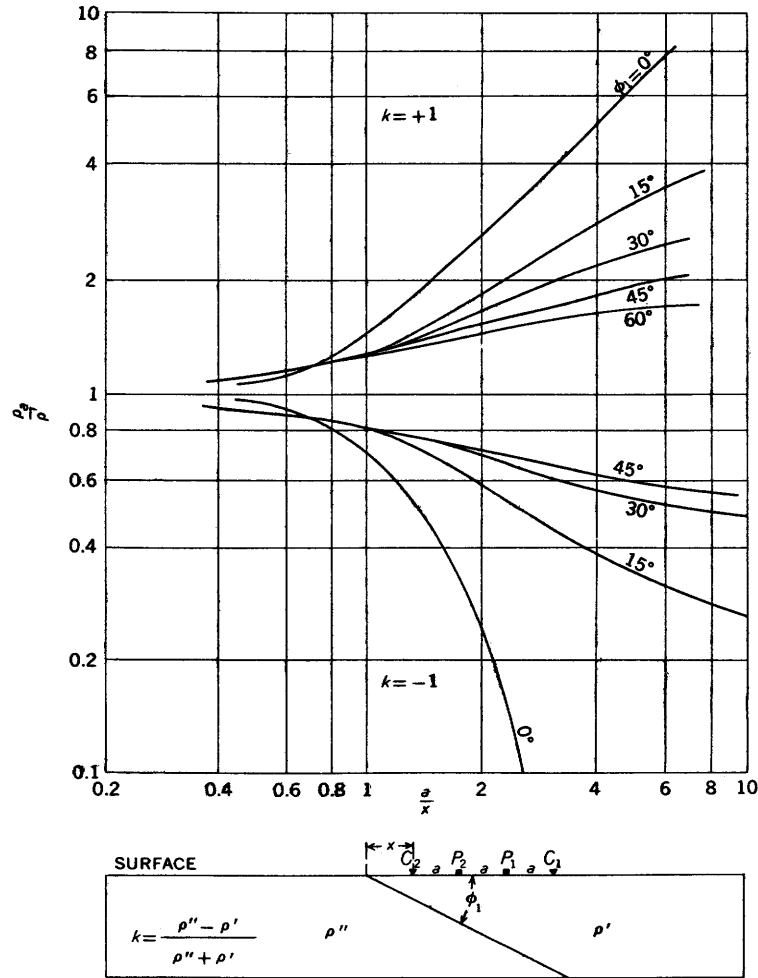
of much higher value than for the vertical fault of the same resistivity contrast.

Figure 136 shows horizontal resistivity profiles across the contact with the Wenner configuration along a traverse perpendicular to the strike of beds of finite-resistivity contrasts ($\rho''/\rho'=10$ and $\rho''/\rho'=1/10$) and dipping at various angles (Huber, 1955). The distance L between the current electrodes is equal to $3a$. For a bottom bed of greater resistivity than the upper bed, the current-converging effect when current electrode C_2 lies near the outcropping trace is pronounced for small and intermediate angles of dip.

VERTICAL PROFILES

Figure 137 shows vertical resistivity profiles with both the Lee and Wenner configurations along a

traverse perpendicular to the strike of a bed or fault dipping 45°. The profiles cross the contact. The resistivity contrast is 1 to 4.

For a station one unit to the left of the outcrop of the fault trace—that is, over the medium of higher resistivity on the updip side—an abrupt decrease in the apparent resistivity occurs for both the Lee and Wenner configurations as current electrode C_1 crosses the fault plane; the minimum of the curve occurs, however, as C_1 lies a short distance to the right of the outcrop of the fault trace. As potential electrode P_1 crosses the contact, a peak occurs in the Wenner curve and in the Lee ρ_1 curve.

For a station one unit to the right of the outcrop of the fault trace—that is, over the medium of lower resistivity on the downdip side—a current-converging peak occurs on both the Lee and Wenner curves
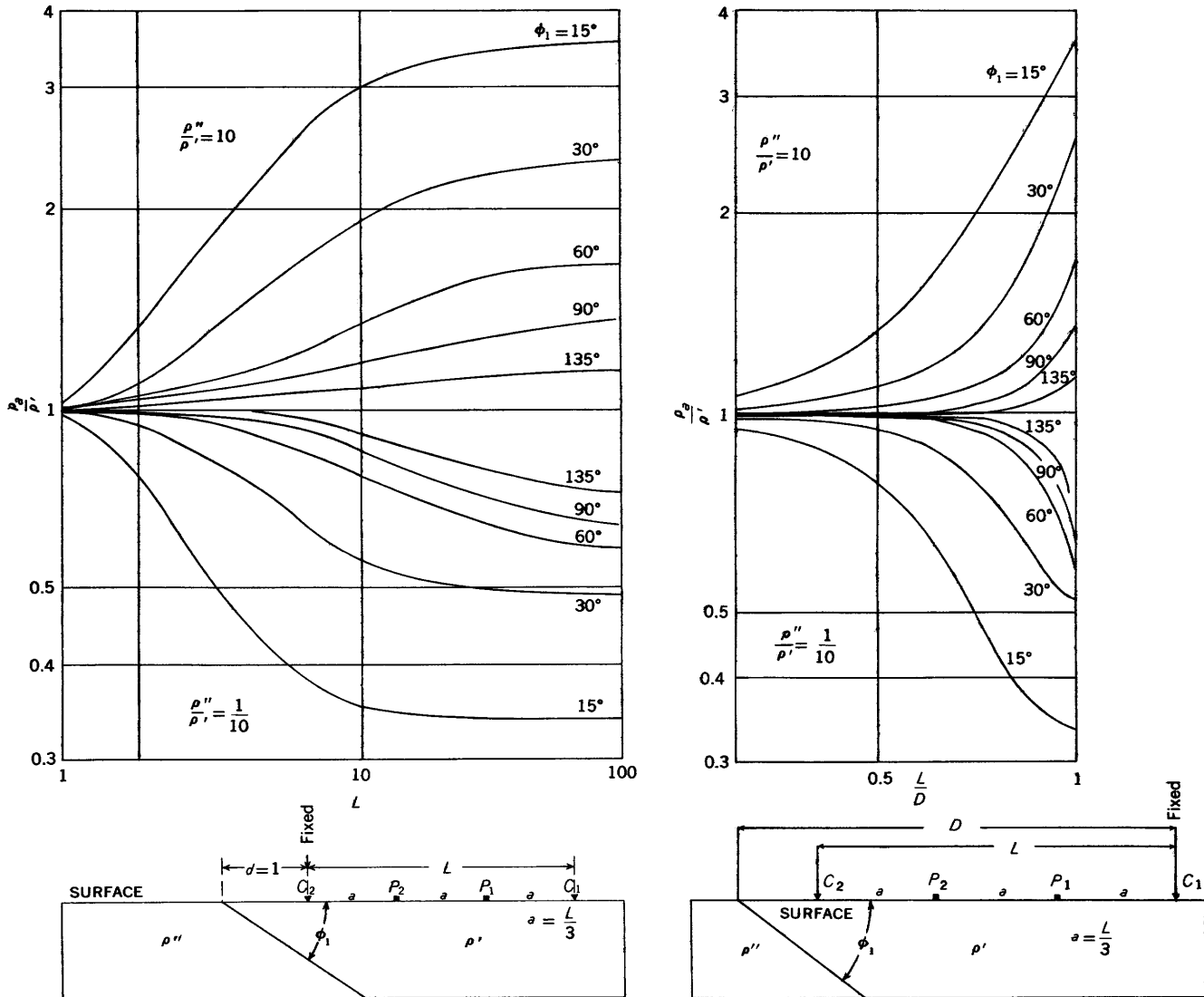
FIGURE 134.—Vertical resistivity profiles along traverse perpendicular to strike of beds of finite resistivity contrasts ($\rho''/\rho'=10$ and $\rho''/\rho'=1/10$) and dipping at various angles ϕ_1, Wenner configuration. Profiles do not cross contact. *Left*, Current electrode C_2 remains fixed. *Right*, Current electrode C_1 remains fixed. Adapted from Huber (1955) by permission of Springer-Verlag, Vienna, Austria.

as current electrode C_2 crosses the outcrop of the fault plane. The discontinuity in slope, which occurs as P_2 crosses the contact, is less pronounced than for a vertical fault. The "plateau" in the apparent resistivity curve in the intervals between the crossing of the contact C_2 and P_2, for both the Lee and Wenner configurations, occurs at a much higher value of apparent resistivity for the inclined fault than for a vertical fault. For the Lee configuration, the "spread" between the ρ_1 and ρ_2 curves in the plateau part of the curves—that is, the difference between the average value of ρ_2 in the plateau area and the average value of ρ_1 in the region beneath this plateau—is about

twice as great for a 45°-dipping fault as for a vertical fault, when the same resistivity contrasts are assumed. (See fig. 59 for comparison with a vertical fault.)

For both the Lee and Wenner vertical profiles the most diagnostic feature to differentiate an inclined fault or bed from a vertical fault or bed is the current-converging peaks and the unusually high values of the apparent-resistivity plateaus. When the Lee configuration is used, the wide spread between the ρ_2 and ρ_1 curves in the plateau region is also of diagnostic value.

Figure 138 shows vertical resistivity profiles across the contact with the Wenner configuration along a
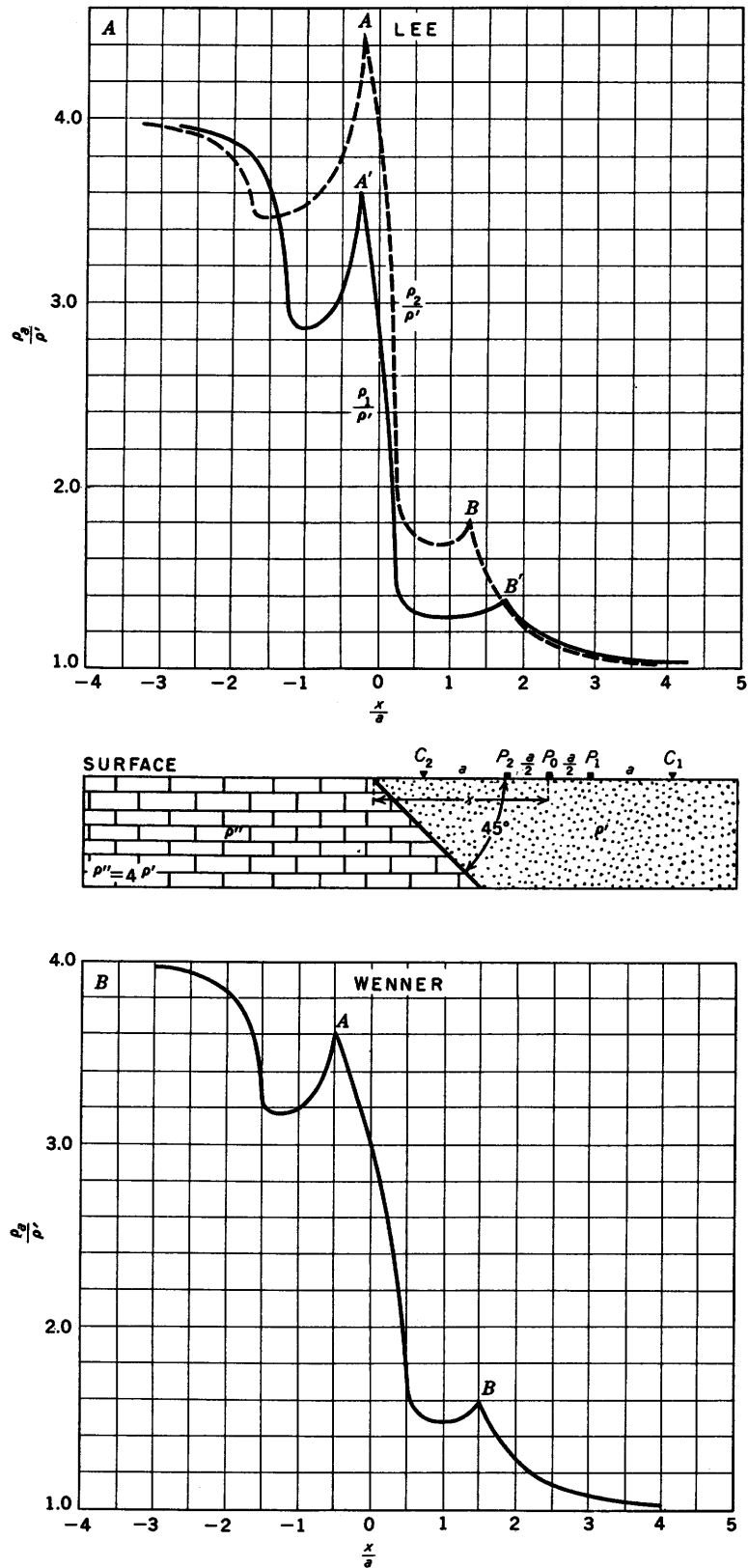
FIGURE 135.—Horizontal resistivity profiles with both the (A) Lee and (B) Wenner configurations along traverse perpendicular to strike of fault dipping 45°. Profiles cross contact. Reflection factor k=+0.6.
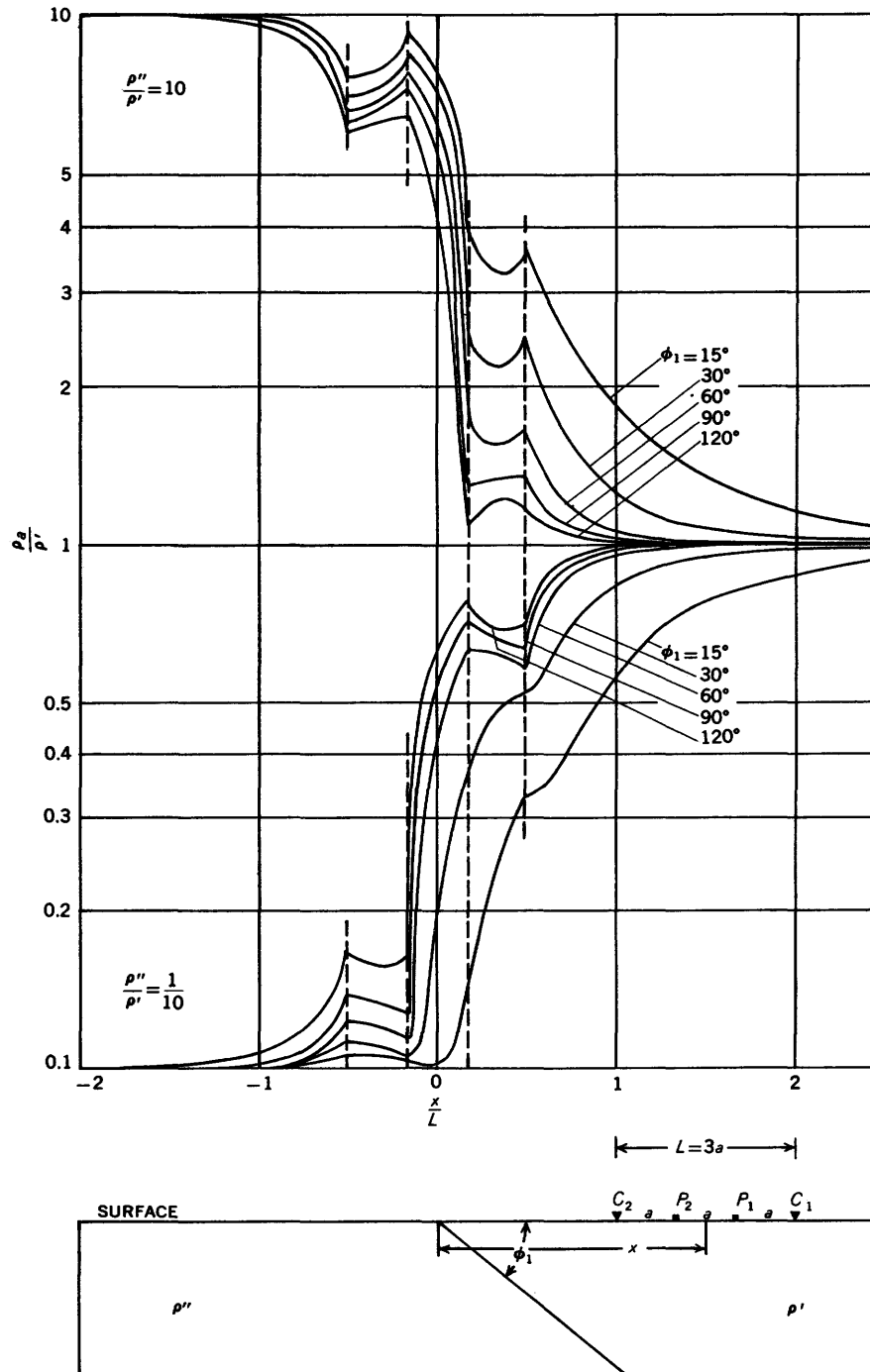
FIGURE 136.—Horizontal resistivity profiles across contact along traverse perpendicular to strike of beds of finite-resistivity contrasts ($\rho''/\rho'=10$ and $\rho''/\rho'=1/10$) and dipping at various angles ϕ_1, Wenner configuration. $L=1$ unit. Adapted from Huber (1955) by permission of Springer-Verlag, Vienna, Austria.

traverse perpendicular to the strike of beds of finite-resistivity contrasts ($\rho''/\rho'=10$ and $\rho''/\rho'=1/10$) and dipping at various angles (Huber, 1955). The station is taken a unit distance from the outcropping trace of the contact. The abscissa is plotted in terms of the distance L between the current electrodes ($L=3a$).

The curves show clearly the current-converging effects for small and intermediate angles of dip.

Figure 139 shows vertical resistivity profiles with the Schlumberger configuration along a traverse perpendicular to the strike of a bed or fault dipping 45° (Chastenet de Géry and Kunetz, 1956). The profiles
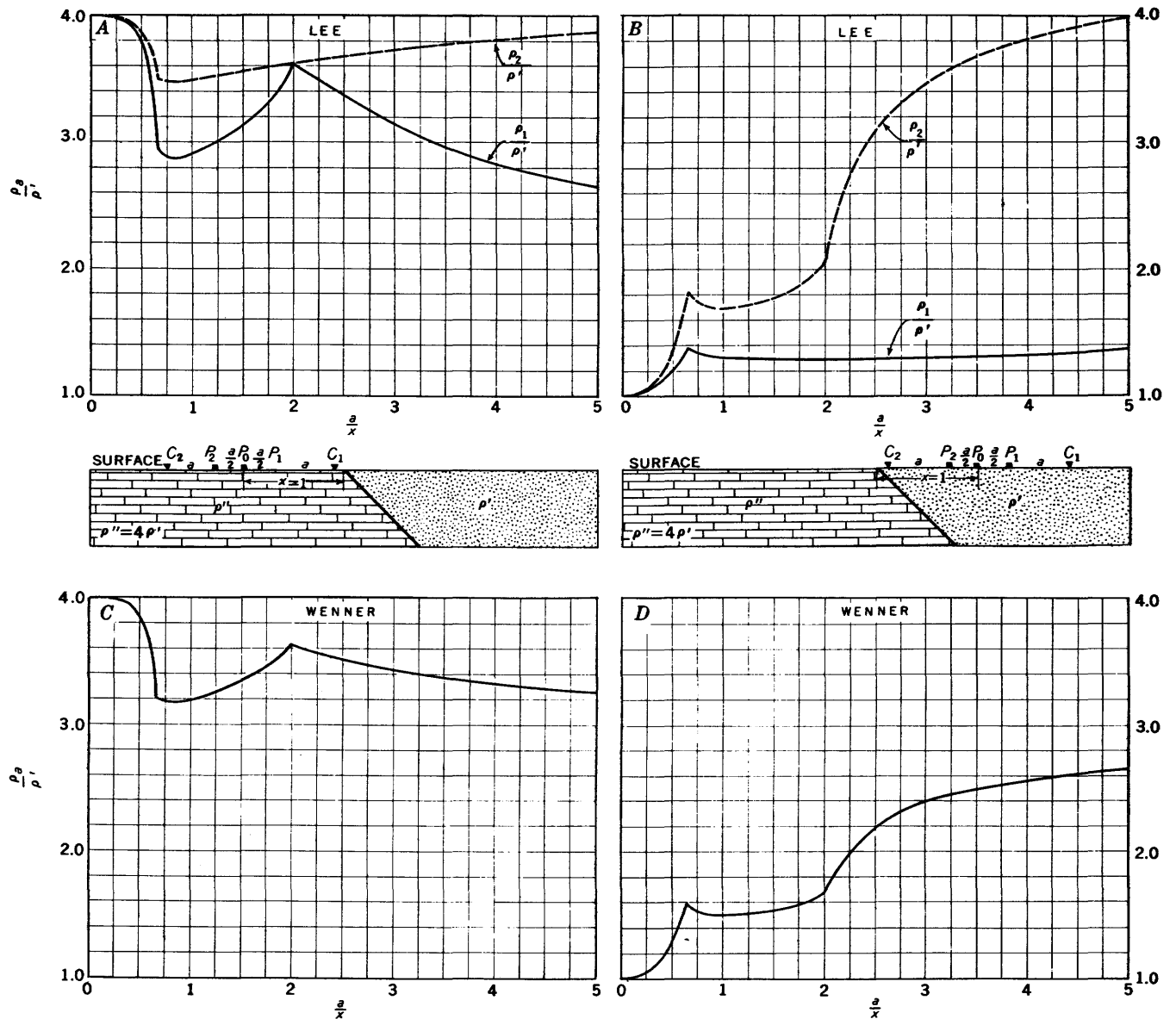
FIGURE 137.—Vertical resistivity profiles with both the (A and B) Lee and (C and D) Wenner configurations along traverse perpendicular to strike of fault dipping 45°. Profiles cross contact. Reflection factor $k=+0.6$.

cross the contact. Various values of k are used. The electrode separations are measured in units of the distance from the surface trace to the center of the configuration. Owing to the geometry of the Schlumberger electrode configuration itself, these curves are paradoxical in that the apparent resistivity approaches either infinity or zero, for large electrode separations, in all of these curves. Let us consider only the case for which $\rho''>\rho'$ (that is, $k>0$). As would be expected, for small electrode separations the curves start out with $\rho_a=\rho'$; and, as the electrode separation is increased, the apparent resistivity increases until the right-hand

current electrode reaches the contact. At this electrode separation, the apparent resistivity is intermediate between ρ' and ρ''. For increasingly larger electrode separations, the apparent resistivity decreases asymptotically to zero.

TRAVERSES AT VARIOUS AZIMUTHS

Huber (1955) computed and plotted the apparent resistivities that would be obtained with the Wenner configuration at a station over the upper bed as the line of electrodes is rotated with constant electrode separation about one of the current electrodes, which is kept fixed. The azimuth angle ω of the line of electrodes is
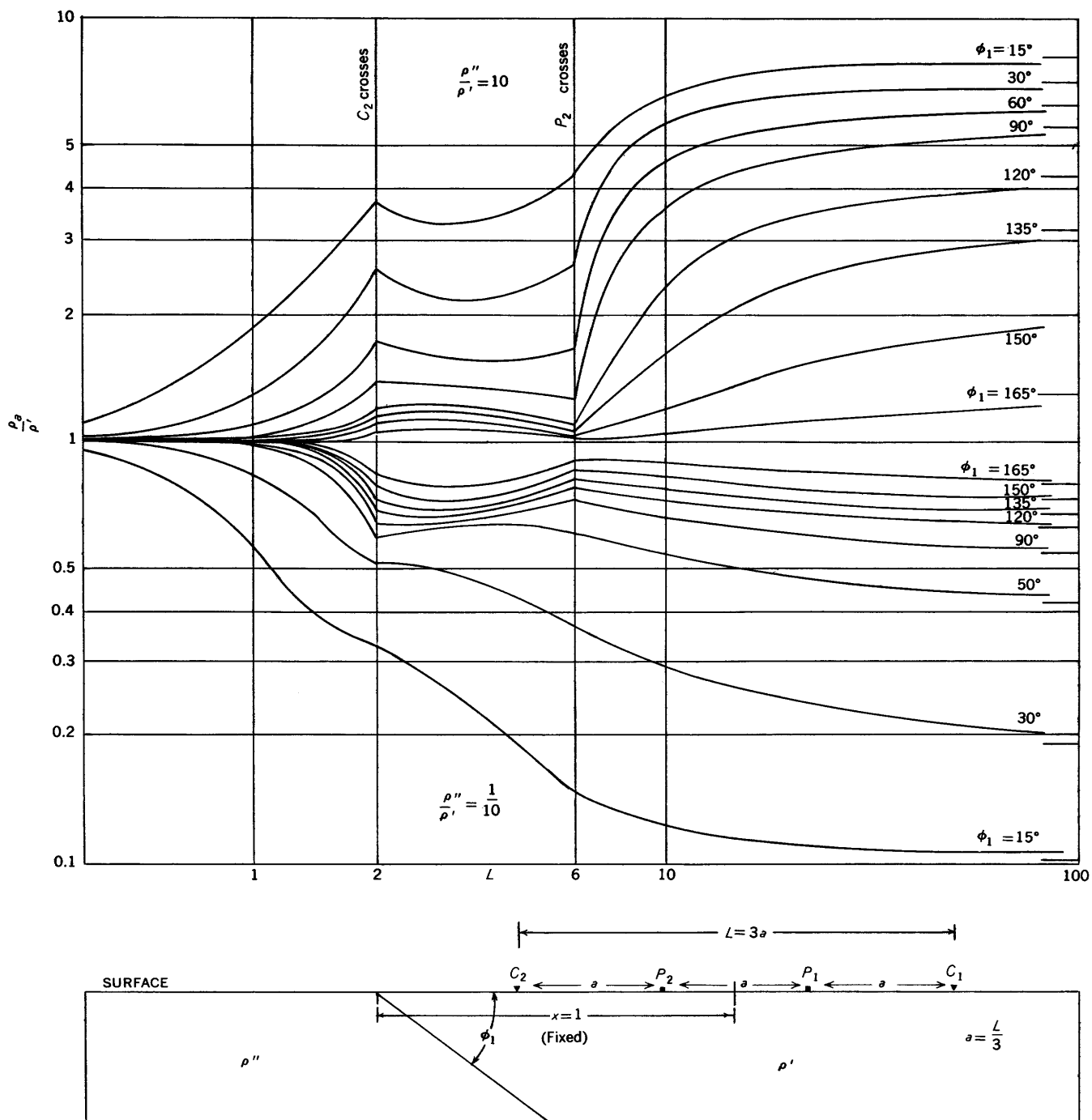
FIGURE 138.—Vertical resistivity profiles along traverse perpendicular to strike of beds of finite-resistivity contrasts ($\rho''/\rho'=10$ and $\rho''/\rho'=1/10$) and dipping at various angles ϕ_1, Wenner configuration. Profiles across contact. $d=1$ unit. Adapted from Huber (1955) by permission of Springer-Verlag, Vienna, Austria.

measured relative to the direction of the horizontal component of the dip vector. The distance between the current electrode acting as the pivot point and the outcropping trace is always made larger than L, the distance between the two current electrodes, so that the line of electrodes does not cross the contact of the beds.

Figure 140 shows the apparent-resistivity values for finite-resistivity contrasts of $\rho''/\rho'=10$ (fig. 140C) and $\rho''/\rho'=1/10$ (fig. 140C) when $d=1$ and $L=0.9$ (Huber, 1955). Various discrete values of dip are taken, and the curves are plotted for values of ω ranging from 0° to 180°.
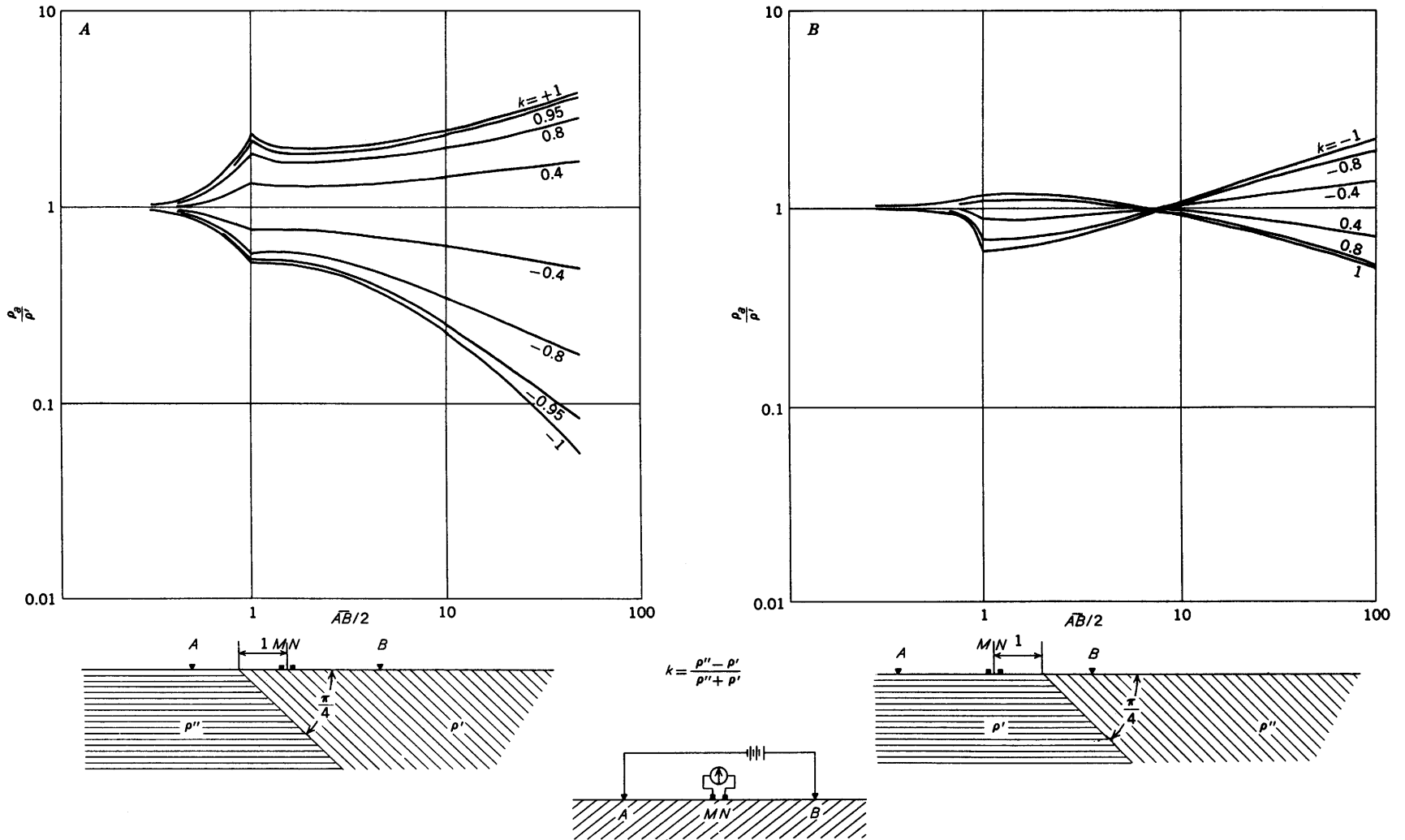
FIGURE 139.—Vertical resistivity profiles with Schlumberger configuration along traverse perpendicular to strike of bed dipping 45°. Profiles cross contact. Various values of reflection factor k. Adapted from Chastenet de Géry and Kunetz (1956).
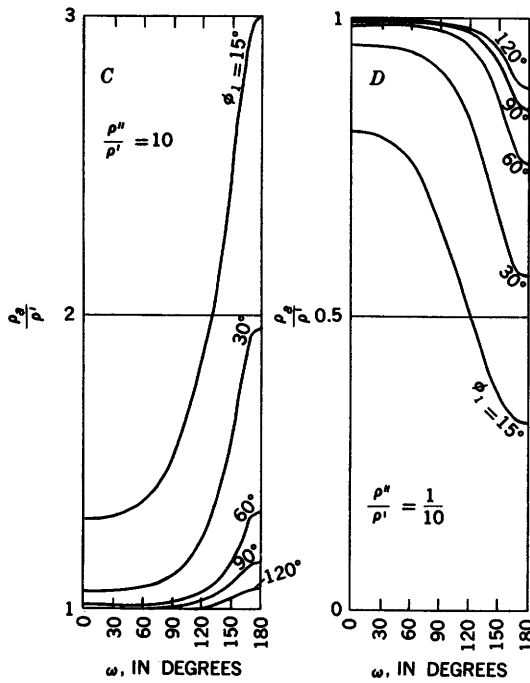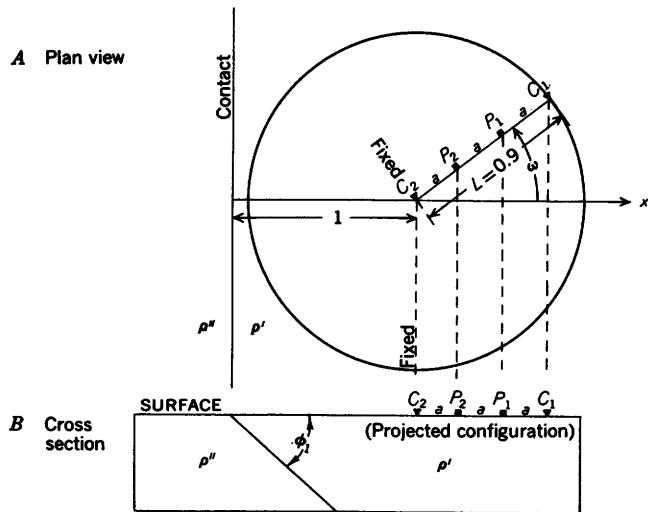
FIGURE 140.—Apparent-resistivity values over the upper bed for traverses oriented at various azimuths ω relative to the direction of dip of beds with finite resistivity contrasts (ρ''/ρ'=10 and ρ''/ρ'=1/10) and dipping at various angles of dip ϕ_1, Wenner configuration. For all curves, d=1 and L=0.9. Adapted from Huber (1955) by permission of Springer-Verlag, Vienna, Austria.

FILLED SINKS AND CHANNELS

An understanding of the interpretation of resistivity data over filled sinks and channels is useful in mining geophysics. As an example, in the Tri-State lead-zinc mining district of Missouri, Kansas, and Oklahoma, ore bodies and mineralized zones are associated with filled sinks, which are locally designated "shale sinks." Under suitable conditions of resistivity contrast, filled sinks lying at shallow depths can be found by resistivity

methods, as was shown in the Tri-State district as early as 1929 (Maillet and Migaux, 1942, p. 73–75; Jakosky and others, 1942).

The objectives of the present section are to summarize the theoretical treatment used in solving the ellipsoidal and hemispherical sink problem; to show how the theoretical results can be used to interpret field data obtained with the Lee and Wenner configurations; and to devise field techniques to discover and outline filled sinks in regions where they probably exist. Although the data and curves shown are specific, the conclusions probably have general utility.

THEORY

To develop the equations on which the theoretical curves in this section are based we divide the theory into two parts, one which depends upon spheroidal coordinates and the second which derives from cylindrical coordinates. The former is used for the filled-sink problem, the latter for the filled-channel problem. Formulas and theoretical curves are given for filled sinks; but only the formulas, without accompanying theoretical curves, are developed for filled channels. If the resistivity contrast is sufficient, shallow filled channels can be detected in a regional survey. More information can then be obtained by taking profiles across the channels perpendicular to their trend. The theoretical curves given in this section for profiles across the center of a filled sink should serve adequately in the detailed work so that the geophysicist can tell whether the linear feature on his regional map is a filled channel or a dikelike body extending infinitely downward. We include the mathematics for the filled-channel problem merely for completeness so that workers may investigate this problem further if they so desire.

FILLED SINKS

The prolate spheroidal coordinate system (fig. 25), with the z-axis oriented vertically, can be used to investigate a sink that is circular in plan view and which has a depth greater than the radius of this circle. The same coordinate system, with the z-axis oriented horizontally, can be used to approximate a sink that is elliptical in plan view and nearly circular in cross-section perpendicular to its major axis. The oblate spheroidal coordinate system (fig. 26), with the z-axis oriented vertically, can be used to approximate a filled sink which is circular in plan and which has a depth less than the radius of this circle. Oblate spheroidal coordinates, with z-axis oriented horizontally, also can be used to approximate a sink that is elliptical in plan view and approximately circular in a cross section taken perpendicular to its minor axis. Both prolate and oblate spheroidal coordinates degenerate into spherical
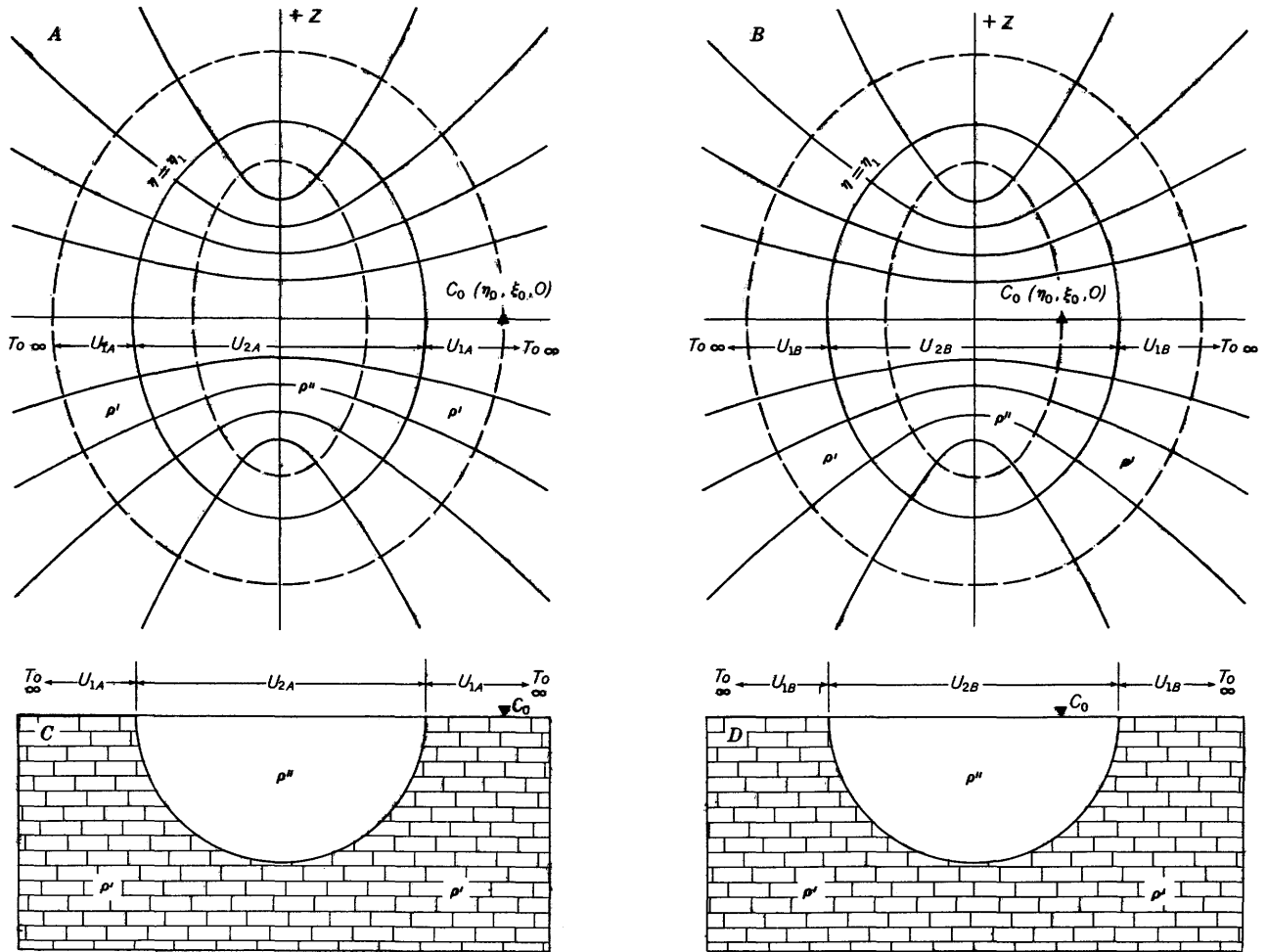
FIGURE 141.—Diagrams showing notations and conventions used in resistivity theory for filled sinks. (A) and (B), Prolate spheroidal coordinates; surfaces of constant third dimension are azimuthal planes through the vertical z-axis. (C) and (D), Cross sections of hemispherical sink with current source outside and inside sink, respectively. Adapted from Cook and Van Nostrand (1954).

coordinates. This latter system can be used to approximate a sink which is nearly hemispherical in shape.

In using any of the above coordinate systems, a given plane is generally designated as the surface of the earth. Usually the plane so chosen must be a plane of symmetry. However, since we will use the solutions developed in this section for another study, it is convenient first to solve the problem of the potential due to a point source of current near a spheroid of one resistivity embedded in an infinite medium of a second resistivity.

Let us consider first a point source of current at a point $C_0(\eta_0, \xi_0, 0)$ in an infinite medium near, and outside of, a prolate spheroid whose surface is described by $\eta = \eta_1$ (fig. 141A). The resistivity of the material within the spheroid is ρ'' and that of the material outside is ρ'. We require two forms for the potential function, one outside the spheroid and the second

inside; from equation 85, these are, respectively,

$$U_{1A} = \frac{I\rho'}{4\pi} \left\{ \frac{1}{R} + \sum_{n=0}^{\infty} \sum_{m=0}^{n} BQ_n{}^m(\eta) P_n{}^m(\xi) \cos m\phi \right\}$$

$$U_{2A} = \frac{I\rho''}{4\pi} \left\{ \frac{1}{R} + \sum_{n=0}^{\infty} \sum_{m=0}^{n} AP_n{}^m(\eta) P_n{}^m(\xi) \cos m\phi \right\}. \quad (207)$$

$P_n{}^m(\eta)$ has been excluded from U_{1A} because it becomes infinite for large η and $Q_n{}^m(\eta)$ is excluded from U_{2A} because it becomes infinite for $\eta = 1$. The subscript notation on U is the same as that used previously (fig. 141).

From the condition that the potential is continuous across the surface $\eta = \eta_1$, we get

$$BQ_n{}^m(\eta_1) = AP_n{}^m(\eta_1). \quad (208)$$

We now substitute for $1/R$ the expansion given in equation 123. We use the form applicable when

$\eta < \eta_0$ because $\eta_1 < \eta_0$. Then, from the condition that the normal component of the current density is continuous across the boundary $\eta = \eta_1$, we get

$$\rho'' B Q_n'^m(\eta_1) - \rho' A P_n'^m(\eta_1) = (\rho' - \rho'') \frac{(2-\delta_{0m})(2n+1)}{b(-1)^m}$$

$$\times \left[\frac{(n-m)!}{(n+m)!}\right]^2 P_n^m(\xi_0) Q_n^m(\eta_0) P_n'^m(\eta_1). \quad (209)$$

Solving equation 208 and 209 as a set of simultaneous equations for A and B, and substituting them into equations 207, we have for the potential functions:

$$U_{1A} = \frac{I\rho'}{4\pi} \left\{ \frac{1}{R} + \frac{(\rho''-\rho')}{b} \sum_{n=0}^{\infty} \sum_{m=0}^{n} \frac{(2n+1)(2-\delta_{0m})}{(-1)^m} \left[\frac{(n-m)!}{(n+m)!}\right]^2 \right.$$

$$\left. \times \frac{\psi_n^m(\eta_1) \psi_n'^m(\eta_1)}{\rho' \psi_n'^m(\eta_1) - \rho'' \psi_n^m(\eta_1)} P_n^m(\xi_0) P_n^m(\xi) Q_n^m(\eta_0) Q_n^m(\eta) \cos m\phi \right\}$$

$$U_{2A} = \frac{I\rho'}{4\pi} \left\{ \frac{1}{R} + \frac{(\rho''-\rho')}{b} \sum_{n=0}^{\infty} \sum_{m=0}^{n} \frac{(2n+1)(2-\delta_{0m})}{(-1)^m} \left[\frac{(n-m)!}{(n+m)!}\right]^2 \right.$$

$$\left. \times \frac{\psi_n'^m(\eta_1)}{\rho' \psi_n'^m(\eta_1) - \rho'' \psi_n^m(\eta_1)} P_n^m(\xi_0) P_n^m(\xi) Q_n^m(\eta_0) P_n^m(\eta) \cos m\phi \right\},$$

$$(210)$$

where

$$\psi_n^m(x) = P_n^m(x)/Q_n^m(x)$$

and

$$\psi_n'^m(x) = P_n'^m(x)/Q_n'^m(x). \quad (211)$$

The primes on $\psi_n^m(x)$, $P_n^m(x)$, and $Q_n^m(x)$ have the usual meaning of differentiation.

When the source is located inside the prolate spheroid of resistivity ρ'' (fig. 141B), the same method is applicable and the following are obtained for the potential functions

$$U_{1B} = \frac{I\rho''}{4\pi} \left\{ \frac{1}{R} + \frac{(\rho''-\rho')}{b} \sum_{n=0}^{\infty} \sum_{m=0}^{n} \frac{(2n+1)(2-\delta_{0m})}{(-1)^m} \left[\frac{(n-m)!}{(n+m)!}\right]^2 \right.$$

$$\left. \times \frac{\psi_n^m(\eta_1)}{\rho' \psi_n'^m(\eta_1) - \rho'' \psi_n^m(\eta_1)} P_n^m(\xi_0) P_n^m(\xi) P_n^m(\eta_0) Q_n^m(\eta) \cos m\phi \right\}$$

$$U_{2B} = \frac{I\rho''}{4\pi} \left\{ \frac{1}{R} + \frac{(\rho''-\rho')}{b} \sum_{n=0}^{\infty} \sum_{m=0}^{n} \frac{(2n+1)(2-\delta_{0m})}{(-1)^m} \left[\frac{(n-m)!}{(n+m)!}\right]^2 \right.$$

$$\left. \times \frac{P_n^m(\xi_0) P_n^m(\xi) P_n^m(\eta_0) P_n^m(\eta)}{\rho' \psi_n'^m(\eta_1) - \rho'' \psi_n^m(\eta_1)} \cos m\phi \right\}.$$

$$(212)$$

Whenever we apply these equations to surface-prospecting problems—that is, when the current electrode is on the surface of the earth, the factor $I/4\pi$ becomes $I/2\pi$. In order to apply these equations to a sink which is circular in plan view and whose semimajor axis is vertical, we choose the plane $\xi = 0$ as the earth's surface. Then $\xi_0 = 0$ and $P_n^m(\xi) = 1$ for all values of m and n. When we apply the equations to a sink which is elliptical in plan view and whose axis

of rotation is horizontal, we let the plane $\phi = 0$, π represent the earth's surface. In such equations, caution must be used in computing potentials for theoretical profiles because ϕ_0 is sometimes zero and sometimes π. Since our equations are set up on the hypothesis that $\phi_0 = 0$, it is sometimes necessary to substitute $\cos m(\phi_0 - \phi)$, or $\cos m(\pi - \phi) = (-1)^m \cos m\phi$, for $\cos m\phi$ in equations 210 and 212. If in the latter case, the point source lies on the polar axis, the equations take on a particularly simple form because the field becomes independent of ϕ, and m is always zero.

The development in oblate spheroidal coordinates follows the same line. However, we prefer to use the substitutions given in equation 89 to transform equations 210 and 212 into similar equations applicable to oblate spheroids. The substitution is straightforward and we obtain

$$U_{1A} = \frac{I\rho'}{4\pi} \left\{ \frac{1}{R} + \frac{i(\rho''-\rho')}{b} \sum_{n=0}^{\infty} \sum_{m=0}^{n} \frac{(2n+1)(2-\delta_{0m})}{(-1)^m} \right.$$

$$\left. \times \left[\frac{(n-m)!}{(n+m)!}\right]^2 \frac{\psi_n^m(i\zeta_1) \psi_n'^m(i\zeta_1)}{\rho' \psi_n'^m(i\zeta_1) - \rho'' \psi_n^m(i\zeta_1)} \right.$$

$$\left. \times P_n^m(\mu_0) P_n^m(\mu) Q_n^m(i\zeta_0) Q_n^m(i\zeta) \cos m\phi \right\}$$

$$U_{2A} = \frac{I\rho'}{4\pi} \left\{ \frac{1}{R} + \frac{i(\rho''-\rho')}{b} \sum_{n=0}^{\infty} \sum_{m=0}^{n} \frac{(2n+1)(2-\delta_{0m})}{(-1)^m} \right.$$

$$\left. \times \left[\frac{(n-m)!}{(n+m)!}\right]^2 \frac{\psi_n'^m(i\zeta_1)}{\rho' \psi_n'^m(i\zeta_1) - \rho'' \psi_n^m(i\zeta_1)} \right.$$

$$\left. \times P_n^m(\mu_0) P_n^m(\mu) Q_n^m(i\zeta_0) P(i\zeta) \cos m\phi \right\}$$

$$U_{1B} = \frac{I\rho''}{4\pi} \left\{ \frac{1}{R} + \frac{i(\rho''-\rho')}{b} \sum_{n=0}^{\infty} \sum_{m=0}^{n} \frac{(2n+1)(2-\delta_{0m})}{(-1)^m} \right.$$

$$\left. \times \left[\frac{(n-m)!}{(n+m)!}\right]^2 \frac{\psi_n^m(i\zeta_1)}{\rho' \psi_n'^m(i\zeta_1) - \rho'' \psi_n^m(i\zeta_1)} \right.$$

$$\left. \times P_n^m(\mu_0) P_n^m(\mu) P_n^m(i\zeta_0) Q_n^m(i\zeta) \cos m\phi \right\}$$

$$U_{2B} = \frac{I\rho''}{4\pi} \left\{ \frac{1}{R} + \frac{i(\rho''-\rho')}{b} \sum_{n=0}^{\infty} \sum_{m=0}^{n} \frac{(2n+1)(2-\delta_{0m})}{(-1)^m} \right.$$

$$\left. \times \left[\frac{(n-m)!}{(n+m)!}\right]^2 \frac{1}{\rho' \psi_n'^m(i\zeta_1) - \rho'' \psi_n^m(i\zeta_1)} \right.$$

$$\left. \times P_n^m(\mu_0) P_n^m(\mu) P_n^m(i\zeta_0) P_n^m(i\zeta) \cos m\phi \right\}. \quad (213)$$

We can obtain the appropriate equations for a hemispherical sink in one of two ways. The most obvious and easiest way is to apply the above technique to the solution of Laplace's equation in spherical coordinates (equation 58). The second way is to examine equations 210 and 212 in the limit as $b \rightarrow 0$, because in that limit the spheroids become spheres. We recall that $\lim_{b \to 0} \xi = \cos \theta$ and $\lim_{b \to 0} \eta = r/b$. We combine with these limits the asymptotic forms of the Legendre functions given in equation 120. The limits of the potential
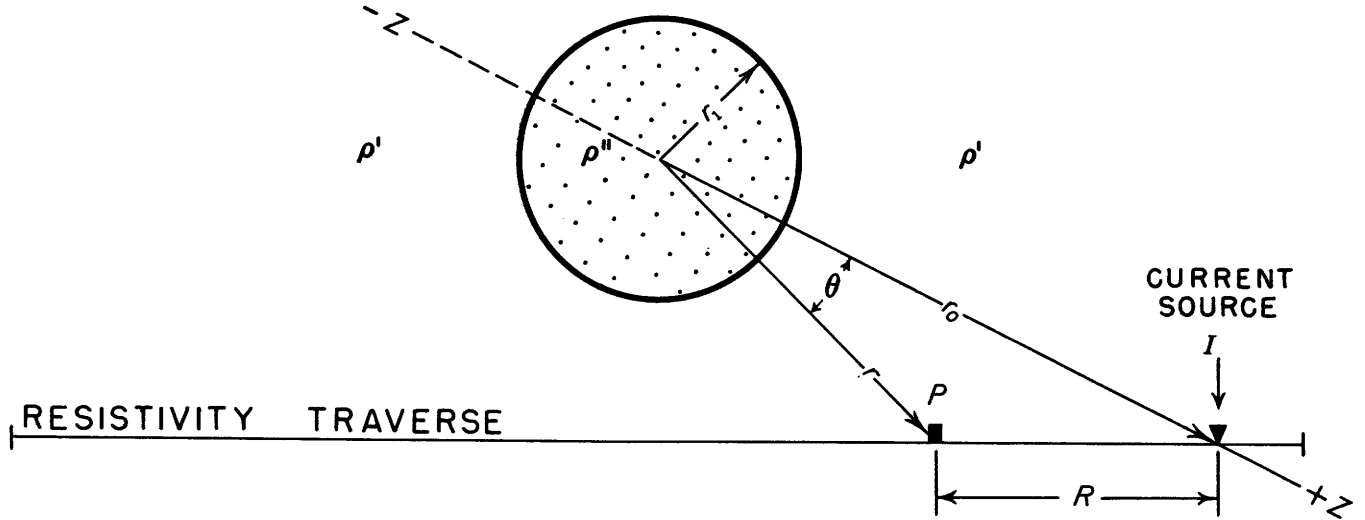
FIGURE 142.—Plan view of hemispherical sink showing relationship with an arbitrary-resistivity traverse. The plane of this figure corresponds to zz-plane in figure 24. Adapted from Cook and Van Nostrand (1954).

functions of equations 210 and 212, as b approaches zero, are then the appropriate forms for the sphere. Either by direct solutions of Laplace's equation or by the limiting process described, we find the potential functions to be as given below, when the source lies on the polar axis as shown in figure 142.

$$U_{1A} = \frac{I\rho'}{4\pi}\left\{\frac{1}{R} + k\sum_{n=0}^{\infty}\frac{2nr_1^{2n+1}}{(2n+1+k)(r_0r)^{n+1}}\,P_n\,(\cos\,\theta)\right\}$$

$$U_{2A} = \frac{I\rho'}{4\pi}\left\{\frac{1+k}{r_0}\sum_{n=0}^{\infty}\frac{(2n+1)}{(2n+1+k)}\left(\frac{r}{r_0}\right)^n P_n\,(\cos\,\theta)\right\}$$

$$U_{1B} = \frac{I\rho''}{4\pi}\left\{\frac{1-k}{r}\sum_{n=0}^{\infty}\frac{(2n+1)}{(2n+1+k)}\left(\frac{r_0}{r}\right)^n P_n\,(\cos\,\theta)\right\}$$

$$U_{2B} = \frac{I\rho''}{4\pi}\left\{\frac{1}{R} - 2k\sum_{n=0}^{\infty}\frac{(n+1)(r_0r)^n}{(2n+1+k)r_1^{2n+1}}\,P_n\,(\cos\,\theta)\right\}.\quad(214)$$

As in the previous cases, if the hemisphere is embedded in the surface of a semi-infinite space and the current electrodes are on the surface of the ground, the factor 4π becomes 2π. This is true for a hemispherical sink, such as those shown in figures 141C and 142. The line joining the current electrode I and the center of the hemispherical sink (fig. 142) is taken as the polar axis, which consequently rotates as the current electrode moves along the traverse. r and r_0 are the distances from the center of the hemisphere to the potential electrode and current electrode, respectively; r_1 is the radius of the hemisphere; θ is the angle subtended at the origin by the line drawn between the current and potential electrodes; and P_n ($\cos\,\theta$) is the Legendre polynomial. All other symbols are identical with those defined above for spheroids.

If we let $\rho''=0$, the solutions in equation 214 are identical to the solutions obtained by the theory of images. Let us consider the expression for U_{2A} only. When $\rho''=0$, then $k=-1$; and the expression for U_{2A}, when considered in the compact form shown, appears to vanish, because of the factor $(1+k)$, which is multiplied by the summation. If we consider the series term by term, however, we see that the zeroth term is $I\rho'/2\pi r_0$; and, since it does not contain k, it is not affected by letting $\rho''=0$. All the remaining terms do vanish; and, therefore, the potential of a perfectly conducting hemispherical sink is $I\rho'/2\pi r_0$, which is the same result as that obtained previously from the theory of images. The same remarks apply to U_{1A} although the limiting process is somewhat more complicated. Summations should be considered term by term whenever a limiting case is being examined.

As r approaches r_0 in magnitude, equations 214 become increasingly unwieldy to use for computations. As an example of how the exact value of the potential in a limiting case may be used to guide the computer, let us consider U_{2A} for a sink of such high resistivity that we can suppose $k=1$. By performing one step of division we find that the quotient is merely the expansion of the reciprocal distance (equation 103) plus a remainder, so that we have

$$U_{2A} = \frac{I\rho'}{2\pi}\left\{\frac{2}{R} - \frac{1}{r_0}\sum_{n=0}^{\infty}\frac{1}{n+1}\left(\frac{r}{r_0}\right)^n P_n\,(\cos\,\theta)\right\},$$

where the factor 4π has been changed to 2π to reflect the fact that we are now considering a hemispherical sink and not a sphere. For a traverse passing through the center of the sink, a current electrode and a potential electrode may simultaneously fall at diametrically

opposing points on the edge of the sink. The $r=r_0$, $\theta=\pi$, $P_n (\cos \theta)=(-1)^n$, and

$$U_{2A}=\frac{I\rho'}{2\pi}\left\{\frac{2}{R}-\frac{1}{r_0}\sum_{n=0}^{\infty}\frac{(-1)^n}{n+1}\right\}.$$

The summation is the Maclaurin expansion of ln 2. Therefore,

$$U_{2A}=\frac{I\rho'}{2\pi}\left\{\frac{2}{R}-\frac{1}{r_0}\ln 2\right\}=\frac{I\rho'}{2\pi r_0}\left\{1-\ln 2\right\},$$

where R, being the distance between the electrodes, is also the diameter of the sink. Likewise r_0 is the radius of the sink.

Whereas the points for which r is close to r_0 in magnitude are difficult to compute because of poor convergence, we now have the limiting value of U_{2A} in a closed form. Thus, we are no longer obliged to calculate data for points for which r approaches r_0 very closely. Other similar computational aids can be devised.

FILLED CHANNELS

We restrict ourselves first to channels that can be approximated by semicircular cylinders. For this purpose we require solutions of Laplace's equation given by equation 76 and an expansion of the reciprocal distance given by equation 111.

Let us consider a point source of current located in an infinite medium, whose resistivity is ρ', near a cylinder of a second material with a different resistivity ρ''. The axis of the cylinder coincides with the axis of cylindrical coordinates, and the surface of the cylinder is described as $r=r_1$. The origin is chosen such that $\phi_0=0$ and $z_0=0$. In the region outside the cylinder, we can discard $I_m(tr)$ from the general solution because it becomes infinite as r approaches infinity. Inside the cylinder, we eliminate $K_m(tr)$ because it becomes infinite on the cylindrical axis. Therefore, the two potential functions outside and inside the cylinder have the forms, respectively,

$$U_{1A}=\frac{I\rho'}{4\pi}\left\{\frac{1}{R}+\sum_{m=0}^{\infty}\cos m\phi\int_0^{\infty}A_mK_m(tr)\cos tz\,dt\right\}$$

$$U_{2A}=\frac{I\rho'}{4\pi}\left\{\frac{1}{R}+\sum_{m=0}^{\infty}\cos m\phi\int_0^{\infty}B_mI_m(tr)\cos tz\,dt\right\}. \quad (215)$$

From the conditions that the potential and the normal component of the current density must be continuous across the surface $r=r_1$, we obtain the following equations:

$$B_m=A_m\psi_m(tr_1)$$

$$\frac{\rho''}{\rho'}A_m\psi_m'(tr_1)-B_m=\frac{2}{\pi}\left(1-\frac{\rho''}{\rho'}\right)(2-\delta_{0m})K_m(tr_0)$$

where

$$\psi_m(tr)=\frac{K_m(tr)}{I_m(tr)}$$

and

$$\psi_m'(tr)=\frac{\partial K_m(tr)}{\partial r}\bigg/\frac{\partial I_m(tr)}{\partial r}.$$

From these equations, we are able to calculate the arbitrary functions A_m and B_m. Substituting the results into equations 215, we obtain for the potential functions:

$$U_{1A}=\frac{I\rho'}{4\pi}\left\{\frac{1}{R}-\frac{2}{\pi}(\rho''-\rho')\sum_{m=0}^{\infty}(2-\delta_{0m})\cos m\phi\right.$$

$$\left.\times\int_0^{\infty}\frac{K_m(tr_0)K_m(tr)\cos tz}{\rho''\psi_m'(tr_1)-\rho'\psi(tr_1)}dt\right\}$$

$$U_{2A}=\frac{I\rho'}{4\pi}\left\{\frac{1}{R}-\frac{2}{\pi}(\rho''-\rho')\sum_{m=0}^{\infty}(2-\delta_{0m})\cos m\phi\right.$$

$$\left.\times\int_0^{\infty}\frac{K_m(tr_0)\psi_m(tr_1)I_m(tr)}{\rho''\psi_m'(tr_1)-\rho'\psi(tr_1)}\cos tz\,dt\right\}. \quad (216)$$

In similar fashion, we can obtain the following potential functions when the source is located within the cylinder:

$$U_{2B}=\frac{I\rho''}{4\pi}\left\{\frac{1}{R}-\frac{2}{\pi}(\rho''-\rho')\sum_{m=0}^{\infty}(2-\delta_{0m})\cos m\phi\right.$$

$$\left.\times\int_0^{\infty}\frac{I_m(tr_0)\psi_m'(tr_1)\psi_m(tr_1)I_m(tr)}{\rho''\psi_m'(tr_1)-\rho'\psi(tr_1)}\cos tz\,dt\right\}$$

$$U_{1B}=\frac{I\rho''}{4\pi}\left\{\frac{1}{R}-\frac{2}{\pi}(\rho''-\rho')\sum_{m=0}^{\infty}(2-\delta_{0m})\cos m\phi\right.$$

$$\left.\times\int_0^{\infty}\frac{I_m(tr_0)\psi_m'(tr_1)K_m(tr)}{\rho''\psi_m'(tr_1)-\rho'\psi(tr_1)}\cos tz\,dt\right\}. \quad (217)$$

If these functions are to be used for a semicircular channel, we let the plane $\phi=0$, π represent the surface of the earth and simply change the factor 4π to 2π in the expressions.

Similar solutions for channels approximated by parabolic or ellipsoidal cross sections can be obtained with appropriate types of cylindrical coordinate systems.

OPEN PITS AND DITCHES

It is sometimes desirable to know the effect on the electrical survey of a nearby open pit or some similar natural feature. The mathematical tools necessary for such a study are contained in the previous two sections. The equations applicable to oblate spheroidal boundaries are used to obtain the effects of shallow depressions; the equations applicable to prolate spheroidal boundaries are used for deep depressions; and the limiting forms for hemispherical boundaries are useful for hemispherical depressions.

Let us consider first the effect of an open pit that may be assumed hemispherical. To ascertain how the pit affects the potential measurements, the potential values along theoretical profiles at various distances from the pit must be determined. Since it is assumed that none of the electrodes enters the pit, only an expression for U_{1A} is needed. The desired expression is obtained from the first of equations 214 when we change 4π to 2π, let $k=1$, and make ρ' equal to the uniform resistivity ρ of the country rock. That equation now becomes

$$U = \frac{I\rho}{2\pi}\left\{\frac{1}{R} + \frac{r_1}{r_0 r}\sum_{n=0}^{\infty}\left(1 - \frac{1}{n+1}\right)\frac{r_1^{2n}}{r_0^n r^n}P_n(\cos\theta)\right\}. \quad (218)$$

A comparison of this equation with equation 103 reveals that the part involving only the "1" in parentheses leads to the existence of an image of strength $(r_1/r_0)I$ located at a distance of r_1^2/r_0 from the origin along a line connecting the origin and the point source of current. This is analogous to the image formed in a sink filled with a perfectly conducting material. However, in the present case, there remains a correction term to the "image solution." Thus, equation 218 becomes

$$U = \frac{I\rho}{2\pi}\left\{\frac{1}{R} + \frac{r_1}{r_0\sqrt{(r_1^2/r_0)^2 + r^2 - 2(r_1^2/r_0)r\cos\theta}}\right.$$

$$\left. - \frac{r_1}{r_0 r}\sum_{n=0}^{\infty}\frac{r_1^{2n}}{(n+1)(r_0 r)^n}P_n(\cos\theta)\right\}. \quad (219)$$

Although it appears simpler to compute the desired potentials from equation 218 rather than from equation 219, the series in the second equation generally converges more rapidly so that fewer terms need to be considered when equation 219 is used.

For a prolate spheroidal depression, the first of equations 210 can be similarly adapted to obtain

$$U = \frac{I\rho}{2\pi}\left\{\frac{1}{R} - \frac{1}{b}\sum_{n=0}^{\infty}\sum_{m=0}^{\infty}\frac{(2n+1)(2-\delta_{0m})}{(-1)^m}\left[\frac{(n-m)!}{(n+m)!}\right]^2\right.$$

$$\left. \times \psi_n'^m(\eta_1)P_n^m(\xi_0)P_n^m(\xi)Q_n^m(\eta_0)Q_n^m(\eta)\cos m\phi\right\}. \quad (220)$$

For an oblate spheroidal depression, a similar equation can be obtained from the first of equations 213. Also the corresponding equations for semicircular ditches can be obtained by treating equation 216 in the same way.

HORIZONTAL PROFILES OVER HEMISPHERICAL SINKS

THEORETICAL AND OBSERVED CURVES

Theoretical horizontal profiles over a filled hemispherical sink for the Lee configuration are shown in figure 143. The electrode separation, a, is taken as half the radius

of the hemisphere, and the resistivity of the material in the sink is one-fifth the resistivity of the surrounding medium. To facilitate the use of the charts for general values of resistivity, subject only to the constant resistivity contrast of 1 to 5, the resistivity values are plotted as ordinates in terms of the ratio of the apparent resistivity to the true resistivity of the medium outside the sink. Because it is convenient to use dimensionless quantities, distances along the traverses are plotted in terms of the electrode separation a and in accordance with the convention of fig. 143G.

For traverse 1 (fig. 143A), which is taken over the center of the sink, each of the apparent-resistivity curves along the horizontal profile displays eight separate discontinuities in slope. Each discontinuity correlates exactly with a position at which either a current electrode or a potential electrode crosses the boundary of the sink. Two maxima and two minima lying on either side of the sink are important features that characterize the horizontal traverse over the filled sink. On the left side of the sink the pronounced peak A and the accompanying lesser peak A' lying directly below it (fig. 143A) lie at a distance of $a/4$ outside of the boundary of the sink. Peak A occurs as the potential electrode P_0 crosses the left edge of the sink and peak A' occurs as the potential electrode P_1 crosses the same edge of the sink. These two maxima, together with their maxima counterparts B and B' on the right side of the sink, greatly facilitate the interpretation of the location of the edges of the filled sink. The minimum at C lies at a distance of $7a/4$ to the left of the boundary, and the minimum at C' lies at a distance of $5a/4$ to the left of the boundary. Thus, the two minima C and C', which occur as the current electrode C_1 crosses the left edge of the sink, are separated by a distance of $a/2$. A corresponding relationship exists between the two minima D and D' lying on the east edge of the sink.

On traverse 1 (fig. 143A), the distance between peaks A and B, or between peaks A' and B', is equal to the sum of the diameter of the sink plus half the electrode separation a.

The deep-resistivity trough that lies over the central part of the sink is a very diagnostic feature. Here the apparent-resistivity values decrease to minima at E and E' (fig. 143A). The gradient of the curve is steep, the total change from the peak at A to the minimum at F occurring over a horizontal distance of half the electrode separation a. At the geometric center of the sink, the ρ_1/ρ' and ρ_2/ρ' curves cross each other symmetrically, and the point of symmetrical crossing is an important interpretative feature except in those cases where field "noise" limits or vitiates its usefulness.
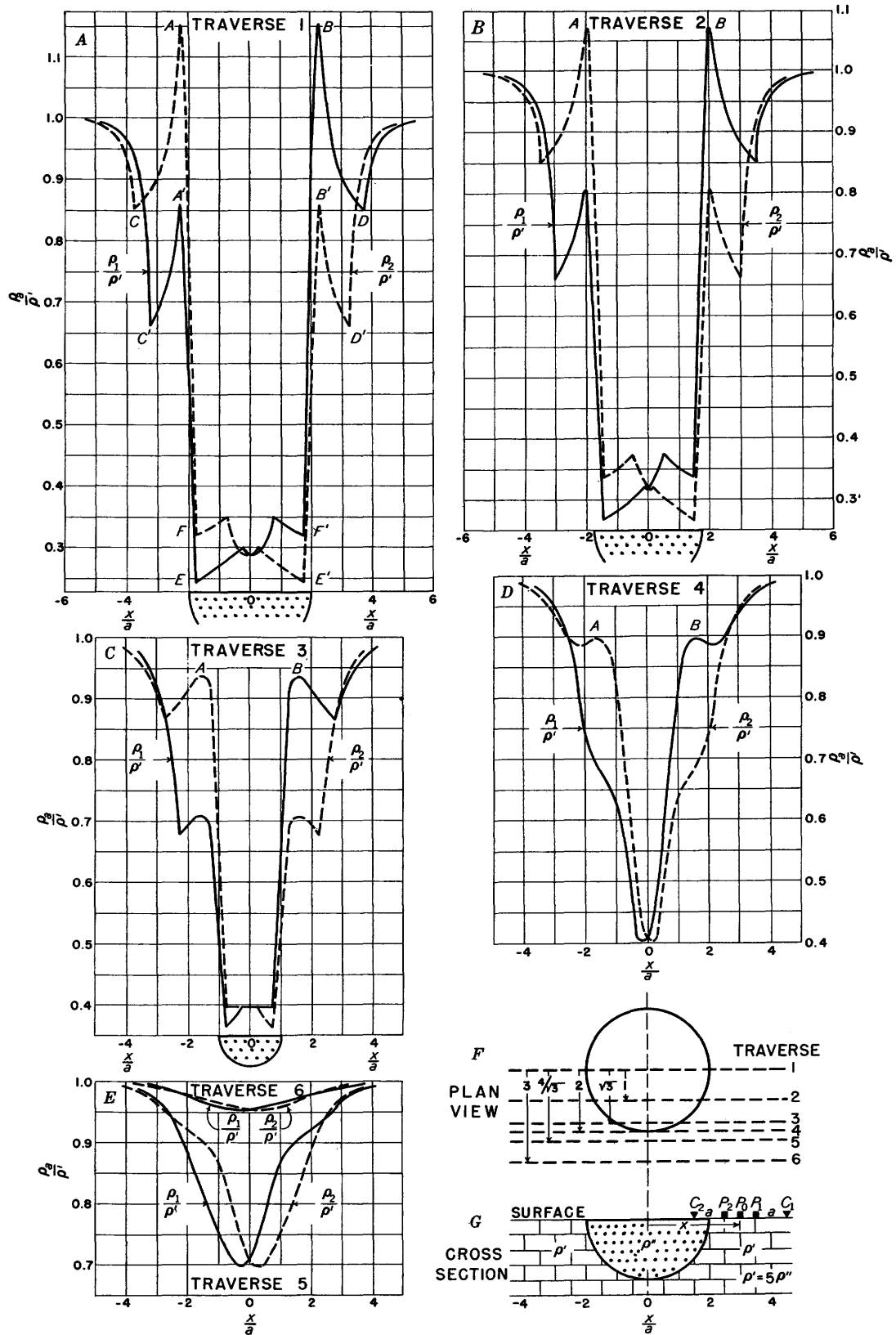
FIGURE 143.—Theoretical horizontal resistivity profiles over hemispherical sink at different distances from center of sink, Lee configuration (offset plotting). Cross sections taken along resistivity traverses. Diameter of hemisphere=4a (each sink size is the same). $\rho''/\rho' = 1/5$. Adapted from Cook and Van Nostrand (1954).

Contrasting features exist between horizontal traverses that cross the sink at different distances from the center. Except for traverse 1, which crosses the center of the sink, the peaks at A and B (fig. 143B–D) display no discontinuity in slope. These peaks persist as maxima through traverse 4 (tangent), and influence the shape of the curves even beyond, actually disappearing only as the anomaly itself becomes very small. Successive traverses at increasing distances from the center of the sink indicate that the distance between peaks A and B diminishes as one goes farther from the center. Minima comparable to those at C, C', D, and D' (fig. 143A) exist for other traverses that cross the sink (fig. 143B, C) but disappear for traverses lying outside of the sink.

In analysis of the theoretical resistivity data for the Lee configuration, the anomaly index as used by us is defined as the maximum value of ρ_1/ρ' minus the minimum value of ρ_1/ρ'. For the Lee. field data, the anomaly index is the ratio:

$$(\rho_{1\,max} - \rho_{1\,min})/\rho_1 \text{ regional.}$$

Similar indices apply to the values of ρ_2. Also similar indices apply for the Wenner configuration by replacing, in the definition, ρ_1/ρ' by ρ_a/ρ' or ρ_1 by ρ_a for theoretical or field data, respectively.

This index number is comparable in some respects to indices already suggested by Lee and Hemberger (1946) and Guyod (1945) for resistivity anomalies. It is to be understood that the "maximum value" as used may sometimes be the regional value itself as, for example, when the value of the peak at A (fig. 143C) falls below the regional value.

The anomaly index is introduced in order to facilitate comparison of curves. In general, the configuration and the traverses chosen in an actual survey will be such that the index will probably be a maximum.

For traverse 1 (fig. 143A) the anomaly index, which is the same for both ρ_1 and ρ_2, is equal to $1.15 - 0.24 = 0.91$. The anomaly indices for all traverses across the hemisphere in figure 143 are given in table 4.

Theoretical horizontal profiles over a filled hemispherical sink for the Wenner configuration are shown in figure 144. The electrode separation a, locations of the traverses, dimensions of the sink, and resistivity contrast are all the same as in the example discussed above in which the Lee configuration was used. For the Wenner data, the apparent resistivities are plotted against the station at which they are determined, that is, at the center of the Wenner configuration used to obtain each data point.

Although the general features of the peaks and troughs in the curves for the Wenner configuration are similar to those for the Lee configuration, important

specific differences exist. For traverse 1 (fig. 144), each peak, A or B, for the Wenner configuration lies at a distance of $a/2$, rather than $a/4$, outside of the boundary of the sink; and the distance between the peaks is equal to the sum of the diameter of the sink plus the whole electrode separation a, rather than half the electrode separation as for the Lee configuration.

The gradient of the curve at the edge of the resistivity trough is less steep for the Wenner configuration than for the Lee configuration, the total change from the peak at A to the minimum at E (fig. 144A) occurring over a horizontal distance equal to the electrode separation a, rather than $a/2$ as for the Lee configuration.

The magnitude of the features for the Wenner configuration is damped in comparison with the Lee configuration. In contrast with the apparent resistivity as measured by the Lee configuration in this particular example, none of the apparent-resistivity values measured by the Wenner configuration rises above the value of the highest true resistivity represented. In a few exceptional cases the Wenner resistivity does rise slightly above the highest true resistivity. Consequently the anomaly index for the Wenner configuration is less than that for the Lee configuration. (See table 4.) This fact is made clearer in the last column in table 4, which gives the ratios of the anomaly indices for the Lee configuration to those for the Wenner configuration. Apparently the ratio is always greater than one.

TABLE 4.—*Comparison of anomaly indices for Lee and Wenner configurations for horizontal profiles over hemispherical sink*

[Data from Cook and Van Nostrand (1954)]

Traverse	Lee	Wenner	Ratio (Lee/ Wenner)
1	0.912	0.712	1.28
2	.792	.692	1.14
3	.637	.605	1.05
4	.597	.546	1.09
5	.306	.261	1.17
6	.048	.044	1.10

Theoretical curves for sinks and channels that are of higher resistivity than the surrounding country rock show characteristics that are analogous to those given here for sinks of low resistivity. In general, apparent-resistivity highs would be obtained where we here obtain apparent-resistivity lows. Abrupt discontinuities in slope would be obtained as certain electrodes cross the contacts; and, as for sinks of low resistivity, the discontinuities in slope can be used to delineate the limits of a sink of high resistivity. These statements apply for both horizontal and vertical resistivity profiles.

In figure 145, a typical field horizontal profile obtained with the Lee configuration over a known shale sink
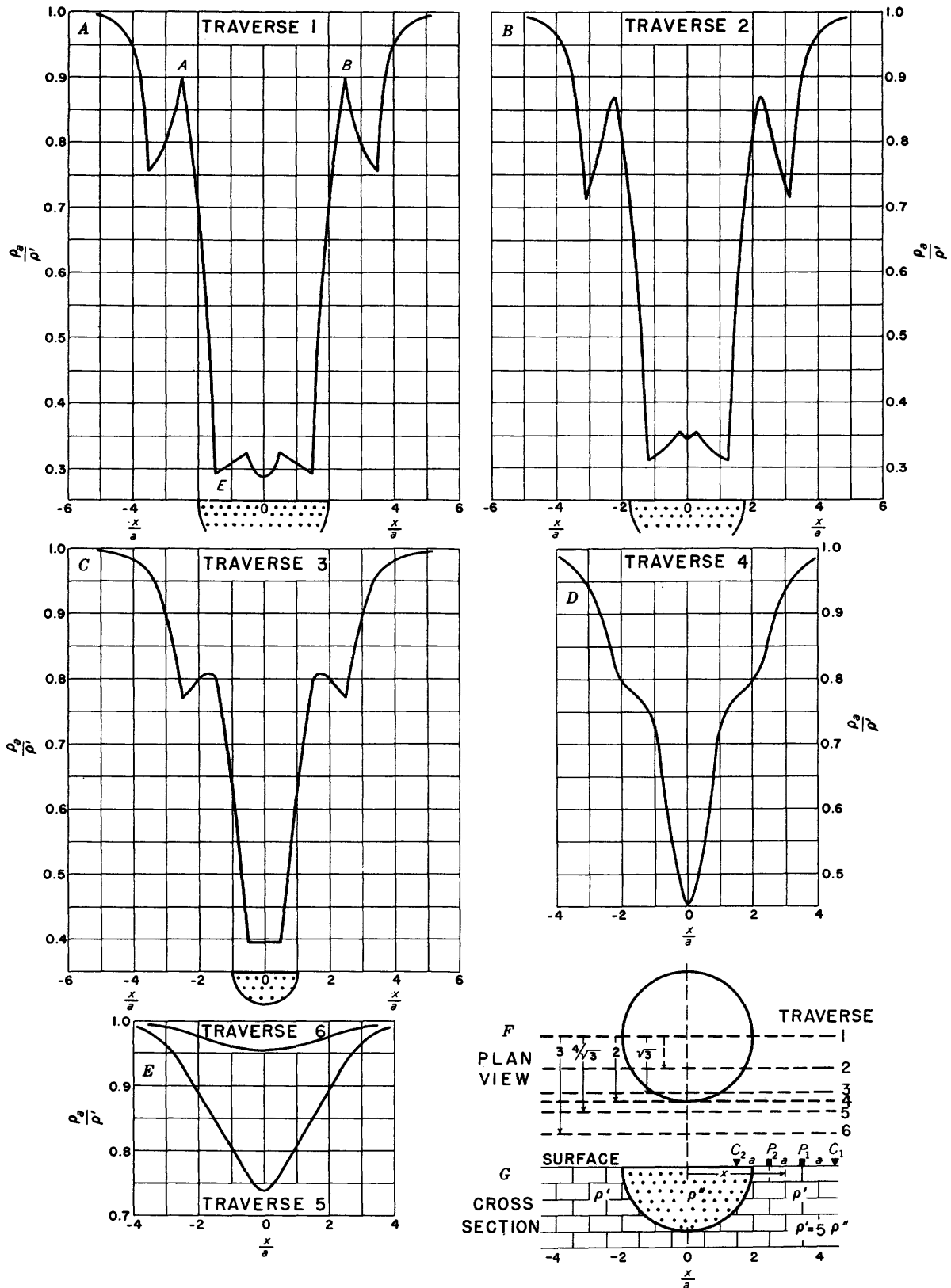
Figure 144.—Theoretical horizontal resistivity profiles over hemispherical sink at different distances from center of sink, Wenner configuration. Cross sections taken along resistivity traverses. Diameter of hemisphere=4a (sink sizes are the same). $\rho''/\rho'=1/5$. Adapted from Cook and Van Nostrand (1954).
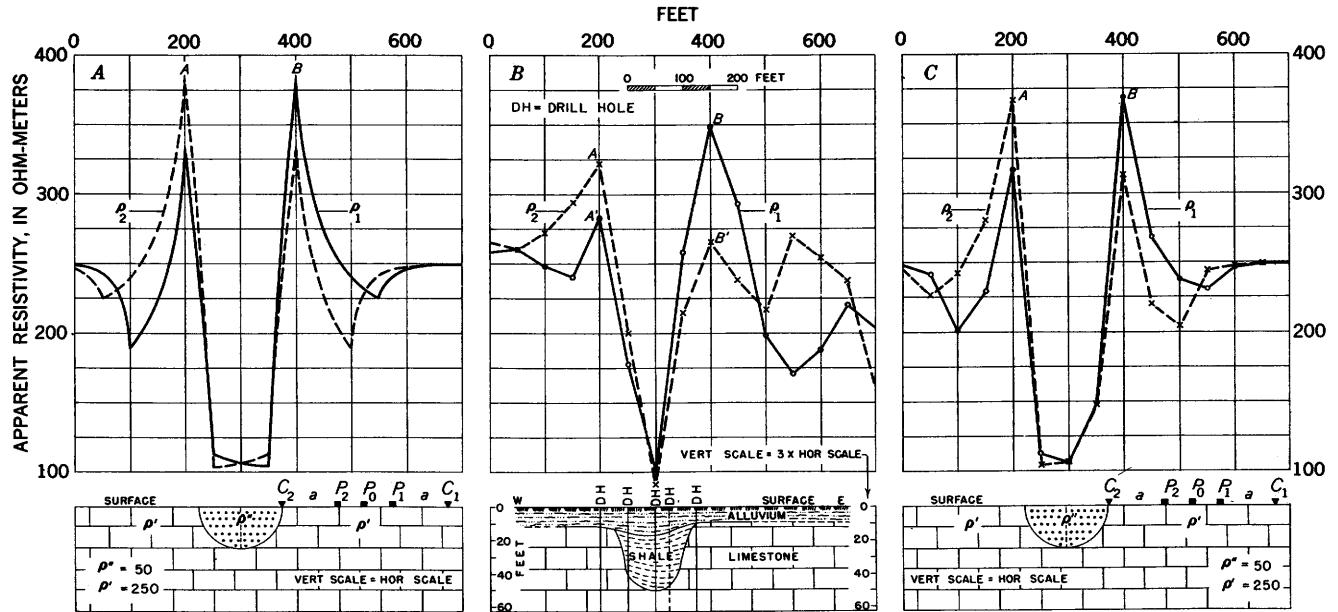
FIGURE 145.—Comparison of theoretical and observed horizontal resistivity profiles over filled sink, Lee configuration (offset plotting). (A) Continuous theoretical curve over hemispherical sink. (B) Observed field curve with geologic cross section. (C) Theoretical field plot over hemispherical sink. Assumed diameter of sink = 3a/2. Assumed $\rho''/\rho' = 50/250$. Adapted from Cook and Van Nostrand (1954).

in Cherokee County, Kans., is compared with two theoretical horizontal profiles over a hemispherical sink. The electrode separation a is 100 feet, and the spacing between successive stations is 50 feet. In all the diagrams, the offset method of plotting is used and the corresponding scales for resistivity and for horizontal distance are used. In order to show the geologic details better, the vertical scale in the geologic cross section in figure 145B is made three times the horizontal scale; in the geologic cross section in figures 145A, C, the horizontal and vertical scales are equal. Except for the easternmost part of the ρ_2 curve, the field horizontal profile shown in figure 145B is typical of that for a filled sink.

It is shown above (fig. 143A) that, for a continuous theoretical curve for a horizontal profile crossing the center of the hemispherical sink, the west margin of the sink lies at a distance of $a/4$, or 25 feet in this case, east of peak A and similarly that the east margin lies 25 feet west of peak B. The peaks A and B on the field horizontal profile (fig. 145B) lie 200 feet apart. Therefore, a filled sink with a diameter of 150 feet is postulated, with certain reservations that are discussed below.

Measurements made in adjacent areas, where excellent geologic control is available, indicate that a resistivity contrast of about 1 to 5 exists between the shale and limestone; and a similar ratio is therefore assumed in computing the theoretical curves of figure 145.

Figure 145A shows a continuous theoretical curve for a filled hemispherical sink with an assumed diameter of 150 feet and a ratio of the resistivity of the material inside the sink to that of the material outside the sink taken as 1 to 5, respectively. The theoretical profile crosses the center of the sink. A proportionality factor of 50 ohm-meters is introduced in order to make the theoretical resistivity values comparable in magnitude to the observed field resistivity values, that is, so that $\rho''/\rho' = 50/250$.

A theoretical field plot, or field plot of the theoretical data, is shown in figure 145C. By definition, the theoretical field plot is obtained from the continuous theoretical curve (fig. 145A) by taking discrete points from the continuous curve and connecting them with straight lines. The spacing of the discrete points is made to conform to the station interval along the horizontal resistivity traverse in the field. In the present example the interval is $a/2$. In order to obtain the closest correspondence between the theoretical field plot and the actual field curve, a template with vertical slits, separated by a scale distance equal to $a/2$ and representing the plotted positions of ρ_1 and ρ_2, is moved along the continuous theoretical profile. In the present example the closest correspondence between the theoretical field plot and actual field plot is obtained in this manner when the plotted points on the theoretical field plot (fig. 145C) lie 5 feet to the east of the center of the continuous theoretical curve (fig. 145A). Greater shifts of the configuration in either direction

FEET
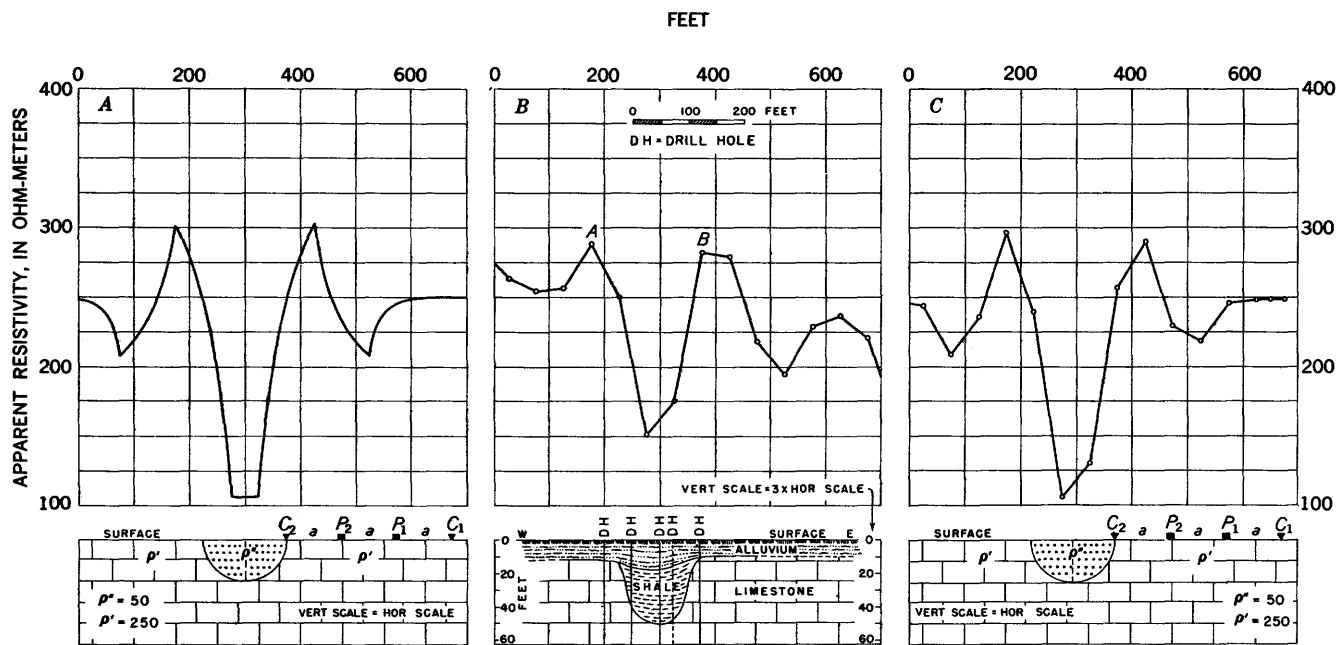
FIGURE 146.—Comparison of theoretical and observed horizontal resistivity profiles over filled sink, Wenner configuration. (*A*) Continuous theoretical curve over hemispherical sink. (*B*) Observed field curve with geologic cross section. (*C*) Theoretical field plot over hemispherical sink. Assumed diameter of sink=3a/2. Assumed $\rho''/\rho'=50/250$. Adapted from Cook and Van Nostrand (1954).

from that chosen in figure 145*C* result in theoretical field plots that depart to a greater degree from the observed field profile shown in figure 145*B*. For this reason, the center of the hemisphere in figure 145*C* is shifted 5 feet to the west of the point midway between peaks *A* and *B*.

It should be emphasized that any theoretical field plot derived from the continuous theoretical curve in figure 145*A* exhibits sharp peaks, corresponding to peaks *A* and *B* (fig. 145*C*), which lie exactly 200 feet apart. Moreover, for any Lee configuration traverse crossing the center of a hemispherical sink whose diameter is an integral multiple of a/2, the distance between the highest peaks on the theoretical field plot (offset plotting) is equal to the diameter of the sink plus half the electrode separation a. The same rule would apply for all sinks if the points on the field curve were infinitesimally close together. However, for any sink of diameter differing from an integral multiple of a/2, the distance between the peaks will vary according to the station interval taken and the locations of the stations in relation to each edge of the sink. Because the ambiguity as to the exact location of the margins of the sink lying between the peaks is related to the spacing of the resistivity stations, the precision of location of the margins of the sink can be increased by taking the stations closer together in the critical regions. Because the results of the horizontal-profile method are very sensitive to the location of the

edges of the sink, the additional information obtained by smaller spacing of the stations is often worth the extra time and trouble.

When the usual irregularities of the field data are discounted, the correlation of the theoretical (fig. 145*C*) and the field (fig. 145*B*) curves is considered to be excellent. The theoretical considerations and interpretative rules outlined above greatly facilitate the testing of shale sinks to obtain a maximum amount of information with a minimum amount of drilling.

In figure 146 the field horizontal profile that would be obtained with the Wenner configuration over the same known shale sink is compared with two theoretical horizontal profiles over a hemispherical sink as before. The Wenner apparent-resistivity values are plotted in the usual maner at the station occupying the midpoint between P_1 and P_2. Although the spacing between successive stations for horizontal profiles with the Wenner configurations is often taken as the whole electrode separation a, the spacing is taken as a/2 in the present example so that a fair comparison can be made between the Lee and Wenner configurations.

In the field example just given, the size of the peaks and the troughs is less pronounced for the Wenner configuration than for the Lee configuration. The anomaly indices, given in table 5, indicate the differences quantitatively. It should be emphasized that, for either the Lee or Wenner configuration, the anomaly indices of both the theoretical field plot and also the actual

Table 5.—*Comparison of anomaly indices for Lee and Wenner configurations over filled sink*

[Theoretical continuous curve and theoretical field plot for hemisphere compared with actual field curve. Assumed regional value of apparent resistivity equals 250 ohm-meters. Data from Cook and Van Nostrand (1954).]

Curve	Lee configuration			Wenner configuration			Ratio, Lee/Wenner		
	p_1	p_2	Average	West peak	East peak	Average	p_1 Wenner west peak	p_2 Wenner east peak	Average
Theoretical continuous curve	1.13	1.13	1.13	0.79	0.79	0.79	1.44	1.44	1.44
Theoretical field plot	1.05	1.05	1.05	.76	.74	.75	1.37	1.43	1.40
Actual field curve	.99	.92	.96	.55	.52	.54	1.80	1.77	1.79

field curve are dependent partly on the locations of the stations in relation to the locations of the edges of the sink. For this reason, the east and west values of the anomaly index are generally unequal.

Because of the modification of peak B in the field curve, it is difficult to assign a value for the probable width of the sink from the Wenner curve alone. Thus an inherent weakness in the Wenner configuration, as used for making width determinations, arises from the possibility that one (or both) of the two peaks may be indefinite, in which case the width cannot be determined accurately. The analysis indicates further that if the Wenner method is used, a spacing of $a/2$ or less between successive stations is desirable for even approximately outlining a sink, rather than a spacing of a. With the Lee configuration, on the other hand, even though one of the two major peaks A and B (fig. 145B) were indefinite, there is still a high probability that the subsidiary peaks A' and B' would be sufficiently pronounced to aid in the interpretation of both the width of the sink and the location of the margins of the sink.

The additional resolving power of the Lee configuration in comparison with the Wenner configuration indicates that for the same number of stations taken along the same horizontal profile, the Lee method can give more detailed information than the Wenner method. Moreover, in certain areas—especially where the sinks are small—this additional information will lead the interpreter to recognize sink features on the Lee profiles that are not recognizable on the Wenner profiles.

Although the mantle of soil and alluvium tempers the resistivity anomalies to some degree, the peaks discussed above are still very pronounced in the observed field curves, especially for the Lee configuration. In the cross sections shown in figures 145B and 146B, the thickness of the alluvium averages about 12 feet and apparently attains a maximum thickness of about 17 feet directly over the sink.

Figure 58 shows horizontal profiles across two shale sinks with the Lee configuration. The observed profiles are somewhat similar to the theoretical profiles, although the silicified limestone complicates somewhat the character of the curves.

Figure 147 shows an observed horizontal resistivity profile with the Lee configuration across two separate shale sinks in the Tri-State lead-zinc mining district, Cherokee County, Kans. The electrode separation is 100 feet, and the station interval is 50 feet. The anomalies are similar to the theoretical curves in figure 143. Pronounced apparent-resistivity lows occur over the shale; and recognizable peaks with apparent-resistivity values that are higher than those of the limestone country rock occur on either side of each shale sink.

Examples of horizontal resistivity profiles with the Wenner configuration over filled sinks and channels associated with karst topography in Hardin County, Ill., and in the area of Chapayevka village, Saratov district, U.S.S.R., are shown in figures 148 and 149, respectively. In figure 148, low apparent-resistivity values are obtained over the clay; whereas high apparent-resistivity values are obtained over the pinnacles and isolated masses of undissolved limestone; apparent-resistivity highs are obtained also over the sinkholes caverns that contain open air spaces of infinite resistivity (Hubbert, 1944). This example demonstrates that a reconnaissance profile can be used to indicate the presence of the sinks and channels. An accurate delineation of them can then be obtained by using a smaller station interval and electrode separation and referring to curves of the type shown in figure 144. In figure 149 a pronounced apparent-resistivity low is obtained over the material filling the sinkhole in comparison with the high resistivity of the surrounding limestone when electrode separations of 30 meters, 50 meters, and 100 meters are used (Khmelevskiy, 1936). In this example the horizontal profiles, rather than being obtained in the conventional manner, are merely lines drawn between apparent-resistivity values obtained at stations which are the same fixed distance apart. Therefore, there is a coincidence of the horizontal position of some of the peaks (fig. 149, at peaks A and C) that would not be so for conventional horizontal profiles with different electrode separations. The peaks closest to the left edge of the sink (fig. 149, at peak B) show how the character of the peak changes for different electrode separations. The peaks and lows farthest to the left of the diagram (fig. 149, near peak A) cannot be related to the clay sink shown in the diagram; they are probably caused by some other lateral resistivity changes in the rock near the left part of the geologic section. The higher peaks at the right part of the sink (fig. 149, at peak C) are possibly caused by the lower dip on this
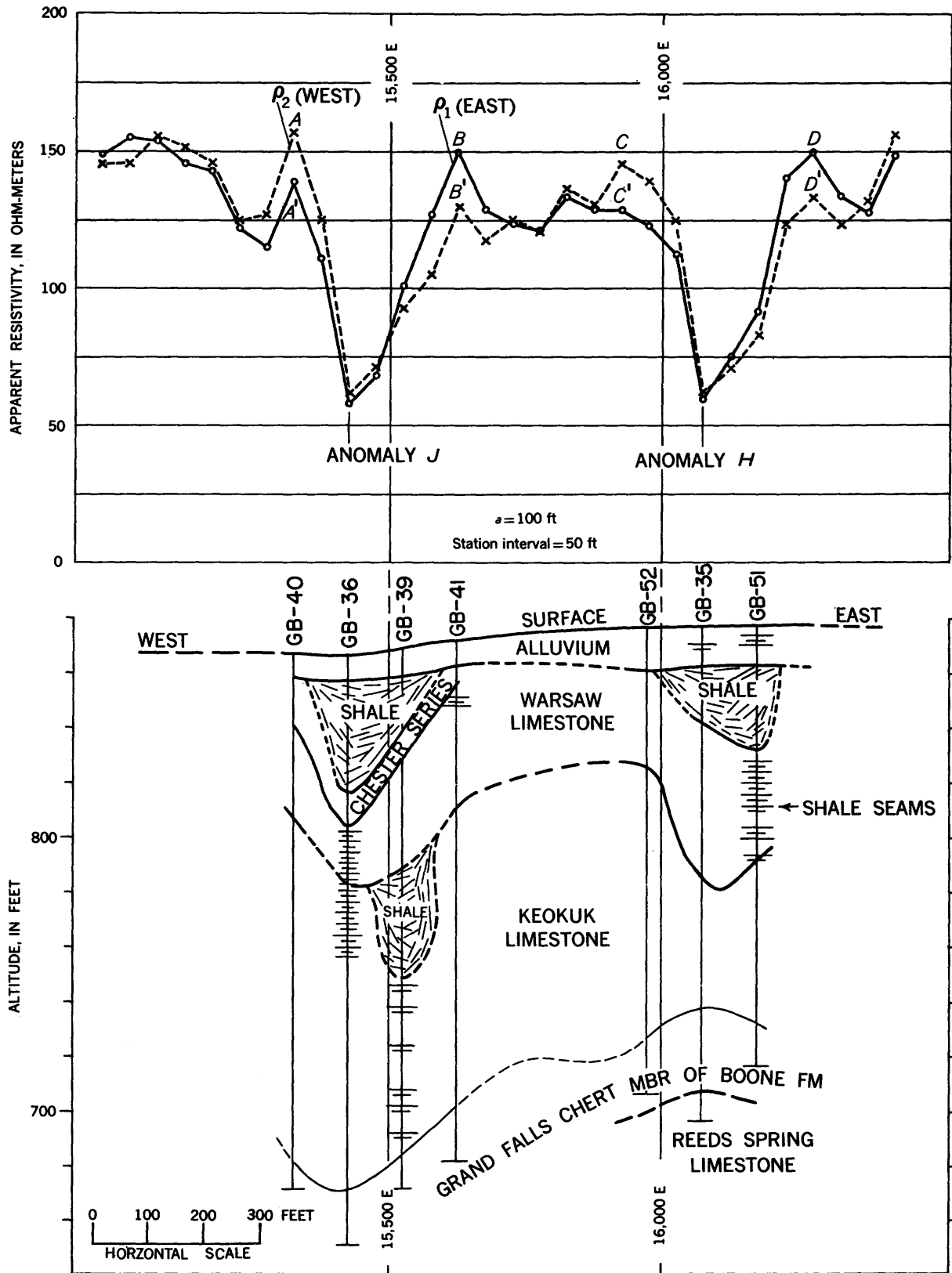
FIGURE 147.—Observed horizontal resistivity profile across two separate shale sinks, Tri-State lead-zinc mining district, Cherokee County, Kans., Lee configuration. Electrode separation a=100 feet; station interval=50 feet. Resistivity data and interpretations by K. L. Cook, 1951-54. Drill-hole data from Brichta and Ryan, 1958.
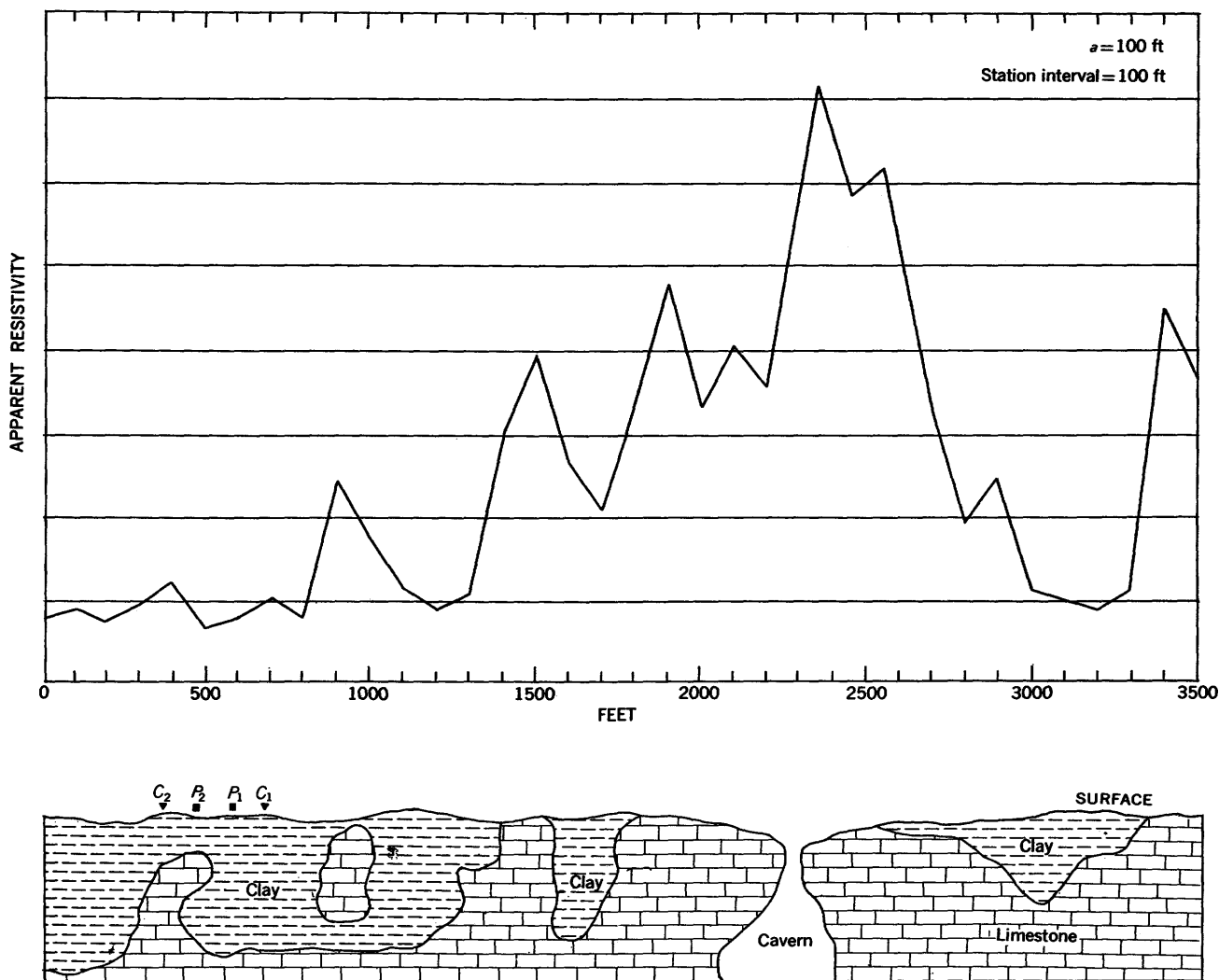
FIGURE 148.—Observed horizontal resistivity profile over karst topography, Hardin County, Ill., Wenner configuration. Electrode separation a = 100 feet; station interval = 100 feet. Adapted from Hubbert (1944).

side of the sink; but the sudden decrease of the curve for a = 100 meters to the right of the peak indicates that other lateral resistivity changes occur in the limestone on the right side of the sink. If our rules are used, we would draw the edges of the sink farther apart than shown in the diagram.

Figure 150 shows an observed horizontal resistivity profile with the Wenner configuration across an artificially made "graben" (actually a cut that had been later filled) of high-resistivity material on a terrace of Kölner Bay, Germany (Stern, 1933a). The electrode separation was 6 meters, and the width of the fill about 18 meters. Thus, the current electrodes cross the edges of the sink simultaneously. The station interval was usually taken as 5 or 6 meters far from the fill; whereas smaller intervals were taken in the areas near and over the fill. A resistivity high occurs over the high-resistivity material.

The lack of symmetry indicates nonuniform packing or some other inhomogeneity of the model, or inhomogeneous surroundings. The apparent-resistivity low and two small peaks obtained over the central part of the fill may be effects as the current electrodes cross either edge of the fill; this effect would be the counterpart of the effect shown in the central part of figure 144B, for a sink of low resistivity. The analogy is not clear cut, however.

VALUE OF VARIOUS APPROXIMATIONS

Filled sinks occur in the field with a wide range of shapes, dimensions, and resistivity contrasts. One of the problems in interpreting resistivity data over filled sinks is to recognize what approximations can be made in order to fit the theoretical data satisfactorily to the field data. Computations of the theoretical resistivity anomalies over hemispheroidal or hemispherical sinks
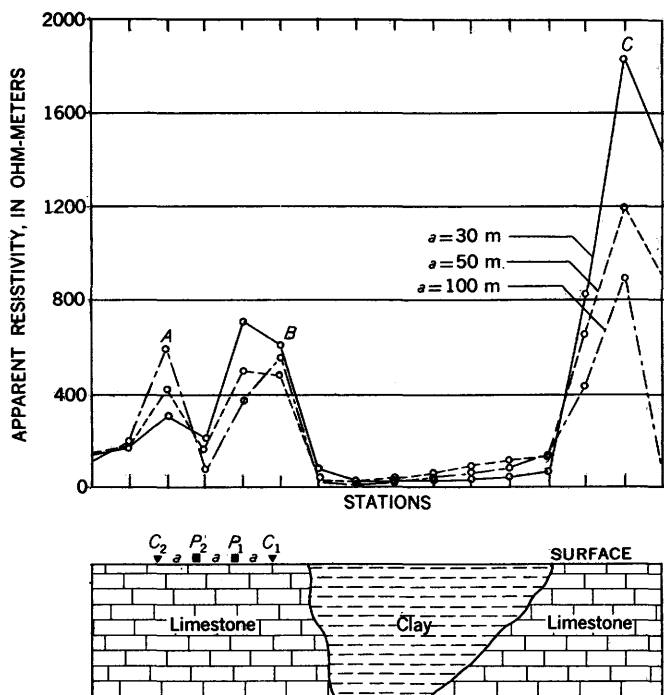
FIGURE 149.—Observed horizontal resistivity profiles over karst topography, area of Chapayevka village, Saratov district, U.S.S.R., Wenner configuration. Various electrode separations and station intervals. Adapted from Khmelevskiy (1936).

FIGURE 150.—Observed horizontal resistivity profile across artificially made "graben" of high-resistivity material on a terrace of Kölner Bay, Germany, Wenner configuration. Electrode separation $a=6$ m.; various station intervals. Adapted from Stern (1933a) by permission of Johnson Reprint Corp., N.Y.

are so tedious that shortcuts or reasonable approximations in interpretational procedures are highly desirable.

To give some notion of the types of approximations that can be made, a comparison of the theoretical results of horizontal resistivity profiles using the Lee and Wenner methods respectively, over an oblate hemispheroidal sink, a hemispherical sink, a vertical dike, and a pair of faults without considering their mutual interaction is given in figures 151 and 152. Each resistivity contrast of the material inside the sink, dike, or faults to the material outside is taken as $1:5$. The diameter of the hemisphere is taken as $3a/2$, where a is the electrode separation. The length of the major axis of the oblate hemispheroid, which is circular in plan view at the surface, is $3a/2$; and the length of the semiminor axis, which is the vertical axis of rotation, is $3a/8$. The width of the dike and the distance between the faults are taken as $3a/2$. The dike and faults are assumed to be of infinite length in the direction of strike and of infinite depth extent.

The horizontal profile is taken along the major axis and diameter, respectively, for the oblate hemispheroid and hemisphere, and along a line perpendicular to the strike for the dike and the faults. Thus, each horizontal traverse crosses the same width ($3a/2$) of low-resistivity medium. It should be emphasized that the theoretical anomaly over each fault is for a single fault with no other fault in the vicinity. Two such faults and their

respective anomalies are merely moved into juxtaposition so that they are separated by a distance of $3a/2$ and can be compared with the other bodies.

The curves of figures 151 and 152 are similar in the following respects:

(1) The general appearance of all curves is the same. The discontinuities in slope of each curve of the Lee set occur at identical points. The same is true within the Wenner set of curves, but the corresponding points in the two sets do not coincide.

(2) Each curve shows a pronounced low-resistivity anomaly over the low-resistivity medium and approaches regional resistivity asymptotically at great distances from the low-resistivity medium.

(3) The Lee curves for ρ_1/ρ' and ρ_2/ρ' cross at the center of the low-resistivity medium.

The curves differ in the following respects:

(1) In the central part of the low-resistivity medium the slopes of the curves differ somewhat because of the different depths and shapes of the bottoms of the low-resistivity media.

(2) The magnitudes of the theoretical anomalies differ with regard to maxima, minima, and hence anomaly indices. The maximum value of ρ_a/ρ' is 1 for the faults and greater than 1 for the other bodies, except for the Wenner curves over the dike. The minimum value of ρ_a/ρ' for the various
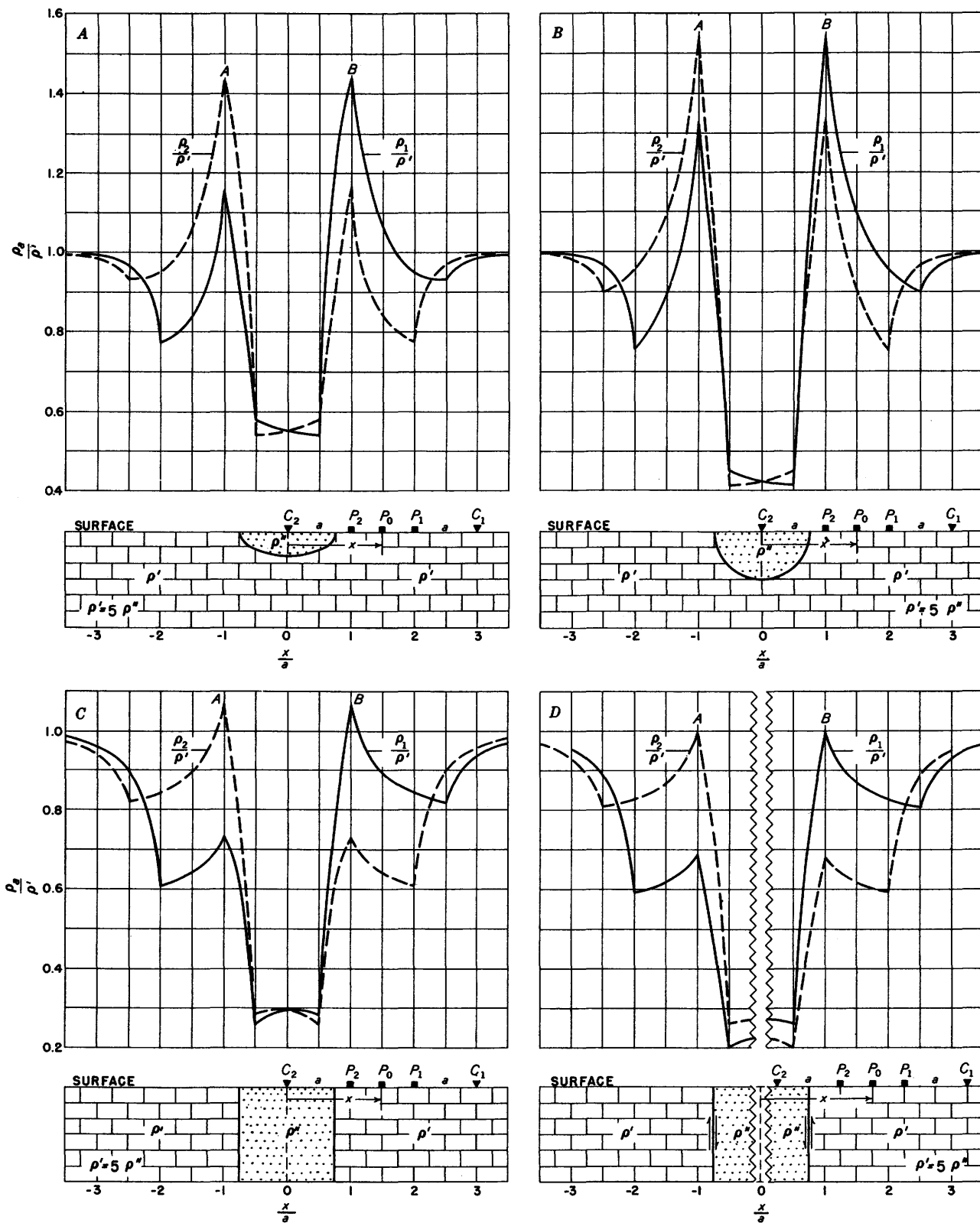
FIGURE 151.—Comparison of theoretical horizontal resistivity profiles over (A) oblate hemispheroid, (B) hemisphere, (C) dike, and (D) pair of faults, Lee configuration (offset plotting). Width at surface=3a/2, $\rho''/\rho'=1/5$. Adapted from Cook and Van Nostrand (1954).
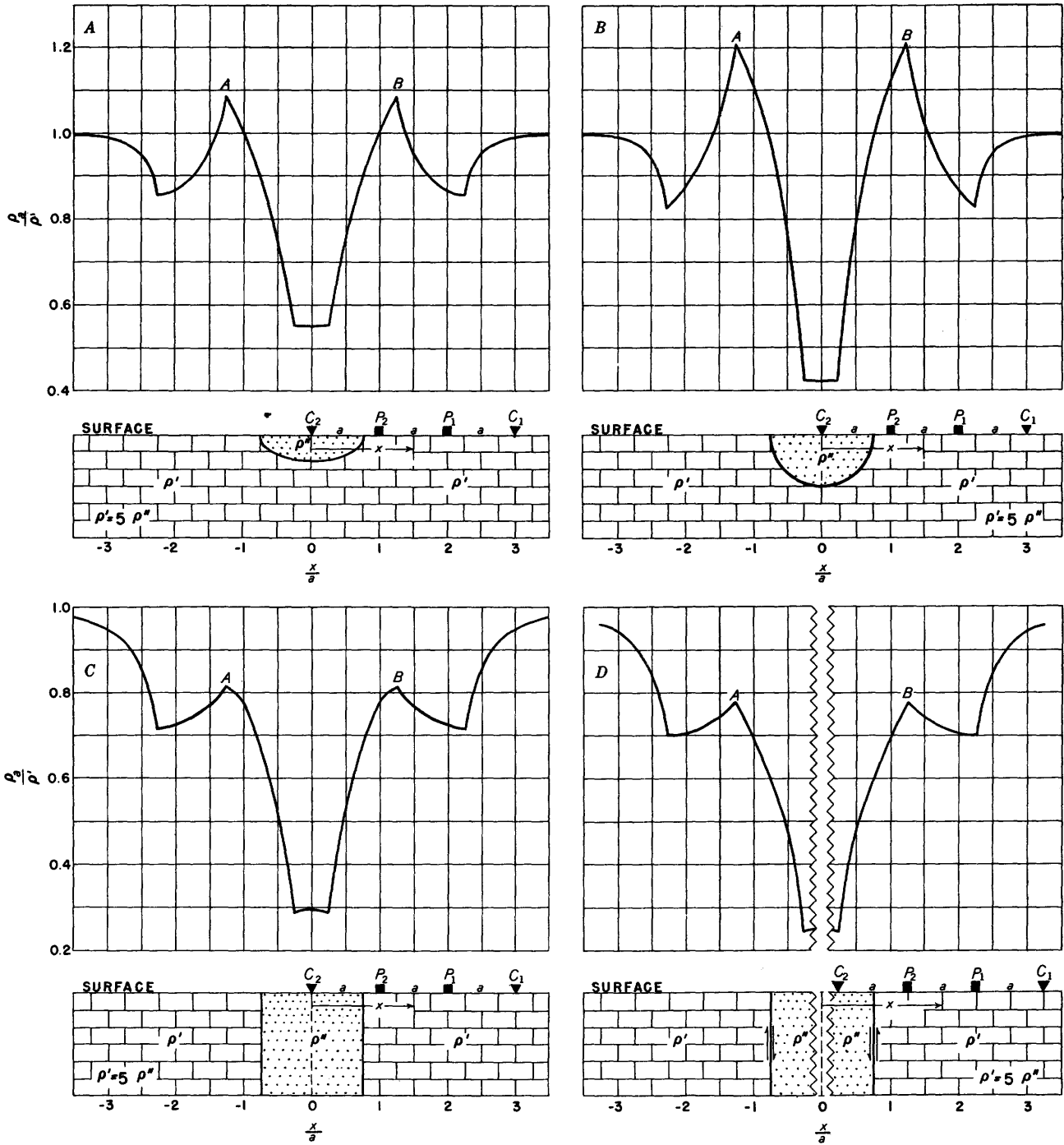
FIGURE 152.—Comparison of theoretical horizontal resistivity profiles over (A) oblate hemispheroid, (B) hemisphere, (C) dike, and (D) pair of faults, Wenner configuration. Width at surface=$3a/2$, $\rho''/\rho'=1/5$. Adapted from Cook and Van Nostrand (1954).

features decreases progressively in the following order: hemispheroid, hemisphere, dike, pair of faults. The anomaly indices are given in table 6. The following generalizations can be made:

(1) The distance between peaks A and B is equal to the width of the body plus half the electrode separa-

tion for the Lee configuration, or the full electrode separation, for the Wenner configuration.

(2) Peaks A and B lie at a distance of $a/4$ outside the margin of the body for the Lee curves and a distance of $a/2$ outside the margin of the body for the Wenner curves.

TABLE 6.—*Comparison of anomaly indices for Lee and Wenner configurations over oblate hemispheroid, hemisphere, dike, and pair of faults*

[Data from Cook and Van Nostrand (1954)]

Figure	Lee configuration	Wenner configuration	Ratio, Lee/Wenner
Oblate hemispheroid	0.90	0.53	1.70
Hemisphere	1.13	.79	1.43
Dike	.81	.71	1.14
Pair of faults	.80	.76	1.05

The following approximations can be made for a horizontal profile that crosses a sink near its center:

(1) If the width of the sink is small in comparison with its length and depth extent, the edge effects are approximately those due to a vertical dike.

(2) If the sink is large in comparison with the electrode separation, the edge effects of the sink are approximately those due to a vertical fault.

VERTICAL PROFILES OVER HEMISPHEROIDAL AND HEMISPHERICAL SINKS

Figure 153 shows the vertical profiles obtained along a traverse TT' over the center of a set of filled sinks taking the forms of a prolate hemispheroid (fig. 153A), a hemisphere (B), and an oblate hemispheroid (C), respectively. Since the traverse TT' coincides with the axis of revolution of each sink, the vertical cross section of each sink along the line SS', which is perpendicular to the traverse, is circular. The vertical cross sections of the sinks along traverse TT' are semielliptical for sinks A and C and semicircular for sink B. For sink A the major axis of the ellipse is parallel to traverse TT' and for sink C the major axis is perpendicular to traverse TT'. If the radius of the hemisphere is taken as unity, the proportion of the three radii of revolution is $r_A : r_B : r_C = 0.553 : 1.000 : 1.944$. The corresponding proportion of the volumes, which vary as the square of the radii, is $0.306 : 1.000 : 3.779$. The ratio of the resistivity of the material within the sink to the resistivity of the surrounding material is $1 : 5$.

For each vertical profile, the center of the electrode configuration is maintained over the geometric center of the theoretical sink. Because of symmetry, it follows that both the Lee and Wenner configurations give the same theoretical vertical profile for a given sink.

The vertical-profile curves display features that are helpful guides in the interpretation of the geology. For small electrode separations, the apparent resistivity is essentially equal to the resistivity of the material within the sink. In the present example, as the electrode configuration is expanded, the apparent resistivity becomes larger. The first breaks in the curves, at A'', B'', and C'' (fig. 153), occur at the point where the
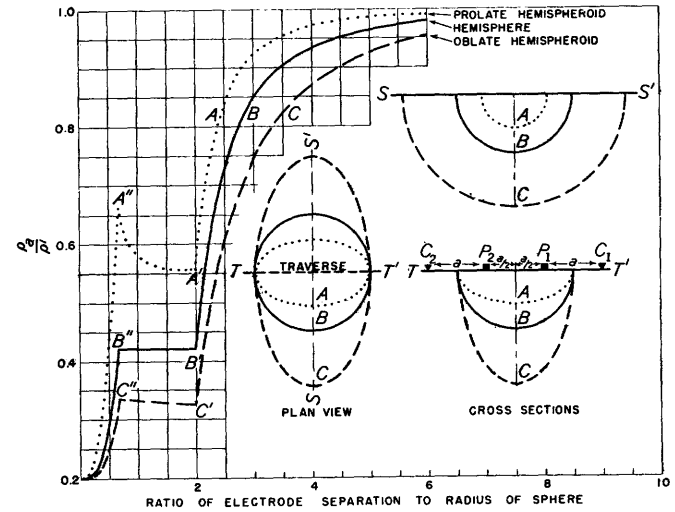
FIGURE 153.—Theoretical vertical resistivity profiles over hemispheroidal sinks. Profiles taken along traverse TT' with center of configuration at center of hemispheroids. $\rho''/\rho'=1/5$. Adapted from Cook and Van Nostrand (1954).

current electrodes simultaneously cross the boundary of the sink. A sharp peak occurs at this point for the prolate hemispheroid only. As the electrode configuration is expanded further, each curve tends to form a plateau. These anomalous features of the curves are due to a converging current effect, which is best displayed by the prolate spheroid.

As the electrode configuration is expanded further, abrupt changes in slope at A', B' and C' (fig. 153) occur at the point where the potential electrodes simultaneously cross the boundary of the sink. This abrupt change is apparently one of the most reliable interpretive features of the vertical profile; and it is very similar to that obtained for a vertical profile over a vertical fault as a potential electrode crosses the fault (fig. 59B).

Finally, for large electrode separations, the curves approach asymptotically the true resistivity value of the material surrounding the sink.

The vertical-profile curves show that the vertical-profile method is very sensitive to the margins of the sinks over a wide range of radii of revolution and indicate that the vertical-profile method should, therefore, be a very valuable tool in outlining a filled sink. In spite of the large differences in volume of the theoretical sinks considered in this example, the general shapes of the curves are similar. For the dimensions and resistivity contrast used, the vertical profile is rather sensitive to variations in the depth of such sinks, that is, to the radii of revolution. The sensitivity manifests itself principally in the plateau part of the apparent-resistivity curve.

Figure 154 shows an observed vertical resistivity profile with the Lee configuration at a station approxi-
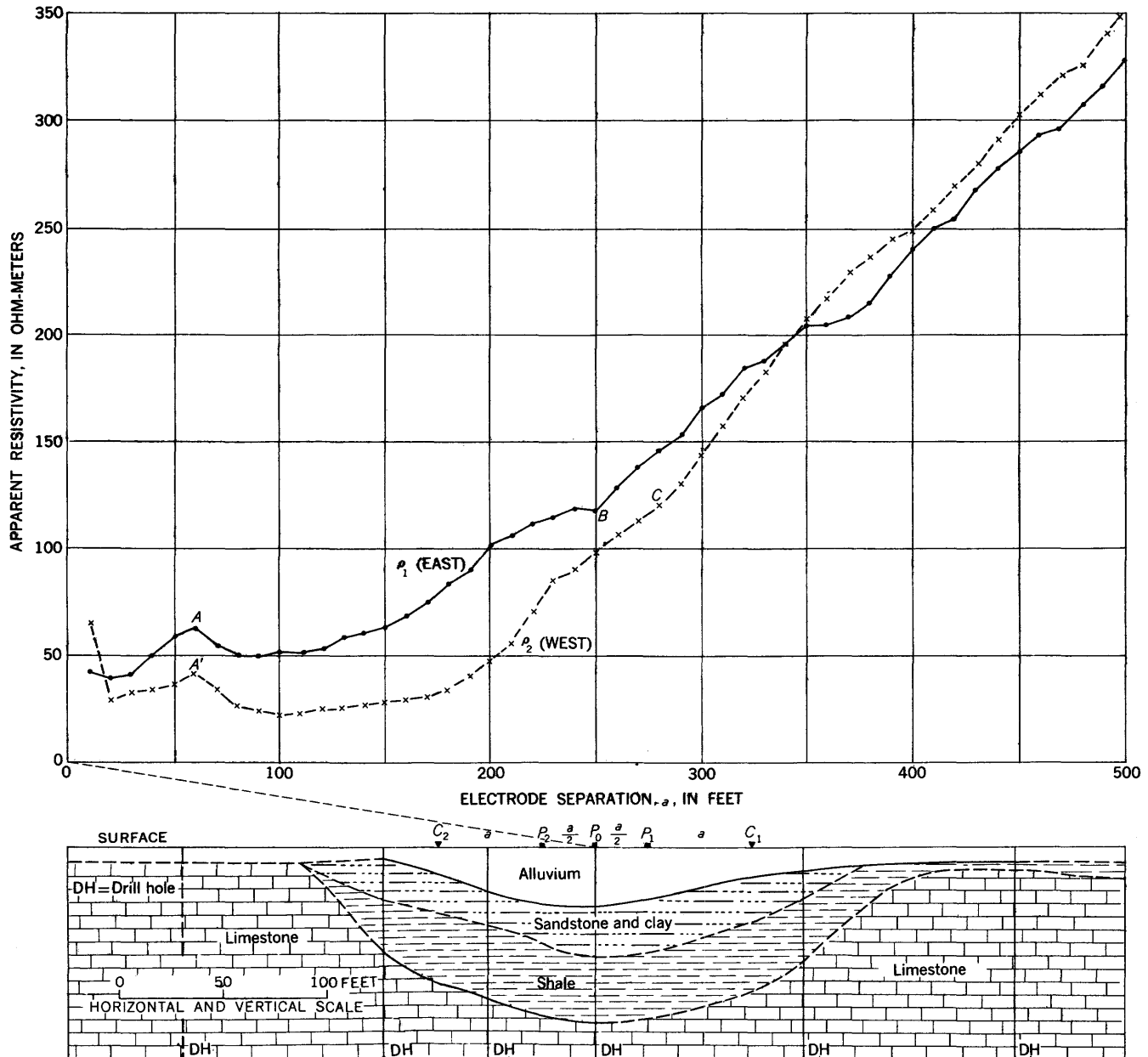
FIGURE 154.—Observed vertical resistivity profile at station approximately over center of hemispheroidal filled sink, Tri-State lead-zinc mining district, Cherokee County, Kan., Lee configuration. Resistivity data and interpretations by K. L. Cook, 1951-54, drill-hole data from Brichta and Ryan (1958).

mately over the center of a hemispheroidal filled sink in the Tri-State lead-zinc mining district, Cherokee County, Kansas. The pronounced peaks A and A' in the ρ_1 and ρ_2 curves, respectively, at $a=60$ feet occur as the current electrodes C_1 and C_2 pass essentially simultaneously over the rim of the alluvium bowl that is found over this sink. At this position of the configuration, the C_2 electrode is about 50 feet east of the shale-limestone contact and the C_1 electrode is about 60 feet west of the west edge of the main limestone shelf on the east edge of the sink. Apparently the additional current-converging effect of the alluvium

bowl causes the peaks to occur at smaller values of a than would have been the case in the absence of the alluvium bowl. For large expansions of the configuration, an abrupt change in slope of the ρ_1 curve at $a=250$ feet (fig. 154, point B) occurs as potential electrode P_1 crosses the "effective" east edge of the main shale sink, which lies about 30 feet west of the west edge of the limestone ridge. A change in slope in the ρ_2 curve at $a=280$ feet (fig. 154, point C), occurs as potential electrode P_2 crosses the west limestone-shale contact as shown in the geologic cross section. Thus, the observed profiles are similar to the theoretical curve
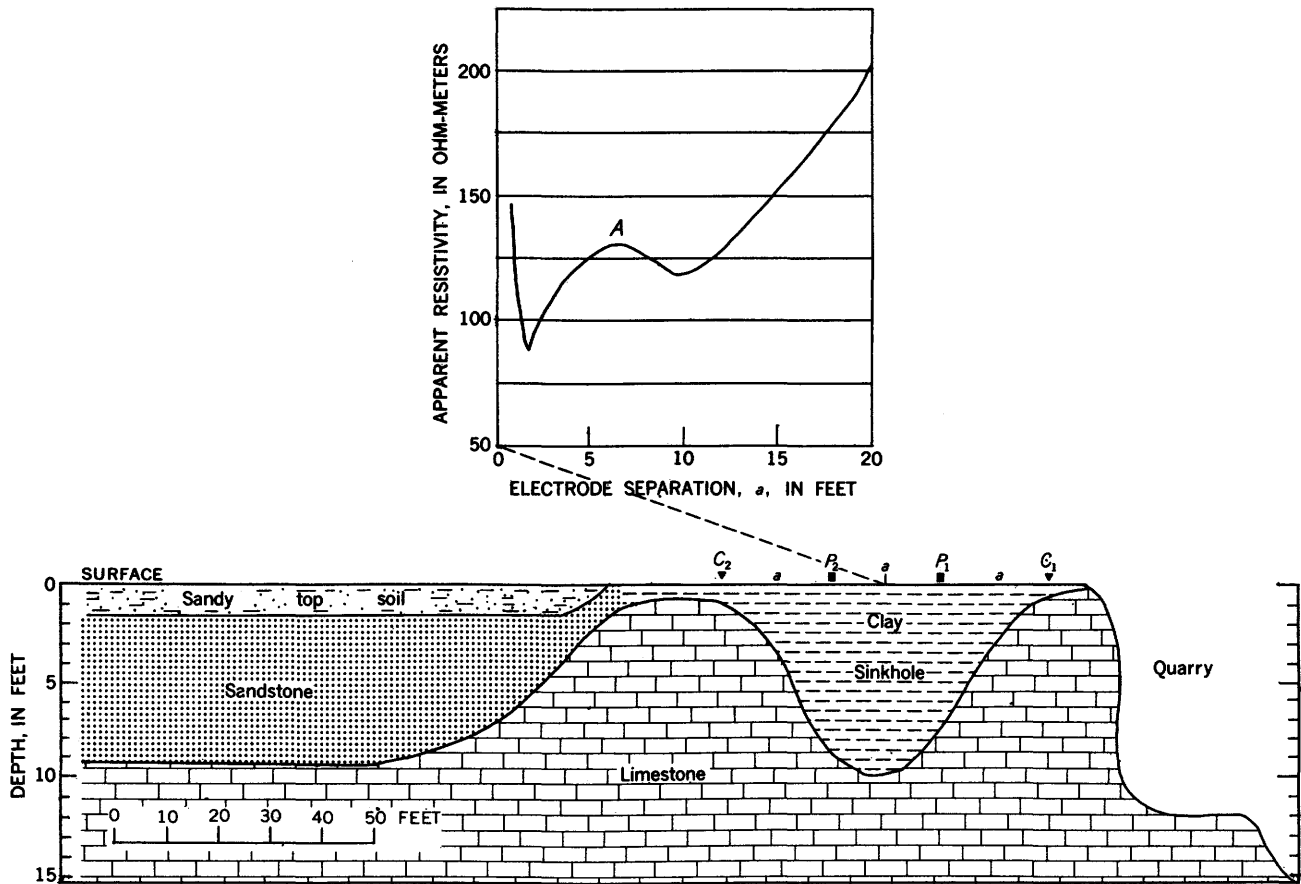
FIGURE 155.—Observed vertical resistivity profile at station approximately over center of hemispheroidal clay-filled sinkhole, western Wisconsin, Wenner configuration. Adapted from Kurtenacker (1934a). Copyright by Am. Inst. Mining Metall. Engineers.

A-A'-A'' in figure 153 for a filled sink whose horizontal dimension greatly exceeds its depth. With further expansion of the configuration beyond $a=280$ feet, the ρ_1 and ρ_2 curves cross at $a=340$ feet and essentially parallel each other for the remaining values of a out to a value of $a=500$ feet.

The term "effective" edge of the shale sink indicates that point where the resistivity effects of the edge of the main filled sink manifest themselves most strongly on the observed apparent-resistivity measurements (Cook, unpublished data, 1954). The actual geologic relationships in the field are often so complex that the main resistivity effects do not manifest themselves exactly at the limestone-shale contact, either because of asymmetrical conditions of the filled sink or because of the complexity of the rocks at the margins of the sink. At the margin of a shale sink, the zone of contact between the shale mass and the limestone—which is often rough, ragged, or irregular, and hence rather ill-defined—consists of limestone boulders, shale boulders, and both large and small blocks of limestone and shale. The blocks of boulders of limestone mixed with the shale at the borders of shale sinks can often cause a

resistivity discontinuity, though geologically the margin of the "shale" is placed at the point where solid limestone is encountered in the drill holes. Thus, the location of the apparent-resistivity discontinuity, designated as the "effective" edge of the shale mass, sometimes differs by as much as 10 to 20 feet or more from the edge of the shale indicated in the geologic cross section. This discrepancy is not considered serious when the heterogeneity of the material often found at the margins of shale sinks is considered. No attempt to sketch these hetereogenous conditions in the geologic cross sections has been made, and a smooth shale-limestone contact is therefore always shown.

Figure 155 shows an observed vertical resistivity profile with the Wenner configuration at a station approximately over the center of a hemispheroidal-shaped clay-filled sinkhole in western Wisconsin (Kurtenacker, 1934a). Peak A, for an electrode separation $a=7$ feet, is probably caused by the current-converging effect as the current electrodes approach the edges of the sinkhole. The "effective" width of the sinkhole, which on the basis of peak A is indicated as about 21 feet, is much less than the width of about

50 feet shown by Kurtenacker. The curve is apparently complicated by the effect of the old quarry face, which causes the apparent-resistivity curve to rise sharply for electrode separations larger than 10 feet.

Figure 156 shows the apparent-resistivity values for theoretical vertical profiles taken on a set of traverses located at different distances from the center of a hemispherical sink. The resistivity contrast is the same as in the previous problem. For the single vertical profile taken on each traverse, the center of the configuration lies along a radial line perpendicular to the traverse and remains fixed as the configuration is expanded. Because of symmetry, the apparent-resistivity values shown apply equally well to both the Lee and Wenner configurations. Except for the scale of plotting, the vertical profile for traverse 1 is comparable to curve B given for the hemisphere in figure 153.

For vertical profiles taken along traverses that intersect the sink, the apparent resistivity for small electrode separations is essentially equal to the true resistivity of the medium lying inside the sink. All such profiles show discontinuities in slope, the most pronounced discontinuity occurring at the point where the potential electrodes cross the boundary. The apparent-resistivity values in the area of the most pronounced discontinuity in slope are nearly the same as the resistivity value constituting the horizontal plateau region $A'A''$ of curve 1 (fig. 156).

For the traverse that is tangent to the hemispherical sink (fig. 156, curve 4), the vertical profile starts for a very small electrode separation with an apparent-resistivity value that is intermediate between the true resistivity of the material within the sink and that of the surrounding material. Further, for an expanding configuration this curve shows a continuous slope, a feature that characterizes the vertical profiles along traverses that do not intersect the sink.

For all vertical profiles taken outside the hemispherical sink, the apparent-resistivity value for small electrode separations essentially equals the true resistivity of the medium outside the sink. For greater electrode separations, the apparent resistivity reaches a minimum value (fig. 156, curve 5), the location of which shifts to the right for succeeding traverses more removed from the sink (fig. 156, curve 6). For very large electrode separations, irrespective of whether the traverses transect the sink, the apparent resistivity approaches asymptotically the true resistivity value of the medium outside the sink. These features of the vertical profiles that pass tangent to or outside of the hemispherical sink can be explained qualitatively on the basis of the ratio of sink material to the total volume of earth within which the field of the current is appreciable.

The corresponding vertical profiles for prolate and oblate hemispheroids would not be identical with those for the hemispherical sink shown in figure 156. However, the latter curves, together with those in figure 153, can be used to determine qualitatively the general character of the former.

Figures 157 and 158 show theoretical vertical resistivity profiles with both the Lee and Wenner configurations at different stations along a traverse passing through the center of a hemispherical sink. The radius of the sink is designated r_1. For all the curves, both Lee and Wenner, the resistivity of the country rock is five times that of the sink material. For both the Lee and Wenner configurations the stations are taken at the center of the sink and at distances of $r_1/2$, $3r_1/4$, r_1— (that is, at the right edge of the sink)—and $3r_1/2$, $2r_1$, and $3r_1$ from the center of the sink. The curves are plotted as the ratio of the apparent resistivity to the resistivity of the surrounding country rock. Distances are plotted as the ratio of the electrode separation a to the radius of the sink r_1.

For a station at the center of the sink (figs. 157A and 158A), the theoretical curves for both the Lee and Wenner configurations are identical; and this curve is identical with curve B–B'–B'' in figure 153 and curve 1 in figure 156.

For a station at a point lying between the center and right edge of the sink (figs. 157B, C, 158B, C), the ρ_1 and ρ_2 curves for the Lee configuration diverge abruptly after current electrode C_2 crosses the left edge of the sink. The apparent-resistivity values for the ρ_1 curve rise abruptly after potential electrode P_1 crosses the right edge to exceed a value of one. A minor current-converging peak occurs in the ρ_2 curve as current electrode C_2 crosses the left edge of the sink; and an abrupt discontinuity in the slope occurs in the ρ_2 curve as potential electrode P_2 crosses the left edge. For corresponding stations with the Wenner configuration, an apparent-resistivity plateau lies at a point corresponding with the electrode separation at which potential electrode P_2 crosses the left edge.

For a station at the right edge of the sink (figs. 157D and 158D), the Lee curves for small electrode separations are separated far from each other; and a more pronounced current-converging peak is obtained both in the ρ_2 and ρ_1 curves as current electrode C_2 crosses the left edge. The values of ρ_1 greatly exceed one. The Wenner curve shows a current-converging peak also, and the apparent-resistivity values slightly exceed one.

For stations lying to the right of the right edge of the sink (figs. 157E, F, G; 158E, F, G), the apparent resistivity of both the Lee and Wenner curves decreases until current electrode C_2 crosses the right edge; then
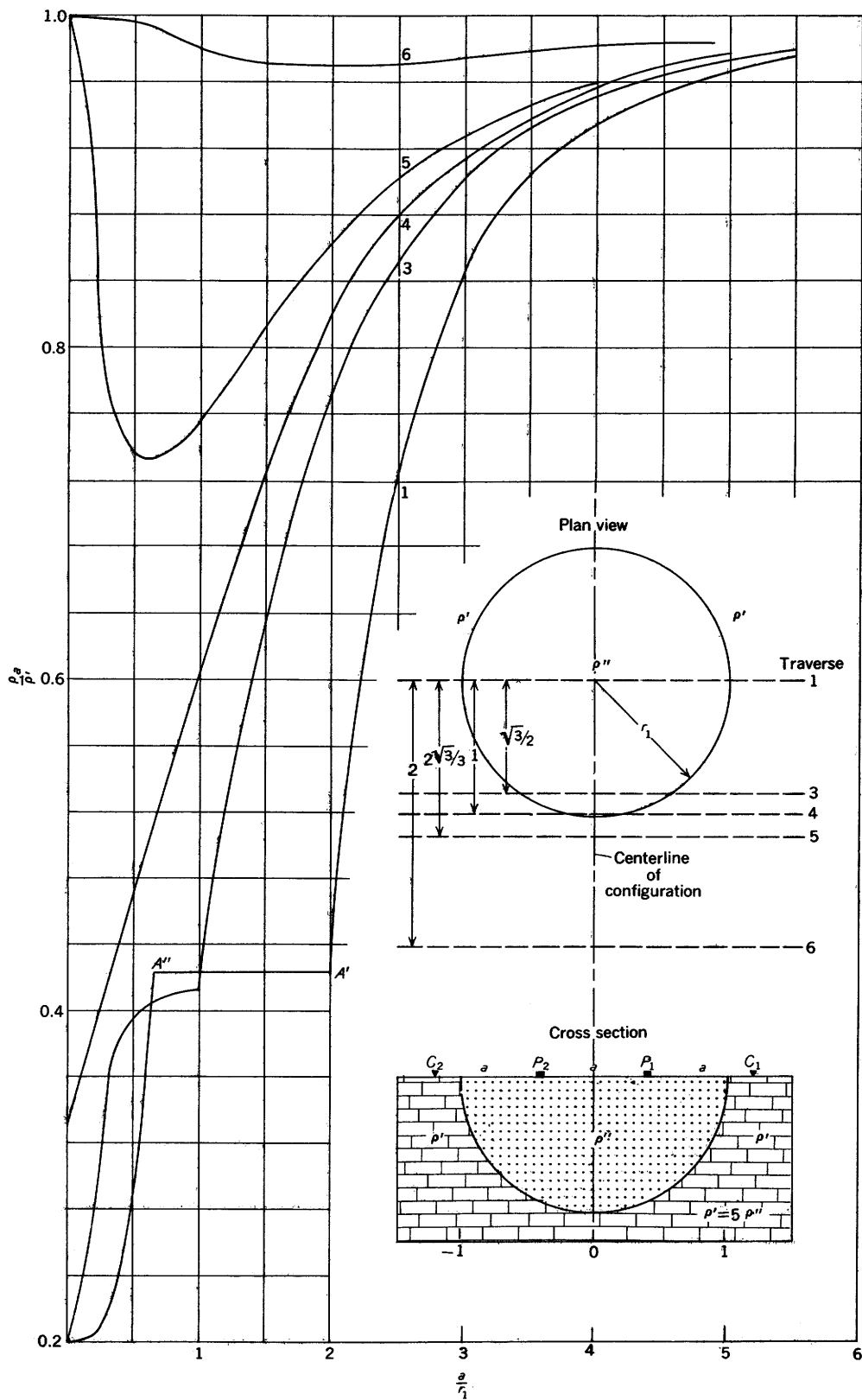
FIGURE 156.—Theoretical vertical resistivity profiles over hemispherical sink, with center of configuration at several distances from center of hemisphere. Adapted from Cook and Van Nostrand (1954).
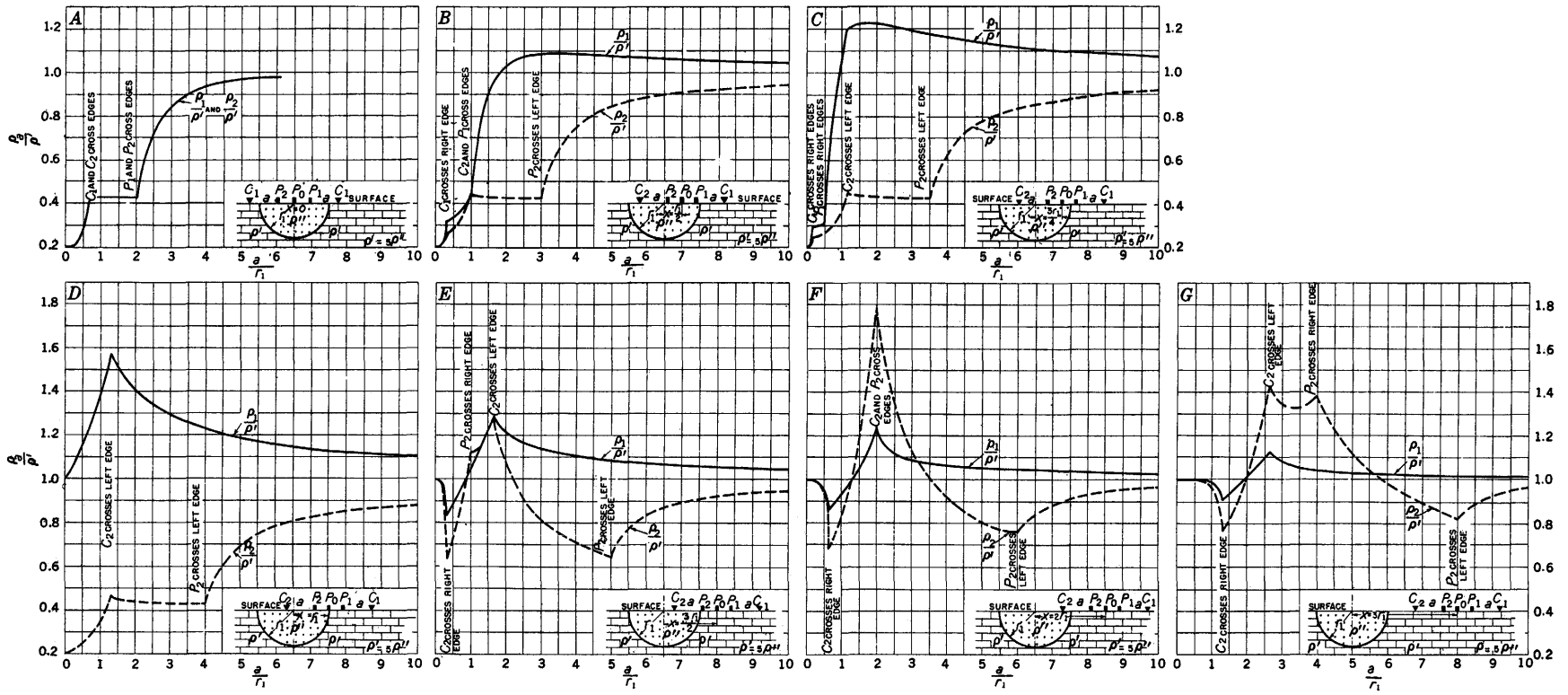
FIGURE 157.—Theoretical vertical resistivity profiles at different stations along traverse passing through center of hemispherical sink, Lee configuration. Radius of sink=r_1; $\rho'=5\rho''$.
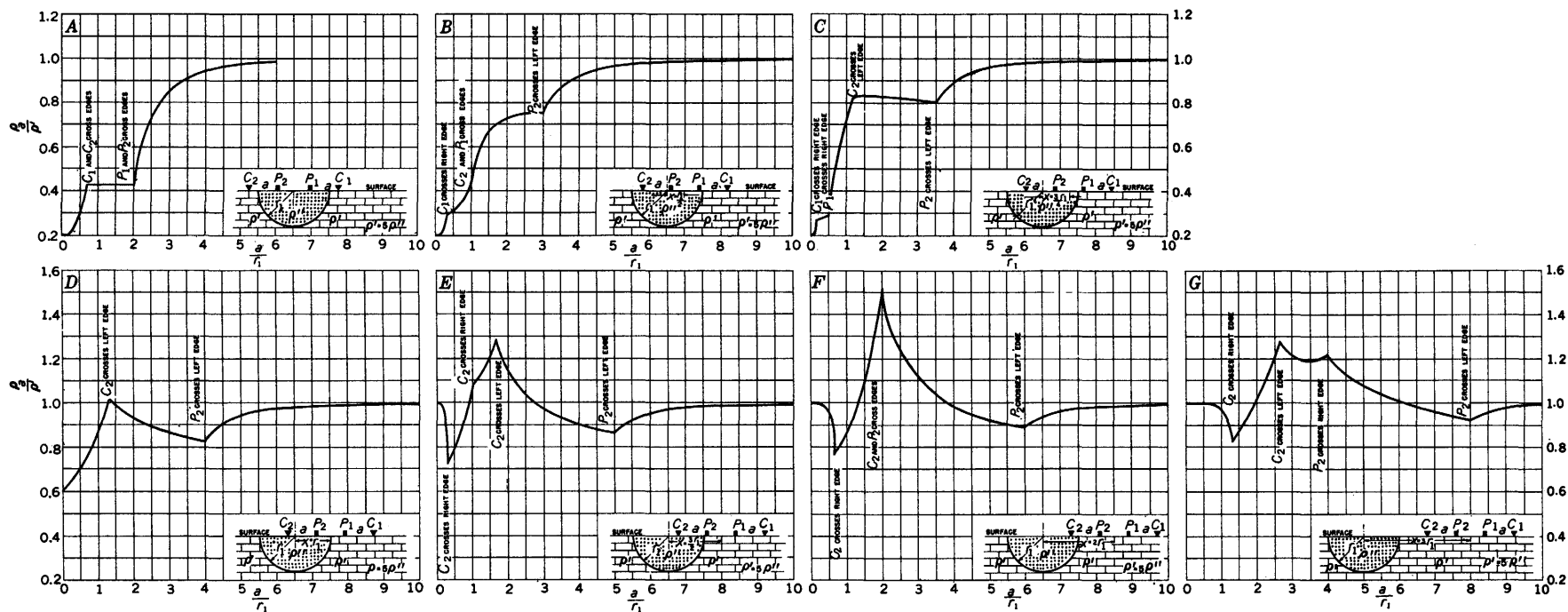
FIGURE 158.—Theoretical vertical resistivity profiles at different stations along traverse passing through center of hemispherical sink, Wenner configuration. Radius of sink $=r_1$; $\rho'=5\rho''$.

the apparent-resistivity values increase rapidly to attain high peaks when the current-converging effect manifests itself most pronouncedly as current electrode C_2 crosses the left edge of the sink. Although the current-converging effect is great for stations lying at distances of $3r_1/2$ and $3r_1$ from the center of the sink, the maximum current-converging effect occurs for a station lying at a distance of $2r_1$ from the center. When this maximum effect occurs, current electrode C_2 crosses the left edge at the same time as potential electrode P_2 crosses the right edge of the sink (see figs. 157F and 158F); and, as a result, a high apparent-resistivity peak is obtained in the ρ_2 curve for the Lee configuration and in the single curve for the Wenner configuration. The values of the current-converging peaks for these stations lying outside the sink at a distance of $2r_1$ from the center attain values of about 1.8 for the Lee configuration and 1.5 for the Wenner configuration.

When vertical resistivity profiles are used to study filled sinks, the apparent-resistivity peaks caused by the current-converging effects are diagnostic features that greatly assist in delineating the edge of the sinks. As emphasized, these peaks occur as the current electrode crosses the side of the sink farthest removed from the station. In addition, the abrupt discontinuities in slope that occur as the potential electrode (or electrodes) cross the edges of the sink are also helpful in the interpretation; yet these discontinuities are relatively minor, and are usually less well-defined in the field data than the current-converging peaks.

Plate 5 shows observed vertical resistivity profiles with the Lee configuration at 18 different stations over and in the vicinity of a known shale sink in the Tri-State lead-zinc mining district, Cherokee County, Kansas. Nine profiles were taken at stations A to I, inclusive, along a traverse that crosses the shale sink in an eastward direction; and nine profiles were taken at stations J to R, inclusive, along a traverse that crosses the shale sink in a northward direction at right angles to the eastward-trending traverse. The two traverses intersect at drill hole 71. The field data were taken so that a comparison could be made between the observed and theoretical curves; accordingly the configurations were expanded sufficiently at some stations so that both potential electrodes P_1 and P_2 passed over the edges of the shale and along the limestone shelves for a distance of 50 feet or more.

The observed features in these profiles are similar in many respects to those in the theoretical curves in figure 157; the reader will find it helpful to refer to the theoretical curves as he studies the observed curves.

Station A (pl. 5), the westernmost station lying over the limestone shelf along the eastward-trending trav-

erse, gives a "normal" vertical resistivity curve for the area under study. With an electrode separation of as much as 200 feet, the apparent resistivity increases almost linearly with the electrode separation because of the high resistivity of the limestone in comparison with that of the alluvium overburden. The apparent-resistivity values for the east side of the configuration, which is the side nearer to the shale mass, are somewhat lower than the values for the west side of the configuration, which is the side farther from the shale mass.

Stations B and C, over the limestone shelf but nearer the west edge of the shale than the previous station, show values of ρ_1 and ρ_2 that are nearly equal for any given value of the electrode separation. At station C, the marked divergence of values of ρ_1 and ρ_2, which starts at $a=100$ feet approximately, is a manifestation of the west edge of the shale sink.

The abnormally high apparent resistivities for small electrode separations that occur on some, but not all, profiles in this area are caused by the dry, caked, and hard condition of the near-surface materials that existed locally in this region during the drought season of 1953 when the measurements were taken. The local high-resistivity layer was generally so thin that its effect on the vertical resistivity profiles is usually negligible for electrode separations exceeding about 20 feet. In the discussion that follows, the few high apparent-resistivity readings obtained at small electrode separations in some of the vertical resistivity profiles will usually not be mentioned unless they appear to distort or change greatly the shape of the apparent-resistivity curve at critical points on the curves that are incident to the analysis of the shale sinks.

Station D gives a fault-type resistivity curve (see fig. 60), if the near-surface high-resistivity effects at $a=10$ feet are neglected. The abrupt change in slope of the ρ_2 curve at $a=50$ feet occurs as potential electrode P_2 crosses the limestone-shale contact as shown in the geologic cross section. The location of the west edge of the shale, as inferred from this vertical profile, agrees well with its location as obtained from the horizontal resistivity profiles. The cause of the second abrupt change in slope in the ρ_2 curve at $a=90$ feet is not known. The persistent low values of ρ_1 are noteworthy. The small, yet recognizable, peak on the ρ_1 curve at $a=150$ feet occurs as current electrode C_1 passes over the east edge of the shale as shown in the geologic cross section.

At station E, the small yet recognizable peaks on both the ρ_1 and ρ_2 curves at $a=40$ feet occur as current electrode C_2 crosses the effective west edge of the shale, which in this case corresponds, within about 15 feet, with the edge shown in the geologic

cross section. The change in the slope of the ρ_2 curve at $a=100$ feet occurs as potential electrode P_2 crosses the effective west edge of the shale, which is about 15 feet from the edge shown in the geologic cross section. The abrupt change in slope of the ρ_1 curve at $a=340$ feet occurs as potential electrode P_1 crosses the east edge of the shale. The change in slope is pronounced probably because of the relatively thin mantle of overburden on the east side of the sink. The thicker the overburden the more the changes in slope tend to be tempered.

At station F, the peaks on the ρ_1 and ρ_2 curves at $a=70$ feet occur as current electrodes C_1 and C_2 pass over the effective edges of the shale sink, which correspond, within about 20 feet, with the margins shown in the geologic cross section. The change in slope in the ρ_1 curve at $a=230$ feet occurs as potential electrode P_1 crosses the east edge of the shale as shown in the cross section. The abrupt change in slope in the ρ_2 curve at $a=260$ feet occurs approximately (within 5 feet) as potential electrode P_2 crosses the west edge of the shale as shown in the cross section.

At station G the peak on the ρ_1 curve at $a=50$ feet occurs as current electrode C_1 passes approximately (within about 15 feet) over the east edge of the sink, and the peak in the ρ_2 curve at $a=100$ feet occurs as current electrode C_2 passes over the effective west edge of the sink, which is about 25 feet east of the west edge shown in the geologic section. The abrupt change in the slope of the ρ_1 curve at $a=140$ feet occurs as potential electrode P_1 crosses the shale-limestone contact at the east edge of the shale as shown in the geologic cross sections. The change in slope of the ρ_2 curve, which is gradual and not pronounced, occurs approximately at $a=310$ feet as potential electrode P_2 crosses the effective west edge of the shale, which is about 20 feet east of the edge shown in the geologic cross section.

At station H, the abrupt divergence of the ρ_1 and ρ_2 curves at small values of a indicates that this station lies near the shale-limestone contact. The peaks on the ρ_1 and ρ_2 curves at $a=130$ feet and $a=140$ feet, respectively, occur approximately as current electrode C_2 passes over the effective west edge of the sink, which is about 15 to 30 feet east of the west edge shown in the geologic cross section.

Station I is centered over the northward-trending limestone barrier that separates the main shale mass from another shale mass to the east. The ρ_1 and ρ_2 curves differ considerably for small values of a and converge for larger values of a, only to cross and diverge at $a=170$ feet approximately, as the effect of the main shale mass manifests itself, to give smaller values for ρ_2.

A comparison of the vertical profiles at the three stations E, F, and G shows clearly the asymmetry of the ρ_1 and ρ_2 curves, which is caused by the different volumes of shale occupying either side of the partitioning plane when the station is on either side of the center of the shale, rather than in the center of the shale. For example, the vertical resistivity profile at station E and that at G are approximate counterparts. At station E, the fact that the values of the ρ_1 curve are much less than those for the ρ_2 curve, even for large electrode separations, indicates that the station is volumewise west of the center of the shale mass. Similarly, at station G, the fact that the values of the ρ_2 curve are much less than those for the ρ_1 curve, even for large electrode separations, indicates that the station is volumewise east of the center of the shale mass. At station F, on the other hand, the fact that the values of the ρ_1 and ρ_2 curves are nearly the same for any given electrode separation, especially for the larger electrode separations, indicates that the station is volumewise at or near the center of the shale mass. The fact that, for small and intermediate electrode separations, the values of ρ_2 are somewhat smaller than those of ρ_1, indicates that station F probably lies slightly east of the center of the shale mass.

The asymmetrical form of the shale mass itself also contributes to the asymmetrical resistivity pattern. In any analysis to locate the center of the shale mass at the surface, therefore, certain limitations are inherent, and certain precautions are necessary. First, if the shale mass is asymmetrical in cross section, as in the present example, the near-surface shale will therefore manifest itself disproportionately on the apparent-resistivity values in comparison with the deeper shale. Second, any asymmetry in the shale mass extending horizontally, in plan view, to the north and south of the eastward-trending geologic cross section in plate 5, will manifest itself on the apparent-resistivity values on the traverse. Thirdly, it is tacitly assumed that the true resistivity of the limestone on one side of the shale is identical with that on the other. This assumption is apparently fulfilled for all practical purposes in the present example along the eastward-trending traverse.

The vertical resistivity profiles at the stations along the eastward-trending traverse provide good agreement between the theoretical and field data. The excellent correlation obtained in this field example is probably attributable to the unusually thin alluvium cover on the east margin of the sink, where the shale-limestone contact is gentle; the steep shale-limestone contact on the west margin of the sink, where the alluvium is relatively thick; and the relatively great thickness of the shale.

For the vertical resistivity profiles at stations along the northward-trending traverse over the same shale

sink, several of the profiles on the south side of the shale have approximate counterparts on the north side. At stations J and R, which are about 110 feet south and 80 feet north, respectively, of the inferred south and north edges of the shale, the profiles are approximate counterparts; except for small values of a, the apparent resistivity generally increases with increasing values of a. At stations K and Q, near the shale-limestone contact at the south and north edges, respectively, of the shale, the profiles are very similar for small values of a, and are approximate counterparts for large values of a only. At stations L and P, over and within the south and north edges, respectively, of the shale, the profiles are approximately counterparts. At station L, the abrupt change in slope of the ρ_2 curve at $a=60$ feet occurs as potential electrode P_2 crosses the south shale-limestone contact as shown in the cross section. At stations M and O, over the interior of the shale, the curves are approximate counterparts, even for large values of a. The divergence of the ρ_1 and ρ_2 curves for station M, with ρ_2 always greater than ρ_1, indicates that the station lies to the south of the center of the shale mass. The divergence of the ρ_1 and ρ_2 curves for station O, with ρ_1 greater than ρ_2 (except for small values of a), indicates that the station lies to the north of the center of the shale mass. At station O, a small current-converging peak in the ρ_2 curve at $a=80$ feet occurs approximately (within 10 feet) as current electrode C_1 crosses the north shale-limestone contact as shown in the cross section.

At station N the low apparent-resistivity values of the order of 25 ohm-meters or less for small values of a, and the close agreement of the ρ_1 and ρ_2 values for any given value of a either small or large, indicate that the station is located over the central part of the shale. For large values of a, the abrupt change in slope of the ρ_2 curve at $a=300$ feet occurs approximately (within 15 feet) as potential electrode P_2 crosses the south shale-limestone contact as shown in the geologic section, and the abrupt change in slope of the ρ_1 curve at $a=350$ feet occurs as potential electrode P_1 crosses the north shale-limestone contact as shown in the geologic section.

The northward-trending traverse on plate 5 passes so close to the western margin of the shale that some unusual lateral effects are produced along the traverse. The effects are provisionally attributed to current-converging effects, although the relations are not entirely clear, principally because insufficient theoretical work has been done to date (1957) for vertical profiles that pass nearly tangent to the edge of the sink. Rather pronounced effects are observed: at station K, where a maximum in the ρ_1 curve occurs at $a=160$ feet; at station L, where a maximum in the ρ_1 curve occurs at $a=120$ feet; at station M, where a maximum in the ρ_1 curve occurs at $a=90$ feet; and at station N, where

maxima in both the ρ_1 and ρ_2 curves occur at $a=60$ feet. These effects occur approximately (within 5 feet) as current electrode C_1 passes over the same point on the surface during the expansion of each of these profiles. This point, although lying about 85 feet south of the north edge of the shale as shown in the geologic cross section, apparently constitutes the effective north edge of the shale, where the resistivity edge effects manifest themselves most pronouncedly.

Other rather pronounced effects provisionally attributable to current-converging effects are observed: at station O, where a barely perceptible maximum occurs in the ρ_2 curve at $a=80$ feet; at station P, where a maximum in the ρ_2 curve occurs at $a=120$ feet; and at station Q, where a maximum in the ρ_2 curve occurs at $a=150$ feet. These effects similarly occur approximately (within 5 feet) as current electrode C_2 passes over the same point on the surface during the expansion of each of these profiles. This point, although lying about 55 feet north of the south edge of the shale as shown in the geologic cross section, apparently constitutes the effective south edge of the shale.

When explained provisionally as above on the basis of current-converging effects, the fact that this effective edge of the sink lies so far from the edge shown in the geologic section—which was inferred principally from horizontal resistivity profiles—is explained possibly by the fact that this traverse passes near the edge of the shale mass.

RESISTIVITY MAPS OVER HEMISPHERICAL SINK

Resistivity maps greatly facilitate the interpretation of resistivity data over filled sinks. The resistivity map is generally obtained by contouring in plan view the values of apparent resistivity for a given electrode separation over the area surveyed. The conventions of contouring are similar to those used for topographic maps. As hachured contours are very common on a resistivity map, it is well to recall that hachured resistivity contours indicate that the apparent resistivity decreases in the direction in which the hachures point.

Figure 159A shows a theoretical resistivity map obtained over a hemispherical sink for the Wenner configuration. The ratio of the resistivity of the material filling the sink to that of the surrounding medium is taken as 1:5—actually 30 ohm-meters:150 ohm-meters—for comparison with a field example later, and the electrode separation a is equal to half the radius of the sink. The contours are based on the same theoretical data which were used to construct the horizontal traverse curves in figure 144. It is to be noted that, near the point of tangency, the traverses are spaced more closely together to provide better definition of the
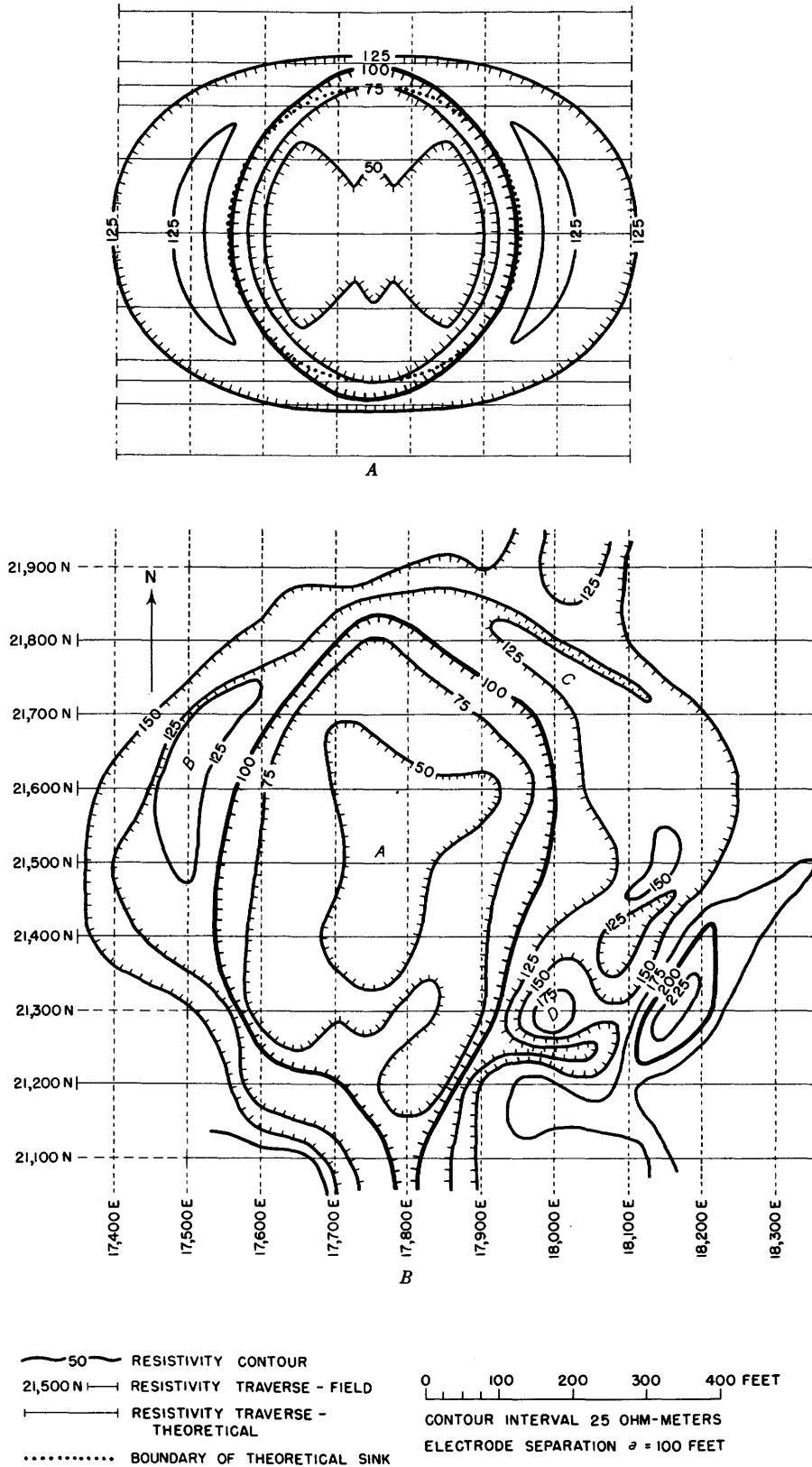
FIGURE 159.—Comparison of (A) theoretical-resistivity map over hemispherical sink (shown in dotted outline) and (B) observed field resistivity map over filled sink, Tri-State lead-zinc mining district, Cherokee County, Kans., Wenner configuration. Resistivity field data by K. L. Cook, 1951–54.

resistivity anomaly in this area where the resistivity changes rapidly.

The theoretical resistivity map is characterized by a large area of low resistivity lying inside the filled sink, and a crescent-shaped high that flanks both the right and left sides of the sink. The low-resistivity area as a whole is elongated in the direction of the traverses and manifests itself far beyond the margin of the hemispherical sink. In view of the symmetry of the sink itself, the oval shape of the outer resistivity contours is a rather striking feature, and is due to the direction in which the profiles are taken.

Figure 160A shows a theoretical resistivity map that was obtained over the same hemispherical sink with the Lee configuration, using the same traverses and station intervals as for the Wenner method. For the contouring of this map, the arithmetic mean of the two offset-plotted Lee partitioning values occupying the same horizontal position for two overlapping stations is computed and plotted at the same position as the two values—that is, midway between P_0 and P_1, or P_0 and P_2. Although this method of averaging the Lee data tempers or vitiates the advantages of detail afforded by the original Lee data along a profile, it is nevertheless the method still in common use today. Any average resistivity value plotted in this manner is generally different from that obtained by merely averaging the apparent-resistivity values on the right- and left-hand sides of the Lee partitioning plane and plotting this value at the position of P_0, which would then be identical to the Wenner plotting discussed above.

Although similar to the map obtained with the Wenner configuration, the theoretical map obtained with the Lee configuration, in spite of the averaging processes discussed above, exhibits characteristics of refinement that are not shown on the corresponding Wenner map. The most striking features of the Lee map in contrast with the Wenner map are: the much steeper gradient (contours closer together) at the right and left margins of the sink on the Lee map; a higher peak on the crescent-shaped high on the Lee map; and the tendency for the hachured 125-ohm-meter contour on the Lee map to be shortened, so that it encloses a smaller area than the similar contour on the Wenner map.

The Wenner and Lee field resistivity maps over a known filled sink in the Tri-State lead-zinc mining district, Cherokee County, Kans., are shown in figures 159B and 160B, respectively. The resistivity data were taken along eastward-trending horizontal profiles spaced 100 feet apart with an electrode separation of 100 feet and a station interval of 50 feet. The ratio of the resistivity of the shale constituting the filled sink to that of the surrounding limestone is known to

be approximately 30 ohm-meters to 150 ohm-meters, or 1:5. Although the shale sink beneath the anomaly is known from drilling data, test pits, and shafts to be somewhat elongate in a northerly direction, the general shape of the sink is sufficiently similar to a hemispherical sink that comparisons of the field data and the theoretical data can be made.

For the Wenner configuration, the area A of low resistivity within the interior of the sink is well shown in the central part of the diagram (fig. 159B). The crescent-shaped resistivity highs B and C are well displayed on the west and east margins, respectively, of the sink. The resistivity high D at the southeast margin of the sink may be due in part to a manifestation of the edge of the sink, but it is probably caused largely by local silicification in the limestone or by some other factor. The resistivity low outside the crescent-shaped high and lying on the east and west sides of the sink tends to be elongate in an east-west direction and to extend far beyond the margin of the sink.

For the Lee configuration, the area A of low resistivity within the interior of the sink is well shown (fig. 160B). The gradient at the margins of the sink is greater than that for the Wenner configuration. The crescent-shaped highs B and C on the west and east margins, respectively, are well defined. The resistivity high D at the southeast margin of the sink may be in part a manifestation of the edge of the sink, but it is probably due largely to local silicification in the limestone or to some other factor.

In the present theoretical and field examples, the difference between the Wenner and Lee resistivity maps is not as striking as in the corresponding theoretical horizontal profiles over a hemispherical sink. In explanation, it should be remembered that the Wenner method is inherently an averaging method whereas the Lee method is inherently a more defining method. Thus, the advantages of the Lee partitioning method are impaired by the necessity of averaging the Lee values to obtain the resistivity maps shown. However, if the averages are taken from the offset-plotted resistivity values in the manner previously described, there still remains some vestige of advantage of the Lee map over the Wenner map.

To maintain on a resistivity map the advantage of greater definition afforded by the Lee partitioning method on profiles, it may be desirable in the future to contour the ρ_1 or ρ_2 apparent-resistivity value separately for the Lee partitioning method. This method has apparently not been tried to date (1957).

In comparing the field resistivity maps shown in figures 159 and 160, one should not hastily conclude that a contour map obtained by the Wenner method
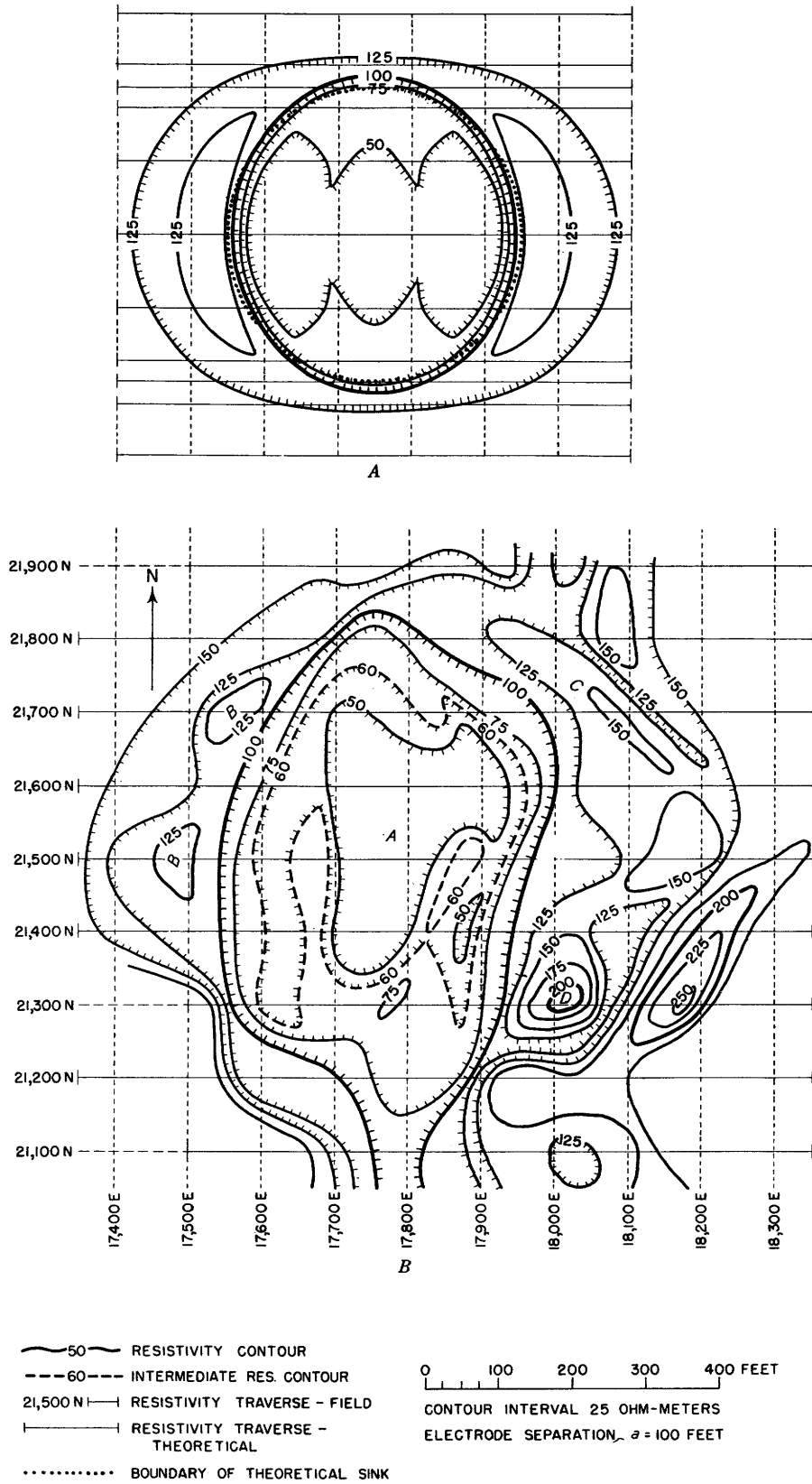
FIGURE 160.—Comparison of (A) theoretical-resistivity map over hemispherical sink (shown in dotted outline) and (B) observed field resistivity map over filled sink, Tri-State lead-zinc mining district, Cherokee County. Kans., Lee configuration. Sinks are identical to those of figure 159. Resistivity field data by K. L. Cook, 1951-54.

is almost as definitive as the map obtained by the Lee method, if the data are averaged in the manner described above. It should be emphasized that the above comparisons assume that the distance between stations for both methods is taken as $a/2$, whereas the station interval for horizontal profiling with the Wenner method is often taken as equal to a. The spacing of stations is an important factor in the comparison.

For detailed information over a hemispherical sink the resistivity profiles using the Lee partitioning method give more diagnostic information than any of the resistivity maps shown. These maps involve methods of averaging the Lee data that temper or vitiate the advantages of detail and resolution afforded by the original Lee data along the profiles.

The resistivity maps as shown help to indicate the trends and general extent of the filled sink and therefore constitute an indispensable tool to the interpreter. However, the details of the filled sink, such as the width and the exact location of the margins of the sink, are better shown in the resistivity profiles.

DETECTABILITY OF HEMISPHERICAL SINK

It can be shown from the basic equations that for traverses outside the sink the value of the electrode separation at the minimum of the curves in figure 156 (curves 5 and 6) is independent of the resistivity contrast. On this basis an equation was established to give the apparent resistivity for the electrode separation at which the minimum occurs in figure 156, curve 6. It can be reasoned that the maximum resistivity anomaly for any Wenner horizontal traverse that passes outside the hemisphere occurs when the center of the configuration is closest to the center of the sink. Therefore, since the curves in figure 156 represent the apparent resistivity for the several values of a at this point of closest approach, they can be used to determine the anomaly index for Wenner horizontal profiles taken at several distances from the center of the sink. Table 7 gives the anomaly indices for several resistivity contrasts when the value of the electrode separation is such that these indices are maximum in absolute value along a traverse that passes at a distance from the center of the sink (fig. 156, traverse 6) that is equal to the diameter of the sink. This electrode separation is about equal to the diameter of the sink.

For the Lee configuration the maximum resistivity anomaly is not found when the center of the configuration is closest to the center of the sink (see fig. 143). However, since the Lee curves for horizontal traverses removed somewhat from the sink have maximum anomalies not greatly different from the Wenner maximum anomalies, the following discussion applies equally well to the Lee data.

TABLE 7.—*Anomaly indices of Wenner horizontal profiles at a distance from the center equal to the diameter of the hemispherical sink with optimum electrode separation*

[Sign added to differentiate between maxima and minima (Data from Cook and Van Nostrand, 1954)]

Sink	k [1]	Anomaly index [2]
Perfect conductor	−1.0	−0.055
Better conductor than country rock	−.8	−.040
	−.667	[3] −.032
	−.6	−.028
	−.4	−.017
	−.2	−.008
Same conductivity as country rock	0	0
Poorer conductor than country rock	+.2	+.007
	+.4	+.013
	+.6	+.019
	+.8	+.024
Perfect insulator	+1.0	+.029

[1] $k=(\rho''-\rho')/(\rho''+\rho)$.
[2] Percent anomaly for traverses outside of sink is obtained by multiplying index number by 100.
[3] Corresponds to minimum in figure 156, curve 6.

For a given value of the electrode separation there is a distance from the hemispherical sink beyond which the sink cannot be detected. Also, in any specific area, depending on the size of the sink and resistivity contrasts involved, there is a most desirable electrode separation as well as an optimum distance between traverses. Both factors can best be determined by a careful study of the curves in figure 156 or from a similar set of curves corresponding to another known resistivity contrast.

When the usual irregularities or noise level of the resistivity readings in the field are taken into account, the anomaly of curve 6 (fig. 156) can scarcely be found. Thus, for the dimensions and resistivity contrast assumed, a traverse that passes a hemispherical filled sink at a distance from its center equal to or greater than its diameter will probably not show a recognizable anomaly. As resistivity contrasts above 5 to 1 fail to make an appreciable increase in the anomaly in such cases, this general rule is valid even for greater resistivity contrasts. Table 7 shows that for a traverse taken at a distance from the center of the sink equal to the diameter of the sink, the anomaly is only 5.5 percent of the regional resistivity value for a perfect conductor and 2.9 percent for a perfect insulator. If the noise level is of this order of magnitude, a hemispherical sink could be missed, even where there are large resistivity contrasts, when successive traverses are spaced as far apart as a distance that equals twice the diameter of the sink.

As a general rule the spacing of successive reconnaissance horizontal profiles should be made approximately equal to the diameter of the expected sink—or the average diameter if the plan of the sink is irregular. This conservative rule can be relaxed in some areas so that the traverses can be spaced with safety at a distance that equals approximately three times the

radius of the sink. A traverse spacing of twice the diameter is regarded as unsafe because a sink could be missed. As implied above, for an anomaly to be observed on at least two adjacent traverses in horizontal profiling, the traverses must be spaced no farther apart than the diameter of the expected sink.

In order to determine the optimum electrode separation to be used along reconnaissance horizontal profiles in a given area, one must compromise between small separations that give better definition across the boundary of the sink and large separations that permit detectability of the sink at greater distances from the sink. As a general rule, the electrode separation a should be made approximately equal to the radius—or one-half the average diameter if the plan of the sink is irregular—of the expected sink. This conservative rule can be relaxed in some areas so that a larger electrode separation may be safely, and perhaps advantageously, used. However, it should be cautioned that as the electrode separation is increased above an optimum amount, the value of the apparent resistivity within the sink increases rapidly. When using this rule, station intervals of $a/2$ or less are recommended for either the Lee or Wenner configuration.

LOCAL INHOMOGENEITIES

Most field men attribute to local inhomogeneities their lack of success in the use of electrical prospecting methods. Although we suspect that failure to differentiate horizontal beds is often due to lateral inhomogeneities not necessarily local, we will try to evaluate the possible effects of literally local inhomogeneities.

Using the results of our studies of filled hemispherical sinks, we can determine how large an inhomogeneity of this shape must be to show an appreciable effect on the apparent-resistivity data obtained by various techniques. It was found that the maximum anomalies occur when one of the electrodes—either a current electrode or a potential electrode—falls on the edge of the sink. The present study is therefore restricted to situations in which one of the electrodes is fixed on the edge of the sink. In order to insure a maximum effect, only inhomogeneities that are either perfectly conducting or perfectly insulating are considered. The case of the conducting inhomogeneity is probably somewhat academic. Nevertheless, the case of the insulating inhomogeneity is practical because it approximates conditions that prevail where there is a boulder near the electrode, where large currents from the current electrode have abnormally dried out the soil surrounding the electrode, or where similar conditions exist.

Five cases have been chosen for study, but only the first of them is discussed in detail. For all, the radius of the hemisphere is taken as the unit of distance.

Case I is designated for that in which current electrode C_2 is fixed on the left edge of the sink (fig. 161). Starting with an electrode separation a equal to 2 units data are computed for increasing values of the electrode separation. As indicated above, the main purpose is to determine how small the inhomogeneity must be in comparison with the electrode separation in order not to influence the resistivity data appreciably. It is therefore convenient to compute the percentage deviation of the apparent-resistivity values from the regional value that is caused by the inhomogeneity. The results are shown in table 8. The percentage-deviation values are listed under ρ_1 and ρ_2 for the Lee configuration and ρ_a for the Wenner configuration. It is noted that the values of ρ_2 are influenced much more than those of ρ_1, because the inhomogeneity is closer to potential electrode p_2 than to the other potential electrodes. It is surprising to find that the electrode separation a must be nearly 15 times the radius of an insulating hemisphere, or more than 20 times the radius of a conducting hemisphere, in order for the effect on P_2 to fall below 5 percent. If the inhomogeneity is less than perfectly conducting or less than perfectly insulating, it follows that the interference which it causes would lie between the values given for the perfect insulator and perfect conductor.

A paramount question in the minds of many field men is whether the greatest interference arises when the current electrode is near the foreign body or when the potential electrode is near the foreign body. In most of our previous theoretical curves, the sharpest anomalies occur when the potential electrodes cross the boundaries. The present example affords an opportunity to study this effect when the dimensions of the foreign body are larger than, comparable to, or smaller than the electrode separation. For a body much smaller than the electrode separation, the answer is obtained immediately from the data in table 8 by comparing cases I to V for an electrode separation of 100 (see also fig. 161). For the Lee configuration, the effect on the apparent resistivity when the small foreign body is near a potential electrode is about twice the effect when the same body is correspondingly near a current electrode (see case III). For the Wenner configuration, the effect on the apparent resistivity when the small foreign body is near the potential electrode is only about 50 percent greater than the effect when the same body is correspondingly near a current electrode.

It should be emphasized that the above rule may not be generalized. The maximum effect is due to the geometry of the electrode configuration and not to the fact that the electrode affected is a potential electrode or a current electrode. For example, if we were to apply the principle of reciprocity and invert the con-
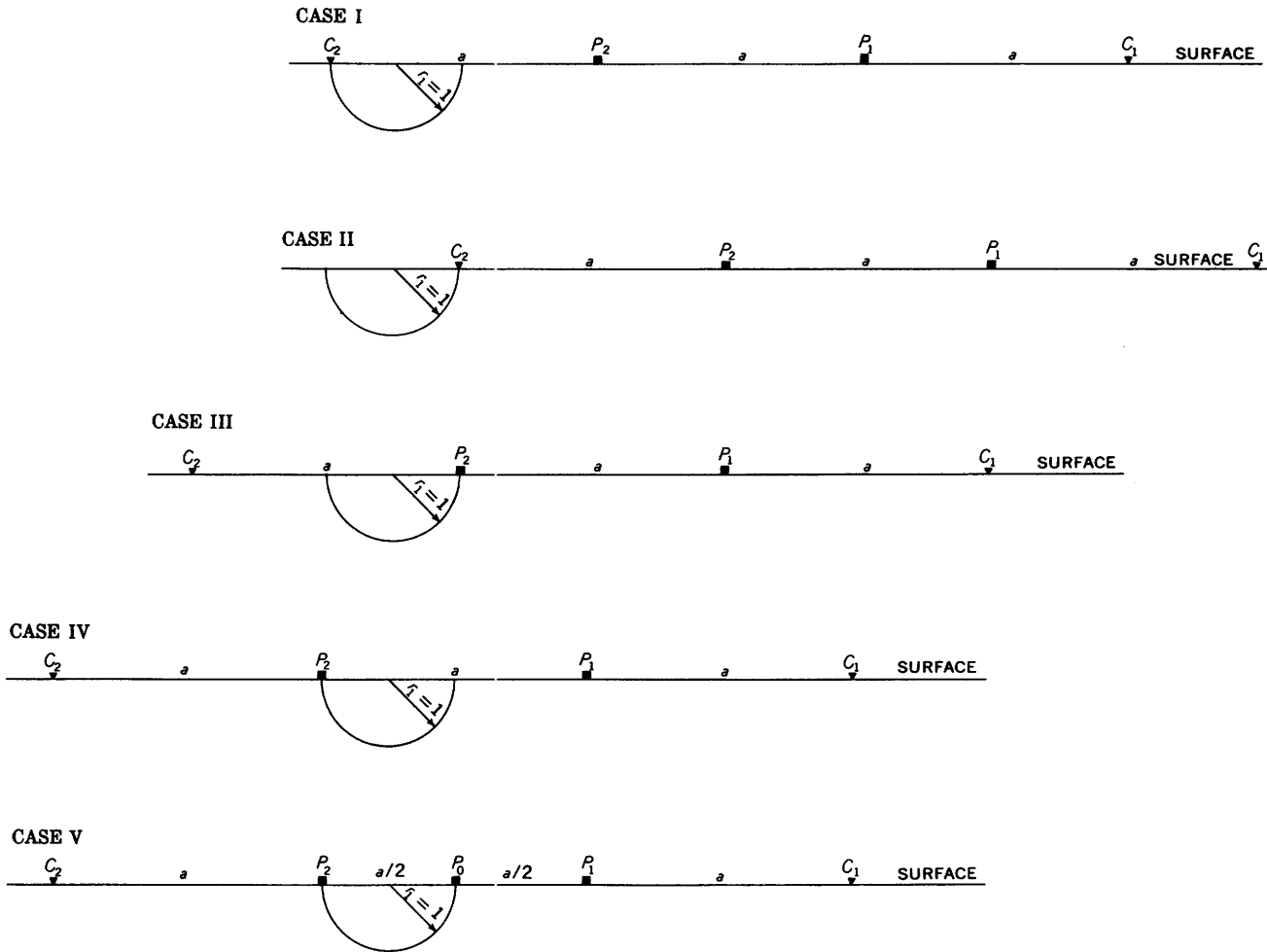
FIGURE 161.—Electrode positions used in the preparation of table 8. Each electrode shown on the edge of the hemisphere is held fixed as the configuration is expanded.

figuration by interchanging all current and potential electrodes, we would find that the greatest effect would occur when the inhomogeneity falls near a current electrode. A general rule to predict this behavior is as follows: If the distance between the potential electrodes is greater than the distance between the current electrodes, then local inhomogeneities will affect the results more where the inhomogeneities are near the current electrodes. If the distance between the current electrodes is greater than that between the potential electrodes, as it is in the usual configurations, the effect on the potential electrodes will be greater. When the rule is stated in this way, the reason becomes obvious: the effect of a foreign body on the resistivity measurement is roughly proportional to the size of the body as compared to the distance between the electrodes through which the disturbing influence is exerted.

The answer to our original question is best found in case III, which apparently yields the maximum effect for all the larger electrode separations. To broaden the meaning of case III, it should be noted that one of

the outside potential electrodes falls on the edge of the inhomogeneity and that the inhomogeneity lies between the potential electrodes and the nearest current electrode. Here, the effect on the Wenner apparent resistivity does not fall below 5 percent until the electrode separation is more than 26 times the radius for a perfectly conducting body or 13 times the radius for a perfectly insulating body. The effect on the Lee apparent resistivity ρ_2 (considering that P_2 is touching the foreign body) is more profound because the measuring electrodes are closer together. For the effect to fall below 5 percent, the electrode separation must be 50 times the radius for a perfect conductor or 25 times for a perfect insulator. For ρ_1, the effect is comparatively very small because none of the electrodes used in this measurement is near the disturbance if the electrode separation is large.

Table 8 also includes data that are valuable in evaluating potential-drop ratios. As previously pointed out, the ratio ρ_2/ρ_1 serves this purpose. The inverse of this ratio, namely, the ratio ρ_1/ρ_2, is used in places to keep

TABLE 8.—*Data showing the effect of local inhomogeneities having the shape of a hemisphere*

[The apparent resistivities are expressed as the percentage deviation from the regional value. The positive and negative columns indicate that the percentage deviation value is either greater or less, respectively, than the regional value. The Lee configuration is inferred by ρ_1 and ρ_2 and the Wenner configuration by ρ_a. The ratio ρ_2/ρ_1 or ρ_1/ρ_2 is comparable to a potential-drop ratio]

a. Perfectly conducting inhomogeneity

Electrode separation a	Case I				Case II				Case III				Case IV				Case V			
	ρ_1	ρ_2	ρ_a	ρ_2/ρ_1	ρ_1	ρ_2	ρ_a	ρ_1/ρ_2	ρ_1	ρ_2	ρ_a	ρ_2/ρ_1	ρ_1	ρ_2	ρ_a	ρ_1/ρ_2	ρ_1	ρ_2	ρ_a	ρ_1/ρ_2
	Positive				Negative				Positive				Positive	Negative			Positive	Negative		
2	35.9	148.9	92.4	1.831	13.1	32.9	23.0	1.295	35.9	148.9	92.4	1.831	-----	-----	-----	-----	-----	-----	-----	-----
3	18.5	63.7	41.1	1.381	9.9	25.6	17.7	1.210	13.0	92.2	52.6	1.702	-----	-----	-----	-----	-----	-----	-----	-----
4	12.4	40.6	26.5	1.251	7.9	20.9	14.4	1.164	6.3	67.7	37.0	1.577	40.3	100.0	29.8	-----	40.4	100.0	29.8	-----
5	9.4	29.7	19.5	1.186	6.5	17.5	12.0	1.133	3.5	53.7	28.6	1.485	14.5	61.4	23.4	2.966	33.1	53.6	10.2	2.868
6	7.6	23.4	15.5	1.147	5.6	15.1	10.4	1.112	2.3	44.8	23.5	1.415	6.1	45.8	19.9	1.959	28.1	37.9	4.9	2.063
8	5.4	16.6	11.0	1.106	4.3	11.8	8.1	1.085	1.1	33.1	17.1	1.317	2.2	31.8	14.0	1.500	21.6	25.0	1.7	1.620
10	4.2	12.8	8.5	1.083	3.6	9.8	6.7	1.068	.6	26.2	13.4	1.254	.8	24.4	11.8	1.333	17.4	18.8	.7	1.445
15	2.8	8.1	5.4	1.052	2.4	6.8	4.6	1.047	.2	17.3	8.7	1.170	.3	16.3	8.0	1.198	11.7	12.2	.2	1.271
20	2.0	5.9	4.0	1.038	1.9	5.2	3.5	1.035	.1	12.9	6.5	1.127	.1	12.2	6.1	1.140	8.8	9.0	.1	1.183
50	.8	2.3	1.5	1.015	.7	2.2	1.5	1.014	0	5.1	2.5	1.050	0	4.9	2.5	1.052	3.6	3.6	0	1.073
100	.1	1.1	.8	1.008	.4	1.1	.7	1.007	0	2.5	1.3	1.025	0	2.5	1.2	1.025	1.8	1.8	0	1.035

b. Perfectly insulating inhomogeneity

Electrode separation a	Case I				Case II				Case III				Case IV				Case V			
	ρ_1	ρ_2	ρ_a	ρ_1/ρ_2	ρ_1	ρ_2	ρ_a	ρ_2/ρ_1	ρ_1	ρ_2	ρ_a	ρ_1/ρ_2	ρ_1	ρ_2	ρ_a	ρ_2/ρ_1	ρ_1	ρ_2	ρ_a	ρ_2/ρ_1
	Negative				Positive				Negative				Negative	Positive			Negative	Positive		
2	15.2	56.8	36.0	1.963	7.4	19.4	13.4	1.112	15.2	56.8	36.0	1.961	-----	-----	-----	-----	-----	-----	-----	-----
3	8.2	26.7	17.5	1.252	5.4	14.3	9.8	1.084	6.1	46.4	23.2	1.576	-----	-----	-----	-----	-----	-----	-----	-----
4	5.7	17.8	11.8	1.148	4.2	11.4	7.8	1.068	3.0	30.9	17.0	1.403	20.7	51.8	15.5	1.914	19.8	50.9	15.5	1.882
5	4.3	13.5	8.9	1.106	3.5	9.5	6.5	1.058	1.7	25.1	13.3	1.312	7.1	31.3	12.1	1.413	16.3	26.6	5.1	1.512
6	3.5	10.9	7.2	1.083	2.9	8.1	5.5	1.050	1.1	21.1	11.1	1.254	3.2	23.3	10.0	1.274	14.0	18.8	2.4	1.382
8	2.6	8.0	5.3	1.059	2.2	6.1	4.2	1.037	.5	16.1	8.3	1.186	1.1	16.0	7.4	1.173	10.7	12.2	.7	1.256
10	2.0	6.2	4.1	1.045	1.8	5.0	3.4	1.031	.2	12.6	6.4	1.142	.2	12.0	5.9	1.122	8.6	9.0	.2	1.192
15	1.4	3.9	2.6	1.027	1.2	3.5	2.4	1.022	.1	8.5	4.3	1.092	.1	8.3	4.1	1.084	5.8	6.1	.1	1.126
20	1.0	2.9	1.9	1.019	.9	2.7	1.8	1.017	0	6.4	3.2	1.067	0	6.5	3.2	1.065	4.5	4.5	0	1.094
50	.4	1.1	.8	1.007	.4	1.1	.7	1.007	0	2.5	1.3	1.025	0	2.5	1.2	1.025	1.8	1.8	0	1.035
100	.2	.6	.4	1.004	.2	.5	.3	1.003	0	1.2	.6	1.021	0	1.2	.6	1.012	.9	.9	0	1.017

the value always greater than unity. For resistivity ratios, case IV offers the greatest effect for a perfect conductor and case III for a perfect insulator; the variation between the two cases is not great for large electrode separations. For the ratio of resistivities, it is found that the disturbance imposes an error of 5 percent when the electrode separation is 50 times the radius for a perfect conductor and 25 times the radius for a perfect insulator.

The restriction on the ratio presentation of the data is the same as the restriction on the most affected potential measurement, or apparent resistivity, that enters into the computation. It therefore follows that the potential-drop-ratio techniques would be less desirable for such applications as vertical profiling for horizontal beds than the corresponding resistivity techniques using comparable electrode configurations. For vertical profiling in horizontal-bed problems, the above results indicate that the technique of using ρ_1 and ρ_2 is preferable to using the ratio ρ_2/ρ_1 because it is possible to distinguish which one of the resistivity curves is affected by local disturbances, if one of the curves *is* so affected. If the Wenner ρ_a curve is added to the plot, the same statement is true when an inhomogeneity is affecting P_0 of the Lee configuration.

The resistivity effects of certain types of local inhomogeneities can be obtained by studying the results based on logarithmic approximations given by Kiyono (1950c). His results are applicable, for example, for a horizontal profile that crosses a small local area which is abnormally dry on the surface but which retains the normal moisture at depth. A similar example would be local areas or lenses of silicification in horizontal beds of limestone. Such features can be represented by a perfectly insulating plate of finite horizontal extent. The horizontal resistivity profiles over such features (figs. 162 and 163), especially the peaks associated with each edge of the plate, show some of the same characteristics as those over vertical dikes of several widths and resistivity contrasts. The difference between these curves and the corresponding ones for vertical dikes lies in the lack of secondary peaks, which appear and disappear as the electrode separation is changed in horizontal profiles over vertical dikes; the secondary peaks do not occur in the curves shown for the local inhomogeneity. A second difference, of course, is found in studying the lateral extent of the features.

The plate of zero depth gives a trivial solution, and therefore is not shown in figure 163. For a plate of horizontal width equal to the electrode separation a and
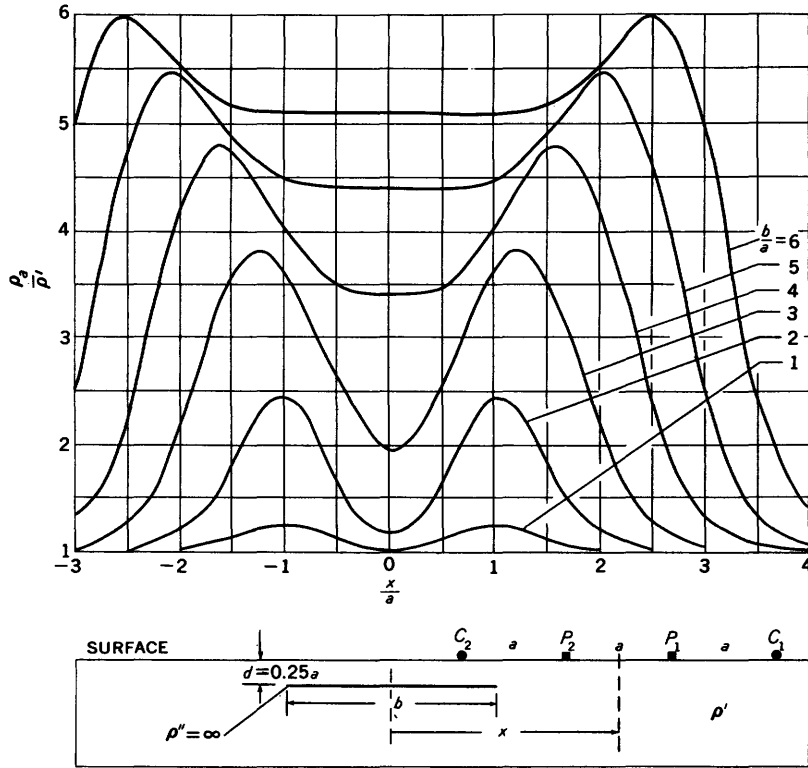
FIGURE 162.—Horizontal resistivity profiles across buried perfectly insulating thin horizontal plates of several widths b, Wenner configuration (two-dimensional approximation). For all curves, depth of overburden $d=0.25$; $a=$unity. Adapted from Kiyono (1950c) by permission of Kyōtō University.
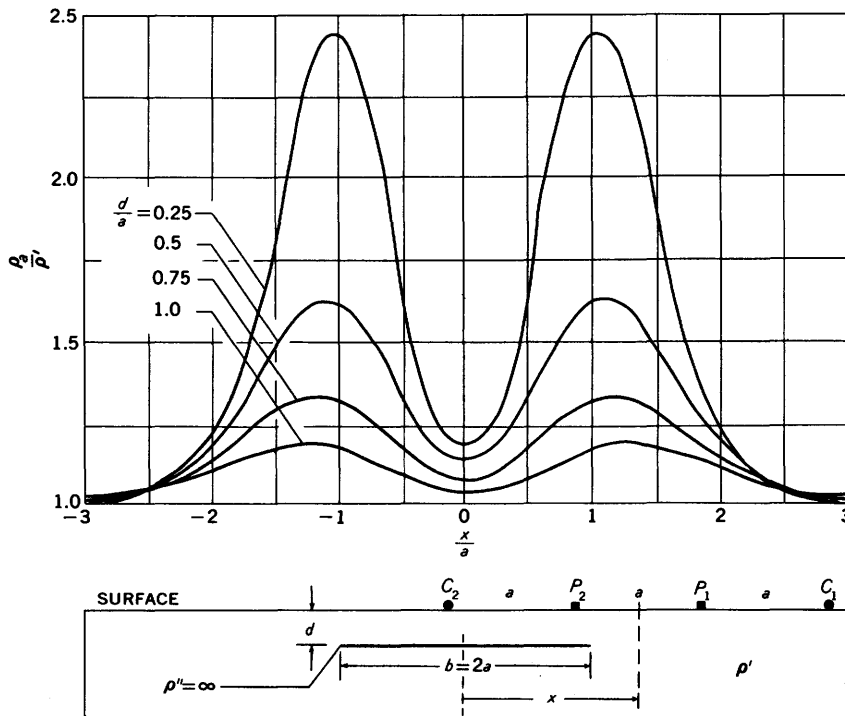
FIGURE 163.—Horizontal resistivity profiles across buried perfectly insulating thin horizontal plates of several depths of overburden d, Wenner configuration (two-dimensional approximation). For all curves, width $b=2$; $a=$unity. Adapted from Kiyono (1950c) by permission of Kyōtō University.
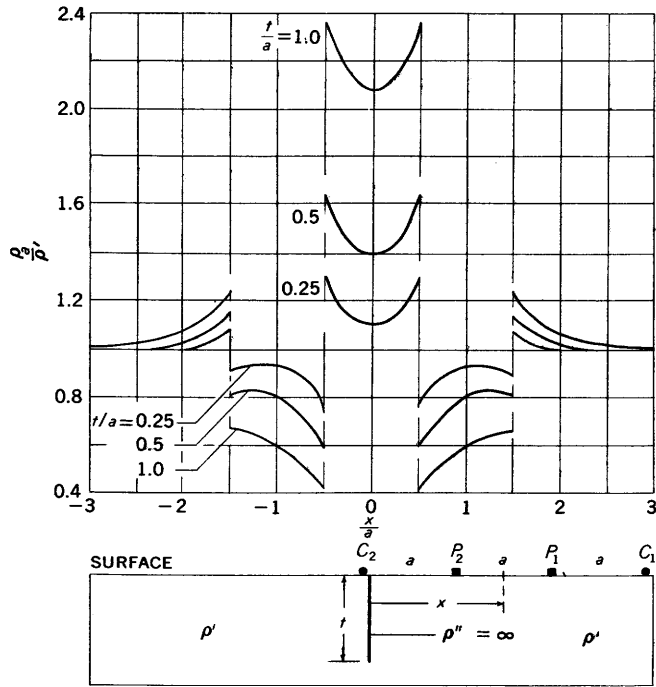
FIGURE 164.—Horizontal resistivity profiles across outcropping perfectly insulating thin vertical plates of different depths t, Wenner configuration (two-dimensional approximation); a=unity. Adapted from Kiyono (1950c) by permission of Kyōtō University.

with a depth of burial equal to $a/4$, the maximum value of the apparent-resistivity anomaly is about 25 percent. of the value of the true resistivity of the country rock. Such a local inhomogeneity would therefore usually be recognizable in the field resistivity measurements. In order for the anomaly due to such a local inhomogeneity to fall below the previously considered "noise" level of 10 percent and thus be unrecognizable, the width of the plate would probably need to be much less than the electrode separation a, provided that the depth of burial remains the same.

Another type of local inhomogeneity, for which the logarithmic approximation is also helpful, is the out-cropping fissure of finite depth. The problem generally concerns the depth of the fissure necessary to adversely affect an electrical survey. Figure 164 shows the approximate horizontal resistivity profiles for the Wenner configuration across outcropping perfectly insulating vertical fissures of several depths (Kiyono, 1950c). It is instructive to compare these curves with the corresponding curve over a vertical fissure of infinite depth given in figure 54A.

The family of curves in figure 164 shows that the interference caused by a surficial crack in the earth that extends to a depth equal to only one-fourth of the electrode separation, for example, is of the order of 20 percent. Since this anomaly is larger than the 10 percent level of noise adopted by us as an arbitrary stand-

ard, we conclude that the depth of cracks in the earth's surface must be considerably less than one-quarter of the electrode separation, or they will affect adversely an electrical survey. The portion of any such cracks that extend below the water table, however, would not ordinarily affect the resistivity measurements adversely.

Another local inhomogeneity which affects results of electrical surveys, especially in mining areas, is an open pit which lies near a given traverse. The usual problem is how close the profile may be to the pit before corrections must be applied; if corrections are necessary, it is desirable to know how to make them readily. The apparent-resistivity curves in the upper part of figure 165 show the effects of such an open pit of hemispherical shape and of infinite resistivity on vertical profiles taken along traverses at different distances from the pit. The curves in the lower part of the same figure are for a corresponding local inhomogeneity of perfect conductivity; but for problems involving disturbing effects, the lower set of curves are not as useful as the upper. Both sets of curves were obtained from equation 219. For profiles that lie completely outside the
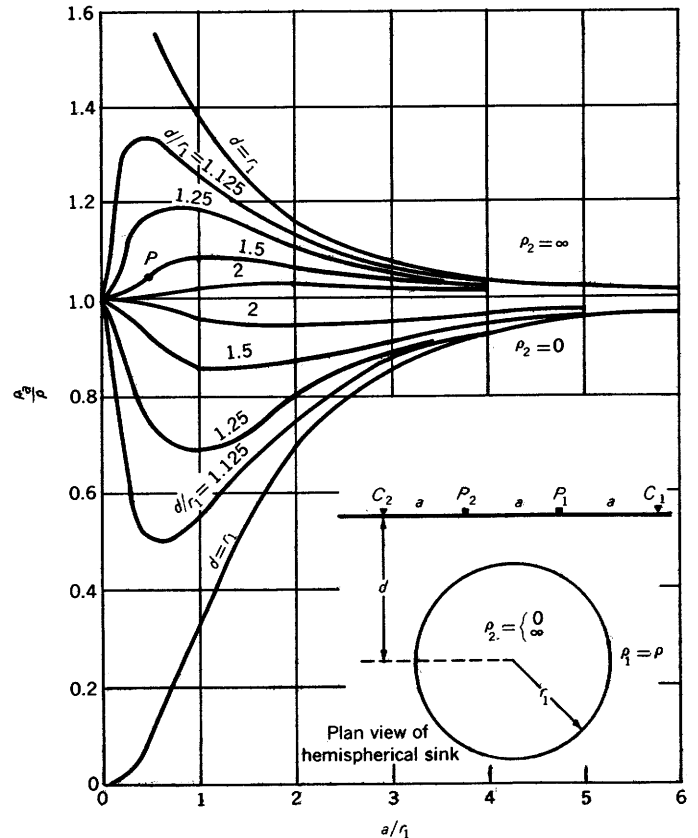
FIGURE 165.—Vertical resistivity profiles taken at several distances from a filled hemispherical sink of radius r_1. Upper curves for perfectly insulating sink; lower curves for perfectly conducting sink; d=perpendicular distance between profile and center of sink.

pit, as in the present example, the maximum effect of the pit occurs when the configuration is symmetrically placed with respect to the pit. Therefore, the curves serve equally well to evaluate the maximum anomalies obtained with horizontal resistivity profiles along the same given traverses.

As an example, suppose an electrode separation of 100 feet is being used in the vicinity of an open hemispherical pit having a radius of 200 feet. The ratio a/r_1 is then $\frac{1}{2}$; therefore, attention is directed to points on the upper set of curves for this value. If it is desired to keep the influence of the pit below a value equal to 5 percent of the regional resistivity value of the surrounding country rock (see fig. 165, point P), the traverse must be taken at least 100 feet from the edge of the pit.

BURIED MASSES AND STRUCTURES

The interpretation of resistivity data over buried three-dimensional masses and structures is difficult. Even for the simplest of buried bodies, the sphere, the mathematics is complex. Only a few papers are available that give an exact theoretical treatment of the problem of buried masses and structures. The exact solutions are limited to bodies of second-order surfaces, such as the sphere, prolate spheroid, oblate spheroid, and similar masses; solutions for these special problems are available even for finite resistivity contrasts. The remaining papers on the subject, also few in number, are restricted to approximate solutions that generally are based on two-dimensional or logarithmic approximations. Further, these solutions generally are limited to buried bodies that are either perfectly conducting or perfectly insulating.

THEORY

In previous problems a single foreign body was assumed to exist within an otherwise infinite and homogeneous space. In the geophysical application of the solution, the surface of the earth was considered as a plane of symmetry passing through the foreign body. Problems in the present section differ in that two identical foreign bodies must now be considered for each case; one body is the mirror image of the other, as if it were reflected from the surface of the earth, which acts as the mirror. The interaction between the original body and its image causes the mathematics to be complex.

As a first approximation, the potential anomaly due to a buried foreign body in the field of a point electrode on the surface of the earth can be considered equivalent to twice the anomaly that would be observed if both the point electrode and the same foreign body were buried in an otherwise infinite and homogeneous earth.

If the foreign body is close to the earth's surface, such an approximation is crude because it does not take into account the interaction between the body and its image. The approximation becomes increasingly valid, however, as the depth of the foreign body increases.

For spheres, Webb (1931a) showed that approximate formulas of this type are sufficiently accurate for computing potentials where the depth of the center of the sphere is greater than three times the radius of the sphere. However, we will show later that this depth is well beyond that at which spheres can ordinarily be detected by electrical methods. Therefore, such approximations are principally of academic interest only.

Another useful approximation to three-dimensional problems is afforded by the logarithmic potential or two-dimensional analysis (see fig. 14). One of the best methods of solving two-dimensional problems is the use of conformal mapping. Therefore, an example of conformal mapping is given as applied to the solution of the buried-vertical-fault problem. In addition, several examples of theoretical curves based on this type of solution are shown.

These approximations form useful tools to study qualitatively the characteristics of resistivity curves. The normal noise level (random variation) in resistivity work is often as high as 10 percent, which is of the same order of magnitude as the error introduced by using the approximations. For quantitative interpretation, however, exact theoretical curves are usually necessary. Proper instruments and field techniques may minimize the random fluctuations in the field curves.

Exact solutions for buried-structure problems usually involve functions that as yet have not been thoroughly investigated. Moreover, numerical tables for most of these functions do not exist, and for many problems the exact solutions themselves have not been worked out. Therefore, we must confine our study of buried-structure problems largely to inductive reasoning based on approximate solutions. There are amenable to exact solution, however, a series of buried-structure problems that may be applied to geologic situations. The exact solutions of these problems are so complicated that they offer little encouragement for large-scale numerical computation. In this study, without sample curves, they are little more than a series of exercises in potential theory, and are included here mainly to offer future workers one more stepping stone toward the eventual realization of useful theoretical curves.

In the special case of the buried conducting sphere, the mathematics is comparatively simple. Therefore, the solution for this problem is developed in detail so that it can be used to draw conclusions concerning the capabilities of electrical prospecting methods in general.

BURIED SPHERES

The general problem of a buried mass involving an arbitrary resistivity contrast between it and the surrounding country rock is especially difficult, owing to the double effect of the inhomogeneity and the earth's surface. Webb (1931a, b) published complete solutions not only to the problem of a buried sphere with an arbitrary resistivity contrast, but also the more general problem of a buried spheroid with arbitrary resistivity contrast. The solutions to the general problem of the spheroid do not lend themselves well to large-scale numerical computations. The solutions for the sphere of arbitrary resistivity are only slightly better in that respect. However, we now offer a new method for solving the special case of a perfectly conducting sphere in order to illustrate a means of circumventing the unique difficulties encountered in this type of problem.

To solve the problem of a buried mass of foreign material that can be approximated by a buried sphere with perfect conductivity (fig. 166), we use bipolar
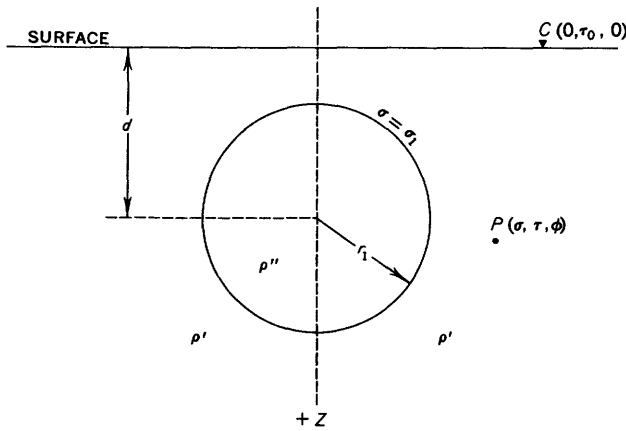

FIGURE 166.—Cross section of a point source of current C on the surface of the earth in the vicinity of a buried sphere of radius r_1.

coordinates and require solutions of Laplace's equation given by equation 96. The surface of the earth, on which is placed the point electrode C, is designated as the xy-plane where $\sigma = 0$. The positive z-axis is downward. The surface of the sphere is described as $\sigma = \sigma_1$. The resistivity outside the sphere is $\rho' = \rho$ ohm-meters and that inside is $\rho'' = 0$. The radius of the sphere, r_1, and the depth of its center, d, can be obtained from the equation for the sphere given immediately prior to equation 90.

In the region outside the sphere, σ ranges only from 0 to σ_1 so that both exponential terms may be retained in the general equation 96. The coefficients of both terms must be equal, however, in order that no current crosses the earth's surface. The expression for the

potential outside the sphere due to a point source of current is, therefore,

$$U = \frac{I\rho}{2\pi} \left\{ \frac{1}{R} + \frac{(1-\cos \tau_0)^{\frac{1}{2}}(\cosh \sigma - \cos \tau)^{\frac{1}{2}}}{b} \right.$$

$$\left. \times \sum_{n=0}^{\infty} \sum_{m=0}^{n} (2-\delta_{0m}) \frac{(n-m)!}{(n+m)!} \right.$$

$$\left. \times A_n{}^m \cosh (N\sigma) \; P_n{}^m (\cos \tau_0) P_n{}^m (\cos \tau) \cos m\phi \right\}, \quad (221)$$

where $N = n + \frac{1}{2}$. We have chosen the form of the expansion in equation 221 to conform to the known expansion for $1/R$. The potential within the sphere has some unknown constant value U_1. We thus have two unknowns, $A_n{}^m$ and U_1, which have to be determined from the boundary conditions.

The first boundary condition is obviously that the potential must equal U_1 at the surface of the sphere where $\sigma = \sigma_1$. If we substitute the expansion for $1/R$ (equation 125), we can write

$$U_1 = \frac{I\rho}{2\pi b} (1-\cos \tau_0)^{\frac{1}{2}} (\cosh \sigma_1 - \cos \tau)^{\frac{1}{2}} \sum_{n=0}^{\infty} \sum_{m=0}^{\infty} (2-\delta_{0m}) \frac{(n-m)!}{(n+m)!}$$

$$\times [e^N + A_n{}^m \cosh N\sigma_1] P_n{}^m (\cos \tau_0) P_n{}^m (\cos \tau) \cos m\phi. \quad (222)$$

We can expand $(\cosh \sigma - \cos \tau)^{-\frac{1}{2}}$ by converting the hyperbolic cosine to its exponential form and by manipulating the expression so that it is analogous to the development in equation 103. Thus we have

$$(\cosh \sigma - \cos \tau)^{-\frac{1}{2}} = \sqrt{2} \sum_{n=0}^{\infty} e^{-(n+\frac{1}{2})\sigma} P_n (\cos \tau). \quad (223)$$

By differentiating both sides of this equation, we obtain a second useful expansion

$$(\cosh \sigma - \cos \tau)^{-\frac{1}{2}} \sinh \sigma = 2\sqrt{2} \sum_{n=0}^{\infty} (n+\frac{1}{2}) e^{-(n+\frac{1}{2})\sigma} P_n (\cos \tau). \quad (224)$$

Dividing both sides of equation 223 by $(\cosh \sigma_1 - \cos \tau)^{\frac{1}{2}}$ and using the first of the above expansions, we obtain

$$U_1 \sqrt{2} \sum_{n=0}^{\infty} e^{-N\sigma_1} P_n (\cos \tau) = \frac{I\rho}{2\pi b} (1-\cos \tau_0)^{\frac{1}{2}}$$

$$\times \sum_{n=0}^{\infty} \sum_{m=0}^{n} (2-\delta_{0m}) \frac{(n-m)!}{(n+m)!} [e^{-N\sigma_1}$$

$$+ A_n{}^m \cosh N\sigma_1] P_n{}^m (\cos \tau_0) P_n{}^m (\cos \tau) \cos m\phi. \quad (225)$$

As the left side of equation 225 contains no terms in which $m \neq 0$, the terms on the right side of the equation in which $m \neq 0$ must vanish if the equality is to hold for all values of ϕ. This can happen only if the term in brackets vanishes separately for each value of m. Thus we find that

$$A_n{}^m = -\frac{e^{-N\sigma_1}}{\cosh N\sigma_1}$$

when m does not equal zero.

We are able to determine the coefficients A_n which remain by applying Gauss's theorem to the sphere. Mathematically, this theorem is expressed as

$$\frac{1}{\rho}\int (\nabla U)_\sigma ds_\sigma = 0,$$

where the integration is to be carried out over the entire surface of the sphere. In physical terms, this integral states that just as much current must flow out of the sphere as flows in. We get $(\nabla U)_\sigma$ and ds_σ from equations 93 and 92, respectively. Substituting for these expressions and canceling factors where possible, we get for the integral:

$$\sum_{n=0}^{\infty}\sum_{m=0}^{n}(2-\delta_{0m})\frac{(n-m)!}{(n+m)!}\int_0^{2\pi}\cos m\phi d\phi \int_0^\pi \sin \tau d\tau$$

$$\times\left[\frac{\sinh \sigma_1}{2(\cosh \sigma_1-\cos \tau)^{3/2}}(e^{-N\sigma_1}+A_n{}^m \cosh N\sigma_1)\right.$$

$$\left.+\frac{N}{(\cosh \sigma_1-\cos \tau)^{1/2}}(-e^{-N\sigma_1}+A_n{}^m \sinh N\sigma_1)\cdot\right]$$

$$\times P_n{}^m (\cos \tau_0)P_n{}^m (\cos \tau)=0. \quad (226)$$

Integrating over ϕ, we find that there persists only the terms for which $m=0$, and we are left with

$$\sum_{n=0}^{\infty}P_n (\cos \tau_0)\int_0^\pi P_n (\cos \tau) \sin \tau\, d\tau \left[\frac{\sinh \sigma_1}{2(\cosh \sigma_1-\cos \tau)^{3/2}}\right.$$

$$\times(e^{-N\sigma_1}+A_n \cosh N\sigma_1)+\frac{N}{(\cosh \sigma_1-\cos \tau)^{1/2}}$$

$$\left.\times(-e^{-N\sigma_1}+A_n \sinh N\sigma_1)\right]=0.$$

The second integration is easily carried out if we substitute the expressions given by equations 223 and 224. After these substitutions are made, equation 226 becomes

$$\sum_{n=0}^{\infty}P_n (\cos \tau_0)\int_0^\infty P_n (\cos \tau) \sum_{j=0}^{\infty}P_j (\cos \tau) \sin \tau d\tau[(j+1/2)$$

$$\times(e^{-N\sigma_1}+A_n \cosh N\sigma_1)+N(-e^{-N\sigma_1}+A_n \sinh N\sigma_1)]e^{-(j+1/2)\sigma_1}=0.$$

In the integration over τ, we make use of the orthogonality of the Legendre polynomials to eliminate all terms for which $n\neq j$. Therefore, we have

$$\sum_{n=0}^{\infty}A_n (\cosh N\sigma_1+\sinh N\sigma_1)e^{-N\sigma_1}P_n (\cos \tau_0)=\sum_{n=0}^{\infty}A_nP_n (\cos \tau_0)=0,$$

which can be true for any value of τ_0 only if A_n is zero. Therefore, we finally have for the potential due to a point source outside a buried conducting sphere:

$$U=\frac{I\rho}{2\pi}\left\{\frac{1}{R}-\frac{2}{b}(1-\cos \tau_0)^{1/2}(\cosh \sigma-\cos \tau)^{1/2}\sum_{n=1}^{\infty}\sum_{m=1}^{n}\frac{(n-m)!}{(n+m)!}\right.$$

$$\left.\times\frac{e^{-N\sigma_1}\cosh N\sigma}{\cosh N\sigma_1}P_n{}^m (\cos \tau_0)P_n{}^m (\cos \tau) \cos m\phi\right\}. \quad (227)$$

An easier form for computations, which is found by using the addition theorem (equation 101) for Legendre polynomials, is

$$U=\frac{I\rho}{2\pi}\left\{\frac{1}{R}-\frac{1}{b}(1-\cos \tau_0)^{1/2}(\cosh \sigma-\cos \tau)^{1/2}\right.$$

$$\left.\times\sum_{n=1}^{\infty}\frac{e^{-N\sigma_1}\cosh N\sigma}{\cosh N\sigma_1}[P_n (\cos \gamma)-P_n (\cos \tau_0)P_n (\cos \tau)]\right\}, \quad (228)$$

where, as in equation 99,

$$\cos \gamma = \cos \tau_0 \cos \tau + \sin \tau_0 \sin \tau \cos \phi.$$

VOLCANIC NECKS AND CONES

Let us assume that a volcanic neck may be approximated by a cone whose apex is at the earth's surface. Obviously such an assumption is not valid in the immediate vicinity of the apex of the volcanic neck, because the apex of an actual volcanic neck is not a definite mathematical point; but the approximation is adequate at short distances from the cone.

To describe the cone we use spherical coordinates with the origin at the apex of the cone (fig. 167). The
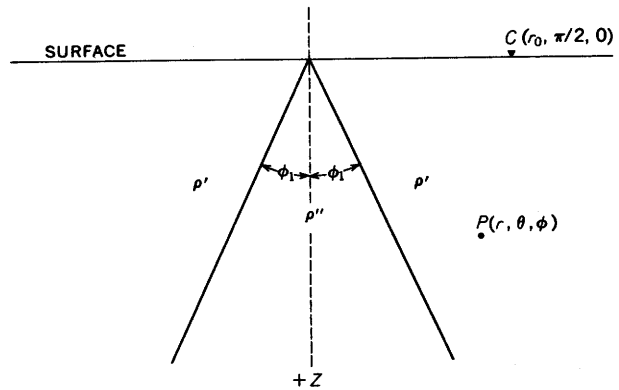
FIGURE 167.—Cross section of a cone-shaped volcanic neck.

surface of the cone is defined by the equation $\theta=\theta_1$. The resistivity is ρ' outside the cone, and ρ'' within the cone. A current electrode is at point $C(r_0, \pi/2, 0)$. We require solutions of Laplace's equation of the form given in equation 63, which contains the cone functions.

In the region of resistivity ρ', which contains no part of the polar axis, both of the Legendre functions must be retained in the solution. The coefficients of both of these Legendre functions must be equal; otherwise there would be a potential gradient (current flow) across the earth's surface. In the region of resistivity ρ'', where $\cos \theta$ becomes plus one, we must discard $P_{ip-\frac{1}{2}}^m (-\cos \theta)$ from the general solution in order to keep the solution finite in the region of interest.

Therefore, the two potential functions are

$$U_{1A}=\frac{I\rho'}{2\pi}\left\{\frac{1}{R}+\frac{1}{\sqrt{r_0 r}}\sum_{m=0}^{\infty}\cos m\phi\int_0^{\infty}A_m(p)[P_{ip-\frac{1}{2}}^m(\cos\theta)\right.$$

$$\left.+P_{ip-\frac{1}{2}}^m(-\cos\theta)]\cos(p\ln r/r_0)\ dp\right\}$$

$$U_{2A}=\frac{I\rho'}{2\pi}\left\{\frac{1}{R}+\frac{1}{\sqrt{r_0 r}}\sum_{m=0}^{\infty}\cos m\phi\right.$$

$$\left.\times\int_0^{\infty}B_m(p)\,P_{ip-\frac{1}{2}}^m(\cos\theta)\cos(p\ln r/r_0)\ dp\right\}.$$

In arriving at the form of the solutions, we have anticipated the dependence on r_0 from our knowledge of the expression for the reciprocal distance in terms of these functions (equation 129). The limits of integration have also been made to conform to that expansion.

Substituting the expansion for $1/R$, applying the boundary conditions that the potential and normal component of the current density must be continuous across the surface $\theta=\theta_1$, and solving the resulting simultaneous equations, we obtain the two arbitrary constants, $A_m(p)$ and $B_m(p)$. Substituting these constants in the original equations, we get the final solutions:

$$U_{1A}=\frac{I\rho'}{2\pi}\left\{\frac{1}{R}+\frac{(\rho''-\rho')}{\sqrt{r_0 r}}\sum_{m=0}^{\infty}\frac{(2-\delta_{0m})\cos m\phi}{(-1)^m}\right.$$

$$\times\int_0^{\infty}\frac{P_{ip-\frac{1}{2}}^m(\cos\theta)+P_{ip-\frac{1}{2}}^m(-\cos\theta)}{\rho'-\rho''+\rho'\psi_p^m(\cos\theta_1)+\rho''\psi_p'^m(\cos\theta_1)}$$

$$\left.\times\frac{\Gamma(\frac{1}{2}+ip-m)}{\cosh n p\Gamma(\frac{1}{2}+ip+m)}\cos(p\ln r/r_0)P_{ip-\frac{1}{2}}^m(0)dp\right\}$$

$$U_{2A}=\frac{I\rho'\rho''}{2\pi\sqrt{r_0 r}}\sum_{m=0}^{\infty}\frac{(2-\delta_{0m})\cos m\phi}{(-1)^m}$$

$$\times\int_0^{\infty}\frac{\psi_p^m(\cos\theta_1)+\psi_p'^m(\cos\theta_1)}{\rho'-\rho''+\rho'\psi_p^m(\cos\theta_1)+\rho''\psi_p'^m(\cos\theta_1)}$$

$$\times\frac{\Gamma(\frac{1}{2}+ip-m)}{\cosh\pi p\Gamma(\frac{1}{2}+ip+m)}$$

$$\times\cos(p\ln r/r_0)P_{ip-\frac{1}{2}}^m(0)P_{ip-\frac{1}{2}}^m(\cos\theta)dp.\quad(229)$$

In the second of these equations, it is more convenient to include the expansion for $1/R$ in the final form. For computational purposes, however, the integral

SURFACE   PIPE $C(r_0, 0, 0)$

ρ' ρ'' ρ' $P(r,\phi,z)$

$\leftarrow r_1 \rightarrow \leftarrow r_1 \rightarrow$

$+Z$

FIGURE 168.—Cross section of a volcanic pipe.

would probably converge faster if $1/R$ were removed as it is in U_{1A}.

A volcanic pipe is essentially a cylindrical mass of igneous material standing vertically. A solution for this problem is obtained simply by an adaptation of equations 216 and 217. The xy-plane ($z=0$) is taken as the surface of the earth, and the positive z-axis is downward (fig. 168). The surface of the cylinder is the surface $r=r_1$. The resistivity of the country rock is ρ' and that of the pipe is ρ''. The modifications necessary in equations 216 and 217 for the present problem are to change 4π to 2π and let $z=0$. The potential functions are then

$$U_{1A}=\frac{I\rho'}{2\pi}\left\{\frac{1}{R}-\frac{2}{\pi}(\rho''-\rho')\sum_{m=0}^{\infty}(2-\delta_{0m})\cos m\phi\right.$$

$$\left.\times\int_0^{\infty}\frac{K_m(tr_0)K_m(tr)}{\rho''\psi_m'(tr_1)-\rho'\psi(tr_1)}dt\right\}.$$

$$U_{2A}=\frac{I\rho'}{2\pi}\left\{\frac{1}{R}-\frac{2}{\pi}(\rho''-\rho')\sum_{m=0}^{\infty}(2-\delta_{0m})\cos m\phi\right.$$

$$\left.\times\int_0^{\infty}\frac{K_m(tr_0)\psi_m(tr_1)I_m(tr)}{\rho''\psi_m'(tr_1)-\rho'\psi(tr_1)}dt\right\}.\quad(230)$$

$$U_{2B}=\frac{I\rho''}{2\pi}\left\{\frac{1}{R}-\frac{2}{\pi}(\rho''-\rho')\sum_{m=0}^{\infty}(2-\delta_{0m})\cos m\phi\right.$$

$$\left.\times\int_0^{\infty}\frac{I_m(tr_0)\psi_m'(tr_1)\psi_m(tr_1)I_m(tr)}{\rho''\psi_m'(tr_1)-\rho'\psi_m(tr_1)}dt\right\}$$

$$U_{1B}=\frac{I\rho''}{2\pi}\left\{\frac{1}{R}-\frac{2}{\pi}(\rho''-\rho')\sum_{m=0}^{\infty}(2-\delta_{0m})\cos m\phi\right.$$

$$\left.\times\int_0^{\infty}\frac{I_m(tr_0)\psi_m'(tr_1)K_m(tr)}{\rho''\psi_m'(tr_1)-\rho'\psi_m(tr_1)}dt\right\}.\quad(231)$$

Equations 230 and 231 are equally applicable to a study of the effect of a perfectly conducting vertical metallic pipe on a resistivity survey. The only modification is to set ρ'' equal to zero. The effects of vertical metallic pipes are sometimes observed in areas where drill tests have been made previously and the drill casing has been left in the ground.

BURIED DOMES

We now study a buried dome with the assumed shape of an inverted hyperboloid of revolution. Mathematically, the relationship between such a dome and the cone previously discussed is that the surface of the hyperboloid approaches asymptotically the surface of a cone at large distances from the origin. Geologically, this means that the resistivity curves for a buried dome will approach asymptotically the corresponding curves for a cone-shaped structure at large distances from the origin for horizontal profiles or at large electrode separations for vertical profiles. It is understandable that
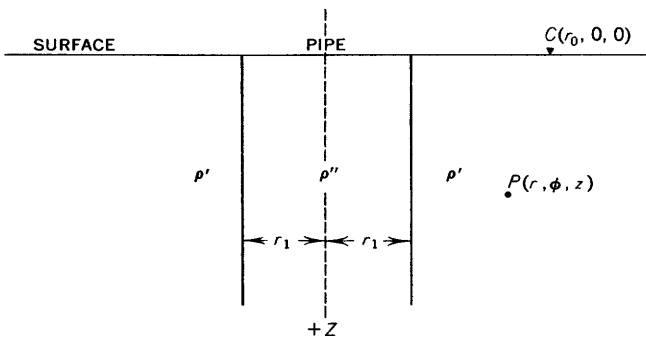
the solutions for the two problems parallel each other closely.

For the dome problem, we use prolate spheroidal coordinates with the positive polar z-axis oriented downward (fig. 169). The surface of the dome is the surface $\xi=\xi_1$. The resistivity of the country rock is ρ', and that within the dome is ρ''. A current electrode is at point $C(\eta_0, 0, 0)$. We require solutions of Laplace's equation of the form given in equation 88 which contains the hyperboloidal functions as well as the cone functions.

In the country rock, ξ ranges from 0 to ξ_1. Therefore, U_{1A} will contain both of the Legendre functions that exist in the general solution. The coefficients of both of the Legendre functions are equal in order to satisfy the condition that no current flows across the earth's surface. Within the dome, where ξ becomes plus one, we must discard $P_{ip-\frac{1}{2}}^{m}(-\xi)$ from the general solution in order to keep the solution finite in the region of interest. Thus, the two potential functions are

$$U_{1A}=\frac{I\rho'}{2\pi}\left\{\frac{1}{R}+\sum_{m=0}^{\infty}\cos m\phi\int_0^{\infty} A_m(p)[P_{ip-\frac{1}{2}}^{m}(\xi)+P_{ip-\frac{1}{2}}^{m}(-\xi)]P_{ip-\frac{1}{2}}^{m}(\eta)dp\right\}$$

$$U_{2A}=\frac{I\rho'}{2\pi}\left\{\frac{1}{R}+\sum_{m=0}^{\infty}\cos m\phi\int_0^{\infty} B_m(p)(P_{ip-\frac{1}{2}}^{m}(\xi)P_{ip-\frac{1}{2}}^{m}(\eta)dp\right\}. \quad (232)$$

Substituting the expansion for $1/R$ (equation 134), applying the boundary conditions that the potential and normal component of the current density must be continuous across the surface $\xi=\xi_1$, and solving the resulting simultaneous equations, we obtain the two arbitrary constants $A_m(p)$ and $B_m(p)$. Substituting these constants in the original equations 232, we get the following final solutions:

$$U_{1A}=\frac{I\rho'}{2\pi}\left\{\frac{1}{R}+\frac{\pi}{b}(\rho''-\rho')\sum_{m=0}^{\infty}(2-\delta_{0m})\cos m\phi\right.$$

$$\times\int_0^{\infty}\frac{p\tanh\pi p}{\cosh\pi p}\frac{\Gamma^2(\frac{1}{2}+ip-m)}{\Gamma^2(\frac{1}{2}+ip+m)}$$

$$\times\left[\frac{P_{ip-\frac{1}{2}}^{m}(\xi)+P_{ip-\frac{1}{2}}^{m}(-\xi)}{\rho'-\rho''+\rho'\psi_p^{m}(\xi_1)+\rho''\psi_p'^{m}(\xi_1)}\right]$$

$$\left.\times P_{ip-\frac{1}{2}}^{m}(0)P_{ip-\frac{1}{2}}^{m}(\eta_0)P_{ip-\frac{1}{2}}^{m}(\eta)dp\right\}$$

$$U_{2A}=\frac{I\rho'}{2\pi}\left(\frac{\pi\rho''}{b}\right)\sum_{m=0}^{\infty}(2-\delta_{0m})\cos m\phi$$

$$\times\int_0^{\infty}\frac{p\tanh\pi p}{\cosh\pi p}\frac{\Gamma^2(\frac{1}{2}+ip-m)}{\Gamma^2(\frac{1}{2}+ip+m)}$$

$$\times\left[\frac{\psi_p^{m}(\xi_1)+\psi_p'^{m}(\xi_1)}{\rho'-\rho''+\rho'\psi_p^{m}(\xi_1)+\rho''\psi_p'^{m}(\xi_1)}\right]$$

$$\times P_{ip-\frac{1}{2}}^{m}(0)P_{ip-\frac{1}{2}}^{m}(\xi)P_{ip-\frac{1}{2}}^{m}(\eta_0)P_{ip-\frac{1}{2}}^{m}(\eta)dp. \quad (233)$$

As in the solution for cones, it is more convenient to express U_{2A} with the expansion for $1/R$ included in the integral. These solutions can be changed to the cone solutions by considering them in the limit as $b\rightarrow0$.

The analysis just used for the buried-dome problem can be used also, with slight modification, for the problem of certain topographic effects on electrical surveys. The effects of hills and depressions, for example, can be obtained by using prolate spheroidal coordinates, provided that the shape of these features approximates a hyperboloid of revolution. The surface
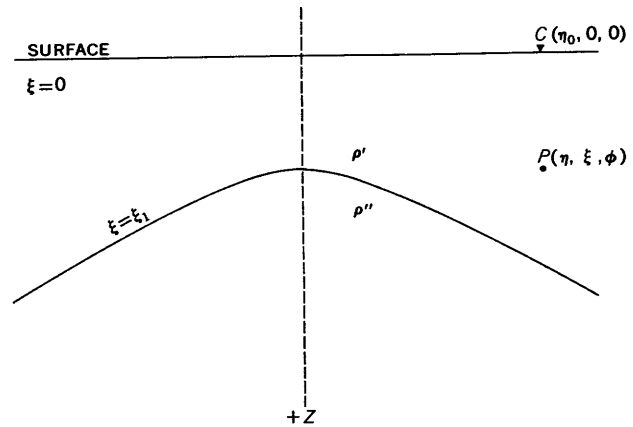
FIGURE 169.—Cross section of a buried dome structure.

of the hill can be described by the surface $\xi=\xi_1$, in prolate spheroidal coordinates (fig. 169), which are oriented with the positive polar axis downward. As usual, $\phi_0=0$, but now the point current electrode is assumed to lie within the earth at the point $C'(\eta_0, \xi_0, 0)$. The resistivity of the earth (where $\xi>\xi_1$) is ρ. Only one potential function is needed in this case, and it is comparatively simple. Since the earth contains points where $\xi=1$, the term containing $P_{ip-1/2}^{m}(-\xi)$ can be discarded from the general solution (equation 88). Therefore, we have

$$U=\frac{I\rho}{4\pi}\left\{\frac{1}{R}+\frac{\pi}{b}\sum_{m=0}^{\infty}(2-\delta_{0m})\cos m\phi\right.$$

$$\times\int_0^{\infty}A_m(p)\frac{p\tanh\pi p}{\cosh\pi p}\frac{\Gamma^2(\frac{1}{2}+ip-m)}{\Gamma^2(\frac{1}{2}+ip+m)}$$

$$\left.\times P_{ip-\frac{1}{2}}^{m}(\xi)P_{ip-\frac{1}{2}}^{m}(\eta_0)P_{ip-\frac{1}{2}}^{m}(\eta)dp\right\}, \quad (234)$$

where the form has been chosen according to the previous knowledge of the expansion for $1/R$ (equation 134). Substituting the expansion for $1/R$ and differentiating with respect to ξ, we obtain the normal com-

ponent of current on the boundary:

$$\frac{\partial U}{\partial \xi}\bigg|_{\xi=\xi_1} = \frac{I\rho}{4\pi}\left(\frac{\pi}{b}\right)\sum_{m=0}^{\infty}(2-\delta_{0m})\cos m\phi$$

$$\times \int_0^\infty \frac{p\tanh \pi p}{\cosh \pi p}\frac{\Gamma^2(\tfrac{1}{2}+ip-m)}{\Gamma^2(\tfrac{1}{2}+ip+m)}$$

$$\times [P_{ip-\nu}^m(\xi_0)\,P_{ip-\nu}'^m(-\xi_1)+A_m(p)\,P_{ip-\nu}'^m(\xi_1)]$$

$$\times P_{ip-\nu}^m(\eta_0)\,P_{ip-\nu}^m(\eta)\,dp.$$

The primes indicate differentiation with respect to ξ.

The derivative of U is equated to zero, in order to apply the boundary condition that no current crosses the earth's surface; and the resulting equation is solved for $A_m(p)$. By substituting the expression into equation 234 and by letting ξ_0 approach ξ_1, we obtain the desired potential function on the surface of the hill:

$$U=\frac{I\rho}{4\pi}\Bigg\{\frac{1}{R}+\frac{\pi}{b}\sum_{m=0}^{\infty}(2-\delta_{0m})\cos m\phi$$

$$\times \int_0^\infty \frac{p\tanh \pi p}{\cosh \pi p}\frac{\Gamma^2(\tfrac{1}{2}+ip-m)}{\Gamma^2(\tfrac{1}{2}+ip+m)}$$

$$\times \frac{P_{ip-1/2}^m(\xi_1)}{\psi_p'^m(\xi_1)}\,P_{ip-\nu}^m(\xi)\,P_{ip-\nu}^m(\eta_0)\,P_{ip-\nu}^m(\eta)\,dp\Bigg\}. \quad (235)$$

A closer examination of the coordinate system reveals that equation 235 serves two purposes. If ξ_1 is positive, the equation applies to a point current electrode near the crest of a hill. If ξ_1 is negative, the equation applies in the same manner to a point current electrode near the bottom of a bowl-shaped depression.

By analogy with the dome problem and its solution it is seen that anticlinal structures can be studied by using a cylindrical coordinate system in which the cross section is similar to that in figure 169. Such systems are called elliptical cylindrical coordinates. Similarly, synclinal structures can be studied by using the same elliptical cylindrical coordinate system when the elliptical cylinders form the boundary surfaces.

BURIED VERTICAL FAULT

Several types of difficult two-dimensional problems, such as the buried vertical fault, can be solved approximately by conformal mapping. The theory of conformal mapping is outlined here to show how it can be used for the buried vertical fault. Specific apparent-resistivity profiles, which are obtained from this type of analysis for several two-dimensional features, will be shown later (p. 268 to 274). Our development of the subject follows that by Kunetz and Chastenet de Géry (1956) in the study of telluric currents over buried structures. For the details of the analysis the reader is referred to any standard text on the subject (for example, Morse and Feshbach, 1953, p. 443–453).

A conformal transformation is an operation that establishes a relation between the points on two different planes, and at the same time preserves the angles; in other words, if two curves intersect at a given angle in one plane, the corresponding curves in the second plane will intersect at the same angle. Analytically, such a transformation is expressed most easily by the aid of complex numbers. The transformation from the coordinates ξ and η in the ζ-plane to the coordinates x and y in the z-plane is represented by a relation of the type $\zeta=f(z)$, where $f(z)$ must be an analytic function. It is recalled that $z=x+iy$ and $\zeta=\xi+i\eta$, where $i=\sqrt{-1}$. Also, where x and y are both considered to be functions of ξ and η, the Cauchy equations have to be fulfilled; that is,

$$\frac{\partial x}{\partial \xi}=\frac{\partial y}{\partial \eta}\quad\text{and}\quad\frac{\partial x}{\partial \eta}=-\frac{\partial y}{\partial \xi}.$$

Since x and y, as functions of ξ and η, obey Cauchy's equations, they also are harmonic and obey Laplace's equation. Thus, we confirm that the potential at a given point in one plane is also the valid potential at the corresponding point in the second plane. This principle will become increasingly clear in a simple example that will be explained before beginning the problem of the buried fault itself.

Several general methods exist for transforming a half plane or the interior of a circle into the interior of an area bounded by a series of curvilinear segments. Most of these methods, however, do not lend themselves well to practical problems. Swartz's method of representing a polygon in a half plane is simple, useful, and usually practical, and it is the most commonly used technique for transformation. Specifically, Swartz's transformation consists of representing the differential of the function $z=f(\zeta)$ in the form of a product

$$dz=(\zeta-a_1)^{-\alpha_1/\pi}(\zeta-a_2)^{-\alpha_2/\pi}(\zeta-a_3)^{-\alpha_3/\pi}\ldots d\zeta, \quad (236)$$

where the a's and α's are real numbers. The a's are chosen so that $a_1>a_2>a_3\ldots$; thus, $\zeta=a_1$, $\zeta=a_2$, $\ldots$ represent successive points on the real axis. Similarly, the α's are angles that lie between $-\pi$ and π.

The meaning of these constants can be best realized by examining this generalized transformation in detail (fig. 170). If, for example, we start at positive infinity on the ξ-axis in the ζ-plane and proceed in the negative direction, our path transforms into the z-plane as shown in the diagram. As we pass each critical point in the ζ-plane, our path in the z-plane turns through an angle α that corresponds to the given point in equation 236. The number and values of the angles are such that our path brings us back to the starting point in the z-plane. In practice the starting point is arbitrary, and for this reason the point in the diagram is chosen off the real axis.
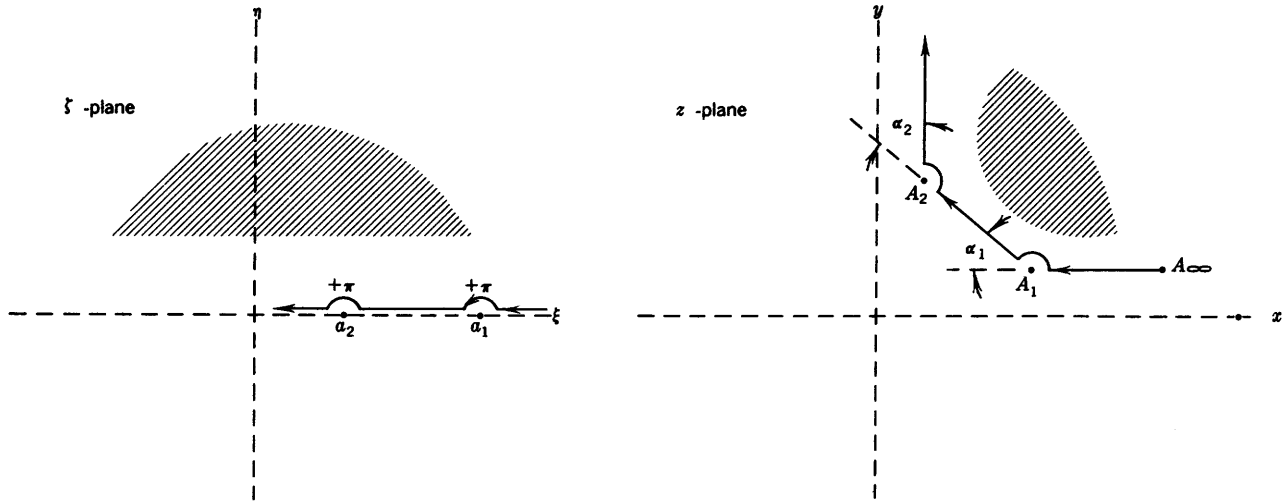
FIGURE 170.—Swartz conformal transformation relating the z-plane to the ζ-plane.
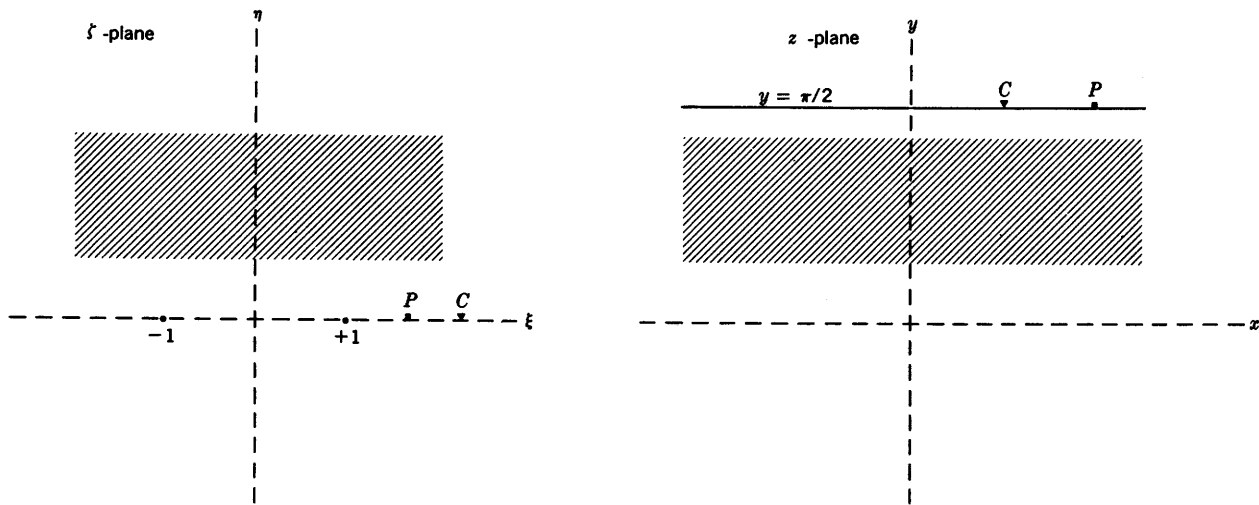
FIGURE 171.—Swartz conformal transformation of the positive half of the ζ-plane into a strip in the z-plane.

To illustrate the Swartz transformation, we use the simple example of describing the potential due to two parallel, infinitely long, grounded wires laid on the surface of the earth. The earth is considered to consist of two layers, the lower of which is infinitely resistant (see the left half of fig. 171). The strip in the z-plane can be considered as a polygon with only two angles, each of which equals π. Since there are only two turning points, both of which are found at infinity in the z-plane, we can specify arbitrarily both of these points in the ζ-plane. The most convenient points to choose are $a_1=1$ and $a_2=-1$. In this case, equation 236, therefore, becomes

$$dz=\frac{d\zeta}{(\zeta-1)(\zeta+1)}.$$

By simple integration it is found that

$$z=\frac{1}{2}\ln\frac{\zeta+1}{\zeta-1} \quad \text{or} \quad \zeta=\tanh z. \tag{237}$$

In order to examine the transformation in detail, it is convenient to put the transformation function in the form

$$z=\frac{1}{2}\ln\frac{1-\xi^2}{(1-\xi)^2}=\frac{1}{2}\ln\frac{\xi^2-1}{(1-\xi)^2}+\frac{i\pi}{2} \tag{238}$$

which is valid for points along the real axis ($\eta=0$) in the ζ-plane only. From this relationship, it is noted that the origin from the ζ-plane transforms into the origin of the z-plane. To the right of the origin towards the point $\zeta=1$, z approaches positive infinity. Thus, the part of the real axis between $\zeta=0$ and $\zeta=1$ transforms into the whole positive real axis in the z-plane. Similarly, the part of the real axis between $\zeta=0$ and $\zeta=-1$ transforms into the whole negative real axis in the z-plane. These relationships have been deduced from the first form of the function in equation 238.

Outside the range $-1<\zeta<1$, the second form of the function in equation 238 must be used. In this case
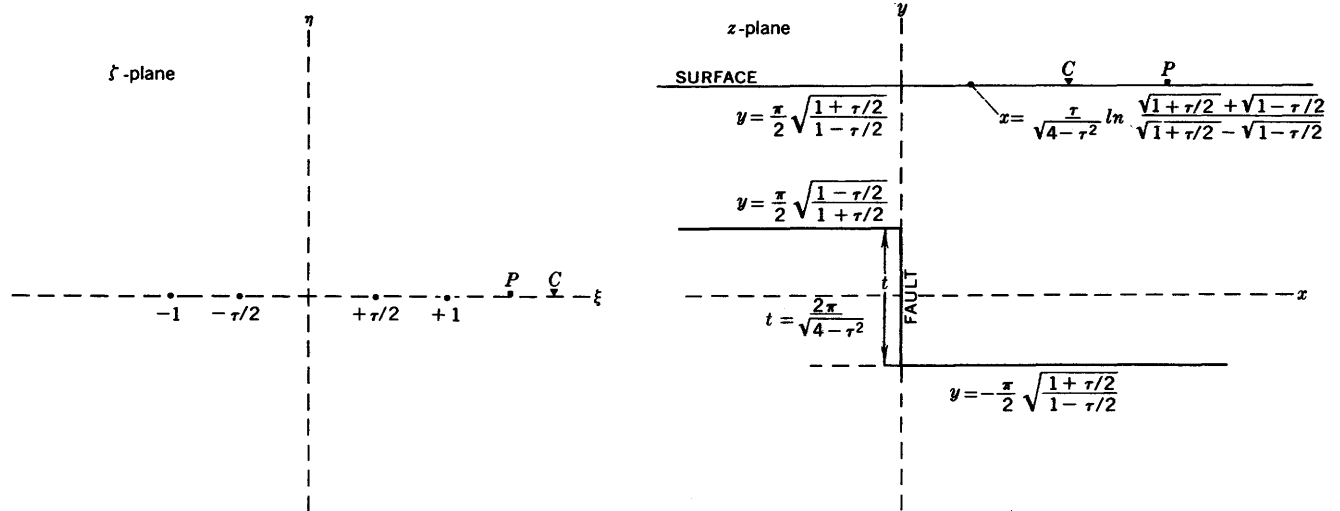
FIGURE 172.—Transformation of a buried fault with finite displacement and overburden of uniform resistivity in the z-plane, into half of the ζ-plane.

all the corresponding points of the z-plane lie along a line parallel to the real axis and are defined by $y=\pi/2$. The points for which $\zeta=\pm\infty$ are seen to transform into the intersection of this line with the imaginary axis in the z-plane.

To solve the two-layer problem with this transformation, as we set out to do, the current electrode is merely placed as shown in figure 171. In order that the upper surface in the z-plane may be used to represent the surface of the earth, the current electrodes in the ζ-plane must be placed outside of the region $-1<\zeta<1$; their exact position depends upon their positions in the z-plane. The thickness of the bed can be changed arbitrarily by changing the scale in the ζ-plane.

The problem of determining the potential distribution in the ζ-plane is a simple one (see equation 20). In order to find the potential at a given point in the z-plane, which is considerably more complicated if attacked directly, we need only find the potential at the corresponding point in the ζ-plane. It should be noted that equation 20 must be used with caution. Because of the unusual characteristics of the logarithmic potential for two or more line electrodes, the same zero for the expressions of potential must be chosen for the separate electrodes. This problem does not exist in three-dimensional problems because zero potential is by convention always set at infinity.

If the potential at the origin is arbitrarily assigned as zero, the potential at point P due to the line electrode C in the ζ-plane along the real axis is (see equation 20) either

$$U=\frac{I\rho}{\pi}\ln\frac{\xi_0}{\xi_0-\xi}\ \text{or}\ U=\frac{I\rho}{\pi}\ln\frac{\xi_0}{\xi-\xi_0}.\qquad(239)$$

The first of these forms is valid for $\xi_0>\xi$ and the second

for $\xi>\xi_0$. Since the potentials are desired along the surface of the earth $(y=\pi/2)$ in the z-plane only, this expression is sufficient. In order to obtain the potentials at corresponding points in the z-plane—that is, at points along the surface of the earth—the appropriate expression from equation 237 is substituted into equation 239 to obtain

$$U=\frac{I\rho}{\pi}\ln\frac{\tanh\ (x_0+i\pi/2)}{\tanh\ (x_0+i\pi/2)-\tanh\ (x+i\pi/2)}$$

$$=\frac{I\rho}{\pi}\ln\frac{\coth x_0}{\coth x_0-\coth x}\qquad(240)$$

for $\xi_0>\xi$.

This expression can be used to determine the potential distribution about a long current electrode laid on the surface of a two-layer earth when the lower layer has a very high resistivity. It can also be used to make a two-dimensional (logarithmic) approximation to the normal three-dimensional Wenner vertical profiles and thus to ascertain in yet another case the value of such approximations. There are a certain number of paradoxes, such as infinite potential at $x=0$, but these vanish in practical cases where two parallel current electrodes are considered.

Having established the principles of conformal transformation involved with a simple problem, we next consider the buried-fault problem. This problem is similar to that given above except that the lower bed has been broken by a vertical fault with finite displacement (fig. 172). The turning points referred to above are chosen to be $\zeta=\pm1$ and $\zeta=\pm\tau/2$ on the real axis in the ζ-plane. Thus, the differential form of the transformation is

$$dz=(\zeta-1)^{-1}(\zeta-\tau/2)^{-1/2}(\zeta+\tau/2)^{-1/2}(\zeta+1)^{-1}d\zeta,$$

which by integration can be shown to be

$$z=\frac{1}{2}\sqrt{\frac{1+\tau/2}{1-\tau/2}}\ln\frac{\sqrt{(1+\tau/2)(\zeta-\tau/2)}+\sqrt{(1-\tau/2)(\zeta+\tau/2)}}{\sqrt{(1+\tau/2)(\zeta-\tau/2)}-\sqrt{(1-\tau/2)(\zeta+\tau/2)}}$$

$$-\frac{1}{2}\sqrt{\frac{1-\tau/2}{1+\tau/2}}\ln\frac{\sqrt{(1+\tau/2)(\zeta+\tau/2)}+\sqrt{(1-\tau/2)(\zeta-\tau/2)}}{\sqrt{(1+\tau/2)(\zeta+\tau/2)}-\sqrt{(1-\tau/2)(\zeta-\tau/2)}}. \quad (241)$$

The transformation can be followed from the ζ-plane to the z-plane in about the same way as in the previous case; but there are some important irregularities that should be noted. For example, the point at real infinity in the ζ-plane no longer transforms into a point on the imaginary axis in the z-plane, as it did previously. Moreover, no part of the real axis in the range $-1<\zeta<1$ transforms into the real axis of the z-plane. The details of the transformation are given in figure 172. Whereas the reverse transformation function in the previous case—that is, ζ as a function of z—was sufficiently simple that the expression could be substituted in the potential function itself, the reverse transformation function in the present case is not conveniently simple. Consequently, a different approach must be used.

Because the potential remains constant during the transformation, the potential at a given point in the z-plane is the same as that at the corresponding point in the ζ-plane. It is, therefore, convenient to determine numerically the corresponding points using equation 241. This process is comparatively simple because all points of interest lie on the earth's surface $(y=(\pi/2)[(1+\tau/2)/(1-\tau/2)]^{1/2})$, which in turn is derived from that part of the ξ-axis outside the range $-1<\xi<1$. Continuous coverage can be obtained by drawing a graph. Once the graph is drawn, the points in the ζ-plane corresponding to the electrode positions in the z-plane can be easily determined; and the desired potential differences can then be calculated.

Thus, we have shown how to compute the logarithmic approximations for resistivity profiles over a buried fault with finite displacement when the faulted bed has a much higher resistivity than the overlying bed. Obviously, an infinite displacement of the fault is obtained by letting $\tau/2$ approach 1. Because the exact three-dimensional solution to this problem is prohibitively difficult, the logarithmic approximation serves a very useful purpose.

To solve a problem involving a finite resistivity contrast, the same approach can be used. The details are much more complicated, however, because essentially three regions must be considered instead of the two regions involved in the example given.

BURIED POCKETS

By buried pockets we mean three-dimensional bodies of finite dimensions in all three directions; these are in contrast with two-dimensional bodies, which are considered of infinite dimension in one or more directions, as, for example, in a buried stream channel or a dike. The mathematics for three-dimensional bodies is exceedingly difficult for all but the simplest problems, and most of our study of such bodies is therefore restricted to those which can be satisfactorily approximated by a sphere.

The location of buried masses and structures was the first object of electrical prospecting, although the subject of horizontal bedding has long since taken the lead with respect to theoretical treatment and publications. Early workers (Sundberg and others, 1923) showed that the homogeneous electrical field due to parallel line electrodes is disturbed proportionally more by buried bodies than the spherical field due to point electrodes. The greater flexibility and convenience in fieldwork with point electrodes, however, is great enough to compensate for the difference. We restrict our discussions to the disturbance of the fields of point electrodes except insofar as logarithmic (two-dimensional) approximations can be used to attain the same end.

The capabilities of electrical methods in general can be roughly appraised by examining the classic problem of a spherical inhomogeneity in a uniform field. Using spherical coordinates (fig. 24) and assuming that uniform current density i is flowing parallel to the polar axis in an infinite and uniform space of resistivity ρ', it can be shown from elementary considerations that the potential is given by $i\rho'r\cos\theta$, where r is the distance from the center of the sphere to the potential electrode and θ is the polar angle.

If, within the material of resistivity ρ', there is now placed a sphere whose center is at the origin, whose radius is r_1, and whose resistivity is ρ'', the potential in the original uniform field will now be disturbed by a perturbation which can be described in terms of equation 58 when $m=0$. The potentials outside and inside the sphere are therefore given, respectively, by

$$\begin{cases} U_1=i\rho'r\cos\theta+\sum_{n=0}^{\infty}B_nr^{-n-1}P_n(\cos\theta) \\ U_2=i\rho'r\cos\theta+\sum_{n=0}^{\infty}A_nr^nP_n(\cos\theta). \end{cases}$$

The application of the boundary conditions is straightforward. All of the coefficients are zero except when $n=1$. After determining A_1 and B_1 and

substituting them into the original expressions, we obtain

$$U_1 = i\rho' r \cos\theta \left[1 + \left(\frac{\rho'' - \rho'}{2\rho'' + \rho'} \right) \left(\frac{r_1}{r} \right)^3 \right]$$

$$U_2 = i\rho' r \cos\theta \left[1 + \frac{\rho'' - \rho'}{2\rho'' + \rho'} \right].$$

The perturbation in each of these equations is such that the effect of the sphere on the potential is constant within the sphere, whereas the effect of the sphere on the potential external to the sphere diminishes as the inverse cube of the distance from the center of the sphere. The inverse-cube law implies that the detection of buried pockets that are removed even relatively short distances from the electrode configuration will be difficult. This fact is paramount even though strictly uniform fields are ordinarily not attained with point-electrode configurations.

It has been pointed out (Sundberg and others, 1923) that the anomaly is independent of the scale of the problem. Although this fact is true with respect to the sphere in a homogeneous field, it is scarcely true in real problems because the finite dimensions of the electrode separation, depth, and size of the buried bodies complicate the problem.

The above analysis can probably be applied exactly if the sphere—or a hemispherical sink on the earth's surface as discussed in an earlier section—exists at moderate depth and approximately midway between two widely spaced point electrodes. In general these principles can be used only as a guide, however, because our problems will not ordinarily satisfy these conditions of symmetry and large electrode separations.

POTENTIAL AND RESISTIVITY OVER BURIED SPHERES

Although relatively few theoretical potential and resistivity curves over buried spheres are available, we have selected for study several typical curves that show diagnostic characteristics for the detection and delineation of buried spheres.

Hummel (1929c, d), by using potential expressions used in hydrodynamics and aerodynamics, developed in simple terms the potential functions for a buried egg-shaped body of "very good conductivity" in an otherwise homogeneous country rock (fig. 173). The shape of this body closely approximates a sphere. The potential V_s at any point P_2 on the surface of the ground over the "sphere" whose center lies a distance d vertically below the midpoint of two fixed current electrodes C_1 and C_2 (fig. 173c) is given by Hummel as

$$V_s = \frac{I\rho}{2\pi} \left[\left(\frac{1}{r_1} - \frac{1}{r_2} \right) + \frac{0.1 L x^2}{r_3^3} \right],$$

where ρ is the resistivity of the country rock; L is the distance between C_1 and C_2; r_1 is the horizontal distance between C_2 and P_2; r_2 is the horizontal distance between P_2 and C_1; r_3 is the distance between P_2 and the center of the sphere; and x is the horizontal projection of r_3. Points C_1, C_2, P_1, and P_2 lie along a straight line over the center of the sphere.

By taking the potential difference between two movable potential electrodes P_2 and P_1, the apparent resistivity can be computed for several positions of the potential electrodes as they are moved across the sphere, keeping C_1 and C_2 fixed. In this technique as used by Hummel, the electrode separation a between P_1 and P_2 is kept equal to the distance between C_2 and P_2, as the potential electrodes are moved over the sphere. Hummel computed the theoretical profile with this technique across the "sphere" shown in figure 173C. The sphere is approximately $0.8d$ in radius and its top is about $0.2d$ below the surface. The distance L is taken as four times the depth to the center of the sphere. Hummel plotted the ratio of the apparent resistivity ρ_a to the resistivity of the country rock versus the ratio a/L (fig. 173A). The smallest value of this ratio is 0.57, which means that the smallest value of the apparent resistivity is 57 percent of the true resistivity of the country rock surrounding the conducting mass.

The equipotential-line pattern that would be obtained at the surface over this "sphere", with two point-current electrodes located symmetrically in relation to its center, identically as described above, is shown in figure 173B (Hummel, 1929c, d). The departure of the equipotential lines from straight lines in the region above the center of the sphere is surprisingly small.

To study the effects observed at the earth's surface over a buried perfectly conducting sphere, it is convenient to chart potential anomalies or anomalous potentials along surface traverses that pass over or near the buried sphere. Figure 174 is one of a set of such profiles prepared by Lipskaya (1949b). Three quantities are represented in these curves: the normal potential U_N, which is the potential produced on the earth's surface by the point-current source for homogeneous ground in the absence of the buried sphere; the total potential U_T, which is the potential actually observed on the earth's surface in the presence of the sphere; and the anomalous potential ΔU, which is the difference between the total potential and the normal potential—that is, $U_T - U_N$—and which is due to the sphere alone. For convenience in plotting, the negative of the quantity ΔU is plotted in figure 174. In studying the profiles, it is convenient to recall that the radius r_1 of the sphere is the unit distance to which all other distances are referred.
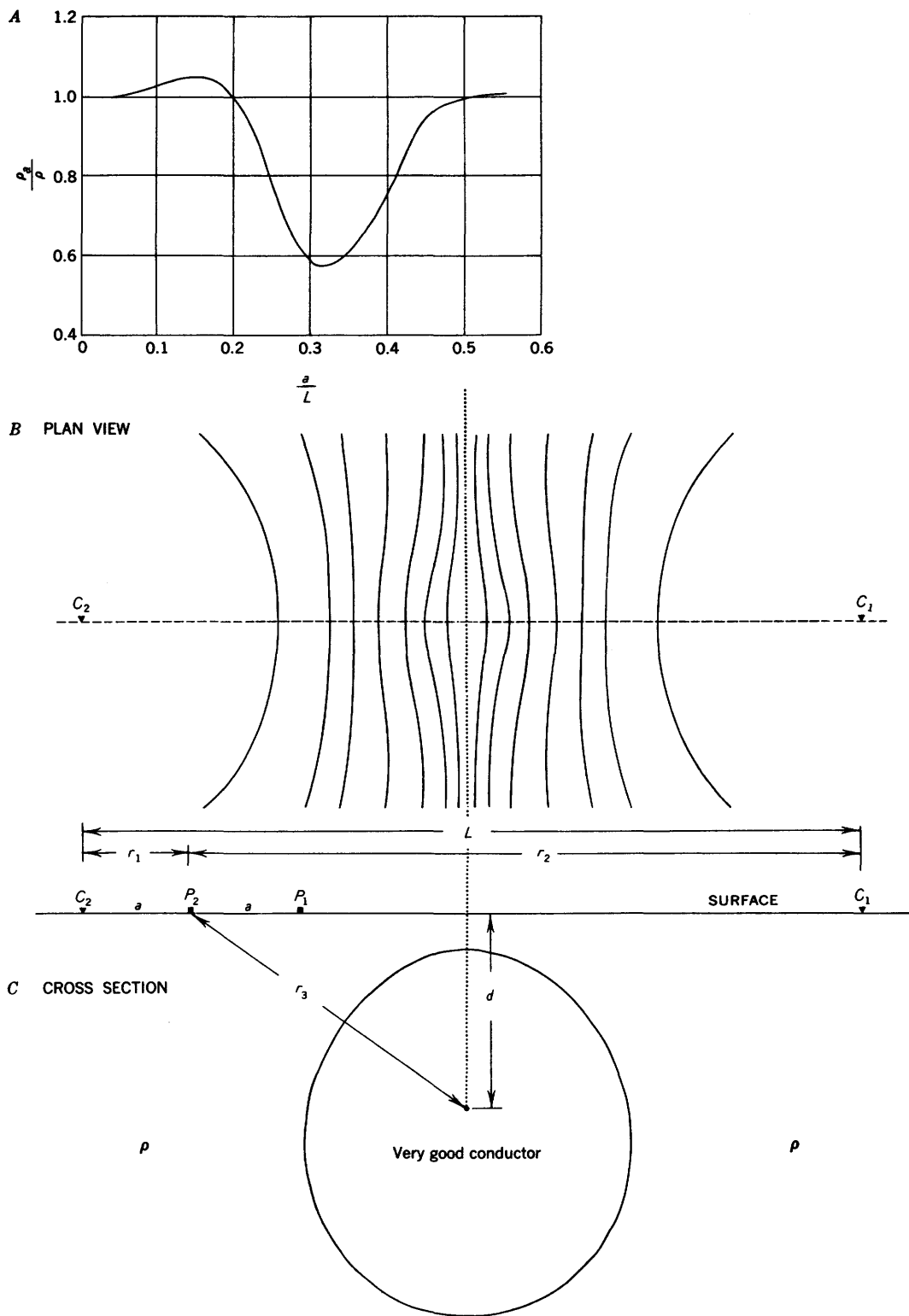
FIGURE 173.—*A*, Curve of apparent resistivity over buried egg-shaped body of "very good conductivity" in otherwise homogeneous country rock. Body closely approximates a sphere. *B*, Equipotential lines at surface over the same body. *C*, Cross section of egg-shaped body. *L*=4*d*. Adapted from Hummel (1929c, d), by permission of Johnson Reprint Corp., New York.
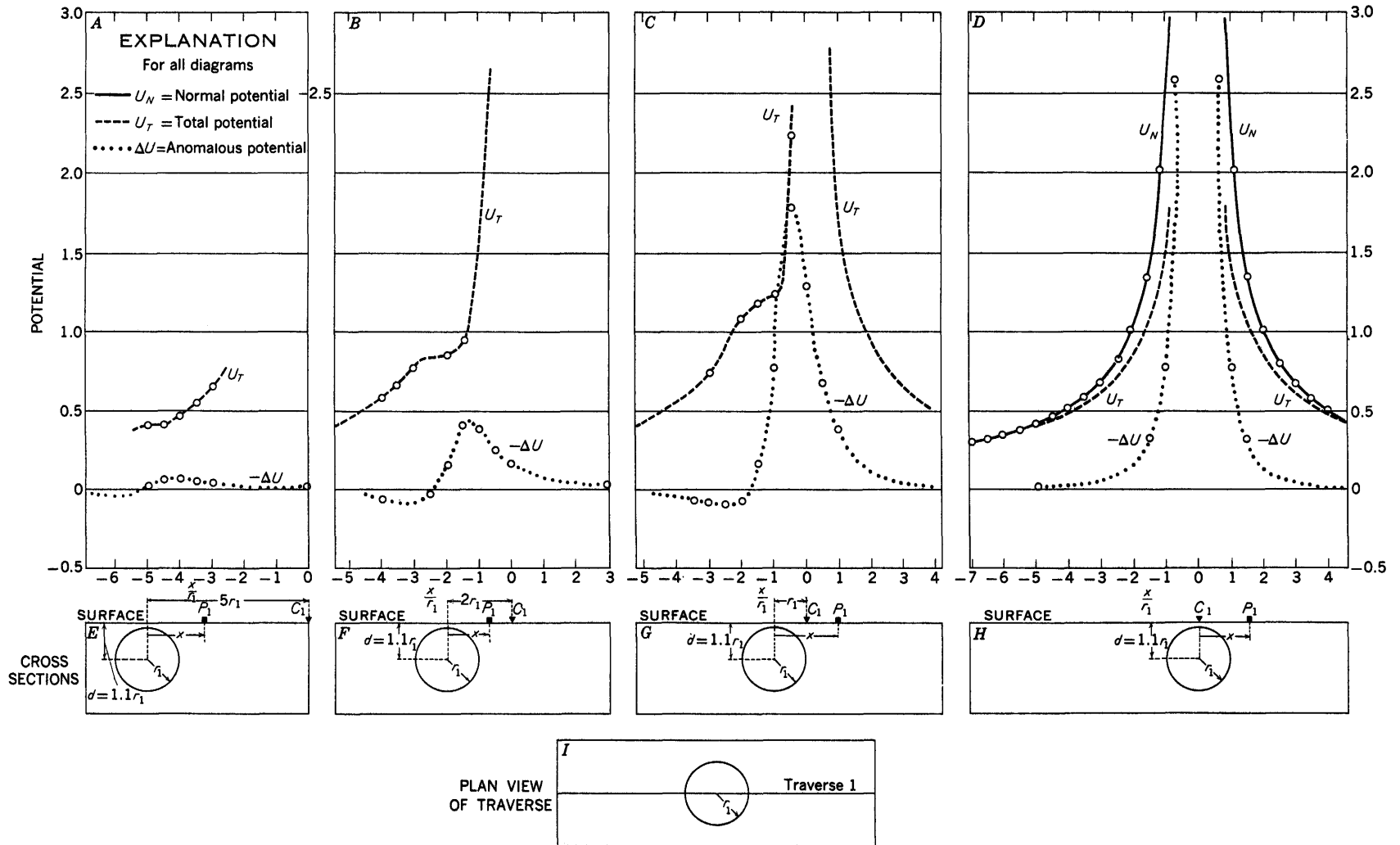
FIGURE 174. Graphs showing the normal potential U_N, total potential U_T and anomalous potential ΔU for profiles along surface traverse passing through epicenter of buried sphere. Depth of center of sphere $d=1.1r_1$. Current electrode C_1 at several distances from epicenter. Adapted from Lipskaya (1949b).

For a buried sphere whose center lies vertically beneath the point-current source (fig. 174H), ΔU is less than zero—that is, $-\Delta U$ is positive—for all points on the profile (fig. 174D). For a sphere removed from the point-current source (figs. 174 B, C), positive values of ΔU appear. For a sphere removed sufficiently far from the source (fig. 174A), the exterior potentials become more and more homogeneous, and the ΔU maximum and minimum become almost equal, making the ΔU curve nearly symmetrical about a vertical axis passing through the center of the sphere; in this respect the ΔU anomaly is analogous to that for a sphere in a constant current.

The negative maximum of ΔU is very large over the sphere when the current electrode is placed at or near the epicenter (fig. 174D). The negative maximum of ΔU increases sharply with the decrease of the depth of the sphere. When the current electrode is removed a short distance from the sphere (figs. 174 B, C), the negative maximum of ΔU lies approximately at the midpoint between the epicenter of the sphere and the current source. The rectilinear portion of the graph with the greatest steepness on the ΔU curve occurs over the sphere.

Graphs of the total potential U_T are obtained by algebraic addition of the normal potential U_N and the anomalous potential ΔU. For a sphere lying vertically beneath the point-current source, the U_T curve is symmetrical about the vertical axis passing though the center of the sphere; and the U_T curve is entirely below the U_N curve. When the current source lies removed from the epicenter of the sphere, the symmetry of the U_T curve is disturbed, and a characteristic flexure appears on one side; the U_T curve descends on the right side of the sphere, crosses the U_N curve, and then surpasses it. The degree of this flexure is dependent upon the depth of the sphere and the distance between the conductive body and the current source.

When the current source is near the body, the value of ΔU can sometimes become very important, but its influence is not very noticeable because of the great steepness of the U_N curve. As the current source moves away from the sphere, the U_N curve becomes flatter, but at the same time the intensity of the anomalous potential decreases. There is a certain optimum distance between the current source and the body at which the distortion of the curves is the greatest.

Figures 175 and 176 show horizontal resistivity profiles with a "two-electrode" configuration taken along the surface of the earth across a buried perfectly conducting sphere (Lipskaya, 1949b). This configuration is comparable to the normal device used in well-logging; it employs the usual single-probe configuration
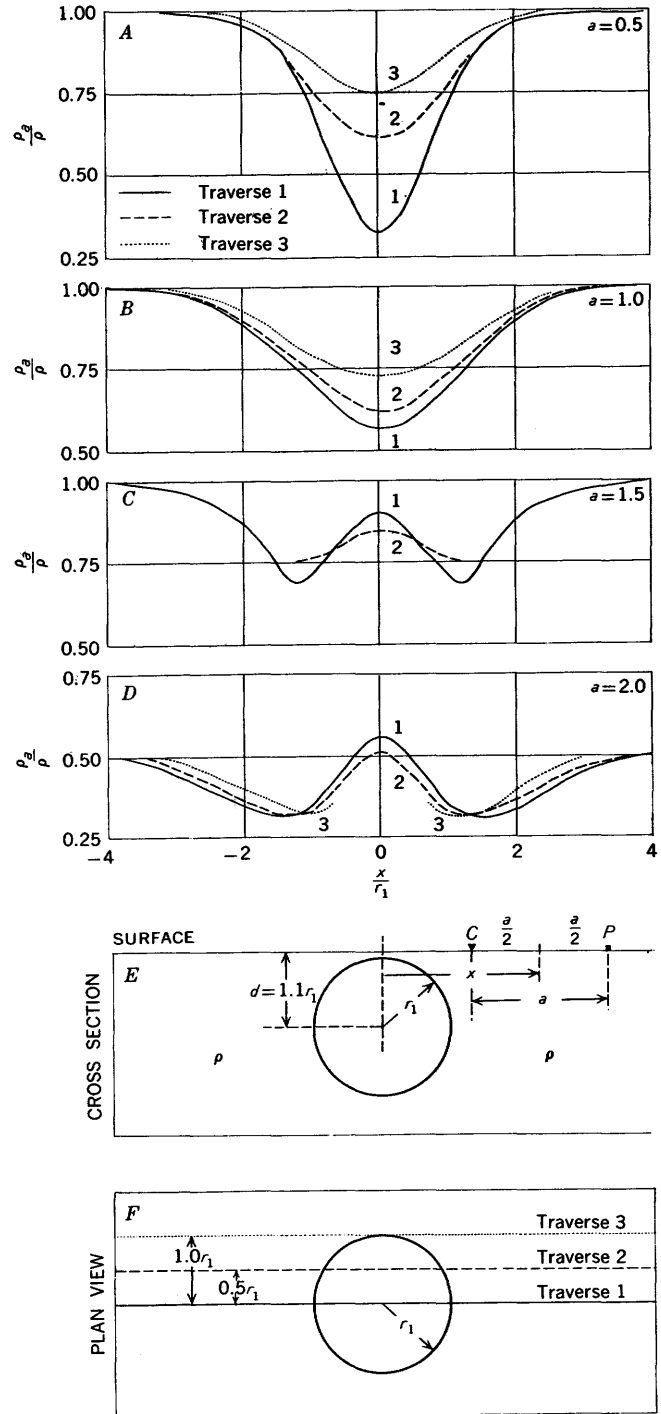
FIGURE 175.—Horizontal resistivity profiles with various electrode separations across buried perfectly conducting sphere along traverses at different distances from epicenter of sphere, "two-electrode" configuration. Depth of center of sphere $d=1.1r_1$. Adapted from Lipskaya (1949b).

with one current electrode and one potential electrode infinitely remote. The profiles for the shallow sphere with depth of center $d=1.1r_1$ are shown in figure 175, and those for the same sphere with depth of center $d=1.5r_1$ are shown in figure 176. The profiles over
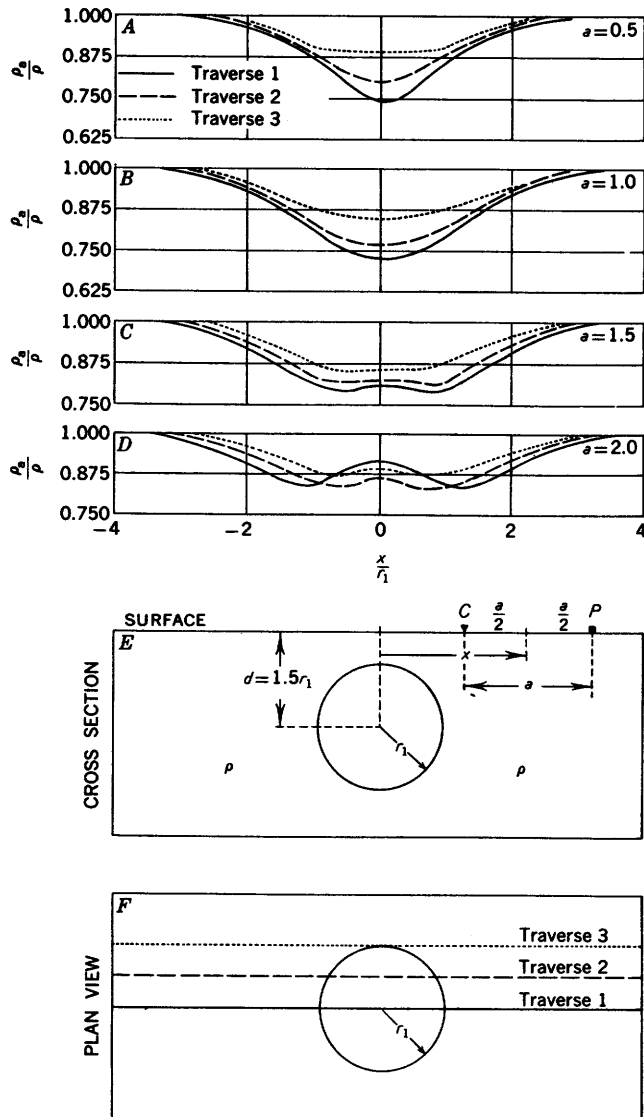
FIGURE 176.—Horizontal resistivity profiles with various electrode separations across buried perfectly conducting sphere along traverses at different distances from epicenter of sphere, "two-electrode" configuration. Depth of center of sphere $d=1.5r_1$. Adapted from Lipskaya (1949b).

each of the two spheres are taken along traverses at distances of zero, $r_1/2$, and r_1 from the epicenter of the sphere. In addition, different electrode spacings are used on individual traverses. As usual, the quantity ρ_a/ρ is plotted on the ordinate, and the distances are measured along the ground from the epicenter of the sphere to the midpoint of the two electrodes.

For a given electrode separation, the computed curves for a traverse over and somewhat removed from the epicenter of the sphere are similar in shape, but the extreme values decrease as the traverses are taken farther from the epicenter. The extreme values also are much less for the deeper sphere than for the shallow sphere. The sharpness of the apparent-

resistivity anomalies is greatly influenced by the appropriate choice of the electrode separation a. For large values of a, W-shaped apparent-resistivity curves are obtained.

Lipskaya (1949b) pointed out that the apparent-resistivity curves shown in figures 175 and 176 compare favorably with the results of model studies by Semenov and Malchevski (1939), who analyzed experimentally the apparent-resistivity effects obtained with a point-current source by a conducting sphere buried near a drill hole.

Figure 177 shows horizontal resistivity profiles with both the Lee and Wenner configurations across a buried perfectly conducting sphere whose depth of center is $1.1559a$ and whose radius is $0.9247a$.[8] For the Lee configuration (fig. 177A), both the ρ_1 and ρ_2 curves show slightly asymmetrical inverted W-shaped curves; the major ρ_2 minimum occurs to the left of the epicenter of the sphere, and the major ρ_1 minimum occurs to the right of the epicenter. The point of symmetrical crossing of the ρ_1 and ρ_2 curves occurs vertically over the center of the sphere.

For the Wenner configuration (fig. 177B), a symmetrical inverted W-shaped curve is obtained. The minimum lies vertically above the center of the sphere. The values of the apparent-resistivity peaks occurring on either side of the sphere greatly exceed one. A curve for the Wenner configuration similar to the one given here was published by Jakosky (1940), apparently on the basis of qualitative reasoning.

Figures 178 and 179 show profiles with the constant-spacing system of the potential-drop-ratio method across a buried sphere of finite resistivity contrasts with the country rock. The diagram in figure 178 shows curves over spheres that are more conducting than the country rock, whereas the diagram in figure 179 is for spheres that are less conducting than the country rock. It should be emphasized that the potential-drop-ratio anomalies over the conducting sphere are greater than those over the insulating sphere of identical size and depth. This property is of fundamental importance in prospecting.

DETECTABILITY OF BURIED SPHERES

Figure 180 shows vertical resistivity profiles with the Wenner configuration over perfectly conducting spheres buried at different depths (Van Nostrand, 1953). The curves are plotted as the ratio of the apparent resistivity to the true resistivity of the country rock versus the ratio of the electrode separation to the radius of the sphere. Each curve represents data for a given

[8] The irrational values of the depth of center and radius resulted from the choice of rational values of the coordinates that were chosen to facilitate computations.
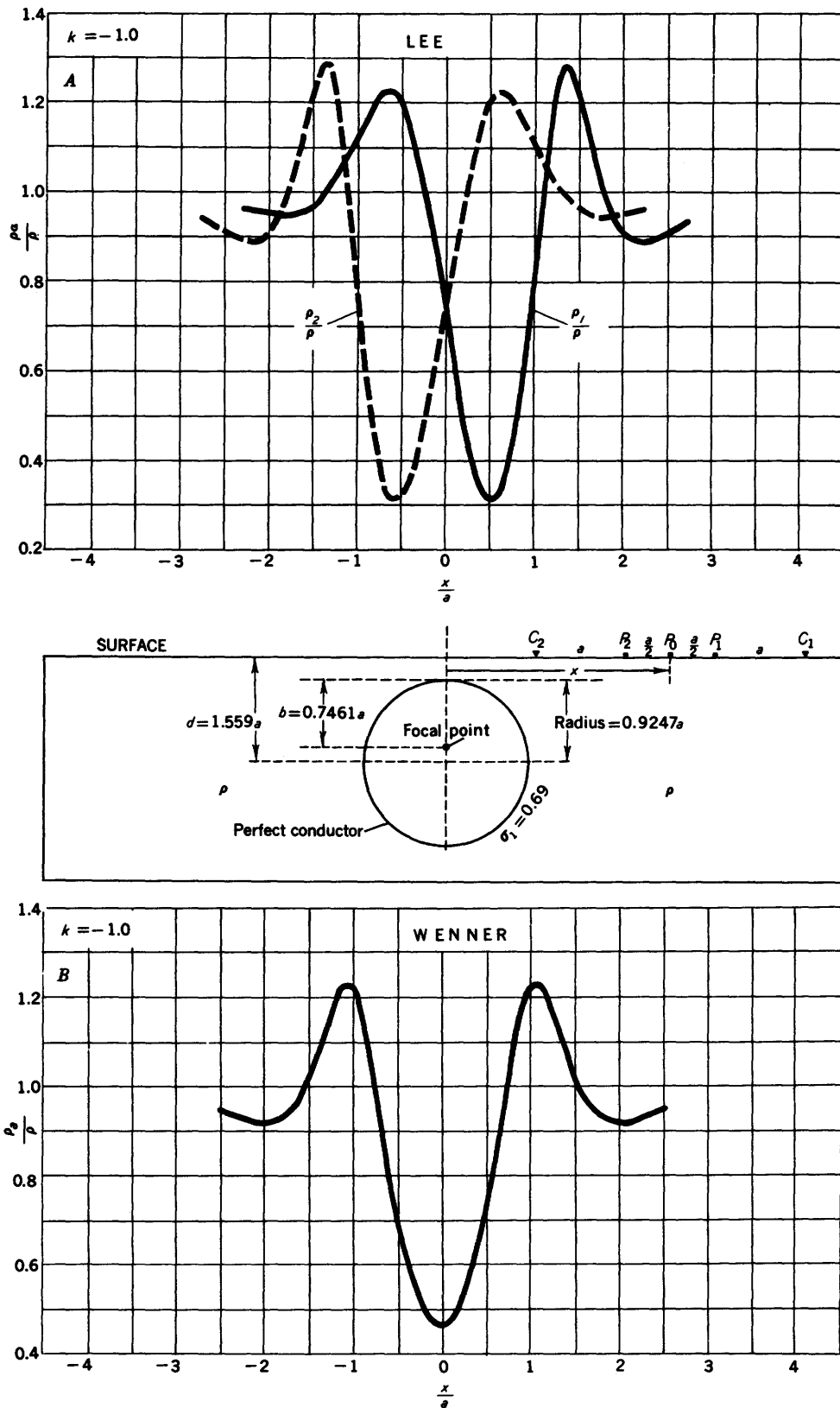
FIGURE 177.—Horizontal resistivity profiles across buried perfectly conducting sphere; (A) Lee configuration (offset plotting); (B) Wenner configuration. Depth to center of sphere=1.559a; radius=0.9247a. (See fig. 27.)
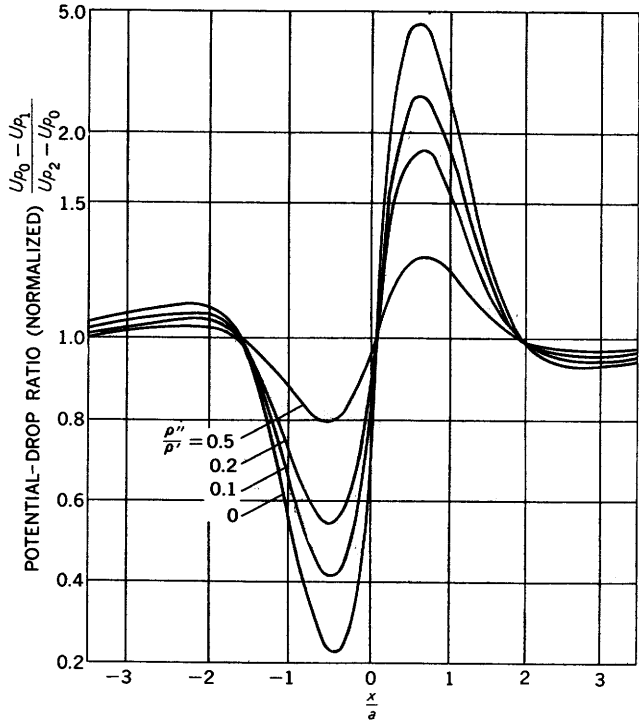
FIGURE 178.—Profiles with constant-spacing system of potential-drop-ratio method across buried spheres of different finite resistivity contrasts with surrounding country rock; spheres more conducting than country rock. Data are normalized. For all curves, $c=10$; $d=1.25r_1=1.25a$; $a=$unity. Adapted from Kiyono (1950c) by permission of Kyōtō University.

buried sphere; the depth to the center of the sphere d is also expressed in terms of the radius of the sphere. Thus, the graph is dimensionless and may be applied to any specific case if the correct scale is introduced.

Two curves of the set are not based on equation 228. That for the hemisphere ($d=0$) is based on the electrostatic analogy which may be found in any intermediate text on electricity (for example, Slater and Frank, 1947); that for the buried sphere which is tangent to the earth's surface ($d=r_1$) has been estimated from the shapes of the other curves shown.

When the sphere is definitely buried, the curve starts for small electrode separation with ρ_a/ρ equal to one. Each curve displays a minimum, which represents the electrode separation at which the sphere produces a maximum effect on the results; and then each curve

trends upward to approach one asymptotically at large electrode separations.

On the other hand, if the sphere is truncated at all by the earth's surface, the corresponding curve starts at zero at the electrode separation equal to the diameter of the circle of truncation, and then rises continuously to approach one asymptotically. The curve for the hemispherical case is one limiting example of this type. The curve representing the other limiting case, that in which the sphere is tangent to the surface of the earth, starts at the origin.

It can be shown that the first five curves in the diagram actually cross the hemisphere curve in the range of the electrode separation between 3.5 and 6, but do not cross each other. This fact implies that the buried spheres have a greater effect at large electrode separations than does the hemisphere, which phenomenon is related to the volume of foreign material which is present in the field and to the ratio of this volume to the volume of space in which the current density is arbitrarily appreciable.

The maximum depth at which a spherical mass can be detected by direct-current methods at the surface is implied in the vertical profile curves in figure 180.
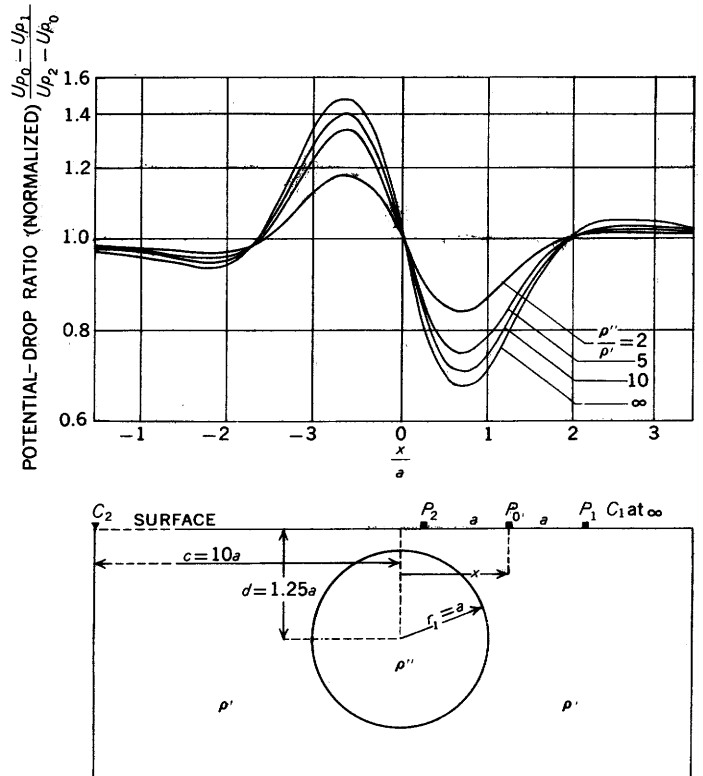

FIGURE 179.—Profiles with constant-spacing system of potential-drop-ratio method across buried spheres of different finite resistivity contrasts with surrounding country rock; spheres less conducting than country rock. Data are normalized. For all curves, $c=10$; $d=1.25r_1=1.25a$; $a=$unity. Adapted from Kiyono (1950c) by permission of Kyōtō University.
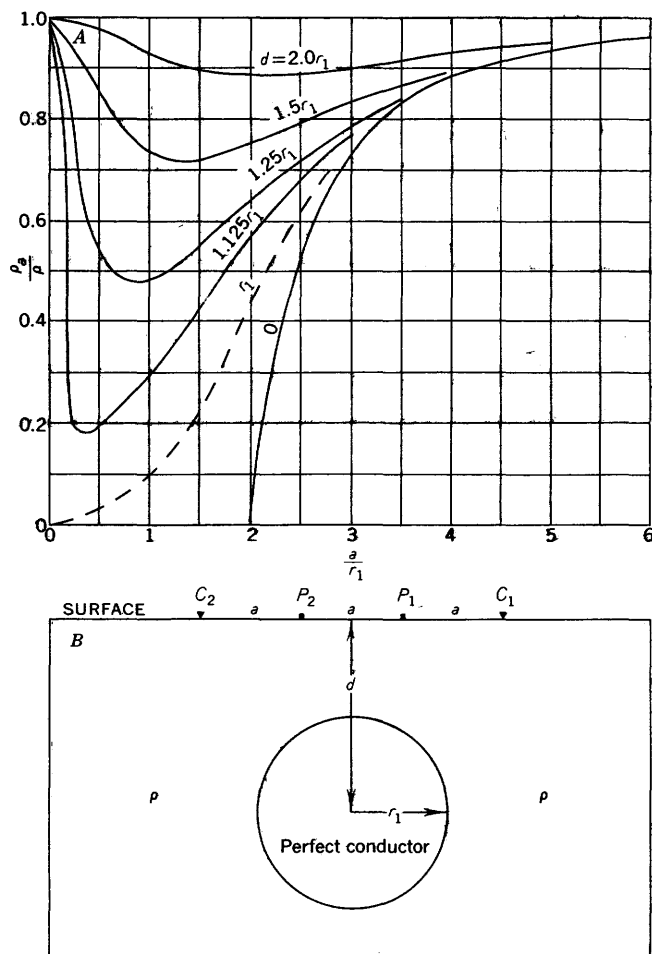
Figure 180.—Vertical resistivity profiles over buried perfectly conducting spheres buried at different depths, Wenner configuration. Adapted from Van Nostrand (1953).

The principal geophysical value of these curves stems from the fact that the disturbing body of zero resistivity has a maximum effect on the measurement of the apparent resistivity for a given geometrical relationship. This fact has been verified, for the case in which the electrodes do not actually fall within the disturbing material, even when comparison is made with a body of infinite resistivity. Of course, the assumption is always valid, even if the electrodes do fall within the disturbing body, when the resistivity of the disturbing body is less than that of the surrounding material.

The curve for which the depth to the center of the sphere is twice the radius of the sphere, has a minimum for which the apparent resistivity varies only 10 percent from the regional value of the true resistivity. Therefore, one is led to the assumption that it would not be safe to depend on finding such a feature when its depth is greater than this value. This result, being in the nature of a guiding principle rather than a fact, may

safely be extended to bodies of arbitrary shape provided that the variation between the maximum and minimum dimensions is not too extreme; a factor of two might well be permissible. In such a case, a maximum depth to the center of the body equal to the mean linear dimension of the body would appear to be in order. As this rule has been based on the limiting case of a conducting sphere, the ability of resistivity methods to locate bodies presenting less than extreme resistivity contrasts would be considerably reduced below the standard set above.

It is recognized that the limits discussed are based only on the direct effects of the disturbing body. It may happen that certain near-surface structural features exist over the disturbing body, and that the detection of such features through electrical means could yield information concerning the presence of a body buried deeper than the above rule permits. A typical associated structure might be a system of fractures due to differential compaction of overlying beds.

We note from figures 175 and 176 that Lipskaya's data are consistent with our own. For example, when the center of the sphere is buried to a depth $d=1.5r_1$ (fig. 176), Lipskaya's anomaly is of the order of 25 percent when the configuration is directly over the sphere. Only for an electrode separation of 0.5 does she get an anomaly (25 percent) essentially different from our own (15 percent). This difference can probably be explained on the basis of the geometries of the two configurations.

The vertical-profile curves in figure 180 can be used also to help establish the proper field techniques for the discovery of a buried sphere. For horizontal-profiling techniques, for example, the curves help in making a choice of the proper electrode separation in a given geologic situation. When one enters a region to perform a survey, he is generally advised by geologists as to the approximate depth at which he should find a certain geologic condition. Suppose, for example, that ore is known to be associated with shale-filled sinks about 200 feet in diameter and 130 feet in vertical dimension, located in an ancient limestone surface which has later been overlain with shale to a depth of 40 feet (fig. 181). Suppose further that the resistivity of the shale is normally much less than one-fifth that of the other materials present.

If this filled sink be approximated by a spherical solid, the mean radius may be thought to be about 82.5 feet and the depth to the center about 105 feet. In the set of curves in figure 180, we imagine the curve for which the depth is about 1.27 times the radius and note that the minimum occurs at an electrode separation about equal to 0.9 times the radius. On

FIGURE 181.—Example of buried body. Adapted from Van Nostrand (1953).

The mathematics already given is equally applicable to the studies of buried ore deposits where the electrodes are sufficiently removed from the surface of the earth. Examples of such studies include the electrical diamond-drill holes and electrical surveys in the underground workings of a mine. Space does not permit giving theoretical curves or practical results of such examples in this report. The potential functions for spherically and spheroidally shaped bodies (see, for example, equations 207 to 214) are especially useful in this respect. Seigel (1952), Clark (1956), and others, show how electrical results from a diamond-drill hole can be used to determine the size and disposition of an ore body. Similarly, the mathematics and results from the sections on vertical faults, fissures, and dikes are by analogy useful in electrical well logging where the holes cut horizontally bedded strata.

In electrical well logging, the electrode separation is usually sufficiently large that the effect of the hole is negligible; if not, the effect of the hole on any given log is constant because the electrode separation is not changed during the run. In electrical surveying in mine workings the same type of problem regarding openings exists, except that this problem is different because the electrode separation is usually changed during the survey in order to study the distance of the ore from the workings, the size of the ore body, and similar problems. In such surveys it is necessary to know the effect of the mine openings themselves, where no ore is present.

Assuming that the same formula for the apparent resistivity is used for all the resistivity data taken in a mine drift, for example, we can readily predict the principal behavior of the apparent resistivity as the electrode separation is expanded. For electrode separations that are small in comparison with the lateral dimensions of the drift, the current behaves as it does in a survey on the surface of the earth. However, for electrode separations that are very large in comparison with the lateral dimensions of the drift—that is, when the potential electrodes are well removed from the current electrodes—the potential at each of the potential electrodes is the same as though the current electrodes were embedded in an infinite earth. Thus, for large electrode separations the potentials and the apparent resistivity will be one-half their value for small separations. This conclusion is based on the assumption that the drift (or shaft) occurs in homogeneous earth; obviously if there is ore nearby, the apparent resistivity will be altered accordingly.

the basis of this information alone, it would be concluded that an electrode separation of about 75 feet would be most useful. However, because a traverse will rarely pass directly over the center of the body, the traverse will normally be farther from the center than the 82.5 feet quoted above. Therefore, an optimum electrode separation is probably larger than 75 feet—perhaps as much as 85 or 90 feet.

In deciding on the appropriate spacing between traverses, one concludes that the rule of permissible depth can be generalized to state that, if an anomaly is to be found along a given traverse, the traverse must pass within a distance from the center of the disturbing body roughly equal to the average dimension of the body. In the above example, this means 165 feet. Therefore, in order for the anomaly in the above example to appear on at least two adjacent traverses, a traverse separation of no more than 127.5 feet could be tolerated.

If the disturbing mass actually crops out, the above discussion must be altered accordingly.

FIGURE 182.—Plots of actual potential U, normal potential U_N, and anomalous potential $\Delta U = U - U_N$ due to point-current electrode C on surface of a perfectly insulating cylinder of infinite length. Potentials are for points also on surface of cylinder, (A) along a circle C' for different values of angle ϕ and (B) along straight line CP for different values of z. Adapted from Huber (1953).

Equation 216 can be used effectively to approximate the manner in which the apparent-resistivity changes from its initial value to its final value as the electrode separation is expanded. We adapt the equation by placing the electrodes on the surface of the cylinder along a directrix ($\phi=0$) and by letting the material within the cylinder assume infinite resistivity in order to represent air. The equation then becomes

$$U_{1A}=\frac{I\rho}{4\pi}\left\{\frac{1}{z}-\frac{2}{\pi}\sum_{m=0}^{\infty}(2-\delta_{0m})\ \cos\ m\phi\int_0^\infty\frac{K_m^2(tr_1)\ \cos\ tz}{\psi'_m(tr_1)}\ dt\right\},$$

where ρ is the resistivity of the homogeneous material surrounding the cylinder and r_1 is the radius of the cylinder. We note also that the interelectrode distance R is now simply equal to z.

Huber (1953) gave curves applicable to this analysis, and we reproduce two of his curves here. Figure 182 shows the potentials at various points P, P', and P'' along the surface of an infinite cylindrical-shaped open tunnel deep within the ground; the point-current electrode is embedded in the rock at the top of the tunnel.

The graphs show the plots of the actual potential U due to the cylinder; the normal potential U_N, which is the potential that would exist if the cylinder were absent; and the anomalous potential $\Delta U=U-U_N$. ΔU is always negative because the actual potential is always less than the normal potential; accordingly it is plotted actually as a "minus" ΔU. Figure 182A shows the potentials for points on circle C' for different values of ϕ; the plane of this circle passes through the point-current electrode C and is perpendicular to the axis of the cylinder. Figure 182B shows the potentials for points along straight line CP, which is the line of intersection of the cylindrical surface $r=1$ and a plane that includes the point-current electrode C and the axis of the cylinder; distances along z are measured in terms of the radius of the cylinder taken as unity.

Figure 183 shows a plot of the values of the actual potential as functions of z and ϕ at points P'' on the surface of the same perfectly insulating cylinder due to a point-current electrode C, also on the surface of the cylinder at the origin $z=0$, $\phi=0$ (Huber, 1953). Although the equipotential lines have been drawn by Huber onto the coordinate system on a plane sheet, it should be emphasized that the plane sheet on which the equipotential lines are drawn is in reality coiled into a semicylindrical surface for the problem at hand; moreover, figure 183 shows only the projection of one of the four semicylindrical quadrant surfaces that actually exist about the point electrode.
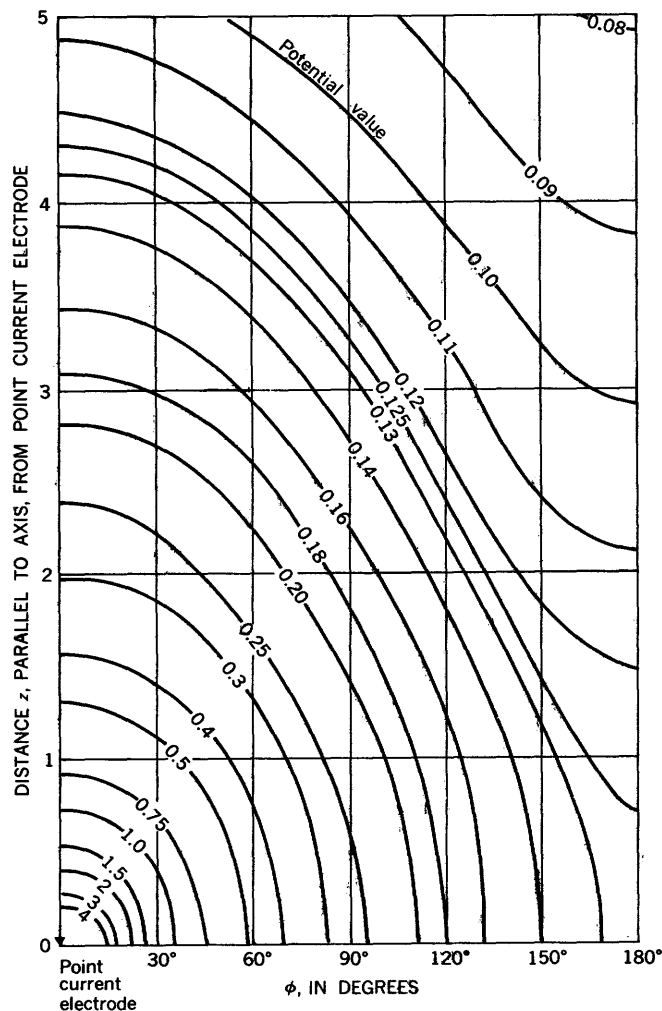
FIGURE 183.—Plot of the values of the actual potential at cylindrical coordinate points z and ϕ on the surface of a perfectly insulating cylinder of infinite length due to point-current electrode C also on the surface of the cylinder at the origin $z=0$; $\phi=0$; radius of cylinder is unity. (See fig. 182.) Adapted from Huber (1953).

GRAPHICAL SOLUTION OF BURIED DOME STRUCTURE

The buried dome structure problem is amenable to an approximate graphical solution, when the boundary of the dome can be approximated by hyperboloids of revolution.[9] The problem is included here to illustrate the technique used in compiling an approximate curve for a problem which is extremely difficult and apparently still unsolved in an exact mathematical form; the final curve obtained actually has little practical utility. As an example, the approximate apparent-resistivity curves for a vertical resistivity profile symmetrically over the center of a buried perfectly conducting dome

[9] Van Nostrand, R. G., 1952, The theory of direct current prospecting in the presence of curved boundary surfaces: Univ. North Carolina [Chapel Hill], unpublished Ph. D. thesis, 107 p.
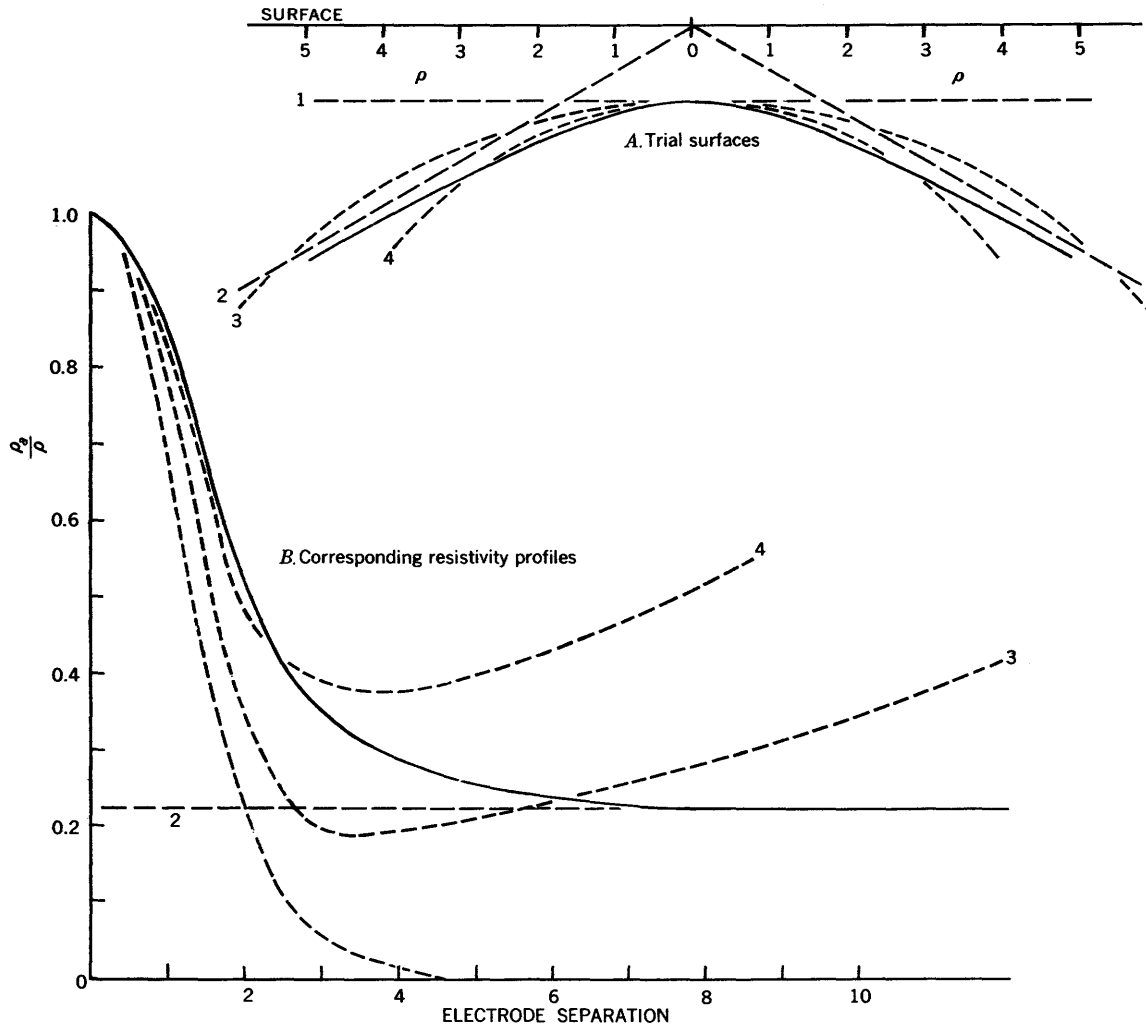
FIGURE 184.—Approximate curve (solid curve) for a vertical resistivity profile symmetrically over center of buried perfectly conducting dome structure, Wenner configuration. Dashed curves are auxiliary curves for features indicated. Adapted from Van Nostrand (1952, Univ. North Carolina [Chapel Hill], unpublished Ph. D. thesis, 107 p.).

structure can be obtained (see fig. 184). Before discussing the profile we will review the reasoning used in obtaining the approximate curve.

For very large or small electrode separations the behavior of the apparent-resistivity curves can be understood by examining qualitatively the limiting cases of the geometric form of a hyperboloid of revolution. For very large electrode separations the behavior is dictated by the asymptotic behavior of the hyperboloid, and the surface of the hyperboloid approaches asymptotically the surface of a cone whose apex is at the origin. Therefore, the apparent-resistivity curve should behave for large electrode separations like the corresponding curve for a conal boundary—which is amenable to solution. For small electrode separations the behavior of the curve is understood by reasoning that the effect of the dome on the apparent resistivity

would always be less than the effect of a horizontal bed of infinite depth, whose upper boundary is a horizontal plane tangent to the dome at its apex.

Besides showing the desired vertical profile over the buried dome structure, figure 184 shows an auxiliary set of vertical-profile curves and the corresponding cross sections used to facilitate the construction of the desired profile. The depth to the top of each auxiliary feature is the same in all cases and is arbitrarily chosen to be a unit distance. The solid line represents a hyperbolic surface, whose flanks dip at an angle of 30° in the one case and the vertical profile over that surface in the other case. The surface labeled "1" is a plane, horizontal boundary; "2" labels the conal asymptote; and "3" and "4" indicate spheres of radii 8 and 5, respectively. The corresponding apparent-resistivity profiles bear the same numbers.

The data for curve 1 are taken from tables published by Roman (1934). Curves 3 and 4 are based on equation 228 and may be thought of as belonging to the set of curves presented in figure 180; the difference between them and those in figure 180 lies in the scale. The unit of distance in figure 180 is the radius of the sphere and in figure 184 is the depth to the top of the dome.

The computations for curve 2, based on equation 229, are more complicated. Making ρ'' equal to zero, and manipulating the potential functions as was done to obtain equation 229, it can be shown that:

$$\frac{\rho_a}{\rho}=1+\frac{32}{\pi\sqrt{3}}\sum_{\substack{m=1\\\text{odd}}}^{\infty}$$

$$\int_0^{\infty}\frac{P_{ip-1/2}^m(\cos\theta_1)P_{ip-1/2}^m(0)\cos(p\ln 3)}{[P_{ip-1/2}^m(\cos\theta_1)+P_{ip-1/2}^m(-\cos\theta_1)]P_{ip-1/2}^m(0)}\,dp.$$

The electrode separation "a" is eliminated from this expression so that the resulting curve is a horizontal line. This property is correct, because the changing of the electrode separation serves only to change the scale of the experimental situation.

Since no tables of cone functions exist, the definitions given by equations 55 and 62 were substituted into equation 229 and as many simplifications as possible were effected before computations were commenced. Fortunately, it was found that only $m=1$ made any appreciable contribution; and values of p, in steps of $\frac{1}{2}$ to as much as 6 were more than adequate.

The results are best appreciated by an examination of the curves themselves. Surface 4 follows the hyperboloid closely until they cross a horizontal distance of 3 from the center. Therefore, curve 4 is used as a basis for the initial behavior of the hyperboloid curve, making allowance for the inexact coincidence of the two surfaces. The next controlling point is furnished by curve 3. Note that surface 2 intersects surface 3 only slightly before surface 3 crosses the hyperboloid. Therefore, it is reasoned that curve 3 intersects the hyperboloid curve at a slightly larger electrode separation than it does in curve 2. This fact is used to estimate how rapidly the hyperboloid curve approaches the cone curve. The results are shown in the diagram.

A natural ambiguity exists in these curves. The hyperboloid curve is very similar to the corresponding curve that represents a horizontal bed with the same boundary as surface 1, but with a resistivity of about one-sixth that of the overlying material; and the two curves approach the same asymptote for large electrode separations. Of course, this ambiguity is removed if the electrode configuration is moved appreciably from its position of symmetry.

MISCELLANEOUS LOGARITHMIC APPROXIMATIONS

Because of the difficulty in solving exactly problems involving buried three-dimensional bodies, Kiyono (1950c) developed logarithmic approximations to many of these problems with two-dimensional analysis. In developing the apparent-resistivity curves for the Wenner configuration, Kiyono assumed that all the electrodes are horizontal line electrodes of infinite length and oriented parallel to the strike of his infinitely long structures. All electrodes are assumed to lie on the earth's surface. Because of the symmetry in the problem, point potential electrodes will yield the same results as the infinitely long potential electrodes; this does not apply, however, to the line current electrodes.

The reader is referred to figure 14 to ascertain the validity of the two-dimensional logarithmic approximation. Kiyono made model experiments which proved that such approximations are sufficiently accurate to make them worth while as a guide in the qualitative interpretation of two-dimensional features—that is, infinitely long in the direction of the strike—when point current electrodes are used with the Wenner configuration. It should be emphasized, however, that the method of conformal transformation, which is used to obtain the logarithmic approximations, is valid only for two-dimensional bodies; and that unfortunately it is useful only for obtaining profiles perpendicular to the strike of the geologic structures. (See p. 252–255.)

Two-dimensional approximations for horizontal resistivity profiles with the Wenner configuration across buried semi-infinite horizontal plates of different thicknesses and depths of overburden are given in figures 185, 186, and 187. These curves are most useful when compared to the curves given in the section on vertical faults.

The distinct peaks and troughs on the previous curves are still recognizable in part (figs. 185 and 187 for perfect conductors), but the sharp discontinuities in slope are now subdued by the overburden. The effect of overburden on horizontal resistivity profiles over vertical faults is best depicted in figure 187. For an outcropping vertical fault ($d=0$), the curve obviously falls to zero as soon as both potential electrodes are in contact with the low-resistivity material; and the sharp peaks are similar to those found on all of the previous curves for vertical faults. With only a small amount of overburden, however, the peaks are rounded. Figure 187 indicates that when the depth of the overburden equals half the electrode separation, the limiting case has been reached. For additional thickness of overburden, the position of the fault could not be readily detected unless a larger electrode separation were used.
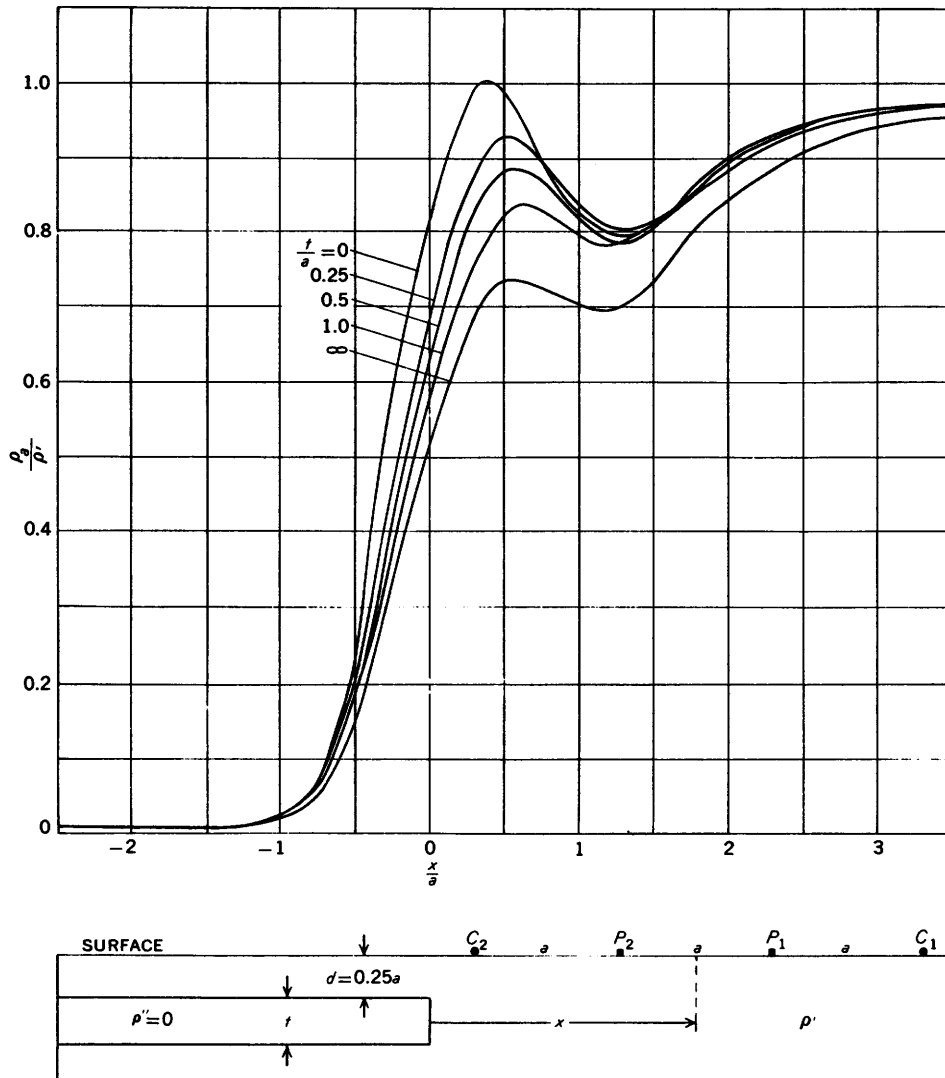
FIGURE 185.—Horizontal resistivity profiles across buried perfectly conducting semi-infinite horizontal plates of different thicknesses t, Wenner configuration (two-dimensional approximation). For all curves, depth of overburden $d=0.25$; $a=$unity. Adapted from Kiyono (1950c) by permission of Kyōtō University.

The overburden over a highly insulating bed (fig. 186) completely subdues the peaks that occur with no overburden; and the effect of the bed is much less pronounced on the downthrown side of the fault than the corresponding effect of the highly conducting material. The curve for infinite thickness in figure 186 can be computed from equation 241.

The horizontal resistivity profiles (two-dimensional approximations) with the Wenner configuration across buried semi-infinite vertical plates of different widths and depths of overburden are given in figures 188, 189, and 190. These curves are most useful when compared to the corresponding curves given in the sections on fissures and dikes.

Figures 189 and 190 show that the effect of overburden is much more for the highly resistant fissure or thin dike than for the corresponding highly conducting feature. In both figures, however, the size of the anomalies indicate that if the overburden thickness is equal to the electrode separation, the fissure would be barely detectable under ordinary field conditions; and this rule may serve as a criterion of the limit of detectability for buried fissures. The secondary peaks and troughs observed in figure 54 have been completely masked by the overburden in figure 190.

Figure 188 illustrates the transition from a paradoxical situation to an intuitively normal situation. The central peak in the curve for zero width corresponds to the same peak in figure 54 which is identical in turn to the curve for zero depth in figure 189. As the width of the dike increases (fig. 188), the central peak is subdued. For a width equal to half the electrode separa-
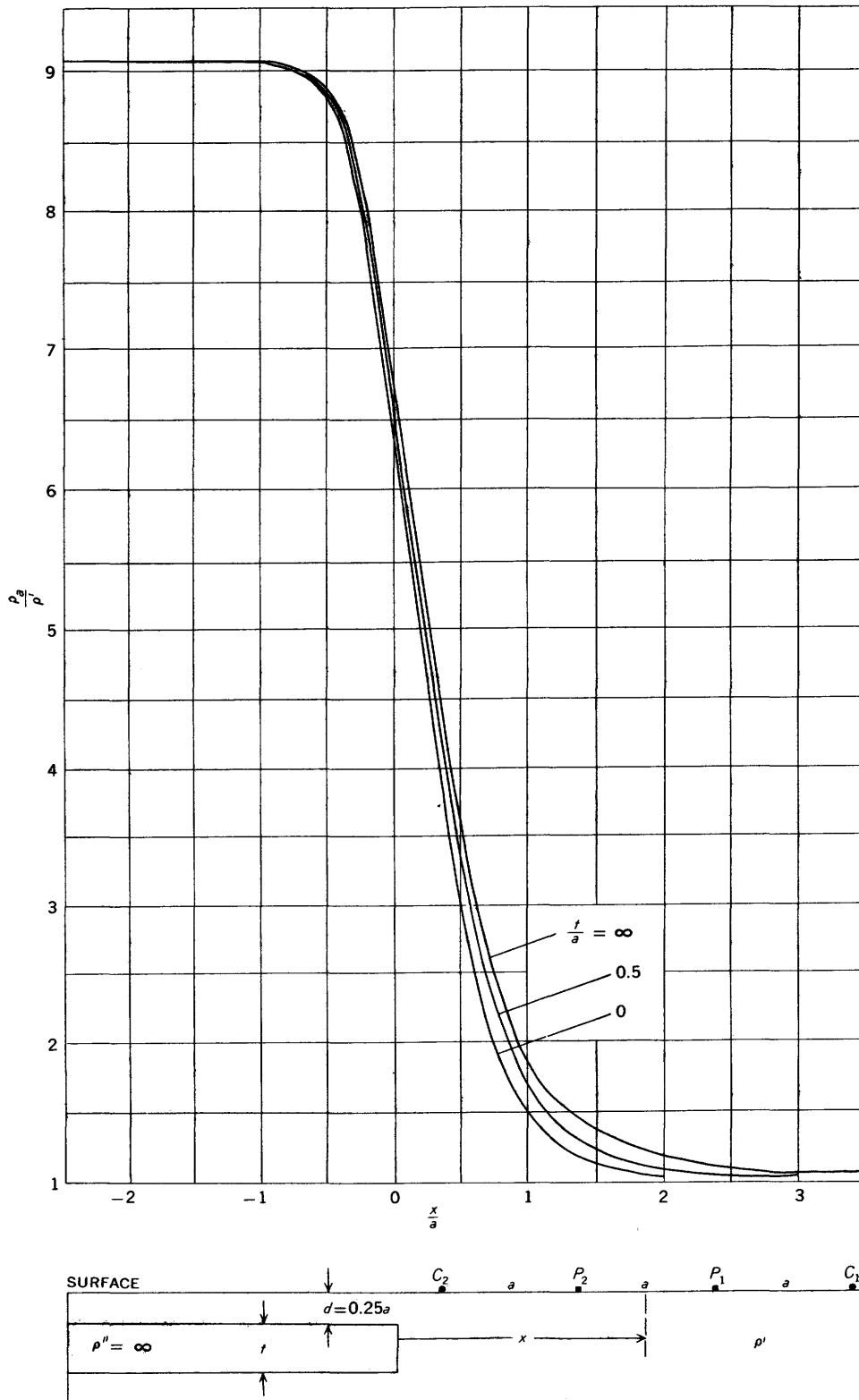
FIGURE 186.—Horizontal resistivity profiles across buried perfectly insulating semi-infinite horizontal plates of different thicknesses t, Wenner configuration (two-dimensional approximation). For all curves, depth of overburden $d=0.25$; $a=$unity. Adapted from Kiyono (1950c) by permission of Kyōtō University.
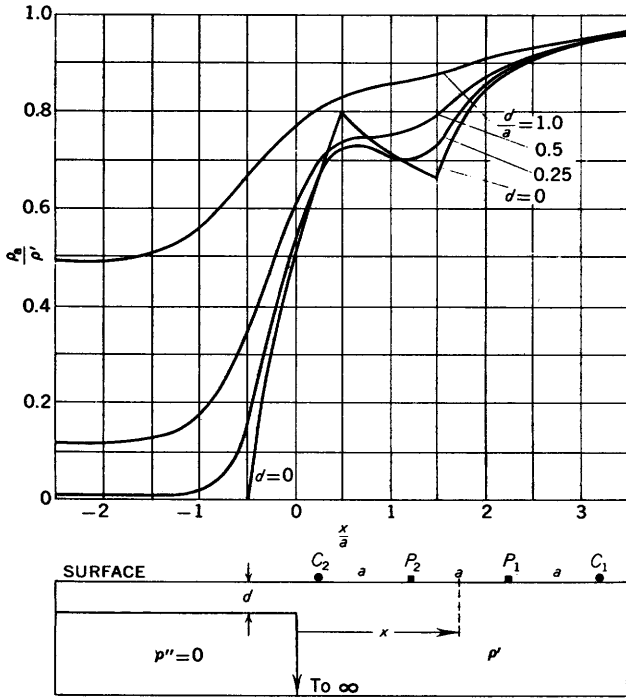
FIGURE 187.—Horizontal resistivity profiles across buried perfectly conducting material, faulted vertically to great depth, for different depths of overburden d, Wenner configuration (two-dimensional approximation). For all curves $a=$unity. Adapted from Kiyono (1950c) by permission of Kyōtō University.

FIGURE 189.—Horizontal resistivity profiles across buried perfectly conducting thin vertical plates of infinite depth extent and different depths of overburden d, Wenner configuration (two-dimensional approximation). $a=$unity. Adapted from Kiyono (1950c) by permission of Kyōtō University.
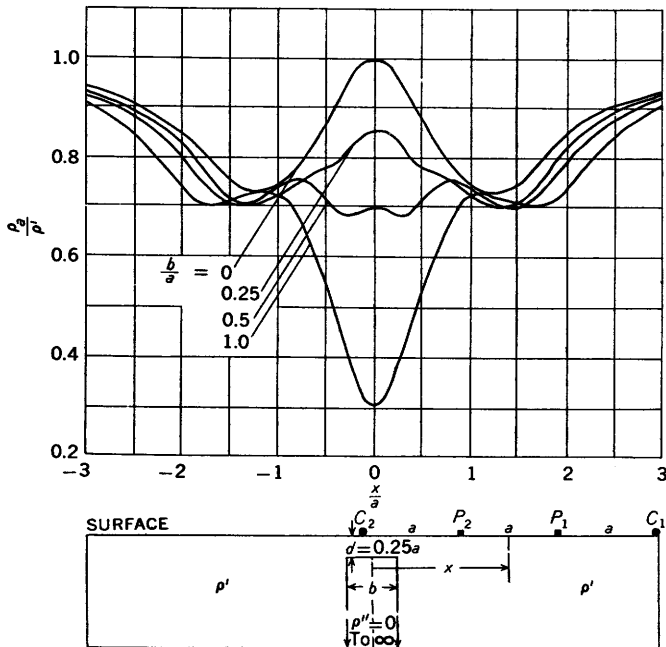
FIGURE 188.—Horizontal resistivity profiles across buried perfectly conducting vertical plates of infinite depth extent and different widths b, Wenner configuration (two-dimensional approximation). For all curves, depth of overburden $d=0.25$; $a=$unity; widths less than electrode separation. Adapted from Kiyono (1950c) by permission of Kyōtō University.
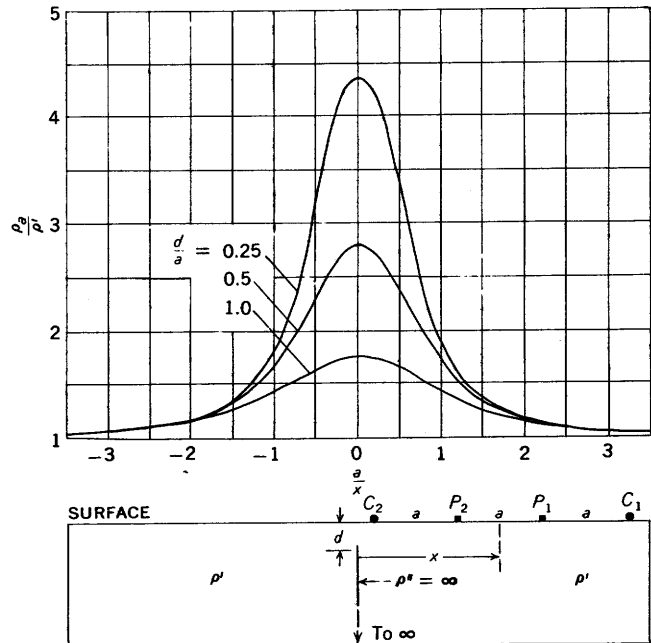
FIGURE 190.—Horizontal resistivity profiles across buried perfectly insulating thin vertical plates of infinite depth extent and different depths of overburden d, Wenner configuration (two-dimensional approximation). $a=$unity. Adapted from Kiyono (1950c) by permission of Kyōtō University.

tion, the curve oscillates for the most part about a medium-low value. This thickness is apparently critical, for with greater thicknesses the curve assumes a distinctly low trough directly over the center of the dike. For thicknesses greater than the electrode separation the curve assumes the aspect of the composite two faultlike curves (in juxtaposition), each of which corresponds to one edge of the dike.
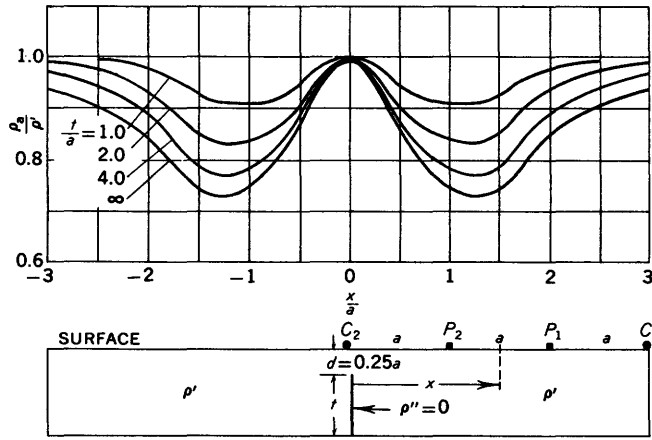
FIGURE 191.—Horizontal resistivity profiles across buried perfectly conducting thin vertical plates of different depth extents t, Wenner configuration (two-dimensional approximation). For all curves, depth of overburden $d=0.25$; a=unity. Adapted from Kiyono (1950c) by permission of Kyōtō University.

The extent to which a perfectly conducting fissure may be considered to be infinite in vertical extent is illustrated in figure 191. It should be remembered that the fissure extends infinitely in a horizontal direction. The rule indicated by the curves is that a fissure which extends downward a distance four or five times the electrode separation can be considered as infinite in vertical extent. Unfortunately, this rule is subject to radical changes depending on the resistivity contrast and the amount of overburden.
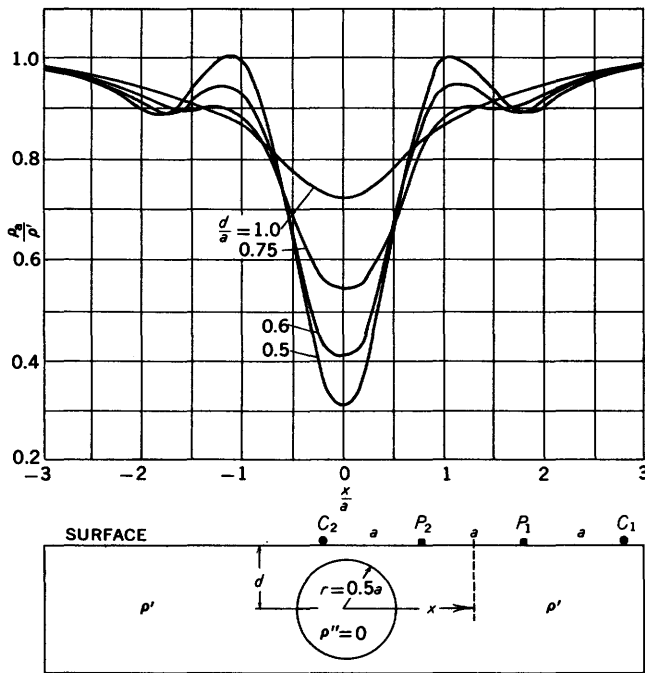
FIGURE 192.—Horizontal resistivity profiles across buried perfectly conducting circular cylinders of different depths to horizontal axis d, Wenner configuration (two-dimensional approximation). For all curves, radius of cylinder $r=0.5$; a=unity. Adapted from Kiyono (1950c) by permission of Kyōtō University.
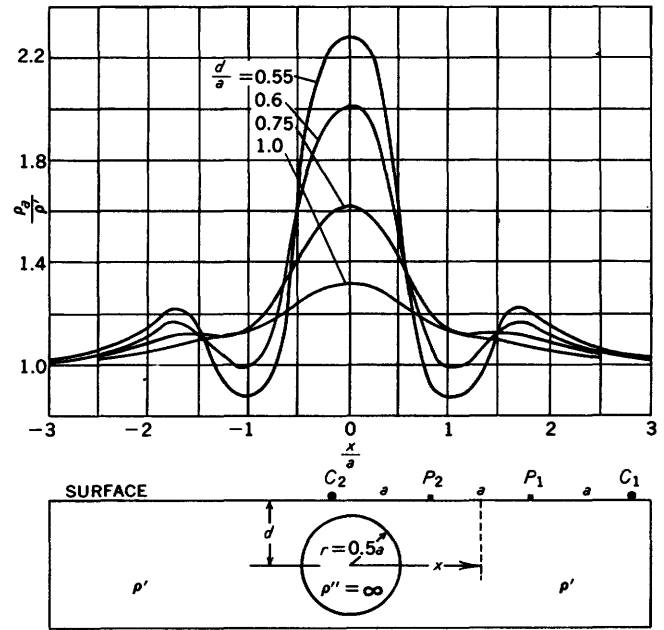
FIGURE 193.—Horizontal resistivity profiles across buried perfectly insulating circular cylinders of different depths to horizontal axis d, Wenner configuration (two-dimensional approximation). For all curves, radius of cylinder $r=0.5$; a=unity. Adapted from Kiyono (1950c) by permission of Kyōtō University.

Horizontal resistivity profiles (two-dimensional approximations) with the Wenner configuration across buried circular cylinders of different depths and various resistivity contrasts are shown in figures 192 to 195, inclusive. Geologically, this geometry may be thought to approximate buried stream channels and caverns. The radius of each cylinder is half the electrode separation. The relationships shown among the various families of curves should be compared with those given for the buried-sphere problem.

For perfectly conducting and insulating cylinders (figs. 192 and 193, respectively), the apparent-resistivity anomalies diminish rapidly with increasing depth of burial of the cylinder. In general, the shape of the curves is the same as that for the corresponding profiles over buried spheres. The cylinder is detectable at slightly greater depths than the sphere, however, provided the same criterion of detectability for the cylinder is used as that for the sphere—that is to say, a 10 percent anomaly. Although the curve is not shown in this set, it can be reasoned that the limiting depth is of the order of twice that of the sphere. At the limiting depth for the sphere (equal to the radius of the sphere from the surface of the earth to the top of the sphere), the anomaly over the cylinder has fallen to only about 30 percent.

The curves for cylinders of various resistivity contrasts (figs. 194 and 195) indicate that for lower resistivity contrasts the detectability of the cylinder is
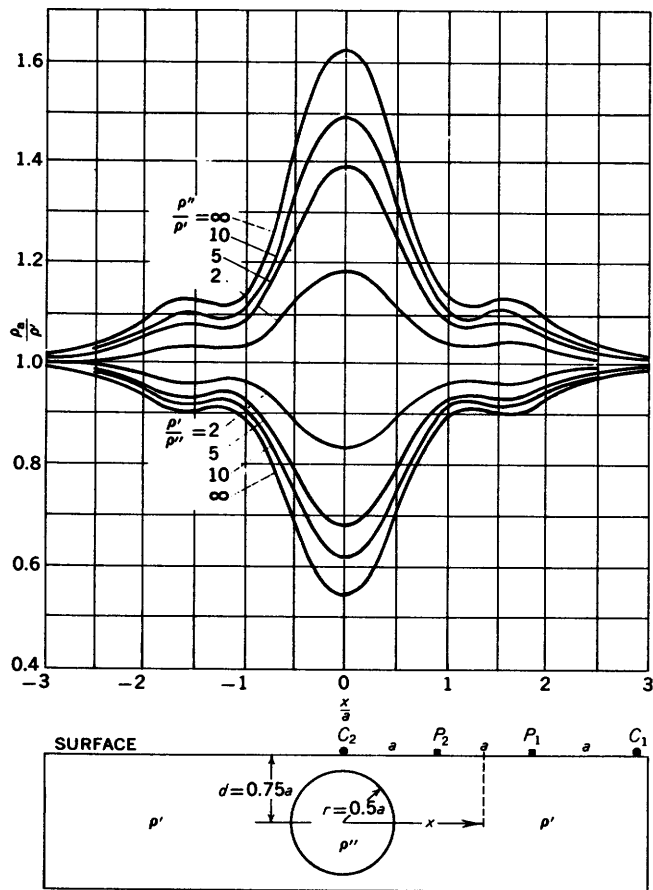
FIGURE 194.—Horizontal resistivity profiles across buried circular cylinders of different resistivity contrasts, Wenner configuration (two-dimentional approximation). For all curves, depth of horizontal axis $d=0.75$; radius of cylinder $r=0.5$; $a=$unity. Adapted from Kiyono (1950) by permission of Kyōtō University.

FIGURE 195.—Horizontal resistivity profiles across buried circular cylinders of different resistivity contrasts. Wenner configuration (two-dimensional approximation). For all curves, depth of horizontal axis $d=1.0$; radius of cylinder $r=0.5$; $a=$unity. Adapted from Kiyono (1950c) by permission of Kyōtō University.
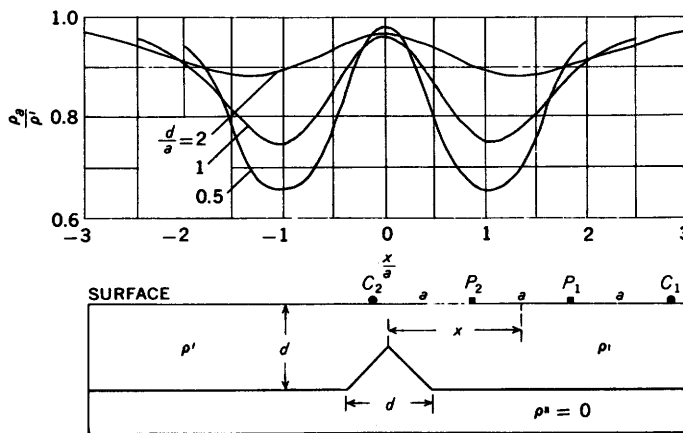
FIGURE 196.—Horizontal resistivity profiles across buried perfectly conducting symmetrical anticlines of different sizes and depths of burial, Wenner configuration (two-dimensional approximation); $a=$unity. Adapted from Kiyono (1950c) by permission of Kyōtō University.

considerably reduced. These same results may also be extended to apply to the buried sphere.

The buried anticline or syncline was approximated by Kiyono by using two inclined planes that intersect each other at a right angle. Figures 196 and 197 show horizontal resistivity profiles (logarithmic approximations) with the Wenner configuration across buried anticlines for different sizes and depths of burial. Following the pattern set previously in this section, the curves for the perfect conductor are W-shaped, whereas those of the perfectly insulating bed are simple symmetrical curves.

Figures 198 and 199 show horizontal profiles across buried synclines. Whereas for the anticlines the ratio of the depth to the width was kept constant, this ratio is varied for buried synclines. As ususal, the curves

over the insulating medium are regular. Over the conducting medium a paradox arises in that the secondary peaks are more pronounced at the intermediate case of $b=2$ and less pronounced for the larger and smaller synclines.
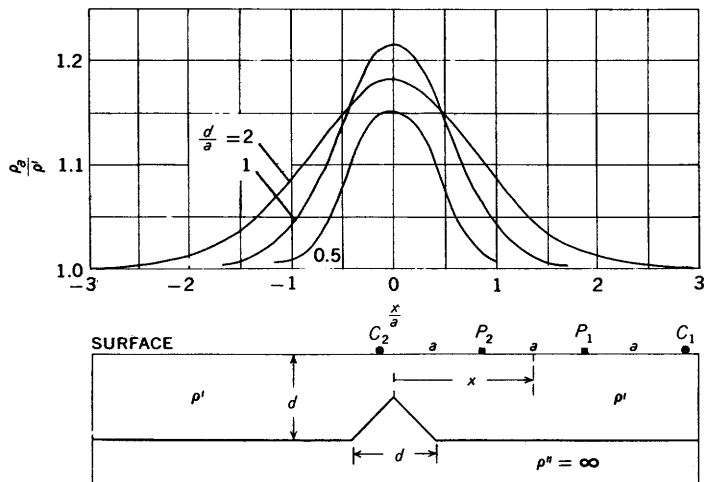
FIGURE 197.—Horizontal resistivity profiles across buried perfectly insulating symmetrical anticlines of different sizes and depths of burial, Wenner configuration (two-dimensional approximation); a=unity. Adapted from Kiyono (1950c) by permission of Kyōtō University.
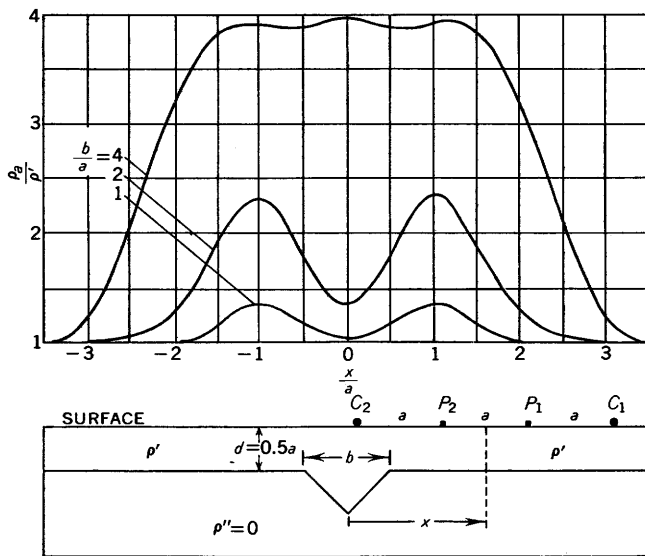
FIGURE 198.—Horizontal resistivity profiles across buried perfectly conducting symmetrical synclines of different sizes, Wenner configuration (two-dimensional approximation). For all curves, d=0.5; a=unity. Adapted from Kiyono (1950c) by permission of Kyōtō University.

BIBLIOGRAPHY

The comprehensive bibliography given below includes most of the important papers on the subject of resistivity methods of prospecting that use steady or commutated direct current. The subject matter is thus restricted to potential mapping, apparent resistivity, potential-drop ratio, spontaneous polarization, telluric currents, and their various modifications. Selected references are included on natural earth currents and potentials as well as on related subjects, because of their direct bearing on the phenomenon of current flow in the ground. All alternating-current techniques that distinctly depend on inductive effects are excluded.
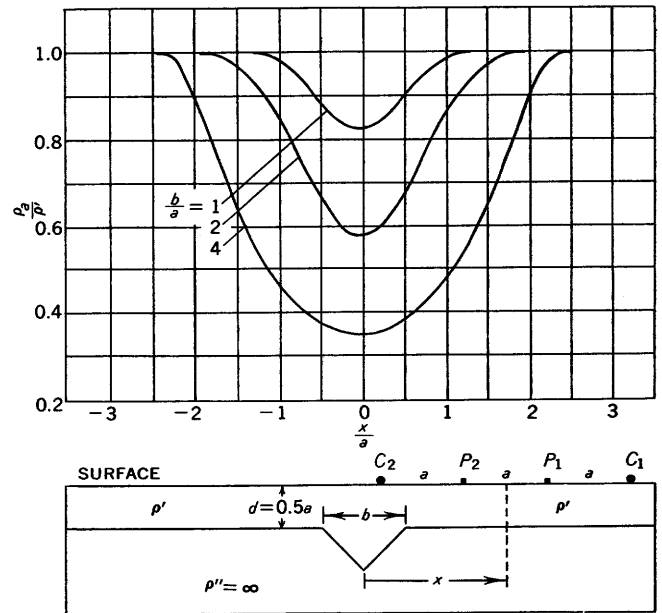

FIGURE 199.—Horizontal resistivity profiles across buried perfectly insulating symmetrical synclines of different sizes, Wenner configuration (two-dimensional approximation). For all curves, d=0.5; a=unity. Adapted from Kiyono (1950c) by permission of Kyōtō University.

Also excluded are radio techniques and the various pulse and transient methods. Certain key references to electrical well logging are included because of the similarity of basic principles and theory of surface and well-logging electrical measurements, but the reader is referred to such works as Guyod (1945), Rothé and Rothé (1952, p. 483), and "Geophysical Abstracts" for exhaustive lists of titles on the subject of well logging.

In this bibliography we have tried to include many papers of historical importance, even though they fail to give facts of great scientific importance, in order that students and investigators can refer to original source material not ordinarily available in texts.

No attempt has been made to include all references on the subject matter. The literature bearing on electrical methods is now so extensive that the compilation of all papers would be a prohibitive task. For an almost complete list of papers on electrical prospecting published prior to 1926, the reader is referred to Ambronn (1926; also to the English translation by Ambronn and Cobb, 1928), which contains about 400 separate papers on the subject, many, but far from all, of which are included here. In the choice of papers covering the period since the advent of the Wenner method in 1915, an attempt was made to include only those papers which make definite contributions to the art or which give critical—as opposed to descriptive—reviews of the subject matter. There is a preponderance of papers in the English language principally because of their availability to the authors as compared with the availability of many foreign papers. Many

foreign papers whose abstracts are not in "Geophysical Abstracts" are omitted from the bibliography because the substance of the paper is not clear from the title alone and the original papers were not available to us. For more exhaustive bibliographies of foreign material, the reader is referred to the three major foreign texts on electrical prospecting by Rothé and Rothé (1952); Krayev (1951), and Fritsch (1949b).

REFERENCES TO "GEOPHYSICAL ABSTRACTS"

Some of the references in the bibliography are annotated to indicate the principal subject matter. The abstract number in "Geophysical Abstracts" (abbreviated "GA" in the bibliography) is given for those papers that have been abstracted. Table 9 is given to help in finding any given abstract. Abstracts published prior to 1931 were not numbered and are given by the proper volume number and pagination in the U.S. Bureau of Mines Information Circular, as for example "GA No. 20, p. 14." Abstracts published during 1931 to 1953, inclusive, are given by a single abstract number only, without reference to volume number, as for example "GA 13950." Abstracts published during 1954 and thereafter are given by two numbers separated by a hyphen, as for example "GA 161–220"; the first number indicates the abstract volume number, the second number is the individual abstract number within the specific volume.

TABLE 9.—*Numbering code of "Geophysical Abstracts"*

[Symbols: IC, Information Circular; GA, Geophysical Abstracts]

Abstract	Month and year	Geophysical Abstracts (No.)	U.S. Bur. Mines publication	U.S. Geol. Survey Bulletin
1929			*IC*	
(¹)	May	1	6120	
(¹)	May	2	6133	
(¹)	July	3	6154	
(¹)	Aug	4	6164	
(¹)	Sept	5	6175	
(¹)	Nov	6	6203	
(¹)	Nov	7	6209	
(¹)	Dec	8	6224	
1930				
(¹)	Jan	9	6233	
(¹)	Feb	10	6253	
(¹)	Mar	11	6273	
(¹)	Apr	12	6287	
(¹)	May	13	6309	
(¹)	June	14	6324	
(¹)	July	15	6341	
(¹)	Aug	16	6355	
(¹)	Sept	17	6366	
(¹)	Oct	18	6393	
(¹)	Nov	19	6403	
(¹)	Dec	20	6422	
1931				
1 to 41	Jan	21	6441	
42 to 82	Feb	22	6452	
83 to 120	Mar	23	6461	
121 to 161	Apr	24	6478	
162 to 197	May	25	6500	
198 to 239	June	26	6511	
240 to 314	July	27	6528	
315 to 351	Aug	28	6547	
352 to 412	Sept	29	6559	
413 to 453	Oct	30	6568	
454 to 503	Nov	31	6575	
504 to 555	Dec	32	6583	

¹ Abstracts published before 1931 are unnumbered.

TABLE 9.—*Numbering code of "Geophysical Abstracts"*—Con.

[Symbols: IC, Information Circular; GA, Geophysical Abstracts]

Abstract	Month and year	Geophysical Abstracts (No.)	U.S. Bur. Mines publication	U.S. Geol. Survey Bulletin
1932			*IC—Con.*	
556 to 604	Jan	33	6593	
605 to 647	Feb	34	6569	
648 to 693	Mar	35	6606	
694 to 748	Apr	36	6620	
749 to 792	May	37	6628	
793 to 840	June	38	6638	
841 to 894	July	39	6646	
895 to 966	Aug	40	6655	
967 to 1023	Sept	41	6669	
			GA	
1024–1079	Oct	42	42	
1080–1119	Nov	43	43	
1120–1172	Dec	44	44	
1933				
1173–1197	Jan	45	45	
1198–1254	Feb	46	46	
1255–1307	Mar	47	47	
1308–1356	Apr	48	48	
1357–1401	May	49	49	
1402–1453	June	50	50	
1454–1495	July	51	51	
1496–1539	Aug	52	52	
1540–1577	Sept	53	53	
1578–1629	Oct	54	54	
1630–1674	Nov	55	55	
1675–1720	Dec	56	56	
1934				
1721–1756	Jan	57	57	
1757–1792	Feb	58	58	
1793–1841	Mar	59	59	
1842–1885	Apr	60	60	
1886–1935	May	61	61	
1936–1977	June	62	62	
1978–2018	July	63	63	
2019–2067	Aug	64	64	
2068–2112	Sept	65	65	
2113–2152	Oct	66	66	
2153–2199	Nov	67	67	
2200–2243	Dec	68	68	
1935				
2244–2279	Jan	69	69	
2280–2319	Feb	70	70	
2320–2378	Mar	71	71	
2379–2434	Apr	72	72	
2435–2486	May	73	73	
2487–2554	June	74	74	
2555–2618	July	75	75	
2619–2686	Aug	76	76	
2687–2751	Sept	77	77	
2752–2817	Oct	78	78	
2818–2885	Nov	79	79	
2886–2944	Dec	80	80	
1936				
2945–2999	Jan	81	81	
3000–3046	Feb	82	82	
3047–3090	Mar	83	83	
3091–3141	Apr	84	84	
3142–3188	May	85	85	
3189–3234	June	86	86	
3235–3524	July–Dec	87		887
1937				
3525–3656	Jan.–Mar	88		895–A
3657–3797	Apr.–June	89		895–B
3798–3933	July–Sept	90		895–C
3934–4103	Oct.–Dec	91		895–D
1938				
4104–4268	Jan.–Mar	92		909–A
4269–4424	Apr.–June	93		909–B
4425–4570	July–Sept	94		909–C
4571–4748	Oct.–Dec	95		909–D
1939				
4749–4886	Jan.–Mar	96		915–A
4887–5005	Apr.–June	97		915–B
5006–5161	July–Sept	98		915–C
5162–5298	Oct.–Dec	99		915–D
1940				
5299–5453	Jan.–Mar	100		925–A
5454–5601	Apr.–June	101		925–B
5602–5742	July–Sept	102		925–C
5743–5876	Oct.–Dec	103		925–D
1941				
5877–5992	Jan.–Mar	104		932–A
5993–6126	Apr.–June	105		932–B
6127–6248	July–Sept	106		932–C
6249–6376	Oct.–Dec	107		932–D

TABLE 9.—*Numbering code of "Geophysical Abstracts"*—Con.

[Symbols: IC, Information Circular; GA, Geophysical Abstracts]

Abstract	Month and year	Geo-physical Abstracts (No.)	U.S. Bur. Mines publica-tion	U.S. Geol. Survey Bulletin
	1942			*GA—Con.*
6377-6499	Jan.-Mar	108		939-A
6500-6586	Apr.-June	109		939-B
6587-6696	July-Sept	110		939-C
6697-6783	Oct.-Dec	111		939-D
	1943		*IC*	
6784-6888	Jan.-Mar	112	7256	
6889-7003	Apr.-June	113	7257	
7004-7132	July-Sept	114	7267	
7133-7252	Oct.-Dec	115	7273	
	1944			
7253-7379	Jan.-Mar	116	7285	
7380-7504	Apr.-June	117	7292	
7505-7643	July-Sept	118	7303	
7644-7785	Oct.-Dec	119	7310	
	1945			
7786-7932	Jan.-Mar	120	7324	
7933-8052	Apr.-June	121	7338	
8053-8185	July-Sept	122	7349	
8186-8326	Oct.-Dec	123	7355	
	1946			
8327-8484	Jan.-Mar	124	7384	
8485-8643	Apr.-June	125	7386	
8644-8806	July-Sept	126	7400	
8807-8962	Oct.-Dec	127	7414	
	1947			
8963-9138	Jan.-Mar	128		957-A
9139-9328	Apr.-June	129		957-B
9329-9518	July-Sept	130		957-C
9519-9707	Oct.-Dec	131		957-D
	1948			
9708-9961	Jan.-Mar	132		959-A
9962-10212	Apr.-June	133		959-B
10213-10472	July-Sept	134		959-C
10473-10736	Oct.-Dec	135		959-D
	1949			
10737-11001	Jan.-Mar	136		966-A
11002-11201	Apr.-June	137		966-B
11202-11441	July-Sept	138		966-C
11442-11678	Oct.-Dec	139		966-D
	1950			
11679-11907	Jan.-Mar	140		976-A
11908-12125	Apr.-June	141		976-B
12126-12339	July-Sept	142		976-C
12340-12513	Oct.-Dec	143		976-D
	1951			
12514-12700	Jan.-Mar	144		981-A
12701-12890	Apr.-June	145		981-B
12891-13092	July-Sept	146		981-C
13093-13283	Oct.-Dec	147		981-D
	1952			
13284-13547	Jan.-Mar	148		991-A
13548-13802	Apr.-June	149		991-B
13803-14003	July-Sept	150		991-C
14004-14183	Oct.-Dec	151		991-D
	1953			
14184-14388	Jan.-Mar	152		1002-A
14389-14598	Apr.-June	153		1002-B
14599-14804	July-Sept	154		1002-C
14805-15026	Oct.-Dec	155		1002-D
	1954			
156-1 to 156-187	Jan.-Mar	156		1022-A
157-1 to 157-201	Apr.-June	157		1022-B
158-1 to 158-227	July-Sept	158		1022-C
159-1 to 159-234	Oct.-Dec	159		1022-D
	1955			
160-1 to 160-203	Jan.-Mar	160		1033-A
161-1 to 161-220	Apr.-June	161		1033-B
162-1 to 162-250	July-Sept	162		1033-C
163-1 to 163-265	Oct.-Dec	163		1033-D
	1956			
164-1 to 164-318	Jan.-Mar	164		1048-A
165-1 to 165-384	Apr.-June	165		1048-B
166-1 to 166-380	July-Sept	166		1048-C
167-1 to 167-291	Oct.-Dec	167		1048-D
	1957			
68-1 to 168-335	Jan.-Mar	168		1066-A

COMPREHENSIVE LIST OF TITLES

Abercrombie, W. F., 1952, The practical value of an earth resistivity method in making subsurface explorations: Am. Soc. Testing Materials Spec. Tech. Pub. 122, p. 136-141. Resistivity. GA 14126.

Akerman, E. A., 1933, Nouvelle méthode de prospections électriques [New method of electrical prospecting]: L'Écho Mines et Métallurgie, v. 61, no. 3149, p. 496-499. GA 1699.

Aldredge, R. F., 1937, The effect of dipping strata on earth resistivity determinations: Colorado School of Mines Quart., v. 32, no. 1, p. 169-186.

Alexanian, C. L., 1932, Traité pratique de prospection géo-physique [Practical treatise on geophysical prospecting]: Paris, Librairie Polytech. Ch. Beranger, 268 p. Textbook. GA 885.

Alfano, Luigi, 1951, Studi sulla interpretazione dei sondaggi electrici verticali [Studies of the interpretation of the electrical resistivity curves obtained in vertical profiling]: Riv. Geofisica Appl., v. 12, no. 1, p. 21-33; v. 12, no. 2, p. 83-106. Resistivity theory. GA 13233 and GA 13731.

Al'pin, L. M., 1937, Differentsial'nyye krivyye zondirovaniya [Differential curves for depth profiles]: Neft. Geofiz. Byull., no. 4, p. 32-48. GA 4497.

——— 1941, Dipol'noe elektricheskoe zondirovaniye [Dipole electrical sounding]: Razvedka Nedr, no. 1, p. 26-35. GA 10866.

——— 1947, Istochniki polya v teorii elektrorazvedki [Sources of the electrical field in the theory of electrical prospecting]: Prikladnaya Geofizika, no. 3, p. 56-100. GA 9597.

——— 1950, Teoriya dipol'nykh zondirovaniy [The theory of dipole sounding]: Moscow, Gostoptekhizdat, 88 p. Mono-graph. GA 12647.

——— 1956, Nesimmetrichnoye (uglovoye) zondiroyaniye [Asymmetric (angular) electrical surveying]: Prikladnaya Geofizika, no. 14, p. 65-96. GA 168-77.

Alty, T., and Alty, S., 1930, The detection of rock salt by the methods of electrical surveying: Canadian Jour. Research, v. 3, no. 6, p. 521-525. Resistivity results. GA 100.

Ambronn, Richard, 1926, Methoden der angewandten Geo-physik [Methods of applied geophysics]: Dresden and Leipzig, Theodor Steinkopff, 372 p. English translation pub. 1928 (see Ambronn and Cobb, 1928). Textbook.

——— 1935, Elektrische Hilfsmittel in der geophysikalischen Bodenforschung [Electrical equipment in geophysical research]: Zeitschr. Elektrotech. v. 56, no. 21, p. 581-585. GA 2723.

Ambronn, Richard, and Cobb, M. C., 1928, Elements of geo-physics: New York, McGraw-Hill, 372 p. This is a trans-lation of Ambronn, 1926. Textbook.

Amirkhanov, Kh. I., 1936, Issledovaniye elektroprovodnosti gornykh porod [An investigation of the electrical conduc-tivity of rocks]: Akad. Nauk SSSR, Trudy Azerbaidzhan-kogo filial, ser. fiz.-khim., Baku, v. 28, p. 99-116.

Antokol'skiy, M. L., 1933, Primeneniye elektricheskoy razvedki dlya inzhenerno-geologicheskikh issledovaniy [Application of electrical methods of prospecting in engineering-geological investigations]: Razvedka Nedr, no. 14, p. 38-40. GA 2411.

Archambault, Jean, 1953, Quelques aspects de la prospection et de l'exploitation des eaux souterraines [Some aspects of the exploration and exploitation of ground water]: Inst. tech. bâtiment et travaux publics Annales, v. 6, no. 67-68, p. 657-672. GA 14854.

Archie, G. E., 1947, Electrical resistivity as an aid in core-analysis interpretation: Am. Assoc. Petroleum Geologists Bull., v. 31, no. 2, p. 350–366.

Arnold, G., 1937, Fehlerquellen bei der Messung von Erdströmen in kurzen Leitungen, untersucht im Taunus-Observatorium [Sources of error in measuring earth-currents in short lines, as observed in the Taunus Observatory]: Gerlands Beitr. Geophysik, v. 49, no. 1/2, p. 140–164. GA 3735.

Aronis, G., 1951, Research on the iron-pyrite deposits in the Hermioni mining district [In Greek with English summary]: Greece Uperesia Ereunon Upedaphous. Ereunai oruktou ploutou tēs Ellados [The Mineral Wealth of Greece]: Athens, G. S. Cristou and Son, v. 1, p. 175–188. GA 14266.

Asahina, T., and Kadowaki, T., 1937, The change of the electrical resistance of soil by freezing [in Japanese]: Meteorology Soc. Japan Jour., 2d ser., v. 15, p. 320–330. Resistivity. GA 4193.

Aynard, Cl., Arnaud, M., and Société Chériflenne des Pétroles, 1954, Etudes par sondages électriques du bassin Miocène du nord du Gharb [Electrical depth profiling studies of the Miocene basin of northern Gharb]: Internat. Geol. Cong., 19th, Algiers 1952, Comptes rendus, sec. 9, pt. 9, p. 217–229. GA 162–82.

Ayvazoglou, W., and Skitsky, V., 1945, Bibliography of Russian literature on geophysical exploration 1929–41: U.S. Bur. Mines Inf. Cir. 7323, 44 p.

Azccara, Gaetano, 1951, L'applicazione del metodo geoelettrico alla ricerca dell'acqua [The application of the geoelectric method in prospecting for water]: Servizio Geol. Italia Boll., v. 72, p. 203–213. Resistivity, example. GA 13955.

Bacon, L. O., 1956, The circular line electrode in equipotential prospecting: Mining Eng. v. 8, no. 2, p. 213–216. GA 165–118.

Ball, H. W., and Garson, M. S., 1951, Geophysical survey of the Blantyre-Limbe area: Nyasaland Geol. Survey Ann. Rept. 1950, p. 10. Resistivity map. GA 13041.

Baranov, V., 1951, Interprétation quantitative des mesures en prospection par courants telluriques [Quantitative interpretation of the data in exploration by telluric currents]: World Petroleum Cong., 3d, [The Hague] Proc., sec. 1, p. 646–653. Self-potential. GA 13734.

Barnes, H. E., 1952, Soil investigations employing a new method of layer-value determination for earth resistivity interpretation: Highway Research Board Bull. 65, p. 26–36. Resistivity. GA 156–70.

Bartley, M. W., 1939, Hematite deposits, Steeprock Lake: Canadian Inst. Mining Metall. Trans., v. 42, no. 327, p. 359–370. Resistivity. GA 5219.

Barton, D. C., 1927, Applied geophysical methods in America: Econ. Geology, v. 22, p. 649–668. Excellent historical review of the development of geophysical prospecting methods.

Barus, Carl, 1882, On the electrical activity of ore bodies, in Becker, George F., Geology of the Comstock lode and the Washoe district: U.S. Geol. Survey Mon. 3, p. 309–367, 400–404.

Bayard-Duclaux, F., 1933, Influence de l'eau d'imbibition des roches sur leur conductibilité électrique [Influence of absorbed water of rocks upon their electrical conductivity]: Acad. Sci. [Paris] Comptes rendus, v. 197, no. 16, p. 854–856. GA 2043.

———— 1936, Recherches sur la conductibilité électrique des roches [Investigations on the electrical conductivity of rocks]: Annales Physique, ser. 11, v. 6, p. 5–107. GA 3374.

Bays, C. A., 1946, Use of electrical geophysical methods in groundwater supply: Illinois Geol. Survey Circ. 122, 35 p. GA 8868.

Bays, C. A., and Folk, S. H., 1944, Developments in the application of geophysics to ground water problems: Illinois Geol. Survey Circ. 108, 25 p. GA 7878.

Běhounck, Rudolf, 1953, Geoelektrické sondovani zakladové půdy přehradniho mista no Vltávě u Zlakovic [Geoelectric exploration for the dam over the Vltava River near Zlakovice]: p. 89–90 in Zoubek, Vladimir, The geological basis for the project of the Orlik dam on the Vltava near Zlakovice: Československá Akad. Věd. Geotechnica, v. 15, 126 p. GA 164–111.

Belluigi, Arnaldo, 1929, Un metodo elettrico d'indagine del sottosuolo [An electrical method of investigation of the substrata]: Mineria Italiana, v. 13, p. 329–331. Resistivity.

———— 1930a, Il problema dell'elettrodi e la misura della conducibilità elettrica delle roccie [The electrode problem in the measurement of rock conductability]: Industria Mineraria, v. 15, no. 1, 8 p.

———— 1930b, Sur les prospections électriques du petrole [On electrical prospecting for oil]: Rev. Pétrolifère, no. 394, p. 1451–1454. GA no. 20, p. 14.

———— 1930c, Nuove vie per lo studio di piccole deformazioni delle linee di corrente sulla superficie d'un suolo elettrizzato [New ways for studying small deformations of the current lines on the surface of an electrified ground]: Cong. Internat. Mines, Metallurgie, Geologie appl., 6th Liege, sec. Geologie, p. 285–287. GA 579.

———— 1932, Determinations of the salt water horizons in large oil bearing anticlines: Beitr. angew. Geophysik, v. 2, p. 337–343.

———— 1933a, Possibilità sperimentali relative ai metodi geoelettrici wenner e racom [Experimental tests regarding Wenner and Racom geoelectric methods]: Soc. Geol. Italiana Boll., v. 52, no. 1, p. 173–180. GA 1599.

———— 1933b, Progressi nelle ricerche elettriche del petrolio [Progress in electrical prospecting for oil]: Industria Mineraria, v. 7, no. 6, 11 p. GA 1600.

———— 1934a, Studio di un profilo qualsiasi di sondaggio elettrico wenner [Study of profiles of any number of layers by Wenner's electrical method]: Beitr. angew. Geophysik, v. 4, p. 126–133. GA 1952.

———— 1934b, Über den Effekt der Anisotropie bei Gleichstrommessungen [On the effect of anisotropy in direct-current measurements]: Beitr. angew. Geophysik, v. 4, p. 400–406. GA 2176.

———— 1934c, Individuazone e determinazione di dicchi e colate basaltische sepolte col metodo geoelettrico wenner [Delineation and determination of buried basaltic dikes and intrusions by the Wenner geoelectric method]: Accad. Naz. Lincei, Atti Cl. Sci. fis. mat. e nat. Rend, ser. 6, v. 19, p. 337–340. GA 2172.

———— 1934d, Sviluppi del problema della conducibilità elettrica dei complessi sedimentari [Development of the problem concerning the electrical conductivity of sedimentary masses]: Soc. Geol. Italiana Boll., v. 53, no. 2, p. 223–231. GA 2721.

———— 1935a, Aufsuchen von erdölhöffigen Strukturen durch Messung des scheinbaren spezifischen Widerstandes [Search for oil-bearing structures by measurement of apparent specific resistivity]: Zeitschr. Petroleum, v. 31, no. 5, p. 1–2. GA 2523.

Belluigi, Arnaldo, 1935b, Sull'impiego delle curve universali di resistività apparente di Hummel [On the application of Hummel's apparent-resistivity universal curve]: Beitr. angew. Geophysik, v. 5, no. 3, p. 296–302. GA 3066.

———— 1936a, Sui Metodi interpretativi delle curve p_s per piu strati paralleli sovrapposti [On the methods of interpreting the p_s curve for several superposed parallel layers]: Beitr. angew. Geophysik, v. 6, no. 1, p. 14–24. Resistivity. GA 3375.

———— 1936b, Theoretical outlines of electrical coring: Beitr. angew. Geophysik, v. 6, no. 1, p. 25–37. Logging method. GA 3376.

———— 1937, Theoretische Grundzüge der Selbstpotential-messungen über Erzlagerstätten [Theoretical foundations of self-potential measurements above ore deposits]: Beitr. angew. Geophysik, v. 7, p. 172–178. Self-potential. GA 4352.

———— 1956a, Su una vexta quaestio di gerarchia nei dispositivi dei sondaggi elettrici [A moot question of the graduated arrangement of electric methods]: Geofisica Pura e Appl., v. 34, p. 51–56. GA 168–80.

———— 1956b, Principi d'equivalenza geoelettrica ed erroneità di alcune leggi di composizione nei sondaggi elettrici su terrenti a piu strati [Principles of geoelectric equivalence and the error of some distribution laws of electric methods for multilayer ground]: Geofisica Pura e Appl., v. 34, p. 57–65. GA 168–79.

Berdichevskiy, M. N., and Petrovskiy, A. D., 1956, Metodika vypolneniya dvustoronnikh ekvatorial'nykh zondirovaniy [Procedures of bilateral equatorial electrical surveying]: Prikladnaya Geofizika, no. 14, p. 97–114. GA 168–78.

Berdichevskiy, M. N., and Zavadskaya, T. N., 1955, K voprosu o stanovlenii elektricheskogo polya v zemle [On the building up of the electric field in the ground]: Akad. Nauk SSSR Izv. ser. geofiz., no. 2, p. 178–180. GA 161–51.

Berel'kovskiy, Ts. Ya, and Zubanov, B. G., 1951, Ob elektro-profilirovanii nad naklonnym kontakon [The determination of an inclined contact by the electrical method]: Akad. Nauk SSSR Izv. ser. geofiz., v. 15, no. 3, p. 16–30. Resistivity theory. GA 13950.

Berg, J. W., Jr., 1952, Conductivity study of aqueous kaolin NaCl mixtures: Producers Monthly, ser. 3, v. 16, p. 36.

Bergström, Gunnar, 1914, Försök med elektrisk malmletning: [Experiments with electrical ore prospecting]: Sveriges Geol. Undersökning, ser. C, no. 259 Årsbok 7, (1913), no. 6, p. 1–9.

Berthelot, Charles, 1933, Recherche du pétrole par l'application de la méthode de la carte de résistivité du sol [Prospecting for oil by the application of the method of the earth-resistivity map]: La Nature, no. 2911, p. 147–150. GA 1698.

Bibikov, N. S., 1940, Opyt primeneniya elektrorazvedki dlya opredeleniya treshchin v gornykh porodakh [A test of the application of the electrical method of exploration to determining the direction of fissures in rocks]: Zhur. Fiziki, Moscow, no. 13, p. 1143–1146.

Bjerkness, V., 1933, Geopotential: Union Geod. Geophys. Internt., no. 2, p. 7–13. GA 2466.

Bleil, D. F., 1953, Induced polarization: A method of geophysical prospecting: Geophysics, v. 18, p. 636–661. GA 14646.

Blondeau, E. E., 1939, Shallow resistivity survey at South Elton, Louisiana: Geophysics, v. 4, p. 271–278. GA 5374.

Bogdanov, A. I., 1940, Graficheskiy metod interpretatsii neko-torykh tipov trekhsloynykh krivykh vertikal'nykh elektri-cheskikh zondirovaniy [Graphical method of interpreting some types of three-layer curves by vertical electric re-sistivity measurements]: Tsentral'nogo nauchno-issledo-vatel'skogo geologo-razvedochnogo instituta Geofizika, v. 8. p. 63–75. Resistivity. GA 5649.

Böhm, Helmut, and Salzman, Günther, 1952, Die geophysi-kalische Untersuchung der Arsenikalkieslagerstätte zu Reichenstein (Schlesien) [Geophysical investigation of arsenical pyrite deposits at Reichenstein (Silesia)]: Zeitschr. Erzbergbau u. Metallhüttenwesen, v. 5, no. 10, p. 400–402. GA 14866.

Boissonnas, Eric, and Leonardon, E. G., 1948, Geophysical exploration by telluric currents, with special reference to a survey of the Haynesville salt dome, Wood County, Texas: Geophysics, v. 13, p. 387–403. Telluric current. GA 10588.

Bondarenko, A. P., 1953, Ob induktsionom elektricheskom polye vertekal'noi sostavlyayushchei geomagnitnykh variatsiy [Electric field induced by the vertical component of geo-magnetic variations]: Akad. Nauk SSSR Doklady, v. 90, no. 3, p. 367–370. Telluric current. GA 14644.

Borrego, Gonzalez, Joaquin, 1951, Nuevo interruptor doble de precisión para compensaciones en el metódo electrico de corriente continua, con potenciómetro de oposición [A new precise two-way switch for compensation in the direct-current electrical method with an opposing potentiometer]: Inst. geol. min. España notas y comunicaciones, no. 24, p. 73–78. Resistivity instrumental. GA 13738.

Bossolasco, Mario, 1940, Sulla prospezione geoelettrica del vulcani [Concerning geoelectrical prospecting of volcanoes]: Geofisica Pura e Appl., v. 2, no. 1, p. 56–59.

———— 1947, Sulle correnti telluriche nelle regioni equatoriali [On telluric currents in equatorial regions]: Geofisica Pura e Appl., v. 10, no. 1–2, p. 41–53. GA 9833.

Breslav, T. B., and Dorokhin, I. V., 1934, Geologo-razvedochnyye i elektro-razvedochnyye raboty na Kizylkiyskom mestoro-zhdenii [Geological and electrical exploration of the Kizilkiisk deposit]: in Nedra Sredney Azii, no. 5–6, p. 45–51.

Breusse, J. J., 1932, Electrical prospecting in Canada: Eng. Mining Jour., v. 133, p. 337–338. GA 999.

———— 1937, Application de la méthode des résistivités dans le bassin pétrolifere roumain [Application of the resistivity method to the Rumanian petroleum basin]: World Petroleum Cong., 2d [The Hague], Proc., v. 1, sec. 1, p. 717–722.

———— 1950, La prospection électrique appliquée aux recher-ches hydrologiques dans la presqu'île de Dakar, A.O.F. [Electrical prospecting applied to ground-water investiga-tions on the Dakar peninsula, French West Africa]: Internat. Geol. Cong., 18th [London], 1948, Proc., pt. 5, sec. D, p. 16–25. Resistivity. GA 12836.

———— 1956, Recherche des gisement de pyrite par prospection électrique [Exploration of pyrite bodies by electrical pros-pecting]: Rev. Industrie Minérale, Recherche minière, spec. no. 1 R, p. 225–232. GA 168–94.

Breusse, J. J., and Huot, G., 1954, Hydrological surveys in the Catania area by means of electrical soundings: Geophys. Prosp., v. 2, p. 227–231. GA 159–80.

Brichta, L. C., and Ryan, J. P., 1958, Practical evaluation of electrical-resistivity surveys as a guide to zinc-lead explora-tory drilling, Badger-Peacock Camp and vicinity, Chero-kee County, Kansas: U.S. Bur. Mines Rept. Inv. 5426, 91 p., 38 figs.

Broderick, T. M., and Hohl, C. D., 1928, Geophysical methods applied to exploration and geologic mapping in the Michigan copper district: Econ. Geology, v. 23, p. 489–514.

Broughton Edge, A. B., 1929, Electrical prospecting: Inst. Mining and Metallurgy [London] Trans., v. 38, p. 323–334; Inst. Mining and Metallurgy [London] Bull. 295, p. 42–53. GA no. 15, p. 13–15.

——— 1932, Geophysical methods of prospecting: Royal Soc. Arts Jour., v. 80, p. 553–579. GA 1190.

Broughton Edge, A. B., and Laby, T. H., 1931, Principles and practice of geophysical prospecting: Cambridge, The Univ. Press, p. 9–134, 236–298. GA 434.

Bruckshaw, J. M., 1933, Electrical methods of geophysical prospecting: Inst. Elec. Engineers Jour., v. 73, p. 521–541. GA 1825.

——— 1939, A new geophysical instrument: Mining Mag., v. 60, no. 5, p. 265–271. GA 5220.

Bruckshaw, J. M., and Dixey, F., 1934, Ground water investigations by geophysical methods: Mining Mag., v. 50, p. 73–84, 147–154. GA 1913.

Bubnoff, Serge von, 1952, Hydrologie, geologische Struktur und elektrische Leitfähigheit des Bodens in Norddeutschland [Hydrology, geologic structure, and electrical conductivity of the ground in northern Germany]: Deutsche Akad. Wiss. Berlin Sitzungsber. Kl. Math.-Naturw., 1951, no. 1, 43 p. Field examples. GA 14464.

Buchheim, W., 1947, Die Bestimmung des spezifischen elektrischen Widerstandes von anisotrop leitenden homogenen Medien nach der Vier-Punkt-Methode [Determination of the resistivity of homogeneous isotropic conducting media using the method of four point reading]: Geofisica Pura e Appl., v. 10, no. 3–4, p. 102–113. GA 9834.

Buckner, G. O., 1954, Sub-surface electrical measurements about two plane interfaces: Geophysics, v. 19, p. 297–309. Resistivity theory. GA 157–53.

Buehler, H. A., 1931, Geophysical prospecting: Missouri Bur. Geology and Mines Biennial Rept. (Rolla), p. 15–16; and App. 3, p. 146–161. Resistivity results.

Buhle, M. B., 1953, Earth resistivity in ground water studies in Illinois: Am. Inst. Mining Metall. Engineers Trans., v. 196, p. 395–399. Field examples. GA 14460.

Bukhnikashvili, A. V., 1938, Experimental'nyye issledovaniya anomal'nykh elektricheskikh poley v tverdoy srede [Experimental investigations of anomalous electric fields in a solid medium]: Tbiliskiy geofiz. Inst. Trudy, Tbilisi, v. 3, p. 43–63.

——— 1940, Elektricheskiye soprotivleniya porod i rud [The electrical resistances of rocks and ores]: Izv. Gruzinskoy Indus. Instituta, Tbilisi, no. 12, p. 1–31.

——— 1955, K voprosuo metodike postanovke elektrorazvedki rudnykh mestorozhdeniy [On the procedure of prospecting for ore deposits by electric methods]: Akad. Nauk Gruzin. SSR Soobshch., v. 16, no. 10, p. 775–779. GA 168–82.

Bukhnikashvili, A. V., and Kebuladze, V. V., 1939, Elektrorazvedka mestorozhdeniya medi v sel. Raro [Electrical prospecting for copper deposits in the village of Raro]: Tbiliskiy geofiz. Inst. Trudy, Tbilisi, v. 4, p. 127–153.

Bulashevich, Yu. P., 1943, K. voprosu ob izuchenii elektricheskikh anomaley po modelyakh [Concerning the question of studying electrical anomalies on models]: Akad. Nauk SSSR Izv., ser. geog. i geofiz., no. 6, p. 354–358. [Russian, English summ.] GA 7700.

Bulashevich, Yu, P., and Zakharchenko, V. F., 1956, Potentsial yestestvenno polyarizovannykh tel ellipsoidal'noy formy [The potential of naturally polarized ellipsoidal bodies]: Akad. Nauk SSSR Izv. ser. geofiz., no. 10, p. 1174–1181. GA 168–84.

Bursian, V. R., 1929, Fizicheskiye osnovaniya metoda ekvipotentsial'nykh liniy [The physical basis of the method of equipotential lines]: Geol. Komitet materialy po obshch. prik. geologii, no. 137, p. 5–35. Equipotential line method. GA no. 12, p. 8–9.

Bursian, B. P., Dedushkevich, S. I., Rodionov, P. F., and Sofronov, N. I., 1929, Fizicheskiye i eksperimental'nyye osnovaniya metoda ekvipotentsial'nykh liniy [Physical and experimental foundations of the method of equipotential lines]: Materialy po Obschchey i Prikladnoy Geologii, Leningrad, no. 137, 48 p.

Cagniard, Louis, 1948, Importance des phénomènes d'anisotropie dans le problème de l'interprétation des données d'un sondage électrique, consequences pratiques [Importance of anisotropy in the interpretation of electrical vertical-profiling data and some practical consequences]: Inst. Physique du Globe Strasbourg Annales, n. s., v. 4, no. 3, p. 3–28. GA 11101.

——— 1950, La prospection géophysique [Geophysical prospecting]: Paris, Presses Universitaires de France, 204 p. GA 12606.

——— 1953, Principe de la méthode magnétotellurique, nouvelle méthode de prospection géophysique [Principles of the magneto-telluric method, a new method of geophysical prospecting]: Annales Geophysique, v. 9. pp. 95–125. Translation published simultaneously as 1953, Basic theory of the magneto-telluric method of geophysical prospecting: Geophysics, v. 18, p. 605–635. Magneto-telluric. GA 14645.

Card, R. H., 1933, Some recent earth resistivity measurements in the United States: Am. Geophys. Union Trans., v. 14, p. 111–115.

——— 1935, Earth resistivity and geological structure: Am. Inst. Elec. Engineers Trans., v. 54, p. 1153–1161. Contains chart showing correlation of resistivities with geological periods and materials. GA 3205.

——— 1937, Correlation of earth resistivity with geological structure and age: Am. Inst. Mining Metall. Engineers Tech. Pub. 829, 19 p.; 1940, Trans., v. 138, p. 380–398. Resistivity. GA 3871.

Carpenter, E. E., and Leonardon, E. G., 1930, Geophysical studies predict rock conditions and tunnel site: Eng. News Record, v. 105, p. 364–365. Resistivity results.

——— 1931, Geophysical investigation at Bridge River tunnel: The Miner, v. 4, p. 11–12. GA 578.

Carpenter, E. W., 1955, Some notes concerning the Wenner configuration: Geophys. Prosp., v. 3, p. 388–402. GA 164–107.

Carpenter, E. W., and Habberjam, G. M., 1956, A tri-potential method of resistivity prospecting: Geophysics, v. 21, p. 455–469. GA 165–120.

Carreño, Alfonso de la O., 1944, A new development of the theory and application of the potential-drop-ratio method of electrical prospecting: Am. Geophys. Union Trans., v. 25, pt. 4, p. 575–584. GA 8244.

——— 1948, The two non-parallel layers problem according to the new development of the potential-drop-ratio method of electrical prospecting: Am. Geophys. Union Trans., v. 29, no. 1, p. 51–58. GA 10078.

Carrette, G., and Kelly, S. F., 1928, Discovery of salt domes in Alsace by electrical exploration: Mining and Metallurgy, v. 9, p. 398–401; 1929, Am. Inst. Mining Metall. Engineers Trans., v. 81, p. 211–220. Resistivity results. GA no. 12, p. 16.

Carslaw, H. S., 1930, Introduction to the theory of Fourier's series and integrals, 3d ed.: London, MacMillan and Co. Ltd., 368 p.

Ceccaty, R. P. de, 1932, Sur l'application des mesures de resistivité électrique du sous-sol aux problèmes stratigraphiques et tectoniques [On the application of measurements of electrical resistivity of the subsoil to stratigraphic and tectonic problems]: Soc. géol. France Bull., ser. 5, v. 2, p. 29–43. GA 2001.

Cechura, F., 1947, Geoelektrické zjist'ovani zlomů v kure zemské odporovým měřením [Determination of geologic faults by the resistivity method]: Věstník Státního Geologického Ústavo Československé Republiky, v. 22, p. 271–276. GA 10342.

Chahnazaroff, D. A., 1954, Investigación de las fundaciones en las construciones de gran peso mediante la aplicación del método geoelectrico [Investigation of the foundations in heavy construction by the geoelectric method]: Mineria y Metalurgia, no. 156, p. 29–32; and no. 158, p. 39–42. Resistivity. GA 159–64.

Chang, T. H., 1949, Application of Wenner's method: Chinese Geophys. Soc. Jour., v. 1, no. 2, p. 228. Resistivity. GA 12057.

Chanturishvili, L. S., 1951, Ob iskazhenii odnorodnogo elektricheskogo polya nerovnost'yu dnevnoy poverkhnosti v vide chetyrekhgrannoy prezmy [On the disturbance of a homogeneous electric field produced by an irregularity having a prismatic cross section]: Akad. Nauk Gruzin. SSR Soobshch., v. 12, no. 10, p. 597–603. GA 156–59.

Chao, J. S., and Kao, S. K., 1948, A field test of the potential gradient method: Chinese Geophys. Soc. Jour., v. 1, no. 1, p. 56–58. GA 11102.

Charrin, P., 1933, Application des techniques électriques aux problèmes de prospection et d'études géologiques [Application of electrical technique to the problems of prospecting and geological studies]: Soc. franc. electriciens Bull., no. 34, p. 1–31. GA 2000.

Chastenet de Géry, Jérôme, and Kunetz, Géza, 1956, Potential and apparent resistivity over dipping beds: Geophysics, v. 21, p. 780–793. GA 166–147.

Chereau, J. Y., and Roger, A. H., 1952, Étude électrotellurique sur la dorsale Ferraraise et comparaison avec les résultats apportes par d'autres méthodes [Electrotelluric survey of the Ferraran ridge and comparison with the results obtained by other methods]: Convegno naz. metano e petrolio, 7mo, Taormina 1952, Atti, v. 1, p. 589–600. GA 159–81.

Chetayev, D. N., 1956, Odna teorema elektrozarvedki [A theorem of electric exploration]: Akad. Nauk SSSR Izv. ser. geofiz., no. 4, p. 473–474. GA 166–141.

Ciuk, Edward, 1951, Geoskop [In Polish with English summary]: Pánstwowy Inst. Geol. Prace, v. 7, p. 65–93. Evaluation of Geoskop instrument. GA 156–62.

Clark, A. R., 1956, The determination of the long dimension of conducting ore bodies: Geophysics, v. 21, p. 470–478. GA 165–121.

Clark, A. R., and Salt, D. J., 1951, The investigation of earth resistivities in the vicinity of a diamond drill hole: Geophysics, v. 16, p. 659–665. Inhole. GA 13234.

Claudet, E., 1932, K voprosu o prirode PS [Concerning the nature of spontaneous polarization]: Azerbaydzhanskoye Neft. Khoz., no. 12, p. 55–61. GA 1373.

Compagnie Générale de Géophysique, La, 1955, Abaques de sondage électrique [Curves of electric profiling]: Geophys. Prosp., v. 3, supp. no. 3, 7 p. Many charts for three-layer case with explanation of Schlumberger configuration.

Conklin, H. R., 1917, Prospecting with electricity: Eng. Mining Jour., v. 104, p. 339–340. Electromagnetic.

Cook, J. C., 1956, An electrical crevasse detector: Geophysics, v. 21, p. 1055–1070. GA 167–98.

Cook, K. L., 1954, Resistivity surveys over slump structures, Tri-State lead-zinc mining district, Cherokee County, Kansas [abs.]: Geophysics, v. 19, p. 631.

Cook, K. L., and Van Nostrand, R. G., 1954, Interpretation of resistivity data over filled sinks: Geophysics, v. 19, p. 761–790. GA 159–68.

Cooper, W. G. G., 1934, Electrical prospecting: Mining Mag. v. 51, p. 275–279. GA 2297.

——— 1949, Electrical aids in water finding: Nyasaland Geol. Survey Bull. no. 7, 23 p. Resistivity, self-potential. GA 12468.

Cox, A. H., 1935, Geophysical surveying in South Wales: Mining Mag., v. 53, p. 73–82. GA 2849.

Cox, A. H., Davies, D. A. B., and Williams, T. G., 1935, Detecting underground water in mining areas—trials of geoelectric methods in South Wales: Colliery Guardian, v. 151, p. 377–380, 427–428. GA 2900.

Craig, R. L., 1938, Testing resistivity of soil: Petroleum Engineer, v. 9, p. 80–86. GA 4656.

Crosby, I. B., 1929, Locating deeply buried bed rock: Eng. and Contracting, v. 68, no. 10, p. 429–430. GA no. 16, p. 10–11.

Crosby, I. B., and Kelly, S. F., 1929, Electrical subsoil exploration and the civil engineer: Eng. News Record, p. 270–273. Resistivity. GA no. 8, p. 10–12.

Crosby, I. B., and Leonardon, E. G., 1928, Eelctrical prospecting applied to foundation problems: Am. Inst. Mining Metall. Engineers Tech. Pub. 131, 12 p.; 1929, Trans., v. 81, p. 199–210. Resistivity results. GA no. 12, p. 15.

Crumrine, K. C., 1950, A method of electrical profiling: Geophysics, v. 15, p. 477–482. Resistivity. GA 12273.

Cummings, J. B., and Romslo, T. M., 1950, Investigation of Twin Buttes copper mines, Pima County, Ariz.: U.S. Bur. Mines Rept. Inv. 4732, 12 p. Resistivity, self-potential. GA 12470.

Currie, B. W., 1939, Earth currents: Royal Astron. Soc. Canada Jour., v. 33, no. 8, p. 313–323. GA 5651.

Dahlberg, R. S., Jr., 1945, An investigation of natural earth currents: Geophysics, v. 10, p. 494–506. GA 8245.

Dakhnov, V. N., 1937, Telluricheskiye toki i puti izucheniya ikh s tsel'ye provedeniya razvedok poleznykb iskopayemykh [Earth currents and ways of studying them in connection with prospecting for ores]: Glavneft NKTP, SSSR, Trans. Vsesoyuznyy Kontory geofizicheskoy razvedki, no. 8, 58 p. Textbook-Telluric current. GA 5652.

——— 1940, O prirode yestestvennykh elektricheskikh poley v iskopayemykh uglyakh [On the nature of the natural electric fields in coal deposits]: Razvedka Nedr, no. 5, p. 48–52. GA 5804.

——— 1951, Elektricheskaya razvedka neftyanykh i gazovykh mestorozhdeniy [Electric exploration of the oil and gas deposits]: Moscow-Leningrad, Gostoptekhizdat, 425 p. Textbook. GA 159–61.

Dakhnov,, V. N., and Ryapolova, V. A., 1952, Metod soprotivleniya ekranirovannogo zazemleniya [The guard-electrode method]: Promyslovaya geofiz., p. 83–103. GA 163–68.

Davidovich, Ya. L., 1933, Elektrorazvedka v Emba-Nefti [Electrical exploration in the Emba petroleum region] in the symposium: Neft. Mestorozhdeniya Uralo-Embanskogo Rayona, Leningrad-Moscow, p. 168–171.

Dedushkevich, S. I., 1929a, Opyty nad modelyami v bake 1924–25 G. [Experiments made on the electric fields in a tank with models of ore bodies, 1924–25]: Geol. Komitet,

materialy po obshch. prik. geologii, no. 137, p. 37–48. Model study using metal plates immersed in water and 50-cycle ac. GA no. 12, p. 9.

Dedushkevich, S. I., 1929b, Opyty nad modelyami razlichnoy provodimosti [Experiments on models of ore bodies of different conductivity in a tank]: Geol. Komitet, materialy po obshch. prik. geologii, no. 137, p. 49–52. GA no. 12, p. 10.

DeMille, J. B., 1929, Geophysical prospecting; its value to the mining geologist: Canadian Mining Jour., v. 50, no. 14, p. 313–315. GA no. 3, p. 8.

—— 1930, Practical results of electrical prospecting at Abana: Canadian Mining Jour., v. 51, no. 14, p. 314–316. GA no. 13, p. 14–15.

Denisevich, V. V., and Gorbenko, L. A., 1937, Kazhushchiyesya soprotivleniya Neftenasyshchennykh peskov produktivnoy tolshchi. [Apparent resistances of oil saturated sands in productive layers]: Azerbaidzhanskoe Neft. Khoz., no. 11–12, p. 63–67.

Deppermann, K., 1954, Die Abhängigkeit des scheinbaren Widerstandes vom Sondenabstand bei der Vierpunkt-Methode [The dependence of the apparent resistivity on the electrode spacing in the four-point method]: Geophys. Prosp., v. 2, p. 262–273. GA 160–60.

Dickey, P. A., 1943, Natural potentials in sedimentary rocks: Am. Inst. Mining Metall. Engineers Tech. Pub. 1625, 10 p.; 1945, Trans., v. 164, p. 256–266.

Diénert, Frédéric, 1941, Méthode différentielle de prospection électrique du sous-sol [Differential method of electrical prospecting of the subsoil]: Acad. Sci. [Paris] Comptes rendus, v. 213, p. 625–627. GA 7848.

Dizioğlu, Mahmet Y., 1953, Orta anadoluda bilhassa elektriki jeofizik usulleriyle yeralti suyu arastirmalari [Underground water investigations by means of geophysical methods (particularly electrical) in the Central Anatolia]: Maden Tetkik ve Arama Enstitüsü Mecmuasi, no. 44–45, p. 63–70; 71–76. Resistivity, Electromagnetic. GA 158–104.

Dmitriev, V. L., and Tolmachev, B. V., 1935, Opyt elektrorazvedki na podzemnye vody [Tests of electrical prospecting for underground waters]: Materialy po gidrogeologii i inzhenernoi geologii S.S.S.R., no. 1, p. 99–104. Resistivity. GA 3380.

Dobrin, M. B., 1952, Introduction to geophysical prospecting: New York, McGraw-Hill, 435 p. Text.

Dolitskiy, V. A., 1936, Karottazh na promysle im. Kaganovicha (Shorsy) [Electrical logging in the Kaganovich mine]: Neftyanoye Khozyaystvo, no. 4, p. 34–43. Logging method. GA 3381.

Doll, H. G., 1948, The S. P. log: Theoretical analysis and principles of interpretation: Am. Inst. Mining Metall. Engineers Tech. Pub. 2463, 40 p.; 1949, Trans., v. 179, p. 146–185.

Drysdale, C. V., and Jolley, A. C., 1924, Electrical measuring instruments: New York, Van Nostrand Co., pt. 2, p. 385–388, 396–399. Description of the Megger.

Duling, J. F., 1935, Geophysics as an aid in gold placer drift mining: Mining Jour., v. 18, no. 21, p. 5–6. GA 2589.

Duschnitz, B., 1931, Hundert Jahre Elektrische Bodenforschung [One hundred years of electrical prospecting for ore]: Kali, v. 25, no. 5 and 6, p. 71–76 and p. 88–92. GA 177.

Dyke, L. J., 1956, An electrical resistivity survey in north-west Ankole: Uganda Protectorate Geol. Survey Dept. Records, p. 61–69, (1954). GA 168–97.

Ebert, Artur, 1927, Möglichkeit der Feststellung des Gebirgsbaues durch elektrogeophysikalische Untersuchungen [The possibility of determining mountain building through geo-

electrical investigations]: Geol. Rundschau, v. 18, no. 5, p. 389–401.

—— 1933a, Apparate und methoden der Elektrischen Wassersuche [Apparatus and methods of electrical water prospecting] Deutsche Geol. Gesell. Zeitschr., v. 85, p. 496–500.

—— 1933b, Elektrische Tiefenmessungen im Thüringer Muschelkalk [Electrical depth measurements in the Thuringian fossiliferous limestone]: Beitr. angew. Geophysik, v. 3, p. 259–260. GA 1377.

—— 1942, Grundlagen zur Auswertung geoelektrischer Tiefenmessungen [Foundations of the evaluation of geoelectric measurements of depth]: Beitr. angew. Geophysik, v. 10, p. 1–17. GA 7702.

Eby, J. B., 1943, Seismic and resistivity geophysical exploration methods: U.S. Waterways Expt. Sta. (Vicksburg) Tech. Mem. 198–1, 90 p. GA 7825.

Edwards, G. J. ,1951, A preliminary report on the electrical resistivity survey at Medicine Lake, Mont.: U.S. Geol. Survey Circ. 97, 16 p. Resistivity vertical profiling. GA 12835.

Ehrenburg, D. O., and Watson, R. J., 1931, Mathematical theory of electrical flow in stratified media with horizontal, homogeneous and isotropic layers: Am. Inst. Mining Metall. Engineers Tech. Pub. 400, 18 p.; 1932, Trans., v. 97, p. 423–442. Resistivity theory. GA 136.

Enenshteyn, B. S., 1947, Rezul'taty primeneniya elektrorazvedki metodom postoyannogo toka v rayonakh vechnoy merzloty [The results of electrical investigations carried out by means of direct current on permanently frozen soils]: Akad. Nauk SSSR Inst. Merzlotovedeniya Trudy, v. 5, p. 36–84. GA 10080.

—— 1948, Odnopolyusnoye elektricheskoye zondirovaniye [Electrical sounding with a single pole]: Akad. Nauk SSSR Izv. ser. geog. i geofiz., v. 12, no. 3, p. 221–230. Electrode configuration similar to half-Wenner. GA 11103.

England, C. M., 1943, A resistivity survey of the Monument oil field: Geophysics, v. 8, p. 14–22. GA 6812.

Enslin, J. F., 1943, Basins of decomposition in igneous rocks: their importance as underground water reservoirs and their location by the electrical resistivity method: Geol. Soc. South Africa Trans., v. 46, p. 1–12. GA 8246.

—— 1948, Lateral effects on electrical resistivity depth probe curves: Geol. Soc. South Africa Trans., v. 51, p. 249–270. GA 11552.

—— 1951, Geophysical methods of tracing and determining contacts of dolerite dykes in Karroo sediments in connection with the siting of boreholes for water: Geol. Soc. South Africa Trans. [1950]., v. 53, p. 193–204. Resistivity, self-potential. GA 13739.

—— 1953, Geophysics as an aid to foundation engineering: South African Inst. Civil Engineers Trans., v. 3, no. 2, p. 49–60.

Eve, A. S., and Keys, D.A., 1927, Geophysical methods of prospecting, a brief and elementary account of the principles involved: U.S. Bur. Mines Tech. Paper 420, 26 p.

—— 1928, Geophysical prospecting: some electrical methods: U.S. Bur. Mines Tech. Paper 434, 41 p. Resistivity results.

—— 1929, Applied geophysics in the search for minerals: Cambridge, The Univ. Press, 253 p.; 1933, 2d ed., 296 p.; 1938, 3d ed., 316 p. GA 1834.

Eve, A. S., Keys, D. A., and Lee, F. W., 1929, Depth attainable by electrical methods in applied geophysics: U.S. Bur. Mines Tech. Paper 463, 58 p. Resistivity results. GA no. 11, p. 20–21.

Eve, A. S., Keys, D. A., Watson, H. C. I., Swartz, J. H., and Mawdsley, J. B., 1931, Geophysical investigations at the Mammoth Caves, Kentucky and in Sudbury Basin district, Ontario: Canada Dept. Mines, Geol. Survey Mem. no. 165, pt. 2, p. 78–160. GA 663.

Evjen, H. M., 1938, Depth factors and resolving power of electrical measurements: Geophysics, v. 3, p. 78–95. GA 4502.

——— 1939, Electrical methods of geophysical exploration: Geologie en Mijnbouw, new ser., v. 1, no. 1, p. 2–8. GA 4940.

——— 1943, Utility of the electric methods in geophysical exploration: Geophysics, v. 8, p. 146–156.

Ewing, Maurice, Crary, A. P., Peoples, J. W., and Peoples, J. A. Jr., 1936, Prospecting for anthracite by the earth resistivity method: Am. Inst. Mining Metall. Engineers Tech. Pub. 683, 36 p.; 1936, Trans., v. 119, p. 443–483. GA 3116.

Ewing, Scott, 1932, Electrical methods for estimating the corrosiveness of soils: Am. Gas Assoc. Monthly, v. 14, no. 8, p. 356–361. GA 1110.

Fedukovich, V. S., 1937, Elektrometrichni rozvidki v USSR i metodichni visnovki z nikh [Electrometric prospecting in the Ukrainian S.S.R.]: Geol. Zhur., v. 3, no. 3–4, p. 83–110, Kiev. Resistivity. GA 3739.

Fedynskiy, V. V., 1944, Geofizicheskaya razvedka na neft' v SSSR za gody otechestvennoy voyiy (1941–43 gg.) [Geophysical exploration for oil in the USSR during the last war 1941–43] [Engl. Summ.]: Akad. Nauk SSSR Izv. ser. geog. i geofiz., v. 8, no. 5, p. 229–243.

Feofilova, A. P., 1940, Opyt primeneniya geofizicheskikh metodov pri geologicheskom kartirovanii [A test of the application of geophysical methods to geological mapping]: Sovetskaya Geologiya, no. 5, p. 153–158.

Fernandez Bollo, Mariano, 1951, Estudio del agua subterránea por prospección geofísica [Exploration for underground water by geophysical methods]: Agricultura (Madrid), no. 227, p. 111–114. Resistivity, self-potential. GA 14855.

Ferreira Gomes, J. C., 1952, A geologia nas barragens [Geology of dam sites]: Univ. Brasil Escola de Minas Rev., v. 17, no. 4, p. 3–18. GA 14268.

Ferris, L. P., 1933, Unit for specifying the electrical resistivity of the earth: Mining and Metallurgy, v. 14, no. 314, p. 99. GA 1322.

Fine, Harry, 1953, An effective ground conductivity map for continental United States: Federal Commun. Comm. Tech. Research Div. T.R.R. Rept., no. 2.1.4 (Revised), 4 p. and map.

Fink, D. G., 1935, Methods of electrical prospecting: Elec. Eng., v. 54, no. 3, p. 293–296. GA 2785.

Flathe, H. 1955a, Possibilities and limitations in applying geoelectrical methods to hydrogeological problems in the coastal areas of north West Germany: Geophys. Prosp., v. 3, p. 95–110. GA 162–72.

——— 1955b, A practical method of calculating geoelectrical model graphs for horizontally stratified media: Geophys. Prosp., v. 3, p. 268–294. GA 163–69.

Foster, J. W., and Buhle, M. B., 1951, An integrated geophysical and geological investigation of aquifers in glacial drift near Champaign-Urbana, Illinois: Econ. Geology, v. 46, p. 367–397. Resistivity, Logging method. GA 13036.

Fox, R. W., 1830, On the electro-magnetic properties of metalliferous veins in the mines of Cornwall: Royal Soc. London Philos. Trans., pt. 2, p. 399–414.

——— 1832, [No title accompanies the paper]: Royal Soc. London Proc., v. 3, no. 10, p. 123–125.

Fox, R. W., 1835a, Account of some experiments on the electricity of the copper vein in Huel Jewel mine: British Assoc. Adv. Sci. Rept., v. 3, p. 572–574.

——— 1835b, Note on the electrical relations of certain metals and metalliferous minerals: Royal Soc. London Philos. Trans., pt. 1, p. 39–40.

——— 1838, Report on some experiments on the electricity of metallic veins and the temperature of mines: British Assoc. Adv. Sci. Rept., v. 6, p. 133–137.

——— 1843a, Notice of some experiments on the electric currents in Pennance mine, near Falmouth: Philos. Mag. and Jour. Sci., v. 23, p. 457–459, London.

——— 1843b, Notice of some experiments on subterranean electricity made in Pennance mine, near Falmouth: Philos. Mag. and Jour. Sci., v. 23, p. 491–496, London.

Frank, Phillip, and von Mises, Richard, 1935, Die Differential- und Integralgleichung der Mechanik und Physik: Braunschweig, Friedn. Vieweg u. Sohn (Reissued 1943, New York, Mary S. Rosenburg by authority Alien Property Custodian), v. 2, 1106 p.

Friedel, Edmond, and Goguel, J. M., 1944, La prospection géophysique du Bas-Dauphiné [Geophysical prospecting in the Bas-Dauphiné]: Annales Mines et Carbur. Mem., ser. 14, v. 4, no. 6, p. 417–432. GA 9414.

Friedel, G., 1927, Sur l'existence d'un dôme de sel dans le bassin potassique oligocène du Haut-Rhin [On the existence of a salt dome in the Oligocene potash basin of the upper Rhine]: Acad. Sci. [Paris] Comptes rendus, v. 184, no. 18, p. 1028–1031.

Friedl, K., 1927, Über die jüngsten Erdforschungen im Wiener Becken [On the most recent investigations in the Vienna basin]: Petroleum, v. 23, p. 189–240.

Fritsch, Volker, 1934, Einiges über die Grundlagen der Funkmutung [Contribution to the fundamental principles of electrical methods of prospecting]: Montan. Rundschau, v. 26. no. 4, p. 1–6. GA 2041.

——— 1937, Der Einfluss des Wassergehaltes auf den Widerstand geologischer Leiter [Influence of the content of water on the resistance of geologic conductors]: Elektrotech. Zeitschr., v. 58, no. 12, p. 319–320, Berlin. GA 3876.

——— 1939, Der Einfluss des Wassergehaltes geologischer Leiter auf deren elektrische Eigenschaften [Influence of the water content of geologic conductors upon their electrical properties]: Schweizer. mineralog. petrog. Mitt., v. 19, no. 1, p. 224–250. GA 6721.

——— 1942, Die Messung von Erdwiderständen [The measurement of earth resistivities]: Braunschweig, Friedr. Viewez und Sohn, 86 p. Resistivity. GA 10871.

——— 1948, Zur Auswertung geoelektrischer Tiefenmessungen [On the value of geoelectric depth measurements]: Bohrtechniker-Zeitung, v. 64, no. 3, p. 12–13. Includes discussion by Bruno Kunz.

——— 1949a, Einige geoelektrische Untersuchungen mit Gleichstrom [Some geoelectrical investigations with direct current]: Geofisica Pura e Appl., v. 14, p. 250–282. Resistivity. GA 13034.

——— 1949b, Grundzüge der angewandten Geoelektrik [Principles of electrical methods in applied geophysics]: Vienna, Manzche Verlags- und Univ. Buchhandlung, 412 p. Text. GA 12267.

——— 1951, Die geoelektrische Überprüfung von Zementinjektionen zur Verfestigung des Baregrundes [Use of geoelectrical testing of cement injections for reinforcement of

the ground]: Geofisica Pura e Appl., v. 19, p. 92–99. Resistivity. GA 13040.

Fritsch, Volker, 1952. Geoelektrik Baugrunduntersuchung [Geoelectrical investigations of ground structure]: Umschau, v. 52, no. 11, p. 330–331. GA 14856.

—— 1954, Einige Probleme der geoelektrischen Bodenverfestigung [Some problems in the geoelectric method in reinforcing the ground]: Geofisica Pura e Appl., v. 28, p. 149–158. GA 160–57.

—— 1956a, Geoelektrische Baugrunduntersuchungen in Jugoslawien und Oesterreich [Geoelectrical foundation investigations in Yugoslavia and Austria]: Geophys. Prosp., v. 4, p. 24–36. GA 165–128.

—— 1956b, Zur geoelektrischen Untersuchung der Zementverpressung von Staumauern und Staudammen [On the geoelectrical investigation of the cement injection of dam walls and reservoirs]: Geofisica Pura e Appl., v. 34, p. 79–100. GA 168–100.

Fujita, Yoshizo, 1926, [Results obtained by the Schlumberger method of electrical prospecting (in Japanese)]: Kyōtō Univ. Faculty Eng. Mem., v. 4, no. 4, p. 63–90.

—— 1931, Experimental studies on the potential method of electrical prospecting: World Eng. Cong. Proc. [Tokyo], v. 37, pt. 5, p. 229–242. GA 1039.

—— 1954, Three-way geophysical method points up huge pyrite deposit: Eng. Mining Jour., v. 155, no. 12, p. 84–88. Resistivity, self-potential. GA 159–82.

Gabriel, V. G., 1944, Electrical resistivity methods of exploration: Petroleum World, Ann. Rev., p. 90–93. GA 7852.

—— 1946, Electrical methods of oil exploration: Petroleum Engineer, v. 18, p. 216–220. GA 9225.

Gage, Maxwell, and McNeill, F. A., 1941, Geophysical investigations in the area between Waiuta and Merrijigs: New Zealand Jour. Sci. Technology, v. 22, no. 3B, p. 155b–165b. GA 6177.

Galbraith, F. M., and Hart, R. C., 1939, Geophysics in exploration at Falconbridge [Ontario]: Canadian Inst. Mining Metallurgy Trans., v. 42, p. 527–531.

Gassmann, Fritz, 1936, Ein geoelektrischer Widerstandsmesser [A geoelectric resistance meter]: Schweizer. naturf. Gesell. Verh., 117. Jahresh., Solothurn, p. 269–270. Resistivity. GA 3877.

—— 1939, Zur Watsonschen Methode der Auswertung geoelektrischer Widerstandsmessungen [On Watson's method of evaluating geoelectric resistivity measurements]: Beitr. angew. Geophysik, v. 7, p. 347–349. GA 5077.

Gavelin, Axel, 1923, Foreword, in Lundberg, Hans, Practical experience in electrical prospecting: Sveriges Geol. Undersökning Årsbok, v. 16 (1922), no. 9, ser. C, (no. 319), p. 3.

Geffrier, R. de, 1938, Les succés de la prospection électrique [Success of electrical prospecting]: Rev. Pétrolifère, no. 773, p. 282–283. GA 4358.

Gella, Norbert, 1928, Geophysikalische Schürfungen auf Erdöl [Geophysical prospecting for oil]: Zeitschr. prakt. Geologie, v. 7, p. 49–54. GA no. 4, p. 11–12.

—— 1930, Geoelectric investigations of nonconductors—Four new examples: Am. Assoc. Petroleum Geologists Bull., v. 14, no. 9, p. 1165–1176. GA no. 18, p. 16.

Gella, Norbert, and Bateman, H. B., 1929, Note on an electrical investigation for copper ores in Roumania; Inst. Mining and Metallurgy [London] Trans., v. 38, p. 362–367; 1929, Inst. Mining and Metallurgy [London] Bull. 295, supp. paper, p. 1–6.

Geneslay, R., and Rouget, F., 1937, Sur l'anisotropie électrique des terrains et le pseudo-anisotropie [On the electrical

anisotropy of formations and pseudoanisotropy]: World Petroleum Cong. Proc., 2d, v. 1, p. 723–739. GA 4359.

Geoffroy, P., and Charrin, P., 1932, Études géologiques et prospections minières par les méthodes géophysiques [Geological studies and mining exploration by geophysical methods]: Service carte géol. Algérie Bull., ser. 4, no. 1, 346 p. Text. GA 1066.

Gibbon, Anthony, 1954, New oil exploration method developed: World Oil, v. 138, no. 6, p. 99–101. GA 157–62.

Gilbert, R. D., 1940, Interpretable method of electrical prospecting: Mining Jour., v. 24, p. 5–7. GA 5807.

Gilchrist, Lachlan, 1931a, Experiments in electrical exploration made in the summer of 1929: Canada Dept. Mines, Geol. Survey Mem., no. 165, pt. 3, p. 161–189. GA 664.

—— 1931b, Measurements of resistivity by central electrode method at Abana mine, northwestern Quebec, Canada: Am. Inst. Mining Metall. Engineers Tech. Pub. 386, 17 p. Resistivity results. GA 135.

—— 1932, Geophysical investigations made in 1930: Canadian Dept. Mines, Geol. Survey Mem., no. 170, pt. 2, p. 65–98. Gilchrist responsible for only one part of Mem. 170. Title of Memoir is "Studies of geophysical methods, 1930" and includes other authors and other than electrical methods.

—— 1940, Recent magnetic and electrical geophysical investigations on the surface and in drill holes in regions containing gas, oil, and other minerals, and the correlation of the results of the investigations: Pennsylvania State Coll. Mineral Industries Expt. Sta. Bull. 30, p. 1–26.

Gilchrist, Lachlan, and Clark, A. R., 1940, The use of mathematics in the delineation of magnetic and electric anomalies: Am. Geophys. Union Trans., v. 21, pt. 4, p. 1072–1081. Resistivity. GA 5400.

Gilchrist, Lachlan, Clark, A. R., and Bernholtz, Ben, 1950, Methods of determination of the average resistivity of a two-layered medium: Canadian Mining Jour., v. 71, no. 1, p. 55–64. Resistivity. GA 12269.

Gilchrist, Lachlan, and Mawdsley, J. B., 1931, Investigations made in cooperation with Radiore Company of Canada, Ltd., Schlumberger Electrical Prospecting Methods, and Swedish American Prospecting Company of Canada: Canada Dept. Mines, Geol. Survey Mem., no. 165, pt. 1, p. 1–77. GA 662.

Gilchrist, Lachlan, Rostoker, Normon, and Bernholtz, Ben, 1950, Distribution of potential in a two-layered medium due to an internal source and sink and the determination of the approximate average resistivity of the medium: Canadian Jour. Research, v. 28, sec. A, p. 1–28. Resistivity. GA 11832.

Gish, O. H., 1923, General description of the earth-currents measuring system at the Watheroo Magnetic Observatory: Terrestrial Magnetism Atmos. Electricity, v. 28, p. 89–108.

—— 1924a, Natural electric currents in the earth's crust: Carnegie Inst. Washington Year Book, no. 23, p. 178–179.

—— 1924b, Preliminary earth-resistivity measurements on the site of the Department of Terrestrial Magnetism at Washington, D.C.: Carnegie Inst. Washington Year Book, no. 23, p. 179–180.

—— 1926, Improved equipment for measuring earth-current potentials and earth resistivity: Natl. Research Council Bull., v. 11, pt. 2, no. 56, p. 86–91.

—— 1928, Depths of ground-water and other subsurface features indicated by earth-resistivity surveys (abs.): Terrestrial Magnetism Atmos. Electricity, v. 33, no. 3, p. 140–141.

Gish, O. H., 1932, Use of geoelectric methods in search for oil: Am. Assoc. Petroleum Geologists Bull., v. 16, no. 12, p. 1337–1348. Reprinted, 1947, *in* Early geophysical papers: Tulsa, Soc. Explor. Geophysicists, p. 497–508. GA 1228.

——— 1936a, Electrical messages from the earth: their reception and interpretation: Washington Acad. Sci. Jour., v. 26, p. 267–289. Telluric current. GA 3388.

——— 1936b, The natural electric currents in the earth: Sci. Monthly, v. 43, p. 47–57. Telluric current. GA 3606.

Gish, O. H., and Rooney, W. J., 1925, Measurement of resistivity of large masses of undisturbed earth: Terrestrial Magnetism Atmos. Electricity, v. 30, p. 161–188. Resistivity.

Glangeaud, Louis; Pezard, Robert; François, Solange; Perrenoud, Marie-Jean; and Toitot, Michel, 1956, Les nappes phréatiques et artésiennes du Jura septentrional (dépt. du Doubs). Leurs relations avec les réseaux karstiques [The phreatic and artesian ground waters of the northern Jura, Doubs. Their relations to the karst system]: Soc. géol. France Bull., ser. 6, v. 6, no. 4–5, p. 531–546. GA 168–99.

Goguel, Jean, 1948, Essai d'interprétation de la prospection géophysique de la Bresse et du Bas-Dauphiné [An interpretation of geophysical prospecting in Bresse and Bas-Dauphiné]: France Bur. Recherches géol. et géophys. Pub. 6, 79 p. Telluric. GA 12277, GA 12059.

Gohara, Yasuma, 1950, On the prospecting for ground water [In Japanese with English summary]: Tokyo Research Inst. Nat. Resources Rept. 16, p. 33–42. Resistivity. GA 13035.

Goldsmith, L. M., 1938, Earth resistivity measurement: Petroleum Engineer, v. 9, p. 68–74. GA 4504.

Golovtsyn, V. N., 1935a, K voprosu o razvedke gluboko zalegayushchikh rudnykh tel kolchedannykh mestorozhdeniy metodami elektrorazvedki [Concerning the exploration of deep pyrite deposits by means of electrical methods]: Akad. Nauk SSSR Ural'sk. filiala Trudy, Ser. obshch., no. 6, p. 93–106.

——— 1935b, O Vozmozhnosti primeneniya elektrometricheskikh metodov k izucheniyu karstovykh yavleniy [On the possibility of application of the electrometric method for studying karst phenomena]: Akad. Nauk SSSR, Seysmol. Inst. Trudy, no. 52, p. 1–65; also 1935, Sverdlovskogo Gornogo Inst. Trudy i Materialy, v. 1, p. 5–34. GA 3742.

——— 1947, Kombinirovannoye pole pri elektrorazvedke polezuykh iskopaemykh [The use of a combined field in the electrical exploration of subsurface resources]: Prikladnaya Geofizika, no. 3, p. 101–105. GA 9837.

Golubiatnikov, D., 1930, Elektrorazvedka v groznenskom rayone [Electrical prospecting in the region of Grozny]: Neft. Piat., no. 11–12, p. 11–14; and also 1930, Azerbaidzhanskoe Neft. Khoz. v. 10, no. 10, p. 51–54. Resistivity results.

Gorbenko, L. A., and Denisevich, V., 1937, K voprosu ob izmenenii soprotivleniya porod po razrezu [Changes of the resistances of rocks along their section]: Azerbaidjanskoe Neft. Khoz., no. 5–6, p. 62–71. GA 4825.

Gorelik, A. M., 1952, Opredeleniye napravleniya techeniya podzemnykh vod po noblyudeniyam elektricheskogo polya fil'tratsii [Determination of the direction of streaming underground water from the observed electric field caused by filtration]: Akad. Nauk SSSR Izv. ser. geofiz., no. 6, p. 55–56. Self-potential. GA 14264.

——— 1955, Ob interpretatsii krivykh elektricheskogo zondirovaniya pri poiskakh vody na nebol'skikh glubinakh [The interpretation of the graphs obtained by electric sounding when prospecting for water at shallow depths]:

Akad. Nauk SSSR Izv. ser. geofiz., no. 4, p. 364–368. GA 163–71.

Gouy, M. G., 1917, Sur la fonction électrocapillaire [On the electrocapillary function]: Annales de Physique, ser. 9, v. 7, pt. 5, p. 129–184.

Graf, A., 1931, Intensitätsgradienten bei elektrischen Aufschlussverfahren [Intensity gradients with electrical methods of exploration]: Ergänz-Hefte angew. Geophysik, v. 1, p. 286–292.

Grand'ry, G. de, 1930, La prospection électrique et ses recents progrès [Electrical prospecting and its recent successes]: Rev. Univ. des Mines, v. 75, ser. 8, no. 5, 7, p. 136–141, 188–198. GA no. 14, p. 14.

Gray, A., Matthews, G. B., and MacRobert, T. M., 1931, A treatise on Bessel functions and their applications to physics, 2d ed.: London, MacMillan and Co., 327 p.

Grigor'yeva, N. P., 1950a, Lineynyy neekvipotentsial'nyy provodnik [Linear nonequipotential conductor]: Vses. nauchno-issled. inst. razved. geofiz. Trudy, no. 2, p. 82–93. GA 158–83.

——— 1950b, Metod combinirovannogo profilirovaniya [The method of composite profiling]: Vses. nauchnoissled. inst. razved. geofiz. Trudy, no. 3, p. 10–32. GA 159–65.

Grinberg, G. A., 1940, O reshenii opredelennogo klassa elektrostaticheskikh i rodstvennykh im problem [On the solution of a certain class of electrostatic and related problems]: Zhur. Eksp. Teoret. Fiziki, v. 10, no. 9–10, p. 1087–1104.

Groot, J. J., and Rasmussen, W. C., 1954, Geology and ground-water resources of the Newark area, Delaware: Delaware Geol. Survey Bull. 2, 133 p. Resistivity. GA 159–77.

Gurevich, B. L., and Zagarmistr, A. M., 1940, Glubinnyye elektricheskiye issledovaniya v svyazi s poiskami neftenosnykh struktur v tsentral'nykh oblastyakh SSSR [Deep electrical depth profiling in connection with the search for oil bearing structures in the central parts of the USSR]: Razvedka Nedr, no. 7, p. 26–31. GA 5941.

Guyod, Hubert, 1945, Electrical well logging: Duncan, Oklahoma, Halliburton Oil Well Cementing Co., 103 p.

——— 1955, Electric analogue of resistivity logging: Geophysics, v. 20, p. 615–629. GA 162–77.

Haalck, Hans, 1929, Die Verwendung der Elektrizität zur Erforschung des Untergrundes [The use of electricity for the exploration of the subsoil]: Gerlands Beitr. Geophysik, v. 23, no. 3, p. 99–143. GA no. 10, p. 16–17.

Habberjam, G. M., and Whetton, J. T., 1954, A resistivity investigation into a washout feature in coal measure strata: Geophys. Prosp., v. 2, p. 24–37.

Haddock, M. H., 1931, Deep borehole surveys and problems: New York, McGraw-Hill, 296 p. Logging method. GA 736.

Hagan, W. W., 1943, Electrical earth resistivity surveys: Indian Acad. Sci. Proc., v. 52, p. 166–168. GA 7303.

Hahnfeld, I., 1932, Untersuchungen über die elektrische Raumladung und das elektrische Feld am Boden [Investigations of the electric space charge and electric field at the ground]: Zeitschr. Geophysik, v. 8, p. 89–106.

Hallenbach, F., 1953, Geo-electrical problems of the hydrology of West German areas: Geophys. Prosp., v. 1, p. 241–249.

Haller, G. P., 1930, The use of geoelectrical methods underground: Mining Jour., v. 14, p. 11, 30. Resistivity. GA 14.

Hatakeyama, H., 1937, Observation of the electrical resistance of frozen and moist soil [in Japanese]: Meteorology Soc. Japan Jour., 2d ser., v. 15, p. 316–320. Resistivity. GA 4198.

Haubner, J., 1882, Über die stationäre Strömung der Elektrizität in flächenförmigen Leitern [On the steady electric current in plane conductors]: Akad. Wiss. Wien Ber., Math.-Naturw. Kl., v. 85, pt. 2, p. 77–97.

—— 1883, Über das logarithmische Potential einer nicht isolierten elliptischen Platte [On the logarithmic potential of a nonisolated elliptical plate]: Akad. Wiss. Wien Ber., Math.-Naturw. Kl., v. 87, pt. 2, p. 412–421.

Hawkins, R. H., 1934, Application of resistivity methods to northern Ontario lignite deposits: Am. Inst. Mining Metall. Engineers Trans., v. 110, p. 76–120. GA 1471.

Hawley, P. F., 1943, Fault location by electrical prospecting—an example: Geophysics, v. 8, p. 291–403. GA 7304.

Hedström, Helmer, 1930a, Electrical survey of structural conditions in Salt Flat field, Caldwell County, Texas: Am. Assoc. Petroleum Geologists Bull., v. 14, no. 9, p. 1177–1185. GA no. 18, p. 16–17.

—— 1930b, Geoelectrical exploration methods used in oil fields: Oil Weekly, v. 58, no. 6 and no. 8, p. 34–37 and p. 32–34. Resistivity results.; GA 17, p. 12; GA 20, p. 11–12.

—— 1932, Electrical prospecting for auriferous quartz veins and reefs: Mining Mag., v. 46, no. 4, p. 201–213. Potential-drop-ratio. GA 928.

Heiland, C. A., 1926, Instruments and methods for the discovery of useful mineral deposits: Eng. Min. Jour., v. 121, p. 47–58.

—— 1929, Geophysical methods of prospecting: Colorado School of Mines Quart., v. 24, no. 1, p. 106–111.

—— 1932a, A demonstration of the geologic possibilities of the resistivity and magnetic prospecting methods: Terrestrial Magnetism Atmos. Electricity, v. 37, no. 3, p. 343–350.

—— 1932b, Advances in technique and application of resistivity and potential-drop-ratio methods in oil prospecting: Am. Assoc. Petroleum Geologists Bull., v. 16, no. 12, p. 1260–1336. Reprinted, 1947, in Early geophysical papers: Tulsa, Soc. Explor. Geophysicists, p. 420–496. GA 1227.

—— 1933, Einige neue Anwendungen der Geophysik bei Talsperren- und Grundwasserproblemen [A new application of geophysics in dam and ground-water problems]: Geol. Rundschau, v. 23a, p. 279–303.

—— 1934, Geophysics in the nonmetallic field: Am. Inst. Mining Metall. Engineers Trans., v. 110, p. 546–577.

—— 1937, Prospecting for water by geophysical methods: Am. Geophys. Union Trans., v. 18, pt. 2, p. 574–588.

—— 1939, Report of the year's activities in electrical, geothermal, radioactive, and soil analysis methods: Geophysics, v. 4, p. 130–137.

—— 1940, Geophysical exploration: New York, Prentice-Hall, 1012 p. Textbook. GA 5844.

—— 1942, Geophysics in war: Colorado School Mines Quart., v. 37, no. 1, 85 p.

Heiland, C. A., Tripp, R. M., and Wantland, Dart, 1945, Geophysical surveys at the Malachite mine, Jefferson County, Colorado: Am. Inst. Mining Metall. Engineers Tech. Pub. 1947, 13 p.; 1945, Trans., v. 164, p. 142–154. Resistivity, self-potential. GA 9040.

Heine, Walther, 1928a, Der gegenwärtige Stand der Elektrischen geophysikalischen Methoden [The present status of electric geophysical methods]: Metall. u. Erz, v. 25, no. 10, p. 238–242. GA no. 5, p. 13–14.

—— 1928b, Elektrische Bodenforschung [Electrical earth-investigation], in Mainka, Carl, Sammlung Geophysikalischer Schriften: Berlin, Gebrüder Borntraeger, no. 8, 223 p. Textbook.

Heine, Walther, 1928c, Zur Theorie elektrischer Bodenforschung [Concerning the theory of electrical prospecting]: Zeitschr. Geophysik, v. 4, p. 109–112. GA no. 5, p. 14.

—— 1930, Praktische Anwendung der elektrischen Methoden [Practical application of electrical methods], in Angenheister, Gustav, Angewandte Geophysik, v. 25, pt. 3 of Wien, W., and Harms, F., Handbuch der Experimentalphysik: Leipzig, Akad. Verlagsgesell., M. B. H., p. 463–515. Resistivity theory.

Heller, J. I., 1931, Methods used in electrical prospecting: Electronics, v. 3, p. 184–185, 214. Equipotential line method and potential-drop ratio. GA 1041.

Henderson, L. H., 1931, A geophysical survey on the Santa Rita orebody: Mining Cong. Jour., v. 17, p. 70–77, 87. Resistivity. GA 527.

Henwood, W. J., 1837, Sur les courants électriques observés dans les filons de Cornouailles [On electric currents observed in Cornwall veins]: Annales Mines Mem., ser. 3, v. 11, p. 585–604. Discusses early work of R. W. Fox.

—— 1841, Experiments on the electric conditions of the rocks and metalliferous veins (lodes) of Longclose and Rosewall Hill mines in Cornwall: Royal Soc. London Proc., v. 4, no. 49, p. 317.

Hobson, E. W., 1931, The theory of spherical and ellipsoidal harmonics: Cambridge, The Univ. Press, 500 p.

Hoffman, R. D., 1932, Bushveld, Transvaal, South Africa in McLaughlin, D. H., and others, Summaries of results of geophysical surveys at various properties: Am. Inst. Mining Metall. Engineers Trans., v. 97, p. 36. GA no. 19, p. 17.

Horvath, Sepp, 1936, The geophysical methods of the Electrical Prospecting Co. of Sweden used in the Aerial, Geological, and Geophysical Survey of Northern Australia: Aerial, Geol., and Geophys. Survey of Northern Australia Rept., Queensland no. 3, 12 p. Self-potential, potential-drop ratio, electromagnetic. GA 3743.

Hotchkiss, W. O., Rooney, W. J., and Fisher, James, 1928, Earth-resistivity measurements in the Lake Superior copper country: Am. Inst. Mining Metall. Engineers Tech. Pub. 82, 15 p.; 1929, Trans., v. 81, p. 51–67. Resistivity results. GA no. 9, p. 19.

Hough, J. M., 1948, Interpretation of data from electrical resistivity geophysical surveys: Nature, v. 161, p. 812–813. Describes graphical method of interpretation for multilayer earth. GA 10591.

Howell, L. G., 1934, Discussion to paper by M. K. Hubbert, in Am. Inst. Mining Metall. Engineers Trans., v. 110, p. 34–37.

Hubbert, M. K., 1932, Results of earth-resistivity survey on various geologic structures in Illinois: Am. Inst. Mining Metall. Engineers Tech. Pub. 463, 23 p.; 1934, Trans., v. 110, p. 9–39; also, 1932, brief summary in Eng. Mining Jour., v. 133, p. 142–143. Resistivity results and theory. GA 669.

—— 1934, Electrical profiles in gaps in New Jersey trap ridges: Am. Jour. Sci., 5th ser., v. 28, p. 65–70. GA 2226.

—— 1937, Theory of scale models as applied to the study of geologic structure: Geol. Soc. America Bull., v. 48, p. 1459–1520.

—— 1944, An exploratory study of faults in the Cave in Rock and Rosiclare districts by the earth-resistivity method, Part 2 of Geological and geophysical survey of fluorspar areas in Hardin County, Ill.: U.S. Geol. Survey Bull. 942, pt. 2, p. 73–147. GA 7563.

Hubbert, M. K., and Weller, J. M., 1934, Location of faults in Hardin County, Illinois, by the earth-resistivity method: Am. Inst. Mining Metall. Engineers Trans., v. 110, p. 40–48. Resistivity results.

Huber, Anton, 1949, Zur Theorie der geoelektrischen Widerstandsmethoden [The theory of geoelectric-resistivity methods]: Archiv Meteorologie, Geophysik, Bioklimatologie, ser. A, v. I, p. 408–420. GA 12459.

——— 1950, Elektrische Ströme in stetig geschichteten Medien [Electric currents in continuous stratified media]: Österreich. Akad. Wiss. Kl. math.-naturw., Erdbeben-Komm. Mitt., Abt. IIa, 159, v. 3, no. 6, p. 71–82.

——— 1951a, Über den Einfluss der Bodenfeuchtigkeit auf geoelektrische Tiefenmessungen [The influence of ground moisture on geoelectric vertical profiling]: Archiv Meteorologie, Geophysik, Bioklimatologie, ser. A, v. 3, p. 330–338.

———1951b, Geoelektrische Tiefenmessungen in Tälern [Geoelectrical vertical profiling in valleys]: Archiv Meteorologie, Geophysik, Bioklimatologie, ser. A, v. 3, p. 464–469. GA 13732.

——— 1952, Einige neuere Fortschritte der geoelektrischen Widerstandsmethoden [Some new developments of the geoelectrical resistance method]: Elektrotech. Maschinenbau, v. 69, p. 1–10.

——— 1953, Die Randwertaufgabe der Geoelektrik für Kugel und Zylinder [The boundary value problem of geoelectrical exploration for a sphere and a cylinder]: Zeitschr. angew. Mathematik Mechanik, v. 33, no. 10–11, p. 382–393. Resistivity theory. GA 156–57.

——— 1955, Der scheinbare spezifische Widerstand einer geneigten ebenen Schichte [The apparent resistivity of an inclined plane layer]: Archiv Meteorologie, Geophysik, Bioklimatologie, ser. A, v. 8, p. 95–112. GA 161–59.

Hummel, J. N., 1928a, Über die Tiefenwirkung bei geoelektrischen Potentiallinienmethoden [The effect of the geoelectric method of potential lines with regard to the depth of an ore body]: Zeitschr. Geophysik, v. 4, no. 1, p. 22–27. Ga no. 3, p. 11.

——— 1928b, Physikalische Grundlagen einer neuen geoelektrischen Aufschlussmethode [Physical principles of a new geoelectric method of prospecting]: Zeitschr. Geophysik, v. 4, no. 2, p. 59–67. GA no. 3, p. 11–12.

——— 1928c, Untersuchung der Potentialverteilung für einen speziellen Fall in Hinblick auf geoelektrische Potentiallinienverfahren [Examination of the distribution of the potential in a special case with regard to the geoelectric method of potential lines]: Zeitschr. Geophysik, v. 4, no. 2, p. 67–76. GA no. 3, p. 10.

———1928d, Beiträge zur geoelektrischen Methode [Contributions to geoelectric methods of prospecting]: Zeitschr. Geophysik, v. 4, no. 4, p. 179–203. GA no. 3, 10–11.

——— 1928e, Theoretische Grundlagen für die Auffindung von Störungskörpern mittels solcher geoelektrischer Methoden, bei denen zwei punktförmige Elektroden zur Erzeugung eines künstlichen Feldes verwandt werden [Theoretical basis for the determination of the interfering bodies by means of geoelectric methods in which the artificial field is produced by two point electrodes]: Gerlands Beitr. Geophysik, v. 20, no. 3–4, p. 281–287. GA no. 3, p. 7.

——— 1929a, Untersuchung der Potentialverteilung um verschiedene Störungskörper, die sich in einem an und für sich homogenen Stromfelde befinden [Researches on the potential distribution about differently formed interference bodies embedded in homogeneous medium]: Gerlands Beitr. Geophysik, v. 21, no. 2–3, p. 204–214. GA no. 3, p. 7.

Kummel, J. N., 1929b, Über die Tiefenwirkung bei geoelektrische. Rahmenmethoden [The effect of the geoelectric framn methods with regard to the depth of an ore body]: Zeitschre Geophysik, v. 5, no. 2, p. 72–80. GA no. 9, p. 21.

——— 1929c, Der scheinbare spezifische Widerstand [The apparent specific resistance]: Zeitschr. Geophysik, v. 5, no. 3–4, p. 89–104. Translated into English by J. A. Malkowsky and T. A. Manhart [A theoretical study of apparent resistivity in surface potential methods]: 1931, Am. Inst. Mining Metall. Engineers Tech. Pub. 418, 31 p.; 1932; Trans., v. 97, p. 392–422; 1932, [Correction to this paper]: Zeitschr. Geophysik, v. 5, p. 249–250. Resistivity theory. GA no. 9, p. 21; GA 1042.

——— 1929d, Der scheinbare spezifische Widerstand bei vier plan-parallelen Schichten [The apparent specific resistance in case of four strata the planes of which are parallel]: Zeitschr. Geophysik, v. 5, no. 5–6, p. 228–238. Translated into English by J. A. Malkowsky and T. A. Manhart [A theoretical study of apparent resistivity in surface potentia. methods]; 1931, Am. Inst. Mining Metall. Engineers Techl Pub. 418, 31 p.; 1932, Trans., v. 97, p. 392–422. Resistivity theory. GA no. 10, p. 15.

——— 1930, Theorie der elektrischen Methoden [Theory of electrical methods], in Angenheister, Gustav, Angewandte Geophysik, v. 25, p. 3 of Wien, W., and Harms, F., Handbuch der Experimentalphysik: Leipzig, Akad. Verlagsgesellschaft, m.b.H., p. 401–462. Resistivity theory. GA no. 9, p. 15–16.

———1931a, A theoretical study of apparent resistivity in surface potential methods: Am. Inst. Mining Metall. Engineers Tech. Pub. 418; 1932, Am. Inst. Mining Metall. Engineers Trans., v. 97, p. 392–422. [A translation by J. A. Malkowsky and T. A. Manhart of two papers published by Hummel as follows: 1929, Der scheinbare spezifische Widerstand: Zeitschr. Geophysik, v. 5, no. 3–4, p. 89–104; 1929, Der scheinbare spezifische Widerstand bei vier plan-parallelen Schichten: Zeitschr. Geophysik, v. 5, no. 5–6, p. 228–238]. Resistivity theory. GA 178.

——— 1931b, Theoretische Grundlagen für die Erforschung des Erdinnern Mittels Gleichstrom [Theoretical foundation for investigation of the interior of the earth by means of direct current]: Zeitschr. Geophysik, v. 7, no. 3–4, p. 182–190. GA 218.

——— 1931c, Die Tiefenwirkung der Potentiallinien- und Rahmenmethoden bei geschichtetem Untergrund [Penetrative effect of the potential line method and of the frame method in the case of a stratified subsoil]: Zeitschr. Geophysik, v. 7, no. 5–6, p. 258–265. GA 472.

——— 1935a, Die Elektrische Leitfähigkeit von Aggregaten in Bezug auf die Leitfähigkeiten ihrer Bestandteile [The electrical conductivity of aggregates with respect to the conductivity of their constituents]: Zeitschr. Geophysik, v. 11, no. 1–2, p. 92–95. GA 2518.

——— 1935b, Die Messung der Elektrischen Strömung im Räumlichen Leiter [Measurement of electric current in a spatial conductor]: Zeitschr. Geophysik, v. 11, no. 6, p. 321–326. GA 3061.

——— 1935c, Unterlagen der Geoelektrischen Aufschliessungsmethoden [Foundations of geoelectrical methods of prospecting]: Beitr. angew. Geophysik, v. 5, p. 32–132. GA 2517.

Hummel, J. N., and Rülke, O., 1936, Der scheinbare spezifische Widerstand in Bohrlöchern [The apparent specific resistance in bore holes]: Beitr. angew. Geophysik, v. 6, p. 89–99. Logging method. GA 3389.

Hummel, J. N., and Rülke, O., 1937, Der Einfluss der Dickspülung auf den scheinbaren spezifischen Widerstand [Influence of mud filling of bore holes on the apparent specific resistance]: Beitr. angew. Geophysik, v. 6, p. 265–270. Logging method. GA 3744.

Hunkel, H., 1928a, Über turbulente Eigenströme der obersten Erdschichten und ihre Beziehungen zu den Gesteinsgrenzen [The turbulent self-exciting currents in the earth's upper layers and their relations to the boundaries of the ore deposits]: Zeitschr. prakt. Geologie, v. 7 and 9, p. 103–109 and p. 143–149. GA no. 3, p. 9–10.

———— 1928b, Zur Streitfrage der direkten Auffindung von Erdöllagerstätten mit Hilfe elektrischer Verfahren [The debated question of the direct discovery of oil deposits with the aid of electrical methods of prospecting]: Petroleum Zeitschr., v. 25, no. 10, p. 293–308. GA no. 4, p. 14–15.

———— 1929, Über den angeblichen geophysikalischen Nachweis von Salzdomen im Oberelsass [On the reported discovery of salt domes in upper Alsace by geophysical prospecting]: Zeitschr. Kali- und Steinsalzindustrie sowie das Salinenwesen, p. 7–10. GA no. 4, p. 13–14.

Hurd, C. O., 1944, Topography's effect in the equipotential line method: Mines Mag., v. 34, p. 15–18, 39, 41. GA 7422.

Ilsley, L. C., Freeman, H. B., and Zellers, D. H., 1928, Experiments in underground communication through earth strata: U.S. Bur. Mines Tech. Paper 433, 60 p.

Ito, Ichiro, 1950, Effects of anisotropy of media on the self-potential curves of electrical prospecting: Kyōtō Univ. Faculty Eng. Mem., v. 12, p. 105–119. Self-potential. GA 13028.

Iwatsu, Jiun, and Ōtsuki, Yoshio, 1952, Revised standard resistivity curves of K. Sundberg for electrical resistivity method [In Japanese with English summary]: Butsuri-Tankō, v. 5, no. 2, p. 87–91.

Jacobson, R. P., 1955, Geophysical case history of a commercial gravel deposit: Mining Eng. v. 7, no. 2, p. 158–161. GA 160–62.

Jakosky, J. J., 1931, Practical aspects of geophysical surveys: Mining Jour., v. 14, no. 16, p. 7–9, 29. Resistivity results.

———— 1934, Geophysical examination of prospects: Canadian Mining Jour., v. 55, no. 1, p. 9–13.

———— 1936, Electrical mapping of oil structures: Mining and Metallurgy, v. 17, no. 353, p. 231–237.

———— 1938, Continuous electrical profiling: Geophysics, v. 3, p. 130–153.

———— 1940, Exploration geophysics: Los Angeles Times Mirror Press, 800 p.; 2d ed., 1950, Los Angeles, Trija Publishing Co., 1195 p. GA 5966.

———— 1949, The economics of geophysics in mining exploration: Am. Inst. Mining Metall. Engineers Trans., v. 184, p. 326–330.

Jakosky, J. J., Dreyer, R. M., and Wilson, C. H., 1942, Geophysical investigations in the Tri-State zinc and lead mining district: Kansas Geol. Survey Bull. 44, 151 p. Resistivity. GA 6961, GA 6823.

Jakosky, J. J., and Hopper, R. H., 1937, The effect of moisture on the direct current resistivities of oils, sands, and rocks: Geophysics, v. 2, p. 33–55. GA 3879.

Jakosky, J. J., and Wilson, C. H., 1933, Geophysical studies in placer and water-supply problems: Am. Inst. Mining and Metall. Engineers. Tech. Pub. 515, 18 p. Excerpt of this paper published 1935, Examining a placer by geophysical methods: Eng. Mining Jour., v. 135, p. 71–74. Resistivity.

———— 1936, Electrical mapping of oil structures: Mining and Metallurgy, v. 17, no. 353, p. 231–237; also 1936, California Oil World, v. 29, no. 2, p. 2–3, 14–16, and v. 29, no. 3, p. 14–15. Resistivity. GA 3390, GA 3391.

Jakosky, J. J., and Wilson, C. H., 1937, Prospecting for oil structures by electrical methods: Petroleum Engineer, v. 8, no. 5, p. 143–149. GA 3745.

Jakosky, J. J., Wilson, C. H., and Daly, J. W., 1932, Geophysical examination of Meteor Crater, Arizona: Am. Inst. Mining Metall. Engineers Trans., v. 97, p. 63–98.

Jameson, M. H., 1941, Effect of dipping strata on determinations of potential-drop ratio: Am. Inst. Mining Metall. Engineers Tech. Pub. 1294, 5 p.; 1945, Trans., v. 164, p. 164–169.

Jensen, Joseph, 1936, Recent developments related to petroleum engineering: Oil and Gas Jour., v. 35, no. 21, p. 44, 48; also Petroleum World, v. 33, no. 434, p. 298–300, London. Method of logging formation through casing known as "Stratigraph," based upon electromotive series of metals. GA 3392; GA 3393.

Jensen, K. D., 1954, Geo-electrical investigations of manganese ore bodies in India: Geofisica pura e Appl., v. 28, p. 91–108. GA 160–65.

Joesting, H. R., 1941, Magnetometer and direct-current resistivity studies in Alaska: Am. Inst. Mining Metall. Engineers Tech. Pub. 1284, 20 p.; 1945, Trans., v. 164, p. 66–87. GA 6080.

Joesting, H. R., Bacon, L. O., and Getz, J. H., 1948, Geophysical investigation of manganiferous iron deposits, Boston Hill, Grant County, New Mexico: U.S. Bur. Mines Rept. Inv. 4175, 12 p. GA 10000.

Johnson, H. N., 1934, Discussion to paper by M. K. Hubbert, 1932: in Am. Inst. Mining Metall. Engineers Trans., v. 110, p. 30–31, 1934.

Johnson, W. R., Jr., MacCarthy, G. R., McCampbell, J. C., and Straley, H. W., 3d, 1937, Tracing a basic dike, near Chapel Hill, NC., by geoelectrical and geomagnetic methods: Am. Inst. Mining Metall. Engineers Contr. 106, 4 p.

Johnson, W. R., Jr., and Straley, H. W., 3d, 1941, Geophysical tracing of pegmatite dikes: Pan Am. Geologist, v. 75, no. 3, p. 161–165. GA 6016.

Jones, B. E., 1937, Results to be expected from resistivity measurements: Am. Geophys. Union Trans., v. 18, pt. 2, p. 399–403.

Jones, W. A., 1947, Experience with some electrical and magnetic methods of prospecting: Canadian Inst. Mining Metallurgy Bull., v. 50, no. 526, Trans. Sec., p. 537–557. GA 10083.

Jung, Karl, 1951, Die Messung der tallurischen Ströme [The measurement of telluric currents]: Umschau, v. 51, no. 3, p. 74–75. Telluric current. GA 14857.

Kalenov, E., 1938, Elektricheskaya razvedka karstovykh obrazovaniy v Donbasse [Electrical prospecting of karst formations in the basin of the Don]: Razvedka Nedr, no. 7, 65–70. GA 4664.

Kamensky, G. M., 1947, Poiski i razvedka podzemnykh vod [Prospecting for underground waters]: Gosudar. Izd. Geol. Lit [State Publ. Co. Geol. Lit.], 313 p. Only part applies to geophysics. Resistivity, logging method. GA 11447.

Kamprath, H. E., 1951, Bemerkungen zu dem Aufsatz von O. Keunecke über: Die Bedeutung von Erzlagerstätten [Remarks on the article by O. Keunecke on: The value of geoelectrical investigations in search and exploration of ore deposits]; Zeitschr. Erzbergbau u. Metallhüttenwesen, v. 4, no. 12, p. 467–468. GA 14655.

Kaneko, Jun, 1951, Electrical and magnetic prospecting on the Sankyo iron mine, Miigata prefecture [In Japanese with English summary]: Japan Geol. Survey Bull., v. 2, p. 38–43. Self-potential. GA 14135.

Kaneko, Jun, 1952, Electrical prospecting in the Shiraoi sulphur mine, Hokkaido [In Japanese with English summary]: Japan Geol. Survey Bull., v. 3, p. 47–51. GA 14468.

Kaneko, Jun, and Honma, Ichiro, 1954, Electrical prospecting of water supply for industrial purposes at Seiban district, Hyogo prefecture [In Japanese with English Summary]: Japan Geol. Survey Bull., v. 5, no. 1, p. 13–22. GA 160–70.

Karcher, J. C., and McDermott, Eugene, 1935, Deep electrical prospecting: Am. Assoc. Petroleum Geologists Bull., v. 19, no. 1, p. 64–77. Reprinted, 1947, in Early geophysical papers: Tulsa, Soc. Explor. Geophysicists, p. 724–737. GA 2357.

Katyev, V. A., 1932, Itogi geoelektrorazvedki v Khakassko-Minusinskoy geologo-razvedochnoy baze za 1931 god. [Results of the geoelectrical survey at the Khakassko-Minusinsk Geologic-Exploration Base during 1931]: Geol.-Razvedochnoe Upravlenie Zapadno-Sibirskoe Otdel. Vestnik, no. 1, p. 56–66.

Keck, W. G., and Colby, W. F., 1942, The depth dependence of earth conductivity upon surface potential data: Jour. Appl. Physics, v. 13, p. 179–188. GA 6529.

Keilhack, Konrad, 1935, Lehrbuch der Grundwasser- und Quellenkunde [Textbook on ground water hydrology]: Berlin, Gebrüder Borntraeger, 3d ed., 575 p. GA 2983.

Keller, Fred, Jr., and Landsberg, Hans, 1941, Geoelectric investigations over Penn's Cave: Pennsylvania Acad. Sci. Proc., v. 15, p. 65–68. Resistivity. GA 6412.

Keller, J. B., 1953, The scope of the image method: Commun. Pure and Appl. Math., v. 6, p. 505–512.

Keller, W. D., 1934, Earth resistivities at depths less than one hundred feet: Am. Assoc. Petroleum Geologists Bull., v. 18, no. 1, p. 39–62. Reprinted, 1947, in Early geophysical papers: Tulsa, Soc. Explor. Geophysicists, p. 561–584. GA 1826.

Kelly, S. F., 1922, Experiments in electrical prospecting: Eng. Mining Jour., v. 114, p. 623–629, 673–676.

────── 1924, Electrical prospecting in Canada: Canadian Inst. Mining Metallurgy Trans., v. 27, p. 278–305; also 1924, Am. Zinc Inst. Bull., v. 7, no. 5, p. 21–39.

────── 1926, The Schlumberger method of electrical prospecting: Canadian Inst. Mining Metallurgy Trans., v. 29, p. 71–76, or Bull., v. 19, no. 175, p. 1154–1159.

────── 1927, Modern methods of prospecting: Canadian Mining Jour., v. 48, no. 47, p. 939–941.

────── 1930, Electrical methods for subsoil investigation: Brooklyn Engineers Club Proc., v. 28, pt. 3, p. 22–41. Resistivity results. GA no. 18, p. 15.

────── 1932a, A uniform expression for resistivity: Am. Inst. Mining Metall. Engineers Trans., v. 97, p. 141–143. Kelly recommended that "ohm-meters" be adopted as the unit of electrical resistivity. GA 666.

────── 1932b, Engineering uses for geophysics: Civil Eng., v. 2, no. 10, p. 628–632.

────── 1935a, Exploring down: Explosives Eng., v. 13, p. 263–270, 303–312.

────── 1935b, The role of geophysics in the exploration for gold: Canadian Mining Jour., v. 56, no. 3, p. 99–105. GA 2521.

────── 1937, Geophysical exploration—Its place in prospecting: Canadian Mining Manual, p. 41–46.

────── 1938a, A perspective of geophysics: Am. Inst. Mining Metall. Engineers Tech. Pub. 950, 11 p.; 1940, Trans., v. 138, p. 23–33. Early history of electrical methods.

────── 1938b, Cutting exploration costs with geophysics: Canadian Mining Manual, 8 p.

Kelly, S. F., 1938c, Geophysical prospecting: Canadian Mining Jour., v. 59, no. 5, p. 260–261. Use of electrical methods on gold-quartz ore. GA 4533.

────── 1939, Geophysical delineation of structure in mining explorations: Am. Geophys. Union Trans., v. 20, pt. 3, p. 245–269.

────── 1940, Geophysics in molybdenite discovery: Mining Jour., v. 23, no. 22, p. 7. Self-potential. GA 5513.

────── 1941, Geological studies of vanadium-uranium deposits by geophysical exploration methods: Mining Cong. Jour., v. 27, no. 8, p. 27–35.

Kelly, S. F., Zuschlag, Theodor, and Low, Bela, 1934, Discovering gold-quartz veins electrically: Mining and Metallurgy, v. 15, p. 251–256. Field examples over dikes. GA 2042.

Kerr, P. F., and Cabeen, C. K., 1925, Electrical conductivity of ore-minerals: Econ. Geology, v. 20, p. 729–737.

Keunecke, O., and Kuhne, R., 1935, Geophysikalische Untersuchung eines Kupfervorkommens [Geophysical investigation of a copper deposit]: Zeitschr. prakt. Geologie, v. 43, no. 3, p. 41–45. GA 2644.

Khalevin, N. I., 1953, Primeneniye elektrorazvedki dlya interpretatsii magnitnykh anomaliy [Employment of electric methods of prospecting for interpretation of magnetic anomalies]: Akad. Nauk SSSR Izv. ser. geofiz., no. 1, p. 61–68.

Khalfin, L. A., 1956a, Pole tochechnogo istochnika v prisutstvii szhatogo i vytyanutogo sferoidov [The field of a point source in the presence of an oblate and a prolate spheroid]: Akad. Nauk SSSR Izv. ser. geofiz., no. 6, p. 657–668. GA 166–129.

────── 1956b, Pole tochechnogo istochnika pri nalichii polusferoidal'noy vyyemki [The field pattern of a point source in the presence of a hemispheroidal indentation]: Akad. Nauk SSSR Izv. ser. geofiz., no. 10, p. 1200–1206. GA 168–76.

Khmelevskiy, I. V., 1936, Opyt primeneniya elektrorazvedki k izucheniyu karstovykh yavleniy [Application of electrical methods of prospecting for studying karst phenomena]: Razvedka Nedr, no. 13, p. 30–32. Resistivity. GA 3396.

Kihlstedt, F. H., 1934, Electrical methods in prospecting for gold: Am. Inst. Mining Metall. Engineers Trans., v. 110, p. 62–74. "Racom" method.

King, L. V., 1933, On the flow of electric current in semi-infinite stratified media: Royal Soc. London Proc., ser. A, v. 139, p. 237–277. Resistivity theory. GA 1734.

────── 1934, On the flow of electric current in semi-infinite media in which the specific resistance is a function of depth: Royal Soc. London Philos. Trans., ser. A., v. 233, p. 327–359. Resistivity theory. GA 2229.

Kislow, Afrikan, 1954, Elektryezhe metody poszukiwawcze [Electric methods of prospecting]: Przeglad geol., v. 5, p. 169–175. Resistivity. GA 164–101.

Kiyono, Takeshi, 1950a, The effects of the non-conducting layer on the apparent resistivity curves [In Japanese]: Butsuri-Tankō, v. 3, no. 1, p. 18–20.

────── 1950b, On the electrical prospecting by the potential-ratio method [In Japanese]: Butsuri-Tankō, v. 3, no. 2, p. 1–7.

────── 1950c, Theoretical study of the ground resistivity method of electrical prospecting: Kyōtō Univ. Faculty Eng., Mem., v. 12, p. 29–59. Resistivity. GA 12051.

────── 1951, The apparent resistivity in a drift [In Japanese with English summary]: Butsuri-Tankō, v. 4, no. 2, p. 71–74. Resistivity. GA 13480.

────── 1952a, A contribution to the theory of electrical prospecting [In Japanese with English summary]: Butsuri-Tankō, v. 5, no. 3, p. 126–129.

Kiyono, Takeshi, 1952b, The topographic effect on resistivity curves [In Japanese with English summary]: Butsuri-Tankō, v. 5, no. 4, p. 178–182.

—— 1953a, Addenda to the paper "Topographic effect on resistivity prospecting" [In Japanese with English summary] Butsuri-Tankō, v. 6, no. 1, p. 51–54.

—— 1953b, On the apparent resistivity curve for two-layer earth [In Japanese with English summary]: Butsuri-Tankō, v. 6, no. 2, p. 83–86.

—— 1953c, Ground resistivity methods [In Japanese with English summary]: Butsuri-Tankō, v. 6, no. 3–4, p. 237–243. GA 165–122.

Kiyono, Takeshi, Inagaki, H., and Shibata, B., 1949, Resistivity curves for a semi-circular disk [In Japanese]: Butsuri-Tankō, v. 2, no. 3, p. 16–17. Resistivity. GA 12053.

Knaebel, C. H., Observation and deduction applicable to measurement of electrical resistivity of large volumes of earth in place: Michigan Coll. Min. Technology Bull., v. 3, no. 2, 31 p. GA 1001.

Koefoed, O., 1955, Resistivity curves for a conducting layer of finite thickness embedded in an otherwise homogeneous and less conducting earth: Geophys. Prosp., v. 3, p. 258–267. GA 163–70.

Koenigsberger, J. G., 1925, Über den Nachweis wasserfuehrender Störungen unter Tage mittels geophysikalischer Methoden [Problem of detecting salt brines in mines by geophysical methods]: Kali, v. 19, p. 353–354. Location of salt brines in salt mines.

—— 1928, Field observations of electrical resistivity and their practical applications: Am. Inst. Mining Metall. Engineers Tech. Pub. 129,; 17 p.; 1929, Trans., v. 81, p. 221–237. GA no. 9, p. 20–21.

—— 1930a, Über geoelektrische Methoden mit direkter Stromzuleitung [On the geoelectric methods with stationary electric current]: Gerlands Beitr. Geophysik, v. 1, no. 1, p. 23–109. Potential drop ratio. GA no. 16, p. 8–10.

—— 1930b, Zur Ermittlung ausgedehnter Schichten verschiedener Leitfähigkeit [On the detection of extensive layers of different conductivity]: Zeitschr. Geophysik, v. 6, no. 2, p. 71–78. Potential-drop ratio. GA no. 14, p. 15.

—— 1933, Aufsuchung von Wasser mit geophysikalischen Methoden [Prospecting for water by geophysical means]: Gerlands Beitr. Geophysik, v. 3, no. 4, p. 463–525; Akad. Verlagsgesell. m.b.H., Leipzig, 63 p. GA 1703, GA 1970.

—— 1934a, Ergänzungen zur Bestimmung des wahren Widerstandes im Erdboden nach dem Zentralinduktionsverfahren und dem 4-Punktverfahren [The determination of the true resistance of the ground by using the central induction method and the four electrode method]: Beitr. angew. Geophysik, v. 4, p. 201–216. GA 1951.

—— 1934b, Angaben und Urteile über die Leistungen der angewandten Geophysik in Russland [Facts and analysis on the productivity of applied geophysics in Russia]: Beitr. angew. Geophysik, v. 4, p. 222–234.

—— 1940, Poverkhnostnaya geologiya i opredeleniye tsentra i glubiny poverkhnosti vozmushchayushchego tela ili poverkhnosti geofizicheskimi metodami po teorii potentsiala [Surface geology and determination of the center and surface depth of a disturbing body, or plane, by geophysical methods based on potential theory]: Internat. Geol. Cong., Moscow, 1937, 17th sess., Reports, v. 4, p. 463–484. GA 7307.

Kondrashev, S. N., 1940, O rezul'tatakh, poluchayemykh s pomoshch'yu metoda zaryazhennogo tela, i o vzaimnoy korreliruemosti kart izoliniy PS i potentsiala zaryadki [Concerning the results obtained by the method of a charged body and the correlation between the maps of PS isolines and the potential of the charge (in electrical prospecting for ores)]: Razvedka Nedr, no. 2–3, p. 49–52.

Kostitzin, V. A., 1935, Théorie générale mathématique des potentiels et résistivités apparentes dans le cas d'un sol constitué par un nombre quelconque de couches horizontales homogènes et isotropes comprises entre un substratum et un supersubstratum indéfini [General mathematical theory of the potentials and apparent resistivities of ground consisting of any number of homogeneous and isotropic horizontal layers and an infinite substratum and topmost stratum]: Annexe mathématique à la note du 10 octobre, Soc. prospection Élec. [Paris], p. 11–29.

Koulomzine, Theodore, and Brossard, Leo, 1947, The use of geophysics in prospecting for gold and base metals in Canada: Geophysics, v. 12, p. 651–662. GA 9758.

Kozhevin, D. V., 1935, Nekotorye voprosy metodiki razvedok ugol'nykh mestorozhdeniy [Questions concerning the methods of prospecting for coal deposits]: Razvedka Nedr, no. 22, p. 26–30. GA 3062.

Kozin, K. P., 1934, Elektricheskaya razvedka mestorozhdeniy redkikh metallov [Electrical exploration for deposits of rare metals]: Redkie Metally, Moscow, no. 3, p. 29–32.

—— 1935, Elektricheskaya razvedka kvartsevykh zhil [Electrical exploration for quartzite veins]: Sovetskaia Zolotopromyshlennost, Moscow, no. 9, p. 3–5.

—— 1936, Elektricheskaya razvedka v vechnoy merzlote [Electrical prospecting in regions with permanently frozen ground]: Neft. Geofiz. Byull., no. 3, p. 31–43. GA 4508.

—— 1937, O sovremennom sostoyanii elektrorazvedki zolotorudnykh mestorozhdeniy [On the present condition of electrical exploration for gold quartz veins]: Tresta Zolotorazvedka i Instituta Nauchno-issled. Geologo-Razved Inst. Zoloto Trudy, no. 4, p. 88–101, Moscow-Leningrad.

—— 1940, Obzor metodov elektricheskoy razvedki v issledovanii zemnoy korozii metallov [A review of methods of electrical exploration for investigating the corrosion of metals underground]: Soveshch. po Vopr. Korrozii i Bor'by s Ney, Trudy, p. 179–201. [Moscow-Leningrad].

Kozin, K. P., and Kalenov, E. N., 1936, Primenenie metodov elektrorazvedki k issledovaniya korrozii podzemnykh tech'-oprovodov [Application of electrical prospecting to the study of underground pipe-line corrosion]: Neft. Geofiz. Byull, no. 3, p. 3–30. GA 4506.

Kozin, K. P., and Mernykh, V. M., 1940, O geofizicheskoy razvedke Zakavkazskikh polimetallicheskikh mestorozhdeniy [On the geophysical exploration of Transcaucasian polymetallic deposits]: Tsvetn. Metally, no. 10–11, p. 12–16, [Moscow-Leningrad].

Kozin, K. P., Ozerskaya, M. L., and Sheynman, S. M., 1937, O novom sposobe polevoy elektrorazvedki [On the new method of electrical prospecting]: Neft. Geofiz. Byull., no. 4, p. 3–31. Telluric current. GA 4507.

Krahmann, Rudolf, 1926, Die Anwendbarkeit der geophysikalischen Lager stättenuntersuchungsverfahren, insbesondere der elektrischen und magnetischen Methoden [The applicability of geophysical methods to the search for ore deposits with special reference to the electric and magnetic methods]: Prakt. Geologie und Bergwirtschaftslehre Abh., v. 3, 40 p. [English translation also issued, same reference, 43 p.] GA 40.

Krajčovič, Silvester, 1956, K hĺbkovemu dosahu geoelektrických odporových metód [On the depth range of the geoelectric resistivity method]: Geol. Práce, v. 5, p. 108–119. GA 166–145.

Krasnow, Shelley, 1937, Discovering underground conditions:. The Constructor, p. 16–19. Resistivity. GA 4041.

Krayev, A. P., 1951, Osnovy geoelektriki [Principles of geo-electric methods of prospecting]: Pt. 1, Moscow, Gostekh-teorizdat, 445 p. Textbook. GA 13728.

Krayev, A. P., Semenov, A. S., and Tarkhov, A. G., 1947, Sverkhglubokoye elektrozondirovaniye [Electrical depth profiling at great depths]: Razvedka Nedr, no. 3, p. 40–41. GA 10084.

Kruger, F. C., and Lacy, W. C., 1949, Geological explanation of geophysical anomalies near Cerro de Pasco, Peru: Econ. Geology, v. 44, p. 485–491. Resistivity, Self-potential. GA 11836.

Ku, Kong-Gyiu, 1948, On some new anomalous results of earth current investigations in mountainous areas of southwest China: Chinese Geophys. Soc. Jour., v. 1, no. 1, p. 30–39. Self-potential. GA 11106.

Ku, K. H., Wang, T. C., and Chang, H. C., 1944, An investigation of the Chaotung lignite field by Wenner's resistivity method of electrical prospecting: China Mineral Explor. Bur., Contr. Econ. Geology, no. 1, p. 111–116. GA 8392.

Kunetz, Gésa, 1954, Enregistrements des courants telluriques à l'occasion de l'éclipse de soleil du 25 février 1952 [Recordings of telluric currents at the time of the solar eclipse of February 25, 1952]: Annales Géophysique, v. 10, p. 262–270. GA 160–51.

——— 1955, Einfluss vertikaler Schichten auf elektrische Sondierungen [Effect of vertical layers on electrical surveys]: Zeitschr. Geophysik, v. 21, no. 1, p. 10–24. GA 165–119.

Kunetz, Gésa, and Chastenet de Géry, Jerome, 1956, La representation conforme et divers problémes de potentiel dans des milieux de "permeabilite" differente [Conformal mapping and various problems of potential in media of different "permeability"]: Rev. Inst. Français du Pétrole, v. 11, no. 10, p. 1179–1192. GA 168–81.

Kunetz, Gésa, and Richard, Henri, 1952, Comparaison des variations rapides du champ tellurique entre stations situées à grande distance [Comparison of rapid variations of the telluric field at stations separated by great distances]: Convegno naz. metano e petrolio, 7mo, Taormina 1952, Atti, v. 1, p. 511–518. GA 159–58.

Kunz, Bruno, 1947, Die Auswertung geoelektrischer Tiefen-messungen [The value of geoelectric depth measurements]: Bohrtechniker-Zeitung, v. 63, no. 5, p. 8–13; no. 9, p. 5–10.

——— 1948, Zur Auswertung geoelektrischer Tiefenmessungen [On the value of geoelectric depth measurements]: Bohrtech-niker Zeitung, v. 64, no. 1, p. 11–13.

Kurata, Nobuo, 1953, On searching for ground water: Butsuri-Tankō, v. 6, no. 3–4, p. 179–185. [In Japanese with English summary] GA 165–130.

Kurata, Nobuo, Ochiai, Toshiro, and Murashita, Toshiō, 1949, Electrical resistivity curves as an index to geological conditions: Butsuri-Tankō, v. 2, no. 3, p. 26–29. [In Japanese]: Resistivity. GA 12054.

Kurdyukov, V. A., and Ryng, S. I., 1936, Poiski pogrebennykh dolin metodami elektrorazvedki [Prospecting for buried valleys by electrical methods]: Razvedka Nedr. no. 14, p. 12–14. GA 3398.

Kurtenacker, K. S., 1934a, Some practical applications of resistivity measurements to highway problems: Am. Inst. Mining Metall. Engineers Trans., v. 110, p. 49–59.

Kurtenacker, K. S., 1934b, Use of resistivity methods for locating and exploring deposits of stone and gravel: Rock Products, v. 37, no. 7, p. 32–35. GA 2531.

Lancaster-Jones E., 1930, The earth-resistivity method of electrical prospecting: Mining Mag., v. 42, no. 6, p. 352–355; v. 43, no. 1, p. 19–29. Resistivity theory: 2-layer case. Resistivity results. GA no. 17, p. 15–16.

Landes, K. K., and Wilson, J. T., 1944, Ground water exploration by earth resistivity methods: Michigan Acad. Sci. Papers, v. 29, p. 345–353. GA 7706.

Langer, R. E., 1933, An inverse problem in differential equations: Am. Math. Soc. Bull., v. 39, p. 814–820.

Lee, F. W., 1928, Measuring the variation of ground resistivity with a Megger: U.S. Bur. Mines Tech. Paper 440, 16 p. Resistivity results.

——— 1930, Comparative advantages of applying several geophysical methods of prospecting to the same territory: U.S. Bur. Mines Inf. Circ. 6235, 11 p.

——— 1936, Geophysical prospecting for underground waters in desert areas: U.S. Bur. Mines Inf. Circ. 6899, 27 p. Resistivity. GA 3399.

——— 1938, A new depth meter for ice and snow: Internat. Assoc. Hydrology Bull. 23, p. 761–771.

——— 1939a, History and activities of the Section of Geophysics of the United States Geological Survey: Am. Geophys. Union Trans., v. 20, pt. 1, p. 280–291. Contains bibliography including many references to electrical prospecting.

——— 1939b, The possibility of electrical stratification in the earth as disclosed by surface measurements of currents and potentials: Am. Geophys. Union Trans., v. 20, pt. 3, p. 383–389.

——— 1941, Geophysical Prospecting, in Peele, Robert, Mining engineer's handbook: New York, John Wiley & Sons, 3d ed. with collaboration of John A. Church, sec. 10–A, p. 10–21.

Lee, F. W., and Hemberger, S. J., 1946, A study of fault determinations by geophysical methods in the fluorspar areas of Western Kentucky: U.S. Bur. Mines Rept. Inv. 3889, 27 p. GA 8714.

Lee, F. W., Joyce, J. W., and Boyer, Phil, 1929, Some earth resistivity measurements: U.S. Bur. Mines Inf. Circ. 6171, 16 p. Resistivity theory. GA no. 9, p. 16–17.

Lee, F. W., Scharon, H. L., and Sandberg, C. H., 1946, Prospecting for mineralization in steeply dipping beds covered by glacial till, talus, and weathered zones: U.S. Bur. Mines Tech. Paper 694, 19 p. GA 8873.

Lee, F. W., and Swartz, J. H., 1930, Resistivity measurements of oil bearing beds: U.S. Bur. Mines Tech. Paper 488, 12 p. Resistivity results. GA no. 21, p. 10.

Lehmann, Martin, 1956, Geomagnetische und geoelektrische Untersuchungen an Lamprophyrgängen in der Lausitz [Geomagnetic and geoelectric investigations on lampro-phyre dikes in the Lausitz massif]: Geologie, v. 5, no. 6, p. 515–527. GA 168–251.

Lelyavin, M. G., 1940, Polevaya elektrorazvedka v usloviyakh tresta Mayneft' [Electrical method of prospecting under the conditions of the Maineft Trust]: Razvedka Nedr, no. 10–11, p. 40–45. GA 6043.

Leonardon, E. G., 1929, Electrical studies in drill holes: Min. Metall. Soc. America Bull., v. 22, no. 10, Bull. 207, p. 150–155. Logging method. GA no. 11, p. 17–18.

——— 1931a, Topographical study of a hidden bed rock surface by resistivity measurements: Eng. Jour., Montreal, v. 14, no. 6, p. 331–335. GA 621.

Leonardon, E. G., 1931b, Electrical exploration applied to geological problems in civil engineering: Am. Inst. Mining Metall. Engineers Tech. Pub. 407, 17 p.; 1932, Trans., v. 97, p. 99–113. Resistivity results. GA 137.

Leonardon, E. G., and Kelly, S. F., 1928a, Exploration for ore by potential methods: Canadian Inst. Mining Metallurgy Bull., no. 189, p. 157–178; Eng. Mining Jour., v. 125, p. 46–49, 163–166.

———— 1928b, Some applications of potential methods to structural studies: Am. Inst. Mining Metall. Engineers Tech. Pub. 115, 18 p.; 1929, Trans., v. 81, p. 180–198. Resistivity results. GA no. 12, p. 15.

Leonardon, E. G., and Schlumberger, Conrad, 1932, Application de la prospection électrique a l'étude des projets de tunnels et de barrages [Application of electrical prospecting to the study of tunnel and dam projects]: Annales des Ponts et Chaussées, v. 102, pt. 2, p. 271–289. GA 1112.

Lepeshinskiy, Yu. N., and Murashov, D. F., 1929, Elektrorazvedka poleznykh iskopaemykh po metody ekvipotentsial'nykh liniy [Electrical prospecting of mineral deposits by the method of equipotential lines]: Geol. Komitet materialy po obshch. prik. geologii, v. 138, 128 p. This publication is one of the series of books on the methods of geophysical prospecting issued by the Geological Committee in Leningrad. Equipotential line method. GA no. 10, p. 17–18.

Lewis, W. B., 1945, Working depths for low frequency electrical prospecting: Geophysics, v. 10, p. 63–75. GA 7994.

Liogen'kiy, S. Ya., 1937, Opredeleniye moshchnosti pegmatitovykh zhil metodom poverkhnostonogo karottazha [Determination of the thickness of pegmatite veins by the superficial coring method]: Razvedka Nedr, no. 24, p. 57–58. GA 4362.

———— 1938, K voprosy opredeleniya glubiny vyklinivaniya pegmatitovykh zhil metodom soprotivleniy [On the question of determining the depth of outcropping pegmatite veins by the resistance method]: Razvedka Nedr, no. 10, p. 44–46. Resistivity. GA 4828.

Lipskaya, N. V., 1949a, O vozmushchenii elektricheskikh poley sfericheskimi neodnorodnostyami (mètod bepolyarnykh koordinat) [The disturbance of electrical fields by spherical inhomogeneities (method of bipolar coordinates)]: Akad. Nauk SSSR Izv. ser. geog. i geofiz., v. 13, no. 4, p. 335–347.

———— 1949b, Pole tochechnogo elektroda, nablyudayemoye na poverkhnosti zemli vblizi pogruzhennoy provodyashchey sfery [The pattern of the electric field produced by a point source as observed on the earth's surface near a buried conductive sphere]: Akad. Nauk SSSR Izv. ser. geog. i geofiz., v. 13, no. 5, p. 409–427. GA 11833.

———— 1953, Anomal'noye pole lokal'noy neodnorodnosti s konechnym znacheniyem elektroprovodnosti [Anomaly field produced by a local heterogeneity of finite electroconductivity]: Akad. Nauk SSSR Izv. ser. geofiz., no. 6, p. 514–522. GA 156–58.

Löhnberg, Alfred, and Loewenstein, A., 1936a, Die geoelektrische Hydrologie als Teilgebiet der Analyse des Untergrundes [Geoelectric hydrology as a special field in analyzing the underground]: Beitr. angew. Geophysik, v. 6, p. 52–88. Resistivity. GA 3401.

———— 1936b, Electrical prospecting for water: Mining Mag., v. 55, no. 3, p. 143–153. GA 3400.

Löhnberg, Alfred and Stern, Walter, 1932, Ein neuer Weg der Karsthydrologischen Forschung durch Anwendung Geoelektrischer Methoden [A new method for investigating the Karst hydrological region by using geoelectrical methods]: Zeitschr. Geophysik, v. 8, no. 6–7, p. 283–305. GA 1141.

Lögn, Örnulf, 1954, Mapping nearly vertical discontinuities by earth resistivities: Geophysics, v. 19, p. 739–760. Resistivity. GA 159–169.

Longacre, W. A., 1941, A study of the problem of depth determination by means of earth-resistivity measurements: Am. Inst. Mining Metall. Engineers Tech. Pub. 1392, 7 p.; 1945, Trans., v. 164, p. 179–185. GA 6413.

Low, Bela, Kelly, S. F., and Creagmile, W. B., 1932, Applying the Megger ground tester in electrical exploration: Am. Inst. Mining Metall. Engineers Trans. v. 97, p. 114–126. Resistivity results.

Löwy, H., 1927, Über das Grundproblem der angewandten Geophysik und den elektrischen Nachweis von Erdöl [On the fundamental problem of applied geophysics and the electrical method of prospecting for oil]: Naturw. v. 15, p. 921. GA no. 12, p. 16–17.

———— 1937, Der Fundamentalsatz der angewandten Geophysik [The fundamental principle of applied geophysics]: Beitr. angew. Geophysik, v. 6, p. 271–276. GA 3746.

Lugeon, M., and Schlumberger, Conrad, 1932, Application des méthodes de prospection électrique a l'étude des fondations de hauts barrages et des ouvrages annexes [Application of electrical prospecting methods to the study of foundations of large dams and to similar works]: Génie Civil, v. 101, no. 66, p. 134–137. GA 1111.

———— 1933, The electrical study of dam foundations: Mining Mag., v. 48, no. 6, p. 340–345. GA 1597.

Lundberg, Hans, 1919, Potentialmetod for elektrisk malmetning [Potential method for electrical prospecting]: Jernkontorets Annaler, p. 203–215.

———— 1923, Practical experience in electrical prospecting: Sveriges Geol. Undersökning Årsbok, v. 16 (1922), no. 9, ser. C, (no. 319), p. 4–37. Contains bibliography of early papers.

———— 1926a, The Swedish methods of electrical prospecting: Canadian Inst. Mining Metall. Bull., v. 19, p. 1139–1147, 1159–1165; Trans., v. 29, p. 56–64.

———— 1926b, Electrical and electromagnetic prospecting: Am. Inst. Mining Metall. Trans., v. 74, p. 3–28.

———— 1928a, Recent results in electrical prospecting for ore: Am. Inst. Mining Metall. Engineers Tech. Pub. 98, 36 p.; 1929, Trans., v. 81, p. 87–124. GA no. 12, p. 14.

———— 1928b, The present status of geophysical methods of prospecting: Canadian Inst. Mining Metallurgy Bull., v. 21, Trans. Sec., p. 693–705; Trans., v. 31, p. 209–221.

———— 1929, The history of magnetic and electrical prospecting for oil: Mining Mag., v. 41, no. 2, p. 73–78.

———— 1937, Recent advances in geophysical prospecting: Canadian Inst. Mining Metall. Trans., v. 40, p. 758–788.

———— 1938, Practical results obtained from geophysical surveys: Am. Inst. Mining Metall. Engineers Tech. Pub. 954, 29 p.

———— 1938, Practical results obtained from geophysical surveys: Am. Inst. Mining Metall. Engineers Tech. Pub. 954, 29 p.

Lundberg, Hans, and Kihlstedt, Folke, 1932, Differential rate of change method; elimination of surface resistivity variations in electrical prospecting: Am. Inst. Mining Metall. Engineers Advance Paper, 4 p., February. Potential-drop ratio.

———— 1933, Geophysics applied to geology: Canadian Mining Jour., v. 54, no. 8, p. 337–342. "Racom" method. GA 1670.

Lundberg, Hans, and Zuschlag, Theodore, 1931, A new development in electrical prospecting: Am. Inst. Mining Metall. Engineers Tech. Pub. 415, 18 p.; 1932, Trans., v. 97, p. 47–62. Potential-drop ratio. GA 176.

Lundberg, Hans, Zuschlag, Theodor, and Kihlstedt, Folke, 1931, Expansion and progress of electrical prospecting: Canadian Inst. Mining Metallurgy Bull. 232, p. 932–962. GA 473.

MacDonald, H. M., 1895, The electrical distribution on a conductor bounded by two spherical surfaces cutting at any angle: London Math. Soc. Proc., v. 26, p. 156–172.

Macelwane, J. B., 1940, Fifteen years of geophysics: A chapter in the exploration of the United States and Canada 1924–39: Geophysics, v. 5, p. 250–258. Contains map of United States and Canada showing (1) locations where electrical methods of prospecting had been applied prior to 1929 and (2) locations where electrical prospecting was done during 1924–39.

Maeda, Katsuro, 1951a, Electrical trenching and its interpretation: Butsuri-Tankō, v. 4, no. 1, p. 16–19. [In Japanese with English summary.]

——, 1951b, Apparent resistivity of dipping strata: Butsuri-Tankō, v. 4, no. 3, p. 103–106; 1952, v. 5, no. 2, p. 57–59. [In Japanese with English summary.]

—— 1955, Apparent resistivity for dipping beds: Geophysics, v. 20, p. 123–139. GA 160–58.

Magnée, Ivan de, 1950, Délimitation géo-électrique du premier pipe de Kimberlite découvert dans les champs diamantifères du Kasaï (Congo Belge) [The delineation by geoelectrical methods of the first pipe of Kimberlite in the diamond fields of Kasai, Belgian Congo]: Internat. Geol. Cong. [London] 18th, Proc., pt. 5, sec. D, p. 52–58. Resistivity. GA 12839.

Magnus, Wilhelm, and Oberhettinger, Fritz, 1949, Formulas and theorems for special functions of mathematical physics: New York, Chelsea Publishing Co., 172 p.

Maillet, Raymond, 1936, Les méthodes de prospection électrique Schlumberger [Schlumberger's methods of electrical prospecting]: Soc. Eng. Civils France Mém. 4, p. 618–641. Self-potential, Resistivity. GA 3609.

—— 1941, La prospection électrique du sous-sol [Electrical prospecting of the sub-strata]: Annales des Mines Mem., ser. 13, v. 18, p. 25–92. Contains list of publications of Conrad Schlumberger and other publications of the Schlumberger school.

—— 1947, The fundamental equations of electrical prospecting: Geophysics, v. 12, p. 529–556. GA 9838.

Maillet, Raymond, and Doll, H. G., 1932, Sur un théorème relatif aux milieux électriquement anistropes, et ses applications à la prospection électrique en courant continu [A theorem relating to electrically anisotropic media and its application to electrical prospecting by direct current]: Gerlands Beitr. Geophysik, v. 3, p. 109–124. Tensorial calculus used in analysis. Resistivity theory. GA 1225.

Maillet, Raymond, and Migaux, Léon, 1942, Conrad Schlumberger et la prospection électrique [Conrad Schlumberger and electrical prospecting]: Paris, Dunod, 190 p. A memorial volume in honor of Conrad Schlumberger. Contains a collection of papers published during 1941 by Maillet and Migaux in Annales des Mines Mem., ser. 13, v. 18, p. 1-190.

Mainguy, M., and Grépin, A., 1953, Some practical examples of interpretation of telluric methods in Languedoc [southeastern France]: Geophys. Prosp., v. 1, p. 233–240.

Makino, Naofumi, 1949, On the apparent resistivity curves for underground layered structures: Butsuri-Tankō, v. 2, no. 3, p. 18–21. Resistivity theory. GA 12052. [Japanese.]

—— 1950, Measurement of the electric resistivity of underground strata: Butsuri-Tankō, v. 3, no. 3, p. 35–37. [In Japanese with English summary.]

Malkowski, Zdzislaw, 1951, Elektrychna metoda oporowa przy stosowaniu pradu stalego w badaniach geofizycznych [Electrical resistivity method with direct current in geophysical explorations]: Państwowy Instyt. Geol. Biul. 63, Ser. geofiz. no. 6, p. 5–31. GA 13947.

Manfredini, Antonio, 1950, Studio geofisico della formazione gessososolfifera Siciliana con il metodo della resistivita elettrica [Geophysical investigation of gypsum and sulfur deposits in Sicily using electrical resistivity methods]: Ufficio Geol. Italia Boll., v. 70, p. 243–246. Resistivity. GA 12466.

—— 1951, Ricerca idrica con mezzi geofisici nel comune di guidonia [Hydrological research with geophysical methods in Guidonia]: Servizio geol. Italia Boll., v. 71, p. 207–215. Resistivity examples. GA 13740.

—— 1952, Investigation of river beds by electric soundings: Servizio geol. Italia Boll., v. 73, p. 371–395. Direct-current resistivity, field examples. GA 14267.

—— 1953, Studie geofiscio del Circeo [Geophysical study of the Circeo]: Servizio geol. Italia Boll., v. 75, no. 1, p. 311–328. Resistivity. GA 157–64.

—— 1954, Alcuni risultat idella campagna geo-elettrica del 1953 [Some results of geoelectric surveying during 1953]: Servizio geol. Italia Boll., v. 75 (1953), no. 2, p. 969–971. GA 161–63.

—— 1955, Su alcuni risultati attenuti nel campo dei metodi elettrici a corrente continua [On some results obtained in the field by the direct current electrical method]: Servizio geol. Italia Boll., v. 76, no. 2, p. 613–614. GA 165–129.

Manhart, T. A. 1937, Model tank experiments and methods for interpretation of resistivity curves: Colorado School of Mines Quart., v. 32, no. 1, p. 139–168. Slightly abridged, but the only published version of original Master's thesis of 1932. Resistivity curves, model tank experiments, and methods of interpretation.

Markov, A., 1938, Poverkhnostnoye raspredeleniye postoyannogo toka v sluchaye naklonnogo provodyashchego sloya [The surface distribution of direct current in the case of an inclined conducting layer]: Tsentr. nauchno-issled. geologo-razvedochnogo Inst. Geofizika, v. 5, p. 40–54. GA 4665.

Mason, Max, 1927, Geophysical exploration for ores: Am. Inst. Mining Metall. Engineers Tech. Pub. 45, 33 p.; 1929, Trans., v. 81, p. 9–43.

Matteucci, M. C., 1865, Sur les courants électriques de la terre [On the electric currents of the earth]: Annales Chimie et Physique, ser. 4, v. 4, p. 177–192.

—— 1867, Sur les courants électriques de la terre [On the electric currents of the earth]: Annales Chimie et Physique, ser. 4, v. 10, p. 148–159.

Maturbara, A. 1937, The electrolytic method of prospecting: Mining Inst. Japan Jour., v. 53, p. 515–528. Self-potential. GA 7057.

Mauchly, S. J., 1918, A study of pressure and temperature effects in earth-current measurements: Terrestrial Magnetism Atmos. Electricity, v. 23, p. 73–91.

Maxwell, James C., 1891, Electricity and magnetism: University Press, Oxford, England, 500 p.; reprinted 1954, Dover Pub., New York, 500 p. This edition (1891) is especially good on the theory of images. GA 845.

Mazzoni, A., and Breusse, J. J., 1954, Application de la prospection électrique à la tectonique pour la recherche de vapeur naturella a Larderello (Italie) [Application of electrical exploration to the structure in the search for natural steam at Larderello (Italy)]: Internat. Geol. Cong., 19th, Algiers, Comptes Rendus sec. 15, pt. 17, p. 161–168. GA 163–74.

McCardell, W. M., Winsauer, W. O., and Williams, M., 1953, Origin of the electric potential observed in wells: Am. Inst. Mining Metall. Engineers Trans., v. 198, p. 41–50.

McCollum, Burton, 1921, Measurements of earth currents: Elec. Railway Jour., v. 58, p. 809–813. Resistivity.

McCollum, Burton, and Ahlborn, G. H., 1916, Methods of making electrolysis surveys: U.S. Bur. Standards Tech. Pub. 28, 84 p.

McCollum, Burton, and Logan, K. H., 1913, Electrolytic corrosion of iron in soils: U.S. Bur. Standards Tech. Pub. 25, 69 p.

—— 1915, Earth resistance and its relation to electrolysis of underground structures: U.S. Bur. Standards Tech. Pub. 26, 48 p.

—— 1927a, Practical applications of the earth-current meter: U.S. Bur. Standards Tech Paper 351, p. 683–727. Resistivities of soils; determination of same.

—— 1927b, Electrolysis testing: U.S. Bur. Standards Tech. Paper 355, p. 15–89.

McCullough, E. J., 1956, Resistivity measurements in cyclothemic sediments: Compass, v. 33, no. 2, p. 115–119. GA 164–112.

McKellar, I. C., and Collins, B. W., 1953, The use of earth resistivity tests in the location of underground water in Canterbury: Pacific Sci Assoc., 7th Cong., Proc., v. 2, p. 129, [1949]. GA 163–75.

McLaughlin, D. H., Bateman, A. M., O'Neill, J. J., Hoffman, R. D., and Dougherty, E. Y., 1930, Summaries of results from geophysical surveys at various properties: Am. Inst. Mining Metall. Engineers Tech Pub. 369, 23 p.; 1932, Trans., v. 97, p. 24–46.

McMurry, H. V., and Hoagland, A. D., 1956, Three-dimensional applied potential studies at Austinville, Virginia: Geol. Soc. America Bull., v. 67, no. 6, p. 683–696. GA 166–164.

Mehler, F. G., 1868, Über die Vertheilung der Statischen Elektrizität in einem von zwei Kugelkalotton begrenzten Körper [On the distribution of static electricity in one of two spherically bounded bodies]: Crelle's Jour. Math., v. 68, p. 134–150.

Meier, Otto, 1933, Some remarks concerning the development of Swedish geoelectric methods of prospecting for oil bearing structures: Petroleum Zeitschr., v. 29, p. 14–16. GA 1423.

Meisser, Otto F., 1943, Praktische Geophysik für Lehre, Forschung und Praxis (Practical geophysics for study, research, and practice]: Dresden und Leipzig, Theodor Steinkopff, 368 p. Reprinted 1946, Ann Arbor Michigan, Edwards Bros., Inc. GA 7754.

Melikian, V., 1931, Elektricheskaia s'emka izvestniakov Biki-Eibatskoi bukhty [Electrical survey of limestones of the Bibi-Eibat Bay]: Azerbaid. Neft. Khoz. (Baku), nos. 9–10, p. 104–108. Resistivity results. GA 624.

Merriam, D. F., 1954, Electrical resistivity studies in the Kansas River valley: Kansas Geol. Survey Bull. 109, pt. 7, p. 97–112. Resistivity. GA 160–61.

Metzger, A. A. T., 1949, Contributions à l'étude électrique des depôts quaternaires [Contributions to the question of electric exploration of Quaternary deposits]: Finlande

Geol. Bull. no. 144, p. 3–8. Resistivity, Potential-drop ratio. GA 11837.

—— 1950, On potential-drop-ratio measurements in structural investigations: Internat. Geol. Cong., 18th, London, 1948, Proc., pt. 5, sec. D, p. 81–84. Potential-drop ratio. GA 12834.

Mielecke, Walter, 1956, Geoelektrische Messungen als Hilfsmittel geologischer Kartierung [Geoelectrical measurements as an aid to geologic mapping]: Zeitschr. angew. Geologie, v. 2, no. 4, p. 154–158. GA 166–156.

Migaux, Léon, 1941a, Conrad Schlumberger: Annales Mines Mem., ser. 13, v. 18, p. 5–23. Biography of Conrad Schlumberger.

—— 1941b, L'exploration électrique et thermique des sondages [Electrical and thermal surveys of bore holes]: Annales Mines Mém., ser. 13, v. 18, p. 93–178. Excellent account of electrical and thermal well logging. Contains list of Conrad Schlumberger's publications on well logging.

—— 1946, Une méthode nouvelle de géophysique Appliquée: La prospection par courants telluriques [A new method of applied geophysics prospecting by telluric currents]: Annales Géophysique, v. 2, p. 131–146. GA 9229.

—— 1950, Quelques exemples d'application de la méthode tellurique [Some examples of the application of the telluric method]: Internat. Geol. Cong., 18th, London, 1948, Proc., sec. D, pt. 5, p. 85–95. Telluric method, Self-potential. GA 12838.

—— 1951, Dix ans d'application de la méthode tellurique [Ten years of use of the telluric method]: World Petroleum Cong., 3d [The Hague], Proc., sec. 1, p. 624–645. Telluric method, Self-potential. GA 13733.

Migaux, Léon, and Kunetz, Géza, 1955, Apports des méthodes électriques de surface à la prospection pétroliere [Contribution of surface electrical methods to petroleum prospecting (with discussion)]: World Petroleum Cong., 4th [Rome], Proc., sec. 1, p. 545–574. GA 168–93.

Militzer, H., 1953, Die elektrische Eigenpotentialmethode in Erzbergbau [The self-potential method in mining industry]: Geologie, v. 2, no. 24, p. 291–292. Self-potential. GA 156–66.

Minakawa, Shinya, and Yamagata, Osamu, 1955, Report on the resistivity survey of Oami landcreep area in Azuma-mura, Higashi-Tagawa-gun Yamagata Prefecture: Butsuri-Tankō, v. 8, no. 2, p. 41–51. GA 166–160.

Mining Magazine, 1923, Schlumberger method of electrical prospecting: Mining Mag., v. 29, no. 4, p. 248–251. Self-potential.

Mitera, Z., 1937, A theoretical and experimental examination of the potential-drop-ratio method: Colorado School of Mines Quart., v. 32, no. 1, p. 187–222.

Mladenović, Milan, 1953, Primena geoelektricne metode otpora na Niksickom Polju [The use of the electrical resistivity method in the investigation of the field of Nikšić (with English summary)]: Serbia Zavod. geol. i geofix. istraživanja Vesnik, v. 10, p. 281–289. Resistivity. GA 157–67.

Mooney, H. M., 1954a, Depth determinations by electrical resistivity: Mining Engineering, v. 6, p. 915–918; 1954, Am. Inst. Mining Metall. Engineers Trans., v. 199, p. 915–918. Resistivity. GA 159–70.

—— 1954b, Effect of a variable surface layer on apparent resistivity data: Mining Engineering, v. 6, p. 1210–1212; 1954, Am. Inst. Mining Metall. Engineers Trans., v. 199, p. 1210–1212. Resistivity. GA 159–71.

Mooney, H. M., and Wetzel, W. W., 1956, The potentials about a point electrode and apparent resistivity curves for a two-, three-, and four-layer earth: Minneapolis, Univ. Minnesota Press, 146 p. and 243 loose sheets of reference curves. GA 166-144.

Moore, James I., and Ebbutt, Frank, 1926, Electrical prospecting at the Britannia mine: Canadian Inst. Mining Metallurgy Trans., v. 29, p. 84-99.

Moore, R. W., 1944, An empirical method of interpretation of earth resistivity measurements: Am. Inst. Mining Metall. Engineers Tech. Pub. 1743, 18 p.; 1945, Trans., v. 164, p. 197-223. GA 7707.

——— 1952a, Earth-resistivity tests applied to subsurface reconnaissance surveys: Am. Soc. Testing Materials, Special Tech. Pub. 122, p. 89-102. GA 14127.

——— 1952b, Geophysical methods adapted to highway engineering problems: Geophysics, v. 17, p. 505-530. Resistivity. GA 13922.

Morgan, Samuel P., Jr., 1947, Tables of Bessel functions of imaginary order and imaginary argument: Pasadena, Calif. Inst. of Technology Bookstore, 61 p. (Limited edition)

Morozov, G. S., 1934, Polevyye elektrometricheskiye raboty v Dagestane v 1932 g. [Electrometric field work in Dagestan in 1932]; Severo-Kavkazskoiye Konferentsii Geologov-Neftyanikov, Trudy, 6 p. 237-268.

Morse, Philip M., and Feshbach, Herman, 1953, Methods of theoretical physics: New York, McGraw-Hill, 2 v., 1978 p.

Mosetti, Ferruccio, 1953a, Su una prospezione geoelettrica in montagna. Rilevamento di falde acquifere fortemente ionizatte [On a geoelectric exploration in mountains. Survey of strongly ionized water-bearing layers]: Osservatorio Geofis. Trieste Pub., no. 31, 7 p. GA 14867.

——— 1953b, Su alcune richerche geoelettriche di zone mineraliz-zate [On some geoelectrical investigations of mineralized zones]: Industria Mineraria, v. 4, no. 12, p. 579-582; Osservatorio Geofis. Trieste Pub., no. 35, 4 p. Resistivity. GA 157-59.

——— 1954a, Misure geoelettriche in zone prevalentemente argillose. Un caso di stratificazione a resistivita non constante [Geoelectric measurements in predominately argillaceous zones. A case of stratification with varying resistivity]: Industria Mineraria, v. 5, no. 5, p. 257-259. GA 161-60.

——— 1954b, Rilievo geoelettrico del delta sotterraneo del Timavo [Geoelectrical survey of the subterranean delta of the Timavo]: Osservatorio Geofis. Trieste Pub., no. 38-39, p. 7-11; from Tecnica Italiana, v. 9, no. 2, p. 115-119. Restistivity. GA 157-66.

——— 1954c, Studio geoelettrico dell'idrologia sotterranea del Friuli orientale [Geoelectrical study of the subterranean hydrology of eastern Friuli]: Osservatorio Geofis. Trieste Pub., no. 42, 7 p., from Tecnica Italiana, v. 9, no. 3. Resistivity. GA 157-65.

Mounce, W. D., and Rust, W. M. Jr., 1943, Natural potentials in well logging: Am. Inst. Mining Metall. Engineers Tech. Pub. 1626, 6 p.; 1944, Trans., v. 155, p. 49-57; 1945, Trans., v. 164, p. 288-294.

Mukhin, A. V., 1947, Geofizicheskiye (elektrorazvedochnye) raboty v zapadnykh oblastyakh USSR [Geophysical (electrical) prospecting in the western region of Ukranian S.S.R.]: Razvedka Nedr, no. 1, p. 31-35.

Mukhina, G. V., 1950a, Ob ekraniruyushchem vliyanii provody-ashchikh sloyev, raspolozhennykh nad kontaktom dvukh ob sred [The screening effect of conductive layers located over a vertical fault]: Akad. Nauk SSSR Izv. ser. geog. i

geofiz., v. 14, no. 4, p. 302-316. Resistivity theory. GA 12460.

Mukhina, G. V., 1950b, Ob ekraniruyushchem vliyanii provody-astichikh sloyev, raspolozhennykh nad vertikal'noy zhiloy [The screening effect of conductive layers located over a vertical vein]: Akad. Nauk SSSR Izv. ser. geog. i geofiz., v. 14, no. 5, p. 392-402. Resistivity theory. GA 12649.

Murakami, Masatuga, 1954, Étude sur l'évolution d'une ancienne lagune selon la mesure de la résistance électrique spécifique du terrain [Study of the evolution of an old lagoon by the measurement of the specific electric resistance of the terrain]: Internat. Geol. Cong. 19th Algiers, Comptes Rendus, sec. 9, pt. 9, p. 211-216. GA 162-84.

Murozumi, Masayoshi, 1951a, Contribution to the electrical prospecting in Shojingawa sulphur mine and Amemasugawa sulphur mine, Hokkaido: Japan Geol. Survey Bull., v. 2, no. 7, p. 21-29. [In Japanese with English summary]. Resistivity, Self-potential. GA 14136.

——— 1951b, Electrical prospecting on Yokota Mine, Fukushima prefecture: Japan Geol. Survey Bull., v. 2, p. 51-64. [In Japanese with English summary.]: Resistivity, Self-potential. GA 13238.

——— 1953, Geophysical prospectings at the Wagasennin iron mine, Iwate prefecture: Japan Geol. Survey Bull., v. 4, no. 10, p. 41-48. [In Japanese with English summary.]: Resistivity, Self-potential, Equipotential line method. GA 159-83.

Muskat, Morris, 1932, Potential distributions in large cylindrical disks with partially penetrating electrodes: Physics, v. 2, p. 329-364.

——— 1933, Potential distribution about an electrode on the surface of the earth: Physics, v. 4, p. 129-147. GA 1474.

——— 1935, Potential distribution about an infinitely extended line electrode on the surface of a horizontally stratified earth (II): Physics, v. 6, p. 14-26. GA 2465.

——— 1944, The interpretation of earth-resistivity measurements: Am. Inst. Mining Metall. Engineers Tech. Pub. 1761, 7 p.; 1945, Trans., v. 164, p. 224-231. GA 7856.

Muskat, Morris, and Evinger, H. H., 1941, Current penetration in direct current prospecting: Geophysics, v. 6, p. 397-427. GA 6415.

Mutch, A. D., 1952, Variation of thermo-electric properties of pyrite in association with gold ore: Am. Inst. Mining Metall. Engineers Trans., v. 193, p. 880-883. Contains references on thermoelectric effect of pyrite.

Nagata, Takesi, 1944, Measurement of earth current in the vicinity of Sikano fault: Imp. Acad. Japan Proc., v. 20, p. 81-85. Self-potential. GA 10346.

Nakabayashi, Kazutaka, 1949, Generating mechanism of spontaneous polarization with some examples in Manchuria: Butsuri-Tankō, v. 2, no. 3, p. 22-25. [Japanese.] Self-potential. GA 12056.

Nakabayashi, Kazutska, and Fujiwara, Takayo, 1950, Generating mechanism of spontaneous polarization: Tokyo Research Inst. Nat. Resources Rept. 13, p. 16 (1949); Rept. 15, p. 6-16. [In Japanese with English summary.] Self-potential. GA 12650.

Nesterov, L. Ya., 1938, Nekotoryye dannyye o vliyanii nanosov pri elektrorazvedke krutopadayushchikh plokhoprovod-yashchikh plastov [Some data on the effect of glacial drift in the electrical prospecting of steeply dipping, poorly conducting layers]: Tsentr. Nauchno-issled. Geol.-Razved. Inst. Materialy, Geofizika, no. 6, p. 1-12. GA 4669.

Nettleton, L. L., 1940, Geophysical prospecting for oil: New York, McGraw-Hill, 444 p. Text. GA 5847.

Neumann, Franz, 1887, Theorie des Potentials und der Kugelfunktionen [Theory of potentials and spherefunctions]: Leipzig, B. G. Teubner, 276 p.

Niem, Günther de, 1937, Feldstärke und Stromdichte eines Dipols im Erdboden [Field intensity and current density of a dipole in the ground]: Beitr. angew. Geophysik, v. 7, p. 162–171. GA 4363.

―――― 1943, Das elektrische und magnetische Feld einer punktförmigen Stromquelle [Electrical and magnetic field of a point source]: Beitr. angew. Geophysik, v. 10, no. 3–4, p. 265–272. GA 12045.

Nikiforov, N. A., 1945, Geofizicheskiye metody kak sredstvo izucheniya i poiskov zolotorudnykh mestorozhdenii [Geophysical methods as means of detecting and studying gold deposits]: Adad. Nauk SSSR Izv. ser. geog. i geofiz., v. 9, no. 4, p. 389–398. [Engl. summ.] GA 8716.

Nippoldt, A., 1936, The secret of earth currents: Terrestrial Magnetism Atmos. Electricity, v. 41, no. 3, p. 261–263. GA 3403.

Nöring, F., 1950, Die geoelektrischen Messungen im Schwankeimer Wald bei Frankfurt a.M. [Geoelectric measurements in the Schwankeimer forest near Frankfurt on the Main]: Bohrtechnik-Brunnenbau, v. 1, no. 10, p. 319–320. GA 14656.

Novitchenko, V. N., 1937, Predvaritel'nyye itogi karottazha v Donbasse [Preliminary results of electrical coring in the Don Basin]: Razvedka Nedr, no. 6, p. 27–34. Logging method. GA 3880.

Noya, R. M., 1945, The application of geophysics to water supply problems: Mine and Quarry Eng., v. 10, p. 15–19, 40–45. GA 8116.

Obara, Nobuhiko, 1955, Geological researches for Takayama dam site, Kyoto Prefecture, accompanied by electric resistivity prospecting: Japan Geol. Survey Bull., v. 6, no. 9, p. 1–10. GA 166–159.

Ogilvi, A. A., 1940, Elektrorazvedka v podzemnykh vyrabotkakh [Electrical prospecting in underground workings]: Razvedka Nedr, no. 7, p. 31–35. GA 5945.

Ollendorff, Franz, 1928, Die Erdströme [Earth currents]: Berlin, Julius Springer, 69 p.

Onodera, Seibe, 1949, Supplement of resistivity curves on Wenner's method [Japanese]: Butsuri-Tankō, v. 2, no. 2, p. 7–10.

Ostermeier, J. B., 1933, Ein neues Messgerät zur Aufsuchung von Edelmetallseifen und erodierten Erzgänger [A new measuring device for discovering precious metal placers and eroded mineral lodes]: Metall. u. Erz, v. 30, no. 2, p. 21–24. Self-potential. GA 1473.

―――― 1934, Erdstrommessungen bei Pfaffenreuth [Earth current measurements near Pfaffenreuth]: Beitr. angew. Geophysik, v. 4, p. 186–200. Self-potential. GA 1954.

―――― 1937, Tektonische Forschung durch quantitative Elektrodenverfahren [Tectonic investigation by quantitative electrode-methods]: Bohrtechniker-Zeitung, v. 55, no. 6, p. 158–164. Resistivity. GA 3881.

Ostermeier, J. B., and Spross, J., 1933, Erdstrommessungen bei Pfaffenreuth [Current measurements near Pfaffenreuth]: Metall u. Erz, v. 30, no. 20, p. 408–412. GA 1737.

O'Sullivan, B. J. C., 1949, Geophysics in the search for water, some development in electrical groundsurvey: Water Eng. v. 52, no. 639, p. 214–234, 236.

Ovchinnikov, I. K., 1950, K teorii effektivnoy elektroprovodnosti $\bar{\gamma}$ magnitnoy pronitsayemosti $\bar{\mu}$, dielektricheskoy postoyannoy $\bar{\epsilon}$ sredy, imeyushchey inorodnye vklyucheniya [On the theory of effective electric conductivity $\bar{\gamma}$, magnetic permeability $\bar{\mu}$, dielectric constant $\bar{\epsilon}$ of a medium containing foreign inclusions]: Vses. nauchn.-issled. inst. razved. geofiz. Trudy, no. 3, p. 33–38. GA 158–87.

Ovchinnikov, I. K., 1953, O vozmushchenii polya postoyannogo toka provodnikami raspolozhennymi v neodnorodnom poluprostranstve [The disturbance of the field of direct current caused by conductors placed in heterogeneous semispace]: Akad. Nauk. SSSR Izv. ser. geofiz., no. 1, p. 48–60. GA 14446.

Ovchinnikov, I. K., and Kilyukova, G. G., 1955, Effektivnarya elektroprovodnost' sredy s vklyucheniyami [Effective electric conductivity of a medium with heterogeneous inclusions]: Akad. Nauk SSSR Izv. ser. geofiz., no. 1, p. 57–59. GA 160–52.

Palmer, L. S., 1954, Location of subterranean cavities by geoelectrical methods: Mining Mag., v. 91, no. 3, p. 137–141. GA 162–70.

Palmer, L. S., and Hough, J. M., 1953, Geoelectrical resistivity measurements: Mining Mag., v. 88, p. 16–22. Direct current resistivity theory and field example. GA 14263.

Parasnis, D. S., 1956, The electrical resistivity of some sulphide and oxide minerals and their ores: Geophys. Prosp., v. 4, p. 249–278. GA 167–100.

Patnode, H. W., and Wyllie, M. R. J., 1950, The presence of conductive solids in reservoir rock as a factor in electric log interpretation: Am. Inst. Mining Metall. Engineers Trans., v. 189, Tech. Pub. 2797, p. 47–52.

Patty, E. N., and Kelly, S. F., 1945, A geological and geophysical study of the Chelan nickel deposit near Winesap, Washington: Am. Inst. Mining Metall. Engineers Tech. Pub. 1953, 10 p.; 1945, Trans., v. 164, p. 155–163.

Paul, Bernt, 1949, Geoelektrische Schlumberger Messungen an der Erdoberfläche and in Bohrloch [Geoelectrical measurements by the Schlumberger method on the surface of the ground and in drill holes]: Erdöl Tektonik Nordwestdeutschland, p. 302–307. Resistivity, Self-potential. GA 12268.

Pautsch, Erich, 1928, Application of electric methods in practical geophysics: Gerlands Beitr. Geophysik, v. 20, p. 85–98.

Paver, G. L. 1944, Application of the electrical resistivity method of geophysical surveying to location of underground water examples from the Middle East: Geol. Soc. London Quart. Jour. Proc., v. 101, p. 46–51.

―――― 1950, The geophysical investigation of underground water supplies—a geological analysis of observed resistivity data: Inst. Water Eng. Jour., v. 4, p. 237–266. Resistivity. GA 12467.

Pekeris, C. L., 1940, Direct method of interpretation in resistivity prospecting: Geophysics, v. 5, p. 31–42. Resistivity. GA 5515.

Pendley, L. C., 1951, Subsurface earth exploration by electrical resistivity method: Kentucky Acad. Sci. Trans., v. 13, p. 189–200. Resistivity. GA 13039.

Perret, W. R., 1949a, Electrical resistivity exploration as a complement to boring in deep alluvial deposits: Internat. Conf. Soil Mechanics and Foundation Eng. 2d, Proc., v. 7, p. 80–84. Resistivity. GA 11838.

―――― 1949b, Electrical resistivity exploration: U.S. Waterways Expt. Sta. (Vicksburg), Bull. 33, 48 p.

Peters, L. J., and Bardeen, John, 1930, The solution of some theoretical problems which arise in electrical methods of geophysical exploration: Univ. Wisconsin Eng. Expt. Sta. Bull. 71, 88 p. Treats multiple layers. For semicylindrical current electrodes parallel to earth's surface, paper treats problems of (1) the dipping bed and (2) buried conducting sphere. Resistivity theory. GA 235.

—— 1932, Some aspects of electrical prospecting applied in locating oil structures: Physics, v. 2, p. 103–122. Reprinted 1947, Early geophysical papers: Tulsa, Soc. Explor. Geophysicists, p. 145–164. Resistivity theory. GA 819.

Petersson, Walfr., 1907, Das Aufsuchen von Erz mittels Elektrizität [The search for ore with electricity]: Glückauf, v. 43, p. 906–910.

Petropavlovskiy, S. A., 1946, Prakticheskiye priyemy detal'noy geofizicheskoy razvedki kolchedannykh mestorozhdeniy Urala [Practical techniques of detailed geophysical exploration of pyrite deposits in the Urals]: Razvedka Nedr, v. 12, no 4, p. 29–32. GA 9418.

Petrowsky, A. A., 1925a, Teoriya izmereniya zemnykh tekov [Theory of the measurements of earth currents]: Inst. Prikl. Geofiziki. Izv., no. 1, p. 73–87. Series of graphs showing electric field near an electrode. GA no. 1, p. 15.

—— 1925b, Yestestvennoye elektricheskoye pole, sozdavayemoye rudnym telom [Natural electric field produced by ore]: Inst. Prikl. Geofiziki Izv., no. 1, p. 87–104. Self-potential theory. GA no. 1, p. 13–14.

—— 1925c, Elektrometricheskiye metody gornoy razvedki i eksperimental'nyye raboty na Ridderskom rudnike letom 1924g. [Electrometric methods in ore prospecting and experimental investigations at Ridder's mine during the summer of 1924]: Inst. Prikl. Geofiziki Izv., no. 1, p. 107–134. Resistivity theory and results. GA no. 1, p. 13.

—— 1926, Osnov rascheta nablyudeniy zemnykh tokov [Basis for calculating the observations of earth currents]: Inst. Prikl. Geofiziki I v., no. 2, p. 124–142. Potential around spherical electrode half sunk in ground. GA no. 2, p. 20.

—— 1927a, On the theory of earth-currents' measurement: Philos. Mag., v. 3, p. 50–62.

—— 1927b, Opredeleniye mesta, glubiny zaleganiya i moshchnosti sfericheskoy zalezhi po nabludeniyam sozdvaymykh yeyu zemnykhtokov [Determination of the location, depth, and thickness of a spherical ore body by observing the earth current produced]: Inst. Prikl. Geofiziki Izv., no. 3, p. 3–36. Self-potential theory. GA no. 1, p. 14.

—— 1927c, Raschet iskusstvennago elektricheskogo polya [Calculations of an artificial electric field]: Inst. Prikl. Geofiziki Izv., no. 3, p. 39–63. Resistivity theory. GA no. 1, p. 15.

—— 1928a, The problem of a hidden polarized sphere—Part I: Philos. Mag., v. 5, p. 334–353; Part II, p. 914–927; Part III, p. 927–933.

—— 1928b, Izolinii yestestvennogo elektricheskogo polya sozdavaymogo sfericheskoy zalezh'yu [Equipotential lines of a natural electric field produced by a spherical ore body]: Inst. Prikl. Geofiziki Izv., no. 4, p. 81–89. GA no. 8, p. 12.

—— 1928c, Elektrometricheskoye issledovaniye Verkhne-Arshinskogo mestorozhdeniya letom 1927g. [Electrometric investigation of the Upper Arshinsk ore-bed accomplished in the summer of 1927]: Inst. Prikl. Geofiziki Izv., no. 4, p. 121–143. GA no. 8, p. 13–15.

—— 1928d, Iskusstvennoye elektricheskoye pole s 21 paroy elektrodov [An artificial electric field with 21 pairs of electrodes]: Inst. Prikl. Geofiziki Izv., no. 4, p. 216–231 GA no. 8, p. 15–17.

Petrowsky, A. A., 1937a, Raschet dielektricheskoy postoyannoy i udel'nogo soprotivleniya po izmerennym: deystvuyushchey ycmkosti i deystvuyushchemu soprotivleniyu [Calculation of dielectric constant and specific resistivity from measurements of effective capacity and resistance]: Akad. Nauk SSSR Petrog. Inst. Trudy, no. 10, p. 153–160. Electromagnetic. GA 4042.

—— 1937b, Teoreticheskiy obosnovaniya izmereniy udel'nogo soprotivleniya merzlykh i talykh gruntov pri pomoshchi dvukhtochechnoy ustanovki postoyannogo toka [The theoretical foundations of the measurement of specific resistances of frozen and thawed grounds by the two-point direct-current method]: Akad. Nauk SSSR Izv., Otdel. obshch. Nauk, no. 3, p. 363–402.

Petrowsky, A. A., and Akimov, A. T., 1938, Instruktsiya po primeneniyu elektrorazvedki postoyannym tokom na vechnoy merzlote [Instruction for applying the direct-current electrical method of prospecting in regions of permanently frozen ground]: Akad. Nauk SSSR, Komitet po vechnoy merzlote sbornik instruktsii i programmnykh ukazanii [Symposium of instructions and directions on the study of permanently frozen grounds and of perma-frost], p. 85–102. GA 5224.

Petrowsky, A. A., and Kramarev, B. N., 1935, Primeneniye elektrometricheskikh metodov razvedki dlya izucheniya karstovykh yavleniy [The application of electrometrical methods of exploration to the study of Karst phenomena]: Adak. Nauk SSSR Ural'sk. filiala Trudy, Ser. obshch., no. 6, p. 65–77.

Petrowsky, A. A., Skaryatin, R., and Kleiman, L., 1927, Elektrometricheskoye issledovaniye Verkhne-Arshinskogo mestorozhdeniya letom 1926 g. [Electrometric investigation of the Upper-Arshinsk (Ural) ore bed, accomplished in summer of 1926]: Inst. Prikl. Geofiz. Izv., no. 3, p. 64–86. GA no. 1, p. 16.

Petrucci, Guiseppe, 1940, Possibilità di applicazione dei metodi geoelettrici di prospezione alla registrazione dei movimenti del magma entro i condotti vulcanici [Possibility of applying geoelectrical methods of prospecting to the registration of the movements of magma inside a volcano]: Geofisica Pura e Appl., v. 2, no. 1, p. 20–28. GA 5654.

—— 1948, L'importanza della rappresentazione dell'andamento del campo elettrico nella prospezione con il metodo dei potenziali naturali [Importance of the analysis of the variation of the electrical field in prospecting by the self-potential method]: Riv. Geomin., v. 9, no. 2, p. 83–88. Self-potential. GA 11834.

—— 1951, Lo studio dei terreni di fondazione per mezzo dei sondaggi elettrici [Exploration of foundation sites by vertical profiling]: Gior. del Genio Civile, v. 89, p. 291–296. Resistivity. GA 13235.

Petsch, B. C., 1948, A geophysical study of the Milbank granite area: South Dakota Geol. Survey, Rept. Inv. 60, 18 p. Resistivity. GA 10347.

Pipes, L. A., 1946, Applied mathematics for engineers and physicists: New York, McGraw-Hill, 618 p.

Pirson, S. J., 1934, Interpretation of three-layer resistivity curves: Am. Inst. Mining Metall. Engineers Trans., v. 110, p. 148–158. GA 2271.

—— 1935, Effect of anisotropy on apparent resistivity curves: Am. Assoc. Petroleum Geologists Bull., v. 19, no. 1, p. 37–57. Reprinted, 1947, in Early geophysical papers: Tulsa, Soc. Explor. Geophysicists, p. 697–717. GA 2356.

Polak, E. J., 1953, The application of resistivity methods in establishing the base of the water-bearing rocks in the Cannock Chase coalfield: Geophys. Prosp., v. 1, p. 197–207.

Poldini, E. M., 1932, Les sondages électriques [Electrical vertical profiling]: Bull. Tech. Suisse Romande, v. 7, 8 p. Resistivity results.

—— 1938, Les phénomènes de polarisation spontanée électrique du sous-sol et leur application a la recherche des gîtes métallifères [Phenomena of electrical spontaneous polarization of the subsoil and their application to prospecting metalliferous deposits]: Soc. vaudoise sci. nat. Mém., v. 6, no. 1, 42 p. Self-potential. GA 4365.

—— 1939, Geophysical exploration by spontaneous polarization methods: Mining Mag., v. 60, no. 1, p. 22–27; no. 2, p. 90–94. Self-potential. GA 4829.

—— 1940, Quelques résultats de prospection électrique [Some results of electrical prospecting]: Univ. Lausanne Bull. 69, 77 p. GA 6660.

—— 1941, La prospection électrique du sous-sol [Electrical exploration of the subsoil]: Lausanne, Librairie F. Rouge et Cie., 94 p. Textbook. GA 6456.

—— 1944, Quelque considérations sur l'interprétation géophysique [Certain considerations relative to geophysical interpretation]: Univ. Lausanne Bull. 79, 8 p. GA 8718.

—— 1947, La prospection électrique du sous-sol [Electrical exploration of the subsoil]: Lausanne, F. Rouge and Co., Revised ed., 119 p.; 1941, 1st ed., 119 p. Textbook. GA 10596.

Poldini, E. M., and Breusse, J. J., 1950, La prospection électrique du sous-sol à faible profondem [Electrical prospecting of shallow sub-strata]: Génie civil, hydrol., mines (Pub. de la Compagnie Générale de Géophysique, Paris), 48 p.

Poole, Granville, Whetton, J. T., and Carr. J., 1933, The location of a concealed thin dike by geophysical surveying: Inst. Mining Engineers [London] Trans., v. 84, p. 198–221. Resistivity model studies. GA 1341.

Poole, Granville, Whetton, J. T., and Taylor, A., 1934a, Earth resistivity surveys on various geological structures related to mining: Inst. Mining Engineers [London] Trans., v. 86, p. 312–335. Resistivity field results. GA 1958.

—— 1934b, Earth resistivity surveys—the location of faults: Colliery Guardian, v. 148, p. 389–390. GA 2092.

Potter, E. V., 1931, Results of electrical resistivity and electrical induction measurements at Abana mine, Quebec, Canada: U.S. Bur. Mines Tech. Paper 501, 28 p. Resistivity results. GA 428.

Powers, Harold, Scharon, H. L., and Tolman, Carl, 1953, Geophysical case history, Fredericktown lead district, Missouri: Am. Inst. Mining Metall. Engineers Trans., v. 196, p. 317–320.

Pulfrey, W., 1936, A geophysical test on a Kenya property: Mining Mag., v. 54, p. 30–32. GA 3069.

Pullen, M. W., 1929, Tentative method for making resistivity measurement of drill cores and hand specimens of rocks and ores: U.S. Bur. Mines Inf. Circ. 6141, 11 p. GA no. 9, p. 17–18.

Pylaev, A. M., 1936, K voprosu ob interpretatsii trekhsloynykh krivykh elektrobureniya pri bol'shikh soprotivleniykh tret'ego sloya [On the interpretation of the curves obtained from electrical investigation of three layers for the case of a high resistance of the third layer]: Zhur. Geofiziki, v. 6, no. 6, p. 526–535. Resistivity. GA 3882.

Rama Rao, B., 1943, Annual report for the year 1941–42, Mysore Geol. Dept. Recs., v. 41, p. 1–15. GA 8249.

Ramachandra Rao, M. B., 1941, Report on the geophysical survey near Guddadarangavvanahalli in Chitaldroog district: Mysore Geol. Dept. Recs., v. 39, p. 75–125. Self-potential. GA 9843.

—— 1942, Notes on the underground water resources near Katharhal for the Chitaldroog water supply project. Explanatory note on the interpretation of the earth resistivity curves, Katharhal area: Mysore Geol. Dept. Recs., v. 40, p. 59–80. GA 9842.

—— 1943, Notes on the underground prospecting work carried out for testing the geophysical indication at Guddadarangavvanahalli, Chitaldroog district: Mysore Geol. Dept. Recs., v. 41, p. 54–57. Self-potential.

—— 1945a, On the electrical prospecting for graphite near Ganacharpur, Kolar district: Mysore Geol. Dept. Recs., v. 42, p. 56–67. Self-potential, Resistivity. GA 10086.

—— 1945b, Spontaneous polarization surveys near Guddadarnagavvanahalli, Chitaldroog, Mysore State, India: Am. Inst. Mining Metall. Engineers Trans., v. 164, p. 107–116. GA 7059.

—— 1946, Geophysical survey report on the Sowanahalli copper ore block, Manjangud Taluk, Mysore district: Mysore Geol. Dept. Recs., v. 43, p. 31–46. Resistivity, Self-potential. GA 10349, GA 9419.

—— 1947, Geophysical investigations for selection of site for Ramapadasagar dam across the Godavari River in Madras, South India: Am. Inst. Mining Metall. Engineers Tech. Pub. 2287; 1949, Trans., v. 181, p. 68–98. GA 10087.

—— 1948, Notes on the geophysical prospecting for graphite: Mysore Geol. Dept. Recs., v. 44, p. 59–72. Resistivity, Self-potential. GA 10874.

—— 1953, Self-potential anomalies due to subsurface water flow at Garimenapenta, Madras State, India: Am. Inst. Mining Metall. Engineers Trans., v. 196, p. 400–403. Field examples. GA 14466.

Ramachandra Rao, M. B., and Negi, B. S., 1952, Geophysical exploration in the arid tracts of Rajputana: Natl. Inst. Sci. India Bull. 1, p. 70–75. GA 167–96.

Rayner, J. M., and Nye, P. B., 1936a, Geophysical report on the Soldiers Cap area, Cloncurry district: Aerial, Geol., and Geophys. Survey of Northern Australia Rept., Queensland no. 4, 15 p. Potential-drop ratio, Electromagnetic, Self-potential. GA 5517.

—— 1936b, Geophysical report on the Trekelano area, Cloncurry district: Aerial, Geol., and Geophys. Survey of Northern Australia Rept., Queensland no. 5, 18 p. Electromagnetic, Potential-drop ratio, Self-potential. GA 5518.

—— 1936c, Geophysical report on the Dobbyn area, Cloncurry district: Aerial, Geol., and Geophys. Survey of Northern Australia Rept., Queensland no. 6, 12 p. Self-potential, Potential-drop ratio, Electromagnetic. GA 5516.

—— 1937a, Geophysical report on the Mount Todd auriferous area, Pine Creek district: Aerial, Geol., and Geophys. Survey of Northern Australia Rept., Northern Terr. no. 6, 7 p. Potential-drop ratio. GA 5519.

—— 1937b, Geophysical report on the Dugald River silver-lead lodes: Aerial, Geol., and Geophys. Survey of Northern Australia Rept., Queensland no. 7, 15 p. Self-potential, Electromagnetic. GA 5520.

—— 1937c, The Fountain Head area, Pine Creek district: Aerial, Geol., and Geophys. Survey of Northern Australia Rept., Northern Terr. no. 7, p. 17–25. Potential-drop ratio. GA 5658.

Rayner, J. M., and Nye, P. B., 1937d, The Yam Creek area, Pine Creek district: Aerial, Geol., and Geophys. Survey of Northern Australia Rept., Northern Terr. no. 9, p. 11–16, 2 pls. Potential-drop ratio. GA 5660.

——— 1937e, The Woolwonga area, Pine Creek district: Aerial, Geol., and Geophys. Survey of Northern Australia Rept., Northern Terr. no. 11, p. 17–22. Potential-drop ratio. GA 5521.

——— 1937f, The Iron Blow area, Pine Creek district: Aerial, Geol., and Geophys. Survey of Northern Australia Rept., Northern Terr. no. 13, p. 15–18. Electromagnetic, Self-potential, Potential-drop ratio. GA 5659.

——— 1937g, Geophysical test surveys on the Britannia, Zapopan and Mount Wells areas, Pine Creek district: Aerial, Geol., and Geophys. Survey of Northern Australia Rept., Northern Terr. no. 15a, p. 13–16. Potential-drop ratio, Self-potential. GA 5656.

——— 1937h, Geophysical report on the Hercules gold mine, Pine Creek district: Aerial, Geol., and Geophys. Survey of Northern Australia Rept., Northern Terr. no. 16, 6 p. Electromagnetic, Self-potential, Potential-drop ratio. GA 5655.

——— 1937i, The Evelyn silver-lead mine, Pine Creek district: Aerial, Geol., and Geophys. Survey of Northern Australia Rept., Northern Terr. no. 26a, p. 9–10. Potential-drop ratio, Self-potential. GA 5657.

Reich, F., 1839, Notiz über elektrische Strömungen auf Erzgängen [Notes on electric currents from mineral veins]: Annalen der Physik und Chemie, v. 48, p. 287–291; reprinted 1840, Edinburgh New Philos. Jour. 28, p. 1–15 and also 1840, Karsten, Archiv. 14, p. 141–158. Discusses early work of R. W. Fox.

Repal, S. N., and Bouchon, M., 1954, Étude tellurique dans le bassin du Hodna [Telluric study in the basin of Hodna]: Internat. Geol. Cong. [Algiers], 19th sess., Comptes Rendus, sec. 9, pt. 9, p. 231–243. GA 161–62.

Rice, S. O., 1940, The electric field produced by a point charge located outside a dielectric wedge: Philos. Mag., v. 29, p. 36–46.

Riznichenko, Yu., 1937, Opredeleniye glubin pri pomoshchi elektroprofilirovaniya [Determination of depths by electroprofiling]: Zhur. Geofiziki (Moscow), v. 7, no. 1, p. 105–128. Resistivity. GA 3883.

Rodionov, P. F., 1937, O technike rabot po metody zaryazhennogo tela i metody izoliniy pri pitanii postoyannym tokom [On the technique of the work applied to the method of a charged body and the method of isolines by using direct current]: Razvedka Nedr, no. 14, p. 42–48. GA 4043.

——— 1938, Electrometriya pri predvaritel'noy i detal'noy razvedke mestorozhdeniy tsvetnykh metallov [Electrometry in the preliminary and detailed exploration for deposits of colored metals]: Tsvetnye Metally, Moscow-Leningrad-Sverdlovsk, no. 6, p. 9–16.

Rodionov, P. F., and Sofronov, N. I., 1929, Opyty nad modelyami 1927–28 g. [Experiments on models carried out in 1927 and 1928]: Geol. Komitet materialy po obshch prik. geologii, no. 137, p. 53–69. GA no. 12, p. 10–11.

Rogers, A. H., 1928, Geophysics and the mining engineer: Am. Inst. Mining Metall. Engineers Tech. Pub. 135, 7 p.; 1929, Trans., v. 81, p. 44–50. Gives cost of electrical surveys.

Roman, Irwin, 1931, How to compute tables for determining electrical resistivity of underlying beds and their application to geophysical problems: U.S. Bur. Mines Tech. Paper 502, 44 p. Resistivity theory. GA 476.

Roman, Irwin, 1933, The calculation of electrical resistivity for a region underlying two uniform layers: Terrestrial Magnetism Atmos. Electricity, v. 38, p. 117–141, 185–202. GA 1700.

——— 1934, Some interpretations of earth-resistivity data: Am. Inst. Mining Metall. Engineers Trans., v. 110, p. 183–200. GA 1860.

——— 1938, Electrical resistivity of snow and ice: Internat. Assoc. Hydrology Bull. 23, p. 483–491, Riga. Resistivity. GA 4946.

——— 1939, Fundamental research in geophysics relating to prospecting: Am. Geophys. Union Trans., v. 20, pt. 3, p. 298–303.

——— 1941, Superposition in the interpretation of two-layer earth resistivity curves: U.S. Geol. Survey Bull. 927–A, 18 p. GA 6302.

——— 1951, Resistivity reconnaissance in Am. Soc. Testing Materials, Symposium on Surface and subsurface reconnaissance: Am. Soc. Testing Materials Special Tech. Pub. 122, p. 171–220. General techniques; excellent bibliography. GA 13945.

——— 1956, Graphical scales for mapping potential functions: Geophysics, v. 21, p. 1041–1046. GA 167–89.

——— 1959, An image analysis of multiple-layer resistivity problems: Geophysics, v. 24, p. 485–509. GA 178–109.

——— 1960, Apparent resistivity of a single uniform overburden: U.S. Geol. Survey Prof. Paper 365, 99 p.

Rooney, W. J., 1927, Earth resistivity measurements in the copper country of Michigan: Terrestrial Magnetism Atmos. Electricity, v. 32, p. 97–126. GA 180.

——— 1931, The use of resistivity measurements in the detection of mineralized areas: Internat. Geod., Geophys. Union Bull. 8 [Paris], Terrest. Magnetism Sec., p. 352–353. Resistivity results.

——— 1937, Earth-current variations with periods longer than one day: Terrestrial Magnetism Atmos. Electricity, v. 42, no. 2, p. 165–172. GA 3884.

Rooney, W. J., and Gish, O. H., 1925a, Measurements of large volumes of undisturbed earth: Phys. Rev., v. 25, p. 254.

——— 1925b, Measurement of the resistivity of large volumes of undisturbed earth: Carnegie Inst. Washington Year Book no. 24, p. 220.

——— 1927, Results of earth-resistivity surveys near Watheroo, Western Australia, and at Ebro, Spain: Terrestrial Magnetism Atmos. Electricity, v. 32, no. 2, p. 49–63; Phys. Rev., v. 2, p. 29, 905.

——— 1930, Earth-resistivity survey at Huancayo, Peru: Terrestrial Magnetism Atmos. Electricity, v. 35, no. 2, p. 61–72. Resistivity. GA no. 19, p. 14.

Rosén, Af. A., 1887, En sats i teorien för konstanta elektriska strömmar: Swenska Vetensk. Akad., Stokholm Öfversight of förhand livgar, no. 4, p. 197.

Rosenzweig, I. E., 1938, A new method of depth determination in earth-resistivity measurements: Am. Inst. Mining Metall. Engineers Tech. Pub. 931, 10 p.; 1940, Trans., v. 138, p. 408–417. GA 4672.

——— 1939, New theory of apparent resistivity of horizontally stratified soils: Am. Inst. Mining Metall. Engineers Tech. Pub. 1102, 23 p.; 1940, Trans., v. 138, p. 418–440. Resistivity. GA 5225.

Rossi, B., 1928a, Studio del campo elettrico nei mezzi omogenei anistropi [Study of electric field in anisotropic homogeneous media]: Sed. Reale Accademia Nazionale dei Lincei Rend., v. 8, no. 3–4, p. 146–154.

——— 1928b, Sopra la distribuzione dell'eletricità nei conduttori immersi in un mezzo omegeneo anistropo [On the distribution

of conductors immersed in anisotropic homogeneous medium]: Sed. Reale Accademia Nazionale dei Lincei Rend., v. 8, no. 5–6, p. 223–228.

Rothé, Edmond, and Rothé, J. P., 1952, Prospection géophysique [Geophysical prospecting]: Paris, Gauthier-Villars, v. 2, p. 185–486. Contains excellent bibliography; field examples. Textbook. GA 14085.

Rothé, J. P., 1932, Application de la prospection électrique à des études de failles et d'horizons d'eau [Application of electrical prospecting to fault and ground-water studies]: Congrès Soc. Savantes, 56th, Tours, p. 544–557.

——— 1938, Courants tellurique [Telluric currents]: Année Polaire Internat., Participation Française, v. 2, p. 53–97.

Rothrock, E. P., and Petsch, B. C., 1935, A shallow water supply for Huron, South Dakota: South Dakota Geol. Survey, Rept Inv. 24, 9 p. GA 2408.

Rougerie, P., 1942, Contribution a l'étude des courants telleriques [Contributions to the study of telluric currents]: Inst. Physique du Globe Paris Annales, v. 20, p. 60–111.

Rowland, E. F., Stolzy, L. H., and Crabb, G. A., Jr., 1955, Frost determined by electrical resistance: Highway Research Board Bull. 100, p. 17–21. GA 162–74.

Rozanov, L. N., and Mazyuk, V. V., 1947, Opyt Korrektirovaniya geologicheskikh kart po materialam elektrorazvedki v Buguruslanskom neftenosnom rayone [An experiment in adjusting geologic maps with the aid of electrical prospecting data in the Buguruslan oil region]: Prikladnaya Geofizika, no. 3, p. 181–194. GA 9839.

Rudnev, V. N., 1937, Elektricheskiy karrotazh na promyslakh yuzhnoy Emby [Electrical logging in the oil-bearing region of sourthern Emba]: Neft. Khoz. no. 7, p. 64–69. Logging method. GA 4044.

Ruedy, R., 1945, The use of cumulative resistance in earth resistivity surveys: Canadian Jour. Research, v. 23A, p. 57–72. GA 8118.

Runge, Hans, 1936, Einige nord- und süddeutsche Erfahrungen mit elektrischen Bohrlochuntersuchungen als stratigraphischem Hilfsmittel [Some experience obtained in north and south Germany with electrical borehole investigations as additional means for stratigraphic determinations]: Öl und Kohle, v. 12, no. 42, p. 890–897. Logging method. GA 3610.

Rust, W. M., Jr., 1938, A historical review of electrical prospecting methods: Geophysics, v. 3, p. 1–6. GA 4366.

——— 1940, Typical electrical prospecting methods: Geophysics, v. 5, p. 243–249. GA 5810.

Safronov, A. P., and Sergeyev, E. A., 1936, Novye geofizicheskiye metody poiskov i razvedki poleznykh iskopayemykh, osnovannye na izuchenii "oreola rasseyaniya" [New geophysical methods of prospecting for deposits based on the study of "aureoles of dissemination"]: Razvedka Nedr, no. 18, p. 24–25. Self-potential. GA 3611.

Sakuma, Shuzo, 1952, Earth current potentials near boundaries of various geological formations: Tokyo Univ. Earthquake Research Inst. Bull., v. 30, p. 25–30. Self-potential. GA 14255.

Samoylov, V. G., and Konshin, G. G., 1956, O primenenii metodov elektrorazvedki pri geologicheskikh issledovaniyakh dlya proyektirovaniya i ṣtroitel'stva vodkhranilishch, prudov i vodoyemov v rayoǹakh s karstuyushchimisya gruntami [The application of the electric method of exploriation to geologic investigations when designing and building reservoirs, ponds, and basins in areas of possible

karst]: Gidrotekhnika i Melioratsiya, no. 1, p. 14–27. GA 164–109.

Samsioe, A. F., 1931, A treatment of the partially penetrating electrode: Zeitschr. angew. Mathematik u. Mechanik, v. 11, p. 124.

Satō, Gekuji, 1952, The electrical survey of a fault at Ashinokuchi, Sendai: Butsuri-Tankō, v. 5, no. 2, p. 67–69. [Japanese with English summary.]

——— 1955, Study on equilibro-four-electrode method (I).— Theoretical curves of apparent resistivity for simple ore models: Butsuri-Tankō, v. 8, no. 3, p. 104–114. GA 166–138.

Satō, Kōnosuke, 1949, On the "mean" 3-electrode method [Japanese]: Butsuri-Tankō, v. 2, no. 2, p. 5–6. Half-Wenner. GA 12055.

Satō, Kōnosuke, and Saitō, Tomosaburō, 1953, Some problems of electrode arrangements of resistivity method: Butsuri-Tankō, v. 6, no. 1, p. 34–44. [Japanese with English summary.]

Satō, Mitsunosuke, and Shibato, Kihei, 1950, Geophysical prospecting in Oshirabetsu mine, Tokaschi province, Hokkaido: Japan Geol. Survey Bull., v. 1, p. 22–28. Resistivity, Self-potential. GA 13239.

Sayre, A. N., and Stephenson, E. L., 1937, Use of resistivity methods in the location of saltwater bodies in the El Paso, Texas, area: Am. Geophys. Union Trans. v. 18, pt. 2, p. 393–398.

Scharon, H. L., 1952, Electrical resistivity geophysical method as applied to engineering problems: Am. Soc. Testing Materials, Special Tech. Pub. 122, p. 104–114. GA 14128.

Scharon, H. L., and Cleaves, A. B., 1951, Geophysics on the Pennsylvania Turnpike: Am. Inst. Mining Metall. Engineers Trans., v. 190, p. 351–355. Resistivity. GA 15038.

Schenk, Erwin, 1942, Über Lagebestimmungen steiler geologischer Grenzflächen im Untergrund durch Gleichstrommessungen [Concerning the location of steep geological boundary-surfaces in the subsoil by means of direct-current measurements]: Zeitschr. prakt. Geologie, v. 50, p. 93–99. GA 8250.

——— 1943a, Untersuchung geologischer Strukturelemente durch Kreissondierungen mit Gleichstrom (Vier-Pol-Methode) [Investigating geologic structure using "circle sounding" with direct current (four-pole method)]: Zeitschr. prakt. Geologie, v. 51, p. 85–90.

——— 1943b, Zur Bedeutung und Auswertung von Unstetigkeiten in Diagrammen geoelektrischer Vertikalsondierungen [The importance and interpretation of discontinuities in graphs obtained in geoelectrical depth profiling]: Beitr. angew. Geophysik, v. 10, no. 3–4, p. 287–307. Resistivity. GA 12049.

——— 1944, Über den Einfluss von Schollengrenzen auf geoelektrische Vertikalsondierungen [The influence of boundaries between layers on depth profiles]: Beitr. angew. Geophysik, v. 11, p. 83–102. Resistivity. GA 12050.

——— 1954, Geoelektrische Untersuchung des Mineralquellengebietes von Selters a. Lahn [Geoelectric investigations of the mineral spring area of Selters on the Lahn]: Oberhess. Gesell, Natur- u. Heilkunde Giessen Ber., naturw. Abt., v. 26, p. 51–69. GA 166–155.

Schlomka, Teodor, 1929, Zur Theorie des elektrischen Feldes der Erde [Contribution to the theory of the earth's electric field]: Gerlands Beitr. Geophysik, v. 24, no. 2–3, p. 241–272. GA no. 11, p. 21–22.

Schlumberger, Conrad, 1920a, Essais de prospection électrique du sous-sol [Analysis of electrical prospecting of the subsoil]: Acad. Sci. [Paris] Comptes rendus, v. 170, no. 9, p. 519–521.

——— 1920b, Étude de la prospection électrique du sous-sol [Study of electrical prospecting of the subsoil]: Paris, Gauthiers-Villars, 94 p. (Reprinted in 1930). Translated into English by S. F. Kelly, under direction of the author. An abstract of the translation (Study of underground prospecting) was published in 1921, Eng. Min. Jour., v. 111, p. 782–788 and p. 818–823. Resistivity theory. GA 194.

——— 1927, Prospection électrique par les procédés Schlumberger [Electrical prospecting with the Schlumberger method]: Soc. Prospection Elec. [Paris], p. 17.

——— 1938, Electrical prospecting for oil: in Dunsau, A. E. and others, The Science of Petroleum, v. 1, London, Oxford Univ. Press, p. 346–350.

Schlumberger, Conrad, and Renaud, P. J. M., 1933, Étude géophysique sous-marine exécutée dans le Port d'Alger [Submarine geophysical study made in the harbor of Algiers]: Ponts et Chaussées Annales, v. 2, no. 4, 15 p. GA 2272.

Schlumberger, Conrad, and Schlumberger, Marcel, 1928, Découverte près de Hettenschlag d'un deuxième dôme de sel sous la plaine d'Alsace [Discovery, near Hettenschlag, of a second salt dome under the Alsace plain]: Acad. sci. [Paris] Comptes rendus, v. 186, no. 7, p. 445–446.

——— 1930a, Depth of investigation attainable by potential methods of electrical exploration: Am. Inst. Mining Metall. Engineers Tech. Pub. 315, p. 3–9; 1932, Trans., v. 97, p. 127–133. GA no. 12, p. 11–12.

——— 1930b, Electrical studies of the earth's crust at great depths: Am. Inst. Mining Metall. Engineers Tech. Pub. 315, p. 10–16; 1932, Trans., v. 97, p. 134–140.

——— 1930c, La méthode de la carte des résistivités et ses applications pratiques [The method of the ground resistivity map and its practical applications]: Annales Mines Mem., ser. 12, v. 18, p. 97–124; 1931, Canadian Mining Metall. Bull. 226, p. 271–294 [English]; discussion, 1931, Canadian Mining Metall. Bull. 236, p. 1413–1414. Resistivity results. GA 101, 219, and 725.

——— 1930d, Sur la détermination électromagnétique du pendage des couches sédimentaires [On the electromagnetic determination of the dip of sedimentary beds]: Acad. sci. [Paris] Comptes rendus, v. 190, no. 18, p. 1064–1066.

——— 1930e, La méthode de la carte des résistivités et ses applications pratiques [The method of resistivity maping and its practical applications]: Cong. Internat. Mines, Métallurgie, Géologie appl., Liege, 6th sec. geol., p. 337–346. Resistivity results.

——— 1935, La prospection électrique du bassin salifère d'Alsace [Electrical prospecting in the salt-bearing basin of Alsace]: Cong. Internat. Mines, Metallurgie, Geologie appl., 7th, Paris, sec. Géologie, v. 2, p. 855–864.

Schlumberger, Conrad, Schlumberger, Marcel, and Charrin, P., 1935, Étude géophysiques par les méthodes électriques in USSR [Geophysical investigations by electrical methods in the USSR]: Rev. Petrolifère, no. 614, p. 77–83; no. 615, p. 110–116. GA 2410.

Schlumberger, Conrad, Schlumberger, Marcel, and Leonardon, E. G., 1932a, Electrical coring; a method of determining bottom-hole data by electrical measurements: Am. Inst. Mining Metall. Engineers Tech. Pub. 462, 38 p.; 1934, Trans., v. 110, p. 237–272.

——— 1932b, Location and study of pipe line corrosion by surface electrical measurements: Am. Inst. Mining Metall.

Engineers Tech. Pub. 476, 24 p. Resistivity results. GA 670.

——— 1933a, A new contribution to subsurface studies by means of electrical measurements in drill holes: Am. Inst. Mining Metall. Engineers Tech. Pub. 503, 18 p.; 1934, Trans., v. 110, p. 273–289.

——— 1933b, Some observations concerning electrical measurements in anisotropic media, and their interpretation: Am. Inst. Mining Metall. Engineers Tech. Pub. 505, 25 p.; 1934, Trans., v. 110, p. 159–182. GA 1563.

——— 1934, Electrical exploration of water-covered areas: Am. Inst. Mining Metall. Engineers Trans., v. 110, p. 122–134. GA 1862.

Schlumberger, Marcel, 1939, The application of telluric currents to surface prospecting: Am. Geophys. Union Trans., v. 20, pt. 3, p. 271–277.

Schlumberger, Marcel, and Kunetz, Géza, 1946, Variations rapids simultanées du champ tellurique en France et à Madagascar [Simultaneous rapid variations in the telluric field in France and Madagascar]: Acad. sci. [Paris] Comptes rendus, v. 223, no. 15, p. 551–553.

Schlumberger Well Surveying Corporation, 1950, Interpretation hand-book for resistivity logs: Houston, Schlumberger Well Surveying Corporation, 148 p.

Schmidt, Adolf, 1940, Zur Frage der hypothetischen die Erdoberfläche durchdringenden elektrischen Ströme [On the question of hypothetical electric currents penetrating the surface of the earth]: Gerlands Beitr. Geophysik., v. 55, no. 2, p. 292–302. GA 5661.

Schneider, Hans, 1953, Kann der speziale Widerstand der geoelektrischen Vermessungen als eine markante hydrologische Kennzahl bezeichnet werden? [Can geoelectric resistivity measurements be considered as an indication of ground water characteristics?]: Bohrtechnik-Brunnenbau, v. 4, no. 3, p. 75–87. Resistivity. GA 14657.

Schofield, R. K., and Dakshinamurti, C., 1948, Ionic diffusion and electric conductivity in sands and clays: Faraday Soc. Discussions, no. 3, p. 56–61. GA 10598.

Schouppé, Alexander, 1952, Elektrische Widerstandsmessungen zur Feststellung der Verbindungswege in Höhlengewässern [Electrical resistance measurements for determination of connecting passages in cavern waters]: Naturwiss. Ver. Steiermark Mitt., v. 81–82, p. 183–186. Resistivity. GA 14465.

Schouppé, Alexander von, 1953, Ein neues Widerstandsmessgerät mit automatischer Umpolung zur Feststellung nicht sichtbarer Verbindungen von Wasserwegen [A new resistivity measuring apparatus with automatic antipolarization for determining concealed connections of water courses]: Neues Jahrb. Geologie u. Paläontologie Monatsh., v. 1953, no. 9, p. 385–390. Resistivity. GA 14850.

Searle, G. F. C., 1911, On resistances with current and potential terminals: Electrician, v. 66, no. 25, p. 999–1002, and no. 26, p. 1029–1033; v. 67, no. 1, p. 12–14, and no. 2, p. 54–58. Proof of theorem of reciprocity for various problems.

Sebestyén, Károly, 1954, Összehasonlító vizsgálatok a vertikális elektromos szondázási görbék kiértékeléséről [Interpretation of resistivity depth curves (with English and Russian summaries)]: Magyar Állami Eötvös Loránd Geofiz. Intézet Geofiz. Közlemények, v. 3, no. 3, p. 31–39. GA 158–100.

Sedlar, Jošica, 1954, Geoelektricna ispitivanja za nalaz vode u krsu na otocima [Geoelectric exploration for water in karst on islands]: Geol. Vjesnik, v. 5–7, p. 217–224 [1951–1953]. GA 160–164.

Seigel, H. O., 1952, Ore body size determination in electrical prospecting: Geophysics, v. 17, p. 907–914. In-hole. GA 14129.

Semenov, A. S., 1937a, Tochnost' izmereniya kazhushchegosya soprotivleniya [The accuracy of apparent resistivity measurements]: Central Geol. and Prosp. Inst. Materials, Geophysics, no. 3, p. 26–43. Resistivity. GA 3886.

————— 1937b, Metod odnoelektrodnogo karottazha dlya izucheniya vodnykh pritokov fil'truyushchikh gorizontov [Method of "one-electrode" logging for studying the influx of water into permeable horizons]: Razvedka Nedr, no. 18, p. 39–41. Resistivity. GA 4203.

————— 1938a, Utechka iz pitayushchey tsepi priyemnyye elektrody [Leakage from the feeding circuit to the electrodes]: Tsentr. Nauchn.-Issled. Geol.-Razved. Inst., Geofizika, v. 5, p. 3–26. GA 4674.

————— 1938b, Bokovye vliyaniya [Lateral effects]: Tsentr. Nauchn.-Issled. Geol.-Razved. Inst., Geofizika, v. 5, p. 27–35. Topographic effects on resistivity surveys. GA 4673.

————— 1938c, Izmereniye elektricheskogo soprotivleniya vod v otkrytykh basseynakh [Measurement of electrical resistivity of water in open basins]: Tsentr. Nauchn.-Issled. Geol.-Razved. Inst., Geofizika, v. 5, p. 36–39. GA 4675.

————— 1947a, Metod zaryazhennogo tela [The method of the charged body]: Razvedka Nedr, no. 4, p. 35–42. GA 10088.

————— 1947b, Kombinirovannoe profilirovaniya v primenenii k provodyashchim zhilam [Combined profiling applied to conducting veins]: Razvedka Nedr, no. 6, p. 45–49. Resistivity. GA 10350.

————— 1948, Teoriya metoda zaryazhennogo tela v primenenii k ekvipotentisial'nym provodnikam [The theory of the method based on charged bodies applied to equipotential conductors]: Vses. Nauchn.-Issled. Geol. Inst. Materialy, Geofizika, no. 13, p. 3–56. Potential fields. GA 12046.

Semenov, A., Ferchev, M., and Mal'chevskiy, V., 1940, k voprosu o primenimosti parametra "PP" v geofizicheskoy razvedke [Contribution to the question of the applicability of the parameter "PP" in geophysical prospecting]: Tsentr. Nauchno-Issled. Geol.-Razved. Inst. Materialy, Geofizika, no. 8, p. 76–84. Induced polarization. GA 5662.

Semenov, A. S., and Mal'chevskiy, V. S., 1939, Primeneniye karottazha dlya poiskov sul'fidnykh rud v rayone skvazhin [Application of electrical logging in the search for sulphide ores within the area of boreholes]: Razvedka Nedr, no. 6, p. 35–43. Logging method. GA 5226.

Shaiderov, A. M., 1930a, Zadachi elektricheskoi razvedki na ploshchadiakh Groynefti [Problems of electrical prospecting on the Grozneft fields]: Azerb. Neft. Khoz., no. 6, p. 58–63. Resistivity results. GA no. 18, p. 14–15.

————— 1930b, O resul'tatakh elektrorazvedki v Novo-Groznenskom rayone [On the results of the electrical prospecting in the region of Novo-Grozny]: Azerbaid. Neft. Khoz., no 9, p. 78–85. Resistivity results. GA 16.

Shakhnes, K. A., 1937, Primeneniye elektrorazvedki k voprosam gidrogeologii [Application of electrical prospecting to hydrology]: Razvedka Nedr, no. 3, p. 19–24. Resistivity. GA 3751.

Shalayev, S. V., 1955, Opredeleniye polozheniya provodyashchego tela v elektrorazvedke [The determination of a conductive body by electrical prospecting methods]: Akad. Nauk SSSR Izv. ser. geofiz., no. 5, p. 468–474. GA 164–104.

Shaw, S. H., 1934, Geophysical prospecting—a study of the resistivity method in connection with the investigation of underground-water supplies in the Nata Reserve, Southern Rhodesia: Inst. Mining and Metallurgy [London] Bull. 361, p. 1–27; discussion on paper pub. 1934, Inst. Mining and Metallurgy [London] Bull. 362, p. 1–18. GA 2228 and GA 2409.

Shchodro, N. K., and Maslov, N. M., 1935, Opredeleniye dielektrichekikh postoyannykh gornykh porod i vliyaniye vlazhnosti na eti konstanty [Determination of the dielectric constants of rocks and of the influence of humidity on these constants]: Akad. Nauk SSSR Izv. 7th ser. Otdel. mat. i yestestven. Nauk, no. 6–7, p. 933–950.

Shepard, E. R., 1935, Subsurface exploration by earth-resistivity and seismic methods: Am. Geophys. Union Trans., v. 16, pt. 1, p. 78–91; 1935, Public Roads, v. 16, no. 4, p. 57–67, 74. GA 2794.

Shibatō, Kihei, 1953, Geophysical prospecting at Noda-Tamagawa Mine, Iwate prefecture: Japan Geol. Survey Bull., v. 4, no. 12, p. 17–34. GA 160–68. [Japanese, English summary.]

————— 1954, Electrical prospectings on sulphur deposit at the Matsuo-Hachimantai district, Iwate prefecture: Japan Geol. Survey Bull., v. 5, no. 1, p. 41–48. GA 160–69. [In Japanese with English summary.]

————— 1955, Geophysical prospecting at Kuga Mine, Yamaguchi Prefecture: Japan Geol. Survey Bull., v. 6, no. 3, p. 19–26. GA 164–113. [In Japanese with English summary.]

Shklyarskiy, F., 1925, O nekotorykh yavleniyakh, nablyudayemykh pri proizvodstve elektricheskikh razvedok [Concerning some phenomena observed during the electrical method of prospecting]: [Russia] Geol. Komitet, Vestnik, no. 2, p. 55–59. Equipotential line method. GA no. 1, p. 10–11.

Shpak, V. A., 1932, Otchet o rabotakh irtyshskoy elektrometricheskoy partii [Report of the work carried out by the Irtysh electrical surveying party]: Vsesoyuznogo Geol.-Razved. Ob'edineniya NKTP SSSR Trudy, no. 211, p. 1–32. GA 1321.

————— 1937, Primeneniye metoda soprotivleniy dlya razvedki krutopadayushchikh linz [Application of the resistivity method to the search for steeply dipping lenses]: Central Geol. and Prosp. Inst. Materials, Geophysics, no. 3, p. 11–26. Resistivity. GA 3889.

Shpak, V. A., and Nesterov, L. Ya., 1935, Primeneniye geofizicheskikh metodov pri razvedke osnovaniy pod gidrosooruzheniya [Application of geophysical methods for prospecting foundations for hydraulic constructions]: Razvedka Nedr, no. 6, p. 12–13. GA 2645.

Simpson, W. H., 1947, An experience with the Megger: Oil and Gas Jour., v. 46, no. 18, p. 192, 292–293. Resistivity survey to detect areas of pipe corrosion. The author suggests that pipe corrosion in one area was apparently caused by galvanic action due to dissimilar soils.

Siñeriz, J. G., 1942, Investigación electrica en Hiendelahencina, determinación del silon "Rico" [Electrical prospecting in Hiendelahencina location of the Rico vein]: Rev. Geofísica, v. 1, p. 51–69.

————— 1946, Investigación hidrologica en Castellón de la Plana por medio del metodo electrico de corriente continua [Ground water investigation in Castellón de la Plana by the direct current electrical method]: Rev. Geofísica, v. 5, p. 153–171. GA 9608.

Skal'skaya, I. P., 1948, Pole tochechnogo istochnika toka, ras-polozhennogo na poverkhnosti zemli nad naklonnym plastom [The field of an electrical point source placed over an inclined layer on the earth's surface]: Akad. Nauk SSSR zhur. tekh. Fiz., v. 18, no. 10, p. 1242–1254. GA 10875.

Skaryatin, R., 1928, Raschet i sravneniye odnorodnosti poley Shlyumberzhe, Lundberga i Petrovskogo [Calculation and comparison of homogeneity of fields of Schlumberger, Lundberg, and Petrowsky]: Inst. prikl. Geofiziki Izv., no. 4, p. 256–265. GA no. 9, p. 22–23.

Slater, John C., and Frank, N. H., 1947, Electromagnetism: New York, McGraw-Hill, 240 p.

Slichter, L. B., 1933, The interpretation of the resistivity prospecting method for horizontal structures: Physics, v. 4, p. 307–322 and 407. Resistivity theory. GA 1706, GA 1771.

——— 1934, Large electrical map of central Massachusetts by the Massachusetts Institute of Technology: Am. Geophys. Union Trans., v. 15, pt. 1, p. 185.

——— 1936, Potential distribution about a leaky cylinder (abst.): Am. Geophys. Union Trans., v. 17, pt. 1, p. 182.

Smith, F. G., 1940, Variation in the electrical conductivity of pyrite: Toronto Univ. Studies, Geol. ser., no. 44, p. 83–95.

Smythe, William R., 1950, Static and dynamic electricity: 2d ed., New York, McGraw-Hill, 616 p.

Snow, Chester, 1942, The hypergeometric and Legendre functions with application to integral equations of potential theory: Natl. Bur. Standards, p. 54.

Solaini, Luigi, 1952, Criteri e problemi costruttivi di strumenti per misure di resistività [Criteria and construction problems of instruments for measuring resistivity]: Annali Geofisica, v. 5, p. 357–365. GA 14449.

Sollner, Karl, and Gregor, H. P., 1950a, The electrochemistry of permselective protamine colloidion membranes; I—Rate studies of the establishment of the concentration potential across various types of permselective protamine colloidion membranes: Jour. Phys. and Colloid Chemistry, v. 54, p. 325–330.

——— 1950b, The electrochemistry of permselective protamine colloidion membranes; II—Experimental studies of the concentration potential across various types of permselective protamine colloidion membranes with solutions of several electrolytes: Jour. Phys. and Colloid Chemistry, v. 54, p. 330–338.

——— 1951, The electrochemistry of permselective membranes; III—The electrical resistance of permselective colloidion membranes in solutions of various electrolytes: Jour. Colloid Sci., v. 6, p. 557–570. Contains bibliography of important electrochemistry papers on this topic.

——— 1952, The electrochemistry of permselective protamine colloidion membranes; III—The electrical resistance of several types of permselective protamine colloidion membranes in solutions of various electrolytes: Jour. Colloid Sci., v. 7, p. 37–52.

Solov'ev A. V., 1937, Opyt geofizicheskoy razvedki pegmatitovykh zhil v rayone Biryusinskikh mestorozhdeniy muskovita [Tests of geophysical prospecting for pegmatite veins in the region of the Biriuzinsk muscovite deposits]: Razvedka Nedr, no. 3, p. 9–12. GA 3753.

Sorokin, L. W. [editor], 1949, Obshchiy kurs razvedochnoy geofiziki dlya tekhnikumov [General course of exploration geophysics for technical schools]: Moscow, Gostoptekhizdat, 408 p.; translated into German by Dr. Barnitzke, 1953,

Lehrbuch der Geophysikalischen Methoden zur Erkundung von Erdölvorkommen: Berlin, VEB Verlag Technik, 579 p. Textbook. GA 12607.

Spicer, H. C., 1941, Earth resistivity as applied to problems of exploration in the potash-bearing region near Carlsbad, New Mexico: Am. Inst. Mining Metall. Engineers Tech. Pub. 1354, 10 p.; 1942, Trans., v. 148, p. 258–267; 1945, Trans., v. 164, p. 88–97. GA 6416.

——— 1947, Electrical resistivity investigations at Memphis and Boliver, Tenn.: U.S. Geol. Survey Geophys. Inv., 60 p. GA 10877.

——— 1950, Investigation of bedrock depths by electrical resistivity methods in the Ripon-Fond du Lac area, Wisconsin: U.S. Geol. Survey Circ. 69, 37 p. Resistivity. GA 12058.

——— 1952, Electrical resistivity studies of subsurface conditions near Antigo, Wisconsin: U.S. Geol. Survey Circ. 181, 19 p. Resistivity examples. GA 14134.

——— 1955, Electrical-resistivity studies in Water resources of southeastern Florida, U.S. Geol. Survey Water-Supply Paper 1255, p. 712–725.

Stefanesco, S. S., 1929, Études théoriques sur la prospection électrique du sous-sol [Theoretical studies on electrical prospecting of the substrata]: Inst. geol. Romaniei, v. 14, pt. 1, p. 1–63.

——— 1935, Sur la mesure des résistivités apparentes par la méthode de la spire circulaire [Measurement of apparent resistivities by the method of a circular current]: Beitr. angew. Geophysik, v. 5, p. 182–192. GA 2854.

Stefanesco, S. S., Schlumberger, Conrad, and Schlumberger, Marcel, 1930, Sur la distribution électrique potentielle autour d'une prise de terre ponctuelle dans un terrain à couchés horizontales homogènes et isotropes [The distribution of electrical potential about a point electrode in an earth of horizontal, homogeneous, and isotropic beds]: Jour. Physique et Radium, ser. 7, v. 1, p. 132–141. Resistivity theory. GA no. 14, p. 15.

——— 1932, Études théorique sur la prospection électrique du sous-sol. 2ᵉ sér. [Theoretical studies on electrical prospecting of the substrata, part 2]: Inst. geol. Romanieri, v. 14, pt. 2, p. 1–128. Resistivity, Electromagnetic theory.

Stefanović, Dragoljub, 1953–54, Primena metode spetsifichnog elektrichnog otpora radi reškavanja nekikh inzhenjersko-geološkikh problema [Application of the electrical resistivity method in the solution of problems in engineering geology]: Beograd Tekh. Velika Škola Zbornik radova geol. i. rudarskog fakulteta, p. 293–301. GA 167–97.

Stefanović, Dragoljub, and Mladenović, Milan, 1952, Geofizivko ispitivanje akumulatsionog bazena Liveroviéi [Geophysical investigation of the storage reservoir near Liveroviéi]: Glasnik Prirod. Mus. Srpske Zemlje, Ser. A, v. 5, p. 225–235. Resistivity. GA 158–103.

Stepanov, G. I., 1936, K voprosu vnedreniya geofizicheskikh metodov razvedki pri inzhenerno-geologicheskikh [On the question of the application of geophysical methods of prospecting in investigations connected with engineering and geology]: Razvedka Nedr, no. 17, p. 38–39. GA 3409.

Stephenson, E. L., 1943, Geophysical surveys in the Ochoco quicksilver district, Oregon: U.S. Geol. Survey Bull. 940C, p. 57–98.

Stern, O., 1924, Zur Theorie der Elektrolytischen Doppelschicht [On the theory of the electrolytic double layer]: Zeitschr. Electrochemie, v. 30, p. 508.

Stern, Walter, 1932a, Beiträge zur Messtechnik und Anwendung der Methode des scheinbaren spezifischen Widerstandes [Contribution to the technique of measurement and application of the method of apparent resistivity]: Zeitschr. Geophysik, v. 8, no. 3–4, p. 181–191. GA 927.

——— 1932b, Über ein geoelektrisches Schürfverfahren zur indirekten Bestimmung der Decken- und Flözmächtigkeit [A geoelectrical method for determining the thickness of the overburden and of the layer]: Braunkohle, v. 31, no. 9, p. 149–152. GA 869.

——— 1933a, Die Bestimmung des Verlaufes geneigter Diskontinuitäts Flaschen (einfallende Schichtgrenzen und Verwerfungen) durch das Widerstands Verfahren [Determination of the attitude of inclined planes of discontinuity (such as bedding planes and faults) by the resistivity method]: Zeitschr. Geophysik, v. 9. p. 1–11. GA 1424.

——— 1933b, Das Widerstandsverfahren zur Untersuchung von Tektonik und Hydrologie des Untergrundes [The resistivity method of prospecting for the structure and hydrology of the earth]: Beitr. angew. Geophysik, v. 3, p. 408–462. Resistivity theory. GA 1739.

——— 1943, Relation between spontaneous polarization curves and depth, size, and dip of ore bodies: Am. Inst. Mining Metall. Engineers Tech. Pub. 1536, 8 p.; 1945 Trans., v. 164, p. 189–196. GA 6813.

Stevens, O., 1937, Die Anwendung eines elektrischen Verfahrens für die Untersuchung von Grundwasserströmungen [Use of electrical methods for investigating the course of underground waters]: Ingenieur, v. 52, no. 17–B 18, The Hague. [Original in Dutch] GA 4205.

Stevenson, A. F., 1934, On the theoretical determination of earth resistance from surface potential measurements: Physics, v. 5, p. 114–124. GA 2044.

——— 1935, On the theoretical determination of earth resistivity from surface potential measurements: Philos. Mag., v. 19, p. 297–306. Resistivity theory. GA 2464.

——— 1936, On the theoretical determination of earth resistance from surface potential measurements: Philos. Mag., v. 21, no. 142, p. 829–830. This is a correction to Stevenson's paper of the same title published in Philos. Mag., v. 19, no. 125, p. 297–306, 1935. (See Geophys. Abstract 2464.) The correction invalidates much of the previous paper. Resistivity. GA 3410.

Stoppel, Rose, 1929, Untersuchungen ueber die Schwankungen der lokalen elektrischen Ladung der Erde [Investigations on the variation of the local electric charge of the earth]: Gerlands Beitr. Geophysik, v. 21, no. 1, p. 116–134. GA no. 11, p. 19–20.

Strombeck, A. V. von, 1833, Über die von Herrn Fox angestellten Versuche in Bezug auf die elektro-magnetischen Äusserungen der Metallgange [The experiments of Mr. Fox concerning the electromagnetic characteristics of metallic ores]: Karsten's Archive, v. 6, p. 431–438.

Sumgin, M. I., and Petrovsky, A. A., 1947, Znacheniye elektricheskikh metodov dlya izucheniya vechnoy merzloty [The importance of electrical methods for the study of permanently frozen ground]: Akad. Nauk SSSR, Inst. Merzlotovedeniya Trudy, v. 5, p. 15–17. GA 10089.

Šumi, Franc, 1953, O mogućnosti odredjivanja nagiba kontakta izmedju dve geološke formatsije pomoću geoelektrične metode [On the possibility of determining the dip of the contact between two geologic formations by the geoelectric method: Serbia Zavod geol. i geofiz. istraživanja Vesnik, v. 10, p. 273–280. [German summary.] GA 157–58.

Šumi, Franc, 1956, Geoelectric exploration of inclined thin beds and ore veins: Geophys. Prosp. v. 4, p. 194–204. GA 166–146.

Sundberg, Karl, 1929, Prospecting by the Swedish geoelectrical methods: Inst. Mining and Metallurgy [London] Trans., v. 38, p. 335–354; 1929, Bull. 295, p. 1–20. GA no. 15, p. 15–16.

——— 1930a, Prospektieren auf Öl elektrischen Methoden [Prospecting for oil by electrical methods]: Petroleum, v. 26, no. 10, p. 317–324. GA no. 13, p. 13.

——— 1930b, Electrical prospecting for oil structure: Am. Assoc. Petroleum Geologists Bull., v. 14, no. 9, p. 1145–1163. Resistivity results. GA no. 18, p. 15–16.

——— 1931, Principles of the Swedish geoelectrical methods: Beitr. angew. Geophysik. v. 1, p. 298–361. Includes direct current methods in part. GA 224.

——— 1932, Effect of impregnating waters on electrical conductivity of soils and rocks: Am. Inst. Mining Metall. Engineers Trans., v. 97, p. 367–391. Contains references on composition of natural waters and on electrolytic dissociation. GA 667.

Sundberg, Karl, and Hedstrom, Helmer, 1929, Communication sur les recherches électriques de minérals et d'huiles [Communication on electrical methods of searching for minerals and oils]: Internat. Congrès Forage, Paris, 2d, p. 16–23; and Special print issued in Saint-Etienne, p. 1–19. GA no. 17, p. 19.

Sundberg, Karl, and Lundberg, Hans, 1929, Some practical results of electrical prospecting for ore: Inst. Mining and Metallurgy [London] Trans., v. 38, p. 368–385; Bull. 296, p. 1–18. GA no. 4, p. 16–18.

Sundberg, Karl, Lundberg, Hans, and Eklund, Jo, 1923, Electrical prospecting in Sweden: Sveriges Geol. Undersökning, Årsb. 17, no. 8, p. 1–74.

——— 1930, Swedish geoelectrical prospecting methods: Mining Mag., v. 43, p. 245–248, and p. 310–313. GA 98.

Sunde, Erling D., 1949, Earth conduction effects in transmission systems: New York, D. Van Nostrand Co., 373 p.

Suyama, Junji, 1953a, Equipment and field techniques of electrical prospecting: Butsuri-Tankō, v. 6, no. 3–4, p. 244–248. [Japanese, English summary.] GA 165–126.

——— 1953b, Electrical prospecting at the Oguchi gold mine, Kagoshima prefecture: Japan Geol. Survey Bull., v. 4, no. 11, p. 35–40. [Japanese, English summary.] GA 160–67.

Suyama, Junji, and Kobayashi, Hajime, 1953, Electrical prospecting at Kasuga gold mine, Kagoshima prefecture: Japan Geol. Survey Bull., v. 4, no. 12, p. 35–46. [Japanese, English summary.] GA 160–66.

Suyama, Junji, Saito, T., and Sugayama, K., 1952, Report of the geophysical prospecting at Yuryō mine, Rhime prefecture: Japan Geol. Survey Bull., v. 3, p. 45–50. [Japanese, English summary.] Self-potential, Direct current, Resistivity. GA 14865.

Swartz, J. H., 1931, Resistivity measurements upon artificial beds: U.S. Bur. Mines Inf. Circ. 6445, 9 p. Resistivity results. GA 102.

——— 1932, Oil prospecting in Kentucky by resistivity methods: U.S. Bur. Mines Tech. Paper 521, 23 p. Resistivity results. GA 1109.

——— 1937, Resistivity-studies of some salt-water boundaries in the Hawaiian Islands: Am. Geophys. Union Trans., v. 18, pt. 2, p. 387–393.

——— 1939, Geophysical investigations in the Hawaiian Islands: Am. Geophys. Union Trans., v. 20, pt. 2, p. 292–298.

Swartz, J. H., 1940a, Resistivity survey of Schofield Plateau: Hawaii Div. Hydrography Bull. 5, p. 56–60. GA 6045.

———— 1940b, Geophysical investigations on Lanai: Hawaii Div. Hydrography Bull. 6, p. 97–115. GA 6044.

Szabadváry, László, 1954, Kutató furásokra tamaszkodó geo-elektromos feltalajhutatás [Geoelectric soil investigations based on several borings]: Magyar Állami Eötvös Loránd Geofiz. Intézet. Geofiz. Közlemények, v. 3, no. 9, p. 121–141. [English and Russian summaries].

Tagg, G. F., 1929, Electrical-resistance method of geophysical surveying: Canadian Mining Jour., v. 50, no. 49, p. 1156–1159. Resistivity results. GA no. 10, p. 13–14.

———— 1930, The earth resistivity method of geophysical prospecting: some theoretical considerations: Mining Mag., v. 43, no. 3, p. 150–158. Resistivity theory. GA no. 20, p. 14.

———— 1931a, Earth resistivity surveying: Eng. Mining Jour., v. 131, p. 325–326. Resistivity methods and instruments. GA 427.

———— 1931b, Practical investigations of the earth resistivity method of geophysical surveying: Phys. Soc. London Proc., v. 43, p. 305–320. Resistivity theory. GA 581.

———— 1932, Interpretation of resistivity measurements: Am. Inst. Mining Metall. Engineers Tech. Pub. 477, 13 p.; 1934, Trans., v. 110, p. 135–147. Resistivity theory.

———— 1935, Earth resistivity surveying: Mining Mag., v. 53, p. 148–154. GA 2904.

———— 1936a, Earth resistivity surveying: Mining Mag., v. 54, p. 27–30. GA 3068.

———— 1936b, Earth-resistivity curves: Mining Mag., v. 55, no. 1, p. 28–31. Resistivity. GA 3411.

———— 1937, Interpretation of earth-resistivity curves: Am. Inst. Mining Metall. Engineers Tech. Pub. 755, 11 p.; 1940, Trans., v. 138, p. 399–407. Resistivity. GA 3616.

Tallquist, Hj., 1935, Sechsstellige Tafeln der 16 ersten Kugel-funktionen $P_n(x)$ [Six-place tables of the first 16 spherical functions $P_n(x)$]: Soc. Sci. Fennic. Acta, Nova Ser. A, v. 2, no. 4, p. 1–43.

———— 1937, Sechsstellige Tafeln der 32 ersten Kugelfunktionen $P_n(\cos \Theta)$ (Six-place tables of the first 32 spherical functions $P_n(\cos \Theta)$: Soc. Sci. Fennic., Acta, Nova Ser. A., v. 2, no. 11, p. 1–43.

Tarkhov, A. G., 1946, O geoelektricheskom pole fil'tratsii [Regarding the geoelectrical field due to filtration]: Akad. Nauk SSSR Izv. ser. geogr. i géofiz., v. 10, no. 5, p. 463–468. GA 9233.

———— 1947, Opyt primeneniya geofizicheskikh metodov krazvedke geologicheskikh struktur Evropeyskogo severa S.S.S.R. [Application of geophysical methods to the exploration of geological structures of the northern part of the USSR]: Vses. Nauchn.-Issled. Geol. Inst. Mater., Geofiz., no. 11, p. 40–57. GA 10649.

Tattam, C. M., 1937, The application of electrical resistivity prospecting to ground-water problems: Colorado School of Mines Quart., v. 32, no. 1, p. 117–138. Slightly abridged, but the only published version of original Doctor's thesis of 1932.

Teisseyre, Roman, 1951, Metody opom pozornego oraz metody, normalnego stosunku napieć w geoelektrycznych pracach poszukiwawczych (Methods of apparent resistivity and of potential-drop ratio in geoelectric prospecting]: Państwowy Insty. Geol. Biul. 63, Ser. geofiz. no. 6, p. 39–50. GA 13946.

Tennberg, C. T., 1929, Electrical prospecting for ore and oil: Chem. Eng. and Mining Rev., v. 22, no. 255, p. 86–90. Historical sketch. GA 11, p. 22.

Tennberg, Ingemar, 1928, Wann und wo soll man elektrisch schürfen [When and where shall the electrical method of prospecting be used]: Berg- u. Hüttenmänn. Monatsh., v. 76, no. 2, p. 53–55. GA no. 2, p. 22–23.

Thiele, Heinrich, 1951, Erfolge und Grenzen der Geoelektrik in der Grundwasserforschung [Results and limitations of geoelectric methods in ground water prospecting]: Bohr-technik-Brunnenbau, v. 2, no. 7, p. 158–166. Field examples, discussion. GA 14462.

———— 1952a, Die Geoelektrik in der Wasserschliessung, in Deutscher Verein von Gas- und Wasserfachmännern, Die Wassererschliessung [Electrical methods of prospecting for water]: Essen, Vulkan-Verlag Dr. W. Classen, pt. 2, p. 287–375. GA 13949.

———— 1952b, Stand der geoelektrischen Methoden in der Grundwassererschliessung—praktische Ergebnisse und Ent-wicklungsmöglichkeiten [State of geoelectrical methods in ground water prospecting—practical results and possibilities for development]: in "Neuere. Methoden der Grundwasser-erschliessung," Symposium of the Deutscher Verein für Gas- und Wasserfachmännern, in Hohensyburg bei Dortmund June 25–26, 1951, Hannover, p. 33–58. GA 14463.

Thiele, Siegfried, 1950, Die Geoelektrik in der Wassererschlies-sung—ein kritische Stellungnahme [Geoelectrical methods in exploration for water—a critical viewpoint]: Bohrtechnik-Brunnenbau, v. 1, no. 4, p. 98–104. Theoretical discussion. GA 14461.

Thoenen, J. R., 1932, Prospecting and exploration for sand and gravel: U.S. Bur. Mines Inf. Circ. 6668, 52 p. GA 1226.

Thomson, Sir William (first Baron-Lord Kelvin), 1884, Reprint of papers on electrostatics and magnetism, 2d ed.: London, Macmillan and Co., 596 p.

Thyer, R. F., Rayner, J. M., and Nye, P. B., 1937, Geophysical report on the Lolworth area, Charters Towers district: Aerial, Geol., and Geophys. Survey of Northern Australia Rept. Queensland no. 24, 8 p. Self-potential, Electro-magnetic, Potential-drop ratio. GA 5523.

Tikhonov, A. N., 1942, K voprosu o vliyanii neodnorodnosti zemnoy kory na pole telluricheskikh tokov [The effect of inhomogeneity of the earth's crust on the field of terrestrial currents]: Akad. Nauk SSSR Izv. ser. geogr. i geofiz., no. 5, p. 207–218. GA 7424.

———— 1946, Ob elektrozondirovanii nad naklonnym plastom [Concerning electrical sounding over an inclined layer]: Akad. Nauk SSSR Inst. Teor., Geofiz. Trudy, v. 1, p. 116–136. GA 9422.

Tikhonov, A. N., and Enenshteyn, B. G., 1953, Fizicheskiye prichiny oshibok, poluchayushchikhsya pri vypolnenii VEZ kompensatsionnym metodom [Physical causes of errors in vertical electrical sounding using the compensating method]: Prikladnaya geofizika, no. 10, p. 74–83. GA 164–106.

Tikhonov, A. N., and Tyurkisher, R. I., 1942, Vliyaniye pro-mezhutochnogo sloya pri vertikal'nom elektricheskom zondirovanii [The influence of an intermediate layer in vertical electrical sounding]: Akad. Nauk SSSR Izv. ser. geogr. i geofiz., no. 5, p. 219–227. GA 7858.

Tölke, F., 1937, Die geophysikalische Baugrunduntersuchung unter besonderer Berücksichtigung der geoelektrischen Aufschlussverfahren [Geophysical investigation of building ground with special consideration of geoelectrical methods of prospecting]: Bauingenieur, v. 18, p. 271–294. GA 4047.

Trudu, Renato, 1952, Curve di resistività per i due strati con contatto piano inclinato rispetto alla superficie del suolo [Resistivity curves for two layers with plane contact slightly inclined with respect to the surface of the earth]: Riv. Geofis. Appl., v. 13, no. 2, p. 95–110. Theoretical. GA 14457.

Tsekov, G. D. 1955, Metodika rascheta krivykh VEZ dlya potentsialustanovki s ispol'zovaniyem krivykh VEZ dlya gradiyent-ustanovki [Method of evaluating curves of the potential variation along a vertical electric profile, using similar curves for the potential-drop arrangement]: Akad. Neft. Prom. Trudy, no. 2, p. 142–149. GA 166–149.

Tsukada, Tadashi; Ochiai, Toshiro; Hasegawa, Kazuo; and Ozawa, Takeo, 1954, Electrical exploration of Isahaya Bay: Butsuri-Tankō, v. 7, no. 4, p. 202–207. GA 165–131.

Tuman, V. S., 1951, The telluric method of prospecting and its limitations under certain geologic conditions: Geophysics, v. 16, p. 102–114. Telluric, Self-potential. GA 12648.

Turlygin, S. Ya., and Karelina, N. A., 1951, Diffuzionnye nepolyarizuyushchiyezya elektrody [Nonpolarizable diffusion electrodes]: Akad. Nauk SSSR Doklady, v. 79, no. 6, p. 965–968.

Tyurkisher, R. I., 1944, Ob odnoy zadache vertikal'nogo elektricheskogo zondirovaniya [A problem in vertical electrical profiling]: Akad. Nauk SSSR Izv. ser. geogr. i geofiz., v. 8, no. 4, p. 154–156. GA 7995.

—— 1945, Elektrokarottazh v anizotropnoy srede [Electric coring in an anisotropic medium]: Akad. Nauk SSSR Izv. ser. geog. i geofiz., v. 9, no. 3, p. 279–287. GA 9046.

—— 1946, Vychisleniye polya tochechnogo istochnika, nakhodyashchegosya nad naklonnym plastom [Calculation of the field of a point-source placed over an inclined layer]: Akad. Nauk SSSR Inst. Teor. Geofis. Trudy, v. 1, p. 137–142. GA 9423.

Uchman, Jan, and Sobieski, Zenon, 1951, Opis aparatury do geofizychnych badán poszukiwawczych metoda oporowa [Description of instruments employed in geophysical exploration by resistivity methods]: Państwowy Instv. Geol. Biul. 63, Ser. geofiz. no. 6, p. 33–38. GA 13948.

Unz, M., 1953, Apparent resistivity curves for dipping beds: Geophysics, v. 18, p. 116–137. Direct current resistivity, theoretical, field problem. GA 14262.

Uryson, V. O., 1956, Ob umen'shenii vliyaniya pomekh na glubokoye elektricheskoye zondirovaniye [On the reduction of the effect of disturbances on deep electric profiling]: Akad. Nauk SSSR Izv. ser. geofiz., no. 7. p. 801–812. GA 167–91.

Uryson, V. O., and Egorov, B. D., 1935, Elektricheskaya razvedka mineral'nykh vod v rayone s Bol'shikh Soley Ivanovskoy Obl. [Electrical exploration of mineral waters in the area of the village of Bolshie Soli, District of Ivanovsk]: Mosk. Geol. gidrolog.-geod. Tresta, Moscow, Izv., v. 3, no. 2, p. 70–80.

Utzmann, R., 1954, Electric and telluric prospecting-studies of small scale models: Franc. Techniciens Petrole Assoc. Bull. 107, p. 347–406, Abstract 1–8204, API Abstracts, v. 1, no. 50.

Vallet, J. M., 1949, Étude des courants électriques naturels liés au carbonifère de la région de Salins-Chandoline-Bramois près de Sion, Valais [Study of natural earth currents associated with Carboniferous rocks in the region of Salins-Chandoline-Bramois near Sion, Valais]: Soc. physique et historie nat. Genève, Archives des Sci., v. 2, p. 22–56. Self-potential. GA 11555.

Van Nostrand, R. G., 1953, Limitations on resistivity methods as inferred from the buried sphere problem: Geophysics, v. 18, p. 423–433. GA 14447.

—— 1954, The orthogonality of the hyperboloid functions: Jour. Math. Physics, v. 33, p. 276–282.

Van Nostrand, R. G., and Cook, K. L., 1955, Apparent resistivity for dipping beds—a discussion: Geophysics, v. 20, p. 140–147. GA 160–59.

Vargas, M. 1941, Nota sobre prospeccao geofisica pelo metodo das resistividades [Note on geophysical prospecting by the electrical resistivity method]: Bol. Depart. Estr. Rodag., v. 7, no. 23, p. 149–160. [Brazil] GA 8719.

Vecchia, Orlando, 1951, Prospezione geofisica su di un filone di Zn e Pb al Mottarone, in Provincia di Novara (Piemonte) [Geophysical exploration of a lead-zinc vein at Mottarone in the province of Novara (Piemonte)]: Riv. Geofis. Appl., v. 12, no. 1, p. 15–20. Resistivity, Self-potential. GA 13236.

—— 1953, Recherches geophysiques pour un barrage au lac de Molvano (Venezia Tridentina) [Geophysical investigations for a dam on the Lake of Molveno (Venezia Tridentina)]: Riv. Geophysica Appl., v. 14, no. 2, p. 73–85. GA 158–105.

Ventocilla, J. F., 1949, La exploración del subsuelo por el metodo eléctroco para localizer los depósitos de grava [Prospecting for gravel deposits by electrical methods]: Soc. ing. Peru Inf. y Mem., v. 50, no. 7, p. 271–281. Resistivity. GA 11556.

Veshev, A. V., Semenov, A. S., and NovoZhilova, M. E., 1952, Novyy vid yestestvennogo elektricheskogo polya v zemle [A new kind of natural electric field in the ground]: Akad. Nauk SSSR Doklady, v. 87, no. 6, p. 939–941. Telluric current. GA 14642.

Vincenz, S. A., 1954, A resistivity survey in Scotland: Colliery Eng., v. 31, no. 362, p. 157–163. GA 162–80.

Volker, A., and Dijkstra, J., 1955, Détermination des salinités des eaux dans le sous-sol du Zuiderzee par prospection géophysique [Determination of the salinity of ground water beneath the Zuiderzee by geophysical exploration]: Geophys. Prosp., v. 3, p. 111–125. GA 162–73.

Walter, A. J. P., 1936, Earth-resistivity measurements: Mining Mag., v. 54, no. 6, p. 341–345. Resistivity. GA 3413.

—— 1937, The probe electrode: Mining Mag., v. 57, no. 3, p. 148–157. GA 4048.

Walters, R. C. S., 1949, Some geophysical experiences in water supply: Inst. Water Eng. Jour., v. 3, p. 436–441. Resistivity. GA 12469.

Wantland, Dart, 1937, Comparison of geophysical surveys and the results of operations at the Roscoe Placer by the Humphreys Gold Corporation, Jefferson County, Colorado: Colorado School of Mines Quart., v. 32, no. 1, p. 95–108.

—— 1952, Geophysical investigations for United States Atomic Energy Commission in the Colorado Plateau area: U.S. Bur. Reclamation Geology Rept. G–119. 141 p. Field examples given. GA 14467.

Watson, G. N., 1952, A treatise on the theory of Bessel functions: 2d ed., Cambridge, The Univ. Press, 804 p.

Watson, R. J., 1934, A contribution to the theory of the interpretation of resistivity measurements obtained from surface potential observations: Am. Inst. Mining Metall. Engineers Tech. Pub. 518, 34 p.; 1934, Trans., v. 110, p. 201–236. GA 1857.

Watson, R. J., and Johnson, J. F., 1938, On the extension of two-layer methods of interpretation of earth resistivity data to three and more layers: Geophysics, v. 3, p. 7–21. Resistivity. GA 4367.

Way, H. J. R., 1941, Geophysical prospecting for water in Uganda: Mining Mag., v. 65, p. 63–69. GA 6304.

────── 1942, An analysis of the results of prospecting for water in Uganda by the resistivity method: Inst. Mining and Metallurgy [London] Bull. 455, p. 1–26. GA 6723.

────── 1944, Reef prospecting by the resistivity method in Uganda: Am. Inst. Mining Metall. Engineers Tech. Pub. 1676, 17 p.; 1945, Trans., v. 164, p. 125–141. GA 7566.

Weaver, Warren, 1928, Certain applications of the surface potential method: Am. Inst. Mining Metall. Engineers Tech. Pub. 121, 16 p.; 1929, Trans., v. 81, p. 68–86. Resistivity theory.

────── 1930, Mathematics and the problem of ore location: Am. Math. Monthly, v. 37, p. 165–181. Resistivity theory.

Webb, J. H., 1931a, Potential due to a buried sphere: Phys. Rev., v. 7, p. 292–302. GA 105.

────── 1931b, Potential due to a buried spheroid: Phys. Rev., v. 38, p. 2056–2068. GA 930.

Weiss, Oscar, 1946, Geophysical prospecting for water in the dolomite: Chem. Metall. Mining Soc. South Africa Jour., v. 47, p. 155–163. GA 9424.

Weiss, Oscar and Frost, A., 1950, Geological results of geophysical prospecting for water on the new gold fields of the Orange Free State of the Union of South Africa: Internat. Geol. Cong. 18th, London, 1948, Proc., p. 5, sec. D, p. 133–137. Resistivity. GA 12837.

Wellman, H. W., 1948, Kawau copper mine—self-potential electrical prospecting: New Zealand Jour. Sci. Technology, v. 29, p. 247–256. GA 10878.

Wells, R. C., 1914, Electric activity in ore deposits: U.S. Geol. Survey Bull. 548, 78 p.

Weng, Wen-Po, 1948, A potential gradient method for electrical survey: Chinese Geophys. Soc. Jour., v. 1, no. 1, p. 51–55. GA 11112.

Wenner, Frank, 1912, The four-terminal conductor and the Thomson bridge: U.S. Bur. Standards Bull., v. 8, p. 559–610. Resistivity theory. Gives proof of reciprocity theorem.

────── 1915, A method of measuring earth resistivity: U.S. Bur. Standards Bull., v. 12, Sci. Paper 258, p. 469–478. Resistivity theory.

West, T. S., 1948, Deep electrical prospecting—a reply: Geophysics, v. 13, p. 97–98. GA 10091.

West, T. S., and Beacham, C. C., 1944, Precise measurement of deep electrical anomalies: Geophysics, v. 9, p. 494–539. Resistolog. GA 7712.

────── 1946, A Resistolog survey of the Loma Alto-Seven Sisters area of McMullen and Duval Counties, Texas: Geophysics, v. 11, p. 491–504. GA 9047.

Wetzel, W. W., and McMurry, H. V., 1937, A set of curves to assist in the interpretation of the three-layer resistivity problem: Geophysics, v. 2, p. 329–341. Resistivity. GA 4206.

Whetton, J. T., 1937, The resistivity method applied to mining problems: Mine and Quarry Eng., v. 2, no. 1, p. 24–28. Resistivity. GA 4049.

Whetton, J. T., and Myers, J. O., 1949a, Earth resistivity measurements, tracing of galena-fluorspar veins at shallow depths: Mine and Quarry Eng., v. 15, p. 37–44. Resistivity. GA 11557.

Whetton, J. T., 1949b, Application of electrical resistivity measurements to the location of coal seams at shallow depth: Leeds Philos. Lit. Soc. Proc., v. 5, p. 263–268. Resistivity. GA 12465.

Whitehead, S., and Radley, W. G., 1948, Interpretation of data from electrical resistivity geophysical surveys: Nature, v. 162, p. 187.

Wiebenga, W. D., 1955, Geophysical investigations of water deposits, Western Australia: Australia Bur. Min. Resources Geology and Geophysics Bull. 30, 48 p., 1955. GA 166–153.

Wilckens, Friedrich, 1956, Geoelektrische Untersuchung der Graphitlagerstätte Kropfmühle im bayerischen Wald [Geoelectrical investigation of the Kropfmuhle graphite deposit in the Bavarian Forest]: Geofisica Pura e Appl., v. 33, p. 91–100. GA 166–154.

Wilcox, S. W., 1935a, Prospecting for road metals by geophysics: Eng. News Record, v. 114, p. 271–275. Resistivity. GA 2591.

────── 1935b, Application of earth resistivity methods to sand and gravel surveys: Minnesota State Highway Dept. Circ., 8. p. GA 2848.

────── 1944, Sand and gravel prospecting by the earth resistivity method: Geophysics, v. 9, p. 36–46. GA 7425.

Wilcox, S. W., and Schwartz, G. M., 1934, Reconnaissance of buried river gorges by the earth resistivity method: Econ. Geology, v. 29, p. 435–453. GA 2136.

Wilson, C. H., 1932, Economic value of geophysics in mining: Mining Jour., v. 15, p. 3–5. GA 830.

Winsauer, W. O., and McCardell, W. M., 1953, Ionic double-layer conductivity in reservoir rock: Petroleum Technology Jour., v. 5, p. 129–134. Theoretical, Experimental. GA 14454.

Winsauer, W. O., Shearin, H. M., Jr., Masson, P. H., and Williams, M., 1952, Resistivity of brine-saturated sands in relation to pore geometry: Am. Assoc. Petroleum Geologists Bull., v. 36, no. 2, p. 253–277.

Witte, Leendert de, 1948, A new method of interpretation of self-potential field data: Geophysics, v. 13, p. 600–608. Self-potential. GA 11313.

────── 1950, Relations between resistivities and fluid contents of porous rock: Oil and Gas Jour., v. 49, no. 16, p. 120–132.

Witte, Leendert de, Fournier, K. P., and Tejada-Flores, Hernan, 1957, Calculation of guard electrode response curves: Geophysics, v. 22, p. 67–74. GA 168–101.

Wood, F. C., Jr., 1936, Prospecting for water by electrical resistivity: Oklahoma Acad. Sci. Proc., v. 17, p. 79–82.

Workman, L. E., and Leighton, M. M., 1937, Search for ground-waters by the electrical resistivity method: Am. Geophys. Union Trans., v. 18, pt. 2, p. 403–409.

Wyllie, M. R. J., 1949, A quantitative analysis of the electrochemical component of the S. P. curve: Jour. Petroleum Technology, v. 1, no. 1, Tech. Paper Sec., Tech. Pub. 2511, p. 17–26; Am. Inst. Mining Metall. Engineers Trans., v. 186, p. 17–26.

────── 1954, The fundamentals of electric log interpretation: New York, Academic Press, 126 p.

Yoshimatsu, Takasaburo, 1954, The local characteristics of earth currents: Kakioka Magnetic Observatory Mem., v. 7, no. 1, p. 15–26. GA 158–85.

Yosikawa, Haruo, 1955, Some example of electrical prospecting in the area bearing black ore ("Kurokō") deposits: Butsuri-Tankō, v. 8, no. 3, p. 95–103. GA 166–158.

Yudkevich, R. V., 1954, Ob otsenke neftenosnosti plastov s malym udel'nym soprotivleniem [The valuation of the oil-bearing potential of reservoirs characterised by low specific resistivity]: Prikl. Geofizika, no. 11, p. 63-71. Defines "coefficient of resistivity increase" of oil-bearing rock as the ratio of its resistivity when filled with oil to that when saturated with water. GA 164-105.

Yüngül, Sulhi, 1948, Deep electrical prospecting—a discussion: Geophysics, v. 13, p. 92-97. GA 10092.

——— 1950, Interpretation of spontaneous polarization anomalies caused by spheroidal bodies: Geophysics, v. 15, p. 237-246. Self-potential. GA 12048.

——— 1954, Spontaneous potential survey of a copper deposit at Sariyer, Turkey: Geophysics, v. 19, p. 455-458. Self-potential. GA 158-106.

Zabelli, Arnaldo, 1931, De l'interprétation des mesures géoelectriques [Interpretation of geoelectrical measurements]: L'Écho Mines et Métallurgie, v. 59, no. 3073, p. 639-642. GA 526.

Zaborovskiy, A. I., 1943, Elektrorazvedka [Electrical exploration]: Moscow, Gos. Nauchn.-Tekhn. Izd. Neft. i Gorn.-Toplivn. Lit., 444 p. Comprehensive textbook includes theoretical foundations and practical methods of electrical prospecting. GA 8120.

Zaccara, Gaetano, 1954, Experimenti geofisica nell'isola di Capri e nella peninsola Sorrentina [Geophysical experiments on the island of Capri and on the Sorrento peninsula]: Servizio geol. Italia Boll., v. 76, no. 1, p. 315-321. GA 162-81.

Zaccara, Gaetano, and Manfredini, Antonio, 1951, Analisi geoelettrica di un terreno di fondazione [Geoelectric investigation of a foundation site]: Servizio geol. Italia Boll., v. 73, p. 125-146. Resistivity. GA 13954.

Zachos, K., 1944, Geophysikalische—magnetische, elektrische und Suszeptibilitäts-Untersuchungen bei Lam, Bayr. Wald [Geophysical investigations in Lam, Bavarian Forest, by magnetic, electrical, and susceptibility measurement]: Beitr. angew. Geophysik, v. 11, p. 1-35. Resistivity. GA 11257.

Zagorac, Željko, 1954, Istrazivanje vode u krsu i upotreba primjenjene geofizike [Prospecting for water in karst and the use of applied geophysics]: Geol. Vjesnik [Zagreb], v. 5-7, p. 201-216 [1951-53]. GA 160-63.

Zheleznyak, A. I., 1937, Elektrokarottazh v Donbas [Electrical coring in the Donbas (in exploring for coal)]: Gornyy Zhurnal, Moscow, no. 14, p. 51-53.

——— 1947, Nekotoryye dannyye o prichinakh vozniknoveniya yestestvennogo elektricheskogo polya na ugol'nykh plastakh Donetskogo basseyna [Certain data on the causes of the formation of a natural electrical field in the coal strata of the Donbas]: Razvedka Nedr, no. 4, p. 43-46. Self-potential. GA 10601.

INDEX

309